Land Subsidence and Mitigation Potential in the Mekong Delta: Extension and Application of Hydrogeomechanical Loading Approaches, Combined with Multi-Parameter Subsurface Monitoring and Numerical Simulations

Zur Erlangung des akademischen Grades eines

DOKTORS DER INGENIEURWISSENSCHAFTEN (Dr.-Ing.)

von der KIT Fakultät für

Bauingenieur-, Geo- und Umweltwissenschaften

des Karlsruher Instituts für Technologie (KIT)

genehmigte

DISSERTATION

von

M.Sc. Felix C. Dörr

Tag der mündlichen Prüfung: 22.05.2026

Referent: Prof. Dr.-Ing. Dr. h.c. mult. Franz Nestmann

Korreferent: Prof. Dr. Stefan Norra

Korreferent: PD Dr. Ulf Mohrlok

Karlsruhe (2026)



This document is licensed under a Creative Commons
Attribution-ShareAlike 4.0 International License (CC BY-SA 4.0):
https://creativecommons.org/licenses/by-sa/4.0/deed.en

Acknowledgements

This work was carried out at the Karlsruhe Institute of Technology, at the Institute of Applied Geosciences and the Institute for Water and Environment, building upon the ViWaT-Engineering project, a joint German–Vietnamese research cooperation funded by the German Federal Ministry of Research, Technology and Space (funding reference: 02WCL1474A). This continuation of the ViWaT research efforts was made possible through the generous support of the Hector Fellow Academy, which funded my position and additional research expenses. Publication fees were covered by the KIT-Publication Fund of the Karlsruhe Institute of Technology.

I would like to express my sincere gratitude to my supervisor Prof. Dr.-Ing. Dr. h.c. mult. Franz Nestmann, who initiated the ViWaT project in the first place, supported me as Hector Fellow in the application of my scholarship and provided exceptionally valuable scientific guidance and personal mentorship throughout my work. For this, I am deeply and sincerely grateful.

Likewise, I am grateful to my co-supervisor, Prof. Dr. Stefan Norra, who welcomed me into his research group and leads it with an exceptionally positive and supportive attitude that fosters genuine scientific curiosity and confidence in the abilities of all team members. Through his leadership within the group and the ViWaT-Engineering project, he continuously encouraged me and established a working atmosphere that I genuinely enjoyed.

In this context, I thank PD Dr. Elisabeth Eiche, who subsequently took over leadership of the KIT branch of our working group with great empathy and dedication, and Prof. Dr. Jochen Kolb, head of the department, for providing the institutional framework.

I would like to sincerely thank PD Dr. Ulf Mohrlok and Prof. Dr.-Ing. Stefan Hinz for joining my committee and for their interest and willingness to evaluate my work. I thank Prof. Dr.-Ing. Hans Henning Stutz for providing access to software packages and to the geomechanical laboratory at the Institute of Soil Mechanics and Rock Mechanics at KIT.

My personal and scientific development was greatly supported by the Graduate School for Climate and Environment (GRACE), which offered valuable courses and training programs and funded a three-month research stay abroad. During this stay, I was warmly welcomed by Dr. Elias Lewi at the Institute of Geophysics, Space Science and Astronomy (IGSSA) at Addis Ababa University, whose scientific and personal perspectives truly inspired me. My time at IGSSA proved to be a highly productive period and fostered valuable scientific and cultural exchange with outstanding Ethiopian colleagues. Also, I thank Dr. Gabriel Rau for his great support and guidance in regard to scientific writing.

I would like to extend special thanks to my close colleague, Dr. Jonas Bauer. When I joined the research group, he helped me to find my way around and introduced me to scientific and institutional workflows. Over the past years, we have worked closely together and published our research findings collaboratively. It was a joy to pursue the path towards PhD together and I am grateful for the friendship that we established beyond scientific collaboration.

Likewise, I thank my colleague Hoan Viet Tran for the amazing times we had during field trips and for introducing me to Vietnamese culture. Without his expertise in groundwater-related fieldwork and practical implementation, many outcomes of this dissertation would not have been possible. I thank my colleague Van Cam Pham for supporting me in my research and for managing translation and communication between German and Vietnamese partners.

I thank Dr. Flavia Digiacomo and Dr. Teba Gil-Diaz for sharing their experiences in scientific career development, for our friendly and fruitful conversations throughout the years and for reviewing this dissertation. Likewise, I want to thank Tino Wilhelm-Degenhardt, who also reviewed my work and, over the years, has become a valued friend.

I thank all current and former colleagues at the Institute of Applied Geosciences, particularly Andre Wilhelms and Dr. Nicolas Börsig, for countless private and work-related discussions and scientific exchanges over the years. Equally I thank all members

of the interdisciplinary ViWaT Team, in particular Dr.-Ing. Andreas Schenk, Dr.-Ing. Nils Dörr, Vu Huu Long, Dr. Moritz Zeemann and Dr.-Ing. Hoang Thai Duong Vu for the amazing cooperation and great times during field trips.

Although no words can fully express my gratitude, I would like to thank my family. My father Helmut, who passed away during the early stage of my PhD, inspired me throughout my life and was, and always will be, a great role model to me. Being exceptionally kind-hearted, bright-minded, and warmly respectful, he was a remarkable scientist, a dear friend to many, and above all, the best father anyone could wish for. I sincerely thank my mother Barbara for always being there for me, in childhood, during my studies and now as a young adult. I thank my sister Christina, her husband Daniel and their daughter Lina, for making my life brighter and always supporting me. I thank my parents-in-law, Carmen and Uwe and my brother-in-law Maximilian, who warmly welcomed me to their family, introduced me to cultural habits and traditions of the Siegerland, and created a sense of belonging that I deeply appreciate. Their support, particularly during the final months of completing my dissertation, by frequently taking care of our son, was invaluable.

Finally, and most importantly, I thank my wonderful wife Katharina and our son Elijah. They make my life complete, remind me of the truly important things in life, and bring joy to each day. I feel incredibly fortunate and grateful beyond words. Thank you!

Declaration of Authorship

I hereby declare that I have written this dissertation independently and have adhered to the principles of the Karlsruhe Institute of Technology for ensuring good scientific practice. All sources and tools used have been fully and accurately acknowledged. In the preparation of this work, ChatGPT was used solely for linguistic revision and improvement of readability. Full responsibility for the entire content of this dissertation rests with me.

Abstract

Land subsidence poses major threats to many river deltas around the world, with severe impacts on their populations and environments. The Vietnamese Mekong Delta ranks among the most critically affected deltas worldwide, facing uncertain long-term viability due to its low elevation and progressive subsidence dynamics. While groundwater depletion is often discussed as the dominant subsidence driver, uncertainties regarding the contributions of groundwater depletion and other processes like autocompaction and structural loading of the built environment persist. This constrains reliable assessments of the effectiveness of potential mitigation and adaptation measures and challenges their implementation.

To address these uncertainties, this dissertation elaborates a high-resolution, process-based approach for investigating subsidence dynamics in the Mekong Delta. This framework advances the understanding of groundwater-depletion-induced subsidence and investigates processes and subsurface parameters relevant to mitigation and adaptation strategies. To overcome limitations of previous delta-wide approaches, a distinctly local yet representative perspective is adopted, providing the data density required for robust and reliable process quantification. The approach integrates depth-differentiated compaction monitoring, continuous groundwater and meteorological observations, geodetic measurements, geomechanical parameterization, physics-informed numerical modelling and passive subsurface characterization.

The results demonstrate that groundwater depletion can be quantified with high reliability as the primary driver of subsidence at the investigated study site, while autocompaction and structural loading of the built environment contribute a secondary yet recognizable share. Observed spatiotemporal heterogeneity and extremes in subsidence rates with high local variance cannot be fully explained by the considered groundwater depletion and surface loading alone. Well-casing failure is therefore proposed and numerically validated as a previously unaddressed anthropogenic

pathway that may locally accelerate subsidence by providing local subsurface drainage pathways and a local equilibration of hydraulic heads between aquitards and the tapped aquifers.

Loading effects are identified to control measured groundwater heads in the Mekong Delta. This novel insight is utilized for passive subsurface characterization, revealing limited rebound and subsidence mitigation potential of deep aquifers. Seasonal surface water loading is shown to mask ongoing groundwater depletion during the rainy season, where rising heads had previously been misinterpreted as indicators of groundwater recharge. This finding underlines the importance of restricting groundwater extraction for preventing advancing depletion and associated subsidence. The management of shallow groundwater resources is identified as a priority mitigation measure, as hydraulic heads in these aquifers largely control the compaction of the overlying soft and highly compressible Holocene strata. Because these shallow waters are often saline and therefore of minor domestic relevance, preventing their depletion may be comparatively achievable.

Beyond the Mekong Delta, the developed framework is transferable to other deltaic systems. The novel integration of ocean and river tide loading into passive subsurface characterization overcomes previous methodological limitations in tide-dominated environments and enables such cost-efficient aquifer parameterization in data-scarce deltaic regions worldwide. The elaborated *recharge-illusion* concept is particularly relevant for deltaic settings, where seasonal inundation, amplified by expanding aquaculture, can generate high-magnitude loading signals in groundwater heads, with great potential for misinterpretation if overlooked. Overall, the results of this local-scale yet largely representative analysis indicate that, despite a significant delay in subsidence response to past groundwater depletion, the existential risk of subsiding below sea level in the near future can be averted if advancing groundwater head depletion is rigorously prevented in the Mekong Delta.

Zusammenfassung

Landsenkungen stellen eine erhebliche Bedrohung für viele Flussdeltas weltweit dar und haben gravierende Auswirkungen auf deren Bevölkerung und Umwelt. Das vietnamesische Mekong Delta zählt zu den am stärksten betroffenen Deltas weltweit und sieht sich aufgrund seiner geringen Höhenlage und fortschreitender Landsenkungsdynamiken mit einer unsicheren langfristigen Zukunftsfähigkeit konfrontiert. Obwohl die starke Grundwasserentnahme häufig als dominanter Faktor für die Landsenkung diskutiert wird, bestehen weiterhin Unsicherheiten und Zweifel hinsichtlich der jeweiligen Beiträge von Grundwasserabsenkung und weiterer Prozesse wie Autokompaktion und Auflasten durch die bebaute Umwelt. Dies schränkt belastbare Bewertungen der Wirksamkeit potenzieller Minderungs- und Anpassungsmaßnahmen ein und erschwert deren Umsetzung.

Um diese Unsicherheiten zu adressieren, entwickelt diese Dissertation einen hochaufgelösten, prozessbasierten Ansatz zur Untersuchung der Landsenkungsdynamik im Mekong Delta. Dieser Rahmen vertieft das Verständnis hinsichtlich grundwasserbedingter Landsenkung und analysiert Prozesse sowie Untergrundparameter, die für Minderungs- und Anpassungsstrategien relevant sind. Um die Einschränkungen früherer deltaweiter Ansätze zu überwinden, wird eine dezidiert lokale, zugleich jedoch repräsentative Perspektive eingenommen, die die für eine robuste und verlässliche Prozessquantifizierung erforderliche Datendichte bereitstellt. Der Ansatz integriert tiefendifferenzierte Kompaktionsmessungen, kontinuierliche Grundwasser- und meteorologische Beobachtungen, geodätische Messungen, geomechanische Parametrisierung, physikalisch fundierte numerische Modellierung sowie passive Untergrundcharakterisierung.

Die Ergebnisse zeigen, dass die Grundwasserentnahme mit hoher Verlässlichkeit als primärer Treiber der Landsenkung am untersuchten Standort quantifiziert werden kann, während Autokompaktion und Auflasten durch die bebaute Umwelt einen sekundären, jedoch erkennbaren Anteil beitragen. Beobachtete räumlich-zeitliche

Heterogenität und extreme Landsenkungsraten mit hoher lokaler Variabilität können nicht allein durch die modelltechnisch abgebildeten Grundwasserabsenkungen und Oberflächenauflasten erklärt werden. Fehlstellen an Brunnenverrohrungen werden in diesem Zusammenhang als bislang unerkannter anthropogener Prozesspfad identifiziert und numerisch validiert, welcher durch ein lokales Angleichen der Grundwasserpotentiale zwischen grundwasserseitig erschlossenen Aquiferen und darüberliegenden Aquitarden, sowie durch die Schaffung von zusätzlichen Drainagepfaden lokal zu einer Beschleunigung und Verstärkung der Landabsenkung führen kann.

Auflasteffekte an der Oberfläche werden als maßgebliche Einflussfaktoren gemessener Grundwasserpotenziale im Mekong Delta identifiziert. Diese neue Erkenntnis wird für die passive Untergrundcharakterisierung genutzt und zeigt ein begrenztes Landhebungs- und Minderungspotenzial tiefer Aquifere. Es wird nachgewiesen, dass Signale von saisonalen Auflasten durch Oberflächengewässer während der Regenzeit fortschreitend fallende Grundwasserdruckspiegel in Messzeitreihen überlagern, wobei steigende Grundwasserpotenziale zuvor häufig als Indikatoren für Grundwasserneubildung fehlinterpretiert wurden. Diese Erkenntnis unterstreicht die Notwendigkeit einer Begrenzung der Grundwasserentnahme, um fortschreitend fallende Grundwasserdruckspiegel und die damit verbundene Landabsenkung zu verhindern. Die Ergebnisse identifizieren das Management flacher Grundwasserressourcen als prioritäre Minderungsmaßnahme, da die hydraulischen Potenziale dieser Aquifere maßgeblich die Kompaktion der darüberliegenden weichen und hochkompressiblen holozänen Sedimente beeinflussen. Da diese oberflächennahen Grundwässer häufig salzhaltig und daher von geringer Bedeutung bei der Bereitstellung von Frischwasser sind, erscheint in diesen Aquiferen die Vermeidung einer weiteren Grundwasserspiegelabsenkung vergleichsweise gut umsetzbar.

Über das Mekong Delta hinaus ist der entwickelte Ansatz auf andere Deltasysteme übertragbar. Die neuartige Integration von Meeres- und Flusstiden in Methoden zur passiven Untergrundcharakterisierung überwindet bisherige methodische Einschränkungen in gezeitenbeeinflussten Umgebungen und ermöglicht so eine kosteneffiziente

Aquiferparametrisierung in datenarmen Deltaregionen weltweit. Das ausgearbeitete „*Recharge-Illusion*“-Konzept ist insbesondere für Deltas von Bedeutung, in denen saisonale Überflutung, verstärkt durch die Ausweitung aquakultureller Landnutzung, starke Auflastsignale in Grundwasserstandsmessungen erzeugen kann, die, sofern sie unbeachtet bleiben, ein erhebliches Fehlinterpretationspotenzial bergen. Insgesamt zeigen die Ergebnisse dieser lokalräumigen, jedoch weitgehend repräsentativen Analyse, dass trotz der deutlich verzögerten Reaktion der Landsenkung auf vergangene Grundwasserspiegelabsenkungen das existenzielle Risiko eines Absinkens unter den Meeresspiegel in naher Zukunft vermieden werden kann, sofern ein fortschreitendes Fallen der Grundwasserdruckspiegel im Mekong Delta konsequent verhindert wird.

Table of Content

1 Introduction 1

1.1 A century of sinking grounds – 100 years of subsidence due to groundwater exploitation and ongoing challenges today 1

1.2 River deltas as hotspots of land subsidence and multi-hazard interactions 4

1.3 Addressing cascading hazards in the Vietnamese Mekong Delta – the ViWaT initiative 6

1.4 Land subsidence in the Vietnamese Mekong Delta 7

1.5 Research focus and objectives 13

2 Materials and Methods 17

2.1 The concept of hydrogeomechanical coupling 18

2.2 Monitoring and data acquisition 19

2.3 Data analysis in time domain 24

2.4 Data analysis in frequency domain 29

2.5 Sample analysis and subsurface parametrization 34

2.6 Numeric simulations 35

3 Scientific Contributions 39

3.1 Concise summary of novel insights and publications 39

3.2 Tidal subsurface analysis provides insights into land subsidence dynamics and mitigation potential 42

3.3 The impact of seasonal surface loading on groundwater heads and recharge analyses 51

3.4 Simulating subsidence due to various drivers 55

3.5 Inferring process dynamics from land subsidence observations 62

4 Synoptic discussion 75

4.1 Groundwater head responses to external forcings and their implications for managing deltaic water resources and subsidence 75

4.2 Anthropogenic drivers for land subsidence in the Mekong Delta 82

4.3 Implications for adaptation and mitigation strategies 86

5 Conclusion 91

References 93

Appendix A First-author publications 103

Appendix B Co-author publications 179

List of Figures

Figure 1: Global extent of land subsidence due to groundwater withdrawal, modified after Gambolati and Teatini (2021). 2

Figure 2: From anthropogenic stressors to cascading hazards in deltaic systems: An overview of anthropogenic stressors and associated activities which disturb the water and sediment balances and trigger cascading hazards. 5

Figure 3: Map of the Vietnamese Mekong Delta. 6

Figure 4: Land subsidence in the Mekong Delta between 2017 and 2022, modified after N. Dörr et al. (2024). 8

Figure 5: Hydrogeological cross-section through the southern Mekong Delta, modified after Hoan et al. (2022) 10

Figure 6: Schematic illustration of the methodological framework. 17

Figure 7: Schematic overview of the ViWaT research site GW1, illustrating the individual monitoring components and subsurface sampling. 20

Figure 8: Photograph of the monitoring site GW1, showing the locations of the soil moisture sensor probe ①, three deep groundwater observation wells ②, the meteorological monitoring station ③, the corner reflector ④ and the land subsidence observatory ⑤. 22

Figure 9: Location of groundwater monitoring sites used within this dissertation. .. 23

Figure 10: Correlation between surface loading and groundwater head dynamics at GW1 (a), modified after Dörr et al. (2026a) and correlation between extensometer signal and groundwater head dynamics (b). 25

Figure 11: Groundwater head response in observation well GW1c to three selected precipitation events, modified after (Dörr et al., 2026a). 26

Figure 12: Barometric response functions and corresponding corrected groundwater heads with and without additional Earth tide consideration. 28

Figure 13: Barometric response functions (a) and corrected groundwater heads (b) for GW1c using single- and multi-factor regression deconvolution. 29

Figure 14: Groundwater head measurements at the monitoring site Q199 (a-b) and the respective amplitude characterization obtained by FFT and HALS (c). ... 31

Figure 15: Simplified workflow of the novel disentanglement of river tide influences in groundwater signals, modified after Dörr et al. (2026a). 33

Figure 16: Compressibility curve (a) and the time compression curve (b) of a sample from 20.7 m depth at GW1 35

Figure 17: Schematic illustration of the extent and mesh of the two-dimensional model domain, together with surface characteristics and the locations of the evaluated reference points. 36

Figure 18: Conceptual illustration of how well-casing failure (b) enhances land subsidence compared with undisturbed subsurface conditions (a) 37

Figure 19: Transient analysis showing groundwater head dynamics (a), periods with all-time minima heads (b), hydraulic head differences between aquifers (c), M_2 phase shift (d) and amplitude response (e) 47

Figure 20: M_2 phase shift dynamics and subsidence trends at the monitoring site IGPVN between 2017 and 2021. 49

Figure 21: Change of void ratio over the past 4,000 years; initial values were calibrated to achieve a good fit of modeled values with recent-day measurements. ... 60

Figure 22: Change of vertical hydraulic conductivity over the past 4,000 years; initial values were calibrated to achieve a good fit of modeled values with recent-day measurements. 60

Figure 23: Simulated future subsidence due to self-weight induced autocompaction of Holocene strata at GW1 (a) and a depth-profile of respective strains (b). 61

Figure 24: Example of the measuring principle of the land subsidence observatory, modified after Dörr et al. (2023). 65

Figure 25: Depth-differentiated compaction monitoring at GW1 between December 2022 and November 2023 alongside observed groundwater heads displaying data of all sensors (a) and data excluding the three uppermost loading-biased sensors (b). 67

Figure 26: Compaction time series of the land subsidence observatory during a pumping test at GW1b alongside drawdown and recovery. 68

Figure 27: Comparison of compaction monitoring at the land subsidence observatory with geodetic levelling measurements during pumping tests (a) and on an annual basis (b). 70

Figure 28: Correlation of InSAR and groundwater time series at the site IGPVN between 2017 and 2022 including individual InSAR time series (a) mean smoothed InSAR time series (b) together with groundwater head time series (c) as well as daily precipitation (d). 72

Figure 29: Schematic illustration of the two complementary phenomena of hydrogeomechanical coupling. 77

Figure 30: Schematic illustration of natural and anthropogenic drivers of land subsidence and their derived contributions in the vicinity of the study site GW1, ... 83

List of Tables

Table 1: Summary of the most commonly investigated frequencies in groundwater analysis (McMillan et al., 2019). 30

Abbreviations

AT	atmospheric tides
BE	barometric efficiency
BRF	barometric response function
ET	Earth tides
FFT	Fast Fourier Transform
GW	groundwater
HALS	harmonic least squares
InSAR	Interferometric Synthetic Aperture Radar
OT_{SE}	ocean tide loading on the solid Earth
PSC	passive subsurface characterization
RT	river tides
SWRC	soil water retention curve

1 Introduction

1.1 A century of sinking grounds – 100 years of subsidence due to groundwater exploitation and ongoing challenges today

Land subsidence caused by groundwater depletion has evolved into a global-scale phenomenon, posing serious threats to human and environmental systems (Galloway and Burbey, 2011; Herrera-García et al., 2021). Its consequences range from damage to civil infrastructure to increased exposure to flooding and progressive land loss in low-elevation settings (Gambolati and Teatini, 2021). A full century has passed since researchers first linked land subsidence to the extraction of groundwater and other subsurface fluids such as oil or gas (Pratt and Johnson, 1926). From a hydro-geomechanical perspective, groundwater overexploitation lowers hydraulic heads in aquifers, thereby increasing effective stresses and generating hydraulic gradients between aquifers and adjacent aquitards. This induces excess pore water pressure in the aquitards relative to the lowered aquifer heads, and its delayed dissipation leads to time-dependent consolidation, sediment compaction, and ultimately land subsidence (Galloway and Burbey, 2011). By the late 1960s these mechanisms of land subsidence due to groundwater exploitation were considered conclusively understood, recognized, and accepted (Gambolati and Teatini, 2021) framed by the benchmark study of Poland and Davis (1969). Over the following decades, methodologies to observe and simulate subsidence dynamics evolved, including advances in numeric modelling (Gambolati and Freeze, 1973; Hoffmann et al., 2003) and the utilization of space-borne observations (Ferretti et al., 2001; Galloway and Hoffmann, 2007). With continuous research efforts, the globally progressing extent of land subsidence due to groundwater depletion was subsequently investigated, revealing land subsidence dynamics of up to 260 mm a^{-1} in Jakarta (Ng et al., 2012), 300 mm a^{-1} in Mexico City (Chaussard et al., 2014) and similarly hazardous subsidence rates in plenty other metropolitan regions around the world. Figure 1 presents a summary of the major regions worldwide affected by anthropogenic land subsidence due to groundwater exploitation.



Figure 1: Global extent of land subsidence due to groundwater withdrawal, modified after Gambolati and Teatini (2021). Point halo size is referenced to maximum reported subsidence rates ranging between 1 and 300 mm a^{-1}.

Despite a hundred years of scientific progress, land subsidence remains an escalating global hazard, with an estimated two billion people around the world living on subsiding grounds (Davydzenka et al., 2024). This underlines the need to pursue more effective and science-informed solutions in the future. Experiences from cities such as Venice and Shanghai have shown that targeted adaptation and mitigation, most notably a strict reduction of groundwater extraction, can effectively halt advancing land subsidence induced by groundwater overexploitation (Gambolati and Teatini, 2021). However, as sustainable groundwater management concepts tend to conflict with increasing water demands linked to population and economic growth, their implementation is often challenged by these competing interests.

Mitigating groundwater-depletion-induced land subsidence requires a reduction of groundwater extraction to sustainable levels, which in turn depends on reliable estimates of groundwater recharge. Where natural groundwater recharge is limited, artificial groundwater recharge constitutes a potential contributing measure to mitigate advancing land subsidence caused by groundwater depletion and has been used to mitigate land subsidence in many regions around the world including Shanghai, Las Vegas, and Mexico City (Seidl et al., 2024). This approach encompasses the seasonal storage of freshwater resources, thereby reducing net annual groundwater withdrawal, and the potential to partially revert compaction by repressurizing confined aquifers.

Understanding land subsidence dynamics, and thus developing effective adaptation and mitigation strategies, becomes increasingly complex when, in addition to groundwater depletion, other superimposed processes contribute to overall subsidence. Such processes include autocompaction (non-anthropogenic self-weight compaction) of young sediments, tectonics, oxidation and consolidation of organic soils as well as surface loading of the built environment (Galloway et al., 2016). Quantifying individual drivers of land subsidence is often challenging, particularly where sparse datasets on subsurface parameters coincide with complex hydrogeological conditions, as is the case in many river deltas, such as the Mekong Delta. Without a robust identification of the relative contributions of individual processes, decision-makers lack the solid scientific basis needed to implement adaptation and mitigation strategies, which are often associated with considerable socio-economic costs and far-reaching societal transformations.

The lack of reliable quantification of individual subsidence drivers, linked to scarce subsurface parametrization and uncertain quantifications of groundwater recharge processes, requires progressive scientific efforts in the context of land subsidence and its mitigation. Therefore, the present dissertation addresses those pending research tasks specifically for the Vietnamese Mekong Delta, as well as on a general basis, as the findings and developed novel method extensions are transferable to similarly affected regions around the world. This work thus builds upon a century of research into groundwater-depletion-induced land subsidence, advancing scientific frameworks that enable more comprehensive process understanding and informed mitigation strategies.

1.2 River deltas as hotspots of land subsidence and multi-hazard interactions

River deltas are highly dynamic systems, shaped and continuously reshaped by complex, interacting balances between water and sediments (Syvitski et al., 2009). This dynamic nature renders them among the most vulnerable landforms to climate change and human intervention (Eslami et al., 2025). Once this fragile balance is disrupted, cascading hazards unfold, including land subsidence, coastal erosion, flooding and saline intrusion into ground- and surface waters (Eslami et al., 2025). As these hazards often exacerbate each other, a sound process understanding is indispensable for understanding such multi-hazard interactions and developing adaptation and mitigation strategies.

Due to their low elevation, climate-change induced sea-level rise poses an obvious and tangible challenge to river deltas. This effect of sea levels rising towards current deltaic surface elevations is intensified by land subsidence, jointly referred to as relative sea-level rise. In many Asian deltas, land subsidence represents the dominant contributor to relative sea-level rise (Becker et al., 2024; Ohenhen et al., 2026).

With an estimated 500 million inhabitants, a large share of the global population lives in deltas (Anthony et al., 2024). Addressing the associated demands for freshwater, energy, construction materials, and flood protection in densely populated deltaic metropolitan regions often comes at the expense of disrupting the deltaic sediment–water balance through groundwater overexploitation, upstream dam construction, and sand mining. The sediment deficit resulting from dam construction and sand mining promotes coastal erosion and prevents the compensation of natural, non-anthropogenic subsidence driven by the compaction of young, shallow sediment strata (Syvitski et al., 2009; Zoccarato et al., 2018).

Figure 2 presents a simplified summary of anthropogenic stressors, associated activities and resulting cascading hazards in deltaic systems. In most deltaic settings, groundwater depletion constitutes the major single driver for land subsidence and

relative sea level rise (Bagheri-Gavkosh et al., 2021; Minderhoud et al., 2025). The presence of soft, unconsolidated, and highly compressible Holocene sediments is characteristic of many deltas (Stanley and Warne, 1994) and largely determines their susceptibility to land subsidence induced by sediment compaction resulting from groundwater overexploitation driven by increasing freshwater demand associated with population growth.

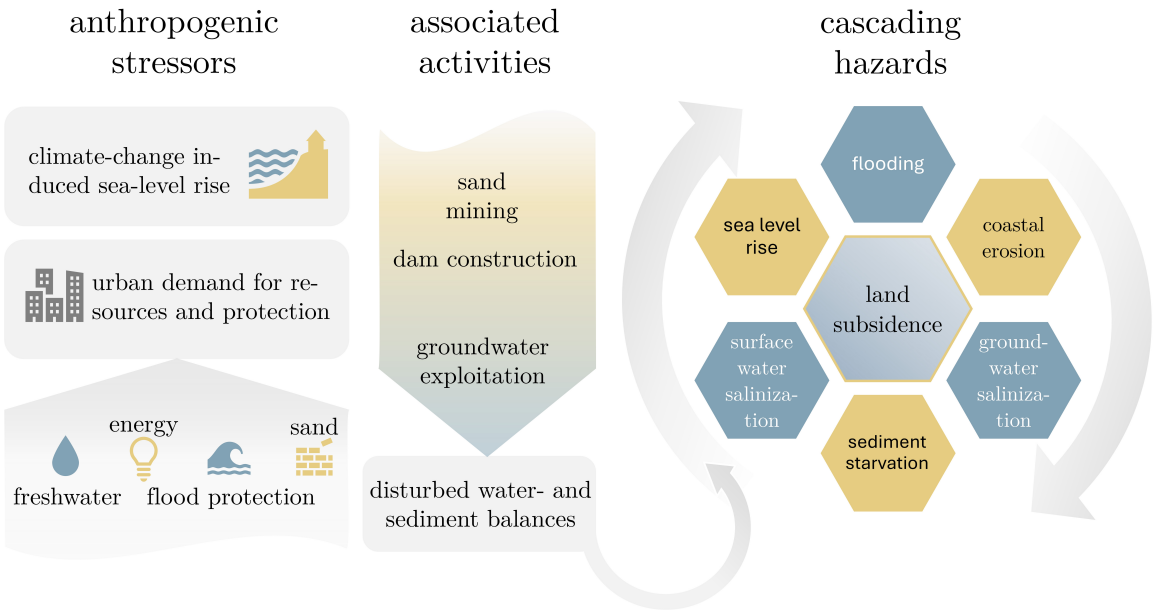


Figure 2: From anthropogenic stressors to cascading hazards in deltaic systems: An overview of anthropogenic stressors and associated activities which disturb the water and sediment balances and trigger cascading hazards.

In light of the outlined stressors, the sustainable preservation and restoration of deltas worldwide present a major global challenge for the decades to come (Huning et al., 2024; Van Engelen et al., 2022), with land subsidence being a central issue therein. Against this background, improving the process-based understanding and quantification of subsidence dynamics is essential for developing effective mitigation and adaptation strategies.

1.3 Addressing cascading hazards in the Vietnamese Mekong Delta – the ViWaT initiative

In regard of the above outlined challenges to deltas around the globe, the Vietnamese Mekong Delta (Figure 3) ranks among the most severely affected deltas worldwide (Kondolf et al., 2022). The southern Mekong Delta, particularly the Ca Mau peninsula, is confronted with increasingly severe environmental challenges like land subsidence, ground- and surface water salinization, coastal erosion and floodings (Khang et al., 2008; Minderhoud et al., 2017; Renaud and Kuenzer, 2012).

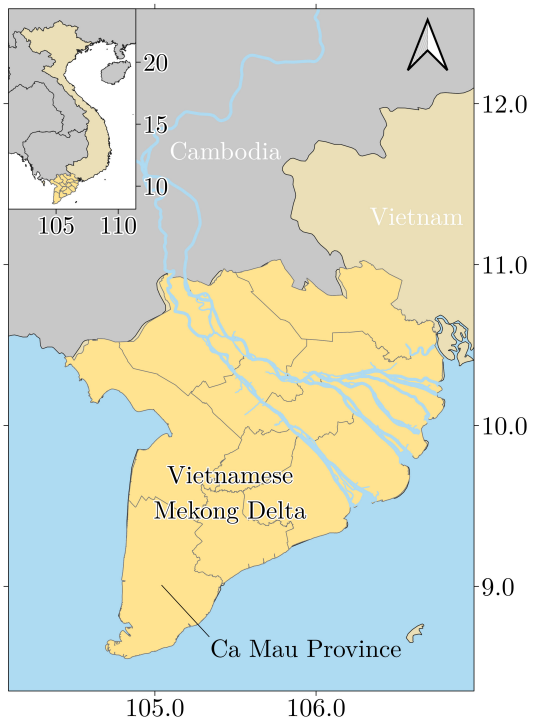


Figure 3: Map of the Vietnamese Mekong Delta.

These cascading hazards in the Vietnamese Mekong Delta, summarized as "loss of land and freshwater" by Bauer et al. (2022), present a substantial threat to the region's viability. Addressing these hazards and developing sustainable mitigation and adaptation strategies was a key focus of the ViWaT (*VietnamWaterTechnologies*) initiative with the associated projects ViWaT-Mekong-GO (2016-2018) and ViWaT Engineering (2018-2022), funded by the German Federal Ministry of Research, Technology and Space (BMFTR, former BMBF). Within these projects and subsequent research efforts, valuable insights into relevant process dynamics were obtained

including insights into (i) groundwater dynamics (Hoan et al., 2022), (ii) climate change related meteorological forecasting (Pham-Thanh et al., 2022, 2020), (iii) coastal erosion (Vu et al., 2025), (iv) salinization of ground- and surface waters (Bauer et al., 2025, 2022; Hoan et al., 2025), (v) changes in land-use (Vu et al., 2022), as well as (vi) social perception and the potential of alternative water resources (Pham et al., 2026, 2023). In the context of land subsidence, the ViWaT-initiative and subsequent research of the involved working groups provided significant insights by introducing and applying improved methods for the evaluation of satellite-based subsidence rates (N. Dörr et al., 2024)* and their evaluation related to droughts (N. Dörr et al., 2025). The findings elaborated in this dissertation complement the research fields addressed within the ViWaT-initiative, with a focus on the process dynamics of land subsidence and mechanisms relevant to associated mitigation strategies.

1.4 Land subsidence in the Vietnamese Mekong Delta

With an average elevation of only 0.8 m above mean sea level in 2018 (Minderhoud et al., 2019), the subsidence rates of locally > 30 mm a^{-1} (Erban et al., 2014; N. Dörr et al., 2024) underline the urgency of investigating the contributing process dynamics and the subsequent development of mitigation and adaptation strategies in the Mekong Delta. Erban et al. (2014) presented the first delta-wide subsidence map of the Mekong Delta based on InSAR (Interferometric Synthetic Aperture Radar) satellite data. Subsequent research of Minderhoud et al. (2017) and Zoccarato et al. (2018) provided first model-based benchmark estimates on the contribution of individual processes to the overall subsidence in the Mekong Delta. Their simulation results suggest that (i) groundwater extraction as well as (ii) autocompaction of Holocene sediments are the two dominant contributors to regional land subsidence dynamics in the Mekong Delta with varying intensity across the delta and with groundwater extraction considered as the greatest single driver among them (Kondolf et al., 2022; Minderhoud et al., 2020).

* For clarity and better distinction, works by Nils Dörr are cited as N. Dörr et al., while those by the author of this dissertation are cited as Dörr et al.

Land subsidence observations

Space-borne methods like InSAR analyses provide valuable data sets on land subsidence dynamics in the Mekong Delta since more than a decade (Erban et al., 2014; N. Dörr et al., 2024). This approach allows the assessment of subsidence dynamics of a great number of individual points by Sentinel-1 satellite data. For example, subsidence dynamics of more than 7 million points were assessed in the Mekong Delta in a study by N. Dörr et al. (2024), who enhanced the evaluation by integrating temporary persistent scatterers into the analysis. Such InSAR methods detect motion of persistent or temporal scatter points like rooftops of buildings or road surfaces. However, they are incapable of detecting subsidence dynamics of natural environments. Therefore, there is an inherent overrepresentation of urban settlements in InSAR-based analyses, posing the question of their representativeness for regional dynamics in non-urban dominated landscapes. It is noted that due to the great number of points, plotting individual InSAR datapoints into a single map is infeasible on a delta-wide scale. Therefore, aggregation of datapoints and their plotting order become necessary, procedures which significantly affect the visualized extent of subsidence – an issue that requires dedicated improvement on a concept level (N. Dörr, 2024). Figure 4 illustrates land subsidence rates derived from InSAR analyses in the Mekong Delta for the period between 2017 and 2022 (N. Dörr, 2024).

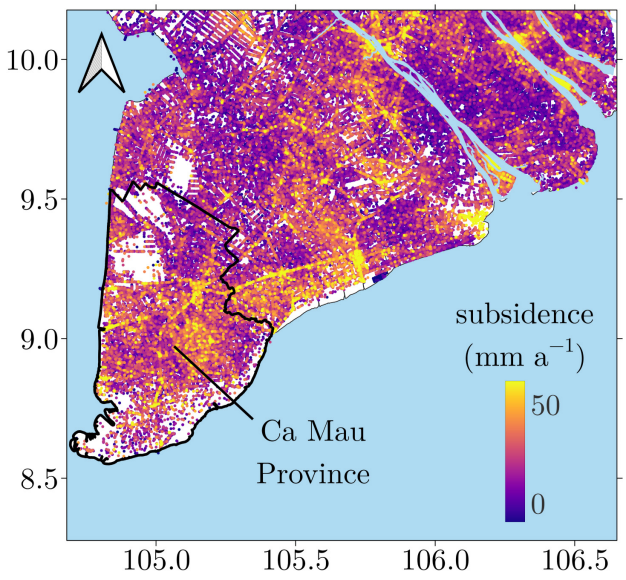


Figure 4: Land subsidence in the Mekong Delta between 2017 and 2022, modified after N. Dörr et al. (2024).

Despite the great spatial coverage of InSAR data, ground-based monitoring of land subsidence dynamics remains essential for the identification of individual drivers, particularly when such monitoring methods permit a depth-association of the measurement data. In the Mekong Delta, only few ground-based subsidence monitoring facilities are available, all limited to single-depth measurements. Surface elevation table measurements with marker horizons have been implemented at four sites in coastal and mangrove environments (Lovelock et al., 2015) showing subsidence rates of 30 - 35 mm a^{-1} in shallow Holocene coastal settings. While this data is valuable for analyzing coastal front sediment balances, it is not representative of inland parts of the peninsula (Zoccarato et al., 2018). Surface elevation table measurements at two stations further inland showed smaller Holocene compaction rates of 6 - 8 mm a^{-1} (Nguyen et al., 2015). Karlsrud et al. (2020) presented preliminary data of three subsidence monitoring stations in Ca Mau Province, measuring subsidence relative to a settlement anchor in 100 m depth, showing rates of 4 - 31 mm a^{-1}.

Neither the data of the ground-based monitoring stations nor the evaluation of satellite data could provide unambiguous quantifications of the contribution of individual drivers. This lack of a solid measurement-based framework for quantifying the contribution of individual drivers is addressed within this dissertation with the land subsidence observatory, which provided the first depth-differentiated compaction monitoring data in the Mekong Delta.

Land subsidence due to groundwater depletion

The Mekong Delta strongly relies on groundwater as its primary freshwater resource (Pham et al., 2023; Bauer et al., 2022; Wagner et al., 2012). An exact quantification of abstraction rates is infeasible, given that the majority of extraction occurs via unlicensed household wells, however, estimates approximate total abstraction rates at 2.5 million m^3 d^{-1} (Minderhoud et al., 2017). These abstractions lead to declines in hydraulic heads throughout the aquifers, a process considered a major driver of ongoing land subsidence in the Mekong Delta.

The Mekong Delta exhibits a complex hydrogeological setting that is commonly conceptualized as a multi-layered aquifer–aquitard system comprising seven aquifers and seven aquitards (Figure 5). Much of the delta is overlain by a Holocene aquitard with locally > 20 m in thickness, while total sediment thickness averages 300 – 400 m (Anderson, 1978; Bauer et al., 2022; Hoan et al., 2022). Whereas early studies reported artesian conditions prior to extensive groundwater abstraction (Anderson, 1978), recent monitoring indicates groundwater head declines of 0.01 – 0.55 m a^{-1} across the aquifers (Duy et al., 2021), with present hydraulic heads locally reaching up to 20 m below ground level.

In the southern Mekong Delta, groundwater abstraction has been most intensive from the upper-middle Pleistocene aquifer qp_{2-3} (Hoan et al., 2022). More recently, however, increasing salinization has led to a growing exploitation of deeper aquifers such as the middle Pliocene aquifer n_2^2 (Hoan et al., 2025). The shallow Holocene aquifer qh is generally highly saline and therefore plays only a minor role in domestic water supply (Pechstein et al., 2018). Nevertheless, despite regulatory restrictions, there are indications that shallow groundwater is being utilized for brackish aquaculture (Van Tuan et al., 2024). Figure 5 illustrates a hydrogeological cross-section through the southern Mekong Delta, modified after Hoan et al. (2022). The introduced color code for the seven aquifers is used throughout all first-authored publications and throughout this dissertation.

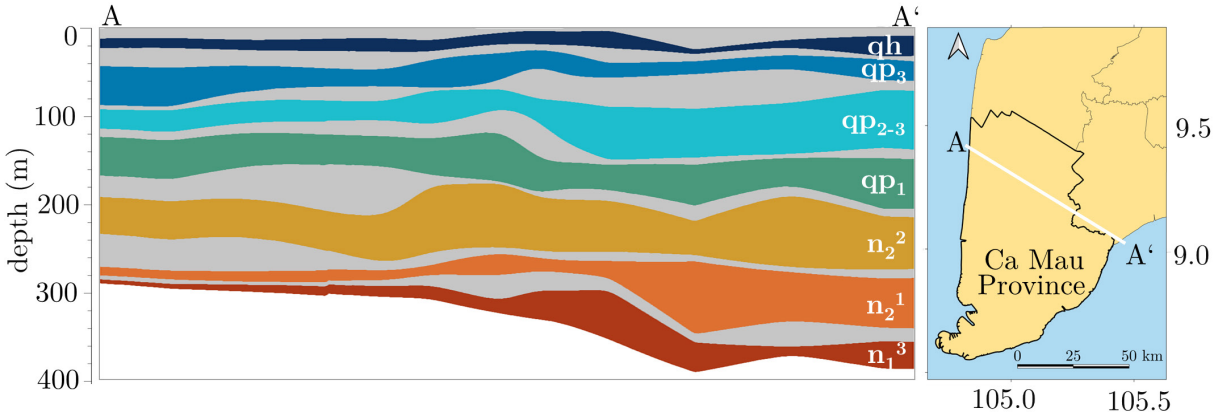


Figure 5: Hydrogeological cross-section through the southern Mekong Delta, modified after Hoan et al. (2022).

First model-based estimates for land subsidence due to groundwater depletion suggest an delta-wide average subsidence of ~180 mm within 25 years with average rates in 2017 varying between 11 mm a^{-1} and locally 25 mm a^{-1} (Minderhoud et al., 2017). This model approach constitutes a valuable first estimate and contributed greatly to awareness creation on land subsidence in the Mekong Delta in scientific and public communities. In recent years the authors themselves and other researchers have addressed limitations of the model (Minderhoud et al., 2024, 2017; Pham et al., 2022). Associated uncertainties and the resulting decrease in confidence in the precision of the model results have been qualitatively discussed. Raised concerns included:

- inconsistencies of hydraulic and geomechanical parameters,
- insufficient vertical aquitard discretization,
- use of vertically averaged geomechanical parameters per lithological unit,
- disregard of the fully coupled (two-way) nature of groundwater flow and sediment compaction.

To erase persistent doubts on the general role of groundwater depletion to land subsidence among decision makers in the Mekong Delta on the one hand and to increase precision and confidence in the quantification on the other hand, more detailed hydrogeomechanical modelling studies are required, with more comprehensive modelling approaches and higher resolution in parametrization. This is addressed in the present dissertation by a numeric study on local scale in unpreceded detail utilizing a subsurface parameterization at high resolution and reliability.

Land subsidence due to autocompaction

Zoccarato et al. (2018) estimated autocompaction processes in the Mekong Delta with a 2-D model, simulating accretion and natural consolidation over the past 4,000 years and for a 100-year prediction period. In line with the delta progradation, the simulated natural compaction is greatest at the present shoreline and decreases towards the upper delta plain. Evaluating two scenarios, considering either (i) 50 % or (ii) 100 % reduction of sediment supply compared to estimated reference values, Zoccarato et al. (2018) estimated a gradual decrease of natural century-averaged compaction rates from (i)

12 mm a^{-1} at the shoreline to 0.8 mm a^{-1} in the upper delta plain and (ii) from 20 mm a^{-1} at the shoreline to 2.4 mm a^{-1} in the upper delta plain, respectively. This 2-D approach was enhanced to a three-dimensional approach (Baldan et al., 2025) confirming the overall range, however with remaining uncertainties regarding lithological heterogeneity, simplified geomechanical characterization and the assumptions made regarding recent sedimentation rates. Overall, autocompaction must be recognized as a driver with potential relevance, however, its actual contribution remains challenging to determine on a spatiotemporal scale with the available model-based analyses.

Other potential drivers of land subsidence

In the Mekong Delta, other subsidence drivers are commonly considered of secondary importance compared to autocompaction of Holocene sediments, local loading of the built environment and compaction induced by groundwater depletion (Zoccarato et al., 2018). This includes, for example, tectonic subsidence, which is considered minor (<1 mm a^{-1}), as the Sunda Shelf, to which the Mekong Delta belongs, has remained tectonically stable from the Quaternary to the present (Hanebuth et al., 2011). Also oxidation of organic matter is often regarded negligible due to the predominantly saturated conditions in the subsurface (Zoccarato et al., 2018), although a more differentiated assessment may be required in areas that are drained for agricultural purposes or beneath extensively sealed urban surfaces.

Mitigation Potential

Four years ago, an interdisciplinary group of scientist joined together for a call for action "*save the Mekong Delta from drowning*" (Kondolf et al., 2022), urging policy makers to effectively address drivers for subsidence in the Mekong Delta. They proposed six measures to safeguard the delta's future, including a reduction of groundwater extraction and various measures to counteract the sediment deficit e.g. by avoiding future constructions of high-impact dams, passing sediment around dams and restricting riverbed sand mining. While these proposed measures undoubtedly will counteract the land subsidence dynamics if implemented, the effectiveness of individual

measures however cannot be quantified without a sound quantification of the main contributing process.

Based on the model of Minderhoud et al. (2017), scenario calculations for various future groundwater extraction rates and the associated evolution of hydraulic heads provided first insights into potential future subsidence dynamics (Minderhoud et al., 2020). These simulations suggest that even if further groundwater depletion is averted, a considerable yet manageable amount of land subsidence must be anticipated in the future. To pursue such stable hydraulic head conditions, more reliable groundwater recharge estimates are needed in order to quantify tolerable groundwater extraction rates. Moreover, methods like *Managed Aquifer Recharge* have been outlined as potential mitigation measures (Minderhoud et al., 2020), however, more accurate investigations are needed to assess the potential of those methods for the challenges in the Mekong Delta.

1.5 Research focus and objectives

In light of the above-outlined state of the art and resulting research gaps regarding land subsidence and associated mitigation potential in the Mekong Delta, this dissertation aims to elaborate a process-based perspective on the governing process dynamics, that enables a robust and reliable quantification of the contributions of individual drivers to past, present, and possible future subsidence dynamics. With this approach the role of groundwater depletion as a dominant subsidence driver can be assessed in more process-based detail than before, therefore persistent uncertainties among decision makers can be reduced and an evaluation and prioritization of potential mitigation and adaptation strategies is enabled. To achieve this, this dissertation pursues two major research foci which are:

- to advance the process understanding of groundwater depletion as the key trigger of land subsidence in the Mekong Delta, among other potential drivers (focus 1).
- to investigate process dynamics and subsurface conditions relevant to associated mitigation strategies (focus 2).

The elaborated insights regarding these two research foci are addressed in the results (section 3) and the synoptic discussion (section 4), in subsections 3.4, 3.5 and 4.2 for focus 1 and in subsections 3.2, 3.3, 4.1 and 4.3 for focus 2, respectively. Overall, the presented findings include a concise summary of the four peer-reviewed research articles (Dörr et al., 2023, 2025, 2026a, 2026b, presented in sections 3.2.1, 3.3.1, 3.4.1 and 3.5.1 respectively) as well as further insights building on these findings, presented in sections 3.2.2, 3.4.2, 3.5.2 and 3.5.3.

To enable the pursued high-resolution process-based approach, this dissertation adopts a distinctly local perspective, as only such a focus provides the data density required for a robust assessment of the relevant processes. This allows an assessment of subsidence-related environmental processes (focus 1) at an unprecedented level of detail for the Mekong Delta and contrasts previous delta-wide study approaches, where data scarcity inevitably introduces uncertainties. Once the governing process dynamics are identified with this proposed approach, the resulting insights can be transferred to large-scale analyses in the Mekong Delta and other deltaic systems.

To facilitate this high-resolution local analysis, this dissertation involves obtaining and evaluating new data from (i) a comprehensive monitoring of groundwater heads, soil moisture and meteorological parameters, (ii) a first-of-its-kind depth-differentiated compaction monitoring in the Mekong Delta, (iii) ground-based levelling campaigns, (iv) a corner reflector for improved satellite evaluation, (v) a characterization of soil-water related properties and (vi) a high-resolution subsurface parameterization based on geomechanical laboratory experiments, as elaborate in detail in section 2.

This dataset is also used to investigate process dynamics related to potential mitigation and adaptation strategies (focus 2), including evaluations of groundwater-recharge related processes, elastic aquifer properties and creep deformation characteristics. In the context of groundwater depletion as trigger for subsidence these assessments provide information on (i) the potential of aquifers to receive water, either by natural recharge or by artificial processes, (ii) their rebound capability and (iii) delayed subsidence to past groundwater depletion. The gained insights provide guidance

regarding the effectiveness and achievability of the most discussed mitigation measure, namely to prevent further groundwater depletion.

With the above-outlined approach, the contribution of groundwater depletion to total subsidence is quantified with high precision on local scale, thereby complementing previous regional studies with process-based detail and enabling an exemplary evaluation and prioritization of mitigation and adaptation strategies. Due to the methodological character of the elaborated approach, insights are conceptually transferable from the local perspective to delta-wide assessments, thereby strengthening confidence in broader application. The developed approach provides a framework for future studies on land subsidence in comparable systems worldwide.

2 Materials and Methods

This section provides a general overview of the methodological approaches employed in this dissertation. It introduces the data acquisition, monitoring infrastructure and summarizes the applied and newly developed methods as presented in the individual first-author publications (see Appendix *A.1* – *A.4*). Figure 6 schematically illustrates the methodological framework in the context of the overarching research objectives.

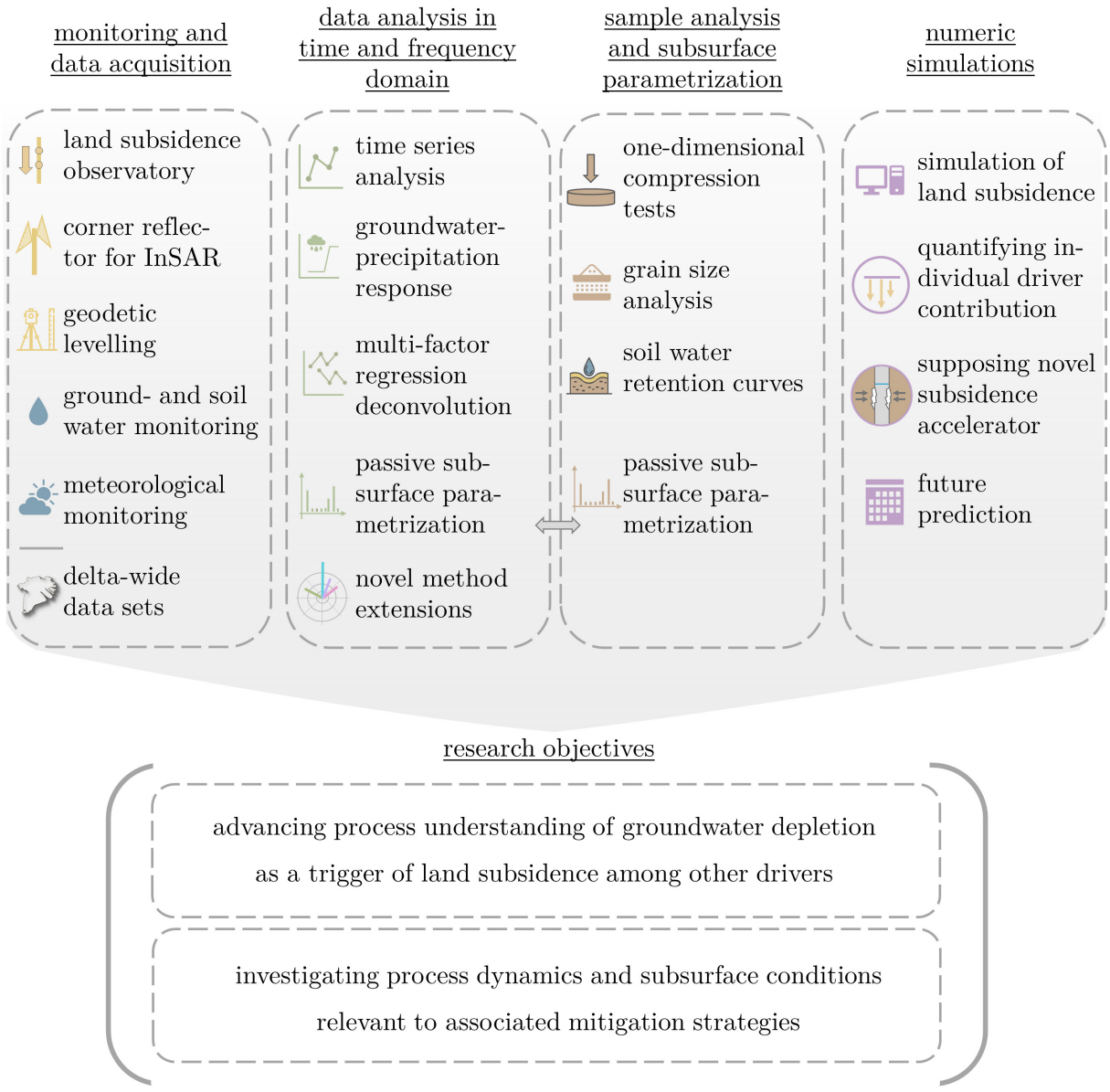


Figure 6: Schematic illustration of the methodological framework.

The applied approaches are grouped into four fundamental categories, each of which is discussed in the following sections: (i) monitoring and data acquisition (section 2.2), (ii) data analysis in time and frequency domain (sections 2.3 - 2.4), (iii) sample analysis and subsurface parameterization (section 2.5), and (iv) numerical simulations (section 2.6).

Prior to these specific elaborations, section 2.1 provides a brief introduction to the framework of hydrogeomechanical coupling, which ultimately governs the sediment compaction and associated land subsidence as well as the groundwater head response to external forcings, which are key concepts addressed in this dissertation.

2.1 The concept of hydrogeomechanical coupling

The concept of hydrogeomechanical coupling acknowledges that groundwater bodies are systems in which geomechanical and hydraulic conditions influence each other: pore fluids carry part of the load, and deformation alters pore space, fluid pressure, and flow (Neuzil, 2003). In the context of land subsidence, groundwater depletion in a confined aquifer causes a reduction in pore water pressure (i.e. hydraulic head), leading to an increase in intergranular effective stress that ultimately triggers compaction in both the aquifer (immediately but typically small) and the aquitard (delayed but commonly greater in magnitude) (Gambolati and Teatini, 2021). As the reduced pore water pressure in the aquifer induces excess pore water pressure in adjacent aquitards, this excess pore water pressure is slowly dissipated through drainage into the aquifer, which governs the delayed character of aquitard compaction and associated subsidence (Galloway and Burbey, 2011).

Land subsidence caused by groundwater depletion represents a fundamental example of hydrogeomechanical coupling, in which changes in hydraulic conditions, namely depleting groundwater heads, induce geomechanical processes such as sediment compaction. However, there are also numerous examples in which the direction of this cause-and-effect relationship is reversed, that is, where (geo-)mechanical processes such as surface loading or subsurface strains induce variations in groundwater heads. Such

phenomena have been recognized and described for more than a century e.g. for groundwater head responses to barometric pressure variations or ocean tides (Klönne, 1880; Veatch, 1906) and are utilized for subsurface parametrization since the 1940's (Jacob, 1940). Beyond barometric pressure variations and ocean tide loading, there is the ubiquitous forcing of Earth tide strains (Bredehoeft, 1967) as well as depending on local conditions, surface loading due to variations in soil moisture, water levels in overlying unconfined aquifers, ponding surface water bodies, snow accumulation and seasonal storage of canopy water (Van Der Kamp and Schmidt, 2017). These forcings can govern hydrogeomechanical responses of groundwater heads across a wide range of time scales and magnitudes.

Despite the long history of scientific investigations, these processes often remain overlooked, resulting in a high potential for misinterpretation of groundwater head time series (Van Der Kamp and Schmidt, 2017). This was the case for the Mekong Delta, which is why the identification and utilization of loading effects in groundwater head time series in the Mekong Delta represent a fundamental achievement of this dissertation.

2.2 Monitoring and data acquisition

Data scarcity is recognized as a central challenge for investigating the multiple hazards in the Mekong Delta. Therefore, generating new comprehensive monitoring data is of essential importance and the installation and maintenance of monitoring equipment represent key contributions of this dissertation. To address the uncertainties associated with land subsidence dynamics in the Mekong Delta and contributing drivers, various environmental processes are monitored at the ViWaT research site GW1, allowing an evaluation of process dynamics in an unprecedented level of detail. Together with the subsurface parameters derived in high vertical resolution from undisturbed drill core samples, a comprehensive dataset of unique coverage was acquired at the research site GW1. Figure 7 illustrates the individual components of the research site GW1.

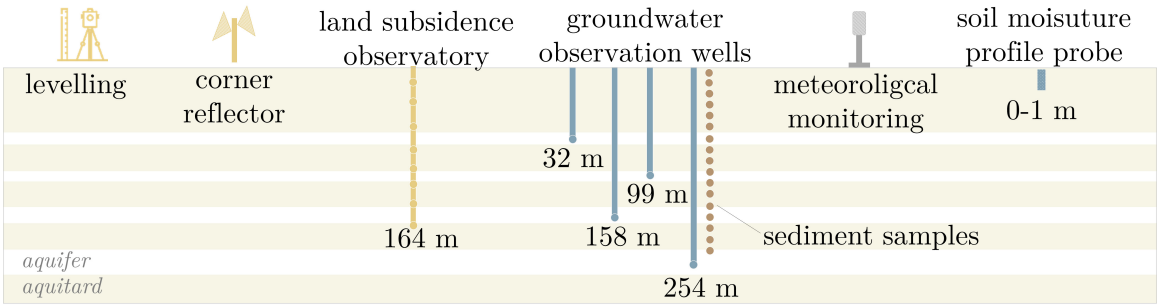


Figure 7: Schematic overview of the ViWaT research site GW1, illustrating the individual monitoring components and subsurface sampling.

During three field trips in the years 2022, 2023 and 2024, the author was actively involved in data acquisition, particularly in regard to the installation and maintenance of the land subsidence observatory, installation of soil moisture and meteorological sensors, maintenance of groundwater pressure sensors, soil sampling and initiating and accompanying geodetic levelling campaigns.

While the high data density achieved at the research site GW1 enabled novel insights into process dynamics, datasets with greater spatial and temporal coverage were evaluated to substantiate the investigated process dynamics on larger scales. This includes datasets of ground- and river water level observations provided by Vietnamese authorities and by other research projects as well as processed InSAR subsidence time series (N. Dörr et al., 2024).

2.2.1 ViWaT research site GW1

Initial monitoring setup

The research site GW1 is located in the southern Mekong Delta, in Ca Mau Province, south of the provincial capital Ca Mau City in Phu Hung Commune (Figure 9). At GW1, three groundwater observation wells were drilled in 2020, screened in the upper-middle Pleistocene aquifer ($qp_{2\text{-}3}$), lower Pleistocene aquifer (qp_1) and middle Pliocene aquifer (n_2^2) at depths of 99 m, 158 m and 254 m respectively. The observation wells were equipped with sensor systems, monitoring groundwater heads and water quality parameters. Moreover, the initial monitoring setup included a corner reflector, installed to enhance InSAR-based subsidence evaluations.

Land subsidence observatory

Addressing the uncertainties of potential contributors to land subsidence in the Mekong Delta, the realization of a sliding-joint multi-extensometer borehole, referred to as land subsidence observatory, was a major achievement, resembling a milestone in subsidence observation in the Mekong Delta. The land subsidence observatory is the first-of-its-kind monitoring facility in the Mekong Delta, providing depth-differentiated compaction data of the subsurface. Initiated and conceptualized by predecessor researchers of the ViWaT projects, in cooperation with an expert company for geotechnical monitoring equipment (SISGEO), the implementation, maintenance and data evaluation of the land subsidence observatory was a key feature associated with the presented dissertation. The first depth-differentiated compaction monitoring data in the Mekong Delta revealed insights into process dynamics governing the land subsidence dynamics and were discussed in a peer-reviewed article (Dörr et al., 2023) and are further presented and discussed in section 3.5.2.

Extension of monitoring setup

Building on the substantial achievements of the ViWaT projects, additional monitoring devices were installed at the ViWaT research site GW1 by the author. This work included the actual installation of the sensor systems, as well as maintenance and programming of data loggers and their remote data transmission. The additionally installed monitoring instruments include a soil moisture profile probe and a meteorological monitoring station. The recorded data of these monitoring systems was used to derive soil and surface water balances, as well as the associated mechanical loading acting on the subsurface (Dörr et al., 2026a).

Recognizing the importance of groundwater dynamics in shallow aquifers for sediment compaction in the highly compressible Holocene strata, an additional groundwater observation well GW1d was drilled in the topmost aquifer qp_3 (32 - 38 m depth) at the research site in 2024, initiated by the author and funded by the *Hector Fellow Academy*. An overview of the monitoring site GW1 and its instrumentation is shown in Figure 8.



Figure 8: Photograph of the monitoring site GW1, showing the locations of the soil moisture sensor probe ①, three deep groundwater observation wells ②, the meteorological monitoring station ③, the corner reflector ④ and the land subsidence observatory ⑤. Photograph by Felix Dörr, 2022.

Soil and sediment samples

The comprehensive set of monitoring data recorded at GW1 is complemented by a sound parametrization of soil and subsurface properties derived from laboratory analyses. Undisturbed sediment samples, obtained from the drilling of the observation well GW1c, permit a detailed geomechanical subsurface parametrization, and were used to characterize geomechanical properties of the highly compressible Holocene and late Pleistocene strata (Dörr et al., 2026b).

Geodetic monitoring campaign

To verify and spatially contextualize the subsidence observations derived from the land subsidence observatory, a local scale geodetic monitoring program was carried out. Over the 12-month observation period (March 2024 until February 2025), 78 monitoring campaigns were conducted. The ground-based surveys were performed by a Vietnamese expert company, with the author accompanying the first three campaigns.

Data availability

To provide the comprehensive dataset obtained from GW1, all monitoring data is made publicly available under the following link: https://doi.org/10.5281/zenodo.18800032.

2.2.2 Delta wide datasets

Groundwater head time series

A comprehensive dataset of groundwater head observations in the Mekong Delta is provided by the Vietnamese National Groundwater Monitoring Network, encompassing groundwater head data since the 1990s at numerous multi-depth monitoring sites. The dataset includes manual measurements of groundwater heads on a daily to monthly basis before 2011, and later groundwater heads measurements at hourly resolution, recorded by automated non-vented pressure transducers. This dataset was used to reveal the presence of loading signals in all screened aquifers throughout the Mekong Delta by frequency analyses (Dörr et al., 2025) and to evaluate long-term trends in groundwater depletion. The locations of the groundwater monitoring sites used in this dissertation are shown in Figure 9.

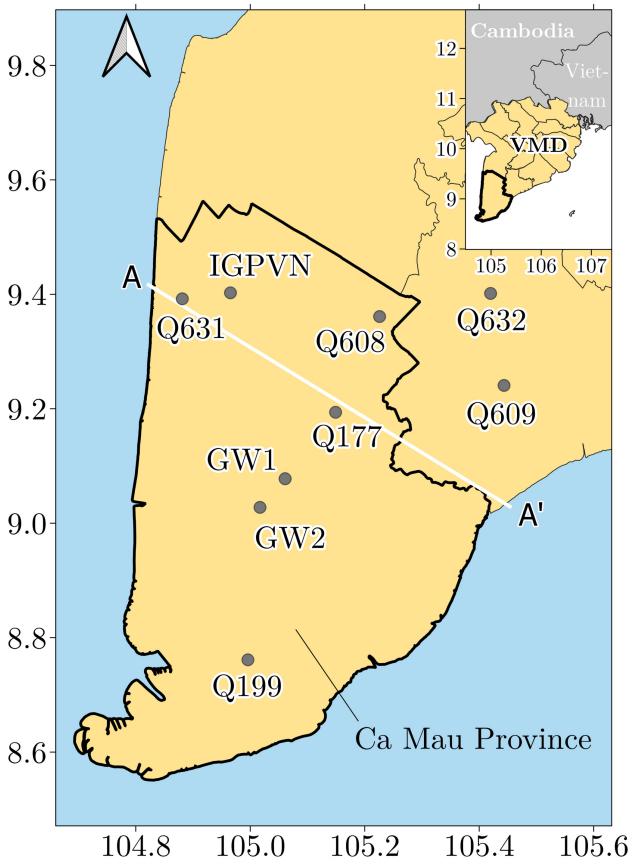


Figure 9: Location of groundwater monitoring sites used within this dissertation.

Complementing the groundwater head data from the national monitoring network and the ViWaT sites, groundwater head time series from the IGPVN research site were

evaluated (IGPVN: Improvement of Groundwater Protection in Vietnam, Federal Institute for Geosciences and Natural Resources (BGR), location: Figure 9). The IGPVN monitoring site was implemented in 2016 and comprises five groundwater observation wells, three of which are screened in the n_2^2 aquifer, two others screen $qp_{2\text{-}3}$ and qp_1 respectively. By encompassing multiple observation wells in a single aquifer, pumping test based subsurface parametrizations at IGPVN are of enhanced reliability compared to single-well pumping tests. Because of the availability of reliable refence parametrization and long-term data, the monitoring site IGPVN was used for an exemplary detailed analysis in the study on passive subsurface characterization (Dörr et al., 2025).

River water level time series

To assess the impact of tidally influenced river water levels on groundwater head dynamics, monitoring data from various gauging stations was evaluated according to their seasonal trend (Dörr et al., 2026a) and according to their harmonic forcings (Dörr et al., 2025, 2026a). The evaluated river water levels encompass data from the stations Ganh Hao, Song Doc, Nam Can and Rach Cui.

InSAR subsidence time series

To contextualize local subsidence observations from the research site GW1, a dataset of InSAR derived subsidence time series covering the period 2017–2022 (N. Dörr et al., 2024) was evaluated locally in the vicinity of the monitoring sites GW1 and IGPVN.

2.3 Data analysis in time domain

The measured time series of monitoring data are analyzed with various comprehensive time series analysis approaches, ranging from conventional time series analysis including qualitative and quantitative comparisons of individual time series (i.e. Dörr et al., 2023) to preprocessing approaches like detrending (Dörr et al., 2025) and more complex approaches like multi-factor regression deconvolution (Dörr et al., 2026a). The following sections provide a concise summary of applied data analysis methods in the time domain.

2.3.1 Time series analysis

Individually measured time series at the monitoring site GW1 are compared to evaluate relationships among the observed processes and derive associated process dynamics. This analysis for instance revealed a clear correlation between surface loading and groundwater head dynamics (Figure 10a, Dörr et al., 2026a), as well as between surface loading and monitored extensometer signals (Figure 10b, section 3.5.2), thereby providing essential insights into process dynamics as well as into validity and potential biases of the compaction measurements.

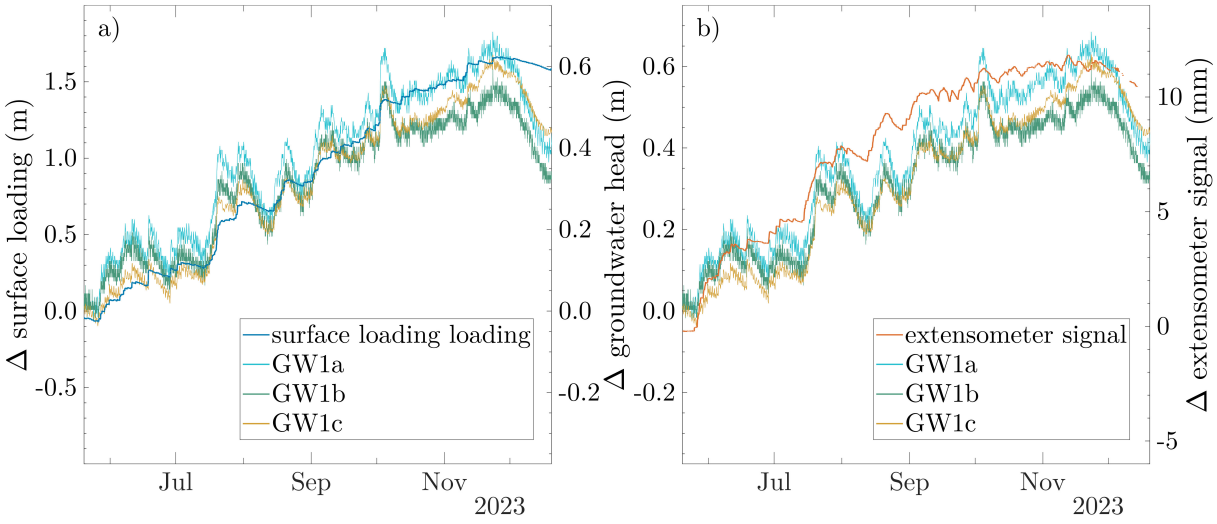


Figure 10: Correlation between surface loading and groundwater head dynamics at GW1 (a), modified after Dörr et al. (2026a) and correlation between extensometer signal and groundwater head dynamics (b).

These correlations between surface loading and groundwater head dynamics are further used to characterize loading imprints in groundwater head observations and to subsequently derive subsurface properties, as elaborated in the following sections.

2.3.2 Groundwater – precipitation response

To initially identify and subsequently characterize the groundwater head response to surface loading, the rise in groundwater heads in response to distinct precipitation events is analyzed. Given that such precipitation events resemble abrupt increases in surface loading (Bardsley and Campbell, 2000), slow processes such as evaporation and (sub-)surface drainage can be neglected when analyzing short-term loading induced groundwater-precipitation response. Under these conditions, the loading efficiency γ (-)

can be estimated from the ratio between accumulated precipitation and the corresponding rise in observed groundwater heads. Figure 11 illustrates exemplary the rise in groundwater heads in 250 m depth at GW1c to three selected precipitation events. The analysis shows a rise in groundwater heads of 64 mm, 202 mm and 45 mm to a respective precipitation of 99 mm, 290 mm and 64 mm. The ratios of these values indicate loading efficiencies of 0.64, 0.70 and 0.72.

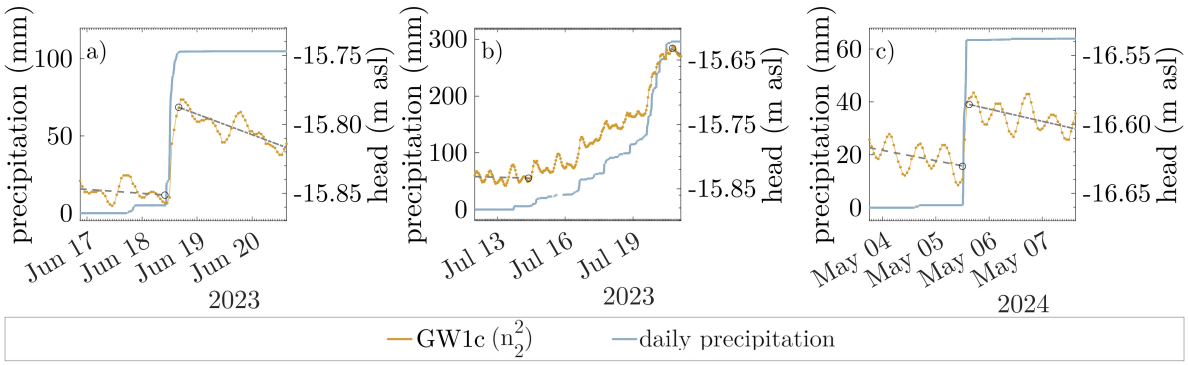


Figure 11: Groundwater head response in observation well GW1c to three selected precipitation events, modified after (Dörr et al., 2026a).

To minimize the impact of sensor accuracy and the influence of tidal variations, linear trends must be fitted to the groundwater head data before and after each precipitation event to obtain reliable start and end values for the groundwater response. This is a disadvantage compared to more sophisticated methods as the multi-factor regression deconvolution (see section 2.3.3) or the frequency domain methods (see section 2.4.2).

2.3.3 Multi-factor regression deconvolution

Within this dissertation a multi-factor regression deconvolution is used to (i) characterize and (ii) remove loading imprints in groundwater heads, resulting from superposing forcings of Earth- and ocean- tide loading, as well as loading of changing river water levels, atmospheric pressure variations and fluctuating pond water levels.

The general regression deconvolution approach is explained below, first for a simpler framework of a single-factor regression deconvolution. The most commonly applied single-factor regression deconvolution in groundwater studies is the barometric response function (BRF). It characterizes the degree to which fluctuations in barometric pressure

are reflected as corresponding changes in monitored well water levels. In this consideration changes in groundwater head at a given time t are expressed as the convolution of changes in barometric pressure before t. This response is captured by instantaneous response coefficients. The cumulative sum of these coefficients is referred to as BRF (Rasmussen and Crawford, 1997). In confined aquifers, the BRF typically rises toward a plateau, whose maximum represents the barometric efficiency BE (Toll and Rasmussen, 2007).

The barometric efficiency BE (-) is inherently coupled with the loading efficiency γ and further with the formation compressibility α (Pa^{-1}) (Eq. (1)), with β (Pa^{-1}) as the water compressibility and θ (-) as the porosity.

$$BE = 1 - \gamma = 1 - \frac{\alpha}{\theta \cdot \beta + \alpha} \tag{1}$$

Therefore, deriving BE is used in this dissertation additionally as a complementary approach to the passive subsurface characterization in frequency domain (section 2.4.2).

Toll and Rasmussen (2007) advanced the outlined regression-deconvolution approach by incorporating Earth tide signals into the regression, treating them as an additional independent driver of well water level fluctuations. After establishing the response function associated with one or several forcings, this function can be used to isolate and remove the respective contributions from the measured groundwater head records.

Figure 12 provides an exemplary illustration of the barometric response function, derived (i) with and (ii) without additional Earth tide consideration, as well as the corresponding corrected groundwater heads. For this example, a dataset from Death Valley (Rau et al., 2020) is utilized, because in contrast to the Mekong Delta, in that region groundwater head fluctuations are governed only by barometric and Earth tide forcing, with no additional superposing drivers.

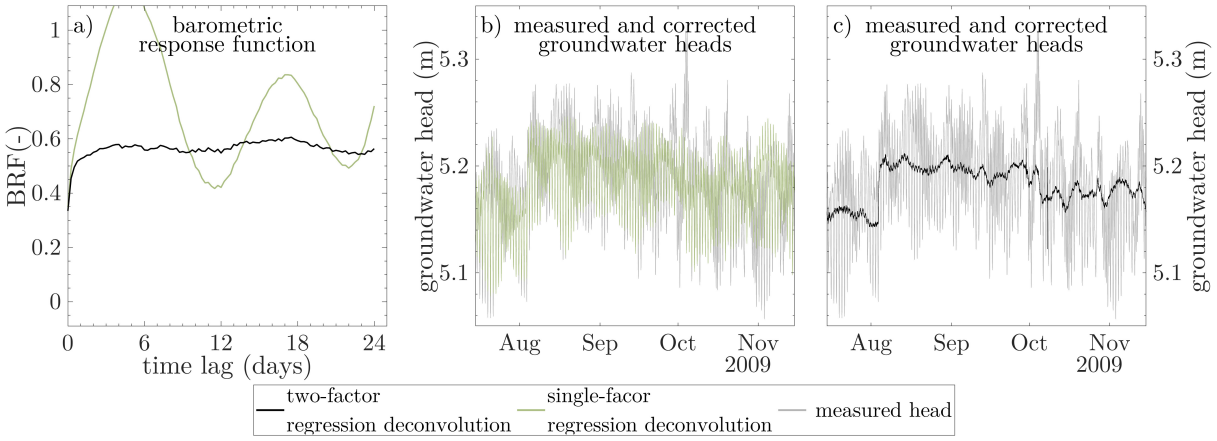


Figure 12: Barometric response functions and corresponding corrected groundwater heads with and without additional Earth tide consideration.

Figure 12 highlights that neglecting relevant forcings has a pronounced impact on the derived response function (Figure 12a) and the corrected groundwater heads (Figure 12b vs. Figure 12c). Therefore, taking the additional superposing forcings of ocean tide loading, as well as loading of river and pond water levels into account, is essential for the Mekong Delta. This is particularly relevant for the correction of groundwater heads, given that unlike the predominantly periodic forcings of barometric pressure and Earth tides, the groundwater system in the Mekong Delta is subject to surface loading of seasonal character, i.e. the variation of pond and river water levels.

This is underscored with Figure 13, showing the barometric response function (Figure 13a) and corrected groundwater heads (Figure 13b) derived for the study site GW1, utilizing (i) only barometric pressure as a considered forcing within a single-factor regression deconvolution and (ii) superposing forcings of barometric pressure, Earth- and ocean- tide loading, and loading of river and pond water levels within a multi-factor regression deconvolution. This multi-factor regression deconvolution approach is used in this dissertation to demonstrate that apparent rising groundwater heads are induced by loading signals and that their removal reveals continuously depleting groundwater heads (Figure 13b, Dörr et al., 2026a).

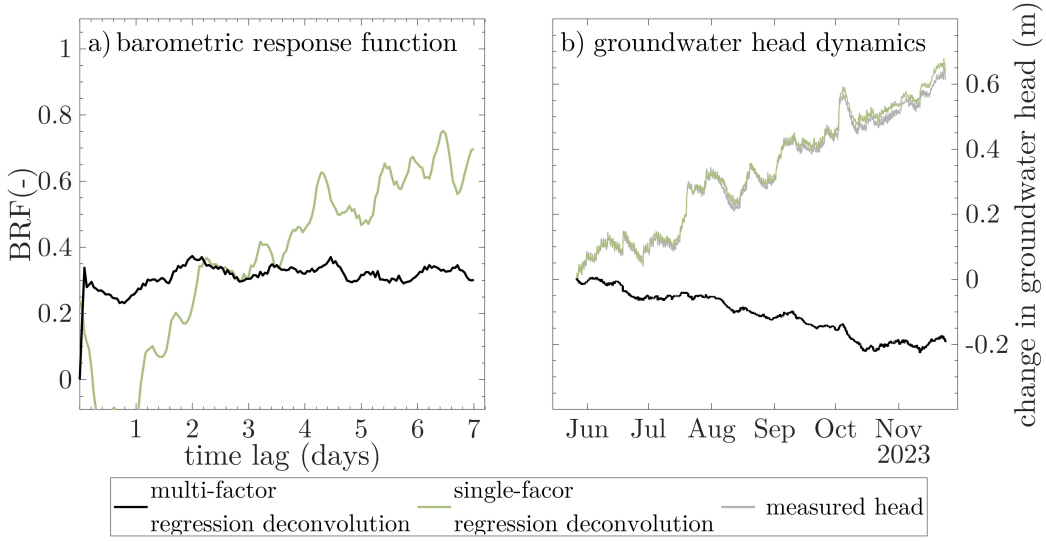


Figure 13: Barometric response functions (a) and corrected groundwater heads (b) for GW1c using single- and multi-factor regression deconvolution. Note that the measured head in (b) is hard to distinguish from the corrected heads using single-factor regression deconvolution.

For assessing the robustness of the loading-corrected groundwater head time series, the results of the multi-factor regression deconvolution model are evaluated within a cross-validation (Dörr et al., 2026a). Within this cross-validation the multi-factor regression deconvolution was applied to 60 sub-datasets of 120 days each, representing different segments of the full observation period.

2.4 Data analysis in frequency domain

2.4.1 Frequency patterns in controlling drivers and resulting groundwater heads

Loading signals of natural drivers like Earth-, ocean-, barometric-, or river tides follow distinct periodic patterns, allowing their evaluation in both the time and frequency domain. By comparing the frequency signatures of these external drivers with those observed in groundwater heads, subsurface properties can be derived (Acworth et al., 2016). These methods are commonly referred to as "*tidal subsurface analysis*" or "*passive subsurface characterization*" (Bastias Espejo et al., 2023; McMillan et al., 2019). To determine amplitude and phase characteristics, the respective time series are evaluated using two independent approaches: (i) the Fast Fourier Transform (FFT) and (ii) the harmonic least-squares (HALS) estimation.

HALS was found to outperform FFT in terms of amplitude and phase estimation accuracy and is furthermore capable of handling gaps in time series (Schweizer et al., 2021). Therefore, amplitudes and phases derived from HALS are used for all respective calculations in this dissertation. FFT, in contrast, is applied for diagnostic frequency analyses, as it provides a complete overview of the underlying spectral amplitudes, whereas HALS only investigates tidal constituents that have been predefined. In this dissertation, the frequencies listed in Table 1 are considered in the HALS analyses, representing the ten most commonly investigated frequencies in tidal subsurface analysis. In tidal groundwater analyses, frequencies with near-diurnal periodicity are commonly denoted in cycles per day (cpd).

Table 1: Summary of the most commonly investigated frequencies in groundwater analysis (McMillan et al., 2019).

Darwin name	frequency (cpd)	Earth tides	atmospheric tides	ocean/river tides
Q_1	0.893244	Yes	-	Yes
O_1	0.929536	Yes	-	Yes
M_1	0.966446	Yes	-	Yes
P_1	0.997262	Yes	-	Yes
S_1	1.000000	-	Yes	-
K_1	1.002738	Yes	-	Yes
N_2	1.895982	Yes	-	Yes
M_2	1.932274	Yes	-	Yes
S_2	2.000000	Yes	Yes	Yes
K_2	2.005476	Yes	-	Yes

Figure 14c exemplary illustrates the results of a frequency analysis of groundwater heads, measured at the monitoring site Q199 in the southern Mekong Delta in 318 m depth (location see Figure 9). In addition to the overall depletion trend (Figure 14a), tidal variations govern the groundwater head dynamics (Figure 14b). The FFT and HALS frequency analyses (Figure 14c) reveal amplitudes at distinct frequencies, most pronounced at the frequencies O_1, K_1, M_2 and S_2. Comparing these amplitudes and their associated phases with those of the governing drivers allows for an evaluation of subsurface parameters like the hydraulic conductivity, the specific storage coefficient or the formation compressibility.

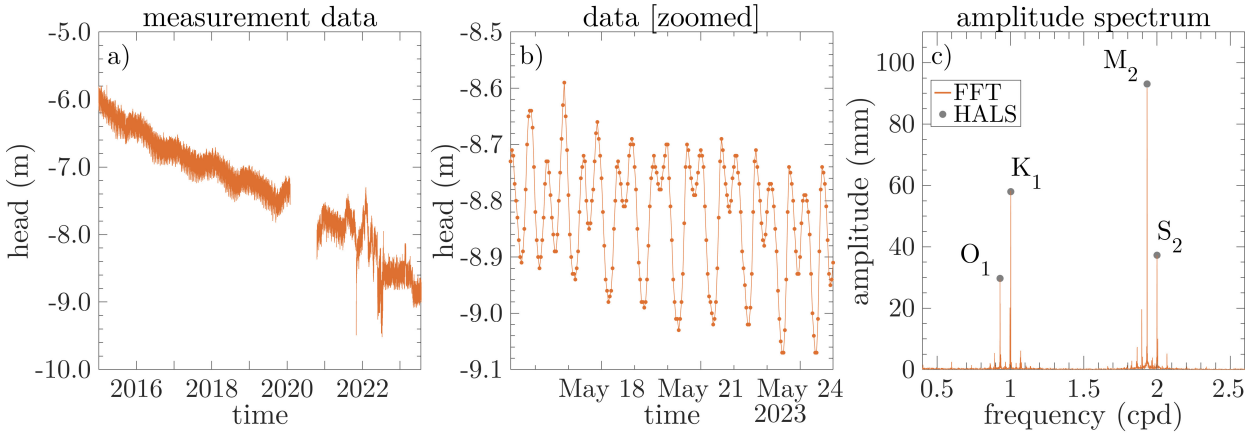


Figure 14: Groundwater head measurements at the monitoring site Q199 (a-b) and the respective amplitude characterization obtained by FFT and HALS (c).

2.4.2 Novel method extensions

Previous passive subsurface characterization methods were only applicable in the absence of river and ocean tide loading (Acworth et al., 2016; Rau et al., 2020), therefore unsuitable for deltaic environments, where tidal forcings from ocean- and river tides are additional superposing drivers to the ubiquitous drivers of Earth- and atmospheric tides. This limitation is overcome by the introduction of two novel method extensions, developed within this dissertation (Dörr et al., 2025, 2026a). Those novel method extensions include:

- integrating subsurface strains due to ocean tide loading on the solid Earth (OT_{SE}) in the analysis (Dörr et al., 2025).
- removing signals of river tide loading using the K_1 tidal constituent (Dörr et al., 2026a).

These novel method extensions require mathematical formulations (Eq. (2)-(6)) which employ complex numbers (denotated by a hat) to represent both the phase and amplitude of each signal z within a single number. In Eq. (2)-(6) and in Figure 15, the different signals are denoted by abbreviations for groundwater (GW), Earth tides (ET), atmospheric tides (AT) and river tides (RT). To integrate OT_{SE} in the analysis, the time series of Earth tide strains and OT_{SE} – strains are added up to a single time series prior to the conducted frequency analysis, further denoted with the superscript $\{ET + OT_{SE}\}$ (Dörr et al., 2025). For the additional removal of river tide contributions

to the M_2 and S_2 signals in groundwater heads, the K_1 component in both river water levels and groundwater heads is used (Dörr et al., 2026a). From the ratio of these K_1 signals, the respective phase shift and amplitude damping are calculated, and subsequently assigned to the M_2 and S_2 signal of the river water levels to estimate the contribution of river water levels on M_2 and S_2 signals in groundwater heads. After this novel signal disentanglement, the barometric efficiency can be calculated based on the S_2 response of groundwater heads to atmospheric tides $BE_{S_2}^{AT}$ (Rau et al., 2020). The introduced novel method extension involves an isolation of river tide signals for M_2 and S_2 frequencies (Eq. (2) and (3)), similar to the M_2–based disentanglement of Earth tides (Rau et al., 2020).

$$\hat{Z}_{M_2}^{\mathrm{GW\cdot RT}} = \frac{\hat{Z}_{K_1}^{\mathrm{GW}}}{\hat{Z}_{K_1}^{\mathrm{RT}}} \hat{Z}_{M_2}^{\mathrm{RT}} \tag{2}$$

$$\hat{Z}_{S_2}^{\mathrm{GW\cdot RT}} = \frac{\hat{Z}_{K_1}^{\mathrm{GW}}}{\hat{Z}_{K_1}^{\mathrm{RT}}} \hat{Z}_{S_2}^{\mathrm{RT}} \tag{3}$$

This formulation involves simplification, assuming insignificant K_1 contribution of Earth tides to groundwater amplitudes ($\hat{z}_{K_1}^{\mathrm{GW\cdot ET}} = 0$) and neglecting the frequency dependency of amplitude damping and phase shifting. It is noted that the validity of this simplified assumption must be assessed for each individual application, as confirmed by Dörr et al. (2026a) for the investigated site in the Mekong Delta. After the isolation of river tide signals, the M_2 response of groundwater to Earth tides and $\mathrm{OT_{SE}}$ can then be calculated by subtracting the river tide contribution (Eq. (3)) from the M_2 signal in groundwater heads:

$$\hat{Z}_{M_2}^{\mathrm{GW\cdot\{ET+OT}_{SE}\}} = \hat{Z}_{M_2}^{\mathrm{GW}} - \hat{Z}_{M_2}^{\mathrm{GW\cdot RT}} \tag{4}$$

Then, the disentanglement of Earth-, atmospheric-, ocean-, and river tide components in S_2 groundwater signals calculates with Eq. (5).

$$\begin{aligned} \hat{Z}_{S_2}^{\mathrm{GW\cdot AT}} &= \hat{Z}_{S_2}^{\mathrm{GW}} - \hat{Z}_{S_2}^{\mathrm{GW\cdot\{ET+OT}_{SE}\}} - \hat{Z}_{S_2}^{\mathrm{GW\cdot RT}} \\ &= \hat{Z}_{S_2}^{\mathrm{GW}} - \frac{\hat{Z}_{M_2}^{\mathrm{GW\cdot\{ET+OT}_{SE}\}}}{\hat{Z}_{M_2}^{\{\mathrm{ET+OT}_{SE}\}}} \hat{Z}_{S_2}^{\{\mathrm{ET+OT}_{SE}\}} - \frac{\hat{Z}_{K_1}^{\mathrm{GW}}}{\hat{Z}_{K_1}^{\mathrm{RT}}} \hat{Z}_{S_2}^{\mathrm{RT}} \end{aligned} \tag{5}$$

After this novel disentanglement of Earth-, ocean-, river- and atmospheric tide signals in groundwater heads, *BE* can be calculated with Eq. (6) (Rau et al., 2020) based on the S_2 response of groundwater heads to atmospheric tides $BE_{S_2}^{AT}$ as:

$$\mathrm{BE}_{S_2}^{\mathrm{AT}} = \frac{1}{A_{S_2}^{r}} \mathrm{abs}\left[\frac{\hat{Z}_{S_2}^{\mathrm{GW \cdot AT}}}{\hat{Z}_{S_2}^{\mathrm{AT}}}\right] \tag{6}$$

with $A_{S_2}^{r}$ as the amplitude response between the measured water levels in an observation well and the actual pore pressure of the surrounding aquifer. $A_{S_2}^{r}$ is a function of well and aquifer parameters and ranges for groundwater wells in confined aquifers with $K > 1 \cdot 10^{-5}$ m s^{-1} typically between 0.99 and 1.00 and is therefore negligible in Eq. (6) (Rau et al., 2020).

Figure 15 presents a visual flow-chart of the introduced disentanglement procedure. This illustration utilizes polar plots for visualization instead of amplitude spectra, as they allow phase and amplitude information to be displayed simultaneously.

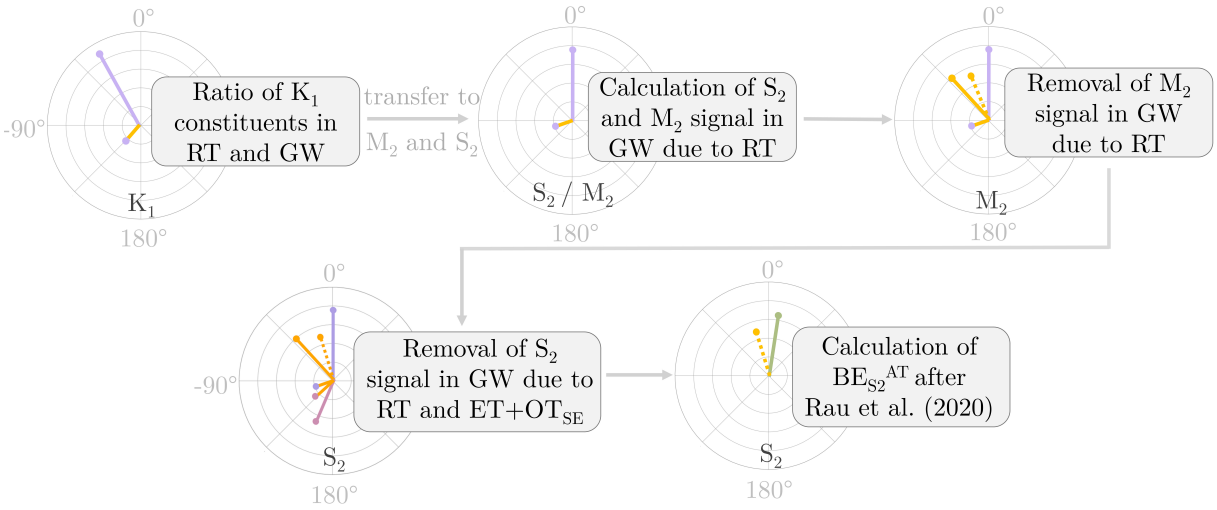


Figure 15: Simplified workflow of the novel disentanglement of river tide influences in groundwater signals, modified after Dörr et al. (2026a). Different signals are denoted by abbreviations for groundwater (GW), Earth tides (ET), atmospheric tides (AT), river tides (RT) and ocean tides on the solid Earth (OT_{SE}).

2.5 Sample analysis and subsurface parametrization

In addition to data-driven approaches for the assessment of subsurface parameters, sediment and soil characteristics were derived from comprehensive laboratory analyses. This includes:

- a geomechanical sediment characterization by twelve one-dimensional compression tests (Oedometer tests) conducted on undisturbed drill-core samples, extracted from various depths (0.9 - 79.2 m) during the drilling of the observation well GW1c.
- a characterization of soil properties under unsaturated conditions, by soil water retention curves (SWRC) derived from 5 undisturbed samples taken from depths between 0.3 m and 1.0 m at GW1.
- a grain-size distribution analysis of 7 samples taken from depths between 0.1 m and 1.0 m at GW1, enabling a comparison of SWRC-derived unsaturated soil properties with values reported in the literature.

From the one-dimensional compression tests, various geomechanical parameters can be derived with standardized evaluation procedures (DIN 18135, 2012). This includes an evaluation of the compression index C_c (-) and the recompression index C_r (-), which both can be derived from the slopes of the linearized sections in the respective semi-logarithmic compressibility curves (Figure 16a). The coefficient of secondary (creep) compression C_α (-) and the coefficient of consolidation c_v ($m^2\ s^{-1}$) as well as the vertical hydraulic conductivity k_v ($m\ s^{-1}$) are derived from the time-compression curve at the load stage representative for the in-situ pressure conditions (Figure 16b). C_α is derived from the gradient of the linearized section in the semilogarithmic time-compression curve. c_v and k_v are derived from mathematical relations with t_{50} (the time at 50 % of primary consolidation) and the incremental change of vertical effective stress and void ratio e, as elaborated by Dörr et al. (2026b). Figure 16 presents an exemplary illustration of the compressibility curve and the time compression curve of a sample from 20.7 m depth.

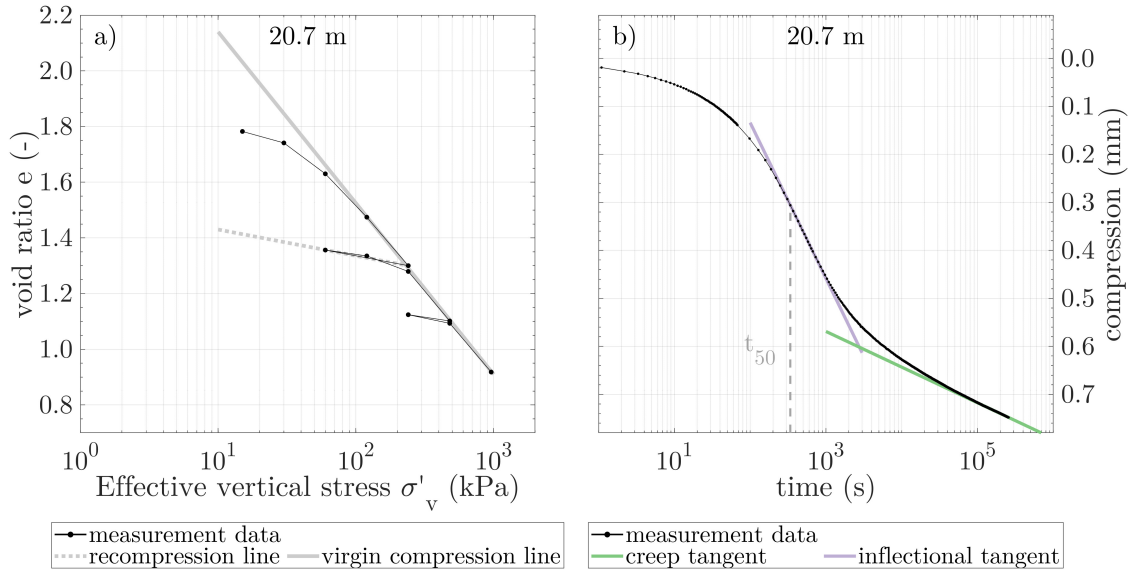


Figure 16: Compressibility curve (a) and the time compression curve (b) of a sample from 20.7 m depth at GW1, where t_{50} denotes the time at which 50% of primary consolidation is reached.

2.6 Numeric simulations

Within the presented dissertation, the first fully-coupled flow-deformation model for the Mekong Delta is developed and employed to simulate subsurface deformation and resulting land subsidence due to depleting groundwater heads and loading of the built environment at the monitoring site GW1 (Dörr et al., 2026b). Within this fully coupled approach, groundwater flow and sediment deformation are computed in an integrated manner, allowing evolving effective stresses and deformations to continuously affect the flow field as well as hydraulic properties (e.g., porosity and permeability), and vice versa. The simulations are carried out with the finite-element–based commercial software PLAXIS 2D (2025), applying the *Soft Soil Creep* model (Vermeer and Neher, 1999), an advanced geomechanical constitutive framework. The simulation utilizes a geomechanical characterization in high vertical resolution as well as observed groundwater head dynamics for pressure head boundary conditions. Seasonal loading dynamics of changing pond water levels are included in the simulation as well as an exemplary urban load of 10 kPa, representative of typical built-environment loading in the Mekong Delta.

While the applied fully coupled flow–deformation framework does not, in itself, provide fundamentally new insights, as coupling effects have been shown to be minor in comparable problem settings (Gambolati et al., 2000), the chosen modelling approach enables the incorporation of surface loading, subsurface drainage via well-casing failures, and a one-dimensional representation of autocompaction, thereby allowing for a more detailed and comprehensive simulation of local subsidence processes and their multiple drivers.

The simulation results are compared to monitored subsidence dynamics from ground-based and InSAR observations. Moreover, the delayed subsidence response to past groundwater head depletion is evaluated with the model, by assuming constant hydraulic conditions in the future. Figure 17 illustrates the model domain, including the range of considered surface characteristics for urban, unsealed, and ponded areas, as well as the location of the implemented road loading and well-casing, together with the finite element mesh, which features refined discretization near the surface and in the vicinity of the well-casing.

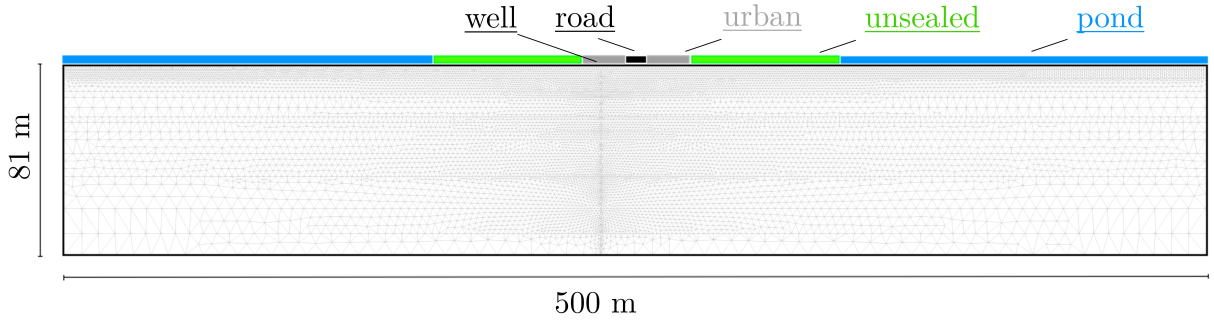


Figure 17: Schematic illustration of the extent and mesh of the two-dimensional model domain, together with surface characteristics and the locations of the evaluated reference points.

The model is further used to explore the possible effect of well-casing failures on local land subsidence dynamics and heterogeneities. The proposed conceptual framework describing the impact of well-casing failures on subsidence dynamics is governed by two main process pathways: (i) accelerated sediment compaction due to additional subsurface drainage pathways, and (ii) increased overall compaction resulting from locally amplified groundwater head depletion. These processes are schematically illustrated in Figure 18 and are discussed in detail below.

Firstly, well-casing failures act locally as additional drainage pathways, allowing excess pore water pressure in aquitard sediments to dissipate laterally into the casing. In undisturbed settings, drainage from aquitards predominantly occurs vertically toward adjacent aquifers, leading to delayed compaction, particularly in thick confining units. The presence of well-casing failures introduces localized, shorter horizontal flow paths, thereby accelerating pore pressure dissipation and associated compaction.

Secondly, well-casing failures may not only affect the timing of compaction but also increase its overall magnitude. In the investigated subsurface setting of the Mekong Delta, compaction of the shallow Holocene strata is primarily controlled by hydraulic head declines in the moderately depleted shallow aquifer. However, in the presence of well-casing failure, the effective reference head for drainage of the Holocene aquitard is locally governed by the water level within the casing, corresponding to the hydraulic head of the deeper tapped aquifer. If this aquifer exhibits lower hydraulic heads than the shallow aquifer, shallow Holocene sediments are locally exposed to increased head depletion, resulting in enhanced subsidence.

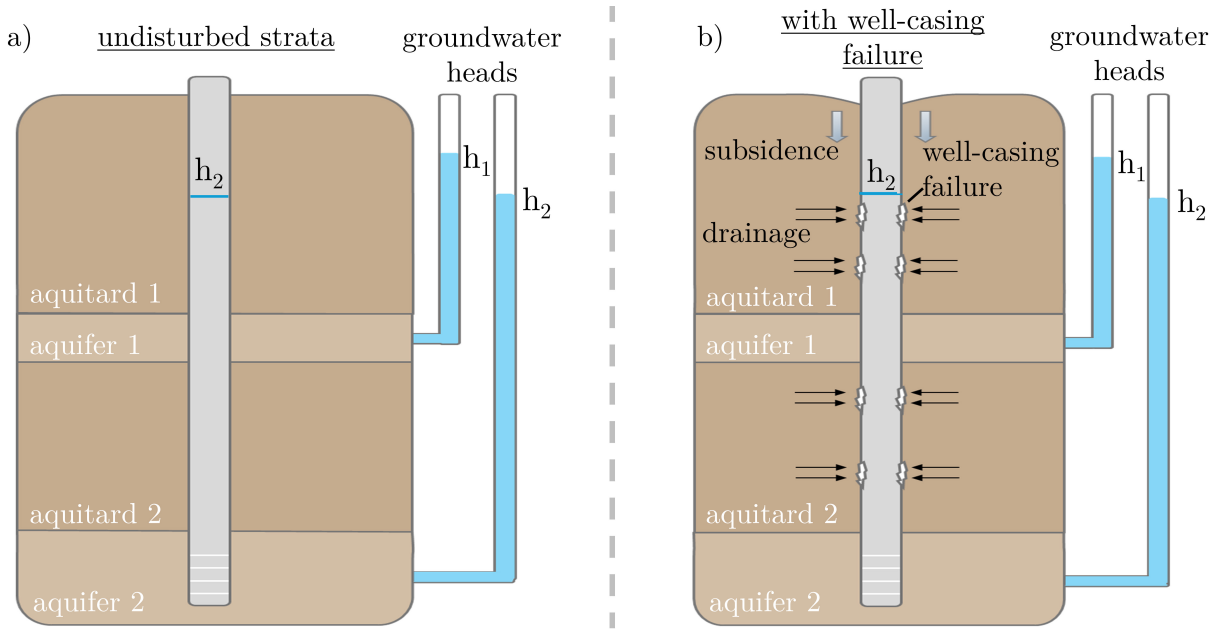


Figure 18: Conceptual illustration of how well-casing failure (b) enhances land subsidence compared with undisturbed subsurface conditions (a), where h_1 denotes the hydraulic head of the shallow aquifer and h_2 that of the deeper aquifer, equivalent to the casing water level.

3 Scientific Contributions

3.1 Concise summary of novel insights and publications

This dissertation advances pending research questions in the context of land subsidence (i) specifically for the Vietnamese Mekong Delta and (ii) more generally by developing broadly applicable methodological approaches and process-based insights relevant to subsidence affected regions worldwide. General methodological advancements of this dissertation include:

- introducing novel method extensions that enable the derivation of hydraulic and geomechanical subsurface parameters through passive subsurface characterization in deltaic systems, where superimposed harmonic drivers have previously limited the applicability of these underutilized methods (Dörr et al., 2025, 2026a).
- demonstrating how seasonal surface loading can induce rising groundwater trends in deltaic aquifers and mask their continuous depletion, thereby highlighting their potential to be misinterpreted as groundwater recharge (Dörr et al., 2026a).
- proposing a previously unaddressed pathway as an additional anthropogenic driver of land subsidence, suggesting that well-casing failures, well-known consequences of subsidence, may in turn accelerate subsidence by facilitating subsurface drainage and local hydraulic head equilibration between aquitards and tapped aquifers (Dörr et al., 2026b).
- advancing tidal subsurface analyses towards inelastic domains, by investigating seasonal variations in M_2 phase shifts and their correlation with dynamics in vertical hydraulic gradients and subsidence observations (section 3.2.2).

Specifically, for the Vietnamese Mekong Delta, this dissertation provides novel insights into land subsidence dynamics and related processes, by:

- unraveling the presence of loading signals in Mekong Delta's groundwater heads (Dörr et al., 2025).
- deriving a low subsidence mitigation potential of deep aquifers in the Mekong Delta by passive methods (Dörr et al., 2025).
- revealing that seasonal surface water loading masks ongoing groundwater depletion during the rainy season, suggesting negligible groundwater recharge and unsustainable groundwater extraction practices (Dörr et al., 2026a).
- presenting depth-differentiated compaction and geodetic monitoring data, showing land subsidence rates at GW1 < 10 mm a^{-1} (Dörr et al., 2023, section 3.5.2).
- quantifying the contribution of groundwater depletion (Dörr et al., 2026b) and autocompaction (section 3.4.2) to overall subsidence with comprehensive numeric modelling and a subsurface characterization in high vertical resolution for the upper 80 m at GW1.
- demonstrating that lateral uniform groundwater depletion and surface loading alone cannot fully explain the spatiotemporal heterogeneity of observed subsidence at GW1 (Dörr et al., 2026b).
- inferring process dynamics with physics-informed evaluations of observed groundwater heads and InSAR subsidence rates (section 3.5.3).

Overall, the key findings of this dissertation are presented in four peer-reviewed first-author research articles. In addition, further insights relevant to the research objectives that have not yet been published are included in this dissertation. The *Results* section 3 is structured such that, within each thematically structured subsection, each sub-subsection 1 presents findings of the first-authored research articles (sections 3.2.1,

3.3.1, 3.4.1 and 3.5.1), whereas subsequent sub-subsections (sections 3.2.2, 3.4.2, 3.5.2 and 3.5.3) provide additional insights that have not yet been published.

The research articles include two publications in the *Journal of Hydrology*, addressing passive subsurface characterization in subsiding deltas (Dörr et al., 2025) and seasonal loading signals and their potential for misinterpretation as groundwater recharge (Dörr et al., 2026a). A third publication discusses the monitoring setup and preliminary results of the land subsidence observatory in the German-language journal *Wasserwirtschaft* (Dörr et al., 2023). The fourth publication explores spatiotemporal heterogeneity and dynamics of land subsidence due to groundwater depletion in the Mekong Delta and was published in *Science of the Total Environment* (Dörr et al., 2026b). The presentation of the first-authored scientific publications in sections 3.2.1, 3.3.1, 3.4.1 and 3.5.1 includes their abstracts, graphical abstracts and highlights (where applicable), authorship statements, and a contextualization of their relevance to the research objectives.

Recognizing the need for multidisciplinary research on the interacting nature of cascading multi-hazards in deltaic systems, co-author contributions to several studies were conducted in collaboration with fellow researchers in the framework of the presented dissertation. This includes studies on social perceptions on land subsidence and water usage (Pham et al., 2023), numeric modelling on groundwater salinization (Hoan et al., 2025), seawater intrusion (Bauer et al., 2025), alternative water resources (Pham et al., 2026) and tidal effects on surface water salinity (Bauer et al., 2026 – under review). A summary of the contribution to each of these research articles and their linkage and relevance to the main objectives of the presented dissertation is presented in Appendix *B.1.* The respective co-author studies are presented in Appendix *B.2 - B.6.*

3.2 Tidal subsurface analysis provides insights into land subsidence dynamics and mitigation potential

The results presented in this section demonstrate how tidal subsurface analysis can be utilized to assess potential land subsidence mitigation strategies. The results include the peer-reviewed research article on passive subsurface characterization (Dörr et al., 2025, section 3.2.1) and further insights into seasonal patterns of groundwater responses to tidal forcings derived from transient frequency analyses (section 3.2.2).

3.2.1 Passive subsurface characterization in subsiding deltas: assessing land subsidence mitigation potential with frequency analyses of groundwater heads and superposing harmonic drivers (Dörr et al., 2025)



Journal of Hydrology 662 (2025) 133844

Contents lists available at ScienceDirect

Journal of Hydrology

journal homepage: www.elsevier.com/locate/jhydrol

Research papers

Passive subsurface characterization in subsiding deltas: assessing land subsidence mitigation potential with frequency analyses of groundwater heads and superposing harmonic drivers

Felix Dörr [a,*], Jonas Bauer [a], Gabriel C. Rau [b], Remi Valois [c], Tran Viet Hoan [a,d], Van Cam Pham [a], Le Thi Mai Van [d], Anke Steinel [e], Franz Nestmann [f], Stefan Norra [g]

[a] Karlsruhe Institute of Technology (KIT), Institute of Applied Geosciences, Kaiserstraße 12, 76131 Karlsruhe, Germany
[b] School of Environmental and Life Sciences, The University of Newcastle, Callaghan, Australia
[c] Avignon University, INRAE, UMR 1114 EMMAH, F-84000 Avignon, France
[d] National Center for Water Resources Planning and Investigation (NAWAPI), No. 93, Lane 95, Vu Xuan Thieu Street, Sai Dong Ward, Long Bien District, Hanoi 100000, Viet Nam
[e] Federal Institute for Geosciences and Natural Resources (BGR), Stilleweg 2, D-30655 Hannover, Germany
[f] Karlsruhe Institute of Technology (KIT), Institute of Water and River Basin Management, Kaiserstraße 12, 76131 Karlsruhe, Germany
[g] Potsdam University, Institute of Environmental Sciences and Geography, Soil Sciences and Geoecology, Campus Golm, Building 12, 14476 Potsdam Golm, Germany

ARTICLE INFO

This manuscript was handled by D. Han, Editor-in-Chief, with the assistance of Xiaolong Geng, Associate Editor

Keywords:
Mekong Delta
Ca Mau
Earth and ocean tides
Tidal subsurface analysis

ABSTRACT

Many of the world's low-lying river deltas are experiencing severe land subsidence, posing significant challenges to sustainable development. Effective mitigation strategies require a thorough understanding of subsurface processes and comprehensive parameterization, which are often hindered by limited investigations and resources. In this context, passive subsurface characterization (PSC) methods are particularly advantageous, as they utilize existing datasets to estimate hydraulic and geomechanical properties of the subsurface. This study conducts a detailed frequency analysis of 43 groundwater head time series in the southern Vietnamese Mekong Delta, revealing harmonic signals and imprints of mechanical loading in groundwater heads. These signals are identified as a superposition of five key drivers: (i) Earth tides, (ii) atmospheric tides, (iii) ocean tides, (iv) river tides, and (v) anthropogenic groundwater extraction. By disentangling Earth and ocean tides from atmospheric tides at the semi-diurnal frequency S_2, the specific storage and elastic formation compressibility of the intensely exploited middle Pliocene aquifer are estimated to 5.9–7.8 · 10^{-6} m^{-1} and 6.4–7.5 · 10^{-10} Pa^{-1}, respectively. This indicates a low land rebound and water storage potential and therefore an insignificant subsidence mitigation potential of this confined aquifer. By revealing that groundwater pumping may leak into amplitude spectra and corrupt quantitative PSC, this study underscores that accurate parameter estimations require a careful disentanglement of various superposing drivers. While the complex interplay of multiple tidal forcings limited previous PSC-applications in subsiding deltas, the novel integration of ocean tide loading on the solid Earth enables PSC-parameter estimations in coastal groundwater systems.

1. Introduction

Land subsidence is a geohazard of global scale and relevance, with nearly two billion people living in affected areas (Davydzenka et al., 2024). Groundwater over-exploitation has been identified as one of the main causes for intensive large-scale land subsidence (Motagh et al., 2008; Sun et al., 1999; Poland and Davis, 1969). Coastal plains and river deltas are particularly vulnerable to subsidence-induced land loss due to

Abbreviations: BE, barometric efficiency; FFT, fast Fourier transform; HALS, harmonic least squares; IGPVN, improvement of groundwater protection in Vietnam; MAR, managed aquifer recharge; NAWAPI, National Center for Water Resources Planning and Investigation, Vietnam; NGMN, National Groundwater Monitoring Network of Vietnam; OT_{SE}, ocean tide loading on the solid Earth; OT_{GW}, ocean tide loading on the aquifer's water; PSC, passive subsurface characterization; PT, pressure transducer; TSA, tidal subsurface analysis; VMD, Vietnamese Mekong Delta.

* Corresponding author.
E-mail address: felix.doerr@kit.edu (F. Dörr).

https://doi.org/10.1016/j.jhydrol.2025.133844
Received 18 February 2025; Received in revised form 11 June 2025; Accepted 5 July 2025
Available online 8 July 2025
0022-1694/© 2025 The Author(s). Published by Elsevier B.V. This is an open access article under the CC BY license (http://creativecommons.org/licenses/by/4.0/).

Paper 1: Published in Journal of Hydrology, 2025, 662.

Authors: Felix Dörr, Jonas Bauer, Gabriel C. Rau, Remi Valois, Tran Viet Hoan, Van Cam Pham, Le Thi Mai Van, Anke Steinel, Franz Nestmann, Stefan Norra.

Journal: Journal of Hydrology, 662.

Availability: Appendix *A.1* and *online* https://doi.org/10.1016/j.jhydrol.2025.133844

Authorship statement: This article, published in a peer-reviewed scientific journal, unravels the presence of loading signals in groundwater head observations in the Mekong Delta. To utilize these imprints of various loadings for the assessment of subsidence mitigation potential in the Mekong Delta and other deltaic aquifer systems, a novel method extension is introduced, integrating ocean tide loading in passive subsurface characterization (PSC),

thereby enabling PSC applicability in near-coastal settings. Tran Viet Hoan, Van Cam Pham and Le Thi Mai Van supported this study by providing time series of groundwater heads, river water levels and groundwater extraction rates. Anke Steinel supported this study by inspiring discussions on the concept of loading signals in groundwater heads and by providing data from the monitoring site IGPVN. With their pronounced experience in passive subsurface characterization, Gabriel C. Rau and Remi Valois contributed to the development of the research concept and the computation of ocean tide loading on the solid Earth. Continuous discussions with Jonas Bauer on the scientific content of this study and his support in preparing a map of the study area were of great importance. This study was supervised by Franz Nestmann and Stefan Norra, who guided the research concept, funding acquisition and project administration. All co-authors contributed to reviewing the scientific content and editorial format of the manuscript.

Relevance for research objectives:

By revealing loading signals in groundwater head observations in the Mekong Delta, this study uncovers the previously overlooked counterpart of hydrogeomechanical coupling. This counterpart represents "*the other side of the same coin*" of the very concept, that ultimately governs the process dynamics of groundwater-depletion–induced land subsidence. Thereby, this study complements the general hydrogeomechanical understanding of coupled surface and subsurface processes in the Mekong Delta and advances a more comprehensive conceptualization of the governing dynamics, which directly supports the outlined research focus 1 by advancing the process-based understanding of the governing subsidence dynamics.

In this study, the newly identified loading signals are fruther utilized for a subsurface parametrization with passive methods, in particular for an assessment of specific storage and elastic formation compressibility. These are key parameters in the context of land subsidence mitigation, as they incorporate information on a confined aquifer's land rebound potential and its capability to receive and store supplemental water resources, i.e. by *Managed Aquifer Recharge*. The evaluation indicates a low subsidence

mitigation potential of deep aquifers in the Mekong Delta. This directly addresses focus 2 of the outlined research objectives, as subsurface conditions relevant to associated mitigation strategies are derived with a previously inapplicable method.

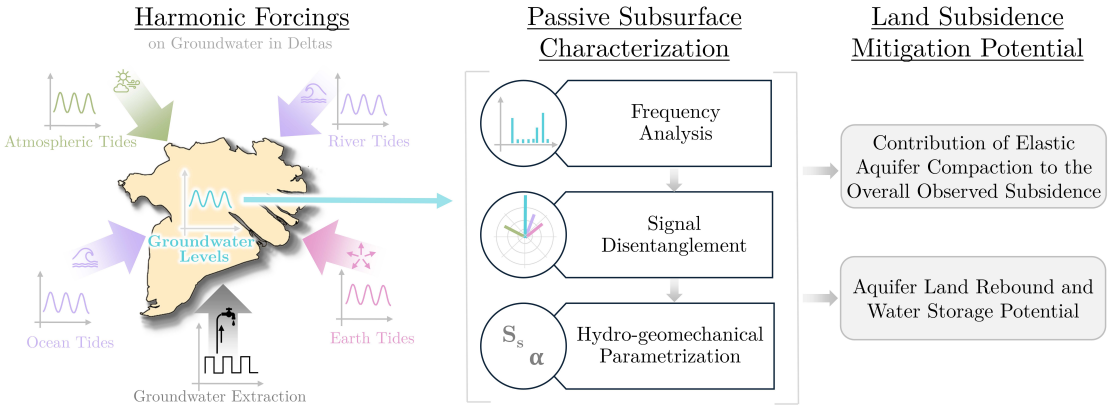
The development of a novel method extension enables the applicability of such passive methods to other subsiding deltas by integrating ocean tide loading on the solid Earth into the frequency-domain analysis. Moreover, the study shows that groundwater pumping, when operated at scheduled intervals, can leak into amplitude spectra derived from water level measurements in nearby observation wells. Thereby this study draws attention to a previously unconsidered factor that can corrupt quantitative passive subsurface characterization and supports the broader applicability of these methods.

Overall, this study provides a process-based quantification of key aquifer properties that directly inform the feasibility and expected effectiveness of groundwater-based mitigation strategies, thereby making a central contribution to focus 2 of the outlined research objectives. With this approach, a low land rebound and water storage potential, and therefore an insignificant subsidence mitigation potential, were derived for the investigated deep aquifers. The proposed methodological extension further enhances the transferability of this approach, enabling its application to other subsiding delta systems beyond the Mekong Delta.

Highlights:

- Novel integration of ocean tides enables near-coast quantitative PSC applicability.
- Groundwater pumping can corrupt quantitative PSC by leaking into amplitude spectra.
- Frequency analyses unravel loading signals in Mekong Delta's groundwater heads.
- Deep aquifers in the Mekong Delta have a low subsidence mitigation potential.

Graphical Abstract:



Abstract:

Many of the world's low-lying river deltas are experiencing severe land subsidence, posing significant challenges to sustainable development. Effective mitigation strategies require a thorough understanding of subsurface processes and comprehensive parameterization, which are often hindered by limited investigations and resources. In this context, passive subsurface characterization (PSC) methods are particularly advantageous, as they utilize existing datasets to estimate hydraulic and geomechanical properties of the subsurface. This study conducts a detailed frequency analysis of 43 groundwater head time series in the southern Vietnamese Mekong Delta, revealing harmonic signals and imprints of mechanical loading in groundwater heads. These signals are identified as a superposition of five key drivers: (i) Earth tides, (ii) atmospheric tides, (iii) ocean tides, (iv) river tides, and (v) anthropogenic groundwater extraction. By disentangling Earth and ocean tides from atmospheric tides at the semi-diurnal frequency S_2, the specific storage and elastic formation compressibility of the intensely exploited middle Pliocene aquifer are estimated to $5.9 - 7.8 \cdot 10^{-6}$ m^{-1} and $6.4 - 7.5 \cdot 10^{-10}$ Pa^{-1}, respectively. This indicates a low land rebound and water storage potential and therefore an insignificant subsidence mitigation potential of this confined aquifer. By revealing that groundwater pumping may leak into amplitude spectra and corrupt quantitative PSC, this study underscores that accurate parameter estimations require a careful disentanglement of various superposing drivers. While the complex interplay of multiple tidal forcings limited previous PSC-applications in subsiding

deltas, the novel integration of ocean tide loading on the solid Earth enables PSC-parameter estimations in coastal groundwater systems.

© The full article is reprinted with kind permission from Elsevier under the Creative Commons Attribution License and is included in Appendix A.1.

3.2.2 Advancing tidal subsurface analysis towards inelastic domains

Context: With the currently available methods, it is infeasible to derive inelastic subsurface parameters from tidal subsurface analyses, as the considered tidal forcings are typically small in magnitude and recur within narrow and constant ranges, thereby remaining in the elastic domain. This presents a major limitation of tidal subsurface analysis in assessing land subsidence, where inelastic aquitard deformation is often the main driver for the compaction processes. However, with the approach described below, tidal subsurface analysis can be advanced to infer aquitard drainage processes and therefore associated inelastic compaction and ultimately subsidence. This approach has not yet been included in the author's peer-reviewed publications.

New findings: By using transient frequency analyses, seasonal trends in M_2 phase shift and amplitude responses of groundwater heads to Earth- and ocean tide loading were discovered, exemplary illustrated for the monitoring site IGPVN in Figure 19d and Figure 19e. In this approach, HALS frequency analyses were conducted for 60-day sub-datasets, scanning the time series between 2016 and 2024 with a moving window. This analysis results in a total of 3,173 independently conducted frequency analyses, each providing a value for phase shift and amplitude within the assessed 60-day period. To simplify the subsequent formulations, the wording "*M_2 phase shift between groundwater heads and Earth- and ocean tide loading*" is shortened to "*M_2 phase shift*". Figure 19d and Figure 19e summarize the temporal variation of phase shift and amplitude response alongside with daily precipitation records. The analyses show pronounced seasonal trends in M_2 phase shift and amplitude response in all three assessed aquifers at the monitoring site IGPVN. During the dry season, an increase in M_2 phase shift to positive

values is evident in all three assessed aquifers. The seasonal variation of M_2 phase shift is most pronounced in IGPVN 1.2 (qp_1) with a spread of approximately ± 40°. In IGPVN 1.3 ($qp_{2\text{-}3}$), and IGPVN 1 (n_2^2) the seasonal M_2 phase shift spread is less pronounced, yet clearly discernible with approximately ± 20° and ± 10° respectively.

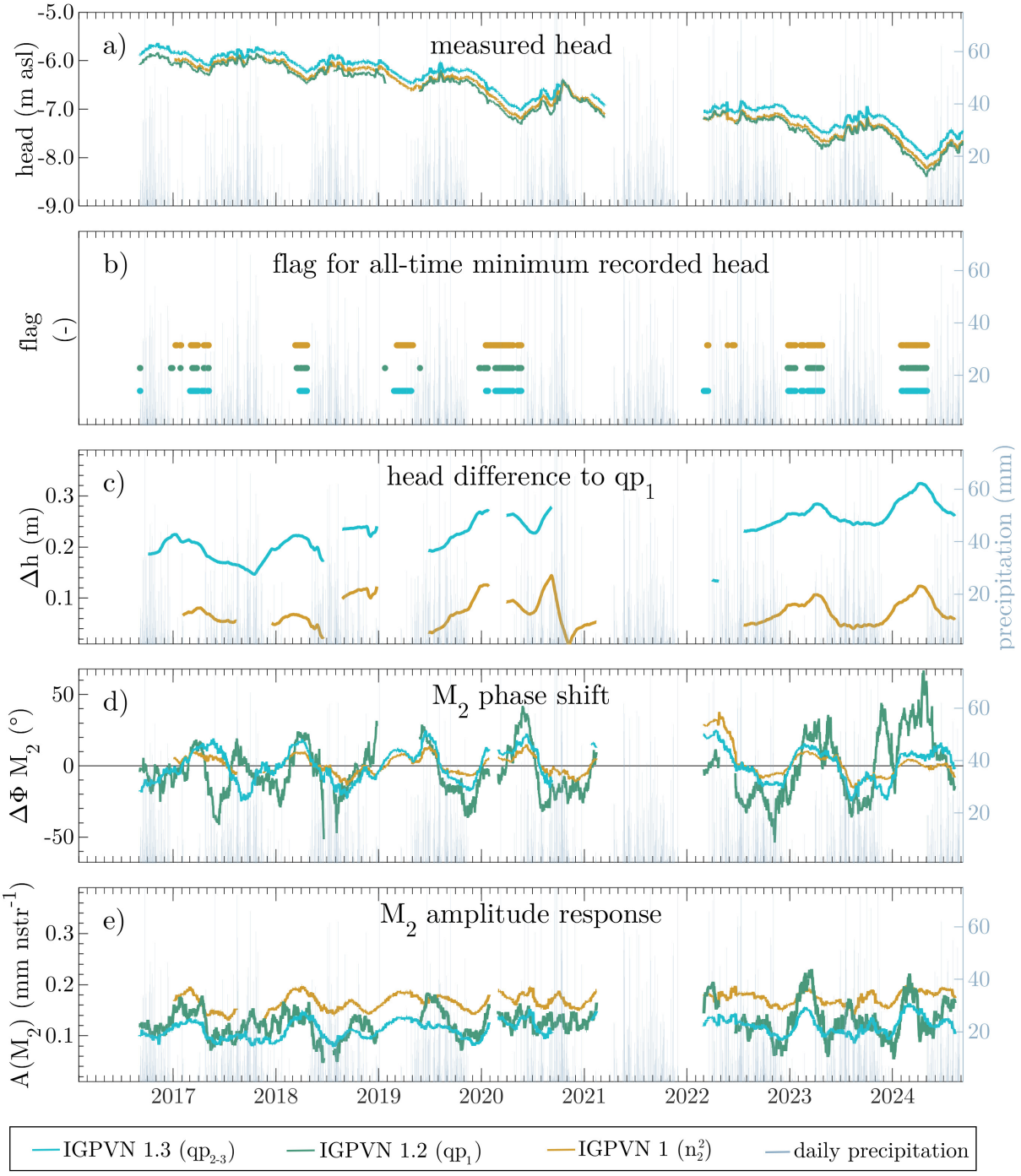


Figure 19: Transient analysis showing groundwater head dynamics (a), periods with all-time minima heads (b), hydraulic head differences between aquifers (c), M_2 phase shift (d) and amplitude response (e) with a 60-day moving window at IGPVN. Results in (d) and (e) are visualized as data points at the center of the 60-day evaluation period.

Seasonality in M_2 phase shift and amplitude response of groundwater heads to Earth tides have only recently been discovered by Liao et al. (2022) at a study site in Southwest China. These seasonal M_2 phase shift variations were interpreted as potential indication for seasonally increasing aquitard leakage. In line with this, the identified seasonal variation in M_2 phase shifts in all three observation wells at IGNPV is interpreted as an increasing contribution of vertical flow from the aquitards to the aquifers. This is also supported by an evaluation of differences in hydraulic head between the locally most exploited aquifer qp_1 and the adjacent aquifers $qp_{2\text{-}3}$ (above) and n_2^2 (below). The head difference between qp_1 and the other two aquifers is illustrated in Figure 19c, showing seasonal variations characterized by an increase during dry season and a decrease during rainy season. This suggests that with advancing depletion during dry season, the vertical hydraulic gradient between qp_1 and the adjacent strata increases, therefore elevating the potential for vertical flow towards the aquifer. This is supported by conducted multi-well pumping tests (Pechstein et al., 2018), characterizing the groundwater system at IGPVN as a leaky aquifer system. Overall, the dynamics of vertical hydraulic gradient as a proxy for increasing vertical flow correlates with changes of the sign of the M_2 phase shift from negative to positive (Figure 19d).

The sign of the M_2 phase shift is commonly used in tidal subsurface analysis to distinguish between vertical and horizontal flow settings: A positive phase shift is indicative of vertical flow as for example in the presence vertical leakage from or through an overlying aquitard, whereas a negative phase shift is associated with horizontal flow in and out of the well, indicating fully confined conditions (Rau et al., 2020; Roeloffs et al., 1989; Rojstaczer, 1988; Xue et al., 2016). Therefore, the positive sign in M_2 phase shift, together with the increasing vertical hydraulic gradient are considered as an indicator for vertical flow from the aquitards to the aquifer.

To substantiate the relationship between phase shift dynamics with groundwater head dynamics (Figure 19a), time periods, in which the groundwater heads reach an all-time minimum, are highlighted in Figure 19b. During these periods, typically occurring in

the second half of the dry season, effective stresses in the sediments reach a historic maximum, marking the tipping point between elastic and inelastic deformation in a normally consolidated setting. Comparing Figure 19b with Figure 19d illustrates the evident correlation between a positive M_2 phase shift and historic minima in hydraulic head.

Finally, the correlation between M_2 phase shift dynamics and subsidence trends is evaluated by illustrating the local InSAR-based subsidence trends (derived from Figure 28) with the M_2 phase shift dynamics (derived from Figure 19d) in Figure 20, showing increased subsidence correlating with positive M_2 phase shift in all years where the two datasets overlap 2017-2021 (periods ①-③).

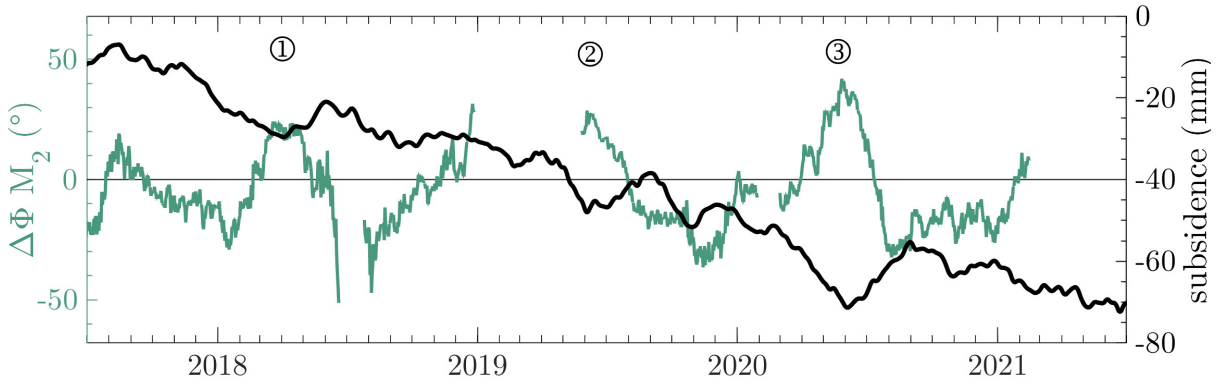


Figure 20: M_2 phase shift dynamics and subsidence trends at the monitoring site IGPVN between 2017 and 2021.

In summary, the seasonal variation in M_2 phase shift changing from predominantly negative in the rainy season to predominantly positive in the dry season is interpreted as an indicator for an increase of vertical flow from the aquitards towards the aquifers, therefore indicating aquitard drainage, inelastic sediment compaction and ultimately subsidence. This is substantiated by (i) an assessment of vertical hydraulic gradients, (ii) an assessment of temporal maxima in effective stresses derived from historic minima in groundwater head observations and (iii) InSAR subsidence observations.

In general, variations of the M_2 phase shift and amplitude response could also be caused by the occurrence of other tidal forcings with seasonally changing impact, e.g. tides of river water levels, with alternating intensity during dry and rainy season. For the assessed monitoring site IGPVN this is considered not to be the driver for the seasonal

variation of M_2 phase shifts given that: (i) river tides have been considered negligible for the site IGPVN as it is located at the border of the freshwater area of U-Minh and the nearby channels are protected from saltwater intrusion and tidal propagation by sluice gates (Dörr et al., 2025); (ii) a forcing acting on the surface like tidal river water influence would act greatest in the topmost aquifer and diminish towards lower aquifers, whereas the evaluation shows the greatest variations in M_2 phase shifts in the central aquifer qp_1.

Implications: These findings provide a framework for advancing tidal subsurface analysis towards inelastic domains, therefore crossing the border of their major limitation in the context of land subsidence investigations. Rather than utilizing tidal subsurface analysis to derive hydrogeomechanical parameters, this procedure contributes to an improved system understanding on a qualitative manner. However, it bears the potential to advance analytical solutions to more robust parameter estimations, as recently derived analytical equations to calculate the aquitard compressibility from groundwater responses to Earth tides (Valois et al., 2024) are challenged by the solution's non-uniqueness.

3.3 The impact of seasonal surface loading on groundwater heads and recharge analyses

In this section, the seasonal rise in groundwater heads is shown to result from seasonal surface loading rather than from groundwater recharge. This finding was presented in a peer-reviewed research article (Dörr et al., 2026a) and was termed the *recharge illusion*. In the context of land subsidence mitigation, this implies that strict limitations on groundwater extraction are required to prevent continued depletion of aquifer heads, thereby directly informing land subsidence mitigation strategies in the Mekong Delta.

3.3.1 The recharge illusion: How seasonal surface loading can hide continuing groundwater resource declines in confined deltaic aquifers (Dörr et al., 2026a)



Journal of Hydrology 665 (2026) 134674

Contents lists available at ScienceDirect

Journal of Hydrology

journal homepage: www.elsevier.com/locate/jhydrol

The recharge illusion: How seasonal surface loading can hide continuing groundwater resource declines in confined deltaic aquifers

Felix Dörr [a,*], Jonas Bauer [a], Gabriel C. Rau [b], Elias Lewi [c], Viet Tran Hoan [a,d], Le Thi Mai Van [d], Remi Valois [e], Anke Steinel [f], Franz Nestmann [g], Stefan Norra [h]

[a] Karlsruhe Institute of Technology (KIT), Institute of Applied Geosciences, Kaiserstraße 12, 76131 Karlsruhe, Germany
[b] School of Environmental and Life Sciences, The University of Newcastle, University Drive, NSW 2308 Callaghan, Australia
[c] Institute of Geophysics, Space Science and Astronomy, Addis Ababa University, Arat Kilo Campus, Addis Ababa, Ethiopia
[d] National Center for Water Resources Planning and Investigation (NAWAPI), No. 93, lane 95, Vu Xuan Thieu Street, Sai Dong Ward, Long Bien District, Hanoi 100000, Viet Nam
[e] Avignon University, INRAE, UMR 1114 EMMAH, F-84000 Avignon, France
[f] Federal Institute for Geosciences and Natural Resources (BGR), Stilleweg 2, D-30655 Hannover, Germany
[g] Karlsruhe Institute of Technology (KIT), Institute of Water and River Basin Management, Kaiserstraße 12, 76131 Karlsruhe, Germany
[h] Potsdam University, Institute of Environmental Sciences and Geography, Soil Sciences and Geoecology, Campus Golm, Building 12, 14476 Potsdam Golm, Germany

ARTICLE INFO

This manuscript was handled by Renato Morbidelli, Editor-in-Chief, with the assistance of Eddie Banks, Associate Editor

Keywords:
Loading efficiency
Mekong delta
Barometric efficiency
Passive subsurface characterization
Groundwater head dynamics

ABSTRACT

Reliable estimates of groundwater recharge are critical for managing water resources and preventing groundwater depletion. However, groundwater recharge estimates can be distorted when loading signals are mistakenly interpreted as signs of groundwater recharge. This study introduces a novel extension to existing frequency-domain methods to quantify loading imprints in groundwater measurements by disentangling superposing signals from Earth, atmospheric, ocean, and river tides, using the K_1 tidal constituent to remove the river tide influence. This approach enables the application of frequency-domain methods for calculating the loading efficiency in deltaic groundwater systems, where superposing multiple forcings govern tidal constituents in groundwater heads. Using multi-factor regression deconvolution analysis, surface loading signals are removed from groundwater head time series. Applying this method to groundwater head data from the southern Vietnamese Mekong Delta strongly suggests that the observed seasonal rise in groundwater heads does not reflect recharge. Instead, the apparent upward trend in uncorrected data is attributed to mechanical surface loading from seasonal surface water accumulation linked to expanding aquaculture. The loading-corrected time series show a consistent decline during both dry and rainy seasons, aligning with observed annual depletion rates. This indicates a deficiency of net effective groundwater recharge throughout the year, reflecting unsustainable groundwater exploitation practices. The methods and findings of this study offer a scientific framework for the analysis of multiple superimposed surface loading processes in deltaic aquifer systems, thereby enhancing groundwater recharge assessments in such hydrogeological environments.

1. Introduction

Global groundwater resources are under increasing stress, and the widespread acceleration of depletion trends underscores the urgent need for effective measures to address ongoing declines (Jasechko et al., 2024). Coastal areas are particularly vulnerable to the impact of groundwater overexploitation, as groundwater depletion promotes seawater intrusion and thus further accelerates the loss of available underground freshwater resources (Konikow and Kendy, 2005). Moreover, in many deltaic lowlands, the depletion of groundwater heads causes notable land subsidence due to the compaction of subsurface sediments (Herrera-García et al., 2021; Davydzenka et al., 2024). The Asian mega-deltas like the Ganges-Brahmaputra Delta, the Yangtze Delta and the Mekong Delta are prominent examples for such subsiding deltas (Syvitski et al., 2009). The southern Vietnamese Mekong Delta (VMD) is subject to land subsidence dynamics with rates locally exceeding 0.03 m a^{-1} (Erban et al., 2014; Minderhoud et al., 2017; Dörr et al., 2024). Given its average elevation of only about 80 cm above mean sea level in 2018 (Minderhoud et al., 2019), such

* Corresponding author.
E-mail address: felix.doerr@kit.edu (F. Dörr).

https://doi.org/10.1016/j.jhydrol.2025.134674
Received 23 July 2025; Received in revised form 26 October 2025; Accepted 24 November 2025
Available online 26 November 2025
0022-1694/© 2025 The Author(s). Published by Elsevier B.V. This is an open access article under the CC BY license (http://creativecommons.org/licenses/by/4.0/).

Paper 2: Published in Journal of Hydrology, 665, 2026.

Authors: Felix Dörr, Jonas Bauer, Gabriel C. Rau, Elias Lewi, Tran Viet Hoan, Le Thi Mai Van, Remi Valois, Anke Steinel, Franz Nestmann, Stefan Norra.

Journal: Journal of Hydrology, 665.

Availability: Appendix *A.2* and *online* https://doi.org/10.1016/j.jhydrol.2025.134674

Authorship statement: This article, published in a peer-reviewed scientific journal, reveals that rising groundwater heads during the rainy season do not reflect groundwater recharge but are due to mechanical surface loading from seasonal surface water accumulation. The finding provides valuable guidance for land subsidence mitigation strategies aimed at

determining sustainable groundwater extraction rates and preventing further depletion in the Mekong Delta and beyond. Tran Viet Hoan and Le Thi Mai Van supported this study by providing measurement data of groundwater heads and river water levels. Anke Steinel supported this study through valuable discussions on the concept of groundwater head responses to precipitation loading. Gabriel C. Rau contributed to this study by validating the introduced method extension. Remi Valois contributed to the study with the computation of ocean tide loading on the solid Earth. Elias Lewi supported this study by sharing inspiring insights into tidal subsurface response from a geophysical perspective. Continuous discussions with Jonas Bauer on the research concept, implications for the study area and the manuscript structure were of great value. Franz Nestmann and Stefan Norra supervised this study, guided the overall research concept, and managed funding acquisition as well as project administration. All co-authors reviewed the scientific content as well as the editorial format of the manuscript.

Relevance for research objectives:

By revealing that rising groundwater heads during the rainy season are caused by mechanical surface loading and therefore do not reflect groundwater recharge, this study provides essential information for determining sustainable groundwater extraction rates and preventing further depletion, a key strategy for mitigating land subsidence and thus directly addresses focus 2 of the outlined research objectives.

By advancing existing methods through a novel integration of river tides into passive subsurface parameterization (introduced in section 2.4.2), this study broadens the applicability of such approaches to deltaic settings in general. By demonstrating the impact of seasonal surface loading on groundwater head dynamics in anthropogenically shaped deltaic systems, this study supports more comprehensive investigations of groundwater resources in such settings.

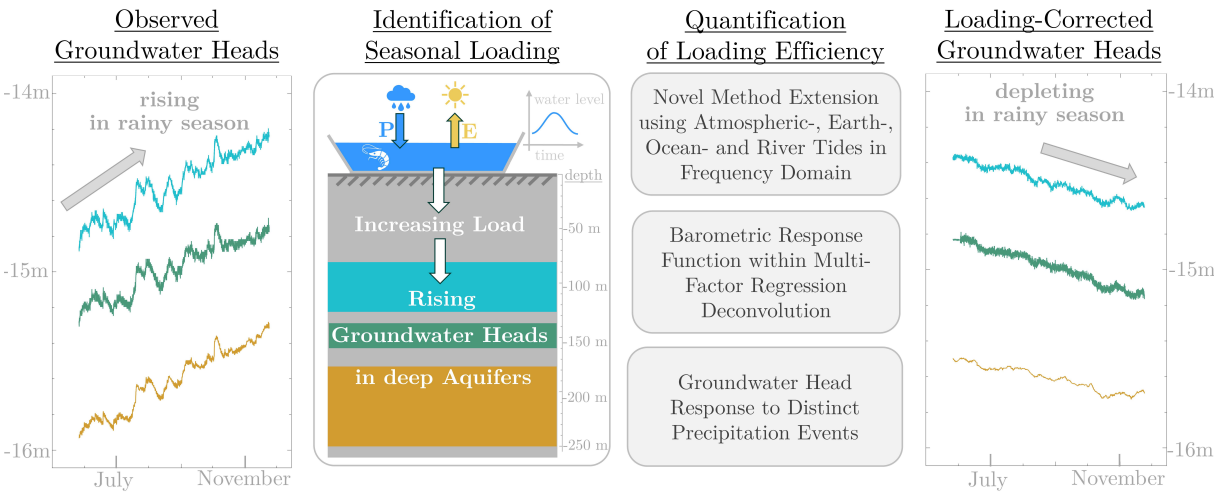
Overall, the study provides a process-based reinterpretation of groundwater head dynamics, indicating a lack of significant groundwater recharge. This implies a limited potential of the aquifer system to recover hydraulic heads or to compensate for

depletion caused by significant anthropogenic groundwater exploitation. Therefore, the findings of this study directly inform the assessment of sustainable groundwater use and associated mitigation strategies, thereby contributing to focus 2 of the outlined research objectives. The proposed methodological advancements further enable the transfer of this approach to other deltaic systems.

Highlights:

- Novel method extension uses ocean and river tides in passive aquifer parametrization.
- Observed groundwater heads in the Vietnamese Mekong Delta rise due to seasonal surface water loading.
- Loading-corrected groundwater heads reveal ongoing depletion during rainy season.
- Surface loading must be considered in deltaic groundwater recharge assessments.

Graphical Abstract:



Abstract:

Reliable estimates of groundwater recharge are critical for managing water resources and preventing groundwater depletion. However, groundwater recharge estimates can be distorted when loading signals are mistakenly interpreted as signs of groundwater recharge. This study introduces a novel extension to existing frequency-domain methods to quantify loading imprints in groundwater measurements by disentangling superposing signals from Earth, atmospheric, ocean, and river tides, using the K_1 tidal constituent to remove the river tide influence. This approach enables the application of frequency-domain methods for calculating the loading efficiency in deltaic groundwater systems, where superposing multiple forcings govern tidal constituents in groundwater heads. Using multi-factor regression deconvolution analysis, surface loading signals are removed from groundwater head time series. Applying this method to groundwater head data from the southern Vietnamese Mekong Delta strongly suggests that the observed seasonal rise in groundwater heads does not reflect recharge. Instead, the apparent upward trend in uncorrected data is attributed to mechanical surface loading from seasonal surface water accumulation linked to expanding aquaculture. The loading-corrected time series show a consistent decline during both dry and rainy seasons, aligning with observed annual depletion rates. This indicates a deficiency of net effective groundwater recharge throughout the year, reflecting unsustainable groundwater exploitation practices. The methods and findings of this study offer a scientific framework for the analysis of multiple superimposed surface loading processes in deltaic aquifer systems, thereby enhancing groundwater recharge assessments in such hydrogeological environments.

© The full article is reprinted with kind permission from Elsevier under the Creative Commons Attribution License and is included in Appendix A.2.

3.4 Simulating subsidence due to various drivers

The results presented in this section address the contributions of individual drivers to total land subsidence based on numerical simulations for the research site GW1. They include results published in *Science of the Total Environment* (Dörr et al., 2026b, section 3.4.1), as well as additional simulations quantifying the contribution of autocompaction to overall land subsidence at GW1 (section 3.4.2).

3.4.1 Land Subsidence Dynamics in the Mekong Delta: Insights from Local High-Resolution Geomechanical Parameterization, Numerical Modelling, and Geodetic Observations (Dörr et al., 2026b)



Science of the Total Environment 1033 (2026) 181850

Contents lists available at ScienceDirect

Science of the Total Environment

journal homepage: www.elsevier.com/locate/scitotenv

Land subsidence dynamics in the Mekong Delta: Insights from local high-resolution geomechanical parameterization, numerical modelling, and geodetic observations

Felix Dörr [a,*], Jonas Bauer [a], Tran Viet Hoan [a,b], Le Thi Mai Van [b], Andreas Schenk [c], Nils Dörr [c], Franz Nestmann [d], Stefan Norra [e]

[a] Karlsruhe Institute of Technology (KIT), Institute of Applied Geosciences, Kaiserstraße 12, 76131, Karlsruhe, Germany
[b] National Center for Water Resources Planning and Investigation (NAWAPI), No. 93, lane 95, Vu Xuan Thieu Street, Sat Dong Ward, Long Bien District, Hanoi, 100000, Viet Nam
[c] Karlsruhe Institute of Technology (KIT), Institute of Photogrammetry and Remote Sensing, Kaiserstraße 12, 76131, Karlsruhe, Germany
[d] Karlsruhe Institute of Technology (KIT), Institute for Water and Environment, Kaiserstraße 12, 76131, Karlsruhe, Germany
[e] Potsdam University, Institute of Environmental Sciences and Geography, Soil Sciences and Geoecology, Campus Golm, Building 12, 14476, Potsdam Golm, Germany

HIGHLIGHTS

- Fully-coupled flow-deformation model used to simulate subsidence in Mekong Delta.
- The Mekong Delta will face delayed subsidence due to past groundwater depletion.
- Well-casing failure can accelerate land subsidence.

GRAPHICAL ABSTRACT

ARTICLE INFO

Keywords:
Land subsidence
Fully-coupled flow-deformation model
Mekong Delta
Groundwater overexploitation

ABSTRACT

Land subsidence poses major threats to human and environmental systems in river deltas worldwide, increasing risks of flooding and damage to civil infrastructure. In deltaic settings, land subsidence can be induced by multiple superimposing processes, including autocompaction, groundwater depletion and infrastructural surface loading. The quantification of each individual process is often uncertain, yet crucial for effective adaptation and mitigation. The Vietnamese Mekong Delta (VMD) is a prominent example of such a subsiding delta, with satellite-derived subsidence rates of up to 30 mm a^{-1} and surface elevations largely below 1 m above mean sea level. By presenting a fully coupled flow-deformation model with geomechanical parameterization at high vertical resolution, this study, supported by local geodetic leveling observations, provides an unprecedentedly detailed local-scale assessment of land subsidence dynamics for the VMD. The simulation results indicate subsidence rates of 5–6 mm a^{-1} due to groundwater depletion and local infrastructure loading. Additionally integrating one or

* Corresponding author.
E-mail address: felix.doerr@kit.edu (F. Dörr).

https://doi.org/10.1016/j.scitotenv.2026.181850
Received 5 January 2026; Received in revised form 25 April 2026; Accepted 30 April 2026
Available online 3 May 2026
0048-9697/© 2026 The Authors. Published by Elsevier B.V. This is an open access article under the CC BY license (http://creativecommons.org/licenses/by/4.0/).

Paper 3: Published in Science of the total Environment, 1033. 2026.

Authors: Felix Dörr, Jonas Bauer, Tran Viet Hoan, Le Thi Mai Van, Andreas Schenk, Nils Dörr, Franz Nestmann, Stefan Norra.

Journal: Science of the total Environment, 1033

Availability: Appendix A.3 and *online* https://doi.org/10.1016/j.scitotenv.2026.181850

Authorship statement: This article has been published in a peer-reviewed scientific journal. Utilizing the high data density obtained from the monitoring site GW1, the publication presents numerical simulations at unprecedented detail for the Mekong Delta, substantiating the role of groundwater depletion as a key driver of land subsidence and addressing potential contributions of surface loading of the built environment and well-casing failures. Throughout the preparation and elaboration of this publication, the results and their implications for interdisciplinary research fields, including inter-aquifer connectivity

and salinization, were discussed with Jonas Bauer. Tran Viet Hoan and Le Thi Mai Van supported this study by providing monitoring data of groundwater heads. In addition, Tran Viet Hoan was involved in fieldwork related to drill-core sampling in 2020 and supported the laboratory work associated with the oedometer tests. Andreas Schenk contributed to the design of the geodetic leveling campaign and to the validation of the corresponding analyses. Nils Dörr provided the processed InSAR observations. The study was supervised by Stefan Norra and Franz Nestmann, who guided the overall research concept and were responsible for project management, administration, and initial funding acquisition. All co-authors reviewed the manuscript.

Relevance for research objectives:

This study advances the process-based understanding of groundwater depletion as a trigger of land subsidence in the Mekong Delta through physics-informed numerical simulations of the governing subsurface processes, thereby directly contributing to focus 1 of the outlined research objectives. By deriving and utilizing a high-resolution subsurface parameterization together with locally recorded groundwater heads within an advanced numerical modeling framework, the simulation results achieve a high level of confidence while agreeing with ground- and satellite- based subsidence observations at the investigated local scale. Thereby, previous concerns among decision-makers regarding the conceptual contribution of groundwater depletion to land subsidence are addressed through a robust quantitative assessment at exemplary level. The presented simulation accounts for groundwater head depletion and nearby urban surface loading in a representative order of magnitude for the delta and successfully reproduces locally observed subsidence rates at GW1 at moderate magnitude <10 mm a^{-1}. This study indicates that locally extreme subsidence rates can be caused not only by commonly considered influences such as urban infrastructure loading and localized peaks in groundwater abstraction and depletion, but also by anthropogenic subsurface disturbances such as well-casing failures.

The good agreement between observed subsidence rates at GW1 and the simulated subsidence dynamics indicates that groundwater depletion is the dominant driver at

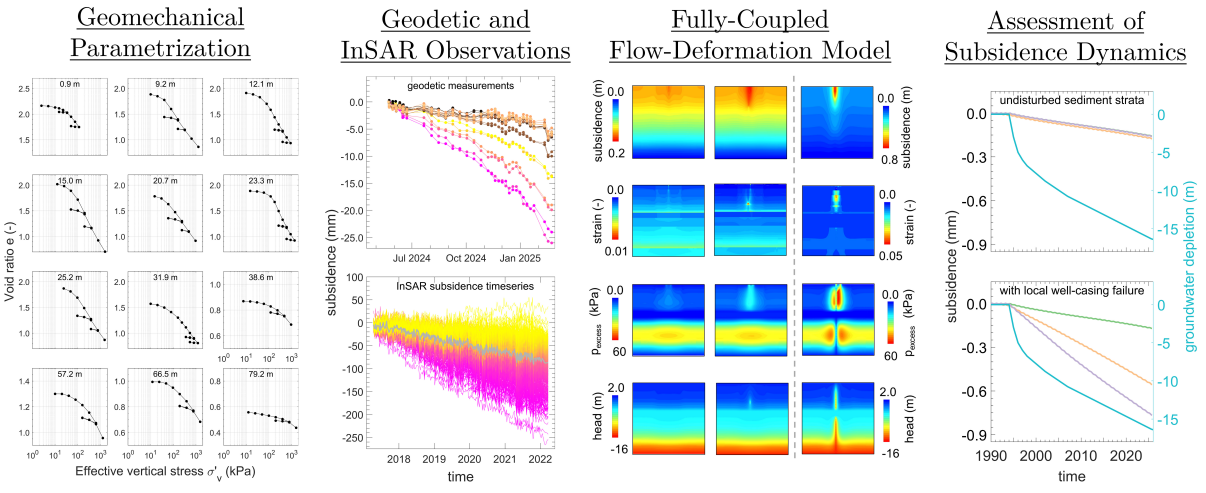
this site. Given that GW1 constitutes a representative setting for the southern Mekong Delta in terms of observed subsidence dynamics, groundwater depletion, and subsurface layering, these findings can be considered exemplary and broadly transferable to other parts of the Mekong Delta. Therefore, this study directly contributes to the outlined research focus 1 by demonstrating that groundwater depletion is the dominant driver of land subsidence at a representative study site.

By introducing well-casing failure as a potential contributor to advancing subsidence dynamics, this study addresses an additional aspect of how anthropogenic interventions in natural systems can accelerate land subsidence processes. The potential impact of well-casing failure on heterogeneous and locally extreme subsidence dynamics is explored through numerical simulations, strengthening the interpretation of this factor as a relevant contribution to spatiotemporal heterogeneity in subsidence patterns in the Mekong Delta and beyond.

Highlights:

- Fully-coupled flow-deformation model used to simulate subsidence in Mekong Delta.
- The Mekong Delta will face delayed subsidence due to past groundwater depletion.
- Well-casing failure can accelerate land subsidence.

Graphical Abstract:



Abstract:

Land subsidence poses major threats to human and environmental systems in river deltas worldwide, increasing risks of flooding and damage to civil infrastructure. In deltaic settings, land subsidence can be induced by multiple superimposing processes, including autocompaction, groundwater depletion and infrastructural surface loading. The quantification of each individual process is often uncertain, yet crucial for effective adaptation and mitigation. The Vietnamese Mekong Delta (VMD) is a prominent example of such a subsiding delta, with satellite-derived subsidence rates of up to 30 mm a^{-1} and surface elevations largely below 1 m above mean sea level. By presenting a fully coupled flow–deformation model with geomechanical parameterization at high vertical resolution, this study, supported by local geodetic levelling observations, provides an unprecedentedly detailed local-scale assessment of land subsidence dynamics for the VMD. The simulation results indicate subsidence rates of 5-6 mm a^{-1} due to groundwater depletion and local infrastructure loading. Additionally integrating one or multiple well-casing failures as localized subsurface disturbances in the model yields spatially heterogeneous subsidence patterns and increases local subsidence rates by an additional 1–20 mm a^{-1}, depending on the number of implemented failures. While well-casing failures are known consequences of land subsidence, this study proposes that such damage can in turn accelerate subsidence by facilitating subsurface drainage pathways and local head equilibration between aquitards and tapped aquifers. Overall, the findings indicate that well-casing failures can be relevant contributors to heterogeneous and locally extreme subsidence dynamics. The results reveal significant delays in subsidence due to past groundwater depletion at the investigated site, underscoring the need for proactive water management strategies in the VMD, supported by comprehensive land subsidence modelling. The insights derived from this localized high-resolution analysis suggest that effective management will require preventing shallow aquifer depletion to avoid triggering the Holocene's pronounced, yet largely inactivated subsidence potential.

© The full article is reprinted with kind permission from Elsevier under the Creative Commons Attribution License and is included in Appendix A.3.

3.4.2 Model-based estimation of autocompaction

Context: In order to complement the high-resolution quantification of groundwater-depletion–induced land subsidence dynamics at GW1 (Dörr et al., 2026b), the available data are also used to numerically estimate the contribution of autocompaction processes to the observed subsidence dynamics. This approach supports the robustness of the results and enables a consistency check of the quantified groundwater-depletion–induced subsidence. The quantification of autocompaction processes at GW1 presented here has not yet been included in the peer-reviewed research articles.

New findings: The 2-D geomechanical model, which was developed to simulate subsidence due to groundwater depletion, surface loading and well-casing failure (Dörr et al., 2026b), was adapted to estimate subsidence caused by autocompaction, i.e. the compaction due to self-weight loading of the Holocene strata. For this purpose, sedimentation and autocompaction over the last 4,000 years were reconstructed. This period represents the second half of the Holocene, the time in which prodelta deposits formed the Ca Mau Peninsula (Zoccarato et al., 2018) and equals the simulation period used by Zoccarato et al. (2018) and Baldan et al. (2025) in their simulation of autocompaction.

To simulate recent autocompaction processes, the Holocene strata was generated in the model by subsequently initiating new model layers over the past 4,000 years. To derive the sedimentation rate at GW1, an initial model simulation was employed, utilizing a sedimentation rates of 6 mm a^{-1}, consistent with estimates for the upper delta plain used by Zoccarato et al. (2018) and Baldan et al. (2025). While this rate produces 24 m of net sedimentation over 4,000 years, reconstructing the present Holocene thickness of ~26 m required an iterative adjustment of the sedimentation rate to 7.5 mm a^{-1} to compensate for the modelled compaction. A total accumulation of 30 m combined with approximately 4 m of simulated compaction ultimately matches the observed 26 m Holocene sequence at GW1.

A similar iterative inverse-modelling procedure was used to estimate the initial void ratio and hydraulic conductivity. As both parameters vary over the course of the fully

coupled simulation, their initial values were iteratively adapted to fit the measured values from samples obtained in 2020 (Figure 21 and Figure 22).

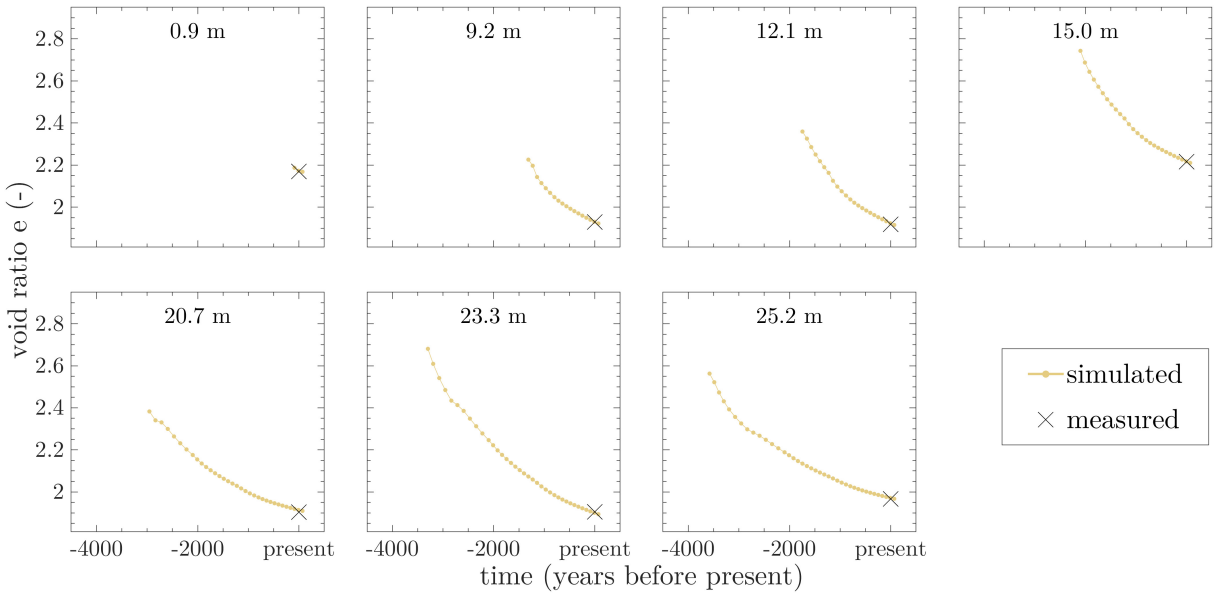


Figure 21: Change of void ratio over the past 4,000 years; initial values were calibrated to achieve a good fit of modeled values with recent-day measurements.

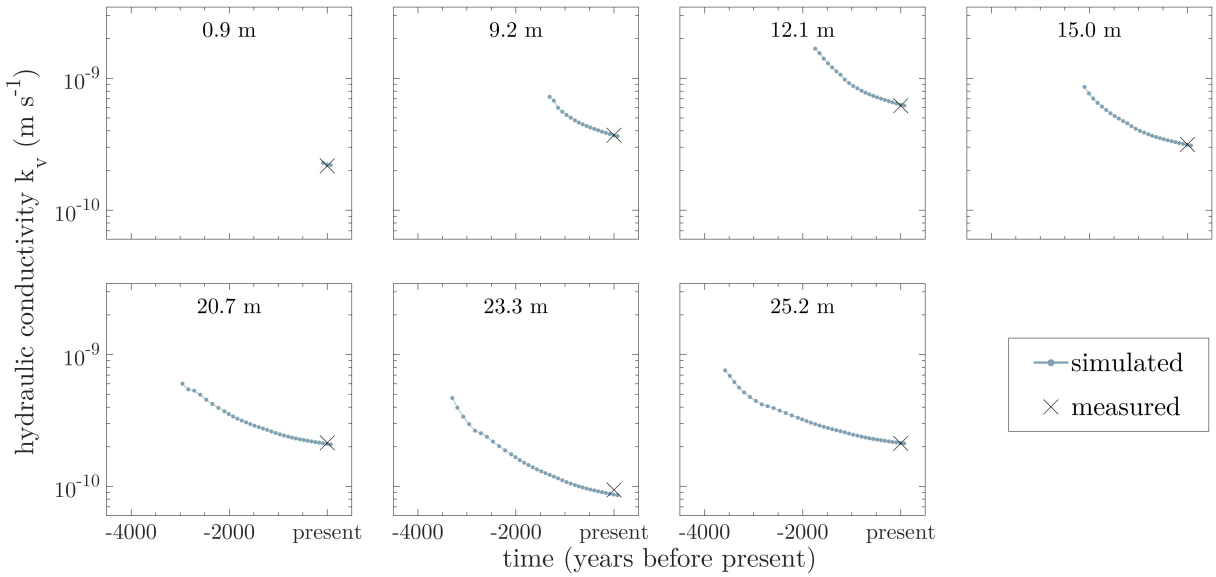


Figure 22: Change of vertical hydraulic conductivity over the past 4,000 years; initial values were calibrated to achieve a good fit of modeled values with recent-day measurements.

Assuming no ongoing sediment deposition, present-day autocompaction at GW1 calculates to 0.8 mm a^{-1}, with a near-constant trend throughout the 21st century (Figure 23a). The calculated vertical distribution of strains for the remainder of the century is

shown in Figure 23b, indicating that the strongest self-weight–induced compaction occurs between depths of approximately 2.5 and 10 m.

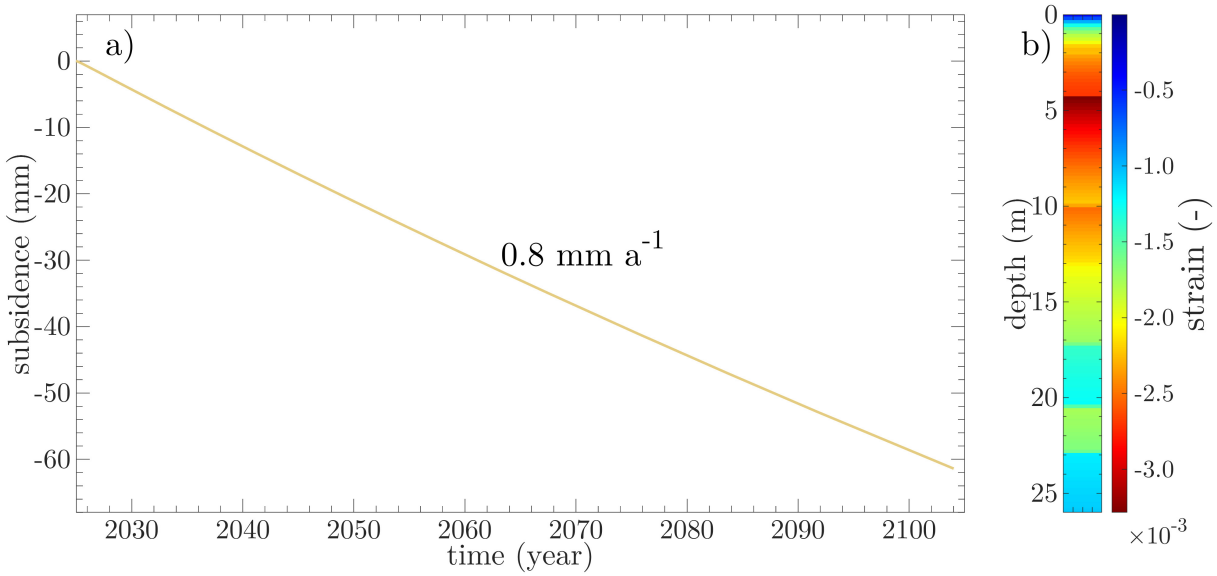


Figure 23: Simulated future subsidence due to self-weight induced autocompaction of Holocene strata at GW1 (a) and a depth-profile of respective strains (b).

Although Zoccarato et al. (2018) did not provide a geographically attributable representation of their simulated autocompaction-induced subsidence, the calculated rate of 0.8 mm a^{-1} (Figure 23a) aligns very well with their reported simulation results for the upper delta plain, which likewise amount to 0.8 mm a^{-1}.

Implications: These simulations enable a robust estimation of the contribution of autocompaction to the overall subsidence. By demonstrating that autocompaction is only a minor driver of land subsidence at GW1, the assessment strengthens the attribution of groundwater depletion as the dominant mechanism for subsidence in the Mekong Delta and underscores the need to prevent further groundwater decline. This finding, derived from a local yet largely representative analysis, is of pronounced relevance for decision makers, as it enables a clear differentiation between mitigatable subsidence induced by groundwater depletion and autocompaction, which represents a natural and largely unavoidable background process.

3.5 Inferring process dynamics from land subsidence observations

This section presents, contextualizes, and discusses observations of land subsidence and governing subsurface compaction, including data from the land subsidence observatory at GW1 (sections 3.5.1–3.5.2) and satellite-based InSAR data for the monitoring site IGPVN (section 3.5.3). For the land subsidence observatory, this comprises the evaluation of preliminary data reported in a peer-reviewed German-language research article (Dörr et al., 2023), as well as a critical assessment of subsequently acquired data, from which additional insights are derived and associated uncertainties are discussed.

3.5.1 Vietnams Mekong-Delta - Landsenkung infolge von Grundwasserübernutzung (Dörr et al., 2023)



FORSCHUNG | WASSERWIRTSCHAFT

Vietnams Mekong-Delta - Landsenkung infolge von Grundwasserübernutzung

Das Mekong-Delta ist Lebensraum für ca. 21,5 Mio. Menschen und sieht sich seit einigen Jahren mit zunehmend existenzbedrohenden Landsenkungsprozessen (bis zu 3 cm/a) konfrontiert. Als einer der Hauptgründe dafür gilt die starke Grundwasserentnahme. Um die Prozessdynamik besser untersuchen zu können, wurde ein im Mekong-Delta bislang einmaliges Messsystem zur tiefendifferenzierten Landsenkungsmessung an einem Pilot-Standort aufgebaut, dessen vorläufige Messdaten eine Korrelation zwischen Landsenkung und dem fallenden Grundwasserspiegel zeigen.

Felix Dörr, Jonas Bauer, Hoan Viet Tran, Stefan Norra und Franz Nestmann

1 Bisheriger Kenntnisstand zur Landsenkung infolge von Grundwasserübernutzung im Mekong-Delta

1.1 Hydrogeologischer Kontext

Das Grundwassersystem (GW-System) des Mekong-Deltas (MD) ist in seiner Gesamtheit noch nicht vollständig verstanden, da vergleichsweise wenig Daten zur Ausdehnung und komplexen Abfolge von GW-Leitern und -Stauern sowie zu deren Interaktion vorliegen. Grundsätzlich wird im MD zwischen sieben GW-Leitern mit jeweils gespannten GW-Verhältnissen differenziert, deren hydraulische Trennung durch GW-Stauer, wie von Hoan et al. [1] dargelegt, meist als durchgehend gewährleistet angenommen wird. Die im südlichen MD häufig >20 m mächtige Tonschicht, die den oberen GW-Leiter überdeckt, verhindert, wie von Bauer et al. [2] erörtert, eine nennenswerte GW-Neubildung. Die Wechselfolge zwischen GW-Leitern und -Stauern endet in 300-400 m Tiefe, doch selbst die tieferen GW-Leiter weisen GW-Druckspiegel von nur 10-20 m unterhalb der Geländeoberkante (GOK) auf. GW-Stand, -Dynamik und -Trends der verschiedenen GW-Leiter sind trotz der hydraulischen Trennung oft nahezu identisch, was auf sogenannte Loading Effects in den gespannten GW-Leitern hinweist.

1.2 Landsenkung im Mekong-Delta

In den vergangenen Jahren wurden im MD u. a. von Erban et al. [3] Landsenkungsraten von bis zu 3 cm/a beobachtet. Da sich die GOK des gesamten MD, wie Minderhoud et al. [4] zeigte, im Mittel nur ca. 0,8 m oberhalb des Meeresspiegels befindet, stellt die Landsenkung in Kombination mit dem stetigen Meeresspiegelanstieg ein akutes existenzbedrohendes Problem für die Bewohner dieser Region dar. Die meisten bislang veröffentlichten Datensätze zu Landsenkung im MD basieren auf der Auswertung von Satellitendaten. Die wenigen bestehenden festinstallierten Monitoring-Systeme, wie von Karlsrud et al. [5] vorgestellt, erlauben keine tiefendifferenzierte Messung der Landsenkung.

1.3 Potenzielle Einflussfaktoren auf die Landsenkung

Landsenkung infolge von sinkenden Grundwasserständen ist ein weltweit bekanntes Phänomen, das bereits seit knapp 100 Jahren untersucht wird [6]. Die extensive GW-Übernutzung von >2,5 Mio. m³/d führt im MD zu einer Senkung der GW-Druckspiegel in den gespannten GW-Leitern, so dass der damit einhergehende sinkende hydrostatische Druck im Untergrund zu einer Erhöhung der effektiven Spannung in den Sedimentschichten führt. Insbesondere in den GW-Stauern kann dies zu einer Kompaktion der tonhaltigen Sedimente führen, woraus letztendlich eine Senkung der Landoberfläche resultiert.

Wie stark die Kompaktion einer Sedimentschicht infolge einer Erhöhung der effektiven Spannung ist, kann durch ihren Kompressionsbeiwert C_c beschrieben werden. Bindige Sedimente, wie beispielsweise Ton, weisen deutlich höhere Kompressionsbeiwerte auf als nicht-bindige Sedimente wie Sand.

Modellbasierten Untersuchungen von Minderhoud et al. [7] zufolge ist das MD aufgrund der GW-Entnahme innerhalb von 25 Jahren um durchschnittlich 18 cm abgesunken. Wie groß der Anteil der aus der GW-Entnahme resultierenden Landsenkung an der gesamten Landsenkung tatsächlich ist, konnte bislang jedoch noch nicht anhand von Messdaten belegt werden.

Ein weiterer möglicher Einflussfaktor auf die Landsenkung im MD könnte das Ausbleiben von großflächigen Überflutungen infolge von Dammbauten sein, da dies die Deposition von neuen Sedimenten verhindert und so möglicherweise natürliche Kompaktionen der jüngsten Sedimentlagen nicht mehr durch neue Ablagerungen kompensiert werden können [8]. Im Weiteren gelten, wie Galloway et al. [9] erörtert, der Abbau von organischen Bestandteilen im Untergrund sowie das Austrocknen

Kompakt

- Erstmalig tiefendifferenzierte Landsenkungsmessung im Mekong-Delta.
- Vorläufige Messdaten zeigen mittlere Landsenkungsraten von 9,5 mm/a in 0 m bis 164 m Tiefe.
- Vorläufige Messdaten zeigen Korrelation zwischen Landsenkung und fallendem Grundwasserspiegel.

52 WasserWirtschaft 11 | 2023 www.springerprofessional.de/wawi

Paper 4: Published in Wasserwirtschaft, 2023, 11.

Authors: Felix Dörr, Jonas Bauer, Tran Viet Hoan, Stefan Norra, Franz Nestmann.

Journal: Wasserwirtschaft, 2023-11.

Availability: Appendix A.4 and *online* http://doi.org/10.1007/s35147-023-1922-3

Authorship statement: This article, published in a peer-reviewed scientific journal, presents the monitoring setup as well as preliminary results of the land subsidence observatory at GW1 in the southern Mekong Delta. The findings constitute correlations between groundwater depletion and land subsidence dynamics and discuss that apparent rising trends in individual sensor time series do not indicate land uplift motion but more likely are induced by downward movement of the respective magnet rings mounted on the sliding-joint casing. During evaluation and data interpretation, insightful discussions with Jonas Bauer were of great value for the

overall research concept. Similarly, discussions with Tran Viet Hoan, who supported the author in the field implementation of the land subsidence observatory, were of particular value regarding installation-related considerations. This study was supervised by Stefan Norra and Franz Nestmann, who guided the research concept, project administration, and funding acquisition. All co-authors reviewed the scientific content and contributed to the editorial improvement of the manuscript.

Relevance for research objectives:

By presenting and discussing the first depth-differentiated compaction monitoring data for the Mekong Delta, this study offers insights at unprecedented vertical and temporal resolution. The evaluation of these data suggests a correlation between subsidence and depleting groundwater heads and indicates that a significant share of the compaction ultimately triggering land subsidence occurs in the upper part of the Holocene strata. These findings provide new process-based insights into the vertical distribution of compaction and its linkage to groundwater dynamics, thereby directly contributing to research focus 1 by advancing the understanding of groundwater depletion as a trigger of land subsidence in the Mekong Delta. Overall, the study provides high-resolution, process-based evidence of subsurface compaction dynamics, thereby strengthening the process-based understanding of different subsidence drivers and their underlying processes in relation to groundwater depletion.

Abstract:

Das Mekong-Delta ist Lebensraum für ca. 21,5 Mio. Menschen und sieht sich seit einigen Jahren mit zunehmend existenzbedrohenden Landsenkungsprozessen (bis zu 3 cm/a) konfrontiert. Als einer der Hauptgründe dafür gilt die starke Grundwasserentnahme. Um die Prozessdynamik besser untersuchen zu können, wurde ein im Mekong-Delta bislang einmaliges Messsystem zur tiefendifferenzierten Landsenkungsmessung an einem Pilot-Standort aufgebaut, dessen vorläufige Messdaten eine Korrelation zwischen Landsenkung und dem fallenden Grundwasserspiegel zeigen.

© The full article is reprinted with kind permission from Springer Nature and is included in Appendix A.4.

3.5.2 Depth-differentiated compaction monitoring: Insights and uncertainties associated with sliding-joint multi-extensometer observations

Context: The land subsidence observatory, a sliding-joint multi-extensometer borehole installed at the monitoring site GW1, provides a unique dataset of depth-differentiated compaction measurements. Building on the preliminary monitoring results reported by Dörr et al. (2023) and summarized in section 3.5.1, this section presents subsequently acquired observations and briefly discusses the associated insights and uncertainties. These considerations have not yet been included in the author's peer-reviewed publications. The acquired dataset includes monitoring data recorded under natural, undisturbed conditions as well as observations obtained during a pumping test, in which groundwater heads were deliberately lowered and the resulting sediment compaction was recorded.

Setup and measurement principle: The land subsidence observatory is a magnet ring-based borehole-extensometer system, installed in a 164 m deep borehole at GW1, comprising a sensor-chain with eight digital extensometers. The sensor chain is freely suspended within a casing that is subdivided into independently movable sections by sliding joints. Magnetic rings are attached to the casing at discrete depth levels. The annulus between the casing and the borehole wall was backfilled with a cement–bentonite grout in accordance with DIN EN ISO 18674. The monitoring setup does not comprise an explicit anchoring of the magnet rings with the surrounding sediment formation.

When compaction occurs within a specific sediment horizon, the entire sensor chain, connected to ground level via the well head, subsides by the magnitude of compaction at that horizon. The casing sections located above the next deeper sliding-joint subside accordingly, resulting in compression of the underlying sliding-joint. In contrast, the casing sections below, including the magnetic rings attached to them, remain stationary. This configuration produces a relative displacement between the magnetic rings and the extensometers along the sensor chain.

Above the compressed sliding-joint, magnetic rings and extensometers move synchronously, such that no relative displacement is recorded. This measurement principle enables a depth-differentiated quantification of compaction between the depth levels of adjacent sliding-joint segments. Compaction occurring between the lowest sliding-joint and the final casing depth results in compression of the lowest segment, whereas compaction below the final casing depth cannot be detected by the system.

The measurement concept is schematically illustrated in Figure 24. In this example, compaction of layer 3 induces relative displacement between extensometer 2 and magnetic ring 2, as well as between extensometer 3 and magnetic ring 3. In contrast, extensometer 1 and magnetic ring 1 move in parallel, and no relative displacement is recorded at that level.

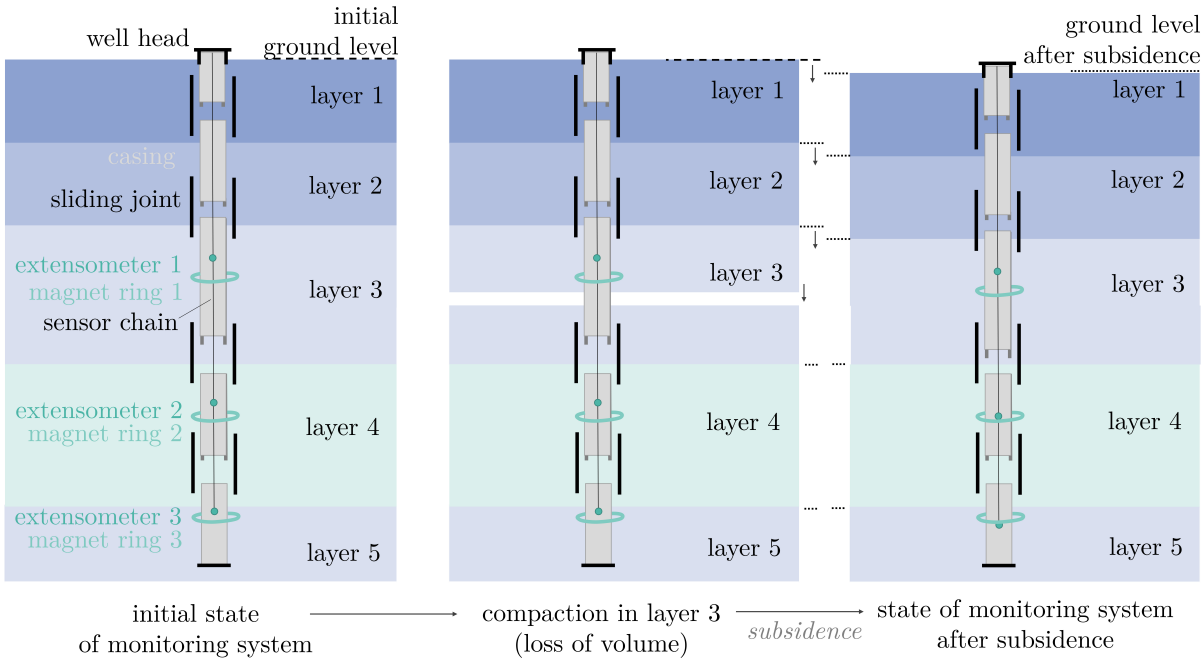


Figure 24: Example of the measuring principle of the land subsidence observatory, modified after Dörr et al. (2023).

Findings: The recorded signals of the extensometer sensors are characterized by a distinct seasonality, suggesting apparent compaction during dry season when groundwater heads decline as well as stagnating or partly even rising trends during the rainy season (Figure 25). Considering the conceptual measurement framework, in which the sensors measure accumulated compaction of the overlying sediment strata, a critical evaluation suggests that the measurement signals are in parts superposed by other

processes in addition to sediment compaction, which can ultimately bias those measured time series. These biases and the underlying process dynamics are discussed below for two selected periods of the monitored data.

The first assessed monitoring period is in the rainy season between April and November 2023, where the three uppermost digital extensometer sensors exhibit upward trends in the monitoring data, distinctly following the dynamics of observed groundwater heads (Figure 25a). In light of the finding that rising groundwater head signals during this period are attributable to surface loading induced by monsoon precipitation and associated increases in surface water levels (Dörr et al., 2026a), the upward trends observed in these three extensometer time series can likewise be attributed to surface loading: the stresses and strains imposed by surface loading affect the entire subsurface, including the grout between the casing and the surrounding sediments. The compression of the grout is transferred to the casing, which is compressed at the sliding-joints and thereby inducing a downward displacement of the magnet rings attached to the casing. As the extensometer sensors record the vertical distance to the nearest magnet ring, a downward movement of the magnet ring produces a sensor response that is indistinguishable from an upward movement of the sensor itself. However, as outlined by Dörr et al. (2023), a true uplift of the land surface would necessarily entail an uplift of the entire measurement chain, which would be reflected consistently across all eight extensometer records. Since this dynamic is observed only in the three uppermost extensometers, it is therefore inferred that the relative movement recorded by these sensors results from a locally constrained downward displacement of the respective magnet rings rather than an upward movement of the measurement chain. Consequently, these measurements do not represent genuine land uplift processes but are most likely caused by movement artefacts within the measurement system itself.

This interpretation is supported by the fact that the backfilling grout used in the upper 40 m was prepared with a different cement–bentonite ratio than the grout filling in the deeper section of the borehole. These ratios were specified during the system design according to normative regulations (DIN EN ISO 18674-1, 2015) to better account for

the different compressibility of the subsurface strata, characterized by higher compressibility in the Holocene and late Pleistocene sediments (0 - 40 m) and lower compressibility in deeper sedimentary units.

The interpretation of the extensometer data presented above suggests that the grout in the upper borehole section is softer and more compressible than the surrounding strata, allowing the grout and the embedded magnet rings to deform and move independently of the sediment formation. Variations in grout and sediment stiffness have previously been recognized as a potential source of error in extensometer measurements (Bayoumi, 2011; Gholinia et al., 2022), particularly in the absence of adequate anchoring between the instrument and the borehole wall. In this derived conceptual framework, actual deformations of the sediment strata are considered to be transferred correctly to the grout and the magnet rings, as they act laterally on the entire grout-sediment interface. In contrast, external forcing such as surface loading may instead induce differential responses in grout and sediment deformation. It is noted that such response to surface loading in the upper sensors seem to halt during rainy season 2024 (Figure 27b), possibly indicating that the respective sliding-joints reach their maximum compression and are closed.

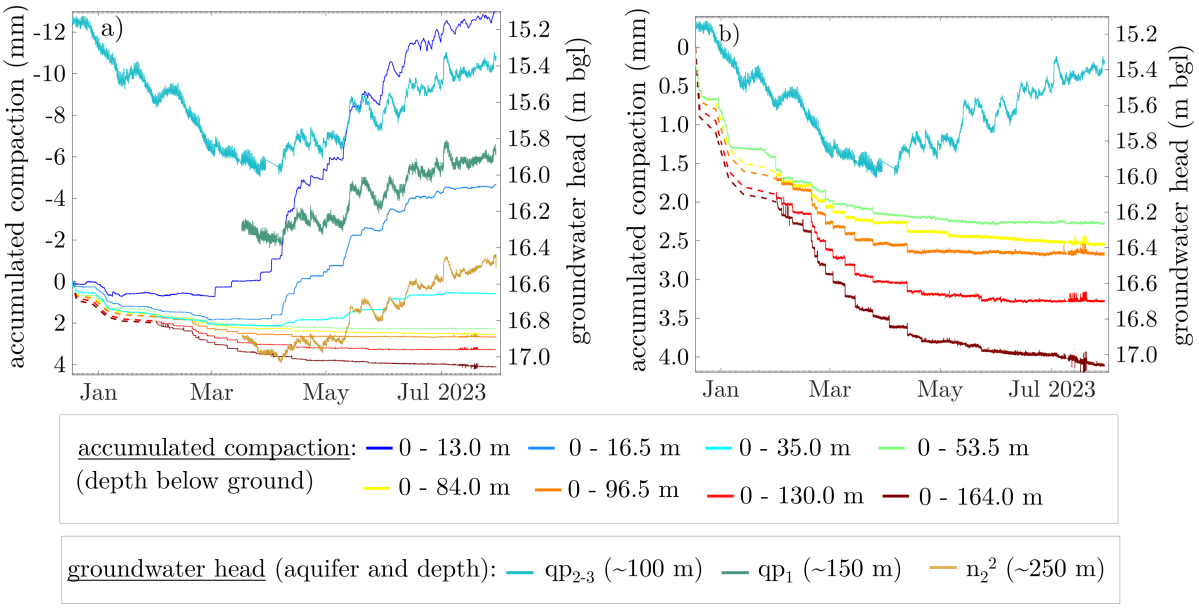


Figure 25: Depth-differentiated compaction monitoring at GW1 between December 2022 and November 2023 alongside observed groundwater heads displaying data of all sensors (a) and data excluding the three uppermost loading-biased sensors (b).

Similar dynamics can be inferred from the monitored extensometer data during the second assessed period, covering the time of the conducted pumping test (Figure 26). The pumping in qp_1 aquifer (~150 m depth) induces compaction between 130 m and 164 m, reflected by an increasing distance between the lowest and the overlying sensor time series (period ①). Conceptually, this observed sediment compaction is consistent with the induced groundwater head depletion. However, during the recovery phase, the monitoring data shows an apparent downward displacement in the several overlying sensors (period ③), with diminishing magnitude from the depth of the pumped aquifer towards shallower layers. Equally, such dynamics are observed during temporary power blackouts when associated pump inactivity induced intermediately rising heads (events ②). Those sensor responses are conceptually inconsistent, given that the recovering groundwater heads would induce elastic rebound and associated uplift motions rather than progressive compaction, and as elaborated above, genuine uplift would need to be reflected in all sensor time series.

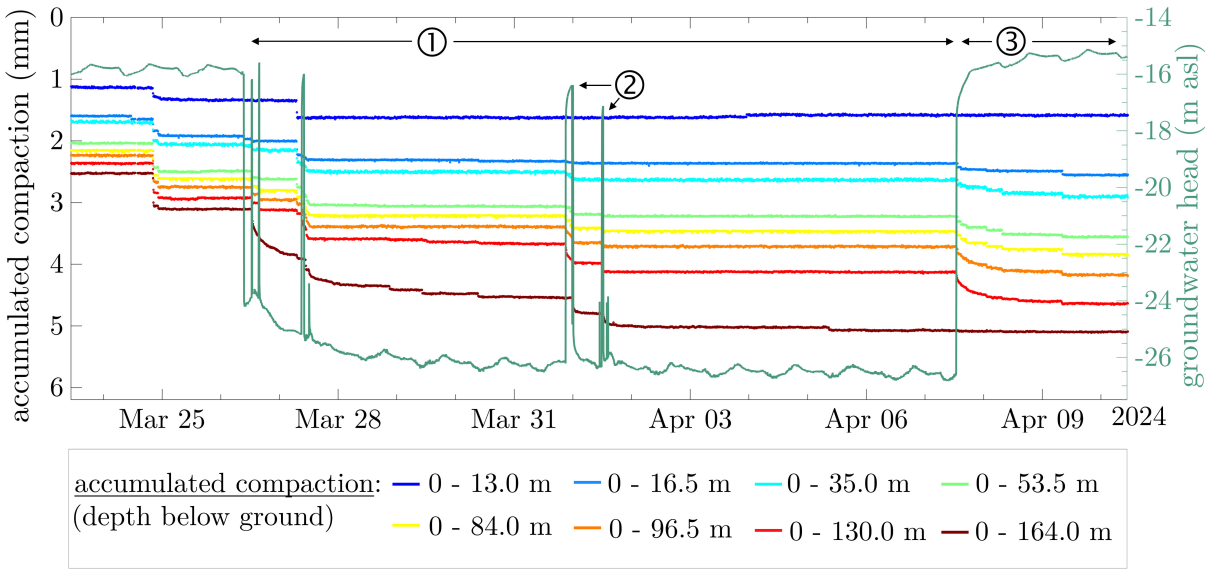


Figure 26: Compaction time series of the land subsidence observatory during a pumping test at GW1b alongside drawdown and recovery.

From a hydrogeomechanical perspective, this implies that recovering groundwater heads cause an elastic rebound of the grout, whereas rebound of the surrounding formation remains negligible. The resulting grout expansion pushes the magnet rings upward, producing the apparent downward trends in the extensometer time series.

Accordingly, similar to the loading-induced downward shift that governs upward trends in near-surface sensors, the downward trend observed during groundwater head recovery (period ③ and ②) is interpreted as a consequence of independent grout deformation rather than sediment deformation. Overall, this interpretation indicates that the land subsidence observatory can reliably capture true sediment compaction, although the measurements may remain susceptible to biases introduced by other processes causing independent grout deformation.

This interpretation is further supported by a comparison between the multi-extensometer records and data from ground-based levelling campaigns, providing additional insights into the validity of the observed signals. Overall, a good agreement is observed between measurements from the land subsidence observatory and independent levelling data during the three pumping test periods (Figure 27a), when groundwater head depletion conceptually governs subsurface deformation. In contrast, a conceptual bias again becomes apparent on a seasonal scale (Figure 27b), with largely stagnant trends in the land subsidence observatory data, whereas the levelling observations indicate more pronounced dynamics.

It is noted that the levelling data acquired at GW1 comprises observations from a total of 13 monitoring points, of which 11 exhibit nearly identical dynamics. In contrast, the two monitoring points which are directly attached to the land subsidence observatory, located at the well head and pedestal of the land subsidence observatory, show distinctly stronger subsidence under conditions of groundwater head depletion. As elaborated in Dörr et al. (2026b), this may indicate that the monitoring facility itself influences the compaction dynamics it is intended to capture, by providing subsurface drainage pathways at casing–joint interfaces. It should be noted that both datasets are inherently relative: the land subsidence observatory is referenced to a depth of 164 m, whereas the levelling data are referenced to the bridge foundation at an estimated depth of 80 m, which further complicates a direct validation.

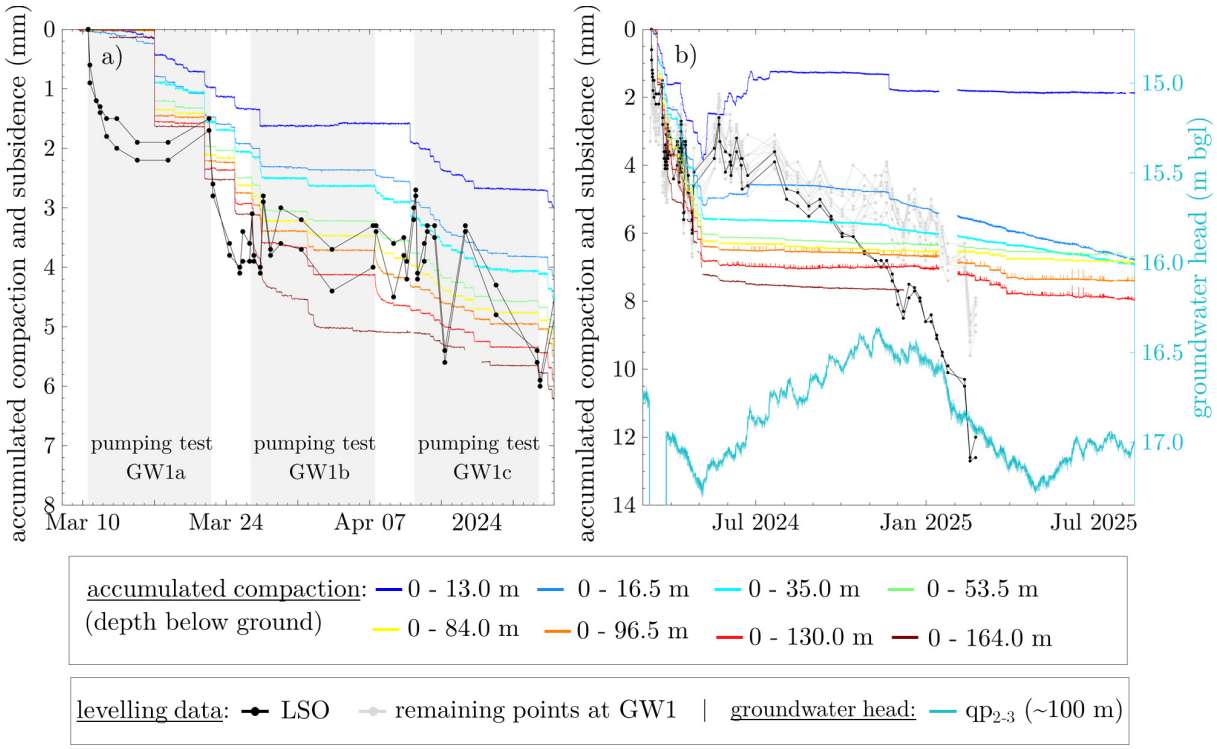


Figure 27: Comparison of compaction monitoring at the land subsidence observatory with geodetic levelling measurements during pumping tests (a) and on an annual basis (b).

Implications and discussion: In general, the elaborated evaluations support the interpretation that the land subsidence observatory records subsidence with validated accuracy during periods when groundwater depletion can be inferred as the dominant driver of land-motion dynamics. In contrast, at the seasonal scale, when surface loading and unloading impose additional stresses and strains on the sedimentary formation and grout, the land subsidence observatory appears incapable of capturing the resulting dynamics accurately.

Further investigations are needed to better assess and validate the reliability of the monitoring data obtained from the land subsidence observatory. Further manual ring measurements can provide more insights into the hypothesized independent movement of magnet rings and further validation with geodetic observations, both ground-based or with remote-sensing approaches and further depth-differentiated observations i.e. by fiber optic sensing. Future implementations of similar systems should ensure adequate anchoring of the magnet rings with the surrounding sediment.

3.5.3 Inferring process dynamics from observed groundwater heads and InSAR subsidence rates

Context: In the Mekong Delta, InSAR analyses have primarily been used to map observed subsidence patterns, while no physics-informed assessments linking InSAR-subsidence dynamics to underlying environmental processes have been proposed. A recent study on drought-induced land subsidence in the Mekong Delta revealed seasonal patterns in the subsidence signals. However, the authors acknowledge that their remote-sensing-based approach cannot identify the governing mechanisms (N. Dörr et al., 2025) beyond showing temporal correlations with the 2020 drought. To propose a first physics-informed interpretation of InSAR subsidence time series, a detailed assessment of groundwater head and InSAR scatterer dynamics was carried out at the local scale in up to 2.5 km distance to the monitoring site IGPVN. This analysis has not yet been included in the author's peer-reviewed publications.

New findings: The analysis of InSAR data in the vicinity of the monitoring site IGPVN reveals a pronounced spatial variability in subsidence rates (Figure 28a), consistent with the assessment of InSAR-derived subsidence near GW1 (Dörr et al., 2026b). Smoothing the mean of all individual time series using a 60-day centered moving-mean window highlights clear seasonal patterns (Figure 28b), in line with the dynamics reported by N. Dörr et al. (2025).

A comparison with groundwater head dynamics in the three aquifers $qp_{2\text{-}3}$, qp_1, and n_2^2 shows a distinct correlation between subsidence rates and groundwater variations (Figure 28c). In 2020, this correlation is particularly pronounced, as illustrated in Figure 28d. Here, subsidence dynamics show a positive correlation with groundwater depletion during the dry season until June 2020 (period ①). With the onset of the rainy season, groundwater heads rise and the InSAR time series show a clear rebound (period ②). These parallel dynamics, however, diminish in period ③ where the time series instead exhibit an inverse, mirrored, relationship.

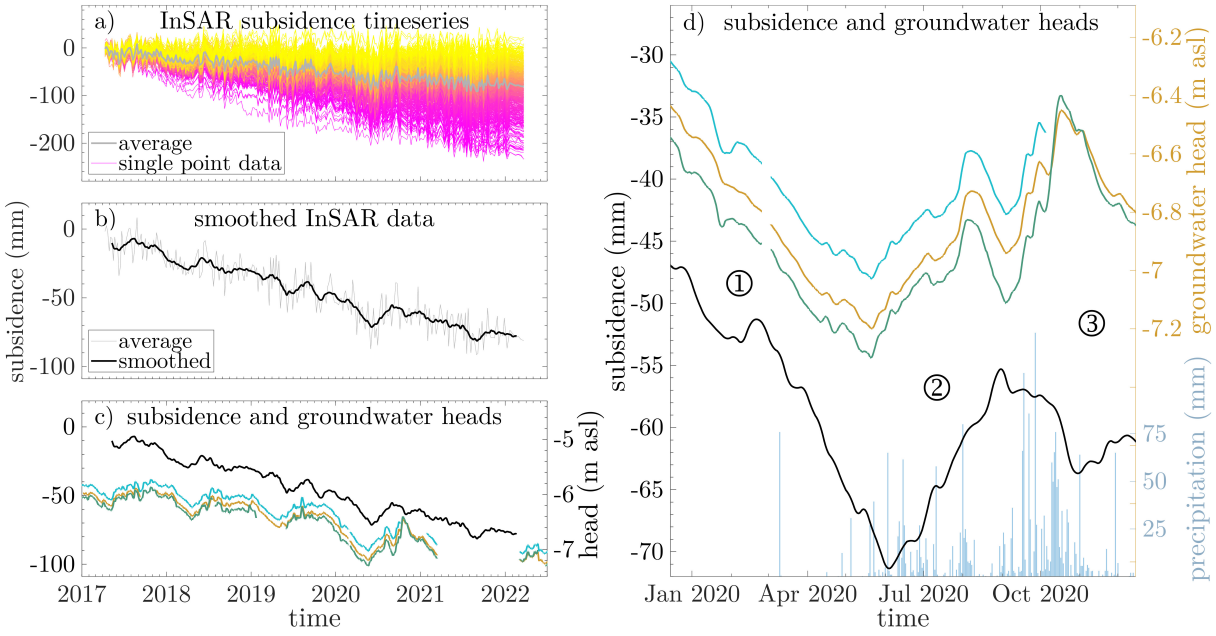


Figure 28: Correlation of InSAR and groundwater time series at the site IGPVN between 2017 and 2022 including individual InSAR time series (a) mean smoothed InSAR time series (b) together with groundwater head time series (c) as well as daily precipitation (d). Groundwater head time series are smoothed with a 5-day moving-mean window to suppress sub-daily and tidal fluctuations for clearer visualization.

Given that the seasonally rising groundwater heads can be attributed to surface loading from accumulating surface-water resources (Dörr et al., 2026a), the inverse dynamics in period ③ can be linked to this surface-water loading, which simultaneously increases hydraulic heads and induces compaction, and thus subsidence. Consequently, the correlation of groundwater heads and subsidence dynamics in period ① is not solely triggered by groundwater depletion but in parts as well by seasonal unloading following declining surface water levels during the dry season, particularly during the 2020 drought. At the onset of the rainy season (period ②), the process of surface loading is superposed by another mechanism which ultimately causes the rebound. In light of the temporal correlation with the rainy season onset, the conceptual framework of loading-induced rising groundwater heads and the resulting dismissal of related groundwater recharge, rewetting of the topsoil appears to be the most plausible cause of this rebound effect. Rewetting reduces matric suction and thereby previously increased effective stresses in unsaturated sediments, consequently promoting elastic rebound (Lu et al., 2010). While mineralogical analyses indicate muscovite–illite-dominated clay minerals at IGPVN with only minor intrinsic swelling potential, a notable organic carbon

content was identified in the topmost aquitard (Pechstein et al., 2018). This organic fraction may contribute to rebound dynamics through hydration of organic matter and aggregate-scale hydro-structural responses (Seidel et al., 2023). At GW1, similar mineralogical compositions and organic contents were found.

This overall interpretation is supported by the observation that the rainy-season rebound is most pronounced following the 2020 drought, the most severe drought during the assessment period, which was also associated with the strongest dry-season subsidence (Figure 28b).

Implications: This physics-informed analysis of InSAR data suggests that the seasonal character of land subsidence dynamics arises from several superposing processes, including (i) the seasonal loading and unloading of surface water bodies and the related sediment compaction, and (ii) rewetting and hydration of organic matter in the topsoil. In addition, (iii) increased groundwater demand and the associated intensified depletion during dry seasons - particularly in severe drought periods - may introduce an additional seasonal component of subsidence. However, in light of recent findings, this contribution is considered less relevant than previously assumed, as the loading-corrected groundwater head dynamics exhibit only minor seasonal variations (Dörr et al., 2026a). Beyond the local analysis in the vicinity of the monitoring site IGPVN, the proposed concept of physics-informed interpretation of InSAR-based subsidence dynamics can be applied to other groundwater monitoring locations where hydraulic head data are available for broader validation.

4 Synoptic discussion

Building on the results presented in section 3, this section synthesizes the key findings within the overarching conceptual framework of land subsidence dynamics in deltaic systems, with particular emphasis on implications for mitigation strategies and on the relevance of these dynamics in the context of multiple, cascading hazards. The discussion highlights the relevance of the findings specifically for the Mekong Delta as well as on a conceptual level for investigations on deltaic groundwater- and subsidence related process dynamics.

4.1 Groundwater head responses to external forcings and their implications for managing deltaic water resources and subsidence

Unlike in most conventional groundwater flow problems, land subsidence induced by groundwater depletion inherently requires a consideration of the coupled nature of groundwater hydraulics and geomechanical processes, as this coupling constitutes the fundamental mechanism driving subsurface deformation (Galloway et al., 2016). While land subsidence has been extensively investigated as a process controlled by groundwater hydraulics in the Mekong Delta (Kondolf et al., 2022; Minderhoud et al., 2020, 2017), the counterpart of this hydrogeomechanical coupling, namely the groundwater head response to mechanical loading and subsurface strains, has remained uncovered. The studies associated with this dissertation (Dörr et al., 2025, 2026a) identify this counterpart and utilize the imprints of these processes to enhance assessments of deltaic water management and land subsidence mitigation strategies, in the Mekong Delta and beyond. Given that disentangling superimposed process dynamics constitutes a fundamental precondition for identifying appropriate mitigation and adaptation strategies in stressed river deltas (Eslami et al., 2025), unraveling the influence of loading signals on groundwater head dynamics advances current system understanding on a fundamental level. Considering the inherently fragile balance between water and sediment fluxes in river deltas (Syvitski et al., 2009), this

advancement in conceptual system understanding constitutes an essential step toward more sustainable delta management.

4.1.1 The overlooked counterpart of hydrogeomechanical coupling in the Mekong Delta: missed opportunities and misinterpretations

It is remarkable that despite the pronounced research attention on land subsidence due to groundwater depletion in the Mekong Delta, the counterpart imprints of this hydrogeomechanical coupling have remained unrecognized and unexplored for so long in evaluations of groundwater head time series. As a result, opportunities to make use of these imprints have been missed in the past, such as utilizing loading effects for aquifer parameterization and assessments of their subsidence mitigation potential, as discussed in section 4.1.3 specifically.

By overlooking this conceptual framework in the Mekong Delta, not only opportunities for its application were missed in the past, but also systematic misinterpretations have emerged: misinterpretations arose particularly in the context of seasonally rising groundwater heads, which previously have been interpreted as indicators for (i) groundwater recharge by precipitation (Van et al., 2023), (ii) recharge by groundwater-surface water interactions (Duy et al., 2021), or (iii) as signals of seasonally varying groundwater extraction rates (Karlsrud et al., 2017; Pechstein et al., 2018). By identifying rising groundwater heads as loading imprints of seasonally accumulating surface water resources (Dörr et al., 2026a), this dissertation contributes to clarify and improve the process understanding governing groundwater head dynamics in the Mekong Delta.

Figure 29 presents a schematic illustration of the two complementary phenomena of hydrogeomechanical coupling in the Mekong Delta: the well-investigated hydraulic control on subsidence and the newly identified groundwater head response to external loading.

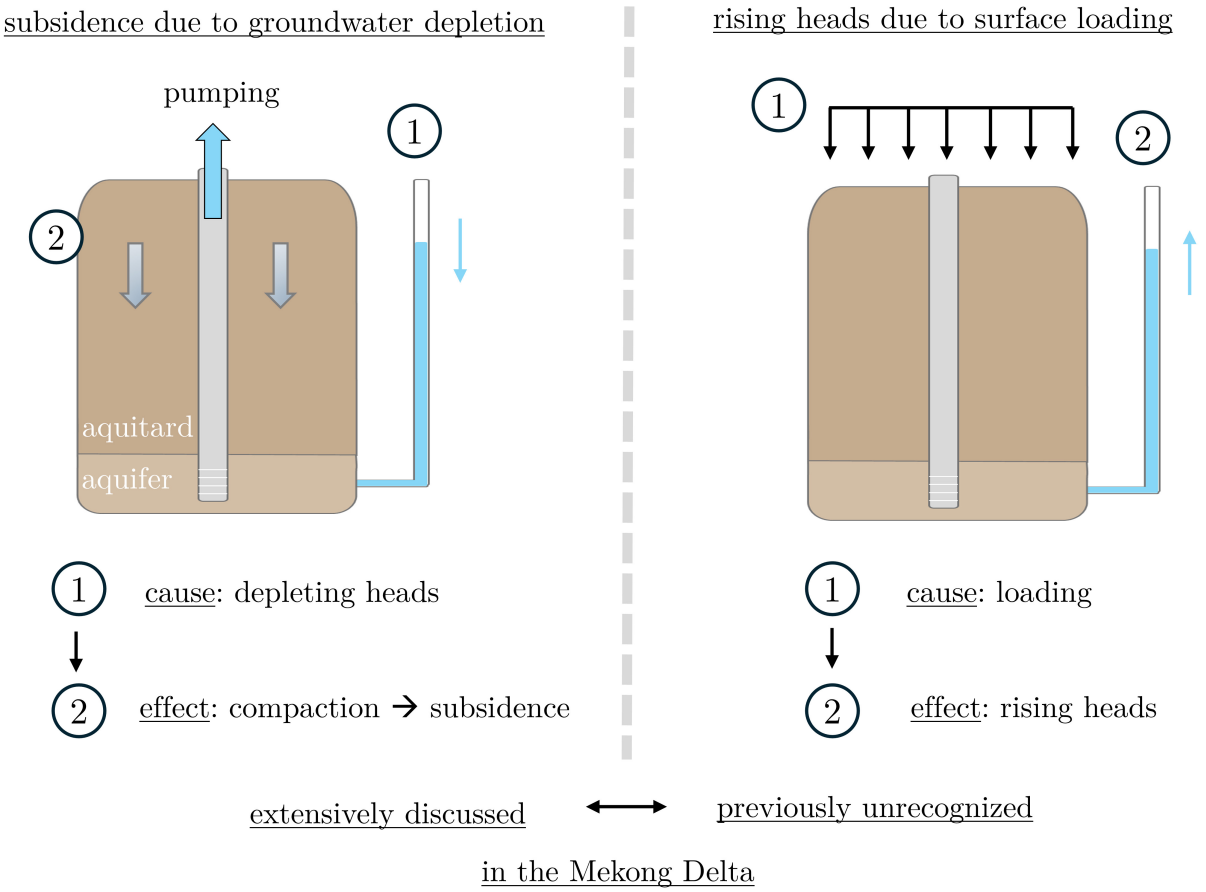


Figure 29: Schematic illustration of the two complementary phenomena of hydrogeomechanical coupling.

Overall, the identification of this previously overlooked counterpart complements the general process understanding of interlinked surface- and subsurface processes in the Mekong Delta and advances a more complete conceptualization of the processes at play. Given that surface water resources are a key characteristic of any river delta, understanding the interaction of surface- and groundwater resources is essential in deltaic groundwater research (Renaud and Kuenzer, 2012; Xu et al., 2021). Therefore, demonstrating that synchronous ground- and surface water dynamics do not necessarily reflect recharge processes challenges oversimplified, yet widespread, interpretations of deltaic groundwater hydrographs and promotes a more robust, process-based assessment of groundwater–surface water interactions.

Moreover, the utilization of frequency-domain methods for loading analyses (Dörr et al., 2025, 2026a) fostered their subsequent application in other research fields in the context of individual and interacting components of cascading hazards in the Mekong

Delta, such as surface-water salinization and seawater intrusion (Bauer et al., 2025; 2026 - under review). This shows how the methods and frameworks developed in this dissertation support the transferability of data-analysis concepts, thereby addressing data scarcity as a key challenge across environmental processes in the Mekong Delta by gaining new insights from available data sets.

4.1.2 Recognizing the blind spot: A call for considering loading effects in deltaic groundwater studies

Despite being ubiquitous in confined aquifers (McMillan et al., 2019) and being exemplary described for barometric effects in most common groundwater textbooks (Van Der Kamp and Schmidt, 2017), loading signals have not only been overlooked in the Mekong Delta but are systematically underrepresented in groundwater studies (Maliva et al., 2011; Pacheco and Fallico, 2015). This results in presumably many cases around the world, where unrecognized loading effects caused misinterpretations of groundwater head data (Van Der Kamp and Schmidt, 2017). The importance of accounting for such effects and the limitations of traditional analyses that ignore them, were pointed out by the few existing studies in hydrogeological settings similar to the Mekong Delta, like the Bengal Basin (Burgess et al., 2017). Their findings highlight that estimates of groundwater recharge and storage changes derived solely from conventional hydraulic analyses of groundwater hydrographs, as well as the calibration of transient groundwater flow models based on such data, may require critical revision as they miss a conceptual component in the governing processes.

By promoting the consideration of loading effects in research on groundwater hydraulics (Dörr et al., 2025, 2026a), this dissertation contributes to overcoming this systematic "*blind spot*", which is of particular importance in deltaic environments, where surface loading associated with seasonal inundation and tidal river water loading are inherent features of deltaic aquifer systems. While in many other hydrogeological settings loading effects stretch over minor temporal and magnitude scales and therefore merely result in a misinterpretation of these signals as noise in observation data (Rasmussen

and Crawford, 1997), the consequences of such misinterpretations are far more severe in deltaic environments, where inundation and river-water loading generate signals of much greater magnitude.

In addition to these natural deltaic loading mechanisms, which have persisted over geological timescales, the rapid expansion of aquaculture ponds has introduced a new, anthropogenically controlled surface-water load, as uncovered in this dissertation (Dörr et al., 2026a). This form of land-use change is widespread across deltaic and coastal regions of Southeast Asia (Luo et al., 2022), highlighting the transferability and broader relevance of the loading-induced *recharge illusion* framework to comparable settings.

4.1.3 Implications of the loading framework and passive methods for subsidence mitigation strategies

A central outcome of this work is the demonstration that passive subsurface characterization methods can be utilized for a process-based assessment of an aquifer's land subsidence mitigation potential (Dörr et al., 2025). Estimating the specific Storage S_s with passive methods directly informs two fundamental components of subsidence mitigation strategies: the potential for elastic aquifer rebound and the storage capacity for seasonal water storage. Applying passive subsurface parametrization methods for the first time in the Mekong Delta (Dörr et al., 2025) reveals a limited subsidence mitigation potential of the assessed Pliocene and Pleistocene aquifers. Therefore, together with the identification of the loading-induced *recharge illusion* (Dörr et al., 2026a), the applied utilization of loading related passive methods implies a limited subsidence mitigation potential of these aquifers in terms of natural or artificial recovery of groundwater heads and elastic aquifer rebound.

In general, passive methods have only been employed rarely in earlier land subsidence-related studies, for example by Sun et al. (1999), who derived the elastic aquifer compressibility from the barometric efficiency. Owing to the inherently elastic character of tidal forcing (Bredehoeft, 1967), passive methods based on such forcings are fundamentally limited to the characterization of elastic subsurface responses. As a

result, inelastic deformation parameters remain inaccessible within the framework of passive subsurface characterization. Accordingly, the role of these methods in subsidence investigations is largely confined to mitigation-related processes (recharge, rebound, and elastic storage), whereas inelastic deformation characteristics - often governing sediment compaction in clay-dominated aquitard settings - cannot be parameterized.

The bounds of these conceptual limitations to elastic process dynamics are pushed by the introduced advancement of tidal subsurface analysis towards inelastic domains (section 3.2.2), as discussed in the following section.

4.1.4 Advancing passive methods for deltaic subsurface parametrization and towards assessments of inelastic subsidence dynamics

In light of the urgency and the limited resources available for targeted subsurface investigations in the Mekong Delta, passive methods are particularly promising approaches, as these approaches utilize existing datasets and no active, often cost-intensive, field investigations are required (Turnadge et al., 2019). However, previous passive approaches were infeasible for application in deltaic environments, where multiple superposing tidal forcings govern tidal constituents in groundwater heads, as those methods did not account for river and ocean tide loading (Acworth et al., 2016; Rau et al., 2020). By the novel integration of ocean- and river tides, the presented dissertation overcomes these limitations and advances the application of this powerful, yet underutilized technique for deltaic aquifer systems.

Considering the substantial share of the global population living in deltaic regions and their increasing dependence on groundwater for freshwater supply (Van Engelen et al., 2022), the introduction of previously inapplicable aquifer parameterization methods to such settings represents a major achievement of this dissertation, particularly as most deltaic aquifer systems lack of proper subsurface parametrization (Van Engelen et al., 2022).

Whereas most passive subsurface parameterization methods are restricted to the estimation of elastic aquifer properties, such as compressibility and storage coefficients, recent studies have introduced analytical solutions to derive aquitard compressibility from groundwater head responses to Earth tides (Valois et al., 2024). This represents a valuable advancement in the context of investigating land subsidence dynamics, where aquitard compressibility often governs total sediment compaction and hence subsidence. However, the solution's non-uniqueness challenges the estimation of reliable parameter values, as there are too many unknown parameters within the set of equations and no singular solution can be obtained. Although a test-wise application of this approach successfully reproduced previously known aquitard compressibility values for the IGPVN site (not explicitly presented in this dissertation), the applied least-squares non-linear parameter optimization showed a pronounced dependency on the choice of initial conditions and parameter bounds, making a meaningful application without a-priori information infeasible. Therefore, quantitative approaches of the studies associated with this dissertation focus on the application of passive subsurface parameterization to elastic aquifer properties and thus address their land subsidence mitigation potential. Future applications could benefit from recent analyses of parameter sensitivity within non-unique solution spaces of tidal groundwater head responses (He et al., 2026), that potentially enhance the robustness of subsurface parameter estimation.

In addition to those quantifications of elastic aquifer properties, the approach presented in section 3.2.2 demonstrates how tidal signals can be exploited to qualitatively diagnose inelastic subsurface processes such as aquitard drainage and their seasonal variability. In doing so, this framework addresses a fundamental limitation of tidal analysis in land subsidence research, namely its restriction to elastic responses. At the same time, this framework outlines a potential pathway for future methodological developments, in which a flexible implementation of the analytical solution proposed by Valois et al. (2024) could be used to quantify the transition from elastic to inelastic aquitard compressibility through the attribution of systematic changes in M_2 phase shift.

4.2 Anthropogenic drivers for land subsidence in the Mekong Delta

4.2.1 Disentangling individual subsidence drivers

A robust understanding of land subsidence in the Mekong Delta requires disentangling the contributions of multiple, interacting drivers. By providing the first high-resolution, process-based quantification of these contributions at the local scale (GW1), this dissertation advances existing delta-wide studies (Minderhoud et al., 2020, 2017; Zoccarato et al., 2018) by achieving the data density required for a reliable quantification of the contributing processes in an exemplary analysis.

By demonstrating that calculated autocompaction rates at GW1 are ~1 mm a^{-1} (section 3.4.2), consistent with modelling results for the upper delta plain by Zoccarato et al. (2018), this analysis underpins the conclusion that subsidence due to groundwater depletion in a commonly exploited aquifer (simulated to ~5 mm a^{-1}) is the dominant contributor to the total subsidence (~8 mm a^{-1}) observed at GW1. The impact of structural loading of the built environment associated with the nearby small urban settlement was calculated to be minor (~1 mm a^{-1}) under undisturbed subsurface settings. Higher subsidence rates of up to ~25 mm a^{-1}, as recorded by levelling and InSAR data in the vicinity of GW1, can occur when the Holocene aquitard is subject to significant groundwater head depletion in the underlying aquifer. This may either result from unlicensed exploitation of brackish shallow groundwater for aquacultural purposes or from well-casing or well-bore failure, which can induce aquifer interconnectivity and lead to a local equalization of hydraulic heads between shallow aquifers and deeper, exploited aquifers, as simulated by Dörr et al. (2026b). These relevant processes and their contribution in the vicinity of the monitoring site GW1 are synthesized in Figure 30.

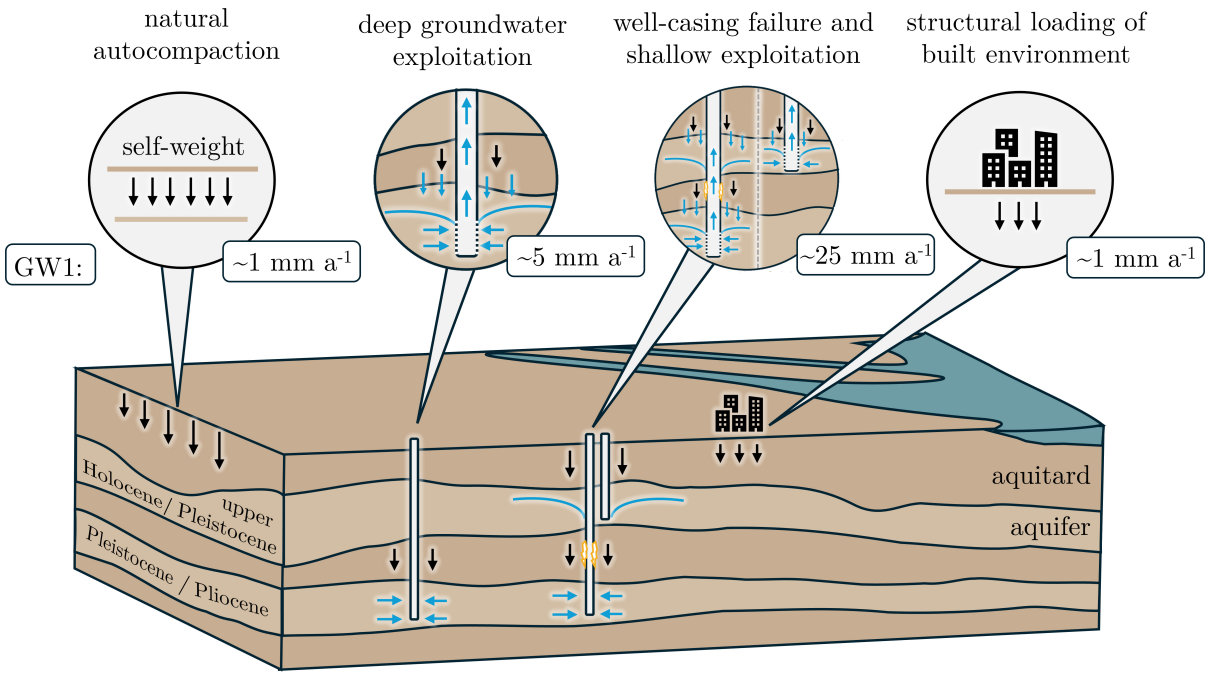


Figure 30: Schematic illustration of natural and anthropogenic drivers of land subsidence and their derived contributions in the vicinity of the study site GW1, based on quantifications by Dörr et al. (2026b) and section 3.4.2.

Although the spatial heterogeneities in subsurface properties and groundwater extraction limit a direct extrapolation of this quantification to the entire delta, the process dynamics identified at GW1 are considered representative of the southern Mekong Delta. This representativeness is supported by the fact that (i) the subsurface stratigraphy at GW1 is in the range of reported layer thicknesses in the southern Mekong Delta (Bauer et al., 2022; Pechstein et al., 2018), (ii) observed groundwater head depletions at GW1 are comparable to those documented in other parts of the southern delta (Dörr et al., 2026b; Duy et al., 2021), (iii) InSAR-derived subsidence rates in the vicinity of GW1 are comparable in magnitude and variability to delta-wide observations (Dörr et al., 2026b; N. Dörr et al., 2024), and (iv) the results are in an overall good agreement with delta-wide modelling studies by Minderhoud et al. (2017) and Zoccarato et al. (2018). Overall, this dissertation identifies groundwater depletion as the dominant driver of land subsidence in the Mekong Delta based on a local, high-resolution, and physics-based analysis, allowing for a process-resolved attribution of the assessed drivers. A recent global-scale study of 40 subsiding deltas published in *Nature* (Ohenhen et al., 2026) independently corroborates this finding for the Mekong Delta

using a large-scale, InSAR-based and artificial-intelligence-supported assessment, albeit at substantially coarser spatial resolution and with a less process-driven methodological focus.

More generally, the holistic character of the applied approach, which integrates multiple monitoring data of subsidence and driving processes, detailed subsurface parameterization, and advanced numerical simulations, provides compelling evidence for the processes at play, indicating that groundwater depletion is the major driver for land subsidence in most parts of the Mekong Delta. Exceptions may be near-coastal settings where autocompaction can reach greater compaction (Zoccarato et al. 2018).

The results show that while groundwater exploitation of the deep and fresh groundwater resources can trigger substantial land subsidence in the Mekong Delta, the subsidence remains moderate unless groundwater head depletion affects the highly compressible shallow Holocene strata. Such pronounced subsidence vulnerability of shallow Holocene aquitards to groundwater depletion were identified in other study areas like in Jakarta (Bakr, 2015) or in Shanghai (Wu et al., 2008), with Shanghai showing a marked decrease in subsidence rates after groundwater extraction was historically shifted from shallow to deeper aquifers. Consequently, a depth-differentiated perspective and targeted management of shallow aquifers are essential for sustainable land subsidence mitigation strategies in the Mekong Delta and comparable hydrogeological settings.

4.2.2 Well-casing and well-bore failures: previously unaddressed anthropogenic accelerators of subsidence

While well-casing failures are long-known consequences of land subsidence (Gambolati and Teatini, 2021; Holzer and Johnson, 1985), the study associated with this dissertation (Dörr et al., 2026b) proposes that such damage may, in turn, contribute to accelerated subsidence by facilitating subsurface drainage pathways and promoting local hydraulic head equilibration between aquitards and tapped aquifers.

In light of the great number of an estimated one million unlicensed groundwater extraction wells in the Mekong Delta (Danh and Khai, 2015), impacts of well-casing failure may scale-up from local to regional significance, representing a potentially relevant contributor to the great spatiotemporal heterogeneity in land subsidence observations. The questionable technical quality of these unlicensed wells favors failures along the well casing, for example at improperly connected pipe joints, and also increases the likelihood of well-bore failure. As the construction of such wells typically involves no backfilling of the annulus beyond a short gravel pack at screen depth, collapsing aquifer material may partially refill the open borehole prior to natural aquitard clay closure. This process can generate vertical hydraulic connections between aquifers (Lacombe et al., 1995), with effects on compaction dynamics similar to those associated with well-casing failure.

Introducing well-casing and well-bore failures as potential additional anthropogenic subsurface control mechanisms in the context of land subsidence offers explanations for other debated research questions, such as inconsistent hydrogeochemical or isotopic signatures across different aquifers (Bauer et al., 2022; Osenbrück et al., 2025) as well as discrepancies between stagnant salinity trends observed in professionally drilled monitoring wells and reported increases in groundwater salinity from farmers' private wells (Hoan et al., 2025).

Therefore, introducing these newly addressed potential control mechanisms affecting subsurface compaction provides new perspectives into interrelated considerations, such as groundwater salinization processes, within the overarching framework of cascading hazards in the Mekong Delta.

4.3 Implications for adaptation and mitigation strategies

4.3.1 Preventing groundwater depletion - The central challenge in mitigating land subsidence and cascading hazards

By high resolution, local-scale compaction monitoring (Dörr et al., 2023) and numeric simulations in unprecedented detail for the Mekong Delta (Dörr et al., 2026b), the findings of this dissertation are based on the data density required for robust and reliable process quantification at local scale and support previous regional studies (Minderhoud et al., 2020, 2017) in their evaluation of groundwater depletion as being a dominant driver for land subsidence in the Mekong Delta.

By revealing that groundwater head depletion persists throughout the year (Dörr et al., 2026a), this dissertation indicates that groundwater recharge plays a negligible role in the governing groundwater balances. As a result, groundwater extraction causes a progressive and uncompensated decline in groundwater heads, even during the rainy season, ultimately triggering sediment compaction and associated land subsidence. Therefore, the results of this dissertation not only reinforce but further intensify the process-based evidence for the need to strictly reduce groundwater extraction, as called for in previous studies (Kondolf et al., 2022).

However, considering the multi-layered character of the aquifer system with its high vertical variation in salinity (Bauer et al., 2022; Hoan et al., 2025), this dissertation offers the first depth-differentiated evaluation, allowing for a better characterization of the subsidence-vulnerability of aquifer exploitation across different depths. Such depth-differentiated analyses have proven highly insightful in other subsiding aquifer systems, such as Shanghai (Wu et al., 2008), where a mere shift from shallow to deep groundwater extraction resulted in reduced subsidence rates.

The findings of this dissertation demonstrate that in the Mekong Delta the greatest subsidence potential lies within the shallow Holocene aquitard sediments (Dörr et al., 2023, 2026b). This underscores the importance of managing shallow groundwater resources for subsidence mitigation, as the hydraulic heads in these aquifers largely

control the compaction of the overlying soft and highly compressible Holocene strata. It is noted that in areas where the shallow Holocene aquifer (qh) is not developed, as is the case in large parts of the southern Mekong Delta (Pechstein et al., 2018), compaction of the shallow Holocene sediments is primarily controlled by the upper Pleistocene aquifer (qp_3), representing the topmost developed aquifer in such areas. Due to their high salinity, these aquifers are of minor relevance for domestic water supply (Pechstein et al., 2018). However, despite existing legal restrictions, there are indications that shallow groundwater is used in brackish aquaculture (Van Tuan et al., 2024).

In light of the high subsidence potential of shallow strata and their minor relevance for domestic water supply, the vertically refined evaluation of this dissertation supports prioritizing the maintenance or restoration of hydraulic heads in shallow aquifers in the context of land subsidence mitigation. This can be achieved through the enforcement and monitoring of existing aquaculture-related abstraction restrictions. Complementary, targeted investigations into *Managed Aquifer Recharge* of shallow aquifers should be pursued, where quality constraints are generally less restrictive than for recharge efforts in aquifers used for domestic water supply.

Importantly, the suggested prioritization of shallow aquifers does not imply that continued deep groundwater extraction is without adverse consequences in terms of future subsidence. In the absence of significant net groundwater recharge, head depletion in deep aquifers will gradually propagate upward as the system approaches hydraulic equilibration (Galloway and Burbey, 2011; Helm, 1975), ultimately exposing shallow layers to increasing effective stresses and promoting advancing land subsidence.

In the context of cascading hazards, excessive groundwater exploitation not only triggers land subsidence and associated hazards such as increased flood risk and relative sea-level rise, but also promotes groundwater salinization (Bauer et al., 2022; Hoan et al., 2022; Osenbrück et al., 2025), ultimately exacerbating the loss of freshwater resources. This underlines that preventing groundwater depletion is a central challenge in addressing the prevailing cascading hazards in the Mekong Delta.

4.3.2 The long-term perspective: the need for alternative water supply concepts

In light of progressive surface water salinization (Bauer et al., 2025) and pollution (Ha et al., 2018), no easily accessible alternative water resources are available in the southern Mekong Delta. Present-day alternative water supply concepts remain underdeveloped and mostly on single household-level (Pham et al., 2026, 2023; Vinh et al., 2024), whereas larger-scale concepts for rainwater storage are challenged by the flat topography (Wagner et al., 2012) and subsurface storage like *Managed Aquifer Recharge* is constrained by low aquifer storage coefficients (Dörr et al., 2025). Despite their conceptual relevance, recent pilot projects on larger-scale rainwater storage supported by the World Bank (2022) and on *Managed Aquifer Recharge* implemented by the Federal Institute for Geosciences and Natural Resources (BGR) (Steinel et al., 2024) remain at an exploratory stage, with no clear indications of planned upscaling or well-defined future perspectives.

Yet, to ensure socio-economic acceptance of the required restriction of groundwater exploitation, alternative water resources must be facilitated. In this context, a centralized water supply infrastructure that conveys and distributes freshwater from distant sources, such as the Hau River, to the southern Mekong Delta could represent a technically feasible, albeit cost-intensive, alternative water supply concept. While this option was addressed during the early phase of the ViWaT Initiative, it has not been pursued further by the responsible decision makers. Given the delayed character of land subsidence to past groundwater depletion, uncertainties regarding the region's long-term viability may have discouraged the consideration of such a cost-intensive concept by decision makers.

Through the quantification of delayed subsidence responses resulting from past groundwater depletion (Dörr et al., 2026b) and autocompaction processes (section 3.4.2) in a representative, high-resolution, local-scale analysis, the findings of this dissertation provide a sound basis for an evidence-based assessment regarding the region's long-term viability, indicating that the existential risk of subsiding below sea level can be averted if further groundwater head depletion is rigorously prevented.

Therefore, this dissertation contributes to more informed decision-making and encourages the consideration of targeted measures, such as investing in a centralized water supply infrastructure alongside the strict prevention of further groundwater head decline.

5 Conclusion

Understanding land subsidence dynamics in deltas requires robust, process-based investigations, as a wide range of interacting drivers can contribute to observed land-motion patterns. These dynamics often exacerbate existential risks in low-lying deltaic regions that host a substantial share of the global population, underscoring the profound societal relevance of deltaic subsidence research. Accordingly, a comprehensive assessment of multifaceted anthropogenic influences, together with a detailed characterization of deltaic subsurface sediments, is essential to reliably interpret subsidence signals and to inform effective mitigation and adaptation strategies.

Against this background, this dissertation demonstrates how previously underutilized information can be extracted from existing datasets in data-scarce deltaic environments. This is achieved by revealing the presence of tidal signals in groundwater head time series in the Mekong Delta and exploring their potential for characterizing aquifer-system properties and process dynamics relevant to subsidence mitigation. Together with the conducted installation of new monitoring equipment, this approach constitutes a valuable contribution to address data scarcity and related uncertainties in process understanding in the Mekong Delta, where comprehensive field data are limited. Enabled by the developed method extensions, this approach introduces a transferable framework for deriving subsurface parameters in the Mekong Delta and other subsiding deltas, independent of costly field experiments, sampling campaigns, or laboratory analyses.

Complementing this methodological approach, the integration of detailed geomechanical parameterization with high-resolution monitoring of subsurface compaction and surface subsidence, together with advanced numerical simulations, enables this dissertation to corroborate previous assessments with enhanced process-based detail and reliability. The results identify groundwater depletion as the dominant driver of land subsidence in the Mekong Delta. Importantly, the depth-differentiated analysis reveals that subsidence vulnerability is strongly controlled by shallow

groundwater heads and their impact on highly compressible Holocene sediments. This vertically refined perspective provides a process-based basis for prioritizing shallow aquifers in targeted groundwater management strategies and underscores the necessity of strict groundwater abstraction control to mitigate ongoing and future land subsidence. In addition to deliberate shallow groundwater abstraction, this dissertation further demonstrates that unintended well-casing and well-bore failures can accelerate and enhance compaction of shallow Holocene sediments, introducing a previously underappreciated anthropogenic control on subsidence dynamics.

The findings further show that groundwater head depletion persists throughout the year and that seasonally rising head trends represent loading artefacts rather than effective recharge. This indicates negligible effective groundwater replenishment and a progressive, uncompensated decline in hydraulic heads that ultimately triggers sediment compaction. In combination with the limited mitigation potential of deeper aquifers, these results emphasize the urgency of rigorously restricting continued groundwater overexploitation.

Extending beyond the Mekong Delta, the explicit consideration of surface-loading effects in the interpretation of groundwater head dynamics helps to overcome a systematic blind spot in evaluations of groundwater hydraulics that is particularly critical in deltaic environments. Seasonal inundation and river-water loading can generate groundwater head signals of substantial magnitude, the misinterpretation of which may lead to biased assessments of recharge processes. In this context, the rapid expansion of aquaculture-driven land-use change in Southeast Asian deltas introduces an additional, anthropogenically controlled surface-water load, underscoring the broader relevance of accounting for loading effects in groundwater and subsidence assessments across comparable deltaic systems.

Taken together, the findings indicate that, despite delayed subsidence responses and ongoing autocompaction, the existential risk of subsiding below sea level in the near future can be averted if further groundwater head depletion is rigorously prevented and alternative water resources are provided.

References

Acworth, R.I., Halloran, L.J.S., Rau, G.C., Cuthbert, M.O., Bernardi, T.L., 2016. An objective frequency domain method for quantifying confined aquifer compressible storage using Earth and atmospheric tides. Geophys. Res. Lett. 43. https://doi.org/10.1002/2016gl071328

Anderson, H.R., 1978. Hydrogeologic Reconnaissance of the Mekong Delta in South Vietnam and Cambodia.

Anthony, E., Syvitski, J., Săinescu, F., Nicholls, R.J., Cohen, K.M., Marriner, N., Saito, Y., Day, J., Minderhoud, P.S.J., Amorosi, A., Chen, Z., Morhange, C., Tamura, T., Vespremeanu-Stroe, A., Besset, M., Sabatier, F., Kaniewski, D., Maselli, V., 2024. Delta sustainability from the Holocene to the Anthropocene and envisioning the future. Nat. Sustain. 7, 1235–1246. https://doi.org/10.1038/s41893-024-01426-3

Bagheri-Gavkosh, M., Hosseini, S.M., Ataie-Ashtiani, B., Sohani, Y., Ebrahimian, H., Morovat, F., Ashrafi, S., 2021. Land subsidence: A global challenge. Sci. Total Environ. 778, 146193. https://doi.org/10.1016/j.scitotenv.2021.146193

Bakr, M., 2015. Influence of Groundwater Management on Land Subsidence in Deltas: A Case Study of Jakarta (Indonesia). Water Resour. Manag. 29, 1541–1555. https://doi.org/10.1007/s11269-014-0893-7

Baldan, S., Minderhoud, P.S.J., Xotta, R., Zoccarato, C., Teatini, P., 2025. Data-driven 3D modelling of long-term Holocene delta evolution and sediment compaction: The Mekong Delta. Earth Surf. Process. Landf. 50. https://doi.org/10.1002/esp.6046

Bardsley, W.E., Campbell, D.I., 2000. Natural Geological Weighing Lysimeters: Calibration Tools for Satellite and Ground Surface Gravity Monitoring of Subsurface Water-Mass Change. Nat. Resour. Res. 9, 147–156. https://doi.org/10.1023/A:1010147527484

Bastias Espejo, J.M., Turnadge, C., Crosbie, R.S., Blum, P., Rau, G.C., 2023. Technical note: Novel analytical solution for groundwater response to atmospheric tides. https://doi.org/10.5194/egusphere-2023-642

Bauer, J., Börsig, N., Pham, V.C., Hoan, T.V., Nguyen, H.T., Norra, S., 2022. Geochemistry and evolution of groundwater resources in the context of salinization and freshening in the southernmost Mekong Delta, Vietnam. J. Hydrol. Reg. Stud. 40, 101010. https://doi.org/10.1016/j.ejrh.2022.101010

Bauer, J., Dörr, F., Duong Vu, H.T., Schenk, A., Tran, H.V., Pham, V.C., Börsig, N., Van Der Linden, R., Nguyen, N.H., Eiche, E., Norra, S., 2025. Seawater intrusion

in river delta systems. Inter-annual dynamics and drivers of salinity variations in the southern Mekong Delta, Vietnam. J. Hydrol. 661, 133745. https://doi.org/10.1016/j.jhydrol.2025.133745

Bayoumi, A., 2011. On the Evaluation of Settlement Measurements Using Borehole Extensometers. Geotech. Geol. Eng. 29, 75–90. https://doi.org/10.1007/s10706-010-9352-2

Becker, M., Seeger, K., Paszkowski, A., Marcos, M., Papa, F., Almar, R., Bates, P., France-Lanord, C., Hossain, M.S., Khan, M.J.U., Karegar, M.A., Karpytchev, M., Long, N., Minderhoud, P.S.J., Neal, J., Nicholls, R.J., Syvitski, J., 2024. Coastal Flooding in Asian Megadeltas: Recent Advances, Persistent Challenges, and Call for Actions Amidst Local and Global Changes. Rev. Geophys. 62. https://doi.org/10.1029/2024rg000846

Bredehoeft, J.D., 1967. Response of well-aquifer systems to Earth tides. J. Geophys. Res. 72, 3075–3087. https://doi.org/10.1029/JZ072i012p03075

Burgess, W.G., Shamsudduha, M., Taylor, R.G., Zahid, A., Ahmed, K.M., Mukherjee, A., Lapworth, D.J., Bense, V.F., 2017. Terrestrial water load and groundwater fluctuation in the Bengal Basin. Sci. Rep. 7. https://doi.org/10.1038/s41598-017-04159-w

Chaussard, E., Wdowinski, S., Cabral-Cano, E., Amelung, F., 2014. Land subsidence in central Mexico detected by ALOS InSAR time-series. Remote Sens. Environ. 140, 94–106. https://doi.org/10.1016/j.rse.2013.08.038

Danh, V.T., Khai, H.V., 2015. Household demand and supply for clean groundwater in the Mekong Delta, Vietnam. Renew. Wind Water Sol. 2, 4. https://doi.org/10.1186/s40807-014-0004-7

Davydzenka, T., Tahmasebi, P., Shokri, N., 2024. Unveiling the Global Extent of Land Subsidence: The Sinking Crisis. Geophys. Res. Lett. 51. https://doi.org/10.1029/2023gl104497

DIN 18135, 2012. DIN 18135: Soil Investigation and testing Oedometer consolidation test.

DIN EN ISO 18674-1, 2015. Geotechnische Erkundung und Untersuchung_- Geotechnische Messungen_- Teil_1: Allgemeine Regeln (ISO_18674-1:2015); Deutsche Fassung EN_ISO_18674-1:2015. https://doi.org/10.31030/2283135

Dörr, F., Bauer, J., Hoan, T.V., Van, L.T.M., Schenk, A., Dörr, N., Nestmann, F., Norra, S., 2026b. Land subsidence dynamics in the Mekong Delta: Insights from local high-resolution geomechanical parameterization, numerical modelling, and geodetic observations. Sci. Total Environ. 1033, 181850. https://doi.org/10.1016/j.scitotenv.2026.181850

Dörr, F., Bauer, J., Rau, G.C., Lewi, E., Hoan, V.T., Van, L.T.M., Valois, R., Steinel, A., Nestmann, F., Norra, S., 2026a. The recharge illusion: How seasonal surface

loading can hide continuing groundwater resource declines in confined deltaic aquifers. J. Hydrol. 665, 134674. https://doi.org/10.1016/j.jhydrol.2025.134674

Dörr, F., Bauer, J., Rau, G.C., Valois, R., Haon, T.V., Pham, V.C., Van, L.T.M., Steinel, A., Nestmann, F., Norra, S., 2025. Passive subsurface characterization in subsiding deltas: assessing land subsidence mitigation potential with frequency analyses of groundwater heads and superposing harmonic drivers. Journal of Hydrology. https://doi.org/10.1016/j.jhydrol.2025.133844.

Dörr, F., Bauer, J., Tran, H.V., Norra, S., Nestmann, F., 2023. Vietnams Mekong-Delta - Landsenkung infolge von Grundwasserübernutzung. WASSERWIRTSCHAFT 113, 52–56. https://doi.org/10.1007/s35147-023-1922-3

Duy, N.L., Nguyen, T.V.K., Nguyen, D.V., Tran, A.T., Nguyen, H.T., Heidbüchel, I., Merz, B., Apel, H., 2021. Groundwater dynamics in the Vietnamese Mekong Delta: Trends, memory effects, and response times. J. Hydrol. Reg. Stud. 33, 100746. https://doi.org/10.1016/j.ejrh.2020.100746

Erban, L.E., Gorelick, S.M., Zebker, H.A., 2014. Groundwater extraction, land subsidence, and sea-level rise in the Mekong Delta, Vietnam. Environ. Res. Lett. 9, 084010. https://doi.org/10.1088/1748-9326/9/8/084010

Eslami, S., Oude Essink, G., Paszkowski, A., Seeger, K., Minderhoud, P.S.J., Sloff, K., Nicholls, R.J., 2025. A systems perspective for climate adaptation in deltas. Nat. Clim. Change 15, 687–691. https://doi.org/10.1038/s41558-025-02368-0

Ferretti, A., Prati, C., Rocca, F., 2001. Permanent scatterers in SAR interferometry. IEEE Trans. Geosci. Remote Sens. 39, 8–20. https://doi.org/10.1109/36.898661

Galloway, D.L., Burbey, T.J., 2011. Review: Regional land subsidence accompanying groundwater extraction. Hydrogeol. J. 19, 1459–1486. https://doi.org/10.1007/s10040-011-0775-5

Galloway, D.L., Erkens, G., Kuniansky, E.L., Rowland, J.C., 2016. Preface: Land subsidence processes. Hydrogeol. J. 24, 547–550. https://doi.org/10.1007/s10040-016-1386-y

Galloway, D.L., Hoffmann, J., 2007. The application of satellite differential SAR interferometry-derived ground displacements in hydrogeology. Hydrogeol. J. 15, 133–154. https://doi.org/10.1007/s10040-006-0121-5

Gambolati, G., Freeze, R.A., 1973. Mathematical simulation of the subsidence of Venice: 1. Theory. Water Resour. Res. 9, 721–733. https://doi.org/10.1029/WR009i003p00721

Gambolati, G., Teatini, P., 2021. Land Subsidence and its Mitigation. The Groundwater Project. https://doi.org/10.21083/978-1-77470-001-3

Gambolati, G., Teatini, P., Baú, D., Ferronato, M., 2000. Importance of poroelastic coupling in dynamically active aquifers of the Po River Basin, Italy. Water Resour. Res. 36, 2443–2459. https://doi.org/10.1029/2000WR900127

Gholinia, A., Nikkhah, M., Naderi, R., 2022. Validation of borehole extensometers results in geotechnical monitoring. Environ. Earth Sci. 81, 312. https://doi.org/10.1007/s12665-022-10422-9

Ha, T.P., Dieperink, C., Dang Tri, V.P., Otter, H.S., Hoekstra, P., 2018. Governance conditions for adaptive freshwater management in the Vietnamese Mekong Delta. J. Hydrol. 557, 116–127. https://doi.org/10.1016/j.jhydrol.2017.12.024

Hanebuth, T.J.J., Voris, H.K., Yokoyama, Y., Saito, Y., Okuno, J., 2011. Formation and fate of sedimentary depocentres on Southeast Asia's Sunda Shelf over the past sea-level cycle and biogeographic implications. Earth-Sci. Rev. 104, 92–110. https://doi.org/10.1016/j.earscirev.2010.09.006

He, G., Shi, Z., Sun, X., Qi, Z., Ye, P., Wang, G., 2026. Stabilizing aquifer permeability time series via parameter sensitivity optimization in groundwater tidal analysis. J. Hydrol. 667, 134874. https://doi.org/10.1016/j.jhydrol.2025.134874

Helm, D.C., 1975. One-dimensional simulation of aquifer system compaction near Pixley, California: 1. Constant parameters. Water Resour. Res. 11, 465–478. https://doi.org/10.1029/WR011i003p00465

Herrera-García, G., Ezquerro, P., Tomás, R., Béjar-Pizarro, M., López-Vinielles, J., Rossi, M., Mateos, R.M., Carreón-Freyre, D., Lambert, J., Teatini, P., Cabral-Cano, E., Erkens, G., Galloway, D., Hung, W.-C., Kakar, N., Sneed, M., Tosi, L., Wang, H., Ye, S., 2021. Mapping the global threat of land subsidence. Science 371, 34–36. https://doi.org/10.1126/science.abb8549

Hoan, T.V., Richter, K.-G., Börsig, N., Bauer, J., Ha, N.T., Norra, S., 2022. An Improved Groundwater Model Framework for Aquifer Structures of the Quaternary-Formed Sediment Body in the Southernmost Parts of the Mekong Delta, Vietnam. Hydrology 9, 61. https://doi.org/10.3390/hydrology9040061

Hoan, T.V., Richter, K.-G., Dörr, F., Bauer, J., Börsig, N., Steinel, A., Le, V.T.M., Pham, V.C., Than, D.V., Norra, S., 2025. The Utilization of a 3D Groundwater Flow and Transport Model for a Qualitative Investigation of Groundwater Salinization in the Ca Mau Peninsula (Mekong Delta, Vietnam). Hydrology 12, 126. https://doi.org/10.3390/hydrology12050126

Hoffmann, J., Leake, S.A., Galloway, D., Wilson, A., 2003. MODFLOW-2000 ground-water model-user guide to the subsidence and aquifer-system compaction (SUB) package.

Holzer, T.L., Johnson, A.I., 1985. Land subsidence caused by ground water withdrawal in urban areas. GeoJournal 11. https://doi.org/10.1007/BF00186338

Huning, L.S., Love, C.A., Anjileli, H., Vahedifard, F., Zhao, Y., Chaffe, P.L.B., Cooper, K., Alborzi, A., Pleitez, E., Martinez, A., Ashraf, S., Mallakpour, I., Moftakhari, H., AghaKouchak, A., 2024. Global Land Subsidence: Impact of Climate

Extremes and Human Activities. Rev. Geophys. 62, e2023RG000817. https://doi.org/10.1029/2023RG000817

Jacob, C.E., 1940. On the flow of water in an elastic artesian aquifer. Eos Trans. Am. Geophys. Union 21, 574–586. https://doi.org/10.1029/TR021i002p00574

Karlsrud, K., Tunbridge, L., Quoc Khanh, N., Quoc Dinh, N., 2020. Preliminary results of land subsidence monitoring in the Ca Mau Province. Proc. Int. Assoc. Hydrol. Sci. 382, 111–115. https://doi.org/10.5194/piahs-382-111-2020

Karlsrud, K., Vangelsten, B.V., Frauenfelder, R., 2017. Subsidence and Shoreline Retreat in the Ca Mau Province – Vietnam. Causes, Consequences and Mitigation Options 48.

Khang, N.D., Kotera, A., Sakamoto, T., Yokozawa, M., 2008. Sensitivity of Salinity Intrusion to Sea Level Rise and River Flow Change in Vietnamese Mekong Delta-Impacts on Availability of Irrigation Water for Rice Cropping. J. Agric. Meteorol. 64, 167–176. https://doi.org/10.2480/agrmet.64.3.4

Klönne, W., 1880. Die periodischen Schwankungen des Wasserspiegels in den inundierten Kohlenschächten von Dux in der Periode vom 8. April bis 15. September 1879. Sitzungsberichte Kaiserliche Akademie der Wissenschaften.

Kondolf, G.M., Schmitt, R.J.P., Carling, P.A., Goichot, M., Keskinen, M., Arias, M.E., Bizzi, S., Castelletti, A., Cochrane, T.A., Darby, S.E., Kummu, M., Minderhoud, P.S.J., Nguyen, D., Nguyen, H.T., Nguyen, N.T., Oeurng, C., Opperman, J., Rubin, Z., San, D.C., Schmeier, S., Wild, T., 2022. Save the Mekong Delta from drowning. Science 376, 583–585. https://doi.org/10.1126/science.abm5176

Lacombe, S., Sudicky, E.A., Frape, S.K., Unger, A.J.A., 1995. Influence of Leaky Boreholes on Cross-Formational Groundwater Flow and Contaminant Transport. Water Resour. Res. 31, 1871–1882. https://doi.org/10.1029/95WR00661

Liao, X., Wang, C.-Y., Wang, Z.-Y., 2022. Seasonal change of groundwater response to Earth tides. J. Hydrol. 612, 128118. https://doi.org/10.1016/j.jhydrol.2022.128118

Lovelock, C.E., Cahoon, D.R., Friess, D.A., Guntenspergen, G.R., Krauss, K.W., Reef, R., Rogers, K., Saunders, M.L., Sidik, F., Swales, A., Saintilan, N., Thuyen, L.X., Triet, T., 2015. The vulnerability of Indo-Pacific mangrove forests to sea-level rise. Nature 526, 559–563. https://doi.org/10.1038/nature15538

Lu, N., Godt, J.W., Wu, D.T., 2010. A closed-form equation for effective stress in unsaturated soil. Water Resour. Res. 46, 2009WR008646. https://doi.org/10.1029/2009WR008646

Luo, J., Sun, Z., Lu, L., Xiong, Z., Cui, L., Mao, Z., 2022. Rapid expansion of coastal aquaculture ponds in Southeast Asia: Patterns, drivers and impacts. J. Environ. Manage. 315, 115100. https://doi.org/10.1016/j.jenvman.2022.115100

Maliva, R.G., Coulibaly, K., Guo, W., Missimer, T.M., 2011. Confined Aquifer Loading: Implications for Groundwater Management. Groundwater 49, 302–304. https://doi.org/10.1111/j.1745-6584.2010.00776.x

McMillan, T.C., Rau, G.C., Timms, W.A., Andersen, M.S., 2019. Utilizing the Impact of Earth and Atmospheric Tides on Groundwater Systems: A Review Reveals the Future Potential. Rev. Geophys. 57, 281–315. https://doi.org/10.1029/2018rg000630

Minderhoud, P., Guzy, A., Baldan, S., Xotta, R., Lexmond, B., Zoccarato, C., Teatini, P., 2024. Improving Subsidence Modelling of Different Depth Domains in the Mekong Delta. https://doi.org/10.31223/x5mt3d

Minderhoud, P.S.J., Coumou, L., Erkens, G., Middelkoop, H., Stouthamer, E., 2019. Mekong delta much lower than previously assumed in sea-level rise impact assessments. Nat. Commun. 10. https://doi.org/10.1038/s41467-019-11602-1

Minderhoud, P.S.J., Erkens, G., Pham, V.H., Bui, V.T., Erban, L., Kooi, H., Stouthamer, E., 2017. Impacts of 25 years of groundwater extraction on subsidence in the Mekong delta, Vietnam. Environ. Res. Lett. 12, 064006. https://doi.org/10.1088/1748-9326/aa7146

Minderhoud, P.S.J., Middelkoop, H., Erkens, G., Stouthamer, E., 2020. Groundwater extraction may drown mega-delta: projections of extraction-induced subsidence and elevation of the Mekong delta for the 21st century. Environ. Res. Commun. 2, 011005. https://doi.org/10.1088/2515-7620/ab5e21

Minderhoud, P.S.J., Shirzaei, M., Teatini, P., 2025. From InSAR-Derived Subsidence to Relative Sea-Level Rise—A Call for Rigor. Earths Future 13, e2024EF005539. https://doi.org/10.1029/2024EF005539

N. Dörr, N., 2024. Robust and Flexible Persistent Scatterer Interferometry for Long-Term and Large-Scale Displacement Monitoring.

N. Dörr, N., Huu, L.V., Schenk, A., Hinz, S., 2025. Drought-Induced Land Subsidence in the Mekong Delta, Vietnam: Insights From SAR Interferometry. Geophys. Res. Lett. 52, e2025GL117096. https://doi.org/10.1029/2025GL117096

N. Dörr, N., Schenk, A., Hinz, S., 2024. Land Subsidence in the Mekong Delta Derived From Advanced Persistent Scatterer Interferometry With an Infrastructural Reference Network. IEEE J. Sel. Top. Appl. Earth Obs. Remote Sens. 17, 12077–12091. https://doi.org/10.1109/jstars.2024.3420130

Neuzil, C.E., 2003. Hydromechanical coupling in geologic processes. Hydrogeol. J. 11, 41–83. https://doi.org/10.1007/s10040-002-0230-8

Ng, A.H.-M., Ge, L., Li, X., Abidin, H.Z., Andreas, H., Zhang, K., 2012. Mapping land subsidence in Jakarta, Indonesia using persistent scatterer interferometry (PSI) technique with ALOS PALSAR. Int. J. Appl. Earth Obs. Geoinformation 18, 232–242. https://doi.org/10.1016/j.jag.2012.01.018

Nguyen, V.K., Le, X.T., Dao, H.H., Do Van, L., 2015. Land surface subsidecne in Mekong delta - due to the groundwater extraction? (In Vietnamese, English summary). Tap Chi Dia Chat 105–110.

Ohenhen, L.O., Shirzaei, M., Davis, J.L., Tiwari, A., Nicholls, R., Dasho, O., Sadhasivam, N., Seeger, K., Werth, S., Chadwick, A.J., Onyike, F., Lucy, J., Atkins, C., Daramola, S., Ankamah, A., Minderhoud, P.S.J., Olsemann, J., Yemele, G.C., 2026. Global subsidence of river deltas. Nature. https://doi.org/10.1038/s41586-025-09928-6

Osenbrück, K., Steinel, A., Montcoudiol, N., Manh, L.V., Bäumle, R., 2025. Geochemical evolution and flow of groundwater impacted by long-term abstraction in the Mekong Delta, Vietnam. J. Hydrol. 655, 132881. https://doi.org/10.1016/j.jhydrol.2025.132881

Pacheco, F.A.L., Fallico, C., 2015. Hydraulic head response of a confined aquifer influenced by river stage fluctuations and mechanical loading. J. Hydrol. 531, 716–727. https://doi.org/10.1016/j.jhydrol.2015.10.055

Pechstein, A., Hanh, H.T., Orilski, J., Nam, L.H., 2018. Detailed Investigations on the hydrogeological situation in Ca Mau Province, Mekong Delta, Vietnam.

Pham, H., Sass, I., Nguyen, O., 2022. Concerns Related to Modelling Land Subsidence of Mekong Delta, in: Ha-Minh, C., Tang, A.M., Bui, T.Q., Vu, X.H., Huynh, D.V.K. (Eds.), CIGOS 2021, Emerging Technologies and Applications for Green Infrastructure, Lecture Notes in Civil Engineering. Springer Nature Singapore, Singapore, pp. 1007–1014. https://doi.org/10.1007/978-981-16-7160-9_102

Pham, V.C., Bauer, J., Börsig, N., Ho, J., Vu Huu, L., Tran Viet, H., Dörr, F., Norra, S., 2023. Groundwater Use Habits and Environmental Awareness in Ca Mau Province, Vietnam: Implications for Sustainable Water Resource Management. Environ. Chall. 13, 100742. https://doi.org/10.1016/j.envc.2023.100742

Pham, V.C., Ho, J., Bauer, J., Börsig, N., Dörr, F., Hoan, T.V., Eiche, E., Tiehm, A., Norra, S., 2026. The potential of collected rainwater as an alternative water resource for domestic purpose to mitigate groundwater overexploitation in terms of water quality and people's acceptance. Environ. Chall. 101443. https://doi.org/10.1016/j.envc.2026.101443

Pham-Thanh, H., Phan-Van, T., Fink, A.H., Van Der Linden, R., 2022. Local-scale rainy season onset detection: A new approach based on principal component analysis and its application to Vietnam. Int. J. Climatol. 42, 3726–3742. https://doi.org/10.1002/joc.7441

Pham-Thanh, H., Van Der Linden, R., Ngo-Duc, T., Nguyen-Dang, Q., Fink, A.H., Phan-Van, T., 2020. Predictability of the rainy season onset date in Central Highlands of Vietnam. Int. J. Climatol. 40, 3072–3086. https://doi.org/10.1002/joc.6383

PLAXIS 2D 2024.3 Reference Manual, 2025.

Poland, J.F., Davis, G.H., 1969. Land Subsidence Due to Withdrawal of Fluids, in: Varnes, D.J., Kiersch, G. (Eds.), Reviews in Engineering Geology. Geological Society of America, pp. 187–269. https://doi.org/10.1130/REG2-p187

Pratt, W.E., Johnson, D.W., 1926. Local Subsidence of the Goose Creek Oil Field. J. Geol. 34, 577–590. https://doi.org/10.1086/623352

Rasmussen, T.C., Crawford, L.A., 1997. Identifying and Removing Barometric Pressure Effects in Confined and Unconfined Aquifers. Groundwater 35, 502–511. https://doi.org/10.1111/j.1745-6584.1997.tb00111.x

Rau, G.C., Cuthbert, M.O., Acworth, R.I., Blum, P., 2020. Technical note: Disentangling the groundwater response to Earth and atmospheric tides to improve subsurface characterisation. Hydrol. Earth Syst. Sci. 24, 6033–6046. https://doi.org/10.5194/hess-24-6033-2020

Renaud, F.G., Kuenzer, C. (Eds.), 2012. The Mekong Delta System: Interdisciplinary Analyses of a River Delta, Springer Environmental Science and Engineering. Springer Netherlands, Dordrecht. https://doi.org/10.1007/978-94-007-3962-8

Roeloffs, E.A., Burford, S.S., Riley, F.S., Records, A.W., 1989. Hydrologic effects on water level changes associated with episodic fault creep near Parkfield, California. J. Geophys. Res. Solid Earth 94, 12387–12402. https://doi.org/10.1029/JB094iB09p12387

Rojstaczer, S., 1988. Determination of fluid flow properties from the response of water levels in wells to atmospheric loading. Water Resour. Res. 24, 1927–1938. https://doi.org/10.1029/WR024i011p01927

Schweizer, D., Ried, V., Rau, G.C., Tuck, J.E., Stoica, P., 2021. Comparing Methods and Defining Practical Requirements for Extracting Harmonic Tidal Components from Groundwater Level Measurements. Math. Geosci. 53, 1147–1169. https://doi.org/10.1007/s11004-020-09915-9

Seidel, R., Dettmann, U., Tiemeyer, B., 2023. Reviewing and analyzing shrinkage of peat and other organic soils in relation to selected soil properties. Vadose Zone J. 22, e20264. https://doi.org/10.1002/vzj2.20264

Seidl, C., Page, D., Wheeler, S.A., 2024. Using managed aquifer recharge to address land subsidence: Insights from a global literature review. Water Secur. 23, 100184. https://doi.org/10.1016/j.wasec.2024.100184

Stanley, D.J., Warne, A.G., 1994. Worldwide Initiation of Holocene Marine Deltas by Deceleration of Sea-Level Rise. Science 265, 228–231. https://doi.org/10.1126/science.265.5169.228

Steinel, A., de Jonge, M., Jansen, S., 2024. Concept for initial water quality assessment and water monitoring plan during implementation for ASR pilot in Hau Giang province.

Sun, H., Grandstaff, D., Shagam, R., 1999. Land subsidence due to groundwater withdrawal: potential damage of subsidence and sea level rise in southern New Jersey, USA. Environ. Geol. 37, 290–296. https://doi.org/10.1007/s002540050386

Syvitski, J.P.M., Kettner, A.J., Overeem, I., Hutton, E.W.H., Hannon, M.T., Brakenridge, G.R., Day, J., Vörösmarty, C., Saito, Y., Giosan, L., Nicholls, R.J., 2009. Sinking deltas due to human activities. Nat. Geosci. 2, 681–686. https://doi.org/10.1038/ngeo629

Toll, N.J., Rasmussen, T.C., 2007. Removal of Barometric Pressure Effects and Earth Tides from Observed Water Levels. Groundwater 45, 101–105. https://doi.org/10.1111/j.1745-6584.2006.00254.x

Turnadge, C., Crosbie, R.S., Barron, O., Rau, G.C., 2019. Comparing Methods of Barometric Efficiency Characterization for Specific Storage Estimation. Groundwater 57, 844–859. https://doi.org/10.1111/gwat.12923

Valois, R., Rivière, A., Vouillamoz, J.-M., Rau, G.C., 2024. Technical note: Analytical solution for well water response to Earth tides in leaky aquifers with storage and compressibility in the aquitard. Hydrol. Earth Syst. Sci. 28, 1041–1054. https://doi.org/10.5194/hess-28-1041-2024

Van Der Kamp, G., Schmidt, R., 2017. Review: Moisture loading—the hidden information in groundwater observation well records. Hydrogeol. J. 25, 2225–2233. https://doi.org/10.1007/s10040-017-1631-z

Van Engelen, J., Essink, G.H.P.O., Bierkens, M.F.P., 2022. Sustainability of fresh groundwater resources in fifteen major deltas around the world. Environ. Res. Lett. 17, 125001. https://doi.org/10.1088/1748-9326/aca16c

Van, L.T.T., Lertsirivorakul, R., Vuong, B.T., Thang, C.H., 2023. Groundwater recharge in Mekong River Delta: An application of the water-table fluctuation method in the Long Xuyen Quadrangle and the Ca Mau Peninsula. Songklanakarin J. Sci. Technol., Songklanakarin Journal of Science & Technology 45.

Van Tuan, P., Jiang, Y., Stigter, T., Zhou, Y., 2024. Understanding groundwater use and vulnerability of rural communities in the Mekong Delta: The case of Tra Vinh province, Vietnam. Groundw. Sustain. Dev. 25, 101095. https://doi.org/10.1016/j.gsd.2024.101095

Veatch, A.C., 1906. Fluctuations of the Water Level in Wells, with Special Reference to Long Island, New York. Water Supply and Irrigation Paper No. 155.

Vermeer, P.A., Neher, H.P., 1999. A soft soil model that accounts for creep, in: Brinkgreve, R.B.J. (Ed.), Beyond 2000 in Computational Geotechnics. Routledge, pp. 249–261. https://doi.org/10.1201/9781315138206-24

Vinh, D.H., Tran, D.D., Cham, D.D., Hang, P.T.T., Man, D.B., Mon, D., Hai Tung, L., Kiem, L.V., Nguyen, T.D., Tuyen, D.T.N., 2024. Integrated Exploitation of Rainwater and Groundwater: A Strategy for Water Self-Sufficiency in Ca Mau Province of the Mekong Delta. Hydrology 11, 55. https://doi.org/10.3390/hydrology11040055

Vu, H.T.D., Tran, D.D., Schenk, A., Nguyen, C.P., Vu, H.L., Oberle, P., Trinh, V.C., Nestmann, F., 2022. Land use change in the Vietnamese Mekong Delta: New evidence from remote sensing. Sci. Total Environ. 813, 151918. https://doi.org/10.1016/j.scitotenv.2021.151918

Vu, H.T.D., Zemann, M., van der Linden, R., Dan, T.C., Oberle, P., Seidel, F., Nguyen, N.M., Tu, L.X., 2025. Modeling Ocean Wave Conditions at a Shallow Coast Under Scarce Data Availability: A Case Study in the Mekong Delta, Vietnam. https://doi.org/10.5445/IR/1000180356

Wagner, F., Tran, V.B., Renaud, F.G., 2012. Groundwater resources in the Mekong Delta: availability, utilization and risks, in: The Mekong Delta System: Interdisciplinary Analyses of a River Delta. Springer, pp. 201–220.

Worldbank, 2022. Climate resiliant rural water supply in the Mekong Delta - Situation analysis and vulnerability report.

Wu, J., Shi, X., Xue, Y., Zhang, Y., Wei, Z., Yu, J., 2008. The development and control of the land subsidence in the Yangtze Delta, China. Environ. Geol. 55, 1725–1735. https://doi.org/10.1007/s00254-007-1123-x

Xu, Z., Hariharan, J., Passalacqua, P., Steel, E., Paola, C., Michael, H.A., 2021. Linking the Surface and Subsurface in River Deltas—Part 2: Relating Subsurface Geometry to Groundwater Flow Behavior. Water Resour. Res. 57, e2020WR029281. https://doi.org/10.1029/2020WR029281

Xue, L., Brodsky, E.E., Erskine, J., Fulton, P.M., Carter, R., 2016. A permeability and compliance contrast measured hydrogeologically on the San Andreas Fault. Geochem. Geophys. Geosystems 17, 858–871. https://doi.org/10.1002/2015GC006167

Zoccarato, C., Minderhoud, P.S.J., Teatini, P., 2018. The role of sedimentation and natural compaction in a prograding delta: insights from the mega Mekong delta, Vietnam. Sci. Rep. 8, 11437. https://doi.org/10.1038/s41598-018-29734-7

Appendix A

First-author publications

A.1. Passive subsurface characterization in subsiding deltas: assessing land subsidence mitigation potential with frequency analyses of groundwater heads and superposing harmonic drivers (Dörr et al., 2025)

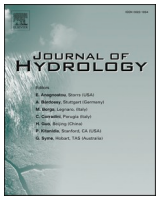
Journal of Hydrology 662 (2025) 133844



Contents lists available at ScienceDirect

Journal of Hydrology

journal homepage: www.elsevier.com/locate/jhydrol



Research papers

Passive subsurface characterization in subsiding deltas: assessing land subsidence mitigation potential with frequency analyses of groundwater heads and superposing harmonic drivers

Felix Dörr [a,*], Jonas Bauer [a], Gabriel C. Rau [b], Remi Valois [c], Tran Viet Hoan [a,d], Van Cam Pham [a], Le Thi Mai Van [d], Anke Steinel [e], Franz Nestmann [f], Stefan Norra [g]

[a] Karlsruhe Institute of Technology (KIT), Institute of Applied Geosciences, Kaiserstraße 12, 76131 Karlsruhe, Germany
[b] School of Environmental and Life Sciences, The University of Newcastle, Callaghan, Australia
[c] Avignon University, INRAE, UMR 1114 EMMAH, F-84000 Avignon, France
[d] National Center for Water Resources Planning and Investigation (NAWAPI), No. 93, Lane 95, Vu Xuan Thieu Street, Sai Dong Ward, Long Bien District, Hanoi 100000, Viet Nam
[e] Federal Institute for Geosciences and Natural Resources (BGR), Stilleweg 2, D-30655 Hannover, Germany
[f] Karlsruhe Institute of Technology (KIT), Institute of Water and River Basin Management, Kaiserstraße 12, 76131 Karlsruhe, Germany
[g] Potsdam University, Institute of Environmental Sciences and Geography, Soil Sciences and Geoecology, Campus Golm, Building 12, 14476 Potsdam Golm, Germany

ARTICLE INFO

This manuscript was handled by D. Han, Editor-in-Chief, with the assistance of Xiaolong Geng, Associate Editor

Keywords:
Mekong Delta
Ca Mau
Earth and ocean tides
Tidal subsurface analysis

ABSTRACT

Many of the world's low-lying river deltas are experiencing severe land subsidence, posing significant challenges to sustainable development. Effective mitigation strategies require a thorough understanding of subsurface processes and comprehensive parameterization, which are often hindered by limited investigations and resources. In this context, passive subsurface characterization (PSC) methods are particularly advantageous, as they utilize existing datasets to estimate hydraulic and geomechanical properties of the subsurface. This study conducts a detailed frequency analysis of 43 groundwater head time series in the southern Vietnamese Mekong Delta, revealing harmonic signals and imprints of mechanical loading in groundwater heads. These signals are identified as a superposition of five key drivers: (i) Earth tides, (ii) atmospheric tides, (iii) ocean tides, (iv) river tides, and (v) anthropogenic groundwater extraction. By disentangling Earth and ocean tides from atmospheric tides at the semi-diurnal frequency S_2, the specific storage and elastic formation compressibility of the intensely exploited middle Pliocene aquifer are estimated to 5.9–7.8 · 10^{-6} m^{-1} and 6.4–7.5 · 10^{-10} Pa^{-1}, respectively. This indicates a low land rebound and water storage potential and therefore an insignificant subsidence mitigation potential of this confined aquifer. By revealing that groundwater pumping may leak into amplitude spectra and corrupt quantitative PSC, this study underscores that accurate parameter estimations require a careful disentanglement of various superposing drivers. While the complex interplay of multiple tidal forcings limited previous PSC-applications in subsiding deltas, the novel integration of ocean tide loading on the solid Earth enables PSC-parameter estimations in coastal groundwater systems.

1. Introduction

Land subsidence is a geohazard of global scale and relevance, with nearly two billion people living in affected areas (Davydzenka et al., 2024). Groundwater over-exploitation has been identified as one of the main causes for intensive large-scale land subsidence (Motagh et al., 2008; Sun et al., 1999; Poland and Davis, 1969). Coastal plains and river deltas are particularly vulnerable to subsidence-induced land loss due to

Abbreviations: BE, barometric efficiency; FFT, fast Fourier transform; HALS, harmonic least squares; IGPVN, improvement of groundwater protection in Vietnam; MAR, managed aquifer recharge; NAWAPI, National Center for Water Resources Planning and Investigation, Vietnam; NGMN, National Groundwater Monitoring Network of Vietnam; OT_{SE}, ocean tide loading on the solid Earth; OT_{GW}, ocean tide loading on the aquifer's water; PSC, passive subsurface characterization; PT, pressure transducer; TSA, tidal subsurface analysis; VMD, Vietnamese Mekong Delta.

* Corresponding author.
E-mail address: felix.doerr@kit.edu (F. Dörr).

https://doi.org/10.1016/j.jhydrol.2025.133844
Received 18 February 2025; Received in revised form 11 June 2025; Accepted 5 July 2025
Available online 8 July 2025
0022-1694/© 2025 The Author(s). Published by Elsevier B.V. This is an open access article under the CC BY license (http://creativecommons.org/licenses/by/4.0/).

their low elevation, and their high demand for freshwater often results in depleting groundwater heads, leading to sediment compaction and causing subsidence (Gambolati and Teatini, 2021). In light of climate change, global economic and population growth, and a resulting increase of groundwater demand and depletion, land subsidence hazards must be expected to exacerbate within the next decades (Herrera-García et al., 2021).

As one of the world's largest deltaic lowlands, the southern Vietnamese Mekong Delta (VMD) is a prominent example for hazardous land subsidence dynamics due to groundwater overexploitation, with rates of more than 3 cm a^{-1} (Erban et al., 2014; Minderhoud et al., 2017; Dörr et al., 2024). Other deltas and their metropolitan cities like the Ganges-Brahmaputra Delta (Dhaka), the Mississippi Delta (New Orleans), the Nile Delta (Alexandria) and the Yangtze Delta (Shanghai) are further examples for deltaic lowlands suffering from land subsidence (Syvitski et al., 2009).

Land subsidence due to groundwater depletion may be mitigated to some extent. However, the effectiveness of mitigation measures varies between the affected regions. In some previously subsiding regions like Tokyo and Osaka, Japan (Sreng et al., 2011), as well as Taipei, Taiwan (Chen et al., 2007), a significant land rebound followed a natural recovery of groundwater heads after a substantial reduction of groundwater extraction. Besides natural groundwater recharge, the injection of water or other fluids into the aquifer, e.g. in the context of managed aquifer recharge (MAR), may yield in significant land rebound, as achieved in the Wilmington oil field, California (Gambolati and Teatini, 2021). In other previously subsiding regions with limited rebound capability, a reduction of groundwater withdrawal substantially reduced further land subsidence, for example in Venice, Italy (Gambolati and Teatini, 2021) and in Shanghai, China (Zhang et al., 2015). In confined aquifer systems, such as in the VMD, the land rebound potential depends on elastic aquifer properties (Allen and Mayuga, 1970) which can be derived from groundwater head responses to harmonic forcings (Merritt, 2004; Cutillo and Bredehoeft, 2011; Rau et al., 2020).

The responses of groundwater heads to external forcings such as barometric pressure variations or ocean tides have been recognized and described long ago (Klönne, 1880; Veatch, 1906) and are used to derive hydro-geomechanical subsurface parameters since the 1940's (Jacob, 1940). Barometric pressure and ocean tides are subject to periodic variations, enabling an assessment of these effects not only in the time domain but in the frequency domain as well. This is equally valid for the response of groundwater heads to Earth tides (Bredehoeft, 1967). Earth tides are caused by small but effectful variations of gravitational potential due to the movement of celestial bodies, inducing motions in the solid Earth (Agnew, 2007). With the given knowledge of the movement of celestial bodies, Earth tide strains can be calculated for any location on the earth's surface and for any point in time.

Since decades methods in time and frequency domain have been developed and improved to derive hydro-geomechanical subsurface parameters like the specific storage S_s (m^{-1}) and the aquifer compressibility α (Pa^{-1}) from groundwater responses to Earth and atmospheric tides, well summarized by Turnadge et al. (2019) and framed by the terms passive subsurface characterization (PSC) and tidal subsurface analysis (TSA). Particularly in the context of land subsidence mitigation, coastal plains and deltaic groundwater bodies would benefit from the application of PSC methods, given that the elastic compressibility of the subsurface is a proxy for (i) the contribution of elastic aquifer compaction to the overall observed subsidence, (ii) the mitigation potential in terms of land rebound capability (Allen and Mayuga, 1970) and (iii) the elastic aquifer storage and therefore the capability to temporarily receive and store surplus water resources by deformation of the aquifer material (Bouwer, 2002).

This study aims to demonstrate the potential of PSC for assessing land subsidence mitigation in deltaic lowlands by estimating elastic geomechanical properties. The southern VMD serves as an ideal study area due to three key factors: (i) tidal signals in groundwater heads have not yet been systematically described in the region, (ii) high land subsidence rates and ongoing land loss necessitate an urgent evaluation of subsurface properties and processes, and (iii) the superposition of multiple harmonic forcings provides a unique opportunity to apply PSC in a complex setting influenced by various tidal drivers. While the application of previous PSC methods was restricted in near-coastal aquifers, the novel integration of ocean tide loading on the solid Earth enhances PSC-parameter estimations in such hydrogeological systems. Therefore, the findings of this study highlight the utility of PSC and its potential applicability to other deltaic aquifer systems.

2. Study area

2.1. Land subsidence and water resources in the southern Vietnamese Mekong Delta

The VMD and its adjacent metropolis Ho Chi Minh City (Fig. 1) are home to more than 21 million people (GSOV, 2024) who have been facing local land subsidence rates >3 cm a^{-1} for several years, amounting to an existential crisis (Erban et al., 2014; Minderhoud et al., 2017; Dörr et al., 2024). With an average elevation of only 80 cm above sea level measured in 2018 (Minderhoud et al., 2019), such high rates of subsidence require an urgent investigation of the process dynamics, parametrization of subsurface properties and the assessment of potential mitigation strategies. Intensive groundwater overexploitation, leading to a continuous decline in groundwater heads throughout the confined multi-aquifer-aquitard system (Duy et al., 2021) and thus increases the effective stresses in the aquifer and aquitard sediments, is considered to be the greatest single driver for land subsidence in the VMD (Minderhoud et al., 2020; Kondolf et al., 2022). In addition, the construction of upstream reservoirs, dams and hydropower plants, along with sand mining activities in the rivers and channels, cause a sediment deficit in the delta plain, contributing to the overall subsidence by failing to compensate non-anthropogenic subsidence due to natural compaction processes of the young delta sediments (Kondolf et al., 2022; Baldan et al., 2024). Moreover, anthropogenic infrastructure, such as urban settlements, bridges and roads exert a surplus load on the subsurface causing localized compaction (Neussner, 2019; Dörr et al., 2021).

The VMD socio-economic activities are highly dependent on water resources, as it is one of Southeast Asia's most productive areas in terms of agricultural and aquacultural food production (Van et al., 2023; Thong et al., 2010; Nguyen et al., 2019). Groundwater resources are extracted at up to half a million licensed and especially non-licensed extraction wells (Danh and Khai, 2015). With increasing trends of surface water salinization and pollution as well as more pronounced droughts, groundwater remains a water resource of major relevance in the VMD (Pham et al., 2023), which is unlikely to be replaced by other water resources in the near future. Therefore, a continuous decline in groundwater heads is anticipated, resulting in further expected land subsidence (Minderhoud et al., 2020).

Due to the low and flat topography, the hydraulic gradients in the rivers are low, enabling upstream propagation of ocean tides, resulting in tidal fluctuations of inland river water levels and salinity (Eslami et al., 2019). In an attempt to control such sea water intrusion and minimize its impact on the tributary channels, sluice gates were constructed in the southern VMD (Di Giusto et al., 2021; Hoanh et al., 2009; Nguyen, 2020), operated on seasonal or tidal scale. Fig. 1 illustrates the southern VMD with its rivers and channel infrastructure, the location of sluice gates in Ca Mau Province and the overall low topography of the VMD.

The VMD's hydrogeological units have been classified into seven aquifers and seven aquitards (Fig. 2). The top Holocene aquitard Q_2 is likely to prevent significant groundwater recharge by infiltration into the Holocene aquifer qh, particularly in the southern VMD, where it has

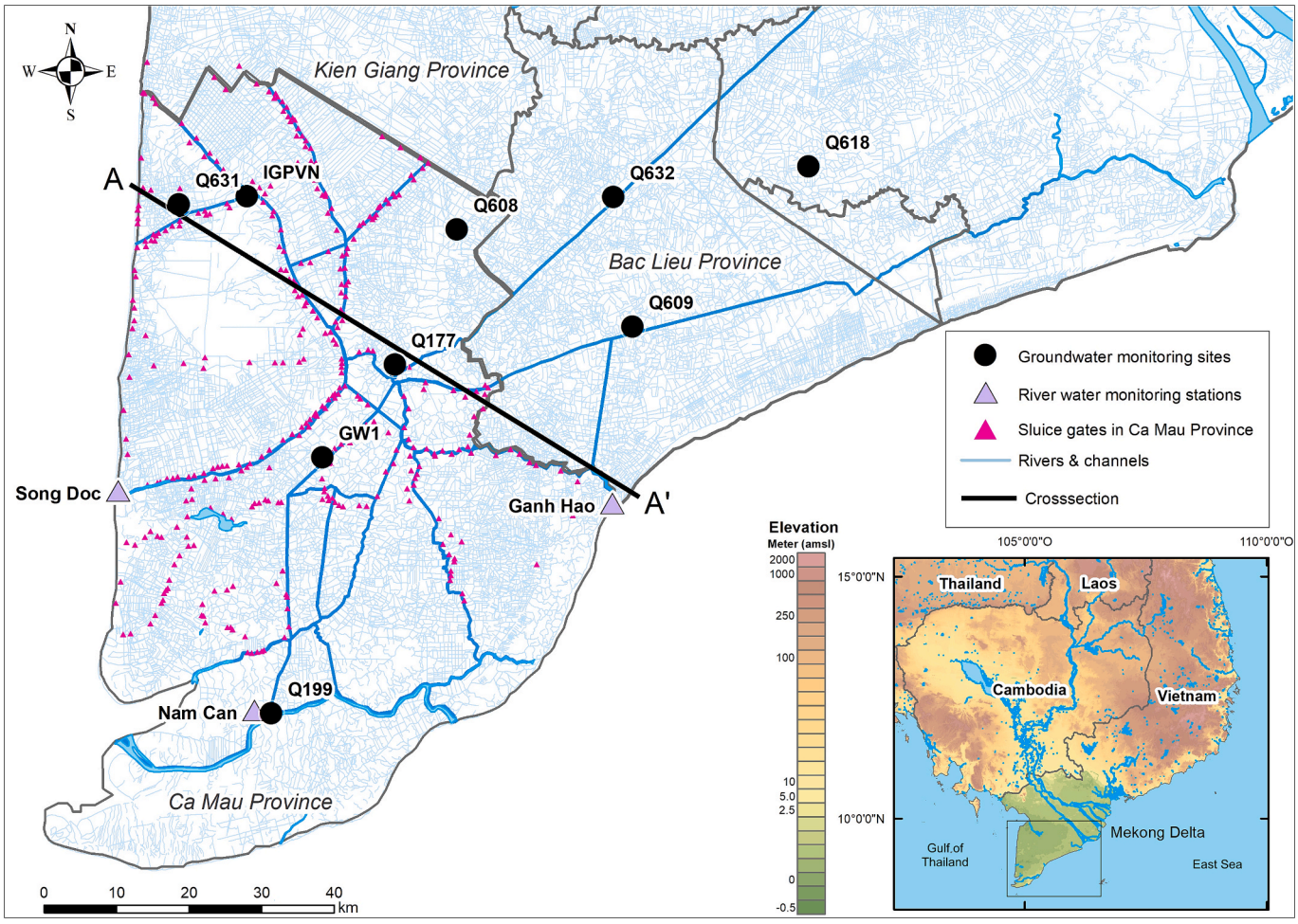


Fig. 1. Study area of the southern VMD, including the rivers and channels (bold and narrow blue lines), the location of the evaluated multi-depth groundwater and river water monitoring sites, and sluice gates in Ca Mau Province. Elevation data in the reference map are based on GTOPO30 (EROS, 2017) and locally for the VMD based on Minderhoud et al. (2019). (For interpretation of the references to color in this figure legend, the reader is referred to the web version of this article.)

a thickness of up to >20 m (Anderson, 1978; Pham et al., 2019; Bauer et al., 2022). At some locations, the qh aquifer is unconfined and hence capable of receiving groundwater recharge, for example, where sand dunes are present in the coastal provinces of Ben Tre, Tra Vinh and Soc Trang (Wagner et al., 2012). Early studies identified artesian conditions prior to significant anthropogenic groundwater extraction (Anderson, 1978), while ongoing groundwater monitoring in the last decade reveals depleting groundwater heads with rates of 0.01–0.55 m a^{-1} in the different aquifers (Duy et al., 2021). The upper, middle and lower Pleistocene aquifers qp_3, qp_{2-3} and qp_1 as well as the middle and lower Pliocene aquifers n_2^2 and n_2^1 and the upper Miocene aquifer n_1^3 are characterized by confined conditions. Fig. 2b illustrates a hydrogeological cross-section through the southern VMD, modified after Hoan et al. (2022). The introduced color code for the seven aquifers will be used henceforth in this study. The location of the cross-section line is marked in Fig. 1. In Fig. 2a, a detailed granulometry profile and the corresponding aquifer categorization of the IGPVN-monitoring site (location see Fig. 1) based on Pechstein et al. (2018) is presented. It shall be noted that the displayed granulometry of the Mesozoic basement (MZ) represents the crushed material rather than the undisturbed sediments. At that monitoring site, the aquifers n_2^1 and n_1^3 are not developed, and the development of the aquifers qh and qp_3 is not clearly distinguishable (Pechstein et al., 2018), indicated by the dashed blue section in the aquifer characterization in Fig. 2a.

2.2. Groundwater and surface water monitoring

The Vietnamese National Groundwater Monitoring Network (NGMN) provides a comprehensive dataset of groundwater head observations (i.e., as measured using well water levels) since the 1990s at numerous multi-depth monitoring sites in the VMD. Initially, these observations entailed manual measurements of groundwater heads on a daily to monthly basis. Since 2011, the NGMN has successively been enhanced by the installation of automated non-vented (i.e., absolute) pressure transducers (PTs) measuring groundwater heads at hourly resolution. The data obtained from the non-vented PTs is compensated for barometric pressure data recorded at each monitoring site by subtraction of the measured barometric pressure from the recorded absolute pressure (sum of water column and barometric loading) (NAWAPI, 2018).

The monitoring sites IGPVN and GW1 have been established by international research projects (IGPVN: Improvement of Groundwater Protection in Vietnam, Federal Institute for Geosciences and Natural Resources (BGR); GW1: ViWaT Engineering, Karlsruhe Institute of Technology (KIT)) complementing the NGMN-wells. At GW1, vented PTs were installed, at IGPVN non-vented PTs were replaced by vented PTs in 2021. Vented PTs are groundwater level sensors which are equipped with a venting tube that connects the submerged PT to the atmosphere, thus enabling a measurement of groundwater heads compensated for atmospheric pressure variations. Further clarification of the term barometric compensation as well as on measurement

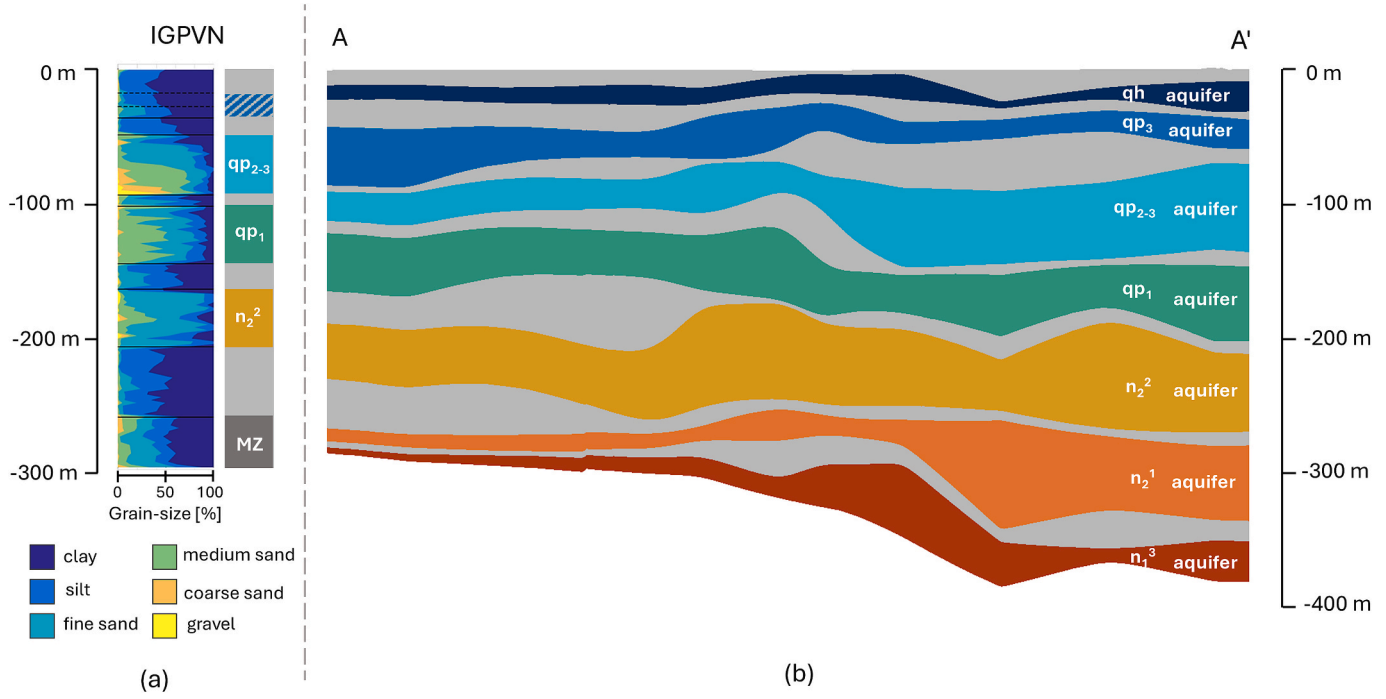


Fig. 2. Granulometry profile and aquifer-aquitard classification at the IGPVN monitoring site (Pechstein et al., 2018) (a) and hydrogeological cross section through the multi-layered aquifer-aquitard system of the southern VMD (Hoan et al., 2022) (b). The locations of the cross-section line and the IGPVN-monitoring site are marked in Fig. 1.

principles of vented and non-vented PTs is provided by Rau et al. (2019).

The IGPVN site comprises a total number of five observation wells, three of which are screened in the n_2^2 aquifer. For the observation wells IGPVN 1.3 ($qp_{2\text{-}3}$), IGPVN 1.2 (qp_1) and IGPVN 1 (n_2^2) data is available from 2016 until 2024, with one major gap of 13 months and several minor gaps. In n_2^2 aquifer two more observation wells IGPVN 1.1 and IGPVN 1.4 recorded groundwater heads from 2016 to 2020 with non-vented PTs. For an assessment of atmospheric loading at IGPVN, two different sources of barometric pressure data are available: (i) hourly barometric pressure records from the IGPVN site, which were also used for barometric compensation before 2021, when non-vented PTs were installed and (ii) hourly barometric pressure data from a meteorological station in Ca Mau City, situated in a distance of 30 km.

In the southern VMD, river water levels are recorded at three gauging stations: (i) Song Doc, located at the estuary of the Ong Doc river into the Gulf of Thailand in approximately 2 km distance to the coast, (ii) Ganh Hao, located at the estuary of the Ganh Hao river into East Sea in approximately 1 km distance to the coast and (iii) Nam Can, located in Nam Can Town in the Cửa Lớn river, a connecting river between the Gulf of Thailand and the East Sea.

In this study, groundwater head data of 35 NGMN wells from seven stations covering six different aquifers are used, as well as of five wells at IGPVN and three wells at GW1. Additionally, records of groundwater extraction rates from a municipal water supply well (G22) in Ca Mau City between December 2023 and January 2024 were provided by the Vietnamese National Center for Water Resources Planning and Investigation (NAWAPI). The location of the groundwater and river water monitoring stations used in this study are illustrated in Fig. 1.

3. Methods

3.1. Frequency analysis

To evaluate the response of groundwater heads to Earth tides, atmospheric tides, ocean tides or river tides, the underlying frequency patterns in the respective time series are analyzed by two independent methods: (i) the Fast Fourier Transform (FFT) and (ii) the harmonic least-squares (HALS) estimation. In FFT analyses, a given time series is decomposed into a linear sum of sinusoidal functions (Acworth et al., 2016), so that the Fourier transform $\mathscr{F}$ of the input signal $s(t)$ reads as

$$\hat{s}(f_k) = \mathscr{F}\{s(t_n)\} = \sum_{n=0}^{N-1} s(t_n) e^{-\frac{2\pi i k n}{N}} \tag{1}$$

where N is the number of observations, k is the frequency index, i is the imaginary unit, n the time index and

$$f_k = k f_s / N \tag{2}$$

with f_s as the sampling rate of the dataset. An alternative approach for the extraction of harmonic components is the application of a harmonic least squares (HALS) estimation (Agnew, 2007):

$$\min_{a_c, b_c} \sum_{n=1}^{N} \left[y_n(t_n) - \sum_{c=1}^{C} \left[a_c \cos(2\pi f_c t_n) + b_c \sin(2\pi f_c t_n) \right] \right]^2 \tag{3}$$

where N is the number of observations, t_n the time, and $y_n(t_n)$ the corresponding observation value, C is the total number of investigated harmonic components c, f_c is the frequency and a_c and b_c are the fitting coefficients.

Both methods yield in complex numbers, which can be decomposed into values of amplitude and phase for the considered frequency. The utilization of complex numbers $\hat{z}$ proves advantageous in the context of PSC analyses, as they encompass information on both the amplitude z and the phase shift ϕ. With the Eq. (4 [1-3]) any of the three values can be calculated from the other two:

$$\hat{z} = z \cdot e^{i\phi}; \quad \phi = \arg\hat{z}; \quad z = abs(\hat{z}) \tag{4 [1-3]}$$

The two methods vary in the requirement of input data quality, as FFT requires continuous data whereas HALS is capable of handling gaps (Schweizer et al., 2021). While FFT yields in amplitude spectra at a fine and constant frequency discretization f_k, HALS takes only predefined frequencies into consideration. Consequently, significant variations

between calculated FFT and HALS amplitudes may suggest that for the HALS analysis, not all relevant frequencies were considered. In this study, for any performed frequency analysis, both methods were applied for validation purposes. HALS outperforms FFT in terms of accuracy in amplitude and phase estimation and therefore is preferable to FFT in PSC (Schweizer et al., 2021). Thus, the amplitudes and phases obtained from HALS were used for the PSC-parameter estimations in this study. For the HALS analyses in this study, the ten most commonly investigated frequencies in groundwater analysis as listed in Table 1 were considered. In tidal analysis, frequencies with near-diurnal periodicity are commonly denoted in cycles per day (cpd).

For the FFT analyses, gaps were filled with an autoregression algorithm (*fillgaps*, MATLAB, 2023), which takes the frequency patterns within the datasets into consideration. To minimize the impact of interpolation on FFT results, subsets of the complete datasets with few or no gaps were selected. The subset durations vary between 0.4 and 5.1 years with an average of 3.1 years. After the selection of groundwater sub-datasets mostly minor gaps of a few hours, e.g. as caused by bi-annual groundwater sampling campaigns, remained and required interpolation. A summary of the subset employed for the frequency analyses and a visualization of the respective time series is provided in the Supplementary information. At all wells >99 % of the data utilized in the FFT analyses is original data with <1 % of interpolated values.

The analyzed river water levels were measured at irregular intervals, on average approximately 6 times per day, requiring an interpolation of a greater fraction of the dataset to obtain a dataset of hourly resolution and thus a more careful comparison of FFT and HALS based amplitudes in the frequency analyses.

3.2. Calculation of Earth and ocean tide strains

Volumetric Earth tide strains, denoted in nanostrain (nstr), were calculated at hourly resolution using *PyGTide* (Rau et al., 2022b), a Python wrapper for *ETERNA PREDICT 3.4* (Wenzel, 1996). Ocean tides may affect tidal signals in inland groundwater heads by two independent processes: (i) by ocean tide loading on the solid Earth (Agnew, 2012), further denoted as OT_{SE}, and (ii) by ocean tide loading on the aquifer's water (Jacob, 1950; van der Kamp, 1972), further denoted as OT_{GW}. OT_{SE} causes strain waves, which propagate from the ocean coast towards the inland by the geologic media, while OT_{GW} is a pressure wave that propagates from the ocean coast towards the inland by the liquid phase (pore water) only. The volumetric strains due to OT_{SE} are calculated with the Fortran-based software package *SPOTL* (Agnew, 2012) at hourly resolution. For an aquifer, which extends below the seabed, the amplitude damping of OT_{GW} in a coastal aquifer can be calculated with Eq. (5) (van der Kamp, 1972):

$$A_{gw}(x) = \frac{1}{2} A_{sw} \gamma e^{-\sqrt{\frac{\pi S_s}{K t_0}} x} \tag{5}$$

where A_{gw} (m) and A_{sw} (m) are the amplitudes in the groundwater and seawater respectively, x (m) is the distance to the shoreline, γ (−) is the uniaxial loading efficiency, t_0 is the tidal period (s), equal to the inverse of the frequency f_c, S_s (m^{-1}) and K ($m\ s^{-1}$) are the specific storage and the hydraulic conductivity of the considered aquifer. Given that the Gulf of Thailand is relatively shallow with an average depth of 45 m, and a maximum depth of 83 m (Aungsakul et al., 2007; Siripong, 1985), it can be reasonably assumed that the investigated aquifers with depths of 101–142 m and 161–202 m respectively at IGPVN extend below the seabed, allowing the application of Eq. (5) for the IGPVN monitoring site.

Table 1
Summary of the ten most relevant frequencies in groundwater analysis after Merritt (2004), McMillan et al. (2019) and Rau et al. (2020).

Darwin name	Frequency (cpd)	Earth Tides	Atmospheric Tides	Ocean and River Tides
Q_1	0.893244	Yes	–	Yes
O_1	0.929536	Yes	–	Yes
M_1	0.966446	Yes	–	Yes
P_1	0.997262	Yes	Yes	Yes
S_1	1.000000	–	Yes	–
K_1	1.002738	Yes	Yes	Yes
N_2	1.895982	Yes	–	Yes
M_2	1.932274	Yes	–	Yes
S_2	2.000000	Yes	Yes	Yes
K_2	2.005476	Yes	Yes	Yes

For the evaluation of the groundwater response to the total volumetric strain caused by OT_{SE} and Earth tides, the two strain time series can be added up to a single time series prior to the conducted frequency analysis. Alternatively, if the well water level response to Earth and ocean tide strains shall be disentangled, the two time series can be considered separately. In accordance with the harmonic addition theorem (Arfken and Weber, 2005), the amplitudes and phases obtained from the merged time series of Earth tides and OT_{SE} (denoted as the complex number $\hat{z}_{f_c}^{\{\mathrm{ET+OT}_{SE}\}}$) equals the sum of the separately calculated amplitudes and phases (each denoted as the complex numbers $\hat{z}_{f_c}^{\mathrm{ET}}$ and $\hat{z}_{f_c}^{\mathrm{OT}_{SE}}$):

$$\hat{z}_{f_c}^{\{\mathrm{ET+OT}_{SE}\}} = \hat{z}_{f_c}^{\mathrm{ET}} + \hat{z}_{f_c}^{\mathrm{OT}_{SE}} \tag{6}$$

It shall be noted here that, depending on the phase shift, amplitudes of Earth tides and OT_{SE} could either add up or counteract each other by causing constructive or destructive interference of the sinusoidal signals.

3.3. Disentanglement of Earth, ocean and atmospheric tides

For the determination of the barometric efficiency *BE* in the frequency domain, the response of groundwater heads to atmospheric tides at S_2 is evaluated. Given that S_2 is present in Earth, ocean and atmospheric tides (Table 1), the S_2 signal in the measured groundwater observation data $\hat{z}_{S_2}^{\mathrm{GW}}$ must be disentangled into its Earth and ocean tide component $\hat{z}_{S_2}^{\mathrm{GW}\cdot\{\mathrm{ET+OT}_{SE}\}}$ and its atmospheric component $\hat{z}_{S_2}^{\mathrm{GW}\cdot\mathrm{AT}}$. Eq. (7) is an adaptation of the formulation by Rau et al. (2020) under additional consideration of ocean tide strains:

$$\hat{z}_{S_2}^{\mathrm{GW}\cdot\mathrm{AT}} = \hat{z}_{S_2}^{\mathrm{GW}} - \hat{z}_{S_2}^{\mathrm{GW}\cdot\{\mathrm{ET+OT}_{SE}\}} = \hat{z}_{S_2}^{\mathrm{GW}} - \frac{\hat{z}_{M_2}^{\mathrm{GW}}}{\hat{z}_{M_2}^{\{\mathrm{ET+OT}_{SE}\}}} \hat{z}_{S_2}^{\{\mathrm{ET+OT}_{SE}\}} \tag{7}$$

The hat denotation indicates complex numbers. After the disentanglement of Earth, ocean and atmospheric tide signals, the barometric efficiency based on the S_2 response of groundwater heads to atmospheric tides $BE_{S_2}^{AT}$ can be calculated after Rau et al. (2020) with Eq. (8) as:

$$\mathrm{BE}_{S_2}^{\mathrm{AT}} = \frac{1}{A_{S_2}^{r}} \mathrm{abs}\left[\frac{\hat{z}_{S_2}^{\mathrm{GW}\cdot\mathrm{AT}}}{\hat{z}_{S_2}^{\mathrm{AT}}}\right] \tag{8}$$

with the amplitude response $A_{S_2}^{r}$ between well water levels and the actual aquifer pore pressure. $A_{S_2}^{r}$ is a function of well and aquifer parameters and can be calculated by using the python package *HydroGeoSines* (HGS, 2023).

3.4. Calculation of formation compressibility and specific storage

In unconsolidated systems like the sedimentary aquifers of the southern VMD, grain compressibility can commonly be neglected as it is much smaller than bulk compressibility (Rau et al., 2022a), so the uniaxial loading efficiency γ (−) and the barometric efficiency *BE* (−) can be expressed with Eq. (9) when undrained conditions are considered for the hydraulic head oscillation at subdiel frequencies (1–2 cpd) (Acworth et al., 2016; Jacob, 1940; van der Kamp and Gale, 1983):

$$BE = 1 - \gamma = 1 - \frac{\alpha}{\theta \cdot \beta + \alpha} \quad (9)$$

α as the formation compressibility (Pa^{-1}), β as the water compressibility ($4.59 \cdot 10^{-10}$ Pa^{-1} at 20 °C for water) and θ (−) as the aquifer porosity. Consequently, once BE and θ have been defined, the compressibility α can be calculated. By considering α as the drained compressibility, the specific storage S_s can be calculated with Eq. (10) (Cooper, 1966; Acworth et al., 2016):

$$S_s = \rho_w g(\theta \cdot \beta + \alpha) \quad (10)$$

ρ_w as the water density (kg m^{-3}) and g as the gravity constant (m s^{-2}) and the assumption of incompressible grains.

Forced by harmonic drivers like Earth or atmospheric tides, a flow between the aquifer and well is induced, that can be used to derive subsurface parameters including the specific storage S_s (Rojstaczer, 1988; Bredehoeft, 1967; Hsieh et al., 1987). Analytic solutions for such groundwater flow problems have been derived for confined conditions (Hsieh et al., 1987) and semi-confined conditions (Rojstaczer, 1988) as a function of well and aquifer parameters, which can be calculated with the python package *HydroGeoSines* (HGS, 2023). The sign of M_2 phase shift $\Delta\phi_{M_2}$(°) between Earth tides and groundwater heads bares information about the flow condition in the absence of borehole skin effects (Valois et al., 2022). For example, a positive M_2 phase shift is indicative of vertical flow as given in the presence of vertical drainage from an overlying aquitard. Conversely, a negative M_2 phase shift could indicate horizontal flow in and out of the well, suggesting fully or semi-confined conditions (Rojstaczer, 1988; Rau et al., 2020; Roeloffs et al., 1989; Xue et al., 2016; Valois et al., 2022). This differentiation, derived from considerations of Earth tides as single drivers for subsurface strains, is equally applicable regardless of the total volumetric strain's origin, i.e., the sum of Earth tide strains and OT_{SE}.

The compaction η (m) of a single confined aquifer can be calculated as the product of the aquifer thickness b (m), the compressibility α (Pa^{-1}), and the change in the effective intergranular stress $\Delta\sigma_z$ (Pa) (Gambolati and Teatini, 2021) to:

$$\eta = b \cdot \alpha \cdot \Delta\sigma_z \quad (11)$$

where $\Delta\sigma_z$ can be calculated from the piezometric decline of water level in the confined aquifer Δz (m) to:

$$\Delta\sigma_z = \rho_w \cdot g \cdot \Delta z \quad (12)$$

3.5. Identification of dominant drivers

For assessing the dominant drivers for the tidal signals in groundwater heads, the S_2 and M_2 ampltiude values as well as the ratio of S_2 and M_2 amplitudes are considered. Given that the S_2 amplitude in atmospheric tides is commonly below 15 mm (Ray and Ponte, 2003) and the diurnal M_2 and S_2 amplitudes in groundwater responses to Earth tides are commonly in a range of maximum 10–20 mm (Bredehoeft, 1967), S_2 and M_2 amplitudes significantly beyond these ranges indicate the presence of additional drivers. In the presence of dominant ocean or river tide loading, the S_2 and M_2 amplitudes in groundwater heads are expected to exceed the aforementioned ranges and occur in a ratio close to that of the driver's amplitudes (Patton et al., 2021). If the groundwater heads are characterized by high S_2 and low M_2 amplitudes, ocean or river tides are unlikely to be the dominant drivers, indicating that other drivers are at play.

3.6. Summary of workflow and applied methods

The presented study utilizes time series of observed groundwater heads, computed subsurface strains due to Earth tides and ocean tide loading on the solid Earth (OT_{SE}), observed barometric pressure, inland river water levels, ocean water levels (derived from estuary river water level observations) as well as groundwater extraction rates and pumping well water level dynamics, for comprehensive frequency analyses. The identified amplitude characteristics of groundwater observation wells are discussed as evidence for the presence of loading signals in groundwater head timeseries. The ratio of M_2 and S_2 amplitudes are used to identify groundwater head timeseries where ocean tides, river tides or groundwater extraction dominate the groundwater amplitude spectra. After a site-specific assessment of potential further forcings, the S_2 signal in groundwater is disentangled into its barometric-, Earth tide- and OT_{SE}–components at a selected groundwater monitoring site. Based on that, the elastic specific storage is derived and discussed as a proxy for elastic compaction, water storage and land rebound potential in the context of land subsidence mitigation measures. Fig. 3 presents a flow chart of the study's methodological approach.

4. Results

4.1. Tidal signals in groundwater and surface water levels

A regional frequency analysis of groundwater heads reveals the presence of distinct amplitudes at characteristic frequencies like S_2 and M_2 with varying intensity. Fig. 4 summarizes the FFT amplitude spectra annotated with HALS amplitudes of the regional frequency analysis, calculated with Eqs. (1)–(3). The analysis shows a good agreement between the HALS-based and FFT-based calculated S_2 and M_2 amplitudes. Note that individual tidal components surrounding 1.00 cpd are not attributed to a specific frequency (e.g., S_1, P_1 and K_1) as they are too close to each other (Table 1) and a differentiation between these frequencies is not considered in this work.

The frequency analyses of recorded river water levels from Ganh Hao (Fig. 5a), Nam Can (Fig. 5b) and Song Doc (Fig. 5c) reveal distinct tidal signals at all three gauging stations with unique amplitude distributions. At Ganh Hao, the tidal regime is characterized by dominant semi-diurnal frequencies with an M_2 amplitude of 925 mm and a K_1 amplitude of 649 mm (Fig. 5a-III). In contrast, at Song Doc, the amplitude at the diurnal frequency K_1 is most pronounced with 226 mm, while the amplitude at the semi-diurnal frequency M_2 is with 111 mm lower (Fig. 5c-III). At Nam Can, the tidal regime is characterized by M_2 amplitudes of 603 mm and K_1 amplitudes of 455 mm (Fig. 5b-III).

Due to the superposition of two different ocean tide regimes from the East Sea and the Gulf of Thailand, Nam Can is characterized by a distinct and unique amplitude distribution which noticeably differs from Ganh Hao and Song Doc. For all three datasets, the HALS-based amplitudes (considering only the irregularly measured raw data) and the FFT-based amplitude spectra (considering the hourly interpolated data) show a good agreement, suggesting that the interpolation of gaps (Fig. 5a-II–c-II) represent the actual river water level dynamics well.

4.2. Characterizing the drivers of tidal signals in groundwater heads

In a preliminary assessment of the dominant drivers of the tidal signals in groundwater heads, the M_2 and S_2 amplitudes obtained from the HALS analyses are summarized in Fig. 6. This preliminiary assessment indicates that the M_2 and S_2 amplitudes of the majority of wells are below 10 mm and thus comply with the range commonly found within impact of Earth tides of approximately maximum 10–20 mm (Bredehoeft, 1967) and atmospheric tides of approximately 15 mm (Ray and Ponte, 2003). However, the potential influence of river or ocean tides, as well as potentially periodic groundwater extraction patterns, cannot be excluded for those locations without a site-specific assessment of the local conditions. In contrast, the M_2 and S_2 amplitudes at the observation wells at the monitoring site Q199, as well as at two observation wells at the monitoring site Q177 and one monitoring well at IGPVN exceed the typical ranges of amplitude responses for Earth and atmospheric tides (Bredehoeft, 1967; Ray and Ponte, 2003), indicating the presence of additional tidal forcings.

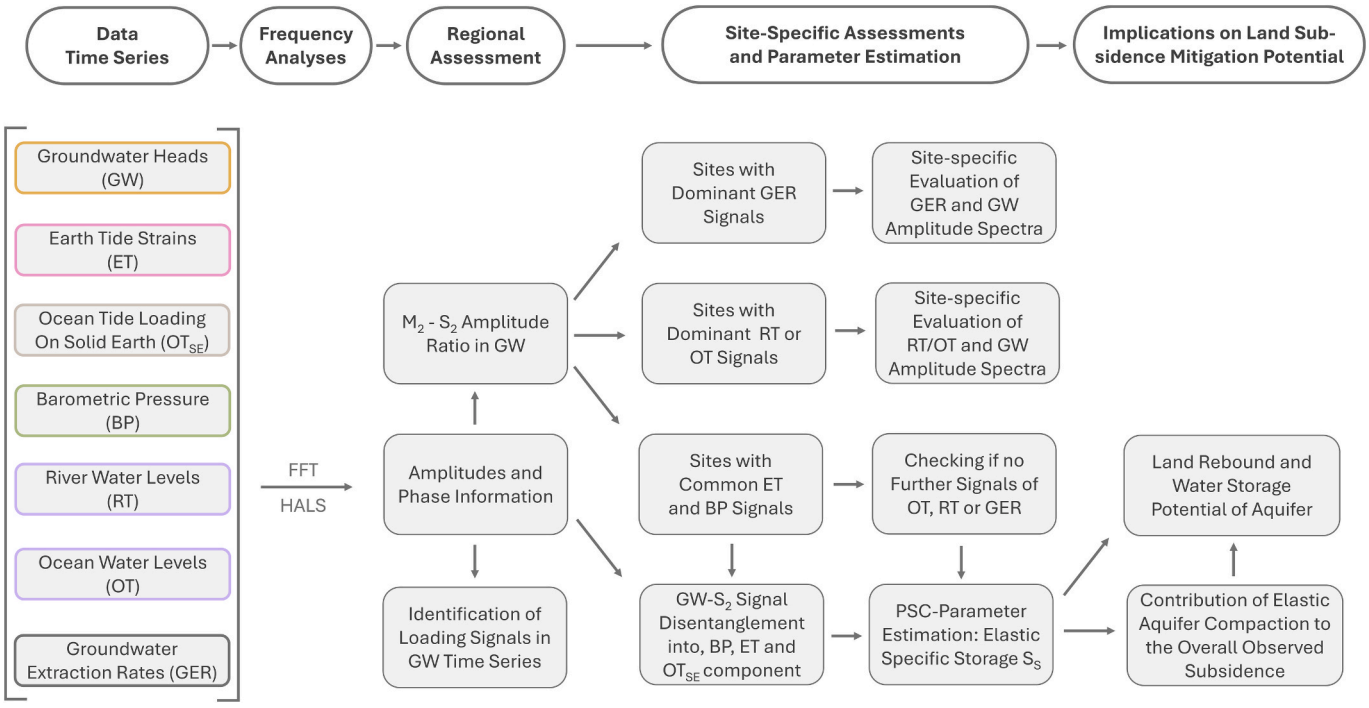


Fig. 3. Overview of the datasets and the workflow that was applied to evaluate and disentangle tidal loading signals and reveal geomechanical properties of the coastal groundwater system in the southern VMD.

At the monitoring sites Q177 and IGPVN some observation wells exhibit uncharacteristically high S_2 amplitudes, while the M_2 amplitudes do not exceed the typical response to Earth tides, indicating that an additional forcing without a M_2 frequency is at play. For those wells, a detailed assessment of the observed groundwater heads in the time domains reveals that the water level fluctuations are induced by periodic groundwater extraction patterns. Q177 is located in 475 m distance to a municipal water supply well (G22) screened in $n2^2$ aquifer, which operates at scheduled intervals. Fig. 7d illustrates the evident correlation of groundwater head variations at Q177 in the $n2^2$ aquifer and the groundwater extraction patterns from G22 (also from $n2^2$ aquifer), characterized by a recovery of groundwater heads in the night, when the operation of the water supply wells is paused. It shall be noted here that the apparent lead of groundwater drawdown and recovery of 3 h compared to the extraction rates in Fig. 7d is considered to be due to a time offset in one of the two recorded datasets.

Fig. 7e visualizes the recorded groundwater heads in the pumping well G22 for the available four-weeks interval between December 2023 and January 2024 showing a drawdown of 4.0 m when the pumping well is operated. The FFT-amplitude spectra of the groundwater heads in the pumping well G22 and in the observation well at Q177 are visualized in Fig. 7f, showing a similar frequency response of both wells, characterized by amplitude peaks at harmonics of S_1 at multiples of 1.00 cpd.

Fig. 7b shows that for the observation well at Q177 in $n2^2$ aquifer, in February and May 2018, the overall groundwater fluctuation magnitude drops from approximately 0.6 m–0.2 m. A similar temporal variation can be observed in qp_1 aquifer at Q177 (Fig. 7c), where between January and May 2022 the overall groundwater fluctuation magnitude is temporarily low and shows a sudden increase after May 2022. This incontinous magnitude in the well water level fluctuations at Q177 in qp_1 and $n2^2$ indicate the presence of anthropogenic influence on the well water level fluctions.

Similarly, the periodic groundwater head variations in the observation well IGPVN 1.2 (qp_1) can be considered to be induced by periodic groundwater extraction patterns of a local water supply well, which is located in 820 m distance, screened in qp_1 aquifer with a licensed pumping rate of 275 $m^3\ d^{-1}$ (Pechstein et al., 2018). Pechstein et al. (2018) had concluded too, that groundwater extraction patterns are the drivers for the strong water level fluctuation in IGPVN 1.2, substantiated by an evaluation of water level variations during a short power blackout, when the water supply well's operation paused off schedule. The close-up visualization of IGPVN 1.2 (qp_1) in Fig. 10f-II underlines that the fluctuations of groundwater heads are caused by non-natural drivers, showing an irregular temporal variation which cannot be attributed to natural processes like Earth and atmospheric tide forcings.

The preliminary assessment of potential drivers (Fig. 6) suggests that ocean or river tide loading are dominant at Q199, given that both, M_2 and S_2 amplitudes exceed the range of common groundwater response to Earth or atmopheric tides. A site-specific analysis reveals that the monitoring site Q199 in Nam Can town is located in less than 100 m distance to the Cửa Lớn river (Fig. 8c). A comparison of the amplitude spectra of groundwater and river water levels (Fig. 8a and b) shows a clear correlation with an average ratio of 1:0.16 between water level amplitudes in the river and in the observation well (Fig. 8d).

4.3. *Disentanglement of well water level responses to harmonic forcings*

In a first step, the presence of OT_{GW} is assessed with Eq. (5) for the monitoring site IGPVN, considering the site's distance to the coast of $x = 15$ km, as well as a hydraulic conductivity and specific storage of $1.1 \cdot 10^{-4}$ m s^{-1} and $6.3 \cdot 10^{-6}$ m^{-1} respectively for the $n2^2$ aquifer (Pechstein et al., 2018). A loading efficiency of $\gamma = 1$ is assumed, to calculate the maximum of expectable OT_{GW} under consideration of the aforementioned parameters. The ocean tide amplitudes (Fig. 9a) were derived from the amplitude spectrum at Song Doc (Fig. 5c-III), representing a good proxy for the ocean tides in the Gulf of Thailand due to its close vicinity to the coast and its good agreement with general tidal characterization of the Gulf of Thailand (Aungsakul et al., 2007; Cui et al., 2019).

Fig. 9b shows the damping of the three strongest ocean tide amplitudes at M_2, K_1 and O_1 frequency, yielding in insignificant OT_{GW} amplitudes (<0.01 mm) at 6.4 km inland and thus being negligible at IGPVN, located 15 km inland. On the contrary, OT_{SE} is not negligible at IGPVN with a volumetric strain amplitude of 2.0 nstr at M_2 (Fig. 10b-III

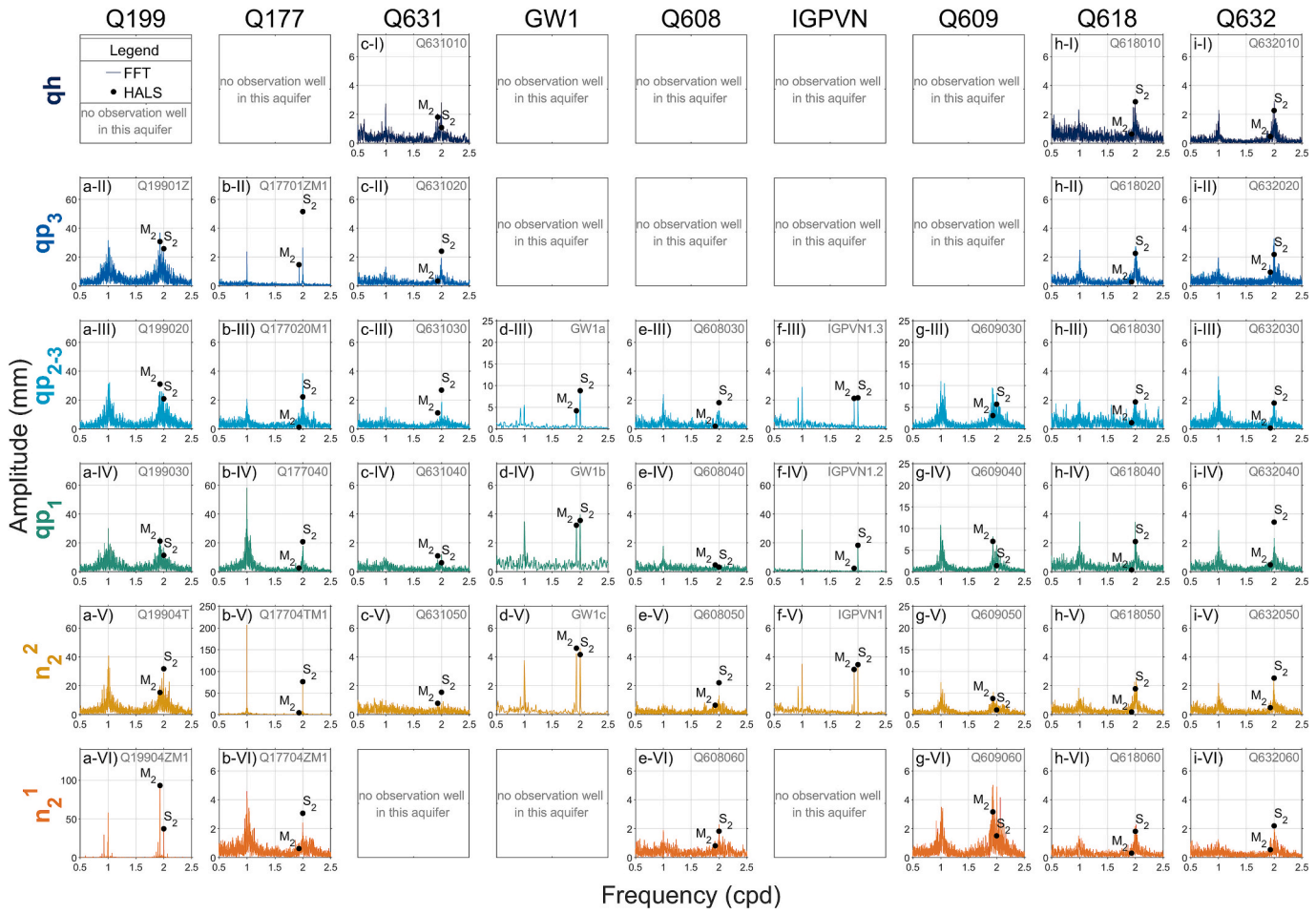


Fig. 4. Frequency analysis of 41 well water level time series in the southern VMD with FFT amplitude spectra (lines) and HALS amplitudes (calculated for the 10 frequencies listed in Table 1, displayed for M_2 and S_2 frequency as dots). The location of the nine multi-depth monitoring sites is shown in Fig. 1. It should be noted that the visualization encompasses distinct y-axis categories, namely 7.5 mm, 25 mm, 75 mm, 125 mm and 250 mm.

and b-IV). For IGPVN, no water level data of rivers or channels in the vicinity is available. Given that the site is located at the border of the freshwater area of U-Minh and the nearby channels are protected from saltwater intrusion and tidal propagation by sluice gates (Fig. 1), river tides are considered as negligible drivers for groundwater heads at IGPVN in this study.

All analyzed data are presented in Fig. 10a-I–i-I, comprising volumetric Earth tide strains (Fig. 10a-I), volumetric strains due to OT_{SE} (Fig. 10b-I), barometric pressure (Fig. 10d-I) and groundwater heads in five observation wells, screened in three aquifers (Fig. 10e-I–i-I). A close-up visualization of the data for a 12-day period in Fig. 10a-II–i-II illustrates the periodic character of each dataset. From a comparison of the measured groundwater heads in the three aquifers (Fig. 10e-II–i-II) no significant effect of the periodic groundwater extraction from qp_1 can be inferred in the adjacent aquifers. Fig. 10a-III–i-III and a-IV–g-IV illustrate the amplitude spectra for 2018 (with non-vented PTs) and 2023 (with vented PTs), both periods are marked in grey in Fig. 10a-I–i-I.

The calculated M_2 amplitudes and phases of the individual volumetric strains due to Earth tides and OT_{SE} as well as their sum are visualized in Fig. 11. The additional consideration of OT_{SE} yields in an increase of the total volumetric strain amplitude at M_2 from 17.0 nstr to 18.6 nstr and a phase shift of 3.6° compared to a consideration of Earth tide strains only.

4.4. Estimation of specific storage and compressibility

For the calculation of the barometric efficiency *BE*, atmospheric tides were disentangled from Earth and ocean tides with Eq. (7) for the monitoring site IGPVN. $A^r_{S_2}$ was calculated to $A^r_{S_2} > 0.99$ for all assessed well water level time series, indicating an insignificant difference between well water levels and pore pressure heads in the surrounding aquifer. The calculated barometric efficiency for the non-vented and vented dataset of observation wells yields in consistent results with $BE = 0.19 \pm 0.02$ in n_2^2 aquifer. Calculation results for the observation well in $qp_{2\text{-}3}$ vary between $BE = 0.12$ and $BE = 0.19$ for the assessed periods of 2018 (non-vented) and 2023 (vented).

In 2023, the phase shift between $BE^{AT}_{S_2}$ in $qp_{2\text{-}3}$ aquifer and the atmospheric driver is with 17° (Fig. 12b-II) significantly greater than the respective phase shift in all four assessed observation wells in 2018 (Fig. 12b-I). For the observation well in qp_1, $BE^{AT}_{S_2}$ was not calculated, given that the S_2 amplitude in groundwater heads is distorted significantly by anthropogenic groundwater extraction patterns (Fig. 7). The calculated barometric efficiency $BE^{AT}_{S_2}$ is summarized in Table 2, alongside with the M_2 amplitude response to Earth tide strains and OT_{SE} (denoted as A_{M2}) and the respective phase shift $\Delta\phi_{M2}$. In Fig. 12 the results are visualized as polar plots.

The M_2 amplitude responses to volumetric strains reveal a variation of 6 % ($\Delta = 0.006$ mm/nstr) at IGPVN 1.3 ($qp_{2\text{-}3}$), 13 % ($\Delta = 0.014$ mm/nstr) at IGPVN 1.2 (qp_1) and 3 % ($\Delta = 0.004$ mm/nstr) at IGPVN 1 (n_2^2) between the vented and non-vented periods, 2018 and 2023. For the calculated *BE*, the variation between the vented and non-vented dataset is 7 % ($\Delta = 0.014$ mm/mm) at IGPVN 1. Given the uncharacteristically high S_2 phase shift of 17° (Fig. 12b-II), the calculated *BE* at IGPVN 1.3 is

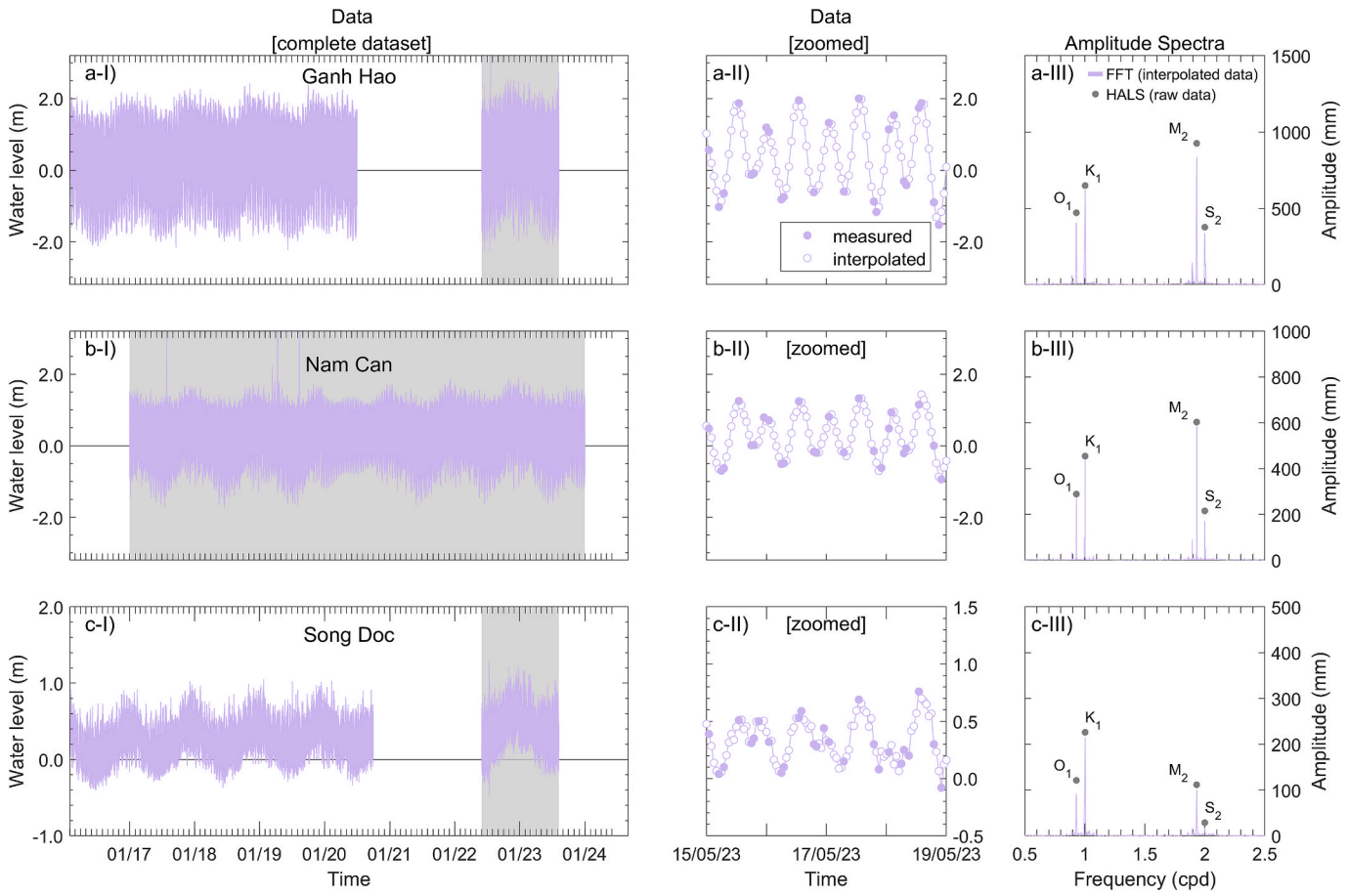


Fig. 5. Frequency analysis of river water levels at Ganh Hao (a), Nam Can (b) and Song Doc (c), including a visualization of the measured river water levels between 2016 and 2024 (I), a close-up visualization of a 4-day period (II), FFT amplitude spectra (lines), and HALS amplitudes (calculated for the 10 frequencies listed in Table 1, displayed for O_1, K_1, M_2 and S_2 frequency as dots) (III). The time periods used for the frequency analyses are highlighted in grey in (I) and were chosen according to the gaps and measurement frequencies in the datasets.

considered to be afflicted by the periodic groundwater extraction patterns in qp_1 and therefore not representative for a comparison. The calculation results indicate a positive M_2 phase shift of 0.9° for IGPVN 1.2 in qp_1 for 2023 (vented) while it was negative in 2018 (non-vented) (Fig. 12a-I and a-II).

The calculated M_2 phase shift between groundwater heads and volumetric strains due to Earth tides and OT_{SE} is negative in $qp_{2\text{-}3}$ and n_2^2 aquifer, indicating horizontal flow between well and aquifer to be dominant. For such flow conditions, the analytical solution of Hsieh et al. (1987) can be applied to calculate the specific storage S_s from well water level responses to volumetric strains without a requirement of a priori information on porosity. This method was applied as implemented in *HydroGeoSines* (HGS, 2023).

At IGPVN, the porosity in $qp_{2\text{-}3}$ and n_2^2 aquifer was determined to $\theta = 0.33$ for both aquifers based on grain size analysis in previous studies (Pechstein et al., 2018). The availability of porosity data allows an alternative calculation of α and S_s based on *BE* with Eqs. (9) and (10). The calculation results for S_s after Hsieh et al. (1987) are summarized in Table 3 alongside the calculation results of S_s based on *BE* with Eqs. (9) and (10). The difference in the S_s estimates of these two passive methods is small (Table 3). More importantly, the results of both passive methods ($5.9\text{–}7.8 \cdot 10^{-6}$ m^{-1}) comply well with S_s estimates from a pumping test conducted independently in the n_2^2 aquifer ($6.3 \cdot 10^{-6}$ m^{-1}, refer to Pechstein et al., 2018). While no hydraulic test was available for the $qp_{2\text{-}3}$ aquifer, the results comply well with regional aquifer parametrization of the study area (DWRPIS, 2010; Pechstein et al., 2018).

From the results in Table 3, the elastic compressibility can be calculated with Eq. (10) as $\alpha = 6.4\text{–}7.5 \cdot 10^{-10}$ Pa^{-1} in $qp_{2\text{-}3}$ and $\alpha = 4.5\text{–}6.4 \cdot 10^{-10}$ Pa^{-1} in n_2^2 aquifer. With thicknesses of $b = 41$ m of each aquifer (Pechstein et al., 2018), an elastic compaction (rebound) η of 0.18–0.30 mm per depletion (recovery) of hydraulic head $\Delta z = 1$ m can be derived for the two considered aquifers from Eqs. (11) and (12).

5. Discussion

5.1. Identification of tidal signals and loading imprints

As shown in the regional frequency analysis presented in Figs. 4 and 6, the groundwater heads in all assessed observation wells in the southern VMD respond to natural forcings, i.e. at M_2 and S_2 frequencies. In the study area, these tidal signals can be attributed to ubiquitous signals of atmospheric loading and Earth tide strains as well as site-specific conditions, such as river tides (Fig. 8), ocean tides (Fig. 11) and periodic groundwater extraction patterns (Fig. 7). The identification of harmonic signals in groundwater heads at S_2 and M_2 frequencies provides compelling evidence that the assessed aquifers in the southern VMD respond to external loading. This finding is not limited to the frequency domain but is evident in the time domain as well, providing a scientific framework for the conclusions of Hoang and Steinel (2021) who attribute temporarily rising groundwater heads at IGPVN during the rainy season to loading effects rather than to groundwater recharge by the means of water volume fluxes into the aquifers. However, to evaluate this specific hypothesis, further studies on seasonal surface loading dynamics are necessary.

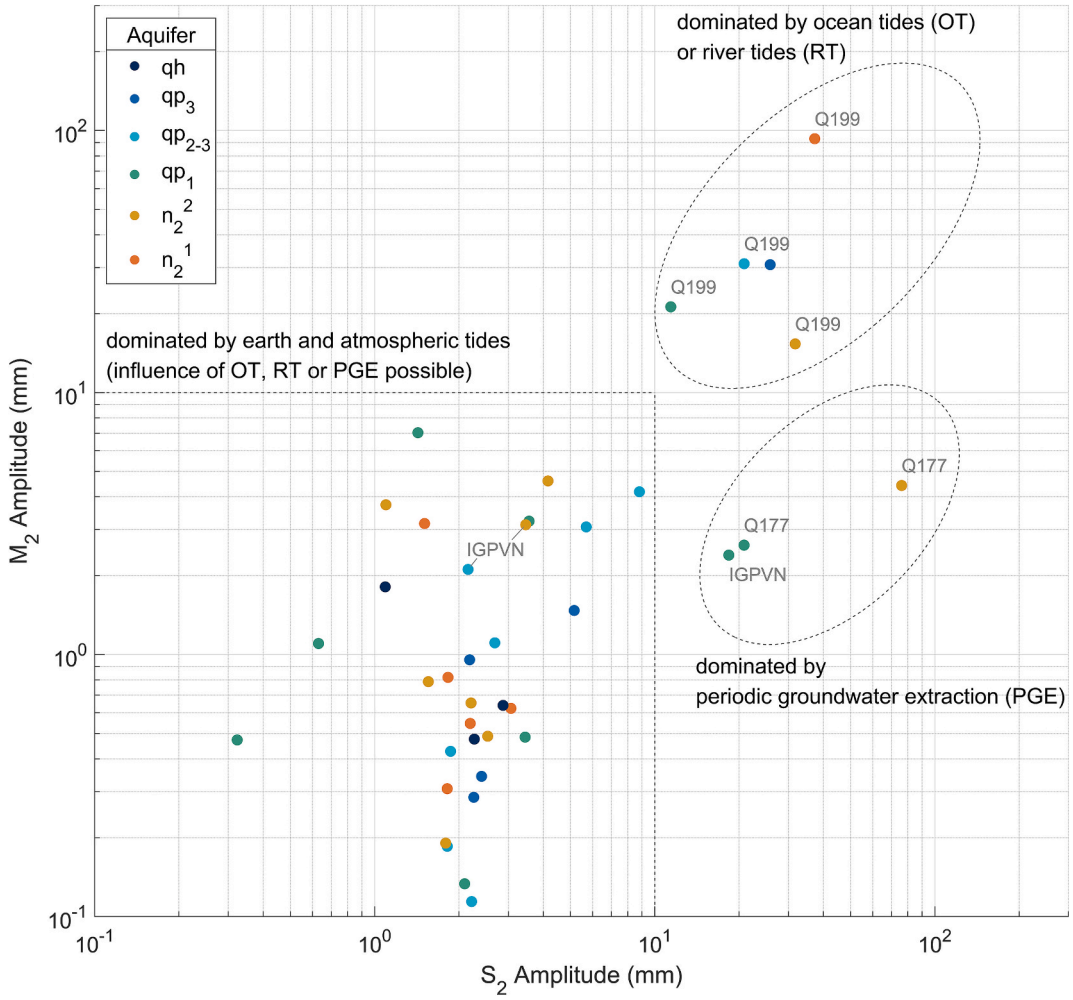


Fig. 6. Preliminary assessment of potential drivers of tidal signals in groundwater heads by a comparison of value and ratio of S_2 and M_2 amplitudes from HALS frequency analyses of 41 observation wells in six different aquifers in the southern VMD.

While the presence of loading signal imprints in groundwater heads is a common feature for confined aquifers (Bredehoeft, 1967), to the authors' best knowledge they have not yet been comprehensively described in the southern VMD. Therefore, the presented study establishes a valuable basis for further research on hydro-geomechanically coupled process dynamics in the study area. By this, the study promotes integrated considerations of hydrogeological and geomechanical problems, of which the observed land subsidence due to groundwater depletion itself is the most prominent example in the study area. In addition, the findings provide a novel perspective on previous studies in the VMD (Duy et al., 2021), which found correlations between ground and surface water levels, without exploring the nature and process dynamics causing the identified correlation.

The southern VMD is a unique study area for PSC-applications in the context of land subsidence due to its complex network of tidally influenced surface water bodies, extensive groundwater extraction and the presence of two distinct ocean tide regimes (Fig. 5). In addition, due to extensive and accelerating land subsidence rates in the low-lying delta, there is an urgent need for hydro-geomechanical subsurface characterization to develop mitigation strategies. If the multiple superposing drivers are carefully disentangled as proposed in this study, the southern VMD and other deltaic groundwater systems bare a high potential to utilize the various tidal forcings for hydro-geomechanical parameter estimations.

5.2. Revelation of multiple influences on groundwater heads

The analyses show that amplitude spectra of groundwater heads can be affected by periodic groundwater extraction patterns (Fig. 7). Demand-oriented operation of municipal water supply wells at scheduled intervals are non-sinusoidal but can leak into FFT-amplitude spectra (Fig. 7f, lines in Fig. 4b-V) at harmonics, i.e., multiples of S_1 and S_2, as well as into HALS-based amplitude characterizations, e.g. at S_2 (dot in Fig. 4b-V). Given that these frequencies are commonly used in PSC, this novel finding highlights the need for careful site-specific analysis prior to PSC applications in densely populated regions with high freshwater demands, such as coastal plains and deltaic lowlands. In the VMD, where up to half a million licensed and unlicensed wells extract groundwater with significant spatiotemporal variability (Danh and Khai, 2015), the potential influence of groundwater extraction patterns on tidal groundwater heads must be carefully considered. Recent applications of time-domain PSC methods have anticipated the effects of groundwater extraction on tidal constituents in groundwater heads (Haehnel et al., 2024). However, to the best of the authors' knowledge, the impact of groundwater extraction patterns on PSC has not yet been demonstrated using actual observational data.

The presented novel approach illustrates that integrating OT_{SE} into PSC enhances the application of PSC in coastal groundwater systems and deltaic lowlands. Here, the consideration of OT_{SE} results in a 10 % increase of volumetric strain from 17.0 nstr to 18.6 nstr and a M_2 phase shift of 3.6° compared to the consideration of only Earth tide strains at

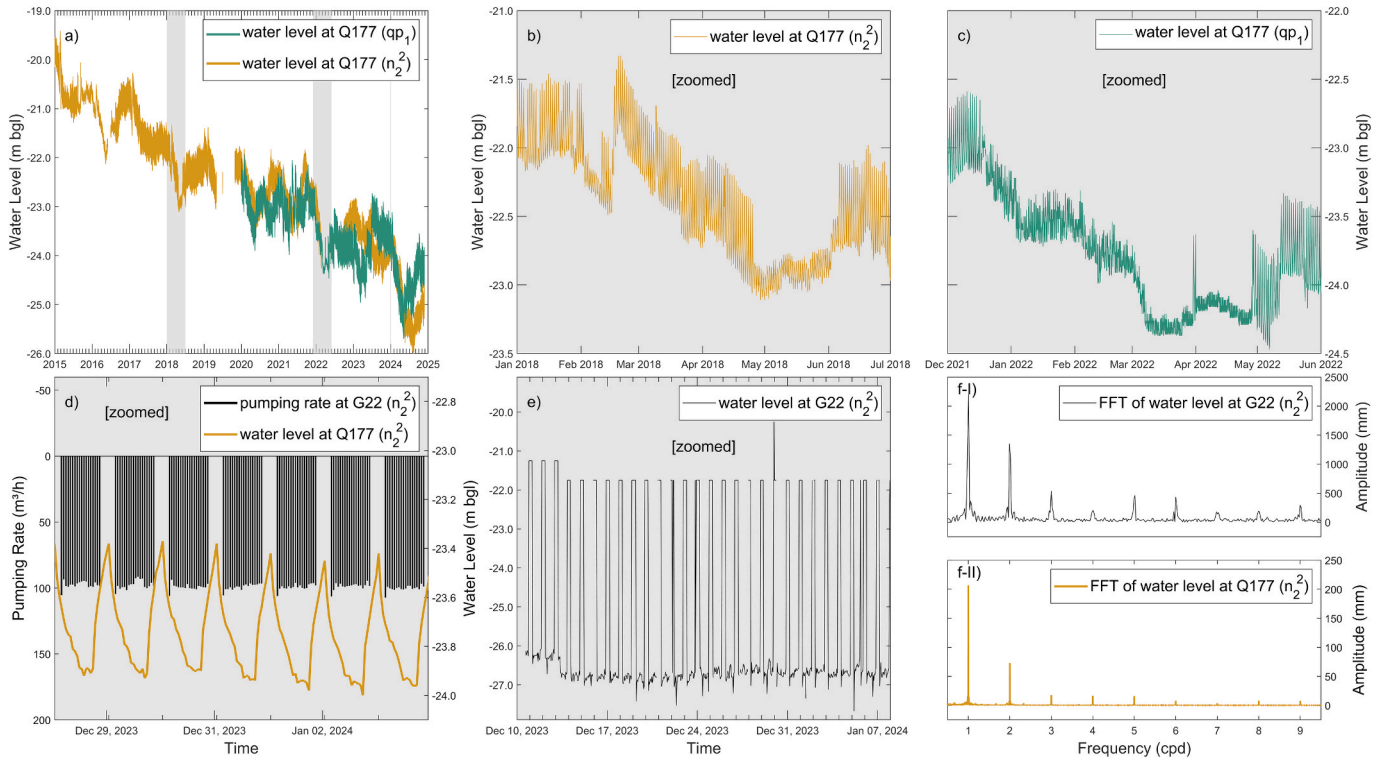


Fig. 7. Groundwater heads in qp_1 and n_2^2 aquifers from 2015 to 2024 at monitoring station Q177 (a), close-up visualization for January to July 2018 in n_2^2 (b) and for December 2021 to May 2022 in qp_1 (c), pumping rates of the water supply well G22 in n_2^2 and groundwater head variations at Q177 in n_2^2 (d), water level dynamics of the pumping well G22 (e) and FFT-amplitude spectra of groundwater heads at G22 (I) and Q177 (II) in n_2^2 aquifer (f).

IGPVN in 15 km distance to the coast (Fig. 11). When OT_{SE} is considered, the phase shift between vented groundwater head records and volumetric strains was determined to be positive in qp_1 aquifer in 2023 (0.9°, Table 2). Given that positive phase shifts are associated with vertical flow in confined systems without borehole skin effects (Valois et al., 2022), this may indicate the presence of aquitard drainage, which is a key process in land subsidence caused by groundwater depletion (Gambolati and Teatini, 2021).

Groundwater pumping for municipal water supply in qp_1 at a distance of 820 m from the observation well could lead to drainage from the adjacent aquitards into the pumped aquifer qp_1 providing a realistic scenario at the investigated study site. The identification of vertical flow using PSC complies with results obtained from a conventional pumping test, characterizing the intermitted aquitard between qp_1 and n_2^2 as leaky at IGPVN (Pechstein et al., 2018).

The study illustrates that careful disentanglement of multiple drivers of tidal signals in groundwater heads is required in regions with multiple tidal forcings. The harmonic forcings of tidally influenced rivers in close vicinity to wells can significantly exceed Earth and atmospheric tidal forcings (Fig. 6), leading to imprints in aquifers at depths exceeding 300 m (Fig. 8). Fig. 8d shows that the groundwater head response at the two major diurnal frequencies K_1 and O_1 is weaker (shifted to the left from the dashed line) compared to responses to the semi-diurnal frequencies M_2 and S_2, which is in line with the known frequency dependency of amplitude damping (Valois et al., 2022). In such settings, where harmonic forcings act on the surface and propagate downwards into the subsurface sediments, a vertically differentiated evaluation of the aquitard hydraulic diffusivity would be possible using an assessment of phase and amplitude difference in the adjacent aquifers (Boldt-Leppin and Hendry, 2003; Larroque et al., 2013).

The aquitard hydraulic diffusivity is equivalent to the consolidation coefficient c_v, a term more commonly used in geomechanical research, describing the delayed compaction response of an aquitard (Gambolati and Teatini, 2021) and is relevant and useful in the context of land subsidence analysis. However, unlike the tidal signals in n_2^1 aquifer (Fig. 4a-VI), the amplitude spectra from the aquifers qp_3, $qp_{2\text{-}3}$, qp_1 and n_2^2 (Fig. 4a-II–a-V) are characterized by a much less precise frequency representation of the river's tidal constituents (Fig. 8a). The cause for the blurred frequency representation (Fig. 4a-II–a-V) needs to be further evaluated before the aquitard hydraulic diffusivity can be assessed using amplitude damping and phase shift. This should include a careful consideration of potential timing errors due to clock drift (Rau et al., 2019).

The novel integration of ocean tide loading on the solid Earth in quantitative PSC parameter estimations enhances the application of such passive methods in near-coastal settings such as deltaic aquifer systems.

5.3. Implications for land subsidence mitigation potential

Given the elastic nature of the tidal forcings at play (Bredehoeft, 1967) it is not possible to quantify inelastic parameters using currently available PSC methods. The differentiation between elastic and inelastic stress regimes as well as the transition between these two end-member conditions is of great importance in land subsidence analyses because (i) unlike elastic deformations inelastic deformations are irreversible (Riley, 1969), and (ii) inelastic deformations can be up to 10–100 times greater than elastic deformation for common aquitard sediments (Riley, 1969; Pavelko, 2004). However, benchmark studies on land subsidence due to groundwater depletion in the VMD (Minderhoud et al., 2017) employ lower ratios between inelastic and elastic compressibility of 5:1 for clay aquitards and 3:1 for sandy aquifers, referring to geotechnical studies in the VMD (Toan and Nu, 2013; Thoang and Giao, 2015). This parameterization indicates that one third of the inelastic aquifer compaction would be reversible, thereby emphasizing the importance of investigating elastic aquifer parameters. This is substantiated by estimations of the overconsolidation ratio *OCR* to approximately 1.6 (Minderhoud et al., 2017) based on a calibrated subsidence model and

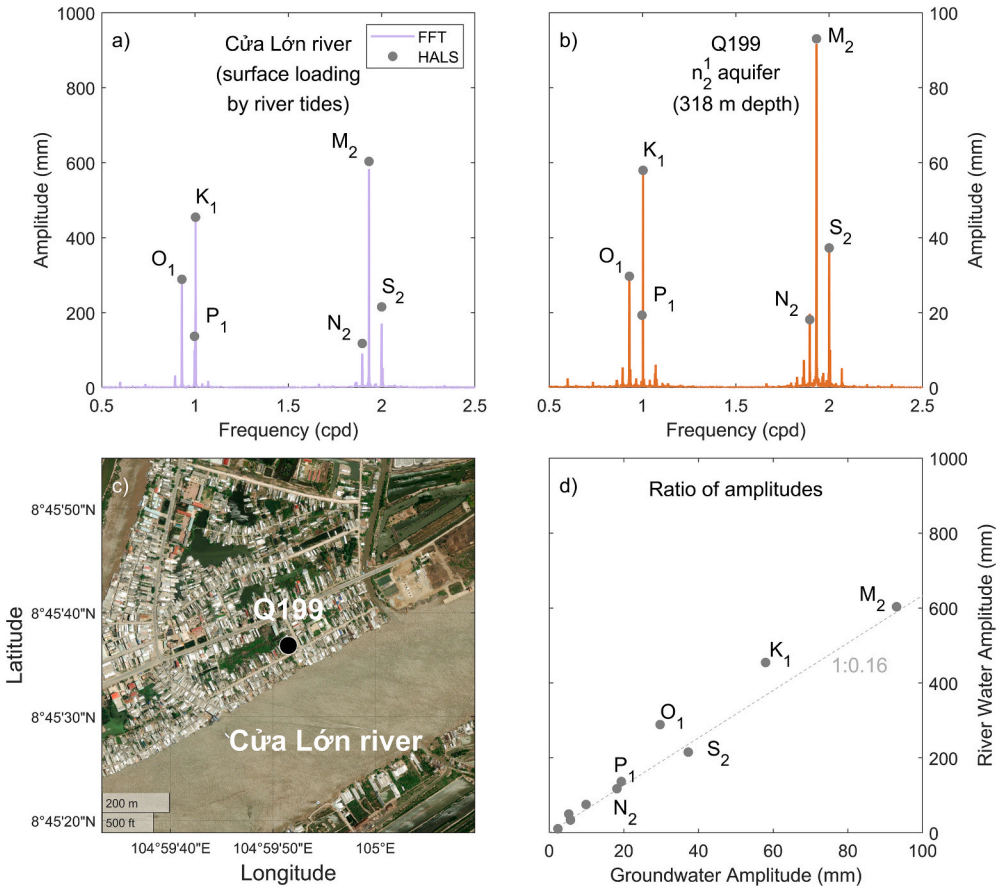


Fig. 8. FFT amplitude spectra (lines) and HALS amplitudes (calculated for the 10 frequencies listed in Table 1, displayed for O_1, K_1, P_1, N_2, M_2 and S_2 frequency as dots) of water levels of the Cửa Lớn river in Nam Can (a) and of groundwater heads in n_2^1 aquifer at monitoring site Q199 (b), satellite image (Esri, 2024) illustrating the location of the groundwater monitoring site and its close distance to the Cửa Lớn river (c), ratio of the HALS amplitudes in groundwater and river water levels of the Cửa Lớn river and n_2^1 aquifer at Q199 (d).

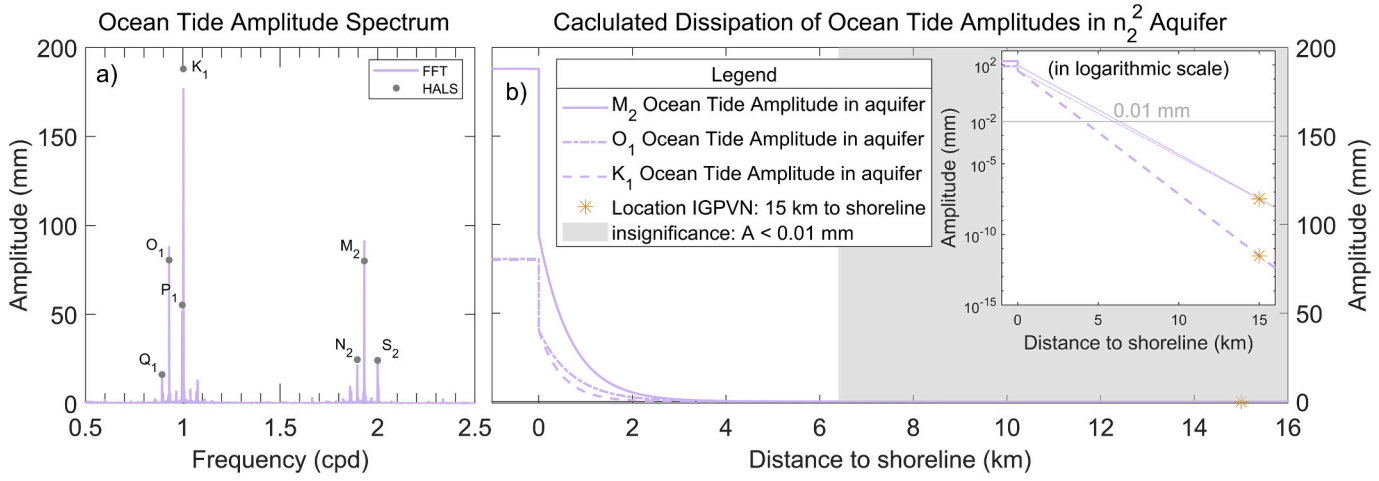


Fig. 9. FFT amplitude spectrum (lines) and HALS amplitudes (calculated for the 10 frequencies listed in Table 1, displayed for Q_1, O_1, K_1, P_1, N_2, M_2 and S_2 frequency as dots) of ocean tides in the Gulf of Thailand, derived from the amplitude spectrum of river water levels at Song Doc (a), calculated amplitude damping of M_2, O_1 and K_1 frequency due to OT_{GW} from the coast towards the inland (b).

the consideration of various geotechnical analyses (Hoang et al., 2016; Thoang and Giao, 2015). Given that $OCR > 1$ is indicative for sediments which have historically experienced stress beyond the current stress, this implies the presence of elastic deformation regimes (Hoffmann et al., 2003).

In the presented study, the elastic specific storage was derived at a selected monitoring site in the southern VMD for $qp_{2\text{-}3}$ and n_2^2 aquifer by two independent PSC methods, i.e., (i) well water level responses to S_2 atmospheric tides ($BE_{S_2}^{AT}$), and (ii) well water level responses to M_2 Earth and ocean tide strains. Both methods deliver consistent results with values between $5.9 \cdot 10^{-6}$ and $8.8 \cdot 10^{-6}$ (m^{-1}) (Table 3). For the n_2^2 aquifer, the S_s estimates from passive methods are verified by

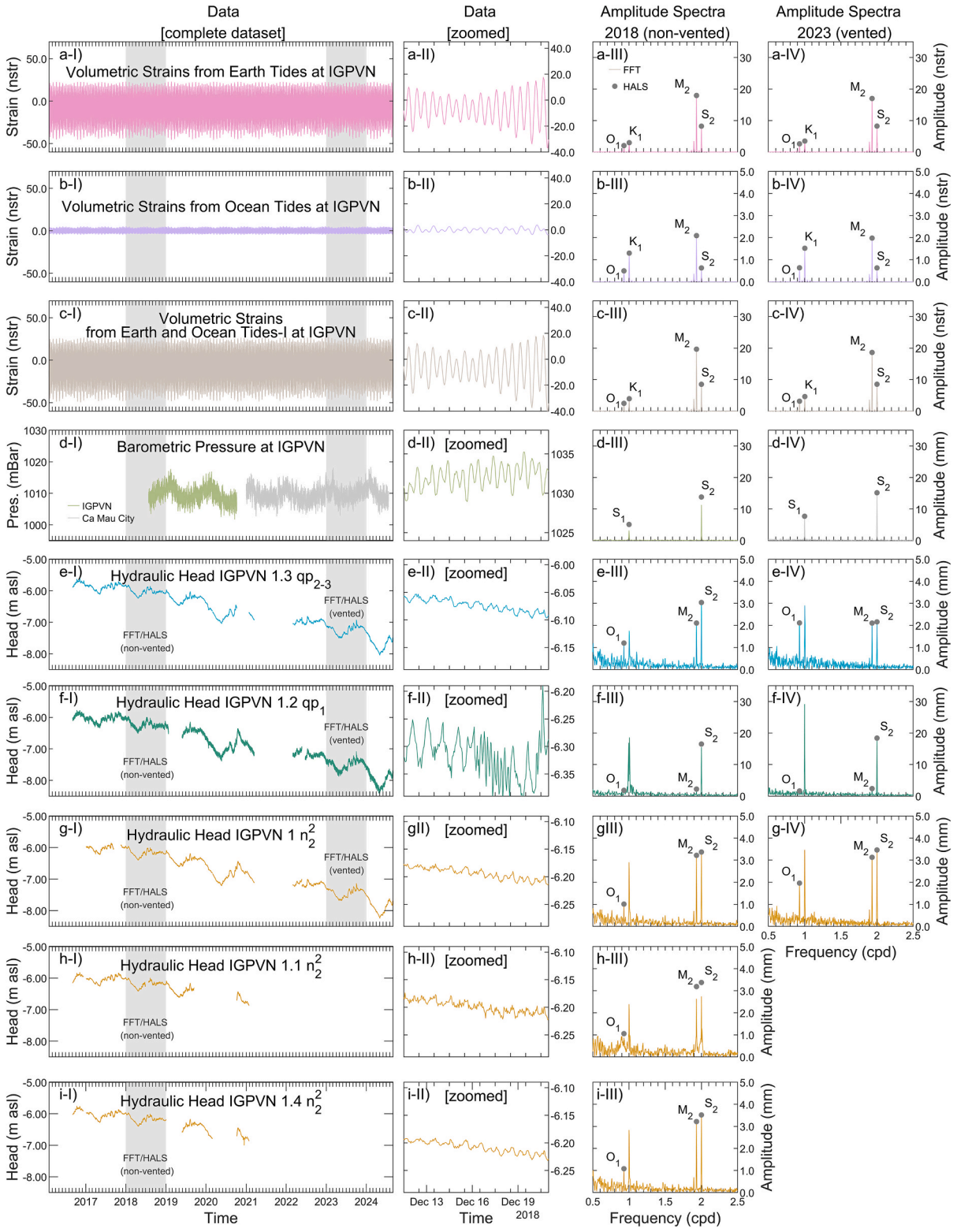


Fig. 10. Employed data (I and II) for the frequency analysis at IGPVN and the resulting FFT amplitude spectrum (lines) and HALS amplitudes (calculated for the 10 frequencies listed in Table 1, displayed for O_1, K_1, S_1, M_2 and S_2 frequency as dots) for 2018 (III) and 2023 (IV), for volumetric Earth tide strains (a) ocean tide strains (b), the sum of Earth and ocean tide strains (c), barometric pressure (d), groundwater heads in the aquifers $qp_{2\text{-}3}$ (e), qp_1 (f) and n_2^2 (g–i).

independently conducted pumping test results of $6.3 \cdot 10^{-6}$ m^{-1} (Pechstein et al., 2018). The derived parameter values are at the lower end of common parameter ranges for aquifers (Domenico and Mifflin, 1965; Rau et al., 2018) and therefore indicate a minimum elastic groundwater storage capacity of the two investigated aquifers. On a regional scale, previous studies derived average parameter values for the storage coefficient S in the n_2^2 aquifer of $1.07 \cdot 10^{-4}$ (–) and an average aquifer thickness of 47.6 m (DWRPIS, 2010; Pechstein et al., 2018). From this, an average specific storage S_s of $2.3 \cdot 10^{-6}$ m^{-1} can be derived, confirming the order of magnitude of the S_s parameter range

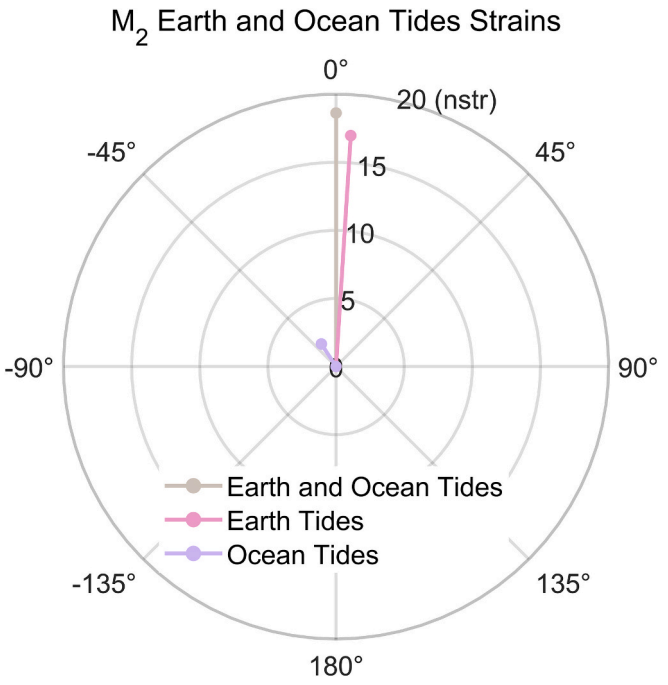


Fig. 11. Polar plot showing M_2 amplitude and phase of volumetric strains due to Earth tides $\widehat{z}_{M_2}^{ET}$ and due to OT_{SE} $\widehat{z}_{M_2}^{OT_{SE}}$ as well as their sum $\widehat{z}_{S_2}^{\{ET+OT_{SE}\}}$ at IGPVN, the phase is referenced to the phase of $\widehat{z}_{S_2}^{\{ET+OT_{SE}\}}$.

between $5.9 \cdot 10^{-6}$ and $7.8 \cdot 10^{-6}$ m^{-1} derived in this study by various passive methods.

The introduction of PSC methods for the estimation of the elastic specific storage is particularly beneficial for the study area, given that the degree of accuracy for S_s-estimates is often below that for transmissivity in pumping tests (Kruseman et al., 1994), particularly in single-well pumping tests. Although the NGMN multi-depth groundwater monitoring sites provide a valuable depth-differentiated dataset in the study area, at most sites each aquifer is only monitored by a single well. In contrast to single-well pumping tests, the deployment of multiple observation wells in one aquifer enhances the reliability of pumping test results (Kruseman et al., 1994), making the parameters derived from pumping test in n_2^2 aquifer at IGPVN a valuable reference for comparison with PSC derived parameters. The good agreement between PSC-based and pumping test-based S_s calculations in n_2^2 at IGPVN demonstrates the usefulness of applying PSC to derive S_s estimations in the southern VMD and other deltaic groundwater bodies.

With the available information of aquifer porosity and thickness, the elastic compaction (and rebound) for $qp_{2\text{-}3}$ and n_2^2 aquifer at IGPVN were estimated with $\alpha = 4.5\text{–}6.4 \cdot 10^{-10}$ Pa^{-1} to 0.18–0.30 mm per meter decline (and recovery) of water level in the confined aquifer. However, observed land subsidence rates are of several mm a^{-1} (Dörr et al., 2024) for a measured groundwater depletion rate of 0.25 m a^{-1} (Hoang and Steinel, 2021). This indicates that the elastic aquifer compaction derived for these two aquifers does not contribute significantly to the observed land subsidence rates. This finding does by no means legitimize a risk-free continuation of groundwater extraction in $qp_{2\text{-}3}$ and n_2^2 aquifer, especially given that a significant part of compaction can be expected to occur in the adjacent aquitards rather than the aquifer (Gambolati and Teatini, 2021).

Governmental circulars and decrees (Circular No. 42/2015/TT-BTNMT, Decree 53/2024/ND-CP, Circular 03/2024/ TT-BTNMT) consider MAR as a potential mitigation measure for land subsidence in the VMD. In general, the injection of water into confined aquifers may prove an efficacious land subsidence mitigation measure in two ways, namely (i) seasonal storage of surplus water resources (Seidl et al., 2024) and (ii) repressurizing of groundwater heads (Gambolati and Teatini, 2021). A seasonal storage of surplus freshwater would reduce the annual net groundwater withdrawal and consequently also the depletion of groundwater heads and associated land subsidence. With large volumes of fresh surface water from the Mekong River and high precipitation rates during the monsoon season, significant freshwater quantities are available in the VMD on an annual basis. However, without sufficient storage capacities in the flat topography, this freshwater cannot be retained for the dry season, leading to substitution sourced from groundwater (Wagner et al., 2012).

Given that truly confined aquifers may only receive surplus water by a deformation of the matrix skeleton or the pore water (Bouwer, 2002), a process inherently contained in the definition of the specific storage S_s (Jacob, 1940), the low estimated specific storage of $<9 \cdot 10^{-6}$ m^{-1} suggests that the considered aquifers are unsuitable for a seasonal freshwater storage based on pressurized water injection.

In addition to the reduction of net annual groundwater withdrawal, MAR can counteract land subsidence by repressurizing targeted confined aquifers (Gambolati and Teatini, 2021) with hydraulic impact zones exceeding the extent of storage zones (Dillon et al., 2009). Based on the estimations of elastic compressibility, the land rebound capability of the two investigated aquifer sediments due to a recovery of groundwater heads is in a range of <3 mm for a 10 m groundwater head increase and therefore insignificant. This emphasizes the urgency to minimize further groundwater depletion to prevent further inelastic land subsidence.

To evaluate the overall rebound capability in the southern VMD, it is essential to characterize shallow aquifer and aquitard sediments. This is particularly important because younger and shallow sediments are generally less consolidated, as indicated by the region's sedimentation history (Zoccarato et al., 2018).

While the presented study focuses on the estimation of elastic aquifer parameters, further research on PSC-based determination of aquitard parameters would be valuable for subsidence-related applications. While recent studies developed analytical solutions to derive the aquitard compressibility from groundwater responses to Earth tides (Valois et al., 2024), the solution's non-uniqueness challenges the estimation of reliable parameter values. Moreover, further investigations that aim to differentiate between elastic and inelastic contributions to land subsidence from groundwater depletion in the southern VMD are required, such as depth-differentiated multi-extensometer compaction monitoring (Dörr et al., 2023).

Given that approximately 25 % of the world's population lives on deltaic lowlands (Tamura et al., 2012) and approximately two billion inhabitants live in areas exposed to potential subsidence (Davydzenka et al., 2024), the presented approach has the potential to be applied in many highly populated coastal plains and deltaic lowlands all around the globe to inform more sustainable groundwater management.

6. Conclusions

The study proves that PSC-methods are valuable tools in the assessment of an aquifer's land subsidence mitigation potential. Imprints of tidal signals in groundwater heads (i.e., as measured using well water levels) carry valuable information about elastic geomechanical subsurface properties and process dynamics and can therefore be used to gain insights of significant relevance for the assessment of land subsidence mitigation potential. The specific storage S_s is a key parameter for an aquifer's land subsidence mitigation potential, as it incorporates the aquifer's elastic deformation characteristics. Therefore, S_s estimates provide relevant information on two key concepts in land subsidence mitigation strategies, (i) an aquifer's land rebound potential and (ii) its capability to temporarily receive and store surplus water resources. Due to the complex interplay of multiple tidal forcings, the application of previously available PSC-based parameter estimation methods for S_s was limited in coastal groundwater and subsiding deltaic aquifer systems.

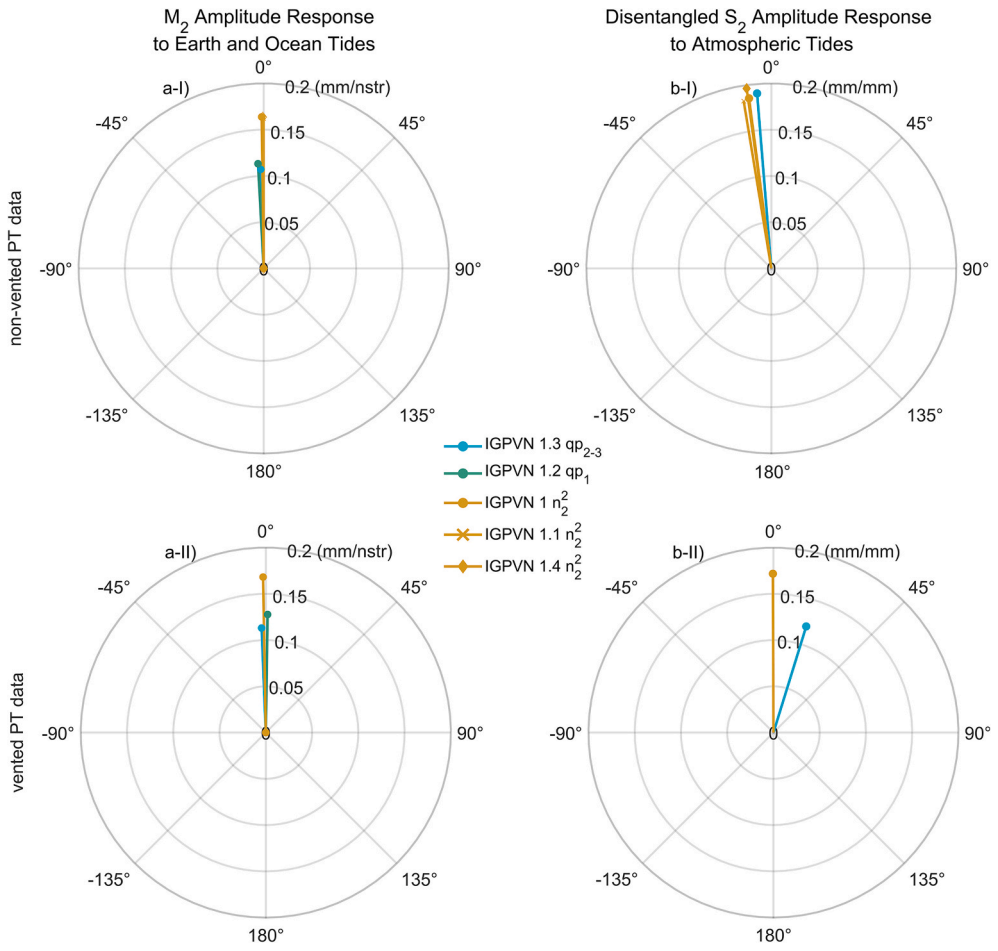


Fig. 12. Polar plots showing amplitude responses to M_2 volumetric strains due to Earth tides and OT_{SE} (a) amplitude response to S_2 atmospheric tides at IGPVN site based on groundwater observation data with non-vented PTs from 2018 (I) and with vented PTs from 2023 (II). It shall be noted that in a-I and b-I, the values for IGPVN 1.1, IGPVN 1.4 and IGPVN 1 are plotted but differ little to insignificantly from each other.

Table 2
Barometric efficiency based on S_2 responses to atmospheric tides BE_{S2}^{AT} as well as M_2 amplitude response A_{M2} and phase shift $\Delta\phi_{M2}$ for wells at the IGPVN site with disentangled Earth and ocean tide influence (calculated values without consideration of ocean tides are additionally displayed in brackets).

	PT	IGPVN 1.3 [qp_{2-3}]	IGPVN 1.2 [qp_1]	IGPVN 1 [n_2^2]	IGPVN 1.1 [n_2^2]	IGPVN 1.4 [n_2^2]
$BE_{S_2}^{AT}$	Non-vented	0.19 (0.19)	–	0.19 (0.18)	0.18 (0.18)	0.20 (0.19)
	vented	0.12 (0.12)	–	0.17 (0.17)		
$\Delta\phi_{M_2}$	Non-vented	−1.7 (−5.3)	−3.1 (−6.7)	−0.8 (−4.4)	−0.1 (−3.7)	−0.3 (−4.0)
	vented	−2.3 (−5.9)	+0.9 (−2.8)	−1.0 (−4.6)		
A_{M_2}	Non-vented	0.11 (0.12)	0.11 (0.12)	0.16 (0.18)	0.16 (0.18)	0.16 (0.18)
	vented	0.11 (0.12)	0.13 (0.14)	0.17 (0.18)		

Table 3
Specific storage at IGPVN derived from PSC and pumping test data.

	BE	θ	S_s (m^{-1}) Earth Tide (Hsieh et al., 1987)	S_s (m^{-1}) Atmospheric Tides Eqs. (9) and (10)	S_s (m^{-1}) Pumping Tests (Pechstein et al., 2018)
IGPVN 1.3 [qp_{2-3}]	0.19	0.33	$8.8 \cdot 10^{-6}$	$7.8 \cdot 10^{-6}$	–
IGPVN 1 [n_2^2]	0.19	0.33	$5.9 \cdot 10^{-6}$	$7.8 \cdot 10^{-6}$	$6.3 \cdot 10^{-6}$

This study demonstrates how to quantitatively disentangle tidal signals in groundwater heads in deltaic aquifer systems, revealing enhanced understanding of subsurface processes and properties in Vietnam's southern Mekong Delta, where loading signals in groundwater heads have not been adequately analyzed before. The findings underscore that further groundwater depletion must be avoided in the Mekong Delta to prevent further irreversible sediment compaction and subsidence. The study emphasizes that PSC-parameter estimations require a careful analysis of local conditions, including groundwater pumping activities, which may corrupt quantitative assessments by leaking into amplitude spectra. Overall, the presented integration of ocean tide loading on the solid Earth enables PSC-parameter estimations in coastal hydrogeological environments.

The presented study is limited to the quantification of elastic aquifer properties. Further research is required to quantify inelastic aquitard compressibility which contributes considerably to the overall observed land subsidence. This could involve the development of new analytical solutions to derive the aquitard compressibility from groundwater responses to cyclic forces.

The methods derived and applied in this study are not limited to the study area of the southern VMD but can be utilized to investigate subsurface hydraulic and geomechanical properties as well as groundwater extraction-related land subsidence in any coastal plain and deltaic lowland. Therefore, this study contributes to inform more sustainable groundwater management in many stressed hydrogeological environments all around the globe.

Overall, this study demonstrates that PSC is a powerful yet underutilized low-cost technique, that may prove particularly valuable for the estimation of hydraulic and geomechanical subsurface properties as well as the evaluation of mitigation strategies in deltas subject to land subsidence due to groundwater depletion.

CRediT authorship contribution statement

Felix Dörr: Writing – original draft, Visualization, Methodology, Investigation, Formal analysis, Data curation, Conceptualization. **Jonas Bauer:** Writing – review & editing, Visualization, Investigation, Formal analysis. **Gabriel C. Rau:** Writing – review & editing, Validation, Methodology, Conceptualization. **Remi Valois:** Writing – review & editing, Software, Conceptualization. **Tran Viet Hoan:** Writing – review & editing, Investigation, Data curation. **Van Cam Pham:** Writing – review & editing. **Le Thi Mai Van:** Writing – review & editing, Project administration, Data curation. **Anke Steinel:** Writing – review & editing, Data curation, Conceptualization. **Franz Nestmann:** Writing – review & editing, Supervision, Resources, Project administration, Funding acquisition, Conceptualization. **Stefan Norra:** Writing – review & editing, Supervision, Resources, Project administration, Funding acquisition.

Declaration of competing interest

The authors declare that they have no known competing financial interests or personal relationships that could have appeared to influence the work reported in this paper.

Acknowledgements

This research was conducted in the frame of the project “ViWaT – Vietnam Water Technologies” funded by the German Federal Ministry of Education and Research (funding reference: 02WCL1474A). Felix Dörr thanks the Hector Fellow Academy for support. We gratefully thank the Vietnamese Ministry of Science and Technology (MOST), the National Center for Water Resources Planning and Investigation (NAWAPI) and the Department of Natural Resources and Environment Ca Mau (DONRE Ca Mau) as well as the Federal Institute for Geosciences and Natural Resources (BGR) who kindly shared the data used in this study. We acknowledge support by the KIT-Publication Fund of the Karlsruhe Institute of Technology, Germany.

Appendix A. Supplementary data

Supplementary data to this article can be found online at https://doi.org/10.1016/j.jhydrol.2025.133844.

Data availability

The well water level data from the sites GW1 and IGPVN (from 2016 to May 2023), as well as the calculated Earth and ocean tide strains for IGPVN and the barometric pressure data used in this study are available at a Zenodo repository: https://doi.org/10.5281/zenodo.14671298. The river water level data, the well water level data from IGPVN after May 2023 as well as the well water level data from the national groundwater monitoring wells are available on request at NAWAPI.

References

Acworth, R.I., Halloran, L.J.S., Rau, G.C., Cuthbert, M.O., Bernardi, T.L., 2016. An objective frequency domain method for quantifying confined aquifer compressible storage using Earth and atmospheric tides. Geophys. Res. Lett. 43, 11671–11678. https://doi.org/10.1002/2016GL071328.

Agnew, D.C., 2007. 3.06 – Earth tides. In: Schubert, G. (Ed.), Treatise on Geophysics. Elsevier, pp. 163–195. https://doi.org/10.1016/B978-044452748-6.00056-0.

Agnew, D.C., 2012. SPOTL: Some Programs for Ocean-Tide Loading, SIO Technical Report. Scripps Institution of Oceanography, UC San Diego, California (last access: 11 November 2024).

Allen, D.R., Mayuga, M.N., 1970. The mechanics of compaction and rebound. International Hydrological Decade, symposium on land subsidence, Tokyo, Japan 17–22 Sept. Wilmington Oil Field, Long Beach, California, USA.

Anderson, H.R., 1978. Hydrogeologic reconnaissance of the Mekong Delta in South Vietnam and Cambodia. Contributions to the hydrology of Asia and Oceania. Geological Survey Water-Supply Paper 1608-R.

Arfken, G., Weber, H., 2005. In: Mathematical Methods for Physicists, 6th ed. Elsevier, Boston, Massachusetts, p. 1182.

Aungsakul, K., Jaroensutasinee, M., Jaroensutasinee, K., 2007. Numerical study of principal tidal constituents in the gulf of Thailand and the Andaman Sea. Walailak J. Sci. Technol. 4 (1), 95–109. https://wjst.wu.ac.th/index.php/wjst/article/view/128.

Baldan, S., Minderhoud, P.S.J., Xotta, R., Zoccarato, C., Teatini, P., 2024. Data-driven 3D modelling of long-term Holocene delta evolution and sediment compaction: the Mekong Delta. Earth Surf. Processes Landf. https://doi.org/10.1002/esp.6046.

Bauer, J., Börsig, N., Pham, V.C., Hoan, T.V., Nguyen, H.T., Norra, S., 2022. Geochemistry and evolution of groundwater resources in the context of salinization and freshening in the southernmost Mekong Delta, Vietnam. J. Hydrol. Reg. Stud. 40. https://doi.org/10.1016/j.ejrh.2022.101010.

Boldt-Leppin, B.E.J., Hendry, M.J., 2003. Application of harmonic analysis of water levels to determine vertical hydraulic conductivities in clay-rich aquitards. Ground Water 41 (4), 514–522. https://doi.org/10.1111/j.1745-6584.2003.tb02385.x.

Bouwer, H., 2002. Artificial recharge of groundwater: hydrogeology and engineering. Hydrgeol. J. 10 (1), 121–142. https://doi.org/10.1007/s10040-001-0182-4.

Bredehoeft, J.D., 1967. Response of well-aquifer systems to Earth tides. J. Geophys. Res. 72 (12), 3075–3087. https://doi.org/10.1029/JZ072i012p03075.

Chen, C.T., Hu, J.T., Lu, C.Y., Lee, J.C., Chan, Y.C., 2007. Thirty-year land elevation change from subsidence to uplift following the termination of groundwater pumping and its geological implications in the Metropolitan Taipei Basin, Northern Taiwan. Eng. Geol. 95, 30–47. https://doi.org/10.1016/j.enggeo.2007.09.001.

Cooper, H.H., 1966. The equation of groundwater flow in fixed and deforming coordinates. J. Geophys. Res. 71 (20), 4785–4790. https://doi.org/10.1029/JZ071i020p04785.

Cui, X., Fang, G., Di, W., 2019. Tidal resonance in the Gulf of Thailand. Ocean Sci. 15 (2), 321–331. https://doi.org/10.5194/os-15-321-2019.

Cutillo, P.A., Bredehoeft, J.D., 2011. Estimating aquifer properties from the water level response to earth tides. Groundwater 49 (4), 600–610. https://doi.org/10.1111/j.1745-6584.2010.00778.x.

Danh, V.T., Khai, H.V., 2015. Household demand and supply for clean groundwater in the Mekong Delta, Vietnam. Renewables 2, 4. https://doi.org/10.1186/s40807-014-0004-7.

Davydzenka, T., Tahmasebi, P., Shokri, N., 2024. Unveiling the global extent of land subsidence: the sinking crisis. Geophys. Res. Lett. 51, e2023GL104497. https://doi.org/10.1029/2023GL104497.

Dillon, P., Pavelic, P., Page, D., Beringen, H., Ward, J., 2009. Managed Aquifer Recharge: An Introduction. ISBN: 978-1-921107-71-9. National Water Commission, Canberra.

Di Giusto, B., Le, T.M.N., Nguyen, T.T.M., Nguyen, T.T.H., Vu, N.U.M., Lavallee, J.P., 2021. Development versus adaptation? Facing climate change in Ca Mau, Vietnam. Atmosphere (Basel) 12. https://doi.org/10.3390/atmos12091160.

Domenico, P.A., Mifflin, M.D., 1965. Water from low-permeability sediments and land subsidence. Water Res. 1 (4), 563–576. https://doi.org/10.1029/WR001i004p00563.

Dörr, N., Schenk, A., Hinz, S., 2021. Analysis of heterogeneous Ps-Insar derived subsidence rates using categorized Gis objects – a case study in the Mekong Delta. Int. Geosci. Remote Sens. Symp. (2021-July), 2655–2658. https://doi.org/10.1109/IGARSS47720.2021.9553297.

Dörr, F., Bauer, J., Tran, H.V., Norra, S., 2023. Vietnams Mekong-Delta – Landsenkung infolge von Grundwasserübernutzung. *Forsch. | WASSERWIRTSCHAFT* 64–68 (in German language). http://doi.org/10.1007/s35147-023-1922-3.

Dörr, N., Schenk, A., Hinz, S., 2024. Land subsidence in the Mekong Delta derived from advanced persistent scatterer interferometry with an infrastructural reference network. IEEE J. Sel. Top. Appl. Earth Obs. Remote Sens. 1–19. https://doi.org/10.1109/JSTARS.2024.3420130.

DWRPIS, 2010. Analysis of the groundwater abstraction status, and assessment of available groundwater resources for water supply, Report 2. Division for Water Resources Planning and Investigation for the south of Vietnam (unpublished).

Erban, L.E., Gorelick, S.M., Zebker, H.A., 2014. Groundwater extraction, land subsidence, and sea-level rise in the Mekong Delta. Vietnam. Environ. Res. Lett. 9. https://doi.org/10.1088/1748-9326/9/8/084010.

EROS, 2017. Global 30 arc-second elevation (GTOPO30). U.S. Geological Survey. [WWW Document]. Earth Resour. Obs. Sci. Cent. https://doi.org/10.5066/F7DF6PQS.

Eslami, S., Hoekstra, P., Nguyen Trung, N., Ahmed Kantoush, S., Van Binh, D., Duc Dung, D., Tran Quang, T., van der Vegt, M., 2019. Tidal amplification and salt intrusion in the Mekong Delta driven by anthropogenic sediment starvation. Sci. Rep. 9, 1–10. https://doi.org/10.1038/s41598-019-55018-9.

Esri, 2024. World Imagery. With assistance of Maxar, Earthstar Geographics, and the GIS User Community, updated on 11/19/2024.
Gambolati, G., Teatini, P., 2021. Land Subsidence and its Mitigation. The Groundwater Project. ISBN: 978-1-77470-001-3.
GSOV, 2024. General Statistics Office of Vietnam. URL (10.2024): https://www.gso.gov.vn/en/homepage/.
Haehnel, P., Rasmussen, T.C., Rau, G.C., 2024. Technical note: removing dynamic sea-level influences from groundwater-level measurements. Hydrol. Earth Syst. Sci. 28 (12), 2767–2784. https://doi.org/10.5194/hess-28-2767-2024.
Herrera-García, G., Ezquerro, P., Tomás, R., Béjar-Pizarro, M., López-Vinielles, J., Rossi, M., et al., 2021. Mapping the global threat of land subsidence. Science 371 (6524), 34–36. https://doi.org/10.1126/science.abb8549.
HGS, 2023. HydroGeoSines, https://github.com/HydroGeoSines/HydroGeoSines (accessed on 9/13/2024).
Hoan, T.V., Richter, K.-G., Börsig, N., Bauer, J., Ha, N.T., Norra, S., 2022. An improved groundwater model framework for aquifer structures of the quaternary-formed sediment body in the southernmost parts of the Mekong Delta, Vietnam. Hydrology 9, 61. https://doi.org/10.3390/hydrology9040061.
Hoang, T.M., van Lap, N., Oanh, T.T.K., Jiro, T., 2016. The influence of delta formation mechanism on geotechnical property sequence of the late Pleistocene-Holocene sediments in the Mekong River Delta. Heliyon 2, e00165. https://doi.org/10.1016/j.heliyon.2016.e00165.
Hoang, T.H., Steinel, A., 2021. Technical Note TN-IV-01. Groundwater level monitoring data at the U Minh well group September 2016 to October 2020. https://www.bgr.bund.de/EN/Themen/Wasser/Projekte/abgeschlossen/TZ/Vietnam/techn_note IV-01_en.pdf?_blob=publicationFile&v=4.
Hoanh, C.T., Phong, N.D., Gowing, J.W., Tuong, T.P., Ngoc, N.V., Hien, N.X., 2009. Hydraulic and water quality modeling: a tool for managing land use conflicts in inland coastal zones. Water Policy 11 (S1), 106–120. https://doi.org/10.2166/wp.2009.107.
Hoffmann, J., Leake, S., Galloway, D., Wilson, A., 2003. MODFLOW-2000 Ground-water model: user guide to the subsidence and aquifersystem compaction (SUB) package. US Geol. Surv. Open-File Rep.
Hsieh, P.A., Bredehoeft, J.D., Farr, J.M., 1987. Determination of aquifer transmissivity from Earth tide analysis. Water Res. 23 (10), 1824–1832. https://doi.org/10.1029/WR023i010p01824.
Jacob, C.E., 1940. On the flow of water in an elastic artesian aquifer. Eos Trans. AGU 21 (2), 574–586. https://doi.org/10.1029/TR021i002p00574.
Jacob, C.E., 1950. Flow of groundwater. Eng. Hydraul. 321–386.
Klönne, F.W., 1880. Die periodischen Schwankungen des Wasserspiegels in den inundieten Kohlenschachten von Dux in der Periode von 8 April bis 15 September 1879. Sitzungsberichte Kaiserliche Akademie Der Wissenschaften.
Kondolf, G.M., Schmitt, R.J.P., Carling, P.A., Goichot, M., Keskinen, M., Arias, M.E., Bizzi, S., Castelletti, A., Cochrane, T.A., Darby, S.E., Kummu, M., Minderhoud, P.S.J., Nguyen, D., Nguyen, H.T., Nguyen, N.T., Oeurng, C., Opperman, J., Rubin, Z., San, D.C., Schmeier, S., Wild, T., 2022. Save the Mekong Delta from drowning. Science (80-.) 376, 583–585. https://doi.org/10.1126/science.abm5176.
Kruseman, G.P., De Ridder, N.A., Verweij, J.M., 1994. Analysis and Evaluation of Pumping Test Data, (Completely Revised). International Institute for Land Reclamation and Improvement, Netherlands.
Larroque, F., Cabaret, O., Atteia, O., Dupuy, A., Franceschi, M., 2013. Vertical heterogeneities of hydraulic aquitard parameters: preliminary results from laboratory and in situ monitoring. Hydrol. Sci. J. 58 (4), 912–929. https://doi.org/10.1080/02626667.2013.783215.
Duy, N.L., Nguyen, T.V.K., Nguyen, D.V., Tran, A.T., Nguyen, H.T., Heidbüchel, I., 2021. Groundwater dynamics in the Vietnamese Mekong Delta: trends, memory effects, and response times. J. Hydrol. Reg. Stud. 33, 100746. https://doi.org/10.1016/j.ejrh.2020.100746.
MATLAB, 2023. MATLAB. Version 23.2.0. (R2023b). The MathWorks Inc., Natick, Massachusetts. Available online at https://www.mathworks.com.
McMillan, T.C., Rau, G.C., Timms, W.A., Andersen, M.S., 2019. Utilizing the impact of earth and atmospheric tides on groundwater systems: a review reveals the future potential. Rev. Geophys. 57, 281–315. https://doi.org/10.1029/2018RG000630.
Merritt, M.L., 2004. Estimating Hydraulic Properties of the Floridan Aquifer System by Analysis of Earth-Tide, Ocean-Tide, and Barometric Effects, Collier and Hendry Counties (No. 3). US Department of the Interior, US Geological Survey.
Minderhoud, P.S.J., Erkens, G., Pham, V.H., Bui, V.T., Erban, L., Kooi, H., Stouthamer, E., 2017. Impacts of 25 years of groundwater extraction on subsidence in the Mekong delta, Vietnam. Environ. Res. Lett. 12 (6), 64006. https://doi.org/10.1088/1748-9326/aa7146.
Minderhoud, P.S.J., Coumou, L., Erkens, G., Middelkoop, H., Stouthamer, E., 2019. Mekong delta much lower than previously assumed in sea-level rise impact assessments. Nat. Commun. 10, 1–13. https://doi.org/10.1038/s41467-019-11602-1.
Minderhoud, P.S.J., Middelkoop, H., Erkens, G., Stouthamer, E., 2020. Groundwater extraction may drown mega-delta: projections of extraction-induced subsidence and elevation of the Mekong delta for the 21st century. Environ. Res. Commun. 2, 011005. https://doi.org/10.1088/2515-7620/ab5e21.
Motagh, M., Walter, T.R., Sharifi, M.A., Fielding, E., Schenk, A., Anderssohn, J., Zschau, J., 2008. Land subsidence in Iran caused by widespread water reservoir overexploitation. Geophys. Res. Lett. 35 (16), L16403. https://doi.org/10.1029/2008GL033814.
NAWAPI, 2018. Report Phase I, Upgrade and Build Groundwater Monitoring Network in the Mekong Delta in the Context of Climate Change. NAWAPI, Hanoi, Vietnam (unpublished).
Neussner, O., 2019. Trouble Underground. Land Subsidence in the Mekong Delta. Deutsche Gesellschaft für Internationale Zusammenarbeit (GIZ).
Nguyen, N.T., 2020. Evolution of water levels at coastal hydrological stations of the Mekong Delta. In: Nguyen, K.D., Guillou, S., Gourbesville, P., Thiebot, J. (Eds.), Estuaries and Coastal Zones in times of Global Change. Springer Water, Singapore, pp. 831–843. https://doi.org/10.1007/978-981-15-2081-5_48.
Nguyen, T.H.O., Tran, T.T.K., Nguyen, C.T.H., 2019. Shrimp yield in relation to the ecological parameters of an organic shrimp model in the Mekong Delta of Vietnam: a case study. Asian Fish. Sci. 32, 154–161. https://doi.org/10.33997/j.afs.2019.32.4.003.
Patton, A.M., Rau, G.C., Cleall, P.J., Cuthbert, M.O., 2021. Hydro-geomechanical characterisation of a coastal urban aquifer using multiscalar time and frequency domain groundwater-level responses. Hydrogeol. J. 29 (8), 2751–2771. https://doi.org/10.1007/s10040-021-02400-5.
Pavelko, M.T., 2004. Estimates of hydraulic properties from a onedimensional numerical model of vertical aquifer-system deformation, Lorenzi site, Las Vegas, Nevada. US Geol. Surv. Water Resour. Rep. 2003–4083. https://doi.org/10.3133/wri034083.
Pechstein, A., Hoang, T.H., Orilski J., Le H.N., Le V.M., 2018. Detailed Investigations on the Hydrogeological Situation in Ca Mau Province, Mekong Delta. Technical Report No III-5. BGR. Ho Chi Minh City. https://www.bgr.bund.de/EN/Themen/Wasser/Projekte/abgeschlossen/TZ/Vietnam/techn_repIII-5_en.pdf;jsessionid=EDD60573B567BB1E9C2B0B5B61478AE1.1_cid331?_blob=publicationFile&v=2.
Pham, V.C., Bauer, J., Börsig, N., Ho, J., Vu, L., Tran, H., Dörr, F., Norra, S., 2023. Groundwater use habits and environmental awareness in Ca Mau Province, Vietnam : implications for sustainable water resource management. Environ. Challenges 13, 100742. https://doi.org/10.1016/j.envc.2023.100742.
Pham, H.V., Van Geer, F.C., Tran, V.B., Dubelaar, W., Oude Essink, G.H.P., 2019. Paleo-hydrogeological reconstruction of the fresh-saline groundwater distribution in the Vietnamese Mekong Delta since the late Pleistocene. J. Hydrol. Reg. Stud. 23, 100594. https://doi.org/10.1016/j.ejrh.2019.100594.
Poland, J.F., Davis, G.H., 1969. Land subsidence due to withdrawal of fluids. GSA Rev. Eng. Geol. 2, 187–269. https://doi.org/10.1130/REG2-p187.
Rau, G.C., Acworth, R.I., Halloran, L.J.S., Timms, W.A., Cuthbert, M.O., 2018. Quantifying compressible groundwater storage by combining cross-hole seismic surveys and head response to atmospheric tides. J. Geophys. Res.: Earth Surf. 123 (8), 1910–1930. https://doi.org/10.1029/2018JF004660.
Rau, G.C., Post, V.E.A., Shanafield, M., Krekeler, T., Banks, E.W., Blum, P., 2019. Error in hydraulic head and gradient time-series measurements: a quantitative appraisal. Hydrol. Earth Syst. Sci. 23 (9), 3603–3629. https://doi.org/10.5194/hess-23-3603-2019.
Rau, G.C., Cuthbert, M.O., Acworth, R.I., Blum, P., 2020. Technical note: disentangling the groundwater response to Earth and atmospheric tides to improve subsurface characterisation. Hydrol. Earth Syst. Sci. 24, 6033–6046. https://doi.org/10.5194/hess-24-6033-2020.
Rau, G.C., McMillan, T.C., Andersen, M.S., Timms, W.A., 2022. In situ estimation of subsurface hydro-geomechanical properties using the groundwater response to semi-diurnal Earth and atmospheric tides. Hydrol. Earth Syst. Sci. 26 (16), 4301–4321. https://doi.org/10.5194/hess-26-4301-2022.
Rau, G.C., Eulenfeld T., Howe D., Rietbroek R., Gosselin J.S., Staniewicz S., 2022b. hydrogeoscience/pygtide: PyGTide v0.7.1, Zenodo [code].
Ray, R.D., Ponte, R.M., 2003. Barometric tides from ECMWF operational analyses. Ann. Geophys. 21 (8), 1897–1910. https://doi.org/10.5194/angeo-21-1897-2003.
Riley, F.S., 1969. Analysis of borehole extensometer data from central California. Int. Assoc. Sci. Hydrol. Publ. 89, 423–431.
Roeloffs, E.A., Burford, S.S., Riley, F.S., Records, A.W., 1989. Hydrologic effects on water level changes associated with episodic fault creep near Parkfield, California. J. Geophys. Res. 94 (B9), 12387. https://doi.org/10.1029/jb094ib09p12387.
Rojstaczer, S., 1988. Determination of fluid flow properties from the response of water levels in wells to atmospheric loading. Water Resour. Res. 24 (11), 1927–1938. https://doi.org/10.1029/wr024i011p01927.
Schweizer, D., Ried, V., Rau, G.C., Tuck, J.E., Stoica, P., 2021. Comparing methods and defining practical requirements for extracting harmonic tidal components from groundwater level measurements. Math. Geosci. 53, 1147–1169. https://doi.org/10.1007/s11004-020-09915-9.
Seidl, C., Page, D., Wheeler, S.A., 2024. Using managed aquifer recharge to address land subsidence: insights from a global literature review. Water Secur. 23, 100184. https://doi.org/10.1016/j.wasec.2024.100184.
Siripong, A., 1985. The Characteristics of the Tides in the Gulf of Thailand. Report. Marine Science Department, Chulalongkorn University, Bangkok.
Sreng, S.L., Sugiyama, H., Kusaka, T., Saitoh, M., 2011. Upheaval phenomenon in clay ground induced by rising groundwater level. Poromechanics 4, 196–203.
Sun, H., Grandstaff, D., Shagam, R., 1999. Land subsidence due to groundwater withdrawal: potential damage of subsidence and sea level rise in southern New Jersey, USA. Environ. Geol. 37 (4), 290–296. https://doi.org/10.1007/s002540050386.
Syvitski, J.P.M., Kettner, A.J., Overeem, I., Hutton, E.W.H., Hannon, M.T., Brakenridge, G.R., et al., 2009. Sinking deltas due to human activities. Nat. Geosci. 2 (10), 681–686. https://doi.org/10.1038/ngeo629.
Tamura, T., Saito, Y., Nguyen, V.L., Ta, T.O., Bateman, M.D., Matsumoto, D., Yamashita, S., 2012. Origin and evolution of interdistributary delta plains; insights from Mekong River delta. Geology 40 (4), 303–306. https://doi.org/10.1130/G32717.1.
Thoang, T.T., Giao, P.H., 2015. Subsurface characterization and prediction of land subsidence for HCM City, Vietnam. Eng. Geol. 199, 107–124. https://doi.org/10.1016/j.enggeo.2015.10.009.

Thong, M.T., Thanh, X., Huyen, V.N., Trung, L.D., Cuong, L.P., Van Hung, L., Hung, C.C., Thi, T., Diep, N., Marcille, J., 2010. Expansion of shrimp farming in Ca Mau, Vietnam Ha Thi Phuong Tien, Nguyen Thu Huong. In: Cook, J.A., Cylke, O., Larson, D.F., Nash, J.D., Stedman-Edwards, P. (Eds.), Vulnerable Places, Vulnerable People Trade Liberalization. Rural Poverty and the Environment, pp. 126–144. https://doi.org/10.4337/9781849805193.00015.

Toan, D.M., Nu, N.T., 2013. Studying on the engineering geological characteristics of Middle-Upper Holocene formation (in Vietnamese, English Summary) Tap chi GIA CHAT, loat A so 333 47–56.

Turnadge, C., Crosbie, R.S., Barron, O., Rau, G.C., 2019. Comparing methods of barometric efficiency characterization for specific storage estimation. Groundwater 57 (6), 844–859. https://doi.org/10.1111/gwat.12923.

Valois, R., Rau, G.C., Vouillamoz, J.M., Derode, B., 2022. Estimating hydraulic properties of the shallow subsurface using the groundwater response to Earth and atmospheric tides: a comparison with pumping tests. Water Resour. Res. 58, e2021WR031666. https://doi.org/10.1029/2021WR031666.

Valois, R., Rivière, A., Vouillamoz, J.-M., Rau, G.C., 2024. Technical note: analytical solution for well water response to Earth tides in leaky aquifers with storage and compressibility in the aquitard. Hydrol. Earth Syst. Sci. 28 (4), 1041–1054. https://doi.org/10.5194/hess-28-1041-2024.

Van, P.D.T., Yarina, L., Nguyen, H.Q., Downes, N.K., 2023. Progress toward resilient and sustainable water management in the Vietnamese Mekong Delta. Wires Water 10 (6), e1670. https://doi.org/10.1002/wat2.1670.

Van der Kamp, G., 1972. Tidal fluctuations in a confined aquifer extending under the sea. In: 24th International Geological Congress, Section 11, pp. 101–106. Montreal, Que., Canada.

Van der Kamp, G., Gale, J.E., 1983. Theory of earth tide and barometric effects in porous formations with compressible grains. Water Resour Res 19 (2), 538–544. ISSN 19447973.

Veatch, A.C., 1906. Fluctuations of the Water Level in Wells, with Special Reference to Long Island, New York. Water Supply and Irrigation Paper No. 155. United States Geological Survey, Government Printing Office, Washington, DC.

Wagner, F., Tran, V.B., Renaud, F.G., 2012. Chapter 7, Groundwater resources in the Mekong Delta: availability. In: Renaud Fabrice, K.C.G. (Ed.), The Mekong Delta System – Interdisciplinary Analysis of a River Delta, first ed. Springer, Dordrecht, pp. 201–220. https://doi.org/10.1007/978-94-007-3962-87.

Wenzel, H.-G., 1996. The nanoGal software: Earth tide data processing package: ETERNA 3.3. Bulletin D'informations Des Marées Terrestres 124, 9425–9439.

Xue, L., Brodsky, E.E., Erskine, J., Fulton, P.M., Carter, R., 2016. A permeability and compliance contrast measured hydrogeologically on the San Andreas Fault. Geochem. Geophys. Geosyst. 17 (3), 858–871. https://doi.org/10.1002/2015gc006167.

Zhang, Y., Wu, J., Xue, Y., Wang, Z., Yao, Y., Yan, X., Wang, H., 2015. Land subsidence and uplift due to long-term groundwater extraction and artificial recharge in Shanghai, China. Hydrogeol. J. 23 (8), 1851–1866. https://doi.org/10.1007/s10040-015-1302-x.

Zoccarato, C., Minderhoud, P.S.J., Teatini, P., 2018. The role of sedimentation and natural compaction in a prograding delta: insights from the mega Mekong delta, Vietnam. Sci. Rep. 8, 11437. https://doi.org/10.1038/s41598-018-29734-7.

A.2. The recharge illusion: How seasonal surface loading can hide continuing groundwater resource declines in confined deltaic aquifers (Dörr et al., 2026a)

Journal of Hydrology 665 (2026) 134674

Contents lists available at ScienceDirect

Journal of Hydrology

journal homepage: www.elsevier.com/locate/jhydrol

The recharge illusion: How seasonal surface loading can hide continuing groundwater resource declines in confined deltaic aquifers

Felix Dörr [a,*], Jonas Bauer [a], Gabriel C. Rau [b], Elias Lewi [c], Viet Tran Hoan [a,d], Le Thi Mai Van [d], Remi Valois [e], Anke Steinel [f], Franz Nestmann [g], Stefan Norra [h]

[a] Karlsruhe Institute of Technology (KIT), Institute of Applied Geosciences, Kaiserstraße 12, 76131 Karlsruhe, Germany
[b] School of Environmental and Life Sciences, The University of Newcastle, University Drive, NSW 2308 Callaghan, Australia
[c] Institute of Geophysics, Space Science and Astronomy, Addis Ababa University, Arat Kilo Campus, Addis Ababa, Ethiopia
[d] National Center for Water Resources Planning and Investigation (NAWAPI), No. 93, lane 95, Vu Xuan Thieu Street, Sai Dong Ward, Long Bien District, Hanoi 100000, Viet Nam
[e] Avignon University, INRAE, UMR 1114 EMMAH, F-84000 Avignon, France
[f] Federal Institute for Geosciences and Natural Resources (BGR), Stilleweg 2, D-30655 Hannover, Germany
[g] Karlsruhe Institute of Technology (KIT), Institute of Water and River Basin Management, Kaiserstraße 12, 76131 Karlsruhe, Germany
[h] Potsdam University, Institute of Environmental Sciences and Geography, Soil Sciences and Geoecology, Campus Golm, Building 12, 14476 Potsdam Golm, Germany

ARTICLE INFO

This manuscript was handled by Renato Morbidelli, Editor-in-Chief, with the assistance of Eddie Banks, Associate Editor

Keywords:
Loading efficiency
Mekong delta
Barometric efficiency
Passive subsurface characterization
Groundwater head dynamics

ABSTRACT

Reliable estimates of groundwater recharge are critical for managing water resources and preventing groundwater depletion. However, groundwater recharge estimates can be distorted when loading signals are mistakenly interpreted as signs of groundwater recharge. This study introduces a novel extension to existing frequency-domain methods to quantify loading imprints in groundwater measurements by disentangling superposing signals from Earth, atmospheric, ocean, and river tides, using the K_1 tidal constituent to remove the river tide influence. This approach enables the application of frequency-domain methods for calculating the loading efficiency in deltaic groundwater systems, where superposing multiple forcings govern tidal constituents in groundwater heads. Using multi-factor regression deconvolution analysis, surface loading signals are removed from groundwater head time series. Applying this method to groundwater head data from the southern Vietnamese Mekong Delta strongly suggests that the observed seasonal rise in groundwater heads does not reflect recharge. Instead, the apparent upward trend in uncorrected data is attributed to mechanical surface loading from seasonal surface water accumulation linked to expanding aquaculture. The loading-corrected time series show a consistent decline during both dry and rainy seasons, aligning with observed annual depletion rates. This indicates a deficiency of net effective groundwater recharge throughout the year, reflecting unsustainable groundwater exploitation practices. The methods and findings of this study offer a scientific framework for the analysis of multiple superimposed surface loading processes in deltaic aquifer systems, thereby enhancing groundwater recharge assessments in such hydrogeological environments.

1. Introduction

Global groundwater resources are under increasing stress, and the widespread acceleration of depletion trends underscores the urgent need for effective measures to address ongoing declines (Jasechko et al., 2024). Coastal areas are particularly vulnerable to the impact of groundwater overexploitation, as groundwater depletion promotes seawater intrusion and thus further accelerates the loss of available underground freshwater resources (Konikow and Kendy, 2005). Moreover, in many deltaic lowlands, the depletion of groundwater heads causes notable land subsidence due to the compaction of subsurface sediments (Herrera-García et al., 2021; Davydzenka et al., 2024). The Asian mega-deltas like the Ganges-Brahmaputra Delta, the Yangtze Delta and the Mekong Delta are prominent examples for such subsiding deltas (Syvitski et al., 2009). The southern Vietnamese Mekong Delta (VMD) is subject to land subsidence dynamics with rates locally exceeding 0.03 m a^{-1} (Erban et al., 2014; Minderhoud et al., 2017; Dörr et al., 2024). Given its average elevation of only about 80 cm above mean sea level in 2018 (Minderhoud et al., 2019), such

* Corresponding author.
E-mail address: felix.doerr@kit.edu (F. Dörr).

https://doi.org/10.1016/j.jhydrol.2025.134674
Received 23 July 2025; Received in revised form 26 October 2025; Accepted 24 November 2025
Available online 26 November 2025
0022-1694/© 2025 The Author(s). Published by Elsevier B.V. This is an open access article under the CC BY license (http://creativecommons.org/licenses/by/4.0/).

Nomenclature

Acronyms and Abbreviations

BE	Barometric Efficiency
BRF	Barometric Response Function
ERF	Earth Tide Response Function
EORF	Earth- and Ocean Tide Response Function
FFT	Fast Fourier Transform
GRACE	Gravity Recovery and Climate Experiment
HALS	Harmonic Least Squares
IRC	Instantaneous Response Coefficient
LULC	Land-Use Land-Cover
MUFACO	Multi-Factor Correction of Groundwater Levels
OT_{GW}	Ocean Tide Loading on the Aquifer's Water
OT_{SE}	Ocean Tide Loading on the Solid Earth
PLRF	Pond Loading Response Function
PT	Pressure Transducer
RRF	River Response Function
VMD	Vietnamese Mekong Delta

pronounced subsidence represents an existential threat to the VMD.

While advancing salinization and increasing pollution often restrain the use of surface water resources in the southern VMD (Bauer et al. 2025; Binh et al. 2025), groundwater remains to serve as a crucial water resource for the region's water dependent socio-economic activities (Hoan et al., 2022, Pham et al., 2023). The overexploitation of groundwater causes an ongoing depletion of the hydraulic heads in the multilayered aquifer-aquitard system with rates of 0.01 to 0.55 m a^{-1} across its seven aquifers (Duy et al., 2021) and sustainable water resource management remains an unsolved challenge.

To prevent further groundwater depletion and associated land subsidence, the determination of sustainable groundwater extraction rates is essential and therefore accurate and reliable groundwater recharge assessments become ever more relevant for the southern VMD and other subsiding deltas.

Despite long-lasting and multidisciplinary research efforts (Anderson, 1978; Pham et al., 2019; Duy et al., 2021; Bauer et al., 2022), groundwater recharge processes in the VMD remain uncertain at the present time. In some coastal provinces of the VMD, the topmost Holocene aquifer (qh) is unconfined and hence generally capable of receiving groundwater recharge (Wagner et al., 2012). However, in most parts of the southern VMD it is overlain by the Holocene aquitard (Q_2). With thicknesses of up to $>$ 20 m (Anderson, 1978; Pham et al., 2019, Fig. 1b) this aquitard constrains significant groundwater recharge by percolation of rain- or surface water resources where present. For the deeper Pliocene, Pleistocene and Miocene aquifers, the intermediate aquitards restrict substantial vertical flow from the qh aquifer to deeper aquifers for which no recharge areas have been identified in the VMD (Pechstein et al., 2018). A potential hydraulic interconnection between the deep aquifers in the southern VMD and outcropping Cambodian alluvial strata remains uncertain and a pending transboundary challenge of essential importance to the VMD's water security (Lee et al., 2018). This is underpinned by recent hydrogeochemical and isotopic analyses across the multilayered aquifer system, suggesting that most groundwater was recharged into the Upper Pleistocene aquifer $qp_{2\text{-}3}$ during the last glacial episode when seawater levels were low (Pham et al. 2019, Bauer et al. 2022, Osenbrück et al., 2025). However, these studies on the other hand indicate that local vertical flow or leakage processes through the aquitards may be present (Bauer et al. 2022, Osenbrück et al., 2025).

Hydrodynamic studies (e.g. Duy et al., 2021) investigated seasonal fluctuations in groundwater levels and their correlation with river water levels, suggesting that the deeper aquifers might receive recharge from upstream areas of the VMD. More recently, Van et al. (2023) applied the water-table fluctuation method (Healy and Cook, 2002) in the southern VMD, a method originally derived for unconfined conditions, to estimate groundwater recharge based on observed seasonally rising groundwater heads and precipitation data.

However, in confined aquifers, groundwater head fluctuations are not solely caused by water mass fluxes, i.e. extraction and recharge, but also by mechanical load acting on the aquifer's confining unit, like for example variations in soil moisture or water levels of surface water bodies (van der Kamp and Maathuis, 1991). Such loading signals bear the potential of being misinterpreted as groundwater recharge, given that they cause an increase of water levels in observation wells (van der Kamp and Schmidt, 2017).

Over the past decade, hydrogeological studies in other subsiding delta systems, such as the Bengal Basin (e.g. Burgess et al., 2017), have identified and investigated loading effects in groundwater observation data. These studies highlight both the importance of accounting for such effects and the limitations of traditional analyses that ignore them, particularly in Southeast Asian mega-deltas. Dörr et al. (2025) uncovered the presence of loading signals in groundwater head time series in the southern VMD, paving the way to assess the contribution of loading signals to apparent seasonally rising groundwater levels in the southern VMD.

The objective of the present study is to identify and quantify the impact of mechanical loading processes due to the accumulation of surface water on seasonally rising groundwater heads in the southern VMD. To achieve this, this study introduces a novel extension to previous frequency-domain methods (Acworth et al., 2016; Rau et al., 2020), which utilize the S_2 frequency (2.00 cycles per day) for the calculation of the loading efficiency γ (−), using K_1 signals for the removal of river tide influence on groundwater head amplitudes. The novel approach expands the applicability of such methods to deltaic groundwater systems, where superposing multiple tidal forcings govern tidal constituents in groundwater heads. While previous methods were only applicable in the absence of river and ocean tide loading (Acworth et al., 2016; Rau et al., 2020), the present method extends the recent inclusion of ocean tide loading (Dörr et al., 2025) by integrating river tide effects and thus, for the first time, enables a quantitative disentanglement of Earth-, atmospheric-, ocean-, and river tide components in groundwater heads.

Evaluating the influence of loading signals on groundwater heads by using the novel extension to existing methods developed in this study enhances the understanding of groundwater response to surface water loading in the study area and supports more accurate groundwater recharge assessments. The insights gained from the case of the VMD are transferable to other delta systems in Southeast Asia and beyond.

2. Materials and methods

2.1. Hydrometeorological data

To assess the potential contribution of loading effects on rising groundwater heads in the southern VMD, this study utilizes hydrometeorological data from the monitoring site GW1 (Fig. 1) in Ca Mau Province in the southern VMD, located in an area dominated by inland aquaculture (Fig. 1a; Vu et al., 2022; Van Binh et al., 2025) and an extensive multi-channel system (Le et al., 2023; Fig. 1c). The monitoring site GW1 was established by the ViWaT Engineering research project by the Karlsruhe Institute of Technology (KIT), the Vietnamese National Center for Water Resources Planning and Investigation (NAWAPI) and the Department of Natural Resources and Environment Ca Mau (DONRE Ca Mau).

At GW1, the top Holocene aquitard Q_2 has a thickness of approx. 32.5 m (Fig. 1b). Like at other study sites in the southern VMD (Pechstein et al., 2018), the development of the aquifers qh and qp_3 is not clearly distinguishable at GW1, indicated by the dashed blue sections in the aquifer characterization in Fig. 1b. The introduced color code for the aquifers will be used throughout this study.

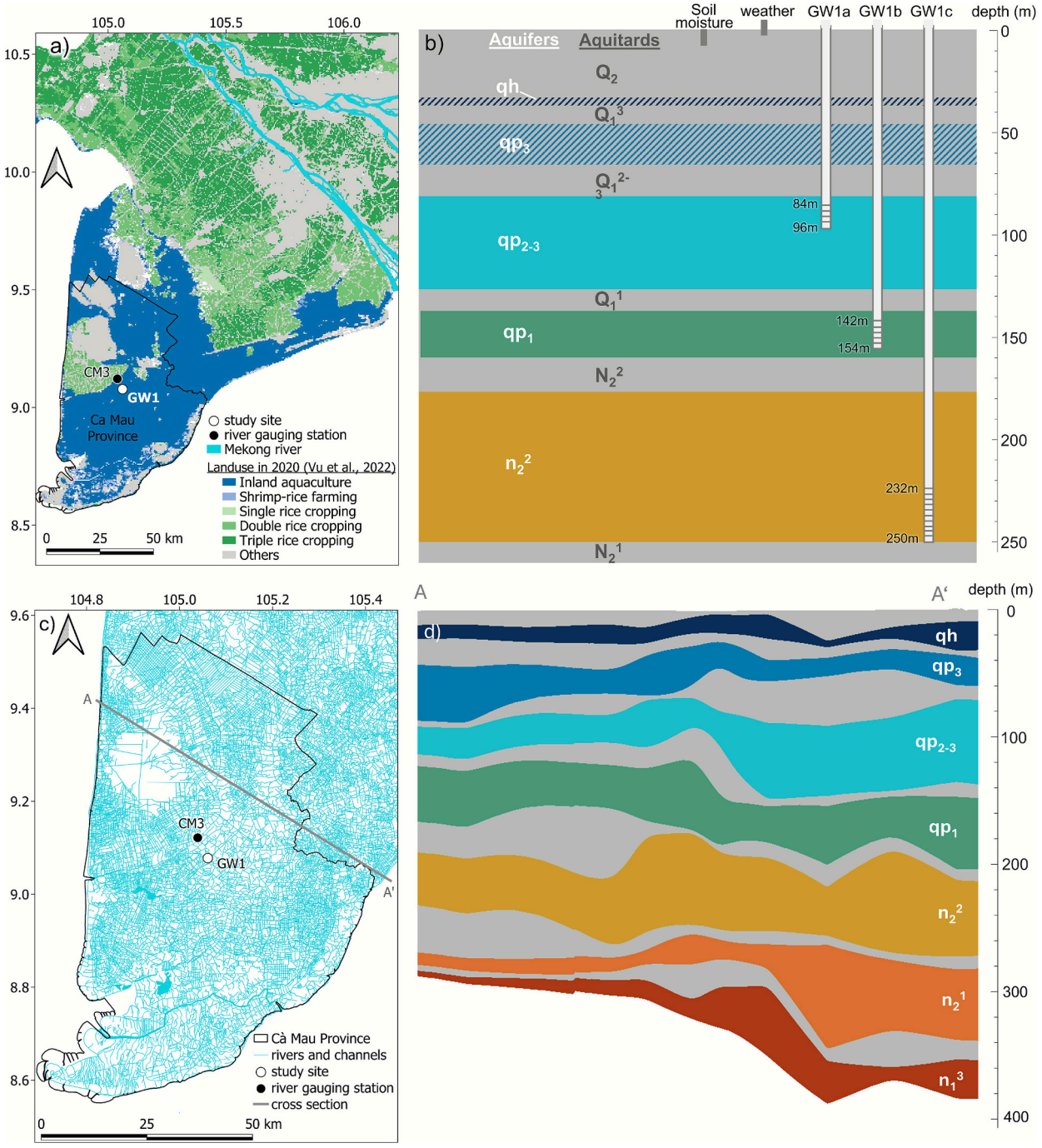


Fig. 1. Study area and location of the CM3 river station and the GW1 hydrometeorological monitoring site in the southern VMD as well as land use map from 2020 (Vu et al., 2022) (a), aquifer-aquitard categorization and screen depths of observation wells at GW1 (b), rivers and channels in the southern VMD (c) and hydrogeological cross section through the multi-layered aquifer-aquitard system of the southern VMD (modified after Hoan et al., 2022) (d). Note that the depth and height of soil moisture and weather sensors in (b) are not scaled.

The following data from GW1 is utilized for the assessment of loading signals in groundwater heads: (i) hourly to 3-hourly groundwater heads obtained using vented pressure transducers (PTs) in three observation wells (GW1a, GW1b, GW1c) screened in the upper-middle Pleistocene aquifer ($qp_{2\text{-}3}$), lower Pleistocene aquifer (qp_1) and middle Pliocene aquifer (n_2^2), respectively (Fig. 2); (ii) 15-minutely observations of the soil's volumetric water content (−) in nine depths between 0.05 and 1.00 m (Fig. 3); (iii) minutely observations from a meteorological station comprising data on air temperature, precipitation, relative humidity, solar radiation, barometric pressure and wind speed (Fig. 4).

The observed hydraulic heads in the confined aquifers $qp_{2\text{-}3}$, qp_1 and n_2^2 (Fig. 2a) show exhibit dynamics, with rising heads between end of May and end of November 2023 (rainy season, see Fig. 4d) and declining heads between end of November 2023 and early May 2024 (dry season, see Fig. 4d).

Fig. 2bI-III illustrates the different resolutions of the PTs of approx. ± 10–15 mm for GW1a and GW1b and approx. ± 2–5 mm for GW1c. The temporal resolution varies between 1 h (GW1b and GW1c, Fig. 2b-II and b-III) and 3 h (GW1a, Fig. 2b-I). The precipitation sensor has a measurement range of 0–400 mm/h and an accuracy of ± 5 % of measurement in the range between 0 to 50 mm/h. Fig. 3 illustrates the soil water content observations at GW1, showing notable variation between the

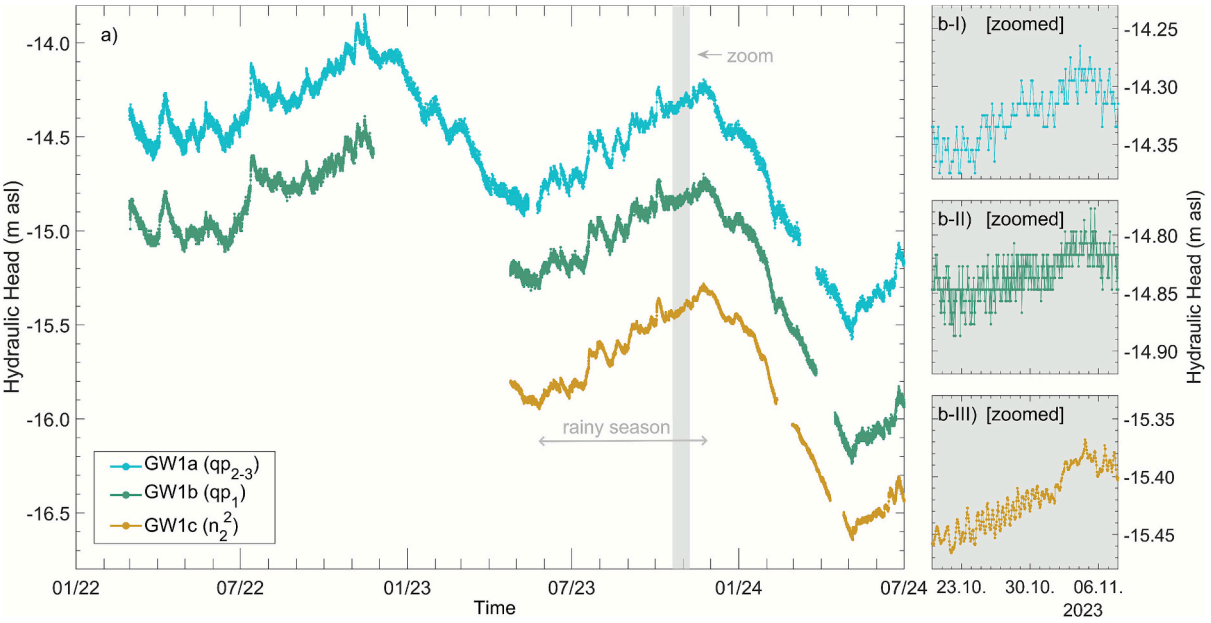


Fig. 2. Hydraulic head observation data of three observation wells at GW1 screened in the upper-middle Pleistocene aquifer ($qp_{2\text{-}3}$), lower Pleistocene aquifer (qp_1) and middle Pliocene aquifer (n_2^2) from January 2022 to July 2024 (a) and a 20-day zoom-in visualization between October and November 2023 (b).

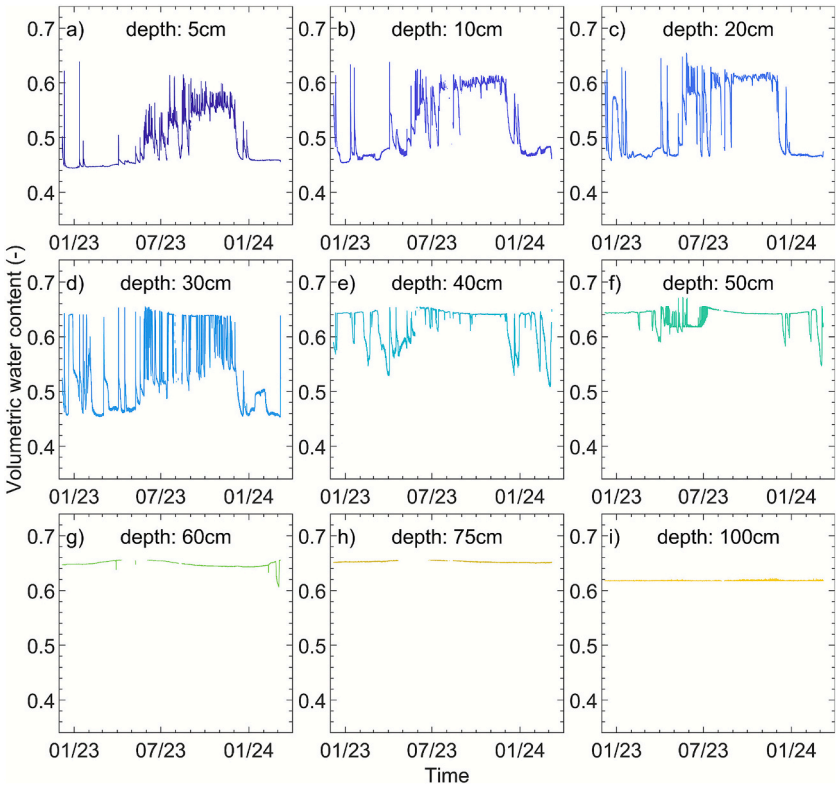


Fig. 3. Observation of soil volumetric water content at GW1 in different depths between 5 cm and 100 cm.

dry and rainy season in depths up to 30 cm (Fig. 3a–c), while below 60 cm a nearly constant volumetric water content is observed (Fig. 3g–i). The sensor was calibrated by a soil specific calibration using laboratory water content analyses of soil samples from each observation depth (Ledieu et al., 1986).

In 5 km distance to GW1 (Fig. 1a), surface water levels are measured at the CM3-Rach Cui station at hourly resolution (Fig. 5). The surface water levels are characterized by seasonal variations with rising water levels between July and November as well as by variations on tidal scale. These seasonal and sub-diel water level dynamics are induced by ocean tides as well as seasonal variations in the upstream feed of freshwater and comply well with the overall reported river water levels dynamics in the southern VMD (Bauer et al., 2025).

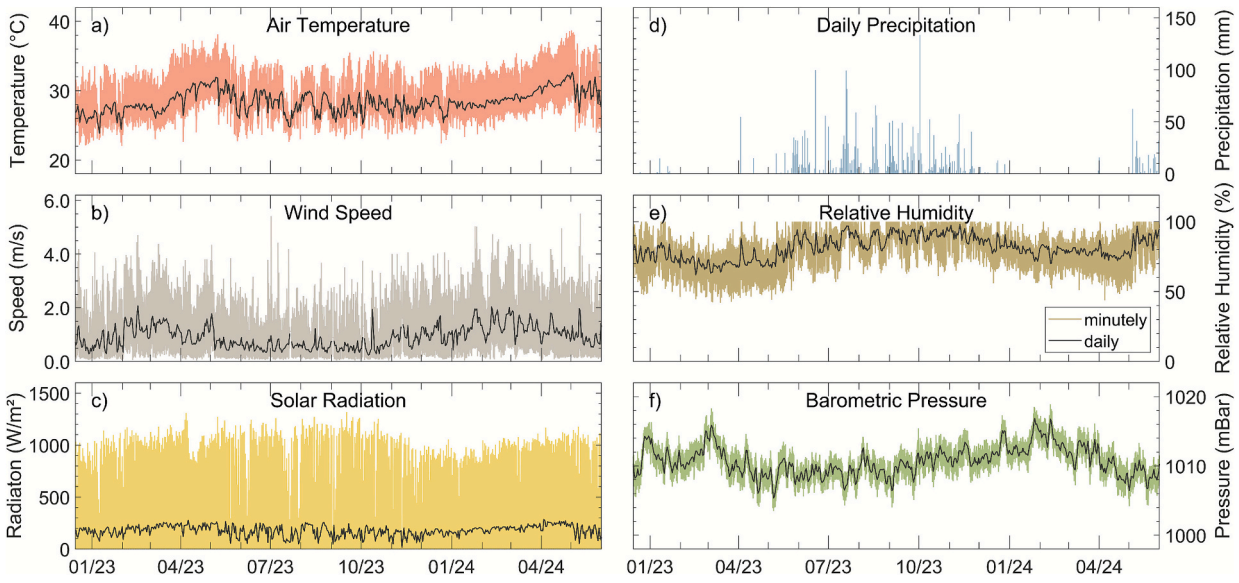


Fig. 4. Measurement data of the meteorological monitoring station at GW1 (colored lines) and daily averages (black lines).

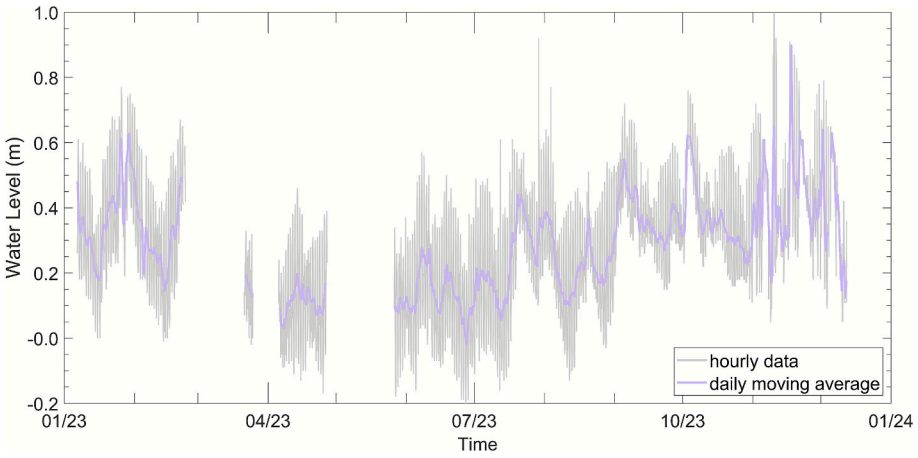


Fig. 5. Hourly data on surface water levels at the gauging station CM3 Rach Cui.

2.2. Water balance and land use land cover classification

For the analysis of seasonal surface loading $\Delta\sigma_L$ (mm), the water balance in the proximity of the study site GW1 is analyzed. In the presented study, the general surface water balance of accumulated precipitation P (mm), accumulated evapotranspiration E (mm) and accumulated runoff R (mm) (Eq. (1)) is considered:

$$\Delta\sigma_L = P - E - R \quad (1)$$

Given that the site exhibits 32.5 m of aquitard at the surface, no actual unconfined aquifer exists at the site (Fig. 1b). Hence, there is no additional loading from unconfined shallow groundwater level changes on the assessed deep aquifers.

The responding area of an observation well to surface loading can be approximated as a circular area with a radius of at least ten times the depth of the observation well (Smith et al., 2017). For the calculations in this study, radii of ten times the depth of GW1a-c are utilized for the estimation of the observation wells' responding area, complemented by an impact assessment of potential uncertainties on the calculation results. Given that actual evapotranspiration and runoff depend on land use and land cover (LULC), in this study four types of LULC-classes are differentiated within the estimated responding surface area: (i) ponds, (ii) vegetated land (iii), sealed surfaces as well as (iv) rivers and channels. These four types of LULC-classes differ in their accumulation of precipitation, their evapotranspiration rates as well as their drainage and runoff behavior.

In this study, based on field observations, LULC-areas identified as ponds are considered as undrained water bodies, supposing that they are not continuously connected to the river and channel network and therefore accumulate precipitation and do not contribute to surface water runoff. In the traditional extensive shrimp farming system, the ponds' water management was on tidal basis, linking the ponds' water levels to water levels in rivers and channels by fortnightly opening and closing of the ponds' sluice gates (Johnston et al., 2000). On the other hand, water level assessments of intensive shrimp farming ponds in the study area showed increasing pond water levels within a production cycle from initially 0.8 – 1.0 m to 1.5 – 2.0 m due to precipitation as well as the addition of supplemental water (Anh et al., 2010). Sources of used supplemental water were not specified by Anh et al. (2010) and are likely to vary according to the availability of different water resources, e.g. harvested rainwater or surface water in sufficient quality. Despite legal restrictions, a survey from Tra Vinh province suggests that also groundwater is used as supplemental water in shrimp farming (Van Tuan et al., 2024). Given that intensive shrimp farming systems account

for the largest share of recent shrimp production in the VMD (Ho et al., 2025), in this study aquaculture ponds near GW1 are considered as intensive shrimp farming ponds, a presumption that matches field observation and is validated by an evaluation of pond sizes within the analysis.

For ponds $\Delta\sigma_L$ is equivalent to variations in the pond water level and is calculated by the difference between accumulated precipitation and evaporation. The evaporation rate for ponds E_w (mm d^{-1}) is calculated with Eq. (2), a simplified form of the Penman (1948) equation derived by Valiantzas (2006) for the application in settings with measurement data from routine meteorological stations:

$$E_w = 0.051(1-\alpha)R_S\sqrt{T+9.5} - 2.4\left(\frac{R_S}{R_A}\right)^2 + 0.052(T+20)\left(1-\frac{RH}{100}\right)(a_U - 0.38 + 0.54u) \quad (2)$$

with α (−) as the albedo (for open water surfaces $\alpha = 0.08$ (Allen et al., 1998)), R_s as the measured solar radiation (MJ m^{-2} d^{-1}), T as the measured air temperature (°C), R_a as the calculated extraterrestrial radiation (MJ m^{-2} d^{-1}) based on the FAO56 method (Allen et al., 1998), RH (%) as the measured relative humidity, $a_U = 1$ according to the original Penman (1948) wind function, and u as the measured wind speed (m s^{-1}).

Areas identified as sealed surfaces like urban settlements do not accumulate water and temporary precipitation loading is completely converted into surface water runoff or evaporation. Therefore, areas classified as sealed surfaces are considered to be fully drained in this study.

The seasonal accumulation of water resources on vegetated land is challenging to determine precisely in the study area, given that several factors such as infiltration, plant water accumulation, inundation, irrigation practices and drainage runoff contribute to this process. On the one hand, the high clay content of the topsoil most likely prevents significant infiltration. In the present study this is assessed by a quantitative evaluation of the soil moisture loading, i.e., the variation of soil water volume, derived from the depth differentiated soil moisture observation at GW1 (Fig. 3). On the other hand, plant- and canopy water accumulation as well as inundation of farmland such as rice paddies add to the overall surface load on vegetated land. Given that these contributions cannot be quantified with the data available, this study does not utilize a single value for $\Delta\sigma_L$ for vegetated land but considers a range of possible values. In this approach a share between 0 % and 50 % of the areas classified as vegetated land are considered to accumulate surface water resources, characterized by the overall water balance dynamics of precipitation and evaporation, equivalent to the loading dynamics of ponds.

For LULC-areas classified as rivers or channels, the loading is directly derived from river water level observations in the proximity of GW1 (Fig. 5). For the LULC-classification, a detailed visual assessment of Google Satellite Imagery, dated to February 2024, was performed, given that remote sensing approaches, for example as used by Vu et al. (2022), have insufficient accuracy for the required site-specific analysis.

2.3. Loading signals in the time domain

Water levels in deep groundwater observation wells in confined aquifers, such as GW1a, GW1b and GW1c respond to variations in the water balance at the surface (van der Kamp and Maathuis, 1991). When hydrometeorological processes like soil moisture variations, ponding of surface water, barometric pressure variations or snow accumulation cause a spatially extensive and uniform surface load, the coupled stress-flow equations can be simplified to a 1D problem and the general relationship between aquifer pore-pressure response and surface loading can be written for saturated, linearly elastic, porous media using van der Kamp and Gale (1983):

$$\frac{\partial u}{\partial t} = \gamma\frac{\partial \sigma_L}{\partial t} + D\frac{\partial^2 u}{\partial z^2} \quad (3)$$

where u is the pore pressure, t is time, γ is the loading efficiency, σ_L is the total stress (mechanical load) acting at the top, D is the hydraulic diffusivity, and z is elevation.

The loading efficiency γ (−) describes the partitioning of external stress that is imposed on an aquifer between the sediment matrix and the pore water (Domenico and Schwartz, 1998). The two terms on the right head side of Eq. (3) represent the two governing key processes, namely the undrained pore-pressure response to changes in mechanical load ($\gamma\frac{\partial\sigma_L}{\partial t}$), and the vertical transient flow of groundwater due to the pore-pressure variations ($D\frac{\partial^2 u}{\partial z^2}$) (van der Kamp and Schmidt, 2017).

While variations of the total stress are instantaneously transmitted into the subsurface to depths of kilometers (Schulze et al., 2000), the transient flow is inherently subject to delay, which is characterized by the time factor T (s) as in Eq. (4) (van der Kamp and Schmidt, 2017)

$$T = \frac{b^2}{D} \quad (4)$$

where b (m) is the thickness of the confining aquitard and D (m^2 s^{-1}) its hydraulic diffusivity. The time factor T scales the time frame for the aquifer-aquitard interaction (van der Kamp and Schmidt, 2017). In an ideal confined aquifer, D converges to zero and the transient flow term is negligible, whereas in leaky aquifer systems a more careful assessment of the contribution of transient flow is necessary. If the duration of a loading signal is much smaller than T, the groundwater response will not be significantly affected by flow through the overlying aquitard (van der Kamp and Schmidt, 2017).

In the present study, the loading efficiency γ was utilized to remove the loading signals due to mechanical loading ($\Delta\sigma_L$) from hydraulic head measurements in three observation wells at the monitoring site GW1. For that, γ was evaluated by three independent methods: (i) the S_2 response of groundwater levels to atmospheric tides $BE^{AT}_{S_2}$; (ii) the groundwater level response to selected distinct precipitation events; (iii) the barometric response function (BRF).

The BRF is calculated using a regression deconvolution approach, where changes in groundwater pressure at a given time t are expressed as the convolution of changes in barometric pressure at times before t, in the form of instantaneous response coefficients (IRC). The cumulative sum of the IRCs is referred to as BRF (Rasmussen and Crawford, 1997). Toll and Rasmussen (2007) enhanced this method by additionally considering Earth tide effects in the regression as an independent driver for variations of well water levels, represented by the Earth tide response function (ERF). Methods like the multi-factor correction of groundwater levels (MUFACO) (Haehnel et al., 2024) generalize the forcings to consider more processes, e.g., ocean tide and precipitation loading, therefore allowing an individual and more flexible consideration of multiple influences.

In aquifers with near-ideally confined conditions, the BRF typically increases towards a plateau. In that case, the BRF's maximum represents the barometric efficiency BE (−) (Toll and Rasmussen, 2007). This is inherently coupled to the loading efficiency γ by Eq. (5) (van der Kamp and Gale, 1983):

$$\gamma = 1 - BE \quad (5)$$

In semi-confined aquifers, the BRF decreases with time, indicating significant contribution of vertical transient flow. Therefore, the shape of the BRF can be used to characterize the aquifer confinement status (Rasmussen and Crawford, 1997; Butler et al., 2011; Spane, 2002). Moreover, once the response function to a certain forcing or multiple forcings are derived, they can be used to remove the imprints of the respective effects in the observed groundwater heads (Rasmussen and Mote, 2007; Toll and Rasmussen, 2007).

In addition to the evaluation of the BRF, the groundwater head re-

sponses to selected distinct precipitation events are used to assess the loading efficiency in this study. Given that short and distinct precipitation events are abrupt increments in the surface loading (Bardsley and Campbell, 2000), slow processes like evaporation as well as surface and subsurface drainage processes can be neglected, Eq. (3) can be simplified and the loading efficiency γ can be calculated with the ratio of accumulated precipitation and increase in observed groundwater heads. To minimize the influence of low sensor accuracy at GW1a and GW1b (Fig. 2 b-I and b-II) and to reduce the impact of tidal forcings (Earth-, ocean-, and atmospheric tides), linear trends were fitted to the groundwater head data before and after each precipitation event. The durations of these trends were selected based on the longest available precipitation-free periods. The resulting start and end values provide a robust basis for the quantitative assessment of γ.

2.4. Multi-factor regression deconvolution

In the present study, a multi-factor regression deconvolution is applied to correct groundwater heads and to derive the BRF. This approach accounts for tidal and seasonal drivers influencing groundwater-head variations at the study site. The considered drivers include the ubiquitous drivers of (i) Earth tides and (ii) atmospheric pressure variations, as well as site-specific drivers including (iii) river water levels, (iv) ocean tide loading on the solid Earth (OT_{SE}), and (v) calculated variations in pond water levels (see section 2.2). Considering the aquaculture-dominated land use and the dense network of rivers and channels in the study area (Figs. 1a and c), pond water loading and river water levels control the seasonal surface loading signals in groundwater heads. The impact of observed river tides at CM3 on groundwater heads at GW1 is assessed using a magnitude-squared coherence analysis based on measured time series of river water levels and groundwater heads at the respective sites.

Volumetric Earth tide strains are computed for the monitoring site GW1 with *PyGTide* (Rau et al., 2022), a Python wrapper for *ETERNA PREDICT 3.4* (Wenzel 1996), under consideration of longitude, latitude and elevation of GW1. The volumetric strains due to ocean tide loading on the solid Earth (OT_{SE}) are calculated with the Fortran-based software package *SPOTL* (Agnew, 2012) at hourly resolution for GW1. OT_{SE} causes strain waves, propagating from the ocean coast towards the inland by the geologic media. In another independent process (denoted as OT_{GW}), ocean tides exert a loading on the aquifer's water (Jacob, 1950; van der Kamp, 1972), causing a pressure wave that propagates from the ocean coast towards the inland by the liquid phase (pore water) only. Dörr et al. (2025) showed that in the southern VMD, groundwater tides due to OT_{GW} reach insignificance (< 0.01 mm) in 6.4 km distance in the middle Pliocene aquifer n_2^2. Given that the study site GW1 is in approx. 28 km distance to the coast, OT_{GW} is considered irrelevant for the tidal composition of groundwater at GW1.

Building on previous studies in the VMD, the hydraulic diffusivity D of the overlying aquitards N_2^2, $Q_1^1$and $Q_1^{2\text{-}3}$ (see Fig. 1b) can be estimated from mean values of the vertical hydraulic conductivity and the specific storage coefficient based on Minderhoud et al. (2017) to $D(Q_1^{2\text{-}3}) = 2.3 \cdot 10^{-3}\ m^2\ s^{-1}$, $D(Q_1^1) = 5.1 \cdot 10^{-4}\ m^2\ s^{-1}$, and $D(N_2^2) = 5.5 \cdot 10^{-4}\ m^2\ s^{-1}$. With aquitard thicknesses of 16.7 m, 9.2 m and 17.8 m at GW1 (Fig. 1b), the time factor T can be estimated with Eq. (4) to be approx. 1.4, 1.9 and 6.7 days, respectively. Based on these time factors, a maximum time lag of 7 days (168 h) was selected in the multi-factor regression deconvolution, to account for potential contributions of vertical flow to the loading-groundwater response.

Within the multi-factor regression deconvolution, uncertainties are assessed in form of the response functions' standard deviations, which are derived from the covariance matrix of the IRC during the regression deconvolution (Haehnel et al., 2024).

2.5. Loading signals in the frequency domain

Complementary to the evaluation of the BRF, this study also assesses *BE* in the frequency domain by an evaluation of groundwater level response to atmospheric tides at S_2 frequency (2.0 cycles per day). For that, the underlying frequency patterns in the time series of Earth-, ocean-, river- and atmospheric tides, as well as groundwater heads are analyzed by two independent methods: (i) the Fast Fourier Transform (FFT); (ii) the harmonic least-squares (HALS) estimation. In this study, HALS analyses are conducted on the ten most studied frequencies in groundwater analysis, as outlined in Table 1. Prior to any performed frequency analysis, the time series are detrended with a 3-day moving window to remove lower frequencies and improve the extraction of the relevant tidal constituents (Rau et al., 2020). Given that HALS outperforms FFT in terms of accuracy in amplitude and phase estimation (Schweizer et al., 2021), amplitudes and phases obtained from HALS are used for the assessment of *BE*. The additional consideration of FFT offers redundancy to the HALS-based amplitude and phase characterization and has the potential to detect amplitudes beyond those listed in Table 1.

Within the HALS estimation of amplitudes and phases, a covariance matrix for the fitted coefficients can be calculated and used to derive the standard deviation (Rau et al., 2020).

2.6. Disentangling Earth and river tides for an improved estimation of barometric efficiency

The barometric efficiency (*BE*) based on the S_2 response of groundwater levels to atmospheric tides (denoted as $BE_{S_2}^{AT}$) is evaluated to derive the loading efficiency with Eq. (5). Given that S_2 signals are present in Earth-, atmospheric-, ocean-, and river tides (Table 1), the S_2 signal in groundwater levels $\hat{z}_{S_2}^{GW}$ needs to be disentangled into its individual drivers before $BE_{S_2}^{AT}$ can be calculated. The mathematical formulation of frequency disentanglement uses complex numbers (denotated by a hat) to account for phase and amplitude information of each signal. For settings without river or ocean tide loading, Rau et al. (2020) introduced a complete tidal disentanglement for S_2 signals in groundwater heads, based on M_2 signals in groundwater and Earth tide strains using:

$$\hat{z}_{S_2}^{GW\cdot ET} = \frac{\hat{z}_{M_2}^{GW}}{\hat{z}_{M_2}^{ET}} \hat{z}_{S_2}^{ET} \tag{6}$$

Recent extensions of this method included OT_{SE} strains in the analysis by a consideration of the total volumetric strain caused by OT_{SE} and Earth tides (Dörr et al., 2025). To achieve this, the two strain time series can be added up to a single time series, further denoted with the superscript $\{ET + OT_{SE}\}$, prior to the conducted frequency analysis (Dörr et al., 2025).

To enable the calculation of $BE_{S_2}^{AT}$ in deltaic groundwater systems, the present study introduces a novel extension of previous methods (Rau

Table 1
Summary of the ten most relevant frequencies in groundwater analysis after McMillan et al., (2019).

Darwin name	Frequency (cpd)	Earth Tides	Atmospheric Tides	Ocean/River Tides
Q_1	0.893244	Yes	–	Yes
O_1	0.929536	Yes	–	Yes
M_1	0.966446	Yes	–	Yes
P_1	0.997262	Yes	–	Yes
S_1	1.000000	–	Yes	–
K_1	1.002738	Yes	–	Yes
N_2	1.895982	Yes	–	Yes
M_2	1.932274	Yes	–	Yes
S_2	2.000000	Yes	Yes	Yes
K_2	2.005476	Yes	–	Yes

et al., 2020; Dörr et al., 2025), which for the first time allows a quantitative disentanglement of Earth-, atmospheric-, ocean-, and river tide components in groundwater heads. To remove the river tide contribution to the M_2 and S_2 response in groundwater heads, the K_1 signal in river tides and groundwater heads is utilized. From the ratio of K_1 signals in river tides and groundwater, the phase shift and amplitude damping of the K_1 signal are calculated, which are then assigned to the M_2 and S_2 signal of the river water levels to estimate the river tide influence on M_2 and S_2 signals in groundwater observation wells. It is noted that this is a simplified consideration assuming insignificant K_1 contribution of Earth tides to groundwater amplitudes ($\hat{z}_{K_1}^{\mathrm{GW\cdot ET}} = 0$) and neglecting the frequency dependency of amplitude damping and phase shifting (Valois et al., 2022; 2024). The applicability of this simplified assumption needs to be validated in any individual application.

Similar to the M_2–based disentanglement of Earth tides (Rau et al., 2020, Eq. (6)), the introduced K_1– based disentanglement of river tides can be formulated with Eqs. (7) and (8) for M_2 and S_2 frequencies.

$$\hat{z}_{M_2}^{\mathrm{GW\cdot RT}} = \frac{\hat{z}_{K_1}^{\mathrm{GW}}}{\hat{z}_{K_1}^{\mathrm{RT}}} \hat{z}_{M_2}^{\mathrm{RT}} \tag{7}$$

$$\hat{z}_{S_2}^{\mathrm{GW\cdot RT}} = \frac{\hat{z}_{K_1}^{\mathrm{GW}}}{\hat{z}_{K_1}^{\mathrm{RT}}} \hat{z}_{S_2}^{\mathrm{RT}} \tag{8}$$

The M_2 response of groundwater to Earth tides and OT_{SE} can then be calculated by subtracting the river tide contribution (Eq. (8)) from the M_2 signal in groundwater:

$$\hat{z}_{M_2}^{\mathrm{GW\cdot\{ET+OT_{SE}\}}} = \hat{z}_{M_2}^{\mathrm{GW}} - \hat{z}_{M_2}^{\mathrm{GW\cdot RT}} \tag{9}$$

Then, the disentanglement of Earth-, atmospheric-, ocean-, and river tide components in S_2 groundwater signals can be formulated with Eq. (10).

$$\begin{aligned} \hat{z}_{S_2}^{\mathrm{GW\cdot AT}} &= \hat{z}_{S_2}^{\mathrm{GW}} - \hat{z}_{S_2}^{\mathrm{GW\cdot\{ET+OT_{SE}\}}} - \hat{z}_{S_2}^{\mathrm{GW\cdot RT}} \\ &= \hat{z}_{S_2}^{\mathrm{GW}} - \frac{\hat{z}_{M_2}^{\mathrm{GW\cdot\{ET+OT_{SE}\}}}}{\hat{z}_{M_2}^{\mathrm{\{ET+OT_{SE}\}}}} \hat{z}_{S_2}^{\mathrm{\{ET+OT_{SE}\}}} - \frac{\hat{z}_{K_1}^{\mathrm{GW}}}{\hat{z}_{K_1}^{\mathrm{RT}}} \hat{z}_{S_2}^{\mathrm{RT}} \end{aligned} \tag{10}$$

After the disentanglement of Earth-, ocean-, river- and atmospheric tide signals, *BE* can be calculated based on the S_2 response of groundwater heads to atmospheric tides $BE_{S_2}^{AT}$ as:

$$\mathrm{BE}_{S_2}^{\mathrm{AT}} = \frac{1}{A_{S_2}^r} \mathrm{abs}\left[\frac{\hat{z}_{S_2}^{\mathrm{GW\cdot AT}}}{\hat{z}_{S_2}^{\mathrm{AT}}}\right] \tag{11}$$

with $A_{S_2}^r$ as the amplitude response between water levels in the observation well and the actual aquifer pore pressure. $A_{S_2}^r$ is a function of well and aquifer parameters and for wells screened in confined aquifers with $K > 1{\cdot}10^{-5}$ m s^{-1}, $A_{S_2}^r$ ranges usually between 0.99 and 1.00 and is therefore negligible in Eq. (11) (Rau et al., 2020).

2.7. Summary of applied methods and workflow

The deep analysis and quantification of loading imprints in groundwater heads utilizes time series of observed groundwater heads, computed Earth tide- and OT_{SE}-strains, measured barometric pressure, river water levels, and precipitation data. A novel method extension is introduced to derive the loading efficiency γ from the S_2 response of groundwater heads to atmospheric tides, using K_1 signals for the removal of river tide signals in groundwater head amplitude spectra. The results are verified using two independent established time domain methods: (i) the barometric response function (BRF) within a multi factor regression deconvolution, and (ii) the groundwater level response to distinct precipitation events. The surface loading dynamics are assessed using an analysis of precipitation-evaporation-driven accumulation of surface water resources in aquaculture ponds, river water level dynamics and a land use land cover classification. Using multi-factor regression deconvolution as well as complementary the quantification of the loading efficiency γ and the derived seasonal loading dynamics, observed groundwater heads are corrected from all loading influences. Fig. 6 presents a flow chart visualizing the study's methodological approach and a concise schematic illustrating the novel tidal disentanglement workflow.

3. Results

3.1. Seasonal surface water loading

A detailed site-specific analysis of satellite imagery agrees with the regional land use classification of Vu et al. (2022) on a local scale for GW1, identifying inland aquaculture as a dominant LULC-class in the proximity of GW1. Fig. 7a shows that the majority of the land area is covered by aquaculture ponds and vegetated land, while rivers, channels and sealed surfaces have a minor contribution to the overall land cover. Most ponds are characterized by sizes of approx. 1 ha, confirming a dominant share of intensive shrimp farming ponds (Ho et al., 2025). Fig. 7b visualizes the change in percentage for each LULC-class relative to the distance from GW1, showing that aquaculture ponds and vegetated land each comprise approximately 40–50 %, sealed surfaces account for 6–15 % and rivers and channels contribute the remaining 0–5 %, depending on the distance to GW1. The responding area of each groundwater observation well, estimated using ten times the depth of their screen casing to approx. 0.9 km 1.5 km and 2.4 km for GW1a, GW1b and GW1c respectively, is illustrated through dashed vertical lines in Fig. 7b. This shows that for GW1c, the share of ponds to the total responding area is greatest with 50 %, whereas for GW1a and GW1b it is closer to 45 %.

The loading due to aquaculture ponds is calculated by the water balance of observed accumulated precipitation (Fig. 4d and Fig. 8a) and the calculated evaporation for open water bodies (Eq. (2) and Fig. 8a) under consideration of the observed meteorological parameters (Fig. 4). Fig. 8b illustrates the seasonal variation of the calculated pond loading, characterized by a decrease (unloading) between December and May, when evaporation exceeds precipitation and an increase (loading) in the remaining months, which are governed by monsoon precipitation.

The calculated soil moisture loading (Fig. 8b) is characterized by seasonal variations of maximum 0.06 m and is therefore negligible compared to the calculated pond water loading. Thus, even though vegetated land covers 40–45 % of the area (Fig. 7b), the effect of soil moisture variations on the groundwater heads is negligible compared to pond- and river water loading effects. The comparison of the calculated pond water loading and the observed groundwater heads at GW1 (Fig. 8c) reveals a pronounced similarity between the calculated loading and the groundwater head dynamics during the rainy season. Fig. 8c also illustrates a correlation between river water level dynamics and groundwater head dynamics, which is particularly well pronounced during extreme events (peaks in timeseries) as well as in February 2023 (highlighted by a gray box in Fig. 8c) and less in the overall trend.

3.2. Groundwater response to distinct precipitation events

The hydrometeorological monitoring station at GW1 recorded distinct precipitation events of 99.0 mm, 289.5 mm and 63.5 mm on 18.06.2023, between 14.07. and 20.07.2023 and on 05.05.2024, respectively. Fig. 9 illustrates the immediate response of groundwater heads in the three observation wells GW1a, GW1b and GW1c to each of these events. Table 2 summarizes the estimated loading efficiency based on the groundwater response to the three precipitation events, calculated as the simple ratio of recorded precipitation and observed groundwater level rise.

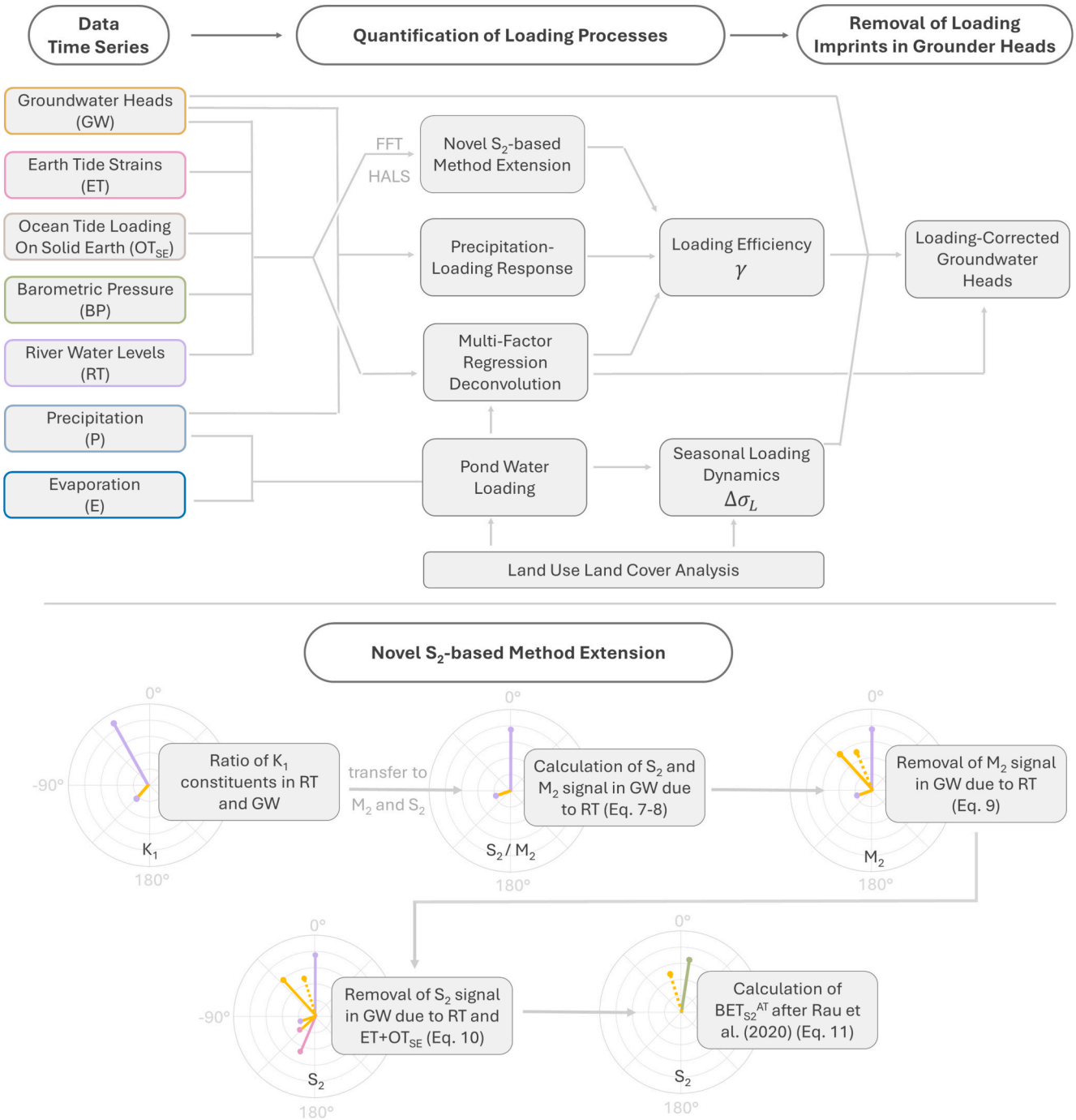


Fig. 6. Overview of the workflow and methods applied in the present study.

The assessment of groundwater head responses to three distinct precipitation events yields loading efficiency ranges of $\gamma_{GW1a} = 0.87 - 0.90$, $\gamma_{GW1b} = 0.68 - 0.79$ and $\gamma_{GW1c} = 0.64 - 0.72$ with corresponding averages of 0.89, 0.72, and 0.69, respectively.

3.3. Loading efficiency from frequency analysis

The loading efficiency was derived in the frequency domain from $BE_{S_2}^{AT}$, i.e., the barometric efficiency based on the S_2 response of groundwater heads to atmospheric tides. $BE_{S_2}^{AT}$ was calculated with the novel method extension introduced in this study (Eq.(10)) utilizing the data presented in Fig. 10 comprising volumetric Earth tide strains (Fig. 10a-I), ocean tide loading on the solid Earth (Fig. 10b-I), river water levels at CM3 Rach Cui (Fig. 10c-I), barometric pressure (Fig. 10d-I) and groundwater heads in three observation wells (Fig. 10e-I to g-I). The FFT amplitude spectra annotated with HALS amplitudes (Fig. 10 e-III to g-III) reveal distinct amplitudes in the groundwater heads at O_1, K_1, M_2 and S_2 frequency, resulting from a superposition of Earth- and ocean-tide amplitudes (Fig. 10a-III and Fig. 10b-III), river tide amplitudes (Fig. 10c-III) and barometric amplitudes (Fig. 10d-III). The sum of Earth tide- and OT_{SE}-strains are dominated by semidiurnal frequencies with a K_1:M_2 amplitude ratio of 0.24 while the river tides are dominated by diurnal frequencies with a K_1:M_2 amplitude ratio of 2.57. In the three groundwater wells the K_1:M_2 amplitude ratio varies between 0.95 (GW1c, 241 m depth), 1.37 (GW1b, 148 m depth) and 1.47 (GW1a, 90 m depth).

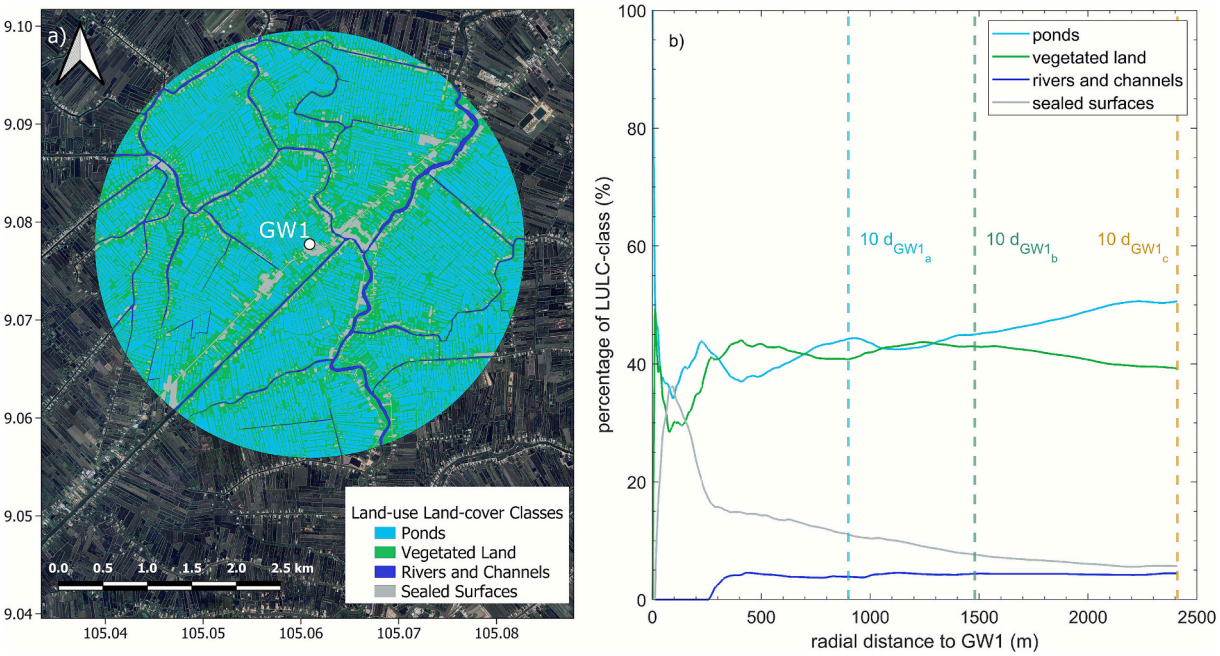


Fig. 7. LULC-classification in the proximity of GW1, Imagery data: Google, © 2024 Maxar Technologies (a) and the change of each LULC-class in radial distance to GW1(b).

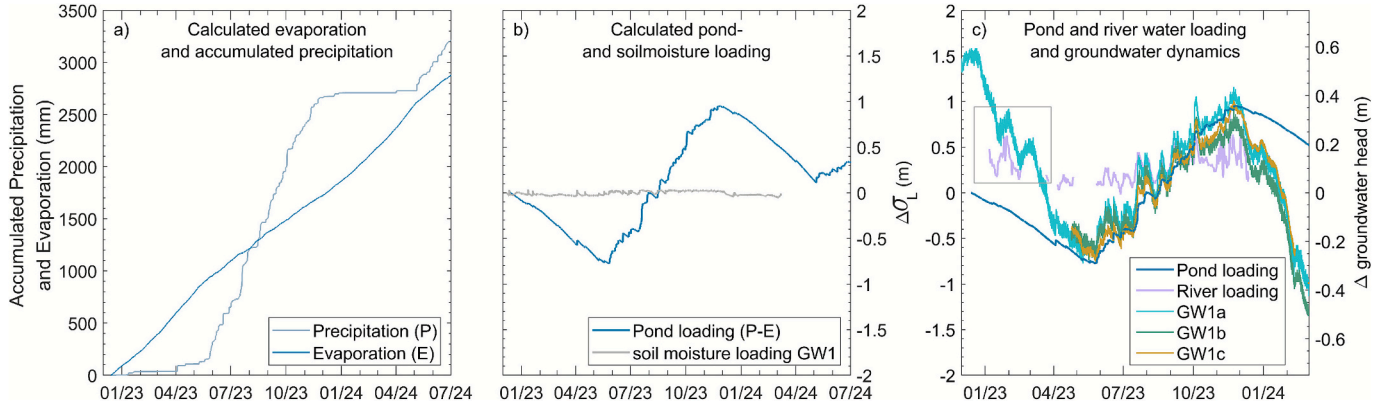


Fig. 8. Accumulated precipitation and accumulated calculated evaporation at GW1 (a), derived surface loading due to variations in pond water levels and soil moisture at GW1 (b) and dynamics of pond loading, river loading and groundwater heads at GW1 (c).

The amplitude spectrum of GW1a (Fig. 10e-III) shows an additional amplitude peak at 3.0 cpd, a frequency which is not present in the drivers amplitude spectra (Fig. 10a-III to d-III). Therefore, GW1 is not used for the quantification of $BE_{S_2}^{AT}$, given that such an amplitude response at 3.0 cpd is indicative for nearby groundwater extraction afflicting the observed S_2 groundwater amplitude (Dörr et al., 2025). For the calculation of the $BE_{S_2}^{AT}$, atmospheric tides were disentangled from Earth-, ocean- and river tides with Eq. (10) for GW1b and GW1c. $A_{S_2}^{r}$ was calculated as 0.99 for GW1b and GW1c, respectively. Table 3 summarizes the HALS amplitudes, phases, and corresponding standard deviations at the O_1, K_1, M_2 and S_2 frequencies for multiple drivers, including Earth tides, OT_{SE}, river water levels, and barometric pressure, as well as for groundwater heads at GW1a–c. The uncertainties in amplitudes and phases of the tidal constituents in the drivers and groundwater heads are generally small to moderate, with standard deviations mostly below 1 % in amplitude and 1° in phase for Earth tides, OT_{SE}, and barometric pressure. Tidal constituents of the river water levels exhibit slightly higher variability, with standard deviations of <4 % and <2.1° for O_1, K_1, and M_2, and up to 15 % and 8.5° for S_2 amplitudes and phases, respectively. For the groundwater data, GW1a and GW1b show larger relative standard deviations compared to GW1c. At GW1c, standard deviations range between 2.5–5.0 % in amplitude and 1.7–2.9° in phase, whereas GW1a and GW1b exhibit higher relative deviations of 5–19 % in amplitude and 3–11° in phase.

The magnitude-squared coherence between river tides at CM3 and groundwater heads in GW1c yielded high values of 0.91, 0.93, and 0.97 for the major tidal constituents O_1, K_1, and M_2, respectively, indicating a significant influence of river tides on groundwater heads.

Fig. 11 visualizes the signal disentanglement of the method extension. Note that the radial axes in the polar plots are in logarithmic scale to provide a comprehensive visualization of the wide range of signal amplitudes. The amplitude damping and phase shift between river tides and groundwater signals at K_1 (Fig. 11a) are projected to M_2 and S_2 frequency, to estimate the river tide contribution in the respective groundwater signals (squares in Fig. 11b and c). The M_2 groundwater signals are displayed in Fig. 11b after removal of the river contribution. Fig. 11c visualizes the S_2 groundwater signals after removal of the Earth tides, OT_{SE} and river tides, i.e. the groundwater response to atmospheric

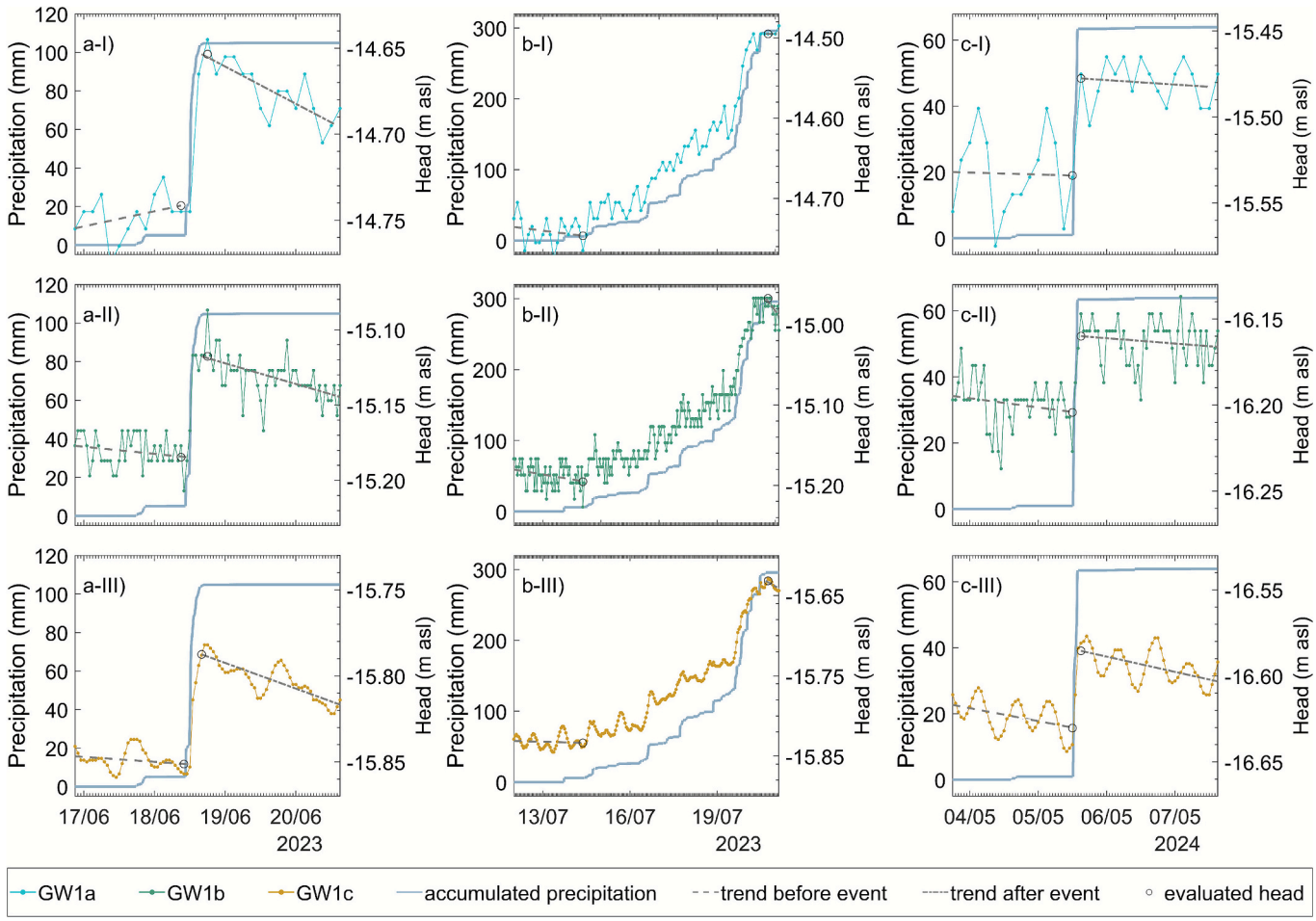


Fig. 9. Hydraulic head response to three precipitation events (a to c) at GW1 site in the observation wells GW1a, $qp_{2\text{-}3}$ (I), in GW1b, qp_1 (II) and in GW1c, n_2^2 (III).

Table 2
Loading efficiency derived from hydraulic head responses to three precipitation events at GW1 in the southern VMD.

	Date & Duration	GW1a	GW1b	GW1c
Precipitation (mm)	18.06.2023	99.0	99.0	99.0
Groundwater response (mm)	[6 h]	88.0	66.9	63.8
Loading Efficiency (−)		0.889	0.676	0.644
Precipitation (mm)	14.-20.07.2023	289.5	289.5	289.5
Groundwater response (mm)	[150 h]	251.6	228.1	202.0
Loading Efficiency (−)		0.869	0.788	0.698
Precipitation (mm)	05.05.2024	63.5	63.5	63.5
Groundwater response (mm)	[2 h]	56.4	44.3	44.9
Loading Efficiency (−)		0.903	0.708	0.718

tides. These values yield in a calculation of $BE_{S_2}^{AT} = 0.31$ for GW1b and $BE_{S_2}^{AT} = 0.30$ for GW1c with Eq. (11). Consequently, the loading efficiency calculates to $\gamma_{GW1b} = 0.69$ and $\gamma_{GW1c} = 0.70$ with Eq. (5), respectively. For comparison, $BE_{S_2}^{AT}$ was additionally calculated after Rau et al. (2020) without a consideration of OT_{SE} and river tides. This calculation results in $BE_{S_2}^{AT} = 0.29$ for GW1b and $BE_{S_2}^{AT} = 0.30$ for GW1c.

3.4. Multi-factor regression deconvolution

Fig. 12 summarizes the response functions to atmospheric tides (Fig. 12a, utilizing data from Fig. 10d-I), (ii) volumetric strains due to Earth tides and OT_{SE} (Fig. 12b, utilizing the sum of timeseries in Fig. 10 a-I and a-II), (iii) pond water loading (Fig. 12c, utilizing data from Fig. 8b) and (iv) river water levels (Fig. 12d, utilizing data from Fig. 10 c-I), obtained from the multi-factor regression deconvolution for GW1a (Fig. 12a-I to d-I), for GW1b (Fig. 12a-II to d-II) and for GW1c (Fig. 12a-III to d-III). This includes an illustration of the calculated uncertainty of each response function. Given that the response functions are the cumulative sum of the respective IRCs, uncertainties of the IRCs accumulate in the response function with increasing time lag consideration.

The response functions of GW1c are characterized by small standard deviations, whereas the multi-factor regression deconvolution yields large standard deviations for GW1a and GW1b. The regression deconvolution yields a good $R^2 = 0.89$ for GW1c. For GW1a and GW1b moderate to poor R^2 of 0.55 and 0.16 are calculated within the multi-factor regression deconvolution.

For GW1c, the BRF approaches a constant value of approx. 0.3 (Fig. 12a-III), from which $\gamma_{GW1c} \approx 0.7$ can be derived with Eq. (5). For GW1a, the BRF varies around an average value of approx. 0.1, suggesting $\gamma_{GW1a} \approx 0.9$ while for GW1b, the BRF approaches a value of approx. 0.3 in the first 48 h of time lag consideration and later approx. 0.4, which would suggest $\gamma_{GW1b} \approx 0.6$–$0.7$. The response function to Earth tide- and OT_{SE}-strains (denoted as Earth- and ocean- tide response function EORF) of all three wells (Fig. 12b) approach constant values <0.01.

The response function from the calculated pond water level, denoted as pond loading response function PLRF, are characterized by an initial rise followed by decreasing trends converging towards a constant value for all three observation wells. For GW1a (Fig. 12c-I), the PLRF peaks at approx. 0.9 and decreases to approx. 0.3, whereas for GW1b (Fig. 12c-II), the PLRF decreases from 0.8 to 0.3. The PLRF of GW1c (Fig. 12c-III) is characterized by less noise and a decrease from 0.75 to approx. 0.4. The river water response functions (Fig. 12d) are characterized by

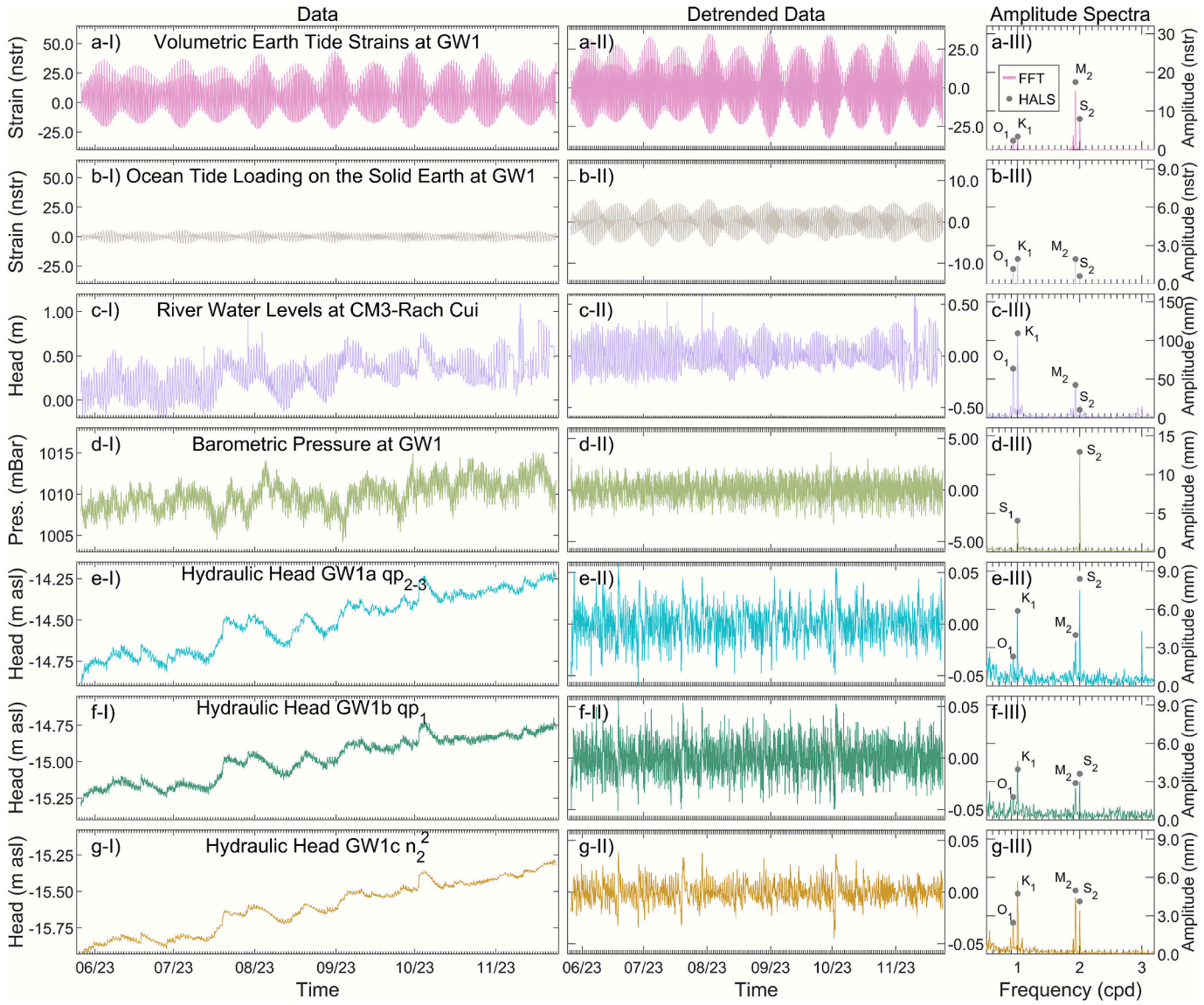


Fig. 10. Employed measurement data (I, left side) and detrended data (II, middle) used for the frequency analysis at GW1 and the resulting FFT amplitude spectrum (lines) and HALS amplitudes (calculated for the 10 frequencies listed in Table 1, displayed for O_1, K_1, M_2 and S_2 frequency as dots) (III, right side), for computed volumetric Earth tide strains (a), computed ocean tide loading on the solid Earth (b), river water levels at CM3 Rach Cui (c), barometric pressure (d), groundwater heads in the aquifers $qp_{2\text{-}3}$ (e), qp_1 (f) and n_2^2 (g).

increasing trends, resulting in plateaus of approx. 0.22 for GW1a, 0.30 for GW1b and 0.17 for GW1c, respectively.

For comparison, the BRF was additionally derived for GW1c with MUFACO considering barometric pressure as the only driver, neglecting Earth-, ocean- and river tides as well as pond loading. This comparative analysis resulted in a distinctly different BRF, characterized by an oscillation and increase up to 0.75 and a poor R^2 of 0.37. The poor R^2 and the resulting high standard deviation in the response functions at GW1a and GW1b are attributable to accumulating uncertainties of the IRC and are a consequence of the low sensor precision of GW1a and GW1b (Fig. 2b).

3.5. Estimated correction of groundwater head data

The observed groundwater head data was corrected from loading signals using the calculated response functions for barometric pressure, volumetric strains due to Earth tides and OT_{SE}, precipitation-evaporation based loading of ponds and river water levels (Fig. 12). Fig. 13 summarizes the obtained estimation of the corrected groundwater heads for the three observation wells at GW1, indicating depleting groundwater levels for all wells, when loading signals are removed from the observation data. For GW1a, GW1b and GW1c, the observed groundwater heads are characterized by increasing trends of 1.29 m a^{-1}, 1.10 m a^{-1} and 1.24 m a^{-1} respectively during the rainy season, whilst the corrected heads indicate depleting trends of −0.59 m a^{-1}, −0.65 m a^{-1} and −0.44 m a^{-1} respectively.

The standard deviations of the response functions (Fig. 12) are projected into the standard deviation of the corrected groundwater levels (Fig. 13). For GW1c (Fig. 13c) the minor standard deviations in the response functions (Fig. 12 a-d III) lead to a moderate standard deviation in the corrected head, encompassing corrected depletion rates ranging from −0.23 m a^{-1} to −0.66 m a^{-1}. For GW1a and GW1b, the high standard deviations of the response functions are transferred into high standard deviations for the corrected heads.

For comparison, the groundwater heads at GW1a, GW1b and GW1c were corrected based on the derived loading efficiencies γ and the area-averaged surface loading $\Delta\sigma_L$ for each of the three wells. Based on the three applied approaches to calculate the loading efficiency, γ_{GW1a} =

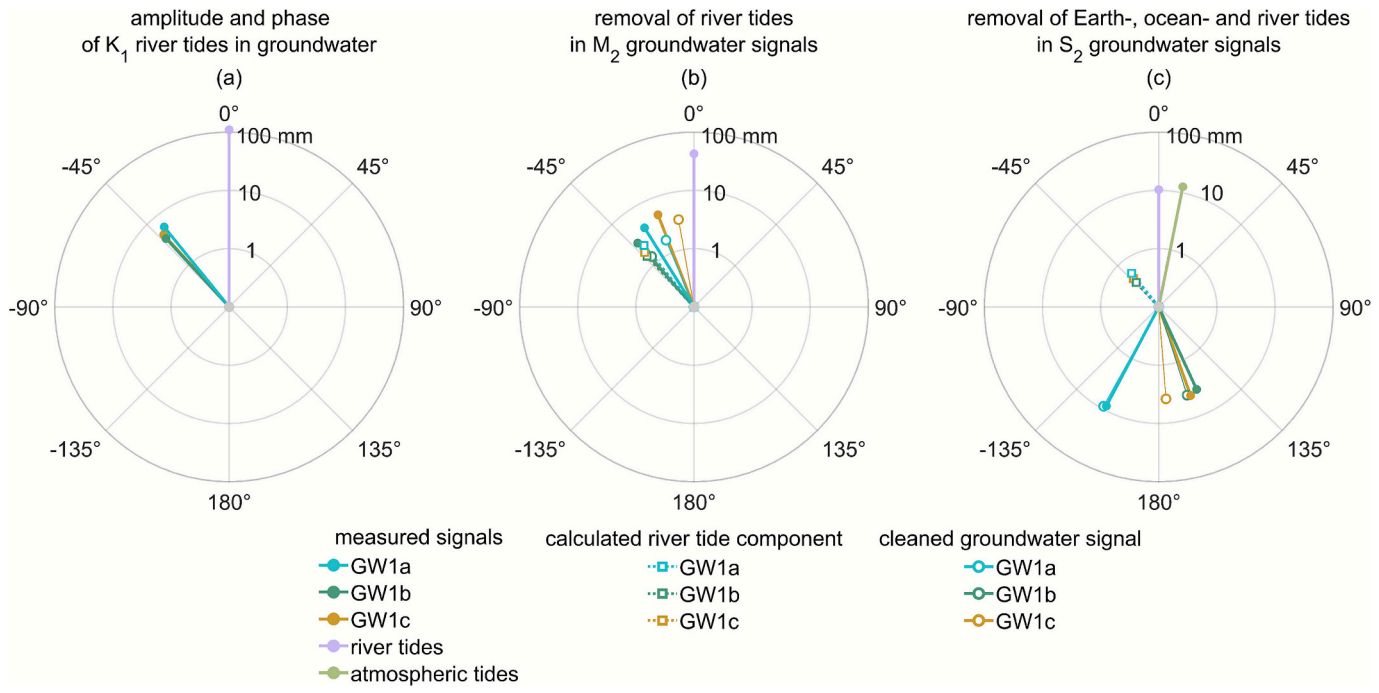


Fig. 11. Results of the signal disentanglement using Eqs. (7)–(10). The signals comprise of amplitude and phase of K_1 river tides in groundwater signals (a), the removal of river tides in M_2 groundwater signals (b) and the removal of Earth tides, ocean tide loading on the solid Earth, and river tides (c). Note the logarithmic scale of radial axes in the polar plots.

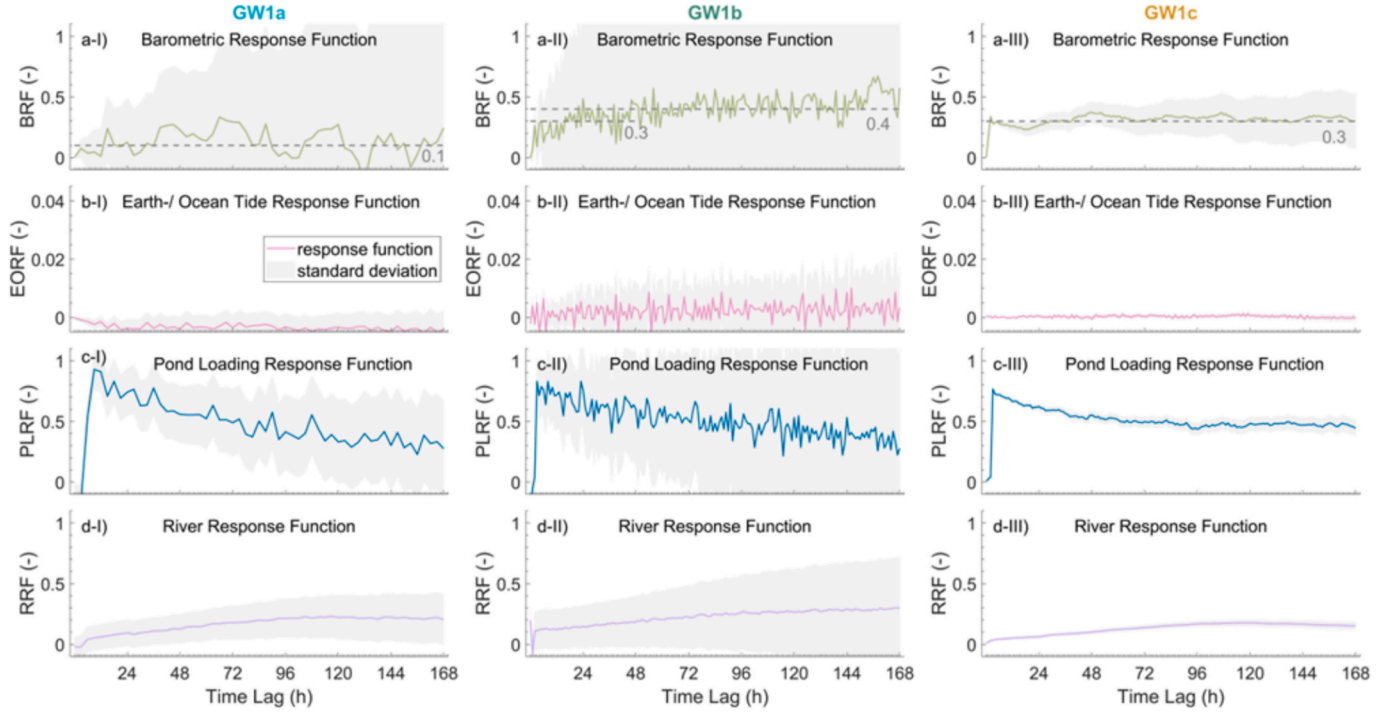


Fig. 12. Response functions obtained from MUFACO for barometric loading (a) Earth tide- and OT_{SE}-strains (b) pond water loading (c) and river water loading (d) for the observation wells GW1a (I), GW1b (II) and GW1c (III) under consideration of maximum time lag of 7 days (168 h).

0.9, $\gamma_{GW1b} = 0.7$ and $\gamma_{GW1c} = 0.7$ were utilized for the correction. Given that the accumulation of water resources on vegetated land cannot be quantified precisely with the data available, the surface loading $\Delta\sigma_L$ and therefore also the corrected groundwater heads are characterized by a value range, depending on the considered share of water accumulation on vegetated land between 0 % and 50 %. Fig. 14 shows that for GW1a, GW1b and GW1c the corrected heads based on γ and $\Delta\sigma_L$ comply best with the deconvolution-based correction for a respective share of water accumulation on vegetated land of 25 %, 46 % and 36 %. These shares imply that depending on the distance to GW1, 54 % – 75 % of the vegetated land discharge surface water out of the wells' responding area, while the remaining fraction underlies the balance of accumulated precipitation and evaporation.

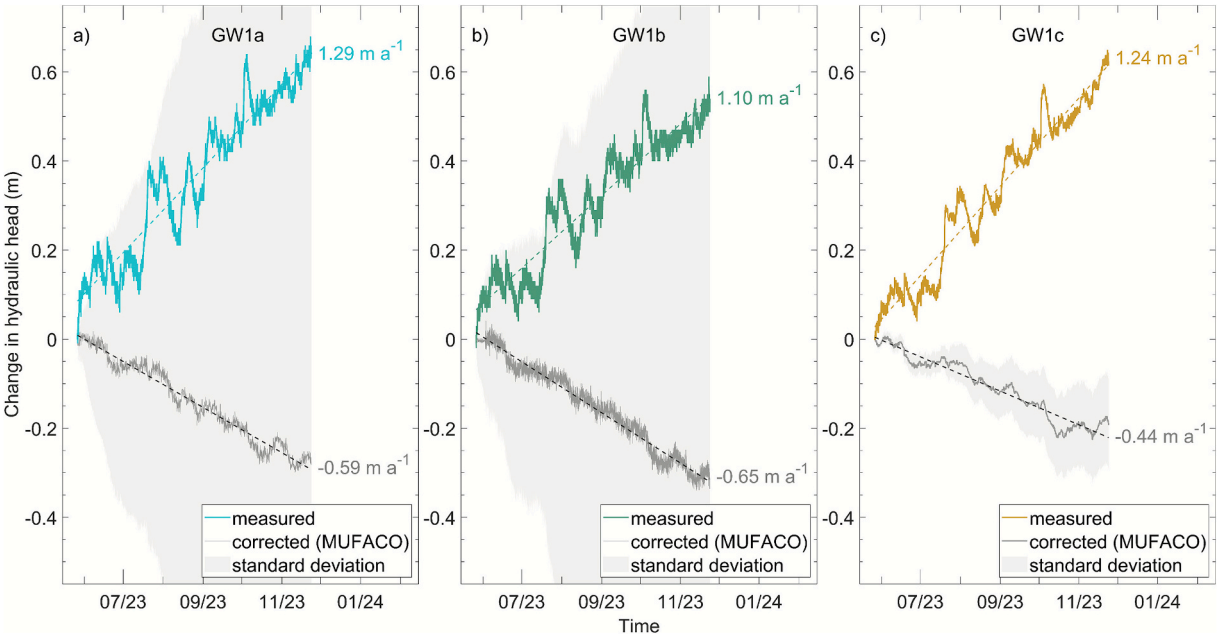


Fig. 13. Corrected groundwater heads for GW1a (a) GW1b (b) and GW1c (c) based on a multi factor regression deconvolution under consideration of barometric pressure, Earth tide- and OT_{SE}-strains, pond water loading and river water levels under a maximum time lag consideration of 7 days (168 h).

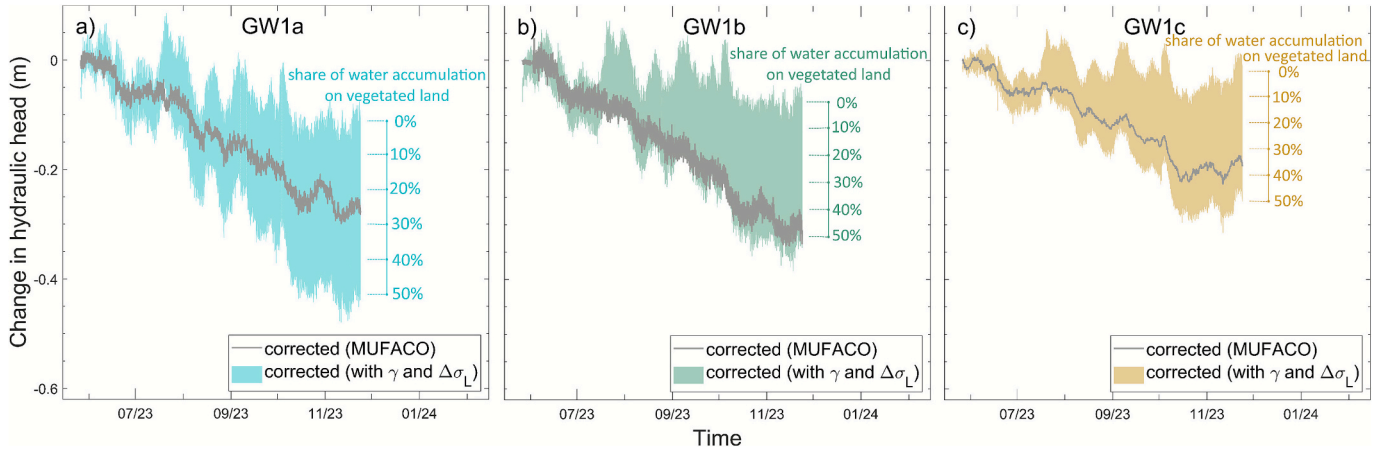


Fig. 14. Corrected groundwater heads for GW1a (a) GW1b (b) and GW1c (c) based on derived loading efficiencies and seasonal surface loading dynamics. For comparison, the corrected groundwater heads based on MUFACO (Fig. 13) are included in the graphs.

4. Discussion

4.1. Quantification of loading signals in deltaic groundwater systems

The loading efficiency γ is derived in the frequency domain using a novel extension of previously introduced methods to assess the S_2 response of groundwater heads to atmospheric tides. While previous frequency-domain methods were only applicable in the absence of river and ocean tide loading (Acworth et al., 2016; Rau et al., 2020), the method extension presented in this work covers a disentanglement of multiple influences, such as Earth-, OT_{SE}-, atmospheric-, and river tides in groundwater heads. The presented K_1-based removal of river tide influences on groundwater head amplitude spectra enables the application of S_2-based methods for the calculation of γ in deltaic groundwater systems, where superposing multiple tidal forcings govern tidal constituents in groundwater heads.

The results of this novel extension are verified using two additional independent methods: (i) the barometric response function (BRF), and (ii) the groundwater head response to distinct precipitation events. All three methods yield consistent results of $\gamma_{GW1a} \approx 0.9$, $\gamma_{GW1b} \approx 0.7$ and $\gamma_{GW1c} \approx 0.7$, confirming that the new frequency-based approach is valid.

The calculated K_1:M_2 amplitude ratio in groundwater heads lie within 0.95–1.47 and therefore between the K_1:M_2 amplitude ratios in Earth tide- and OT_{SE}-strains (0.24) and the K_1:M_2 ratio in river water levels (2.57). This, together with the conducted magnitude-squared coherence analysis, indicates the presence of river tide imprints in groundwater head amplitude spectra and underlines the necessity to disentangle these influences with the introduced novel approach (Eqs. (7)–(10)).

The method's presumption of insignificant K_1 contribution from Earth tide- and OT_{SE}-strains to groundwater signals is evaluated by a multiplication of the K_1:M_2 amplitude ratio in Earth tide- and OT_{SE}-strains (0.24) with the M_2 amplitude in groundwater due to Earth tide- and OT_{SE}-strains (1.7 mm, 1.3 mm, 3.3 mm, see Fig. 11b). This simplified consideration results in calculated amplitudes of 0.4 mm, 0.3 mm, 0.8 mm, which equals a share of 7 %, 8 % and 17 % of Earth tide- and OT_{SE}-strain contribution to the K_1 signal in groundwater heads. While these contributions are minor compared to the river tide signals, they

might not per se be considered negligible. However, given that the complementary calculation of *BE* without consideration of river tides and OT_{SE} based on the method of Rau et al. (2020) shows minimal variations of *BE* (0.00–0.02), inaccuracies due to simplifications within this method are negligible for the application with the given tidal composition at the study site. The uncertainties in the HALS-based estimation of tidal constituents (Table 3) are generally low, and given the consistency with loading efficiencies derived from other methods, uncertainties in the tidal constituents are considered to have a negligible effect on the calculated $BE_{S_2}^{AT}$ and γ.

The investigation of rainfall loading responses in deep observation wells is an established method for the assessment of loading signals in groundwater head data (Sophocleous et al., 2006; Bardsley and Campbell, 2000; Jan et al., 2007) and is suitable to verify the results of the novel approach that disentangles multiple influences. In assessments of rainfall loading responses, uncertainties may originate from limitation of the groundwater level and the accuracy of the precipitation monitoring instrument. While more intense precipitation events result in a clearer groundwater level response, there is a concomitant decrease in the accuracy of the recorded precipitation. Moreover, intense precipitation events, which typically occur in the tropical monsoon rainfall environment of Southeast Asia, commonly underly high spatiotemporal variation (Mandapaka et al., 2017), highlighting the need for on-site precipitation records when evaluating groundwater head responses to precipitation loading. The minor to moderate variations in the calculated loading efficiency of ± 0.02 to ± 0.06 across three independent precipitation events (Table 2) align well with estimates of γ based on BRF and $BE_{S_2}^{AT}$. In contrast to the first and third precipitation events, which lasted approximately 2 and 6 h respectively, the second event extended over a substantially longer period of about 150 h. Given the derived time factors and the general assessments of Smith et al. (2017), such long-duration precipitation events may allow for pore pressure dissipation through groundwater flow, whereas the shorter events can be considered instantaneous in terms of loading. Accordingly, the two short events are more appropriate for estimating the loading efficiency γ. The long-duration event yields a notably higher γ at GW1b, whereas γ values at GW1a and GW1c remain in the range of those derived from the shorter events. Overall, the results support the method's applicability in the study area, particularly for short-term precipitation events, and underline its potential for application in other deltaic aquifer systems in Southeast Asia with similar hydrometeorological and hydrogeological settings.

Calculating the BRF is a well-established method for the estimation of *BE* and γ (Furbish 1991; Rasmussen and Crawford, 1997; Turnadge et al., 2019). The present study derives the BRF within a multi-factor regression deconvolution, and not only from barometric and groundwater observations. The consideration of all relevant loading signals within MUFACO proved essential, given that a comparative analysis considering barometric pressure as the only driver suggested distinctly different values for *BE* and γ compared to the complete consideration with additional Earth-, ocean- and river tides as well as pond loading. To the authors' best knowledge, this study is first to consider multiple forcings, such as Earth-, ocean- and river tides as well as seasonal surface water accumulation, when calculating BRF, *BE* and γ. This allows application in more settings such as deltaic aquifers.

Oscillating BRF-patterns as in BRF_{GW1a} (Fig. 12a-I) are indicative for non-constant groundwater extraction influencing the regression deconvolution (Haehnel et al., 2024). Dörr et al. (2025) showed that periodic groundwater extraction can leak into amplitude spectra of observation wells at harmonics, i.e., multiples of S_1, including S_2 and S_3. Therefore, the presence of the S_3 amplitude peak (Fig. 10d-III) and the oscillating BRF-pattern at GW1a are indicators for nearby groundwater extraction, afflicting the observed S_2 groundwater amplitude.

Overall, the results demonstrate the presence of loading signals in observed groundwater heads across the three aquifers in the southern VMD and establish a solid quantification of γ. This is supported by independent analyses in both the frequency domain (Fig. 10) and the time domain, covering periods from a few hours (Fig. 9a) to days (Fig. 9b) and months (Fig. 8c). Furthermore, the findings align with recent research (Hoang and Steinel, 2021; Dörr et al., 2025) in identifying loading signals in the southern VMD. For the first time, this study provides a quantification of the loading efficiency of γ for three vertically stacked and highly exploited aquifers in the deltaic aquifer of the southern VMD. Further applications in the study area would benefit from more multi-parameter monitoring stations comprising observations of groundwater dynamics, soil moisture and meteorological parameters, such as the here utilized study site GW1.

4.2. Seasonal loading characteristics

The dynamics of observed groundwater heads have an evident correlation with the calculated loading due to pond water level dynamics in the rainy season (May to November, Fig. 8c). Based on the elaborated framework of groundwater-loading response for confined groundwater systems (Eq. (3)), the local aquifer-aquitard stratification (Fig. 1b), as well as the time scale of the groundwater-loading responses (Fig. 9,

Table 3
Calculated HALS amplitudes and phases for multiple drivers and groundwater heads at GW1 for O_1, K_1, M_2 and S_2 frequency including the calculated standard deviation (±σ).

	Drivers							
Frequency	Earth tides		OT_{SE}		River water levels		Barometric pressure	
	Amplitude ± σ (nstr)	Phase ± σ (°)	Amplitude ± σ (nstr)	Phase ± σ (°)	Amplitude ± σ (mm)	Phase ± σ (°)	Amplitude ± σ (mm)	Phase ± σ (°)
O_1	2.34 ± 0.02	10.3 ± 0.6	1.17 ± 0.01	152.7 ± 0.2	63.45 ± 1.52	310.8 ± 1.4	–	–
K_1	3.42 ± 0.04	103.7 ± 0.7	1.95 ± 0.01	222.6 ± 0.3	109.2 ± 2.73	38.4 ± 1.4	–	–
M_2	17.49 ± 0.02	22.4 ± 0.1	1.94 ± 0.01	183.7 ± 0.1	42.42 ± 1.52	201.6 ± 2.1	–	–
S_2	7.97 ± 0.02	182.2 ± 0.2	0.61 ± 0.01	323.3 ± 0.5	10.28 ± 1.52	244.9 ± 8.5	12.67 ± 0.09	256.3 ± 0.4

	Groundwater response					
Frequency	GW1a		GW1b		GW1c	
	Amplitude ± σ (mm)	Phase ± σ (°)	Amplitude ± σ (mm)	Phase ± σ (°)	Amplitude ± σ (mm)	Phase ± σ (°)
O_1	2.31 ± 0.44	276.2 ± 10.9	1.8 ± 0.28	273.1 ± 8.9	2.45 ± 0.12	261 ± 2.9
K_1	5.88 ± 0.78	359.2 ± 7.6	3.96 ± 0.5	355.6 ± 7.2	4.73 ± 0.22	356.2 ± 2.7
M_2	3.99 ± 0.44	169.5 ± 6.3	2.89 ± 0.28	160.1 ± 5.5	4.97 ± 0.12	180.2 ± 1.4
S_2	8.39 ± 0.44	92.9 ± 3	3.61 ± 0.28	40.2 ± 4.4	4.12 ± 0.12	45.1 ± 1.7

Fig. 12) this correlation strongly suggests, that loading effects cause the apparent seasonal rise in groundwater heads.

Directly after precipitation events, the load of the fallen rainwater exerts a spatially extensive and uniform load (Fig. 9 and peaks in Fig. 8c), as well as equally rising river water levels (Fig. 8c). Given that the river water levels regulate the responding area's drainage dynamics, the correlation of increasing and decreasing groundwater head dynamics after intensive precipitation events (peaks in Fig. 8c) with the river water level dynamics is associated to drainage and temporary loading–unloading dynamics. Therefore, the correlation of river water levels and groundwater heads is particularly well pronounced when heads peak and decrease due to distinct intensive precipitation events and the subsequent drainage (Fig. 8c).

The rise in pond water levels, calculated by means of accumulated precipitation and evaporation, complies well with reported seasonally rising water levels in intensive shrimp farming ponds in the study area, as observed by Anh et al. (2010). However, in the absence of direct monitoring data on pond water levels and records of supplemental water use, a more precise characterization of water level dynamics in the aquaculture ponds is not feasible for the investigated study site. Considering legal restrictions on groundwater abstraction for aquaculture (Van Binh et al., 2025) and the declining quality of surface water, the availability of suitable water sources for supplemental use appears limited. The overall good agreement between the precipitation–evaporation-based estimates and both reported seasonal pond water level trends and the loading efficiencies derived from the PLRF and other approaches in this study supports the validity of using precipitation and evaporation as proxies for pond water levels in the study area. Future investigations would benefit from continuous monitoring of pond water levels and quantification of supplemental water use in aquaculture systems. Given the rapid expansion of coastal aquaculture in Southeast Asia (Luo et al., 2022), precipitation accumulation in such ponds likely represents a significant surface loading process influencing groundwater head dynamics in confined deltaic aquifer systems across the region.

Whilst the accumulation of surface water induces an increase in observed groundwater levels during the rainy season (May to November in Fig. 8c), declining surface water levels in the dry season, e.g. due to pond water evaporation and significantly lower river water levels due to reduced upstream discharge of the Mekong River, equally cause a decline of observed groundwater heads. However, due to the lack of longer (i.e., complete annual) datasets, the present analysis is largely restricted to evaluating loading dynamics during the rainy season, which curtails the full potential of the presented approach. Multi-year time series encompassing several seasonal loading and unloading cycles would provide a valuable basis for future investigations aiming to correct groundwater head variations for surface loading effects in the VMD. In the absence of continuous dry-season observations, unloading dynamics can only be addressed qualitatively for short subperiods in this study. For instance, the short temporary rise in observed groundwater levels at GW1 during the dry season in February 2023 shows an evident correlation with the river water level dynamics (highlighted by a square box Fig. 8c). This is interpreted to be due to unloading caused by a temporary hydraulic connection of aquaculture ponds and the multi-channel system, as a result from pond flushing activities, a common practice for sludge removal between production cycles during this time (Anh et al., 2010).

A comparison of the response functions to river water levels (Fig. 12d) and pond water loading (Fig. 12c) shows a stronger response to the calculated loading of ponds than to the river water levels. Together with the evaluation of pond sizes, field observations, and the elaborated interpretation of the PLRF, this supports the assumption that the majority of the aquaculture ponds within the study area are operated as intensive shrimp farming ponds and accumulate water from precipitation.

The identification of surface loading as a major contributor to rising groundwater heads in the southern VMD enables a more refined evaluation of groundwater responses to periods of extreme hydrological conditions, such as dry-season droughts or exceptionally wet rainy seasons. Within this framework, severe groundwater depletion during droughts can be attributed not only to increased water demand but also to exceptionally low surface water levels and the associated unloading effects. Similarly, rainy seasons with exceptionally high precipitation and the resulting elevated surface water levels induce a more pronounced seasonal rise in groundwater heads compared to rainy seasons with average rainfall.

4.3. *Aquifer confinement status: Surface water drainage vs. Aquitard leakage*

The pond loading response functions obtained from the multi-factor regression deconvolution are characterized by an initial rise and a subsequent decrease with increasing time lag consideration (Fig. 12c). The initial peaks represent the loading efficiency as they feature the groundwater responses to precipitation events, which exert a uniform loading within the entire responding area of the observation well at first. These peak values comply well with the loading efficiency derived from BRF, $BE_{S_2}^{AT}$ and the response to the selected distinct precipitation events. Whilst aquaculture ponds are considered to accumulate precipitation and hence the load, urban areas and parts of vegetated land drain the rainwater into the multi-channel systems, from where it is discharged from the responding area of the observation well. This causes a decrease of the overall load, which manifests as a decrease in the PLRF curve. Understanding the decreasing trends of the PLRF curves as unloading signals due to surface water drainage, the values towards which the PLRF converges are associated with the product of the loading efficiency and the percentage of area, which accumulates water resources over the rainy season. For all PLRF curves (Fig. 12c), this complies well with the derived LULC-classification considering ponds and parts of vegetated land (Fig. 7b) and loading efficiencies, in particular for GW1c (Fig. 12c-III), where due to a good sensor resolution, the uncertainty of the response function is minimal. This suggests that the various surface loading of individual LULC can be simplified to a uniform loading based on their share of land cover. However, unless the accumulation of water resources can be formulated precisely for all LULC-classes, the removal of loading signals based on γ and $\Delta\sigma_L$ can only provide a range of possible corrected groundwater heads (Fig. 14) depending on the accuracy of $\Delta\sigma_L$ estimates for each LULC-class and the representativeness of the responding area. With regard to the latter, Fig. 7b shows minor variations in the spatial distribution of LULC-class, thereby indicating that imprecise estimates on the size of the responding area would have little impact on the corrected groundwater heads.

While decreasing trends in response functions are commonly indicative for semi-confined conditions (Butler et al., 2011; Hussein et al., 2013), the obtained decreasing trends of the pond loading-response functions are attributed to surface drainage processes in the study area. A misinterpretation of the decreasing trends in response functions as an indicator for aquitard leakage or aquitard drainage would be precarious in the context of land subsidence due to aquitard compaction. Further investigations on the correlation of groundwater depletion and sediment compaction due to aquitard drainage are required, such as depth-differentiated multi-extensometer compaction monitoring (Dörr et al., 2023).

With the available data, an independent quantitative consideration of these drainage-induced temporary loading–unloading processes is not possible beyond the presented descriptive assessment. Further studies, aiming to enhance the assessment of seasonal loading signals by the calculation of a uniform loading time series for the loading response areas of the groundwater wells, need to consider and verify the water balance of all LULC-classes. This would include a quantification of plant and canopy water accumulation as well as multi-year time series encompassing measurements of pond water levels, temporary

inundation levels of vegetated land as well as investigations on the source and use of supplemental water in aquacultural practices.

For barometric as well as Earth- and ocean tide loading signals, which are predominantly characterized by (semi-)diurnal loading cycles, the vertical transient flow of groundwater due to the pore pressure in Eq. (3) may be neglected, as the estimated time factors of 1.4 to 6.7 days are greater than the (semi-)diurnal loading duration (van der Kamp and Schmidt, 2017). This is substantiated by the shape of the BRF and EORF curves (Fig. 12a and b) which are characterized by plateaus and therefore indicate confined conditions, i.e. no vertical flow from an overlying aquitard due to the processes under consideration.

Conversely, for longer loading cycles like the seasonal pond water loading, the vertical transient flow of groundwater may generate a certain flow. The time factor T describes the duration in which 93 % of the consolidation and associated drainage processes are completed (Shukla et al., 2009; Terzaghi, 1943). Therefore, using a time lag of 7 days (168 h) is sufficient to capture potential contributions of vertical flow to the groundwater-loading response within the multi-factor regression deconvolution for the study area, where T was estimated between 1.4 and 6.7 days. However, as the shape of the PLRF curve is governed by drainage processes of surface water resources, which equally cause a declining trend in the response function, the present study cannot provide evidence for or against aquitard leakage processes based on the shape of response functions.

4.4. Corrected groundwater heads and implications for groundwater recharge

Regression deconvolution has been applied in multiple previous studies to remove diverse influences on groundwater heads, e.g., barometric pressure (Furbish 1991; Rasmussen and Crawford, 1997), Earth tides (Toll and Rasmussen, 2007), soil moisture and variations in surface water storage (van der Kamp and Maathuis, 1991), river water levels (Spane and Mackley, 2011), sea levels (Haehnel et al., 2024) or to evaluate aquifer hydraulic conductivity with atmospheric slug test (Valois et al., 2022; 2023).

The multi-factor regression deconvolution applied in this study allows an individual and more flexible consideration of multiple influences (Haehnel et al., 2024) and is therefore suitable for the assessment and removal of multiple forcings on observed groundwater levels as given in deltaic groundwater systems. To the best of the authors' knowledge, this study is the first to consider a variety of natural forcings in the correction of observed groundwater heads, including Earth, ocean and river tides, barometric pressure variations as well as surface water accumulation in anthropogenically managed environments.

In the study area, the removal of loading signals during the rainy season reveals corrected groundwater heads with downward trends, whilst the observed (uncorrected) groundwater heads show rising trends. The estimated corrected depletion rates during the rainy season of -0.59 m a^{-1}, -0.65 m a^{-1} and -0.44 m a^{-1} are below the annual average depletion rates of -0.70 m a^{-1}, -0.97 m a^{-1} and -0.73 m a^{-1} for the three assessed observation wells calculated between rainy season onsets 2023 and 2024 (Fig. 2a).

The corrected groundwater heads derived from the multi-factor regression deconvolution are subject to uncertainties. The illustrated standard deviations in the results demonstrate that the measurement precision and resolution of groundwater level sensors exert a pronounced influence on the magnitude of these uncertainties. At observation wells GW1a and GW1b, groundwater heads were recorded with low precision (Fig. 2b), resulting in equally imprecise response coefficients. The uncertainties of the response coefficients accumulate in the response function and ultimately manifest in the uncertainties of the corrected groundwater heads. Fig. 12 and Fig. 13 illustrate that both response functions and corrected heads exhibit substantial uncertainties at GW1a and GW1b, where sensor resolution is low, whereas uncertainties are minimal to moderate at GW1c, where measurements were obtained with higher precision. This pattern is also reflected in the R^2 of the regression deconvolution, characterized by good R^2 of 0.89 for GW1c and moderate to poor R^2 of 0.55 and 0.16 for GW1a and GW1b respectively. Despite their low R^2 values and high standard deviations, the response functions and corrected heads at GW1a and GW1b are considered reliable, supported by the consistency of groundwater dynamics (Fig. 2a) and response functions (Fig. 12) with those of GW1c, as well as their overall agreement with other methods applied in this study. In addition to uncertainties arising from sensor resolution, uncertainties in the estimation of pond water loading, derived here from a precipitation–evaporation-based approach, contribute to the overall uncertainty of the corrected heads. To reduce these effects in future studies, continuous monitoring of pond water levels is recommended.

Within a cross-validation framework, the performance of the multi-factor regression deconvolution was evaluated exemplarily for GW1c. For this purpose, a set of response functions was derived from 60 sub-datasets, each covering 120 days of the complete observation period, and subsequently applied to correct the full groundwater head time series. Fig. 15 illustrates that all 60 corrected time series consistently confirm the overall depletion trend, albeit with a less pronounced decline compared to the correction based on the full dataset. This result supports the interpretation of persistent groundwater depletion and, at the same time, emphasizes the importance of long-term records comprehensive model validation for a more accurate quantification of the depletion rate.

In light of the outlined uncertainties, independent validation is necessary to strengthen the presented conclusions regarding persistent groundwater depletion. Such validation could involve analyses of mass variations derived from the Gravity Recovery and Climate Experiment (GRACE) satellite mission (Tapley et al., 2004), combined with observations of pond and river water levels and detailed records of groundwater extraction rates at monthly or higher temporal resolution. Considering legal restrictions on groundwater use for large-scale rice farming and aquaculture (Van Binh et al., 2025), it is reasonable to assume that a substantial share of groundwater extraction meets seasonally independent demands, such as domestic water use. Considering the long-term annual-average groundwater depletion rates of recent years and decades together with the conceptual framework presented here,

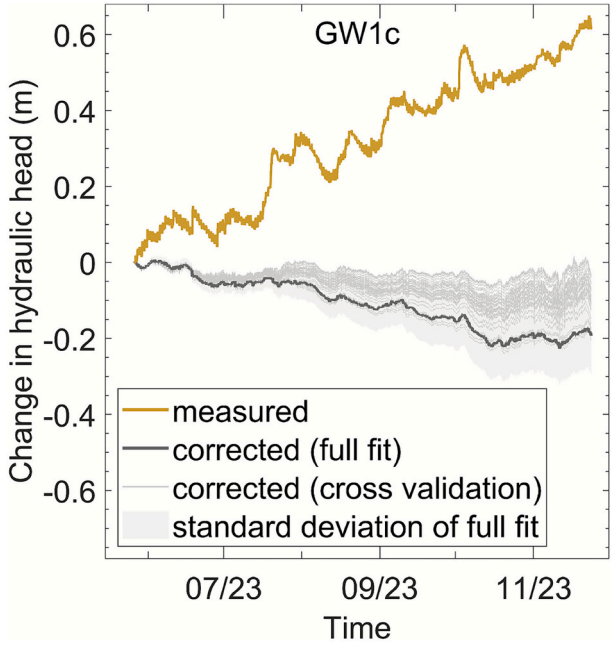


Fig. 15. Measured and corrected groundwater heads for GW1c, including 60 corrected time series derived within the cross-validation framework.

which attributes seasonally rising groundwater heads to surface loading, a persistent decline in loading-corrected groundwater heads throughout the seasons appears realistic. Thus, the smaller yet pronounced depletion rates obtained from the corrected groundwater heads during the rainy season appear reasonable compared to the annual-average groundwater depletion rates. Depending on the underlying uncertainties, the magnitude of these depletion rates may vary, yet the overall pattern is consistently reproduced.

Overall, the evaluation of uncertainties in the corrected groundwater heads indicates that the derived depletion rates may not accurately represent the actual loading-corrected groundwater dynamics. Nevertheless, they support the overall conclusion that loading-corrected groundwater heads decline during the rainy season, whereas the measured data show a rising trend.

In addition to the loading correction by multi-factor regression deconvolution (Fig. 13), groundwater heads were corrected based on the derived loading efficiency γ and the change of the area-averaged surface load $\Delta\sigma_L$ (Fig. 14). Due to the uncertainty about surface water accumulation on vegetated land, groundwater heads corrected by this method are characterized by a high uncertainty. A comparison with the groundwater head correction by MUFACO suggests that 25 % (GW1a), 46 % (GW1b) and 36 % (GW1c) of the vegetated land accumulate water resources based on the balance of precipitation and evaporation, while the remaining share of vegetated land is drained. Given that unintended flooding and inundation of agricultural farmland can be counteracted relatively effectively in the VMD by its complex multi-channel system of irrigation and drainage channels (Le et al., 2023), this is in a reasonable order of magnitude and substantiates the correction based on MUFACO.

The comparison of the two approaches for the correction of loading signals underlines that, unless a precise water balance within the loading response area of an observation well can be formulated, a correction of groundwater heads by multi-factor regression deconvolution is preferable to a correction based on calculated values for γ and derived surface loading timeseries.

Overall, the evaluation of loading-corrected groundwater heads indicates that groundwater recharge, if present, is insufficient to compensate for extractions in the assessed aquifers. This aligns with the local and regional thicknesses of the Holocene Q_2 aquitard of approx. 20–30 m (Fig. 1b; Anderson, 1978; Pham et al., 2019; Bauer et al., 2022), through which percolation of surface water is considered unlikely at the timescale considered in this study. By the multi-factor regression deconvolution, any significant rise in observed heads was attributed to local loading processes on the ground surface. The loading-corrected time series therefore contain no indication for possible recharge at potential aquifer outcrops, which have been shown to propagate as pressure signals through confined aquifers (Armstrong & Narayan, 1998).

In previous studies (Duy et al., 2021), a relationship between groundwater and river water levels in the VMD was identified using time series analysis. However, as the authors acknowledge themselves, the applied black-box correlation is incapable of exploring the causes for the observed relationship. Therefore, considering the present results, the postulation of possible groundwater recharge to shallow and deep aquifers during the flood season should be reconsidered. The present analysis shows that the observed groundwater dynamics can be consistently explained by mechanical loading responses rather than by actual infiltration and recharge. Data-driven approaches can provide valuable insights into process dynamics, but their interpretation must remain embedded within a consistent physical framework. In the context of this study, that framework is the groundwater response to mechanical surface loading. When recharge is postulated, as in Duy et al. (2021), its plausibility should be evaluated in light of the actual hydraulic gradients and transmissivities controlling recharge flow processes.

Furthermore, the applicability of the water-table-fluctuation method must be carefully reconsidered wherever the investigated aquifer is confined or not developed, such as at the monitoring sites Q177 and Q199 in the southern VMD analyzed by Van et al. (2023). The water-table-fluctuation method attributes rising groundwater heads to groundwater recharge. While this approach is feasible for unconfined aquifers, its application in confined settings is inappropriate and can lead to a misinterpretation of loading-induced head increases as recharge. Under such conditions, the observed rise in groundwater heads in the southern VMD most likely reflects hydro-geomechanical responses to surface loading rather than actual infiltration or recharge.

Overall, this study challenges previous interpretations by Duy et al. (2021) and Van et al. (2023), which attributed groundwater responses to precipitation and river water levels as indicators of recharge without appropriately accounting for surface loading effects.

This study highlights the importance of identifying and removing loading signals from groundwater head data for strongly confined aquifers in aquaculture-dominated deltaic systems to achieve an accurate understanding of water resource dynamics. It emphasizes that reliable groundwater recharge assessments in such environments must account for these loading effects. By doing so, the findings provide valuable guidance for efforts to determine sustainable groundwater extraction rates and preventing further depletion. Future research could combine the presented data-driven approach with physically based methods to further assess potential groundwater recharge and verify both local and regional water balances. In particular, obtaining reliable groundwater extraction data for use in comprehensive water balance analyses, together with a delta-wide hydro-geomechanically coupled groundwater model that accounts for surface loading, would provide a sound framework for more holistic recharge assessments. Such integrative approaches would enable a more detailed understanding of the spatial and temporal variability of actual recharge processes and surface loading, as well as the associated groundwater head dynamics, thereby supporting the validation of recharge estimates derived from the groundwater-loading analysis presented in this study.

By showing that groundwater recharge, if present at all, is insufficient to compensate for the current exploitation, the present study highlights the necessity for developing alternative freshwater resource strategies as essential concepts for the region's sustainable development.

5. Conclusion

Observed rising trends in groundwater heads within confined aquifers may not necessarily indicate groundwater recharge, as these trends can also be attributed to mechanical loading at the surface. A comprehensive analysis of loading signals in groundwater heads in the southern VMD between 2023 and 2024 strongly suggests that the seasonal rise in groundwater heads is primarily due to the accumulation of surface water in aquaculture ponds during the rainy season. By removing these loading signals from groundwater observation data, the trend reverses, showing declining groundwater heads. This implies that not only in dry but also in rainy season, groundwater recharge, if present, is incapable of compensating for the groundwater exploitation in the study area. Independent validation, for example using GRACE-based mass balances, is essential to substantiate the conclusions on persistent groundwater depletion.

The influence of temporary flooding and inundation on surface loading processes in deltas has been a persistent phenomenon over the course of geological history. However, the recent rapid expansion of aquaculture ponds has introduced a new infrastructure capable of holding substantial surface water volumes. This shift in land use and land cover is a common feature in many deltaic and coastal zones across Southeast Asia, highlighting the broader relevance of this study beyond the southern VMD. Future research would greatly benefit from monitoring data on pond water level dynamics, solid quantification of hydraulic properties, water balances and other factors contributing to seasonal surface loading to improve the correction of groundwater heads in confined aquifers beneath.

Data-driven approaches to groundwater recharge assessment must

be firmly grounded in a consistent physical framework. Purely statistical correlations between surface and groundwater levels may lead to misinterpretations of recharge processes. The preconditions for applying easy-to-use methods, such as the water table fluctuation method, must be carefully evaluated, as these methods are not suitable for confined aquifer systems. Within the framework of groundwater-loading response in confined aquifers, the analysis of groundwater head responses to distinct precipitation events represents a straightforward and effective diagnostic indicator of loading effects. A sound quantification of surface and, where present, unconfined aquifer water balances provide an essential foundation for the (multi-)seasonal correction of groundwater head time series for loading signals. Combined with a robust definition of loading efficiency, or integrated within a multi-factor regression deconvolution, these water balances constitute key input parameters for isolating and removing loading signals from groundwater head time series on (multi-)seasonal time scales. Furthermore, the reliability of such deconvolution-based corrections strongly depends on the availability of long-term observation records and should be systematically tested, for example through cross-validation, to ensure robust and transferable conclusions.

The method of calculating an aquifer's loading efficiency from the groundwater head responses to atmospheric tides at the S_2 frequency has seen significant development over the past decade. Unlike earlier approaches limited to areas without river and ocean tidal influences, the current method incorporates these additional tidal drivers into the analysis, representing a novel advancement. This advancement enables the calculation of loading efficiency using S_2-based methods in deltaic groundwater systems elsewhere, where multiple tidal forcings influence the tidal constituents in groundwater heads.

These findings provide valuable insights for groundwater recharge assessments and play a critical role in shaping sustainable water resource management strategies in the southern Mekong Delta and other confined deltaic aquifers. By evaluating loading signals within groundwater time series, this study advances a more holistic understanding of groundwater dynamics – especially the coupling between hydrological and geomechanical processes – in confined deltaic aquifer systems.

CRediT authorship contribution statement

Felix Dörr: Writing – original draft, Visualization, Methodology, Investigation, Formal analysis, Data curation, Conceptualization. **Jonas Bauer:** Writing – review & editing, Validation, Investigation, Formal analysis. **Gabriel C. Rau:** Writing – review & editing, Validation, Methodology, Conceptualization. **Elias Lewi:** Writing – review & editing, Methodology. **Viet Tran Hoan:** Data curation, Investigation, Writing – review & editing. **Le Thi Mai Van:** Writing – review & editing, Project administration, Data curation. **Remi Valois:** Writing – review & editing, Software. **Anke Steinel:** Writing – review & editing, Conceptualization. **Franz Nestmann:** Writing – review & editing, Supervision, Resources, Project administration, Funding acquisition. **Stefan Norra:** Writing – review & editing, Supervision, Resources, Project administration, Funding acquisition.

Declaration of competing interest

The authors declare that they have no known competing financial interests or personal relationships that could have appeared to influence the work reported in this paper.

Acknowledgements

This research was conducted in the frame of the project "ViWaT – Vietnam Water Technologies" funded by the German Federal Ministry of Education and Research (funding reference: 02WCL1474A). Felix Dörr thanks the Hector Fellow Academy for support. We gratefully thank the Vietnamese Ministry of Science and Technology (MOST), the National Center for Water Resources Planning and Investigation (NAWAPI) and the Department of Natural Resources and Environment Ca Mau (DONRE Ca Mau) as well as the Federal Institute for Geosciences and Natural Resources (BGR) for the good cooperation and providing data. We acknowledge support by the KIT-Publication Fund of the Karlsruhe Institute of Technology, Germany. We acknowledge the developers of the software tools PyGTide, HydroGeoSines, and Groundwater.app for making their applications and methods publicly available, which supported parts of the data analysis in this study.

Data availability

The data used in this study are available at a Zenodo repository: https://doi.org/10.5281/zenodo.17279956.

References

Acworth, R.I., Halloran, L.J.S., Rau, G.C., Cuthbert, M.O., Bernardi, T.L., 2016. An objective frequency domain method for quantifying confined aquifer compressible storage using Earth and atmospheric tides. Geophys. Res. Lett. 43, 11671. https://doi.org/10.1002/2016GL071328.

D.C. Agnew SPOTL: some programs for ocean-tide loading, SIO technical report, Scripps Institution of Oceanography 2012 UC San Diego, California 954322pg (last access: 22 May 2025.

R.G. Allen L.S. Pereira D. Raes M. Smith Crop evapotranspiration: guidelines for computing crop water requirements FAO Irrigation and Drainage Paper 56 1998 Rome, 300 pp.

Anderson, H. R.,1978: Hydrogeologic Reconnaissance of the Mekong Delta in South Vietnam and Cambodia. Contributions to The Hydrology of Asia and Oceania, Geological Survey Water-Supply Paper 1608-R.

Anh, P.T., Kroeze, C., Bush, S.R., Mol, A.P., 2010. Water pollution by intensive brackish shrimp farming in south-east Vietnam: causes and options for control. Agric. Water Manag. 97 (6), 872–882. https://doi.org/10.1016/j.agwat.2010.01.018.

Armstrong, D., Narayan, K., 1998. The basics of recharge and discharge. CSIRO, Collingwood, Victoria.

Bardsley, W.E., Campbell, D.I., 2000. Natural geological weighing lysimeters: calibration tools for satellite and ground surface gravity monitoring of subsurface water-mass change. Nat. Resour. Res. 9, 147–156. https://doi.org/10.1023/A:1010147527484.

Bauer, J., Börsig, N., Pham, V.C., Hoan, T.V., Nguyen, H.T., Norra, S., 2022. Geochemistry and evolution of groundwater resources in the context of salinization and freshening in the southernmost Mekong Delta. Vietnam. J. Hydrol. Reg. Stud. 40. https://doi.org/10.1016/j.ejrh.2022.101010.

Bauer, J., Dörr Vu, F., Duong, H.T., Schenk, A., Tran, H.V., Pham, V.C., Börsig, N., Van Der Linden, R., Nguyen, N.H., Eiche, E., Norra, S., 2025. Seawater intrusion in river delta systems. Inter-annual dynamics and drivers of salinity variations in the southern Mekong Delta Vietnam. J. Hydrol. 661, 133745. https://doi.org/10.1016/j.jhydrol.2025.133745.

Binh, D. Van, Tran, D.D., Thái Dương, V.H., Bauer, J., Park, E., Loc, H.H., 2025. Land use change in the Vietnamese Mekong Delta: Long-term impacts of drought and salinity intrusion using satellite and monitoring data. iScience 28. https://doi.org/10.1016/j.isci.2025.112723.

Burgess, W.G., Shamsudduha, M., Taylor, R.G., Zahid, A., Ahmed, K.M., Mukherjee, A., et al., 2017. Terrestrial water load and groundwater fluctuation in the Bengal Basin. Sci. Rep. 7 (1), 3872. https://doi.org/10.1038/s41598-017-04159-w.

Butler, J.J., Jin, W., Mohammed, G.A., Reboulet, E.C., 2011. New insights from well responses to fluctuations in barometric pressure. Ground Water 49 (4), 525–533. https://doi.org/10.1111/j.1745-6584.2010.00768.x.

Davydzenka, T., Tahmasebi, P., Shokri, N., 2024. Unveiling the global extent of land subsidence: the sinking crisis. Geophys. Res. Lett. 51, e2023GL104497. https://doi.org/10.1029/2023GL104497.

Domenico, P.A., Schwartz, F.W., 1998. Physical and chemical hydrogeology, 2nd ed. Wiley, Chichester, USA.

Dörr, F., Bauer, J., Rau, G.C., Valois, R., Hoan, T.V., Pham, V.C., Van, L.T.M., Steinel, A., Nestmann, F., Norra, S., 2025. Passive subsurface characterization in subsiding deltas: assessing land subsidence mitigation potential with frequency analyses of groundwater heads and superposing harmonic drivers. J. Hydrol. https://doi.org/10.1016/j.jhydrol.2025.133844.

Dörr, N., Schenk, A., Hinz, S., 2024. Land subsidence in the mekong delta derived from advanced persistent scatterer interferometry with an infrastructural reference network. IEEE J. Sel. Top. Appl. Earth Obs. Remote Sens. 1–19. https://doi.org/10.1109/JSTARS.2024.3420130.

Dörr, F., Bauer, J., Tran, H.V., Norra, S., Nestmann, F., 2023. Vietnams Mekong-Delta - Landsenkung infolge von Grundwasserübernutzung. Forsch. | WASSERWIRTSCHAFT 64–68. (In German language) http://doi.org/10.1007/s35147-023-1922-3.

Duy, N.L., Nguyen, T.V.K., Nguyen, D.V., Tran, A.T., Nguyen, H.T., Heidbüchel, I., 2021. Groundwater dynamics in the Vietnamese Mekong Delta: trends, memory effects, and response times. J. Hydrol.: Reg. Stud. 33, 100746. https://doi.org/10.1016/j.ejrh.2020.100746.

Erban, L.E., Gorelick, S.M., Zebker, H.A., 2014. Groundwater extraction, land subsidence, and sea-level rise in the Mekong Delta Vietnam. Environ. Res. Lett. 9. https://doi.org/10.1088/1748-9326/9/8/084010.
Furbish, D.J., 1991. The response of water level in a well to a time series of atmospheric loading under confined conditions. In Water Res. 27 (4), 557–568. https://doi.org/10.1029/90WR02775.
Haehnel, P., Rasmussen, T.C., Rau, G.C., 2024. Technical note: Removing dynamic sea-level influences from groundwater-level measurements. Hydrol. Earth Syst. Sci. 28 (12), 2767–2784. https://doi.org/10.5194/hess-28-2767-2024.
Healy, R.W., Cook, P.G., 2002. Using groundwater levels to estimate recharge. In Hydrogeology Journal 10 (1), 91–109. https://doi.org/10.1007/s10040-001-0178-0.
Herrera-García, G., Ezquerro, P., Tomás, R., Béjar-Pizarro, M., López-Vinielles, J., Rossi, M., et al., 2021. Mapping the global threat of land subsidence. Science 371 (6524), 34–36. https://doi.org/10.1126/science.abb8549.
Ho, T.Q., Do, H.L., Eggert, H., 2025. Shrimp farming industry in Vietnam: An aquaculture performance indicators approach. In *Aquaculture Economics & Management*, pp. 1–24. https://doi.org/10.1080/13657305.2024.2449410.
Hoan, T.V., Richter, K.-G., Börsig, N., Bauer, J., Ha, N.T., Norra, S., 2022. An improved groundwater model framework for aquifer structures of the quaternary-formed sediment body in the southernmost parts of the mekong delta Vietnam. Hydrology 9, 61. https://doi.org/10.3390/hydrology9040061.
Hoang, T.H., Steinel, A., 2021. Technical Note TN-IV-01. Groundwater level monitoring data at the U Minh well group September 2016 to October 2020. https://www.deutsche-rohstoffagentur.de/EN/Themen/Wasser/Projekte/abgeschlossen/TZ/Vietnam/techn_noteIV-01_en.pdf?_blob=publicationFile&v=4.
Hussein, M.E., Odling, N.E., Clark, R.A., 2013. Borehole water level response to barometric pressure as an indicator of aquifer vulnerability. Water Resour. Res. 49 (10), 7102–7119. https://doi.org/10.1002/2013WR014134.
Jacob, C.E., 1950. Flow of groundwater. Engineering Hydraulics 321–386.
Jan, C.-D., Chen, T.-H., Lo, W.-C., 2007. Effect of rainfall intensity and distribution on groundwater level fluctuations. J. Hydrol. 332 (3–4), 348–360. https://doi.org/10.1016/j.jhydrol.2006.07.010.
Jasechko, S., Seybold, H., Perrone, D., Fan, Y., Shamsudduha, M., Taylor, R.G., Fallatah, O., Kirchner, J.W., 2024. Rapid groundwater decline and some cases of recovery in aquifers globally. Nature 625, 715–721. https://doi.org/10.1038/s41586-023-06879-8.
Johnston, D., Trong, N.V., Tien, D.V., Xuan, T.T., 2000. Shrimp yields and harvest characteristics of mixed shrimp–mangrove forestry farms in southern Vietnam: factors affecting production. Aquaculture 188, 263–284. https://doi.org/10.1016/S0044-8486(00)00348-3.
Konikow, L.F., Kendy, E., 2005. Groundwater depletion: a global problem. Hydrgeol. J. 13, 317–320. https://doi.org/10.1007/s10040-004-0411-8.
Ledieu, J., De Ridder, P., De Clerck, P., Dautrebande, S., 1986. A method of measuring soil moisture by time-domain reflectometry. J. Hydrol. 88, 319–328. https://doi.org/10.1016/0022-1694(86)90097-1.
Lee, E., Jayakumar, R., Shrestha, S., Han, Z., 2018. Assessment of transboundary aquifer resources in Asia: Status and progress towards sustainable groundwater management. J. Hydrol.: Reg. Stud. 20, 103–115. https://doi.org/10.1016/j.ejrh.2018.01.004.
Le, H.-A., Nguyen, T., Gratiot, N., Deleersnijder, E., Soarez-Frazão, S., 2023. The multi-channel system of the Vietnamese Mekong Delta: Impacts on the flow dynamics under relative sea-level rise scenarios. Water 15 (20), 3597. https://doi.org/10.3390/w15203597.
Luo, J., Sun, Z., Lu, L., Xiong, Z., Cui, L., Mao, Z., 2022. Rapid expansion of coastal aquaculture ponds in Southeast Asia: patterns, drivers and impacts. J. Environ. Manage. 315, 115100. https://doi.org/10.1016/j.jenvman.2022.115100.
Mandapaka, P.V., Qin, X., Lo, E.Y.M., 2017. Analysis of spatial patterns of daily precipitation and wet spell extremes in Southeast Asia. Intl Journal of Climatology 37 (S1), 1161–1179. https://doi.org/10.1002/joc.5073.
McMillan, T.C., Rau, G.C., Timms, W.A., Andersen, M.S., 2019. Utilizing the impact of earth and atmospheric tides on groundwater systems: a review reveals the Future potential. Rev. Geophys. 57, 281–315. https://doi.org/10.1029/2018RG000630.
Minderhoud, P.S.J., Erkens, G., Pham, V.H., Bui, V.T., Erban, L., Kooi, H., Stouthamer, E., 2017. Impacts of 25 years of groundwater extraction on subsidence in the Mekong delta Vietnam. Environ. Res. Lett. 12 (6), 64006. https://doi.org/10.1088/1748-9326/aa7146.
Minderhoud, P.S.J., Coumou, L., Erkens, G., Middelkoop, H., Stouthamer, E., 2019. Mekong delta much lower than previously assumed in sea-level rise impact assessments. Nat. Commun. 10, 1–13. https://doi.org/10.1038/s41467-019-11602-1.
Osenbrück, K., Steinel, A., Montcoudiol, N., Manh, V., Bäumle, R., 2025. Geochemical evolution and flow of groundwater impacted by long-term abstraction in the Mekong Delta Vietnam. J. Hydrol, 132881. https://doi.org/10.1016/j.jhydrol.2025.132881.
Pechstein, A., Hoang, T.H., Orilski, J., Le, H.N., Le, V.M., 2018. Detailed investigations on the hydrogeological situation in Ca Mau Province, Mekong Delta. Technical Report No III-5. BGR. Ho Chi Minh. City. https://www.pebs-eu.de/EN/Themen/Wasser/Projekte/abgeschlossen/TZ/Vietnam/techn_repIII-5_en.pdf?_blob=publicationFile&v=3.
Penman, H.L., 1948. Natural evaporation from open water, bare and grass. Proc. R. Soc. Lond. Ser. A 193, 120–145. https://doi.org/10.1098/rspa.1948.0037.
Pham, V.C., Bauer, J., Börsig, N., Ho, J., Vu, L., Tran, H., Dörr, F., Norra, S., 2023. Groundwater use habits and environmental awareness in Ca Mau Province, Vietnam: implications for sustainable water resource management. Environ. Challenges 13, 100742. https://doi.org/10.1016/j.envc.2023.100742.
Pham, H.V., Van Geer, F.C., Tran, V.B., Dubelaar, W., Oude Essink, G.H.P., 2019. Paleo-hydrogeological reconstruction of the fresh-saline groundwater distribution in the Vietnamese Mekong Delta since the late Pleistocene. J. Hydrol.: Reg. Stud. 23, 100594. https://doi.org/10.1016/j.ejrh.2019.100594.
Rasmussen, T.C., Crawford, L.A., 1997. Identifying and removing barometric pressure effects in confined and unconfined aquifers. Groundwater 35 (3), 502–511. https://doi.org/10.1111/j.1745-6584.1997.tb00111.x.
Rasmussen, T.C., Mote, T.L., 2007. Monitoring surface and subsurface water storage using confined aquifer water levels at the savannah river site, USA. Vadose Zone J. 6 (2), 327–335. https://doi.org/10.2136/vzj2006.0049.
Rau, G.C., Cuthbert, M.O., Acworth, R.I., Blum, P., 2020. Technical note: Disentangling the groundwater response to Earth and atmospheric tides to improve subsurface characterisation. Hydrol. Earth Syst. Sci. 24, 6033–6046. https://doi.org/10.5194/hess-24-6033-2020.
Rau, G.C., Eulenfeld T., Howe D., Rietbroek R., Gosselin J.S., Staniewicz S., 2022. hydrogeoscience/pygtide: PyGTide v0.7.1, Zenodo [code].
Schulze, K.C., Kümpel, H-J., Huenges, E., 2000. In-Situ Petrohydraulic Parameters from Tidal and Barometric Analysis of Fluid Level Variations in Deep Wells: Some Results From KTB. In Ingrid Stober, Kurt Bucher (Eds.): Hydrogeology of Crystalline Rocks. Dordrecht: Springer (Springer eBook Collection, 34), pp. 79–104 https://doi.org/10.1007/978-94-017-1816-5_4.
Schweizer, D., Ried, V., Rau, G.C., Tuck, J.E., Stoica, P., 2021. Comparing methods and defining practical requirements for extracting harmonic tidal components from groundwater level measurements. Math. Geosci. 53, 1147–1169. https://doi.org/10.1007/s11004-020-09915-9.
Shukla, S., Sivakugan, N., Das, B., 2009. Methods for determination of the coefficient of consolidation and field observations of time rate of settlement — an overview. Int. J. Geotech. Eng. 3 (1), 89–108. https://doi.org/10.3328/IJGE.2009.03.01.89-108.
Smith, C., van der Kamp, G., Arnold, L., Schmidt, R., 2017. Measuring precipitation with a geolysimeter. Hydrol. Earth Syst. Sci. 21 (10). https://doi.org/10.5194/hess-2017-174.
Sophocleous, M., Bardsley, W.E., Healey, J., 2006. A rainfall loading response recorded at 300 m depth: implications for geological weighing lysimeters. J. Hydrol. 319, 237–244. https://doi.org/10.1016/j.jhydrol.2005.06.031.
Spane, F.A., 2002. Considering barometric pressure in groundwater flow investigations. Water Res. 38 (6). https://doi.org/10.1029/2001WR000701.
Spane, F.A., Mackley, R.D., 2011. Removal of river-stage fluctuations from well response using multiple regression. Ground Water 49 (6), 794–807. https://doi.org/10.1111/j.1745-6584.2010.00780.x.
Syvitski, J.P.M., Kettner, A.J., Overeem, I., Hutton, E.W.H., Hannon, M.T., Brakenridge, G.R., et al., 2009. Sinking deltas due to human activities. Nature Geosci. 2 (10), 681–686. https://doi.org/10.1038/ngeo629.
Tapley, B.D., Bettadpur, S., Watkins, M., Reigber, C., 2004. The gravity recovery and climate experiment: mission overview and early results. Geophys. Res. Lett. 31, 2004GL019920. https://doi.org/10.1029/2004GL019920.
Terzaghi, K., 1943. Theoretical soil mechanics. Wiley, Chichester, UK.
Toll, N.J., Rasmussen, T.C., 2007. Removal of barometric pressure effects and earth tides from observed water levels. Ground Water 45 (1), 101–105. https://doi.org/10.1111/j.1745-6584.2006.00254.x.
Turnadge, C., Crosbie, R.S., Barron, O., Rau, G.C., 2019. Comparing methods of barometric efficiency characterization for specific storage estimation. Groundwater 57 (6), 844–859. https://doi.org/10.1111/gwat.12923.
Valiantzas, J.D., 2006. Simplified versions for the Penman evaporation equation using routine weather data. J. Hydro. 331 (3–4), 690–702. https://doi.org/10.1016/j.jhydrol.2006.06.012.
Valois, R., Rivière, A., Vouillamoz, J.M., Rau, G.C., 2024. Analytical solution for well water response to Earth tides in leaky aquifers with storage and compressibility in the aquitard. Hydrol. Earth Syst. Sci. 28 (4), 1041–1054. https://doi.org/10.5194/hess-28-1041-2024.
Valois, R., Derode, B., Vouillamoz, J.M., Valerie Kotchoni, D.O., Lawson, M.A., Rau, G.C., 2023. Use of atmospheric tides to estimate the hydraulic conductivity of confined and semi-confined aquifers. Hydrgeol. J. 31 (8), 2115–2128. https://doi.org/10.1007/s10040-023-02715-5.
Valois, R., Rau, G.C., Vouillamoz, J.M., Derode, B., 2022. Estimating hydraulic properties of the shallow subsurface using the groundwater response to Earth and atmospheric tides: a comparison with pumping tests. Water Resour. Res. 58 (5), e2021WR031666. https://doi.org/10.1029/2021WR031666.
Van Tuan, P., Jiang, Y., Stigter, T., Zhou, Y., 2024. Understanding groundwater use and vulnerability of rural communities in the Mekong Delta: the case of Tra Vinh province Vietnam. Groundwater for Sustainable Development 25, 101095. https://doi.org/10.1016/j.gsd.2024.101095.
Van, L.T.T., Lertsirivorakul, R., Vuong, B.T., Thang, C.H., 2023. Groundwater recharge in Mekong River Delta: an application of the water-table fluctuation method in the Long Xuyen Quadrangle and the Ca Mau Peninsula. Songklanakarin J. Sci. Technol. 45 (1), 51–58.
van der Kamp, G., 1972. Tidal fluctuations in a confined aquifer extending under the sea, 24th International Geological Congress, Section 11 (pp. 101–106). Montreal, Que., Canada.
van der Kamp, G., Gale, J.E., 1983. Theory of earth tide and barometric effects in porous formations with compressible grains. Water Resour. Res. 19 (2), 538–544 ISSN 19447973.
van der Kamp, G., Schmidt, R., 2017. Review: Moisture loading—the hidden information in groundwater observation well records. Hydrgeol. J. 25 (8), 2225–2233. https://doi.org/10.1007/s10040-017-1631-z.

van der Kamp, G., Maathuis, H., 1991. Annual fluctuations of groundwater levels as a result of loading by surface moisture. J. Hydrol. 127, 137–152. https://doi.org/10.1016/0022-1694(91)90112-U.

Vu, H.T.D., Tran, D.D., Schenk, A., Nguyen, C.P., Vu, H.L., Oberle, P., et al., 2022. Land use change in the Vietnamese Mekong Delta: new evidence from remote sensing. Sci. Total Environ. 813, 151918. https://doi.org/10.1016/j.scitotenv.2021.151918.

Wagner, F., Tran, V.B., Renaud, F.G., 2012. Chapter 7, Groundwater resources in the Mekong Delta: availability. In: Renaud Fabrice G., K.C. (Ed.), The Mekong Delta System - Interdisciplinary Analysis of a River Delta, 1st ed. Springer, Dordrecht, pp. 201–220. https://doi.org/10.1007/978-94-007-3962-87.

Wenzel, H.-G., 1996. The nanoGal software: Earth tide data processing package: ETERNA 3.3. Bulletin D'informations Des Marées Terrestres 124, 9425–9439.

A.3. Land Subsidence Dynamics in the Mekong Delta: Insights from Local High-Resolution Geomechanical Parameterization, Numerical Modelling, and Geodetic Observations (Dörr et al., 2026b)

Science of the Total Environment 1033 (2026) 181850

Contents lists available at ScienceDirect

Science of the Total Environment

journal homepage: www.elsevier.com/locate/scitotenv

Land subsidence dynamics in the Mekong Delta: Insights from local high-resolution geomechanical parameterization, numerical modelling, and geodetic observations

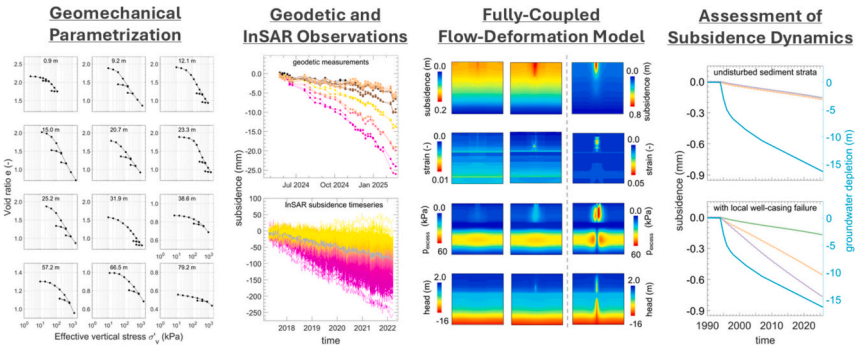
Felix Dörr [a,*], Jonas Bauer [a], Tran Viet Hoan [a,b], Le Thi Mai Van [b], Andreas Schenk [c], Nils Dörr [c], Franz Nestmann [d], Stefan Norra [e]

[a] Karlsruhe Institute of Technology (KIT), Institute of Applied Geosciences, Kaiserstraße 12, 76131, Karlsruhe, Germany
[b] National Center for Water Resources Planning and Investigation (NAWAPI), No. 93, lane 95, Vu Xuan Thieu Street, Sai Dong Ward, Long Bien District, Hanoi, 100000, Viet Nam
[c] Karlsruhe Institute of Technology (KIT), Institute of Photogrammetry and Remote Sensing, Kaiserstraße 12, 76131, Karlsruhe, Germany
[d] Karlsruhe Institute of Technology (KIT), Institute for Water and Environment, Kaiserstraße 12, 76131, Karlsruhe, Germany
[e] Potsdam University, Institute of Environmental Sciences and Geography, Soil Sciences and Geoecology, Campus Golm, Building 12, 14476, Potsdam Golm, Germany

HIGHLIGHTS

- Fully-coupled flow-deformation model used to simulate subsidence in Mekong Delta.
- The Mekong Delta will face delayed subsidence due to past groundwater depletion.
- Well-casing failure can accelerate land subsidence.

GRAPHICAL ABSTRACT



ARTICLE INFO

Keywords:
Land subsidence
Fully-coupled flow-deformation model
Mekong Delta
Groundwater overexploitation

ABSTRACT

Land subsidence poses major threats to human and environmental systems in river deltas worldwide, increasing risks of flooding and damage to civil infrastructure. In deltaic settings, land subsidence can be induced by multiple superimposing processes, including autocompaction, groundwater depletion and infrastructural surface loading. The quantification of each individual process is often uncertain, yet crucial for effective adaptation and mitigation. The Vietnamese Mekong Delta (VMD) is a prominent example of such a subsiding delta, with satellite-derived subsidence rates of up to 30 mm a^{-1} and surface elevations largely below 1 m above mean sea level. By presenting a fully coupled flow–deformation model with geomechanical parameterization at high vertical resolution, this study, supported by local geodetic leveling observations, provides an unprecedentedly detailed local-scale assessment of land subsidence dynamics for the VMD. The simulation results indicate subsidence rates of 5–6 mm a^{-1} due to groundwater depletion and local infrastructure loading. Additionally integrating one or

* Corresponding author.
E-mail address: felix.doerr@kit.edu (F. Dörr).

https://doi.org/10.1016/j.scitotenv.2026.181850
Received 5 January 2026; Received in revised form 25 April 2026; Accepted 30 April 2026
Available online 3 May 2026
0048-9697/© 2026 The Authors. Published by Elsevier B.V. This is an open access article under the CC BY license (http://creativecommons.org/licenses/by/4.0/).

multiple well-casing failures as localized subsurface disturbances in the model yields spatially heterogeneous subsidence patterns and increases local subsidence rates by an additional 1–20 mm a^{-1}, depending on the number of implemented failures. While well-casing failures are known consequences of land subsidence, the hypothesis-driven exploratory simulations employed here indicate that such damage may in turn accelerate subsidence by facilitating subsurface drainage pathways and local head equilibration between aquitards and tapped aquifers. This suggests that well-casing failures could contribute to heterogeneous and locally extreme subsidence dynamics. The results reveal significant delays in subsidence due to past groundwater depletion at the investigated site, underscoring the need for proactive water management strategies in the VMD, supported by comprehensive land subsidence modelling. The insights derived from this localized high-resolution analysis suggest that effective management will require preventing shallow aquifer depletion to avoid triggering the Holocene's pronounced, yet largely inactivated subsidence potential.

1. Introduction

Many of the world's coastal plains and river deltas are threatened by relative sea level rise, a combined effect of actual sea level rise due to global warming and land subsidence (Syvitski et al., 2009). While the actual sea level rise is in a range of approx. 3 mm a^{-1} on a global average, land subsidence rates can exceed these rates by 1–2 orders of magnitude (Davydzenka et al., 2024). This emphasizes the hazardous character of land subsidence and the urgent need for action in coastal settings. Consequences of land subsidence in delta systems range from increased exposure to flooding and seawater intrusion, loss of land and damages on civil infrastructure including bridges, roads and casings of water supply wells (Gambolati and Teatini, 2021; Holzer and Johnson, 1985).

The Vietnamese Mekong Delta (VMD) is a prominent example of a delta that is confronted with hazardous land subsidence rates. With an average surface elevation of approx. 0.8 m above mean sea level in 2018 (Minderhoud et al., 2019) and subsidence rates locally exceeding 30 mm a^{-1} (Erban et al., 2014; Dörr et al., 2024), these dynamics pose a substantial threat to the region's viability. In delta systems like the southern VMD, land subsidence can be induced by various superimposing processes including natural processes like autocompaction of shallow sediments (Zoccarato et al., 2018; Baldan et al., 2025), as well as anthropogenically triggered processes like sediment compaction due to groundwater extraction (Minderhoud et al., 2017, 2020). Furthermore, loading of civil infrastructure can additionally cause local sediment compaction below buildings and roads (Minderhoud et al., 2018).

Understanding the relative contributions of individual processes to total land subsidence is fundamental, as effective adaptation and mitigation strategies depend on identifying the governing mechanisms driving subsidence.

Most of the previous studies that aimed to quantify the contribution of either autocompaction or groundwater depletion to the overall subsidence are based on delta-wide numeric modelling (Baldan et al., 2025; Minderhoud et al., 2020, 2017; Zoccarato et al., 2018). These modelling approaches provided important first-order estimates and have significantly raised awareness of land subsidence in the Mekong Delta within both scientific and public communities. In light of the large size of the study area together with the high vertical and horizontal heterogeneity of the sediment strata, the limited availability of data for geomechanical parameterization represents an inherent challenge for large-scale subsidence models in the VMD.

In contrast to those delta-wide analyses, this study presents a local site-specific analysis, utilizing (i) InSAR and ground-based geodetic spatiotemporal subsidence observations, (ii) observed groundwater head data, and (iii) a detailed geomechanical subsurface parametrization based on incremental-loading oedometer tests on undisturbed drill-core samples for a fully-coupled flow-deformation simulation of land subsidence due to groundwater depletion and surface loading in the southern VMD.

This study elaborates numeric simulations for a process-based exploration of local land subsidence dynamics in an unprecedented level of detail for the southern VMD, providing new insights into process dynamics of land subsidence due to groundwater depletion and explores new potential factors for the spatiotemporal heterogeneity of observed subsidence rates. The analysis focuses on quantifying the contribution of various subsidence drivers at a non-urban research site with relatively high data density and explores additional mechanisms that may contribute to spatially heterogeneous subsidence rates in the immediate vicinity. In this context, the study proposes the hypothesis that well-casing failures, i.e. cracks and ruptures in the casing material, represent a previously unexplored mechanism potentially contributing to locally extreme and spatially heterogeneous subsidence rates in addition to those induced by groundwater depletion, surface loading, autocompaction and heterogeneous sediment characteristics. Such well-casing failures, long known consequences of land subsidence induced by groundwater depletion (Gambolati and Teatini, 2021; Holzer and Johnson, 1985), may additionally accelerate subsidence by facilitating subsurface drainage pathways and enabling local hydraulic head equilibration between aquitards and tapped aquifers.

2. Materials and methods

2.1. Hydrogeology and groundwater depletion

The VMD is characterized by a complex hydrogeological stratigraphy, which is commonly conceptualized as a multi-layered aquifer-aquitard system comprising seven aquifers and seven aquitards (Hoan et al., 2022, Fig. 1c). In the southern VMD, the topmost Holocene aquifer *qh* is not continuously developed (Dörr et al., 2026) and the clay-silt sequences of the Holocene and Pleistocene aquitards Q_2 and Q_1^3 can merge, forming a single aquitard above the upper Pleistocene aquifer qp_3. In Ca Mau Province, the southernmost province of the southern VMD, the Holocene-Pleistocene interface is located at a depth of approx. 20 m (Mi et al., 2023). In this region, the qp_3 aquifer is the first continuously developed aquifer, yet it is rarely utilized for groundwater extraction (Hoan et al., 2022). The highest groundwater extraction rates have been reported for the upper-middle Pleistocene aquifer qp_{2-3} (Hoan et al., 2022), whereas more recently deeper aquifers like the middle Pliocene aquifer n_2^2 are subject to increasing exploitation due to salinization processes in the upper aquifers (Hoan et al., 2025).

Prior to significant anthropogenic groundwater extraction, early studies documented artesian groundwater heads in the southern VMD (Anderson, 1978). Since 1995, groundwater head measurements provided by the Vietnamese National Groundwater Monitoring Network (NGMN) have documented a continuous decline in groundwater heads over the past three decades. At the study site GW1 (Fig. 1b), groundwater heads have been monitored since 2022 in several aquifers, including an observation well (GW1a) screened in the upper–middle Pleistocene aquifer (qp_{2-3}), and, temporarily between May and August 2024, in an observation well (GW1d) screened in the upper Pleistocene aquifer (qp_3). The monitoring site GW1, located in Ca Mau Province, was established in collaboration of the Karlsruhe Institute of Technology (KIT), the National Center for Water Resources Planning and Investigation (NAWAPI) and the Department of Natural Resources and Environment Ca Mau (DONRE Ca Mau) as part of the German-Vietnamese

ViWaT-Engineering research project funded by the Vietnamese Ministry of Natural Resources and Environment and the German Ministry of Research, Technology and Space.

Fig. 1a illustrates groundwater head data for the monitoring site Q177 in Ca Mau city for the period 1995 until 2025 as well as for the monitoring site GW1 from 2022 until 2025, respectively. It is noted that despite its attribution to the Holocene aquifer *qh* in the NGMN database and in previous studies (e.g. Van et al., 2023), the monitoring well Q17701T is not screened in Holocene aquifer *qh*. A review of the respective drilling profile (see supplementary information S3) indicates that this observation well is screened in 2.5–8.5 m depth, clearly within the Holocene aquitard Q_2. Therefore, the stagnant trend with seasonal variations in the observation data cannot be interpreted as hydraulic head but rather as an indicator for constant saturation in the top of the Holocene aquitard Q_2 and an influence of seasonal surface water loading.

The seasonal rise in groundwater heads at GW1 (Fig. 1a) was identified to be due to surface loading effects, driven by a seasonal accumulation of water resources in the surrounding aquaculture ponds (Dörr et al., 2026). A removal of these loading effects for the rainy season 2023 revealed a continuous groundwater depletion in qp_{2-3} (Dörr et al., 2026). For the employed numeric simulation of sediment compaction at GW1, annual average, therefore loading independent, groundwater head depletion rates are utilized. For the model implementation, hydraulic head boundary conditions are derived from locally observed groundwater heads at GW1 between 2022 and 2025, while earlier depletion trends between 1995 and 2022 are approximated based on groundwater head trends at Q177 (dashed lines in Fig. 1a).

2.2. Subsurface characterization

The geomechanical subsurface parametrization for GW1 is derived from a total number of twelve one-dimensional compression tests using undisturbed drill core samples from distinct depths between 0.9 m and 79.2 m, obtained from the drilling of the observation well GW1c in the southern VMD. For each sample, the compression index C_c (−) and the recompression index C_r (−) are derived from the slopes of the linearized sections in the obtained compressibility curves. From the time-compression curve at the load stage representative for the in-situ pressure conditions, the coefficient of secondary (creep) compression C_α (−) and the coefficient of consolidation c_v ($m^2\ s^{-1}$) as well as the vertical hydraulic conductivity k_v ($m\ s^{-1}$) are calculated. C_α is derived from the gradient of the linearized section in the obtained semilogarithmic time-compression curve. c_v is calculated with the *Casagrande Logarithm of Time Fitting Method* by Eq. (1) to

$$c_v = 0,196 \cdot \frac{(h/2)^2}{t_{50}} \tag{1}$$

where h (m) is the sample's height and t_{50} (s) is the time at 50% of primary consolidation. k_v is calculated with Eq. (2), where γ_w is the unit weight of water (~ 10 kN m^{-3}) and m_v (kPa $^{-1}$) is the coefficient of volume compressibility, which is derived with Eq. (3), where $\Delta\sigma'_{v,i}$ (kPa) is the vertical effective stress increment at the loading step i, Δe_i (−) is the change of void ratio during the loading step i and e_{i-1} (−) is the void ratio in the previous loading step.

$$k_v = c_v m_v \gamma_w \tag{2}$$

$$m_{v,i} = \frac{\Delta e_i}{\Delta\sigma'_{v,i}(1 + e_{i-1})} \tag{3}$$

The preconsolidation stress σ'_p (kPa) is derived from the experimental data with the opensource software tool *pySigmaP* (Montoya-Araque et al., 2022), which incorporates several established methods e.g. the approaches of *Casagrande*, *Pacheco Silva* and *Boone*. The method of Boone provides an alternative to the historically established methods of Casagrande and Pacheco Silva, aiming to overcome uncertainties due to the graphical approximations used in those methods. The method of Boone takes the in-situ effective vertical stress σ'_{v0} (kPa) as well as C_c (−) and C_r (−) into account and was used to derive σ'_p in this study. From σ'_p and σ'_{v0} the overconsolidation ratio *OCR* (−) is calculated to

$$OCR = \frac{\sigma'_p}{\sigma'_{v0}} \tag{4}$$

For each sample, the void ratio e (−) and the unit weight γ (kN m^{-3}) were determined based on weighing the undisturbed and dried sample.

To characterize the soil's properties under unsaturated conditions,

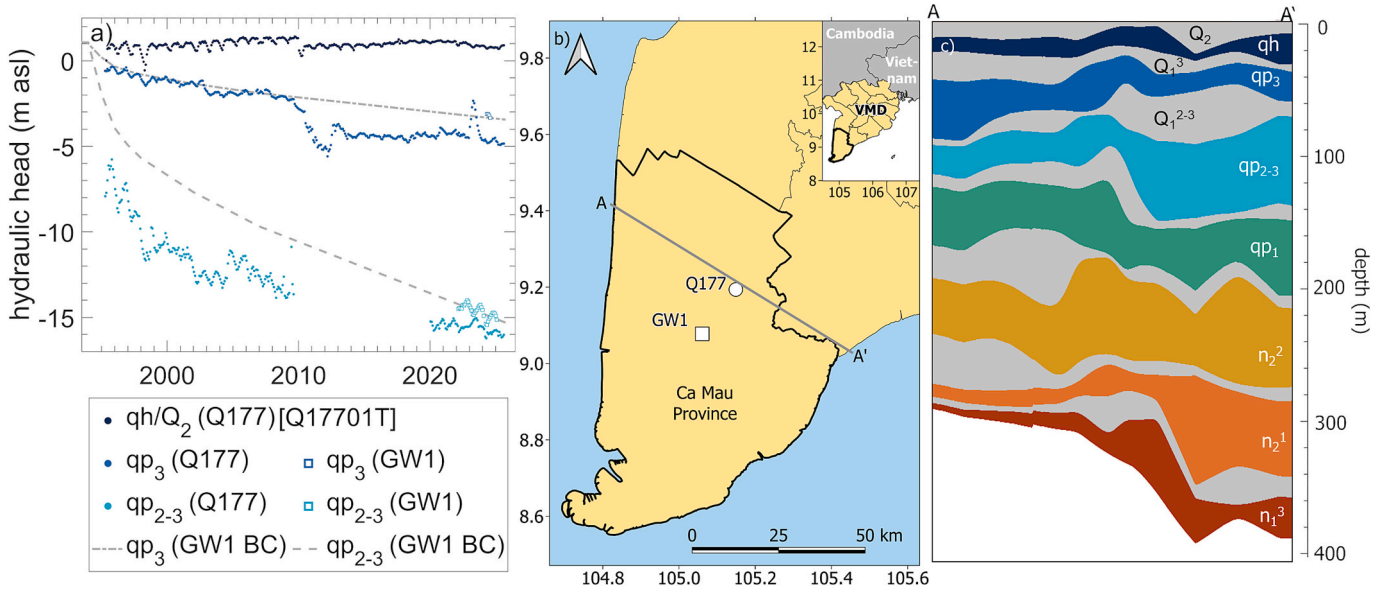


Fig. 1. Hydraulic head observations from the monitoring site Q177 in Ca Mau city from 1995 until 2025 and from the monitoring site GW1 between 2022 and 2025, in the aquifers qp_{2-3} and qp_3, respectively. Additionally, observation data from the observation well Q17701T screened in the Holocene aquitard at the monitoring site Q177 is included, denoted as qh / Q_2. Data displayed as monthly mean values (a). Map of the study area in the southern VMD including the locations of the monitoring sites GW1 and Q177 (b) and hydrogeological cross-section (Hoan et al., 2022) with aquifers in colors and aquitards in gray (c).

the soil water characteristic curves (SWCC) are derived for GW1 in five depths between 0.3 m and 1.0 m. For that, undisturbed soil samples were analyzed in the laboratory by measuring the volumetric water content θ (−) and the corresponding matric potential Ψ (kPa). Based on the measurement data, the Van Genuchten parameters α (kPa^{-1}) and n (−) are derived, providing a mathematical representation of the SWCC. Additionally, the grain size distribution is analyzed for seven samples at depths between 0.1 m and 1.0 m. The obtained soil classes are used to compare the calculated values for α and n with standard literature values for specific soil and sediment classes (Tuller and Or, 2005).

2.3. Leveling and InSAR monitoring

Between May 22, 2024, and February 23, 2025, a total of 35 geodetic monitoring campaigns were carried out in the vicinity of GW1. Each campaign comprised (i) 13 measurement points located at the GW1 site, (ii) one monitoring point positioned on the pile foundation of a nearby bridge, and (iii) six additional points situated between the bridge and GW1, adjacent to the road and neighboring urban dwellings. The location of the monitoring points is visualized in the supplementary information S2 and in the presented results. The leveling results are referenced to the monitoring point located on the bridge foundation, assuming the bridge's deep piled foundation to be stable and unaffected by Holocene and shallow Pleistocene compaction. This approach is generally consistent with that of Dörr et al. (2024), who used bridge foundations as reference networks for InSAR analyses in the southern VMD, with estimated foundation depths of approximately 70 m. The geodetic leveling was conducted in closed loops, allowing for assessment of the vertical misclosure. The median misclosure in the 35 geodetic monitoring campaigns is low with 0.29 mm and presented in detail in the supplementary information S1.

The geodetic monitoring network at GW1 comprises the points PW3–PW8 on the well head and pedestal of the three observation wells (GW1a, GW1b, and GW1c), points CR10–CR14 on the pedestal and metal plates of the corner reflector, and points PW1–PW2 on the well head and pedestal of the sliding-joint-based multi-extensometer drilling. The location of geodetic monitoring points on the site GW1 is illustrated in the supplementary information S2. The points P102–P105 are located within one to three meters of the road lane and thus are presumably still positioned on the road embankment. The points P100 and P101 are located in a driveway and within a sealed courtyard.

To contextualize the geodetic leveling results, these observations from 2024 to 2025 are compared with InSAR-derived subsidence time series of persistent scatterers in the vicinity of GW1, extracted from a dataset covering the period 2017–2022 (Dörr et al., 2024). Although the time series do not overlap, and the exact locations of the geodetic points are not resembled in the InSAR data, similarities in trends, spatial heterogeneity, and seasonal patterns allow for a qualitative assessment of consistency and plausibility.

2.4. Subsidence model

In the present study, a fully coupled flow-deformation model is employed to simulate subsurface deformation and resulting land subsidence due to depleting groundwater heads at the monitoring site GW1 in the southern VMD. Within this framework, groundwater flow and mechanical deformation are solved simultaneously, allowing changes in effective stress and deformation to dynamically influence flow and hydraulic properties such as porosity and permeability, and vice versa. For this, the finite-element based commercial software tool *PLAXIS 2D* is used, utilizing the *SoftSoilCreep* model (Vermeer and Neher, 1999), which is an advanced geomechanical constitutive model.

The *SoftSoilCreep* model is capable of simulating time-dependent processes of consolidation and creep and was applied in previous studies to simulate settlement processes due to surface loading and groundwater level variations (Lee et al., 2018; Feng et al., 2019). Considering such time-dependent processes is essential, given that delayed compression of soils and sediments such as creep is a well-recognized process contributing to land subsidence (Qi et al., 2025), although creep is neglected in many studies on groundwater-depletion-induced subsidence (Kooi and Erkens, 2020).

The effects of saturation on the subsurface stresses are integrated in the PLAXIS implementation with the *Bishop stress formulation*

$$\boldsymbol{\sigma} = \boldsymbol{\sigma}' + \boldsymbol{m}(\chi p_w + (1-\chi)p_a) \quad (5)$$

where σ (kPa) is the tensor of total stresses, σ' (kPa) is the effective stress tensor, m is a tensor with unity terms for normal stress components and zero terms for the shear stress, χ (−) is the matric suction coefficient p_w (kPa) and p_a (kPa) are the pore water pressure and the pore air pressure (Galavi, 2010). In PLAXIS, the matric suction coefficient is internally calculated from the effective saturation, which is governed by the soil water characteristic curve model, here the Van Genuchten model and its corresponding parameters (Galavi, 2010). Additionally, the model considers a reduction of the hydraulic conductivity with advancing consolidation by the permeability change index C_k (−) which is estimated to $C_k \cong 0.5\, e_0$ (Tavenas et al., 1983). The model parameters are derived from the geomechanical characterization described above.

The 2D cross-sectional model developed in this study encompasses a lateral extent of 500 m and a vertical extent of 81 m (Fig. 2). The bottom of the model domain equals the interface between the middle Pleistocene aquitard Q_1^{2-3} and the highly exploited upper-middle Pleistocene aquifer qp_{2-3}. Therefore, the groundwater depletion in qp_{2-3} represents a model boundary condition, which is implemented by a transient Dirichlet boundary condition with a depletion rate derived from recent local and historic regional groundwater head data (Fig. 1a). The vertical model discretization covers 13 layers and was derived from sampling depths and sediment classifications. The finite-element mesh discretization includes 45,192 nodes and 22,275 triangular elements. The intermediate aquifer qp_3 is implemented in the model by a linear-elastic constitutive model. Similar to qp_{2-3}, the groundwater depletion in qp_3 is implemented by a transient Dirichlet boundary condition with a depletion rate derived from recent local and historic regional groundwater head data (Fig. 1a). This boundary condition is realized in the model on the aquifer's lateral boundary. The aquifer's hydraulic conductivity, which is of secondary importance for the simulated subsidence response compared to the locally derived aquitard deformation parameters, was determined to $3.2{\cdot}10^{-4}$ m s^{-1} based on regional aquifer parametrization and a calibrated groundwater flow model (Hoan et al., 2022). For the aquitards, an anisotropy ratio of hydraulic conductivity (k_h/k_v) of 3 was adopted, consistent with the parametrization in a recent study on Holocene sediments in the VMD by Baldan et al. (2025).

By covering a variety of land use and land cover (LULC) types including aquaculture, vegetation, road infrastructure and urban settlements adjacent to the road, the model comprises a typical representation of surface characteristics in the southern VMD. These various LULC types locally influence the hydraulic interaction between surface water resources and subsurface sediments and are hence differentiated in the assignment of hydraulic boundary conditions in the model. The road near GW1, QL1, is a historically used route, with an estimated age of up to 200 years and underwent several upgrades during colonial history (Logan, 2002). Assuming intermediate road rehabilitation to have negligible impact on the road's self-weight loading, consolidation processes related to the road construction itself are considered completed in this study. Sealed surfaces of roads and urban settlements locally prevent infiltration or rewetting processes and are therefore implemented in the model by no-flow Neumann boundary conditions, a reasonable consideration if the sediment strata is topped by a completely impermeable layer (Baú et al., 2004). For the spatially extensive aquaculture ponds however, which are commonly not lined with plastic foil, the ponds' water levels maintain the hydraulic conditions on the surface and can therefore be represented by a constant or transient Dirichlet

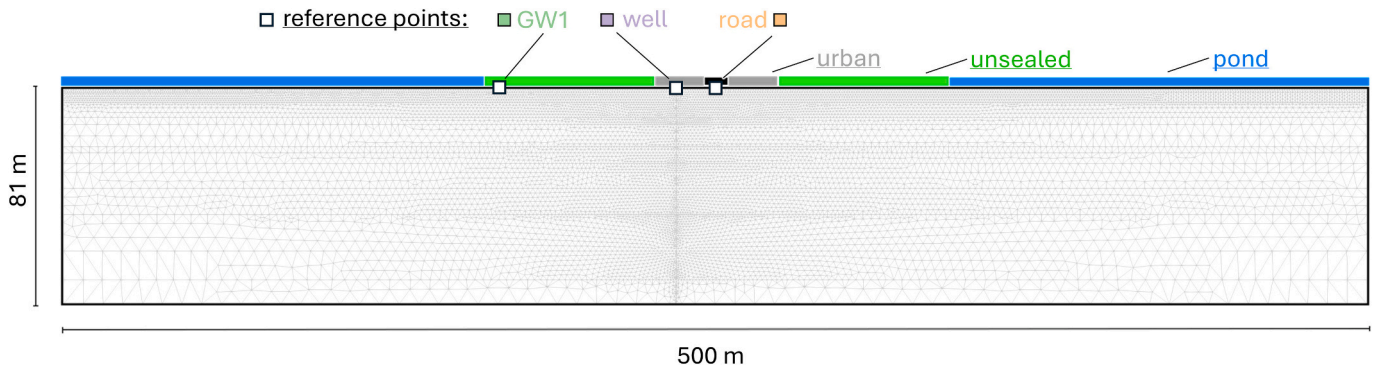


Fig. 2. 2-D Model domain illustrating the mesh and the spatial extent of surface boundary conditions for urban (gray), unsealed (green) and ponded (blue) surfaces as well as the road (black) in the center. Reference points for the site GW1, the urban well and the road which are used later on for the evaluation of computed subsidence time series are included.

boundary condition, e.g. as applied in analytical calculations by Gambolati and Teatini (2021). To account for the seasonal loading effects due to variations of surface water levels in aquaculture ponds near GW1, the Dirichlet boundary condition for aquaculture ponds are implemented as sinusoidally harmonic head variations with an annual oscillation period and an amplitude of 0.5 m. Such seasonal water level variations comply well with seasonal water level variations in aquaculture ponds in the study area (Dörr et al., 2026).

Vegetated surfaces, as well as a 1-m wide drainage channel situated on either side of the road, are implemented in the model by seepage boundary conditions. Such seepage boundary conditions locally permit water flow and therefore the dissipation of excess pore pressure toward the surface. On the road, a vehicle load of 10 kPa is applied according to Vietnamese standards referenced by Mi et al. (2023). Loads of buildings are not included in the calculations. To provide a contextualization of this consideration, the local loading of the predominantly one-story residential buildings is estimated to be within the range of the applied vehicle load (Xu et al., 2025).

It should be noted that the implemented surface load does not aim to accurately represent the actual loading conditions in the vicinity of GW1, but rather to capture a representative order of magnitude of typical urban surface loading in the VMD. By assuming design vehicle loads to be constant and neglecting the loading from residential buildings, this simplified representation of urban loading is considered reasonable within the context of this study.

To evaluate the hypothesis that damaged well casings may affect the spatiotemporal dynamics of land subsidence due to groundwater depletion, damaged casing segments of an exemplary well are implemented in the model by drainage boundary conditions within exploratory scenario simulations. Two main scenarios are considered: (i) a single well-casing failure located at depths of highest subsurface strain, and (ii) multiple failures implemented at regular intervals along the casing. In the latter case, damaged casing segments are introduced at intervals of 3 m, representing the typical length of casing pipe segments and failures at their interconnecting joints. In the main scenarios, individual failures are represented by 0.1 m long damaged casing segments. In addition, a sensitivity analysis is conducted to evaluate the influence of both the number of failures and the assumed failure length, reducing the latter from 0.1 m in the main scenarios to 0.05 m and 0.01 m in additional comparison simulations. At the drain boundary conditions, water outflow from the model is permitted and controlled by a specified reference head. The reference head of these drain boundaries corresponds to the water level within the well casing, and thus to the hydraulic head in the tapped aquifer. Since PLAXIS does not allow a fully dynamic implementation of reference heads in drain boundary conditions, they were incorporated into the model as annually constant values, discretely representing the depletion of the tapped aquifer as illustrated in the supplementary information S4. This approximation leads to a small offset relative to the hydraulic heads that would correspond to the casing water levels under the applied modelling concept, and therefore to a slight overestimation of the hydraulic head gradients and drainage. Moreover, this approach does not capture short-term fluctuations in hydraulic heads and casing water levels. Such variations have been shown to result predominantly from surface loading effects at GW1 (Dörr et al., 2026), which induce transient pressure responses in the aquifer system and can influence drainage dynamics.

Fig. 2 visualizes the model domain, including the variety of implemented surface boundary conditions for urban, unsealed and ponded surfaces and the finite element mesh, which is characterized by grid refinement close to the surface and near the implemented well casing.

In the *SoftSoilCreep* model, the initial creep deformation is overestimated if sediments are parametrized as ideally normally consolidated sediments (OCR = 1.0), as this would imply that the sediments have experienced their complete primary loading, i.e. the self-weight of any overlying sediment layers, within the preceding 24-h period prior to the start of the simulation. This is unrealistic in the context of geological formation history, where in most depths, the sediment strata have experienced loading for thousands of years already. To avoid such overestimated initial creep deformations to bias the calculation results, a 100,000-year period with constant hydraulic and geomechanical conditions is included in the simulation, prior to the calculation of compaction due to groundwater depletion and surface loading. To verify that the initial creep deformation reached insignificance, the simulated deformation rate prior to evaluation period starting from 1990 was checked to be <0.01 mm a^{-1}.

During the fully-coupled simulation, initially defined state variables like the void ratio as well as related parameters like the hydraulic conductivity change dynamically over the course of the simulation period. Since the model parameters were derived from samples collected in 2020, the initial parameterization was iteratively adjusted to ensure consistency with the 2020 reference state in the model.

3. Results

3.1. Observed subsidence rates

The observed land subsidence rates measured with ground-based leveling between May 2024 and February 2025 are characterized by a distinct spatial heterogeneity with higher subsidence rates near the road and adjacent urban settlements and lower subsidence rates at GW1 (Fig. 3a). The subsidence rates show temporal variations, with higher subsidence rates observed during the dry-season surveys (Fig. 3a-b), when groundwater heads and surface water levels decline. The greatest subsidence rates are measured at P101 with a subsidence rate of 50 mm a^{-1} in the dry season and 25 mm a^{-1} in the rainy season (Fig. 3b). At GW1, eleven of the thirteen subsidence observation points show very

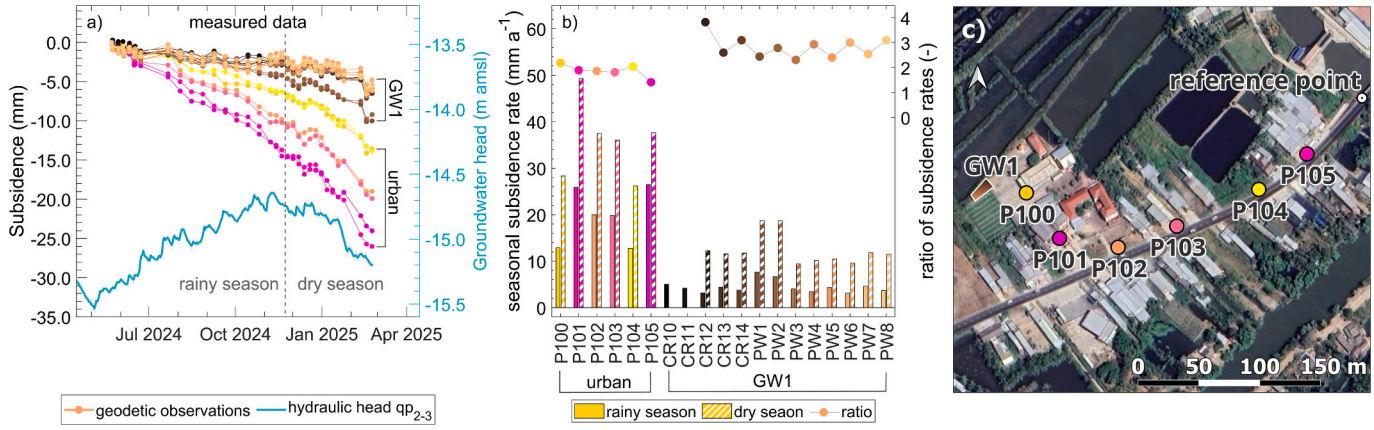


Fig. 3. Measured land subsidence rates and observed groundwater heads at GW1 (a), seasonal trends and ratio between dry season and rainy season subsidence (b), and location of subsidence observation points (c). In (c), individual measurement locations are omitted and only the spatial extent of monitoring site GW1 is shown; see Supplementary Information S2 for detailed locations.

similar dynamics (Fig. 3a), with an annual-average subsidence rate of 8 mm a^{-1} and trends between approx. 10 mm a^{-1} in the dry season and approx. 3 mm a^{-1} in the rainy season (Fig. 3b). Only the points PW1 and PW2, located at the well head and pedestal of the sliding-joint multi-extensometer drilling, show increased subsidence rates of approx. 13 mm a^{-1} and seasonal trends between approx. 18 mm a^{-1} in the dry season and approx. 8 mm a^{-1} in the rainy season (Fig. 3a-b).

Fig. 4 presents the InSAR-based subsidence observation in the vicinity of GW1, comprising (i) all individual subsidence time series and their average (Fig. 4a), (ii) a statistical summary of the corresponding subsidence rate distribution (Fig. 4b), (iii) a smoothed subsidence time series obtained from a 60-day moving-mean window of the averaged subsidence time series of all InSAR points (Fig. 4c), and (iv) a map showing the spatial distribution of the InSAR scatterers (Fig. 4d), color-coded in accordance with Fig. 4a-b). The subsidence dynamics are characterized by a pronounced variability (Fig. 4a-b) with a median subsidence rate of 15.7 mm a^{-1} (Fig. 4b). The averaged and smoothed subsidence time series reveals seasonal patterns with temporal rebound phases (Fig. 4c).

In the vicinity of GW1, 89% of the InSAR-derived scatterers (Fig. 4b) exhibited subsidence rates between 2017 and 2022 that exceeded the geodetically measured annual-average depletion rate of 8 mm a^{-1} at GW1 in 2024–2025.

3.2. Geomechanical subsurface characterization

The compression and recompression indices are derived from the compressibility curves of the one-dimensional compression tests for twelve distinct depths between 0.9 m and 79.2 m (Fig. 5). The results are summarized in depth profiles (Fig. 7) and show a high compressibility in the Holocene aquitard Q_2 and the upper Pleistocene aquitard Q_1^3 with compression indices between 0.59 and 1.06 (Fig. 7e) and a mean value of 0.77. The middle Pleistocene aquitard Q_1^{2-3} is characterized by distinctly lower compression indices between 0.21 and 0.46 (Fig. 7e). Similarly, the recompression indices are greater in Q_2 and Q_1^3 with values between 0.04 and 0.09, whereas in Q_1^{2-3} C_r varies between 0.02 and 0.07 (Fig. 7f). The ratio of C_c and C_r varies between 9.0 and 15.8 in Q_2 and Q_1^3. Fig. 5l shows that for the sample at 79.2 m depth, the maximum applied load of 1600 kPa, limited by the load capacity of the used oedometer apparatus, was possibly insufficient to clearly define the slope of the linear portion of the compressibility curve, thereby introducing uncertainty to the derived C_c value.

The compressibility curves of some samples (Fig. 5 b, d, f) show a lower gradient at higher stress stages after the linear trend in the semilogarithmic e- σ'_v plot. Such trends in compressibility curves have been observed for sensitive clays and are attributed to a greater degree of particle interaction and stronger resistance to structure compression (Boone, 2010). This aligns with previous findings (Giao et al., 2008), characterizing the soft clay sediments in Ca Mau as medium to very sensitive clay.

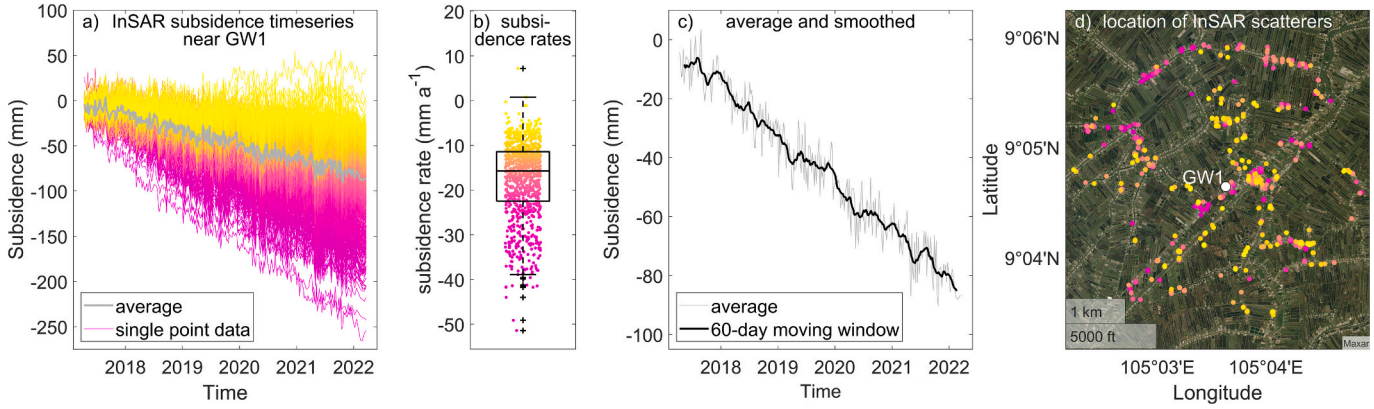


Fig. 4. InSAR-derived subsidence dynamics between 2017 and 2022 near GW1, comprising all individual time series and average (a), a distribution of annual subsidence rates (b), a 60-day moving-mean smoothed subsidence time series (c) and a spatial distribution of the InSAR scatterers (d). Note that the color scale in (d) is identical to that in (a) and (b), indicating observed subsidence magnitudes from low (yellow) to high (magenta).

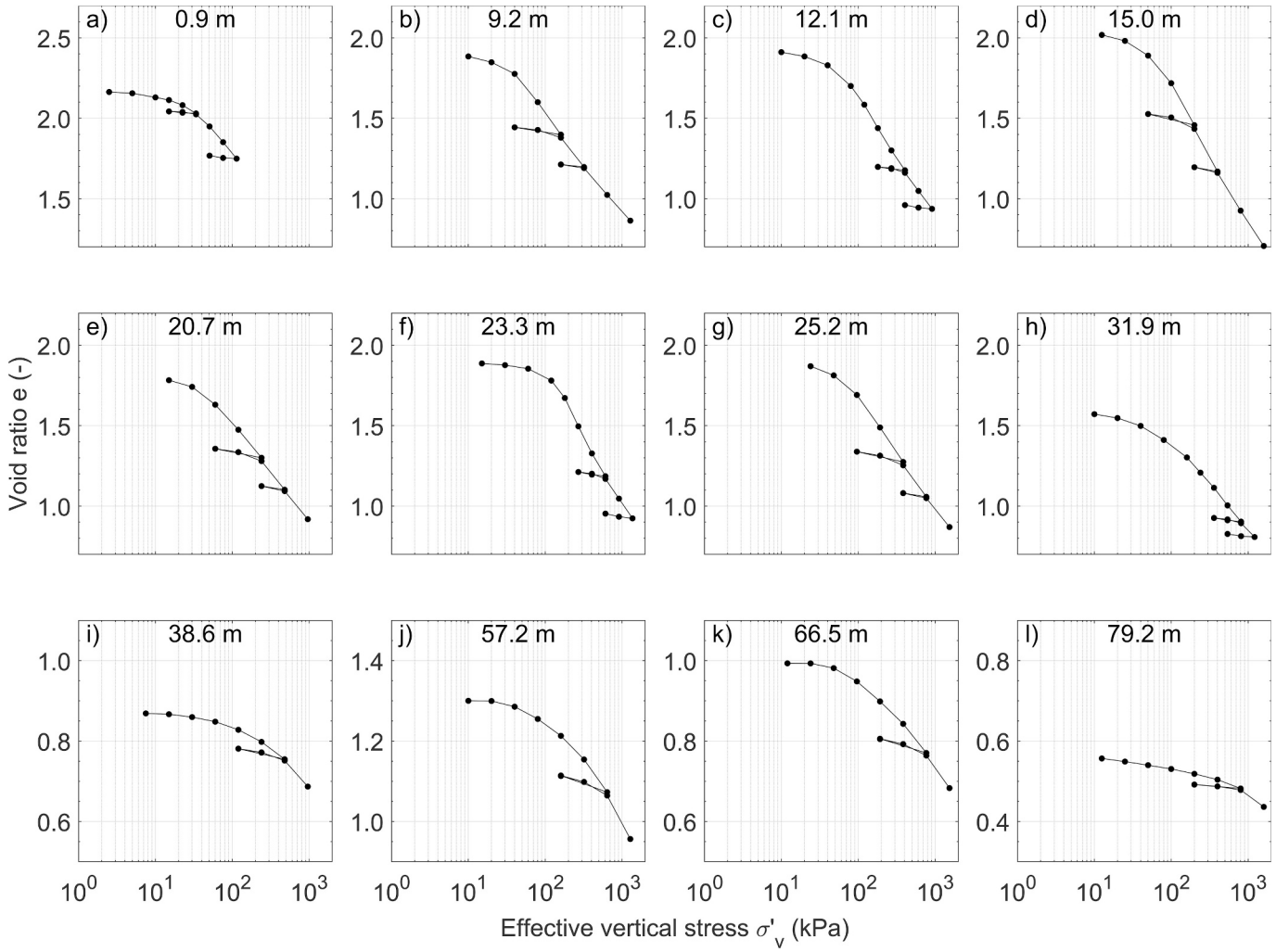


Fig. 5. Compressibility curves from twelve one-dimensional compression tests on undisturbed drill core samples from GW1 between 0.9 m and 79.2 m depth.

The secondary (creep) compression C_α (−) is derived from the time compression curves of the one-dimensional compression tests at a load stage representative for the in-situ effective stress at the corresponding depth. In Fig. 6, the twelve time-compression curves used for the calculation of C_α are summarized. Each time-compression curve is characterized by a distinct linear trend in the semilogarithmic plot, from which C_α is derived.

In Fig. 7, the obtained parameters for GW1 are visualized in profiles. This includes profiles of the samples' void ratio e (Fig. 7c) and unit weight γ (Fig. 7d), the compression index C_c (Fig. 7e), the recompression index C_r (Fig. 7f), the creep compression index C_α (Fig. 7g), the over-consolidation ratio OCR (Fig. 7h), the coefficient of consolidation c_v (Fig. 7i) and the vertical hydraulic conductivity k_v (Fig. 7j). In Fig. 7a, the sediment characterization is presented in form of a grain size distribution estimation based on an on-site evaluation of the drill cores during drilling. Based on the sediment characterization and the parameterization, a stratigraphic classification is derived and illustrated in Fig. 7b.

Except for the topmost sample (0.9 m depth) the overconsolidation ratio implies normally consolidated conditions in the Holocene aquitard Q_2 and the upper Pleistocene aquitard Q_1^3, with ranges of OCR between 1.04 and 1.19. In 0.9 m depth, OCR = 5.3 implies overconsolidated sediments in the topmost strata. The coefficient of consolidation varies between 1.2 $\cdot 10^{-8}$ and 5.4 $\cdot 10^{-8}$ $m^2\ s^{-1}$ in Q_2 and Q_1^3 and between 5.3 $\cdot 10^{-8}$ and 9.6 $\cdot 10^{-7}$ $m^2\ s^{-1}$ in Q_1^{2-3} (Fig. 7i).

Overall, the geomechanical characterization presented in Fig. 7 reveals a clear differentiation between the upper aquitard (comprising Q_2 and Q_1^3 sediments) and the lower investigated aquitard (Q_1^{2-3}). The upper aquitard is characterized by higher void ratios, lower unit weights, higher compression indices, and lower coefficients of consolidation compared to the lower aquitard.

Grain-size analyses of seven samples collected between 0.1 and 1.0 m depth at site GW1 indicate that the top soil is dominated by medium to fine silt and clay fractions. (Fig. 8a). For silt, standard values for the Van Genuchten parameters α and n are reported to 0.06 kPa^{-1} and 1.53 along with a residual water content of θ_r (−) of 0.123 (Tuller and Or, 2005). In Fig. 8b to f, the measured SWCC are presented for the samples between 0.3 and 1.0 m. Note that only a subset of the measured data was used for the fits of the Van Genuchten parameters to prevent the large number of measurements (>100) at low matric potential Ψ, from disproportionately dominating the information content of the single measurement at higher Ψ (see Fig. 8). Based on these characterizations, Van Genuchten parameters of α = 0.04 kPa^{-1} and $n = 1.4$ are utilized for the model with a residual water content of θ_r (−) of 0.123.

3.3. Numeric simulation of land subsidence

The numeric simulation of land subsidence due to groundwater depletion at the monitoring site GW1 in the southern VMD provides calculated subsidence dynamics along the modeled 500 m × 81 m cross-section for the period 1990–2025. In the present study, three distinct simulations are employed, either supposing (i) undisturbed subsurface

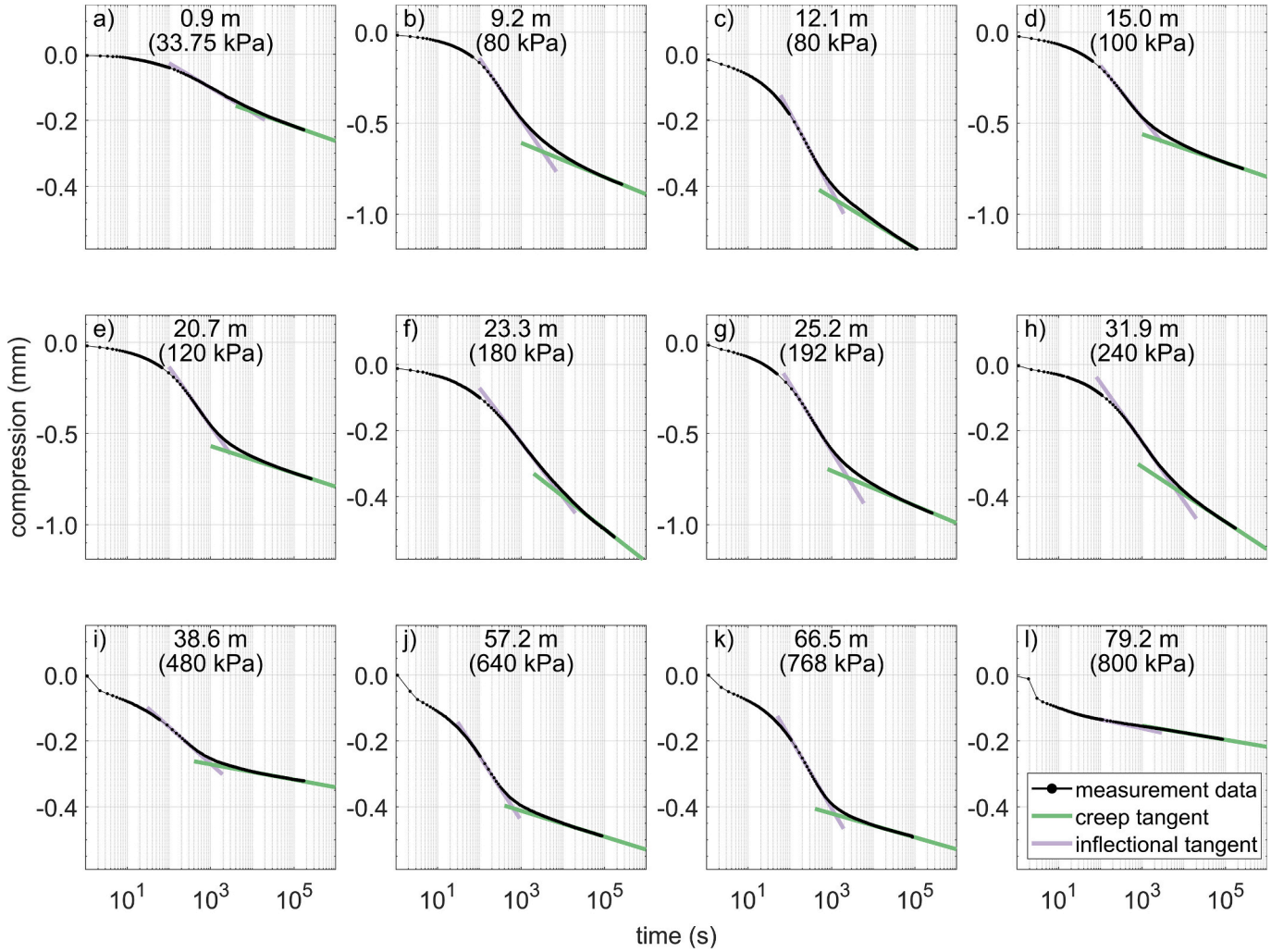


Fig. 6. Time-compression curves from twelve one-dimensional compression tests on undisturbed drill core samples from GW1 between 0.9 m and 79.2 m depth. The respectively evaluated incremental load stages are displayed in brackets below the samples' depth information.

sediment strata, (ii) subsurface disturbances due to a single well-casing failure or (iii) subsurface disturbances due to multiple well-casing failures implemented into the model in 3 m intervals along the casing.

Fig. 9 illustrates calculated subsidence dynamics for the simulation period 1990–2025. The degree of spatiotemporal heterogeneity in computed subsidence rates varies significantly between the three simulations employed for the period 1995–2025, during which groundwater depletion occurs. In the simulation which considers undisturbed subsurface strata, a subsidence rate of 5.1 mm a^{-1} (Fig. 9a) is calculated for the monitoring site GW1, which is situated in approximately 5 m distance to an aquaculture pond. An equal subsidence rate of 5.1 mm a^{-1} is calculated for an urban area, whereas the road experiences lightly elevated subsidence rates of 5.7 mm a^{-1} due to the vehicle load of 10 kPa (Fig. 9a). The calculated subsidence rates show seasonal variations, which are induced by the implemented sinusoidal water load of the aquaculture ponds.

Including a local subsurface disturbance in form of a single well-casing failures into the model yields in notably different spatiotemporal subsidence dynamics, increasing calculated subsidence rates to 6.3 mm a^{-1} and 6.5 mm a^{-1} for the well and road location respectively (Fig. 9b).

Including local subsurface disturbances in form of multiple well-casing failures, implemented into the model in 3 m intervals along the casing, yields in significantly more expressed spatiotemporal subsidence dynamics (Fig. 9c). For the monitoring site GW1, the calculated subsidence rates increase only marginally from 5.1 mm a^{-1} to from 5.6 mm a^{-1} under consideration of multiple well-casing failures in a well in the nearby urban area. Conversely, the road is subject to significantly elevated subsidence rates of 18.1 mm a^{-1}, representing an increase by a factor of 3 compared to the simulation of undisturbed subsurface sediment strata. The impact of the local well-casing failure on calculated subsidence rates peaks at the location of the implemented well, with calculated subsidence rates of 25.0 mm a^{-1} and a corresponding increase by a factor of 5 compared to the simulation of undisturbed subsurface sediment strata, with multiple well-casing failures implemented into the model at 3 m intervals along the casing.

Fig. 10 visualizes the results for the end of the simulation period in 2025, including the spatial distribution of computed subsidence (Fig. 10a), subsurface vertical strains (Fig. 10b), excess pore pressure (Fig. 10c) and hydraulic head (Fig. 10d) for the respective simulations of undisturbed sediment strata (Fig. 10a to d-i) and local subsurface disturbances due to a single well-casing failure (Fig. 10a to d ii) and multiple well-casing failures in 3 m intervals along the casing (Fig. 10a to d iii).

Fig. 10a-i shows a near-uniform horizontal distribution of land subsidence with a maximum subsidence below the road and minimum subsidence below the ponds. Conversely, the implementation of local subsurface disturbances due to well-casing failure induces a local peak maximum of subsidence at the well location, resulting in a horizontally heterogeneous subsidence distribution (Fig. 10a-ii and Fig. 10a-iii).

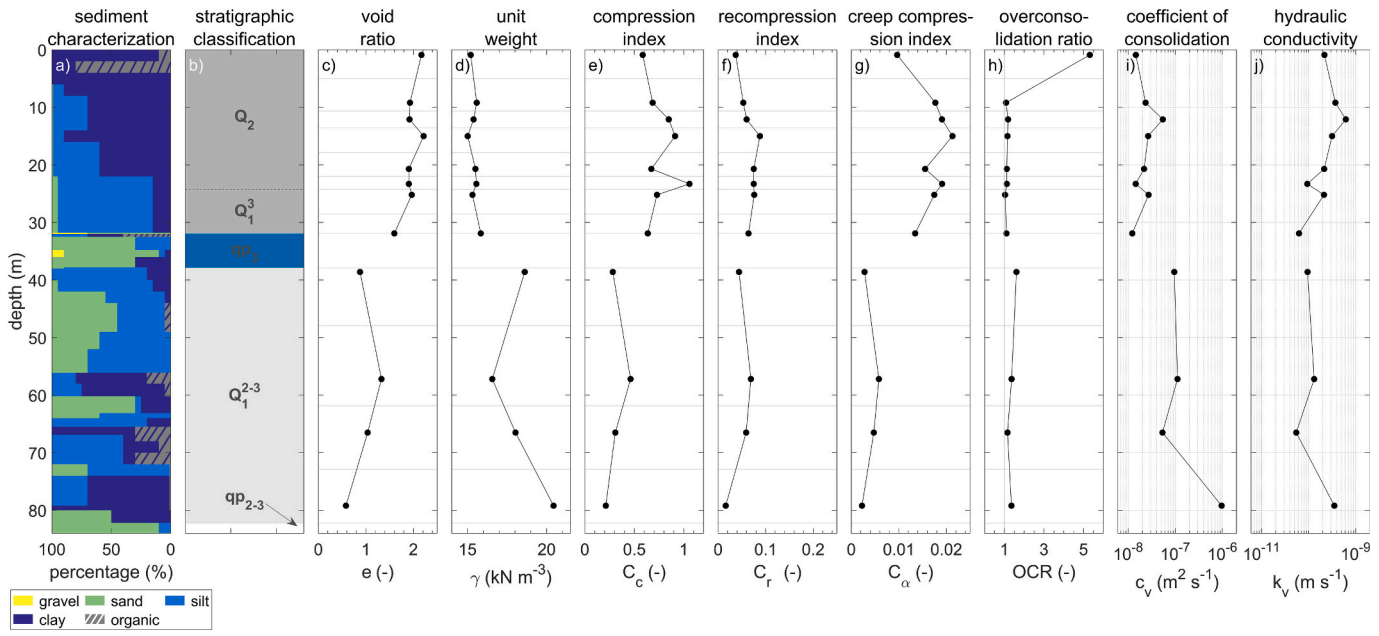


Fig. 7. Profiles showing the geomechanical characterization of the study site GW1 in the southern VMD including a sediment characterization visualized as a stacked percentage of each sediment class (a), a stratigraphic classification (b), and a parameterization void ratio (c), unit weight (d), compression index (e), recompression index (f), creep compression index (g), overconsolidation ratio (h), coefficient of consolidation (i) and vertical hydraulic conductivity (j).

The spatial distribution of subsurface strains is visualized in Fig. 10b and enables a depth-dependent assessment of the sediment compaction, which ultimately induce the subsidence of the groundwater surfaces. Fig. 10 b-ii shows that when a single well-casing failure is implemented in the model, strains are greatest in the vicinity of the failure. Fig. 10 b-iii illustrates that in the presence of multiple damaged well-casing segments, the greatest strains occur in approx. 10–12 m and in 21–23 m depth, where the sediments are highly compressible with high compression indices of C_c = 0.85–1.0 (Fig. 7e). Conversely, in the simulation of undisturbed sediment strata, strains are greatest in the second lowest layer of Q_1^{2-3} aquitard, where the compression index is significantly lower with $C_c = 0.31$. These distinct strain distributions are induced by the specific hydraulic head distributions (Fig. 10d) within the two simulations. In the simulation of undisturbed sediment strata, a predominantly uniform distribution of hydraulic head is computed (Fig. 10d-i), whereas at each implemented damaged casing segment the hydraulic head is locally determined by the reference head of the implemented drain boundary condition (Fig. 10d-ii and Fig. 10d-iii). This reference head corresponds to the water level within the casing and is equivalent to the head of the tapped aquifer qp_{2-3}. Given that the dissipation of excess pore pressure is associated with drainage and associated compaction, the excess pore pressure is indicative for pending compaction and hence subsidence, which has to be anticipated as a delayed response to past groundwater depletion. It is noted that in the employed fully coupled flow-deformation model, the excess pore pressure is defined by the difference between the actual pore water pressure and the pore water pressure in a steady-state flow condition. An individual presentation of these pressure distributions is presented in supplementary information S5. In the simulation of undisturbed sediment strata, in 2025 the excess pore pressure is greatest in approx. 60 m depth (Fig. 10c-i), where hydraulic conductivity is low and the distance to the draining aquifers qp_3 and qp_{2-3} is large (Fig. 7b and j). Fig. 10c-ii and Fig. 10c-iii show that at each implemented damaged casing segment, the excess pore pressure equals to zero, given that water can be drained from the subsurface sediments into the well-casing. The vehicle load on the road as well as the distribution of sealed surfaces (no-flow boundary conditions) and vegetated surfaces (seepage boundary conditions) leads to the complex distribution of excess pore pressure as illustrated in Fig. 10c-ii and Fig. 10c-iii. It is noted that for a direct comparison of the simulated excess pore pressure distributions (Fig. 10 c), it must be considered, that due to the well-casing failure, the steady-state groundwater flow conditions differ between the simulations, given the local assimilation of hydraulic heads in the aquitard layers toward the head in the tapped aquifer qp_{2-3}.

The contribution of suction pressure to the total effective stress is minor, remaining below 2 kPa in the simulation with undisturbed sediment strata (Fig. 11a) but increases locally to approx. 3.5 and 10 kPa beneath sealed surfaces in the simulation that additionally accounts for single or multiple well-casing failures respectively (Fig. 11b and c).

To provide a quantitative assessment of model performance, the simulated subsidence time series are compared with the observed subsidence data at monitoring site GW1 and its vicinity (Fig. 12). The scenario with multiple well-casing failures is shown explicitly in the comparison. As demonstrated in the evaluation of the different simulation scenarios (no well-casing failure, single well-casing failure, and multiple well-casing failures), the simulated subsidence behavior at the non-urban monitoring location GW1 remains nearly identical across all scenarios, whereas pronounced spatial variability emerges mainly in the vicinity of the implemented well casing. Consequently, the comparison illustrates both the subsidence dynamics at GW1 and the potential for strong local heterogeneity represented by the multiple well-casing failure scenario. The root mean square error (RMSE) is calculated to 1.1 mm for monitoring site GW1 using the average of the measured subsidence time series at GW1 and the corresponding simulation results for the same location. Compared with the median vertical measurement misclosure of 0.29 mm across the 35 geodetic monitoring campaigns, the RMSE of 1.1 mm indicates that model deviations exceed the internal survey precision but remain relatively small in absolute magnitude. It should be noted that this evaluation is site-specific to GW1 and does not assess predictive model performance with respect to spatial variability beyond this location. In addition, residual deviations at GW1 may partly reflect processes not explicitly represented in the model, such as auto-compaction. The model should therefore be understood primarily as a process-based exploratory tool rather than a precise predictive framework for total land subsidence arising from all contributing drivers.

It should be noted that the aim of the modelling is not to claim that

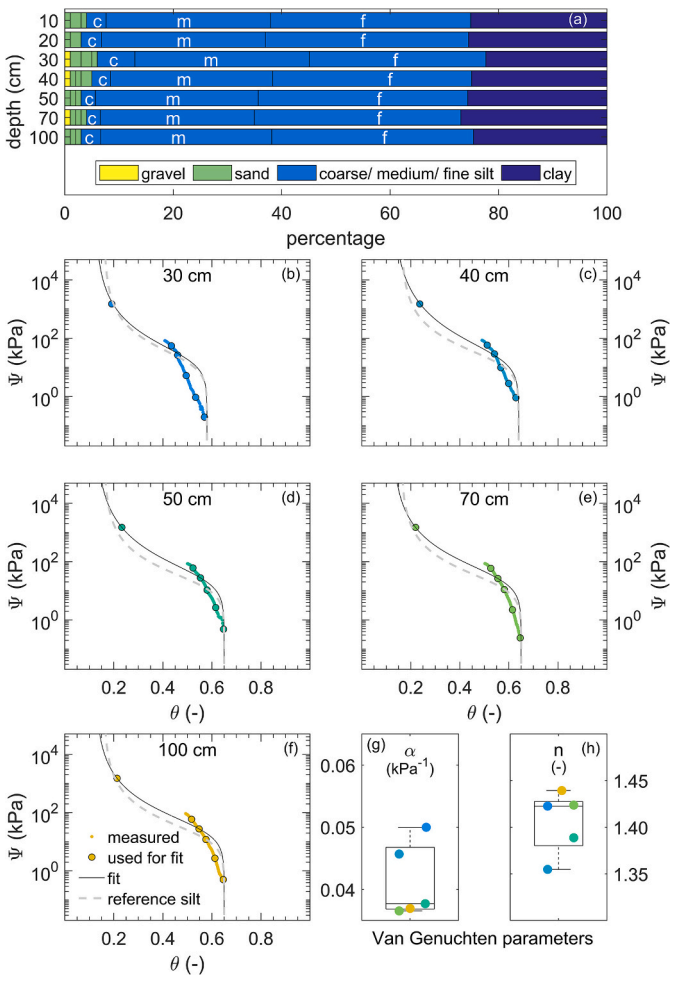


Fig. 8. Grain size distribution (a) and soil water characteristic curves (b-f) for soils in the top first meter at GW1 and resulting Van Genuchten parameters (g-h).

the observed spatial heterogeneity in subsidence rates must necessarily be explained solely by well-casing failures. Rather, the modelling follows an exploratory approach. It demonstrates that the observed subsidence trend and parts of the temporal dynamics at the GW1 site, represented in the model through sinusoidal surface loading variations, can be reproduced in the correct order of magnitude, while acknowledging that additional processes, such as heterogeneity in geomechanical properties and spatially and temporally variable groundwater depletion, also influence the real subsidence dynamics.

This comparison shows that seasonal surface loading due to variations in surface water levels can influence subsidence dynamics in a manner comparable to seasonal variations in groundwater extraction. At the same time, the simulations illustrate that well-casing failures, depending on their extent, may represent a plausible mechanism contributing to the development of pronounced spatial heterogeneity and local extremes in subsidence rates.

The future contribution of delayed subsidence resulting from previous groundwater depletion is assessed in a scenario simulation assuming stable groundwater heads after 2025. As shown in Fig. 13a considering undisturbed sediment strata, the delayed subsidence response leads to an additional increase of 0.14–0.18 m yielding and a total subsidence of 0.30–0.35 m by 2100, with only minor differences between non-urban and urban landscapes. The simulations that account for single and multiple well-casing failures (Fig. 13b and c) yield comparable cumulative subsidence for the non-urban monitoring site GW1. Conversely, the well-casing failure and the associated assimilation of hydraulic heads in the aquitard layers toward the head in the tapped aquifer $qp_{2–3}$ exacerbate urban subsidence, yielding a calculated cumulative subsidence of 0.42–0.44 m by 2100 for single well-casing failure and 1.15–1.35 m when considering multiple well-casing failures.

4. Discussion

4.1. Geomechanical subsurface characterization and implications on subsidence dynamics

The results show a high compressibility of the Holocene and Pleistocene aquitards Q_2 and Q_1^3, indicating their high potential for compaction and land subsidence. The depth-differentiated mean value of $C_c = 0.77$ in these aquitards at GW1 (Fig. 7e) exceeds reported spatial mean compression indices of $C_c = 0.66$ for soft clay Holocene deposits in the VMD (Baldan et al., 2025). The variation of C_c along the presented depth profile (Fig. 7e) underscores that utilizing mean values for C_c within hydrogeological units in geomechanical simulations is a simplification, which may require careful reconsideration for accurate and high-resolution simulations.

The geomechanical characterization reveals predominantly normally consolidated conditions along the depth profile in the Holocene aquitard Q_2 and the upper Pleistocene aquitard Q_1^3. Only in the topmost

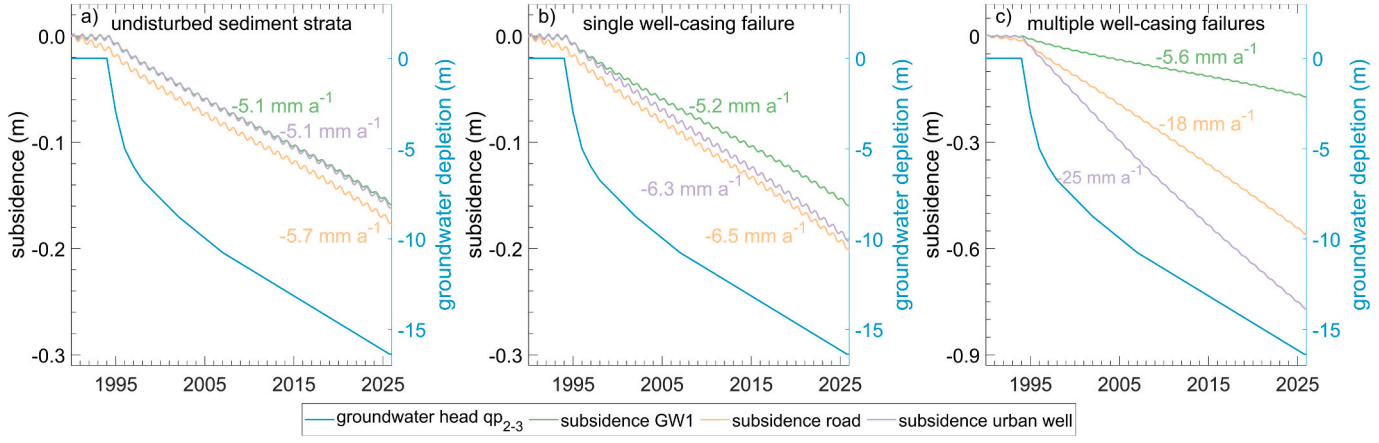


Fig. 9. Simulated land subsidence induced by groundwater depletion and local surface loading along a road (a), and with additional consideration of a single well-casing failure (b), and multiple well-casing failures (c) for the period 1990–2025 at monitoring site GW1 in the southern VMD. Note that in (a) the time-series of subsidence at GW1 and at the urban well are nearly equal, therefore hard to distinguish. Also note the different y-axis scale in (c) and that additionally to groundwater head depletion in $qp_{2–3}$ the model considers groundwater depletion in qp_3 aquifer (see Fig. 1a).

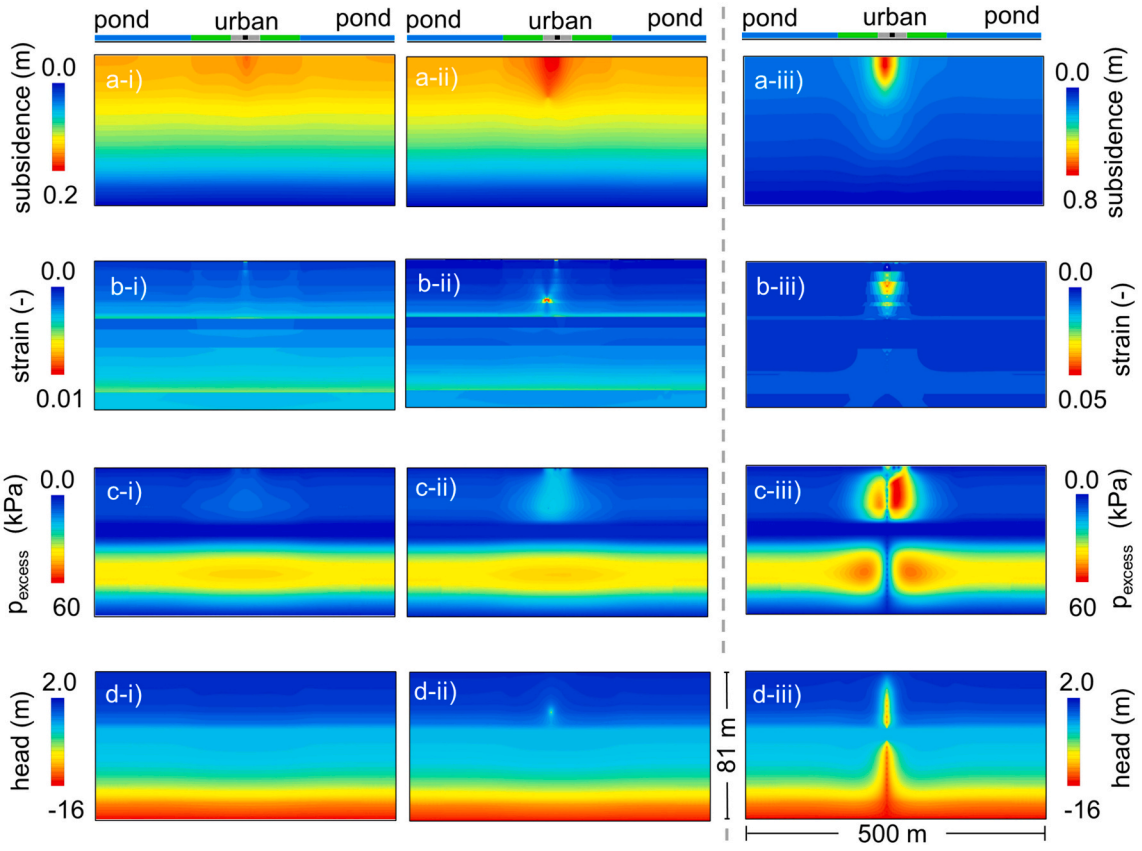


Fig. 10. Simulated state variables at the end of the simulation period (2025), showing vertical displacement (i.e., subsidence) (a), vertical strain (b), excess pore pressure (c), and hydraulic head (d), for scenarios with groundwater depletion and surface loading from a road (i), and with additional consideration of a single well-casing failure (ii) and multiple well-casing failures (c). Note that the y-axis scales in (a-iii) and (b-iii) differ from those in (a-i) to (b-ii). Surface land-use characteristics are schematically shown in the upper part of the figure (see Fig. 2 for details).

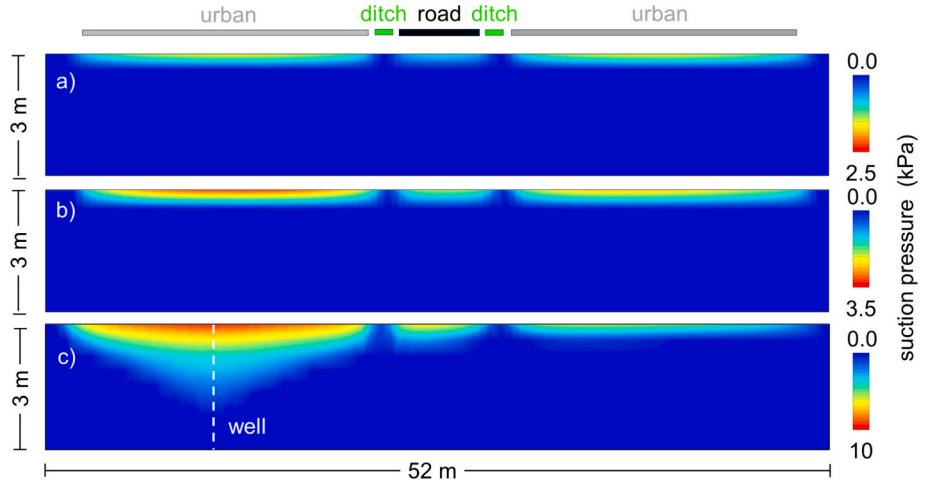


Fig. 11. Calculated suction pressure at the end of the simulation period (2025) for scenarios with groundwater depletion and surface loading from a road (a), and with additional consideration of a single well-casing failure (b) and multiple well-casing failures (c).

meters, the sediments are characterized by overconsolidated conditions. Similar *OCR*-profiles have been reported by Mi et al. (2023) for Holocene deposits in the southern VMD, characterized by lightly to moderately overconsolidated conditions in the top 4–5 m thick weathered crust and a convergence of *OCR* toward unity with increasing depth. The *OCR*-profile at GW1 implies that except for the top meters, deformation processes are characterized by the compression index C_C and therefore must be anticipated to be only marginally reversible. The potential of sediments to revert compression when the effective stresses are reduced is characterized by the recompression index (Allen and Mayuga, 1970). The results show that the compression index exceeds the recompression index by a factor of 9.0 to 15.8. This indicates that once the sediments undergo inelastic deformations, the land rebound potential is limited to approx. 6–11% (inverse of 9.0 and 15.8) of the inelastic deformation.

The derived vertical hydraulic conductivity for GW1 (Fig. 7j) varies between 6.3 $\cdot 10^{-11}$ and 6.2 $\cdot 10^{-10}$ m s^{-1} along the vertical profile,

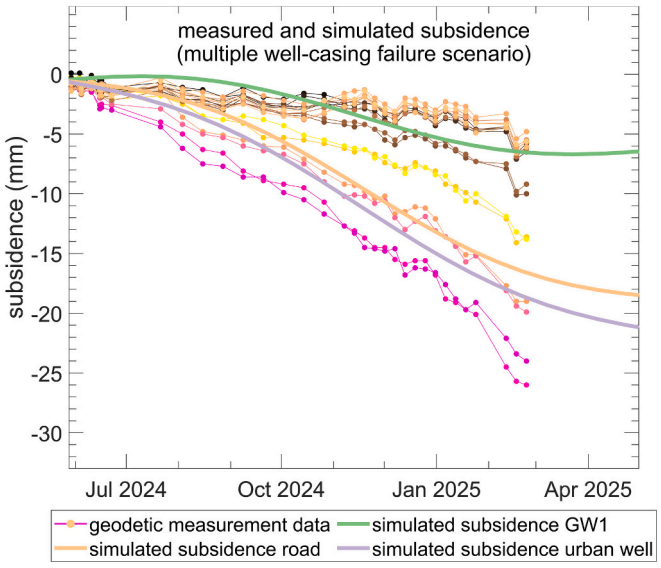


Fig. 12. Comparison of measured and simulated subsidence dynamics for the multiple well-casing failure scenario.

thereby agreeing with literature values for unweathered marine clay (Domenico and Schwartz, 1998) like the Q_2 and Q_1^3 deposits in the southern VMD (Wagner et al., 2012). Due to the low hydraulic conductivity in combination with the aquitard thicknesses of 31.9 m and 44.3 m, dissipation of excess pore pressure and the associated aquitard drainage are slow processes, and a delayed subsidence response to past groundwater depletion must be anticipated. This is also manifested in the coefficient of consolidation, c_v, a parameter which describes the rate of sediment compaction. The calculated values of c_v between $1.2 \cdot 10^{-8}$ and $5.4 \cdot 10^{-8}$ $m^2\ s^{-1}$ in Q_2 and Q_1^3 (Fig. 7i) corroborate previous analyses of c_v in the study area Ca Mau, characterized by a range of $c_v = 2.9 \cdot 10^{-8}$ to $1.1 \cdot 10^{-9}$ $m^2\ s^{-1}$ in the Holocene aquitard Q_2 (Nguyen Thi et al., 2020). The distinct variation in parameter characteristics between the upper and lower aquitard is consistent with classifications of very soft to soft clay in the near-surface aquitard and medium to stiff clay in the lower aquitard (Mi et al., 2023), reflecting differences in depositional history and consolidation characteristics.

The high compression indices together with the predominantly normally consolidated conditions characterize the high potential of the Holocene sediments for land subsidence due to groundwater depletion in the southern VMD. However, with the relatively weak depletion rate in the adjacent aquifer qp_3 (Duy et al., 2021; Fig. 1a) the increase in effective stress within the Holocene deposits over recent decades has remained moderate, leaving the Holocene's high potential for land subsidence largely inactivated. Within the scope of this local-scale study, these findings underline that particularly the exploitation of shallow aquifers (< 40 m depth) and the resulting exposure of the highly compressible sediments to increasing effective stresses must be prevented to avert exacerbating subsidence dynamics. Therefore, this local-scale analysis highlights that informed sustainable water resource management is essential with a particular emphasis on the regulation of shallow aquifers, which are of particular interest for aquaculture due to their predominantly brackish water quality. Given the low hydraulic conductivity and substantial thickness of the aquitards, a considerable portion of the subsidence will occur with delay, emphasizing the necessity for proactive water management practices.

Beyond the presented local geomechanical parameterization in high vertical resolution, a spatially extensive depth-differentiated mapping of geomechanical properties is crucial for robust predictions of delta-wide subsidence in the southern VMD. Despite seemingly similar lithologic compositions, Holocene sediments can exhibit spatially highly heterogenous geomechanical characteristics, governing their consolidation behavior and additionally contributing to the spatial complexity of observed subsidence patterns (Buffardi et al., 2025). This highlights the need for improved geomechanical parameterization at higher vertical and horizontal resolution in the VMD, to support both high-resolution modelling and the derivation of representative parameters for more generalized approaches.

4.2. Spatiotemporal dynamics of observed land subsidence rates

The two evaluated subsidence datasets of geodetic leveling data (Fig. 3) and InSAR-derived subsidence rates (Fig. 4) show consistent patterns of spatial heterogeneity of comparable order of magnitude. As these datasets cover non-overlapping time periods and the geodetic leveling data cover only a subset of the spatial extent of the local InSAR data, the agreement between them remains qualitative in nature, with no possibility of direct comparison. Nevertheless, both datasets exhibit similar characteristics with regard to the magnitude and extent of subsidence heterogeneity, which supports their interpretation as plausibly consistent. While the geodetic leveling data show moderate subsidence rates <10 mm a^{-1} at the non-urban monitoring site GW1, approximately 90% of the individual InSAR scatterers in the vicinity of GW1 show subsidence rates greater than those derived from leveling at GW1. This local analysis may indicate that the InSAR-based assessments of land subsidence are not necessarily representative for non-urban landscapes in the southern VMD. In addition, even within urban areas, high variability in InSAR-based subsidence rates have been reported earlier (e.g.

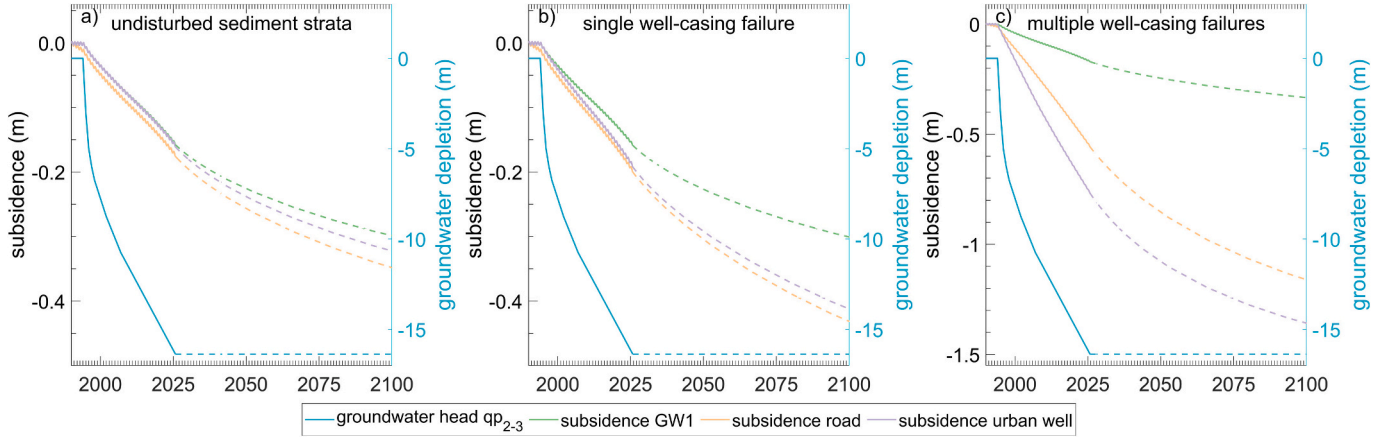


Fig. 13. Simulated delayed future subsidence assuming no further groundwater depletion for the period 2025–2100 at monitoring site GW1 in the southern VMD (a) and with additional consideration of a single well-casing failure (b) and multiple well-casing failures (c). Note the different y-axis scaling in (c).

Minderhoud et al., 2018), particularly in urban areas, where this variance has been attributed to buildings' specific type and depth of foundations and previous land use (De Wit et al., 2021). While the present geodetic leveling results also reveal a similarly high variability in subsidence, the monitored points are not directly located on surfaces exposed to loading, such as roads or buildings, but rather in intermediate and adjacent zones without direct surface loading. The ground-based geodetic data, albeit limited to only a few points, does not show a correlation between elevated subsidence rates and distances to loading infrastructure e.g. the road or buildings. This suggests that, in addition to groundwater depletion and surface loading, other contributing processes or environmental conditions with high spatial variability could be at play, inducing the hazardous subsidence rates derived from delta-wide InSAR analyses. Future research would benefit from more extensive geodetical monitoring campaigns, allowing for a statistically sound evaluation of potential relationships between subsidence dynamics and distances to certain infrastructures or land use types.

The subsidence rates derived from the geodetic monitoring campaign are subject to uncertainties, as the depth of the bridge's pile foundation, and thus the depth datum representing the zero level of the subsidence measurements, is uncertain. Consequently, any sediment compaction occurring below the bridge's foundation level, and the associated land subsidence, are not captured in the geodetic observation data. While using the nearby bridge as a stable reference point follows the general approach of Dörr et al. (2024), who employed larger (~200 m) bridges together with solid rock outcrops as reference networks for InSAR analyses in the southern VMD, the bridge in this study is shorter (~50 m). Nonetheless, the agreement between the subsidence rates derived from the geodetic monitoring campaign (Fig. 3) and the InSAR satellite data (Fig. 4) suggests that the bridge at the study site serves as a reasonably reliable reference point for subsidence observations. For future studies, it is recommended to obtain and incorporate actual data on bridge foundation depths to clarify the corresponding depth datum, while GNSS (Global Navigation Satellite System) measurements could additionally be employed to provide an absolute vertical reference.

Overall, for the observation of land subsidence dynamics, space-borne methods have become indispensable, providing valuable datasets on spatiotemporal subsidence dynamics in the VMD since more than a decade (Dörr et al., 2024; Erban et al., 2014). However, such methods are limited to the observation of persistent or temporal scatter points like rooftops of buildings or road surfaces and are incapable of monitoring subsidence dynamics of natural environments like vegetated surfaces. The local-scale study supports the interpretation, that the inherent overrepresentation of anthropogenically shaped land in delta-wide InSAR-based subsidence analyses possibly undermines their representativeness for regional dynamics in non-urban dominated landscapes. This potential limitation of InSAR based observations underscores the relevance of ground-based monitoring as well as physic-informed modelling, as proposed in this local-scale investigation.

The spatial heterogeneity of subsurface properties and groundwater extraction patterns limits a direct extrapolation of the process quantification at GW1 to the entire delta and limits overgeneralizing the derived management implications. However, the process dynamics identified at GW1 can be considered broadly representative of the southern VMD for several reasons: (i) The stratigraphy at GW1 falls within the range of reported layer thicknesses and lithological configurations documented for the southern VMD (e.g., Wagner et al., 2012; Duy et al., 2021; Mi et al., 2023) and compression indices are broadly comparable to those reported by Baldan et al. (2025). (ii) The observed groundwater head declines at GW1 are comparable to those reported from other parts of the southern delta (Duy et al., 2021; exemplary also Fig. 1a). (iii) The aquaculture-dominated land use, with minor adjacent urban infrastructure along a road corridor, reflects typical land-use and land-cover characteristics of large parts of the southern VMD. (iv) InSAR-derived subsidence rates in the vicinity of GW1 are comparable in magnitude and spatial variability to delta-wide observations (Dörr et al., 2024). (v) The quantified subsidence dynamics due to groundwater depletion are in overall agreement with results from delta-wide numerical modelling studies (e.g., Minderhoud et al., 2017). Together, these aspects support the relevance of the identified hydro-geomechanical process dynamics beyond the immediate study site, while acknowledging that local variability across the delta may lead to differences in the relative contribution and timing of individual drivers.

4.3. Simulated land subsidence due to groundwater depletion

This study presents a fully-coupled flow-deformation model that applies geomechanical parameterization at high vertical resolution to simulate local land subsidence dynamics in the southern VMD. Utilizing this advanced simulation approach at local scale for a detailed 2-D cross-sectional model complements delta-wide benchmark simulations on land subsidence due to groundwater depletion in the VMD by Minderhoud et al. (2017, 2020). Overall, the presented local-scale modelling results support the validity of the delta-scale estimates of land subsidence due to groundwater depletion introduced by Minderhoud et al. (2017), thereby countering previously raised concerns regarding model-structural uncertainties and the resulting skepticism toward their projections. This interpretation is consistent with recent investigations by Lexmon et al. (2025), which demonstrate that vertical aquitard discretization exerts a negligible influence on subsidence estimates at the delta scale in the VMD.

In the model simulation for fully undisturbed sediment strata, a land subsidence rate of 5.1 mm a^{-1} is calculated for the non-urban monitoring site GW1. This simulated rate represents the lower bound of subsidence values observed in delta-wide (Dörr et al., 2024) and local (Fig. 4) InSAR analyses, but is generally consistent with computed subsidence rates by Minderhoud et al. (2017), who calculated an average delta-wide subsidence due to groundwater depletion of 18 cm over 25 years, equivalent to a rate of 7.2 mm a^{-1}. However, a direct comparison is not feasible because the model domains differ in their vertical extent and Minderhoud et al. (2017, 2020) report total subsidence without depth differentiation of the governing compaction processes. By presenting the first depth-differentiated simulation results of subsidence caused by groundwater depletion in the Mekong Delta, this local-scale study illustrates how depth-differentiated simulations can support more robust assessments of how the exploitation of specific aquifers can affect subsidence vulnerability (see Section 4.6).

The difference between the simulated (5.1 mm a^{-1}) and observed (8 mm a^{-1}) subsidence rates at GW1 might be attributed to process dynamics not captured with the proposed model, e.g. autocompaction. However, without reliable information on the depth of the bridge's pile foundation, and thus the reference depth of the subsidence measurements, this attribution remains uncertain.

In the simulation results, the influence of locally unsaturated conditions on shallow compaction is minor and mainly restricted to sediments below sealed surfaces, as the aquaculture ponds maintain fully saturated conditions in the soils below. The limited impact arises from the shallow depth range affected by the lowering of the phreatic water level within the Holocene aquitard, resulting in only minor and spatially restricted increases in effective stress (Fig. 11a). It is noted that the adopted van Genuchten parameters do not optimally reproduce the measured $\Psi - \theta$ relationship in the near-saturation range, but were selected to represent literature values typical for the local silt-dominated sediments. However, as the sediments remain almost fully saturated in all three employed simulations (minimum saturation $> 95\%$), the influence of the resulting slight overestimation of suction pressure on the simulated subsidence dynamics is minor. The largely saturated conditions are controlled by the low vertical hydraulic conductivity and the anisotropy ratio (k_h/k_v), which together restrict vertical percolation and promote shallow lateral flow from fully saturated sediments beneath aquaculture ponds toward the unsaturated zones below sealed surfaces. In urban settings, however, such as in the provincial capital Ca Mau City,

the extent of sealed surfaces is considerably larger, lateral flow becomes less effective and declines in the phreatic water level within the Holocene aquitard may be anticipated. This would in turn induce spatially more pronounced unsaturated conditions, thereby exerting a greater influence on sediment compaction and resulting land subsidence. The quantified impact of unsaturated conditions substantiates the discussions of De Wit et al. (2021), who postulate that urbanization may accelerate subsidence due to lowered phreatic groundwater levels.

The land subsidence time series computed in the present study exhibit seasonal variations (Fig. 9), consistent with seasonal patterns observed in local InSAR data (Fig. 4c). Indications of temporal variability are also visible in the geodetic leveling data at GW1 (Fig. 3b), although the available observation period is too short to robustly resolve a seasonal signal. In the simulation results, the seasonal variations are attributable to the sinusoidal representation of water load fluctuations in aquaculture ponds acting on the ground surface. This indicates that a correlation between the seasonal characteristics of subsidence and groundwater dynamics does not necessarily imply a causal relationship, as both processes are governed by the same seasonal surface load variations. Imprints of this interrelation can also be inferred on sub-seasonal scales from observed subsidence rates and groundwater heads e.g. during January and February 2025 (Fig. 3a), for instance during periods of temporarily rising or rapidly declining groundwater heads. In addition to loading-induced seasonality captured in the model, seasonal groundwater abstraction for agriculture or domestic water supply may also contribute to seasonal variations in groundwater heads and associated subsidence dynamics. In the present modelling framework, groundwater extraction is represented through annual average depletion rates, which simplifies potential seasonal variability in pumping-induced head dynamics. Recent analyses for the investigated pilot site GW1 (Dörr et al., 2026) indicate that the majority of the observed seasonal variability in groundwater heads is induced by loading effects, whereas loading-corrected, and therefore abstraction-induced, seasonal fluctuations appear to have a comparatively minor influence on the annual variation of groundwater head dynamics at this local setting.

The implementation of a vehicle load of 10 kPa does not result in significant additional subsidence of the road (see Fig. 9a). Building loads, which are not included in the simulation, likely exert a similar magnitude of loading as the implemented 10 kPa vehicle loads (Xu et al., 2025). This suggests that the evaluated combination of laterally uniform groundwater depletion and local urban surface loading alone is insufficient to either explain the spatially heterogeneous patterns of observed subsidence (Fig. 3 and Fig. 4) or the regionally reported hazardous subsidence rates of up to 30–50 mm a^{-1} (Dörr et al., 2024; Erban et al., 2014) under the assumption of laterally uniform parametrization and boundary conditions utilized in the present model. In addition to the numerically assessed impact of well-casing failure, other localized drivers and subsurface heterogeneities not explicitly represented in the modelling framework are likely to contribute to the observed subsidence patterns, such as shallow drainage, historical land-use changes, spatially variable groundwater head depletion, or small-scale heterogeneities in geomechanical properties and layer thickness.

The simulation results reveal a pronounced delayed subsidence response to past groundwater depletion, amounting to an additional 0.14–0.18 m and a total subsidence of 0.30–0.35 m by 2100 (Fig. 13a). This projection is consistent with the M2-scenario of Minderhoud et al. (2017), who estimated a comparable future subsidence of approx. 0.20 m and a total subsidence of approx. 0.40 m by 2100 under the assumption that groundwater depletion ceased in 2018. It should be noted that the assumption of stable groundwater heads after 2025 represents an optimistic and most likely unrealistic groundwater management scenario given current extraction trends. In this study, the assumption primarily serves to isolate and quantify the delayed subsidence response to groundwater depletion that has already occurred in the past. The magnitude and temporal evolution of this delayed response may differ under alternative groundwater management scenarios, such as continued business-as-usual depletion or a recovery of groundwater heads, for example through managed aquifer recharge.

4.4. Well-casing failure as a potential factor for spatiotemporal heterogeneity in subsidence dynamics

To explore potential factors contributing to the pronounced spatiotemporal heterogeneity in observed subsidence rates, the possibility is examined that failures in borehole casings can provide local subsurface drainage pathways and hydraulic interconnectivities, thereby facilitating accelerated aquitard drainage and compaction. In general, well-casing failures and ruptures in borehole casings are well known consequences of land subsidence induced by groundwater depletion (Gambolati and Teatini, 2021; Holzer and Johnson, 1985). However, to the best of the authors' knowledge, it has not yet been proposed that once such casing damage occurred, it can also accelerate subsequent subsidence by providing local subsurface drainage pathways and a local equilibration of hydraulic heads between the aquitard and the tapped aquifer.

By implementing damaged well casing segments into the model, spatially heterogeneous subsidence rates were simulated, with peak subsidence occurring at the locations of the failed well-casings. The simulated local subsidence peaks in the vicinity of the well are caused by two processes, namely (i) acceleration of compaction processes by provision of drainage facilities and (ii) locally increased groundwater head depletion. Firstly, within this proposed conceptual framework, compaction processes are locally accelerated because well-casing failures provide additional drainage pathways for excess pore water pressure from aquitard sediments into the well casing. In undisturbed settings, aquitard drainage is predominantly directed vertically toward the adjacent aquifer, which can result in a pronounced delay in the presence of thick confining units. In contrast, where well-casing failures occur, drainage is accelerated due to additional, localized, and shorter horizontal flow paths toward the casing. Secondly, this process not only alters the time dependency of compaction but may also affect its overall magnitude. In the present setting, compaction of the shallow Holocene strata is primarily controlled by hydraulic heads in the moderately depleting shallow aquifer. However, drainage toward a well-casing failure is governed by the hydraulic head within the casing, which corresponds to the hydraulic head of the deeper aquifer in which the well is screened. This process is also evident in the computed hydraulic heads in the simulation results (Fig. 10 d).

These processes are schematically visualized in Fig. 14, illustrating how well-casing failure creates drainage pathways for excess pore water pressure dissipation in aquitards and locally exposes aquitard sediments to the lower hydraulic head of the tapped aquifer (denoted as reference head h_2 in Fig. 14) at the casing–aquifer interfaces.

Overall, the simulation results show that damaged well casing segments can potentially provide subsurface drainage pathways and locally accelerate sediment compaction and resulting land subsidence. The simulation results show that the magnitude of this effect strongly depends on the number of well-casing failures considered. To constrain the possible range of impacts, two end-member scenarios were therefore simulated: a single well-casing failure at depths of highest subsurface strain, and multiple failures implemented at 3 m intervals along the casing, conceptually representing failures at each casing joint.

This relationship was further investigated through a sensitivity analysis, in which the magnitude of simulated subsidence was evaluated by varying the number of implemented broken well-casing segments, reducing it from 25 (every 3 m) to 13 (every 6 m), to 6 (every 12 m), and finally to only 2 segments and 1 segment (placed at depths where strains are greatest and casing rupture is therefore most likely). Fig. 15a illustrates the resulting variation in calculated subsidence at the well location at the end of 2025 for different numbers of broken well-casing segments implemented in the model. The results indicate that the magnitude of locally elevated subsidence increases with the number of

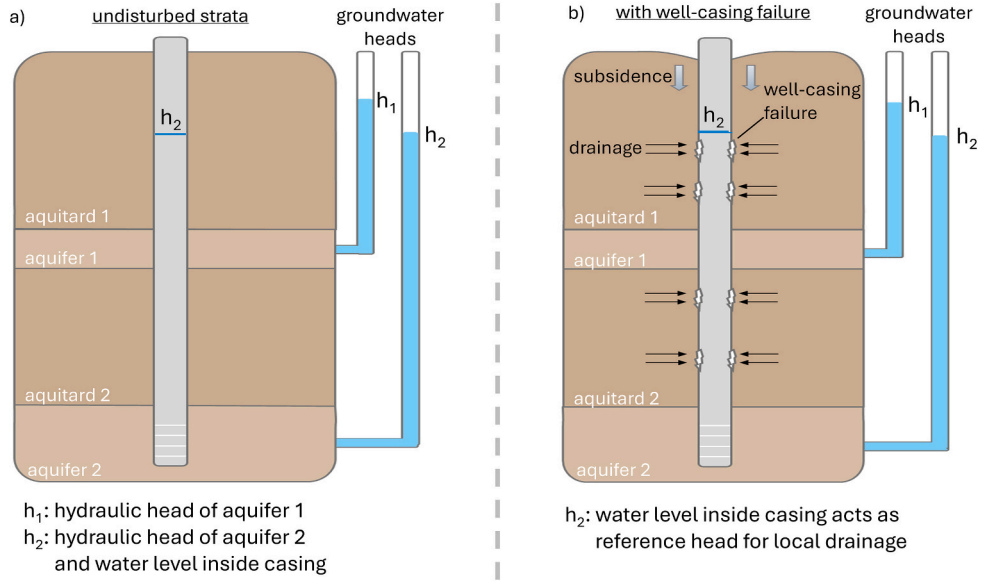


Fig. 14. Schematic illustration of how well-casing failure (b) can accelerate land subsidence compared to an undisturbed subsurface setting (a).

casing failures, highlighting the overall importance of casing integrity and installation quality. An additional sensitivity analysis with respect to the length of the implemented casing-failure segments showed only minor differences in the resulting subsidence when failures were considered every 3 m (Fig. 15b), indicating that the model results are largely insensitive to the exact segment length for the failure spacing considered here.

The scenario assuming casing failures at 3 m intervals represents damage occurring at each casing joint, which can constitute structural weak points of well casings when improperly installed. Such a high number of failures reflects a maximum-impact scenario and would likely require severely compromised casing integrity, for example in cases where the commonly used PVC joints between the 3 m pipe segments in unprofessionally constructed household wells are only loosely fitted or inadequately glued. Previous studies have also addressed the possibility that such household tube wells in the VMD may lose casing integrity over time and thereby potentially affect groundwater quality (Danh and Khai, 2015). Therefore, this scenario is considered to represent a high, yet not necessarily implausible, level of casing damage in individual wells, given the questionable technical quality of unlicensed groundwater extraction wells in the VMD, where improper installation or subsequent weakening of casing joints may result in failures at multiple casing connections within a single well.

Overall, the magnitude and spatial relevance of well-casing failures for subsidence dynamics under field conditions remain difficult to quantify and are subject to considerable uncertainty given the limited availability of observational field evidence. Future field investigations could help test this numerically derived hypothesis, for example through camera inspections of abandoned wells combined with comparisons to InSAR-derived subsidence patterns.

In the VMD, an estimated number of up to half a million to one million unlicensed groundwater extraction wells (Danh and Khai, 2015) provides a spatially extensive and unsupervised subsurface infrastructure of questionable technical quality, with a potential to scale well-

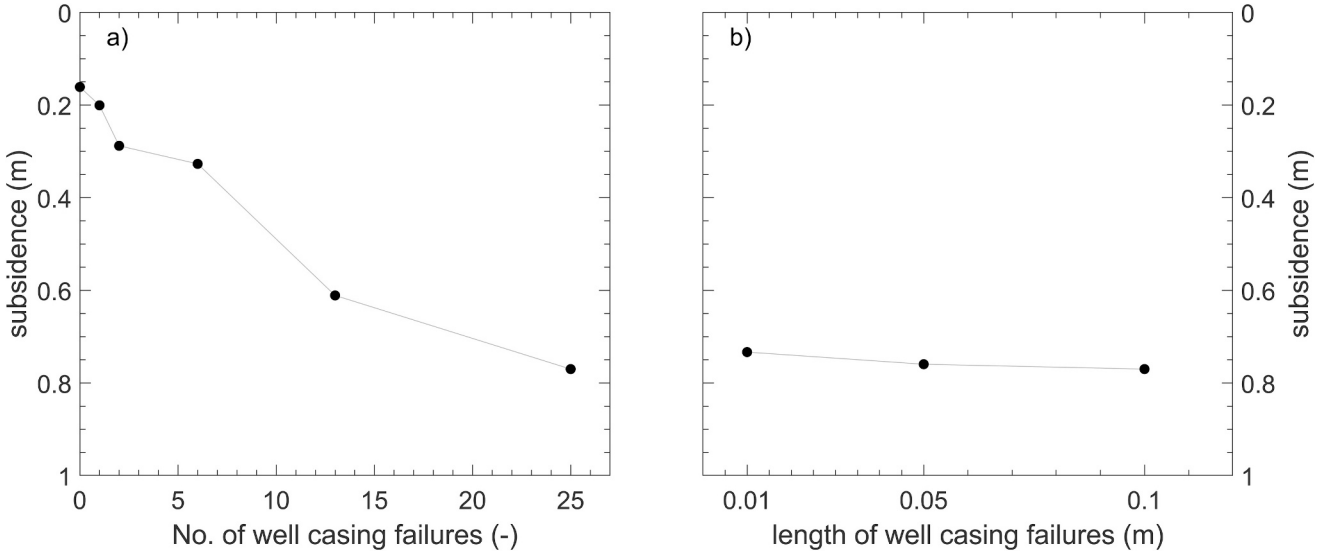


Fig. 15. Calculated subsidence at the well location at the end of 2025 for varying numbers of broken well-casing segments implemented in the model with a constant failure length of 10 cm (a), and for varying well-casing failure lengths with a constant failure spacing of 3 m (b).

casing failure from a local to a regional effect. The proposed process pathway of well-casing failure as land subsidence accelerator may have remained unrecognized because such effects are difficult to infer from surface observations alone, as groundwater wells commonly coincide with local subsidence maxima associated with groundwater depression cones.

The numerically assessed hypothesis of broken well-casings and the resulting interconnectivity of aquifers/aquitards could also offer explanations for other unresolved questions, such as inconsistent hydrogeochemical or isotopic signatures across different aquifers (Osenbrück et al., 2025), and discrepancies between stagnant salinity trends observed in professionally drilled monitoring wells of the NGMN and reported increases in groundwater salinity from farmers' private wells (Hoan et al., 2025). To further evaluate this hypothesis, camera inspections of abandoned wells are recommended. Moreover, mapping the spatial distribution of such wells together with InSAR-derived subsidence scatterers could provide an effective means of validation. Overall, future investigations of well-casing failure effects on land subsidence would benefit from three-dimensional simulations to adequately resolve casing-failure geometries and the resulting localized flow and stress redistribution processes.

While broken well-casing segments would represent unintended subsurface drainage pathways, such drainage effects are recently induced deliberately in the context of road construction in the VMD through the installation of prefabricated vertical drains (PVDs) below newly constructed road embankments (Mi et al., 2023). These are installed to accelerate soil and sediment consolidation immediately after construction and thereby reduce the proportion of compaction and subsidence occurring during operation.

The subsidence observations from the monitoring site GW1 (PW1 and PW2 in Fig. 3 a-b) appear to indicate the presence of potential casing drainage pathways, revealing locally elevated subsidence rates at the multi-extensometer borehole, which is equipped with a sliding-joint casing. Due to the requirement for the sliding-joint casing segments to exhibit flexibility in movement, they are not sealed off against water, therefore representing a small-scale drainage opportunity for the surrounding aquitard sediments. This local drainage to the sliding-joint casing segments is most likely distinctly less pronounced than a potential casing rupture as implemented into the model for an exemplary unlicensed urban production well. This finding supports the hypothesis that well-casing failure accelerates subsidence and, at the same time, raises concerns about the measurement concept of sliding-joint extensometer boreholes, as it suggests that the monitoring facility itself may alter the very compaction dynamics it is designed to observe. Although an additional load from the monitoring installation cannot be fully excluded, the pronounced settlement during the dry season points toward drainage-driven subsurface processes as a likely contributing mechanism.

Overall, the present study corroborates the conclusion of Yuill et al. (2009) that changes in surface and subsurface drainage pathways must be investigated to understand land subsidence and its spatial heterogeneity. With depths of commonly below 3–5 m (Le et al., 2023), the various channels represent possible drainage pathways for the upper few meters of the Holocene deposits in the southern VMD. Therefore, the characteristic street bumps at bridge onsets in the southern VMD (Dörr et al., 2024) may not only be attributable to differential subsidence between the stable bridges' piled foundations and regional subsidence, but also to surface drainage opportunities, accelerating near-surface dissipation of excess pore pressure and associated elevated compaction and subsidence close to the channel bank.

4.5. Capabilities and limitations of the applied modelling framework

The local-scale modelling approach applied here builds upon previous regional modelling studies on groundwater-depletion–induced land subsidence in the VMD (Minderhoud et al., 2017, 2020) by incorporating surface loading from structural loads of the built environment and changing surface water levels, as well as potential anthropogenic subsurface drainage pathways. This enables a process-based exploration of multiple drivers of local subsidence dynamics and their spatiotemporal variability. It should be noted that the implementation of a fully coupled flow–deformation framework per se did not yield fundamentally new insights, as coupling effects have been shown to be minor in comparable problem settings (Gambolati et al., 2000). However, this modelling framework enabled the implementation of surface loading and potential subsurface drainage toward well-casing failures, which, together with the high-resolution, site-specific parameterization, allows for a more detailed investigation of local subsidence processes and their potential drivers.

The employed modelling framework is primarily intended for a process-based exploration of compaction and subsidence mechanisms, whereas precise predictions are constrained particularly due to limited lateral sampling of geomechanical properties. Despite the relatively high vertical data density employed for the geomechanical parameterization, derived from consolidation tests on multiple samples from a single borehole (GW1), the assumption of laterally uniform geomechanical properties within the 500 m lateral model domain represents a simplification, given the inherently heterogeneous geomechanical properties of deltaic sediments (Buffardi et al., 2025). Such unresolved lateral variability in sediment properties, together with possible local variations in groundwater depletion, may affect both the magnitude and spatial distribution of subsidence dynamics beyond the numerically implemented drivers. These assumptions of lateral uniformity limit the generality of the presented results even at the considered local scale.

Overall, the *SoftSoilCreep* model is well suited to simulate the key processes relevant in this study, namely the time-dependent deformation of sediments under groundwater depletion and surface loading (Lee et al., 2018; Feng et al., 2019). However, this constitutive model does not explicitly account for deformation mechanisms associated with cyclic loading. Consequently, deformations due to seasonal loading and unloading of surface water bodies may not be fully captured, representing a limitation of the present simulations. This shortcoming could be addressed in future work by employing constitutive models that incorporate a dedicated description of cyclic deformation behavior.

A general limitation of this study arises from the depth range covered by the available datasets, which only extend to the upper ~80 m of the aquifer system. Consequently, potential contributions to overall subsidence from deeper aquifers and aquitards are not explicitly represented in the model. It should be noted, however, that this depth range corresponds to the portion of the subsurface reflected in the evaluated subsidence observations. In particular, the presented local leveling data is referenced to a bridge foundation that likely extends to comparable depths. Similarly, the InSAR dataset (Dörr et al., 2024) incorporated bridges with deep piled foundations, in addition to rock outcrops, into the reference network. As a result, these observations primarily reflect deformation within the upper ~70–80 m of the subsurface, where most of the measured subsidence was also inferred to originate (Dörr et al., 2024). The focus of the model domain on the upper 80 m and the associated choice of the lower hydraulic head boundary condition limit not only the simulation of compaction in deeper layers but also the assessment of how deep groundwater extraction may influence compaction in shallower strata. This is particularly relevant given the likely limited groundwater recharge (Dörr et al., 2026), as pressure declines induced by deep pumping may progressively affect overlying layers, increasing effective stresses and contributing to land subsidence. To better assess the potential impact of deeper strata on subsidence dynamics, future studies should therefore extend the presented modelling framework to include deeper strata below the upper Pleistocene and evaluate the contribution of deeper groundwater exploitation and aquitard compaction to overall land subsidence.

4.6. Implications for informed mitigation strategies

In subsidence threatened deltas, adaptation and mitigation strategies strongly rely on (i) accurate and representative quantifications of land subsidence across the delta and (ii) a sound process understanding of the driving forces behind land subsidence. Both aspects are essential for reliable predictions of expected future subsidence under various scenario considerations. The present study introduces a high-precision fully-coupled flow-deformation model, exemplary applied on local-scale, as a suitable tool for integrated assessments of land subsidence in the VMD. This study promotes future applications on delta-wide scale that allow the consideration of multiple drivers to support more comprehensive simulation of land subsidence dynamics in the VMD.

The findings of the present local-scale analysis suggest that, to prevent the highly compressible Holocene sediments from being exposed to increasing effective stresses and consequent land subsidence, particularly a depletion of the shallow aquifers *qh* and qp_3 must be avoided. In settings where shallow groundwater is used e.g. for brackish aquaculture, the combined effects of aquifer exploitation and the disconnection of Holocene sediments from surface water through urban sealed surfaces make these areas highly susceptible to intensified land subsidence.

Inter-aquifer connectivity, either caused by natural conditions like faults or hydrogeological windows or by anthropogenic interventions like failures of well-casings or well-bores, can accelerate the assimilation of hydraulic heads in shallow, more compressible strata, toward those of the highly exploited aquifers. Nonetheless, in light of insufficient groundwater recharge (Dörr et al., 2026), even in the absence of inter-aquifer connectivity, the exploitation of deep aquifers and associated head depletions will gradually propagate upward to shallow sediment layers, ultimately exposing them to increasing effective stresses and promoting land subsidence. The findings imply a considerable portion of delayed subsidence to past groundwater depletion at the investigated site in the VMD consistent with previous studies (Minderhoud et al., 2020), emphasizing the overall need for proactive water management strategies demonstrated here through a high-resolution local-scale analysis.

While the presented results highlight potential implications for groundwater management, they are derived from a local-scale analysis and cannot be directly extrapolated to delta-wide conditions. Accordingly, the proposed management implications should be viewed as exploratory rather than prescriptive and require validation at broader spatial scales.

5. Conclusion

The present study substantiates that a detailed depth-differentiated subsurface parameterization is indispensable for accurate simulations of deltaic land subsidence and a reliable subsequent identification of the governing driving processes. Utilizing such sound parameterization in the presented fully coupled flow–deformation model framework provides a comprehensive approach for subsidence simulations, as it enables the integration of various potential drivers and process pathway.

Whilst urban dwellings provide a suitable infrastructure for satellite-based subsidence observations, their influence on compaction processes may concomitantly distort the representativeness of those observations for delta-wide evaluations. This study suggests that beyond the commonly considered effects of urban infrastructure loading and local anomalies in groundwater demand and depletion, sediment compaction below urban areas may also be influenced by anthropogenic subsurface disturbances like damaged well casings. The employed hypothesis-driven exploratory simulations indicate that such local disturbances could accelerate and intensify compaction by creating additional drainage pathways and increasing effective stresses in aquitards through a local assimilation of hydraulic heads toward those of the tapped aquifers. The impact of such effects depends locally on the number and extent of well-casing failures as well as on subsurface characteristics, particularly the aquitard thickness and hydraulic conductivity and at larger scales on the number of affected wells. However, the magnitude of these effects remains uncertain due to limited observational field evidence. Therefore, validation of this numerically assessed hypothesis is recommended, for example, through camera inspections of abandoned wells and their mapping together with InSAR-derived subsidence scatterers.

To mitigate the exposure of the highly compressible Holocene sediments to increasing effective stresses and the associated land subsidence, depletion of the shallow aquifers must be prevented in the Mekong Delta and other deltaic aquifer systems worldwide. In settings where economic activities rely on brackish water from these shallow aquifers, a particular vulnerability to advancing land subsidence must be anticipated. The derived portion of delayed subsidence to past groundwater depletion at the investigated site underscores that proactive water management strategies are crucial for the viability of the southern Mekong Delta.

Abbreviations

GNSS	Global Navigation Satellite System
InSAR	Interferometric Synthetic Aperture Radar
LULC	Land Use and Land Cover
NGMN	Vietnamese National Groundwater Monitoring Network
OCR	Overconsolidation ratio
PVD	Prefabricated Vertical Drains
RMSE	Root Mean Square Error
SWCC	Soil Water Characteristic Curves
VMD	Vietnamese Mekong Delta

CRediT authorship contribution statement

Felix Dörr: Writing – original draft, Validation, Methodology, Investigation, Formal analysis, Data curation, Conceptualization. **Jonas Bauer:** Writing – review & editing, Investigation, Formal analysis. **Tran Viet Hoan:** Writing – review & editing, Investigation, Data curation. **Le Thi Mai Van:** Writing – review & editing, Project administration, Data curation. **Andreas Schenk:** Writing – review & editing, Data curation. **Nils Dörr:** Writing – review & editing, Methodology, Formal analysis. **Franz Nestmann:** Writing – review & editing, Supervision, Resources, Project administration, Funding acquisition. **Stefan Norra:** Writing – review & editing, Supervision, Resources, Project administration, Funding acquisition.

Declaration of Generative AI and AI-assisted technologies in the writing process

During the preparation of this work the author(s) used ChatGPT in order to improve language and readability of the manuscript text. After using this tool/service, the authors reviewed and edited the content as needed and take full responsibility for the content of the published article.

Declaration of competing interest

The authors declare that they have no known competing financial interests or personal relationships that could have appeared to influence the work reported in this paper.

Acknowledgements

This research was conducted in the frame of the project “ViWaT – Vietnam Water Technologies” funded by the German Federal Ministry of Research, Technology and Space (funding reference: 02WCL1474A). Felix Dörr thanks the Hector Fellow Academy for support. We gratefully thank the Vietnamese Ministry of Science and Technology (MOST), the

National Center for Water Resources Planning and Investigation (NAWAPI) and the Department of Natural Resources and Environment Ca Mau (DONRE Ca Mau) for the good cooperation and providing data. We thank the KIT Institute of Soil Mechanics and Rock Mechanics (KIT-IBF) for providing access to the geotechnical laboratory facilities, and Hauke Sattler of the Institute of Environmental Sciences and Geography, Soil Sciences and Geoecology at the University of Potsdam for determining the soil-water characteristic curves. We acknowledge support by the KIT-Publication Fund of the Karlsruhe Institute of Technology, Germany.

Appendix A. Supplementary data

Supplementary data to this article can be found online at https://doi.org/10.1016/j.scitotenv.2026.181850.

Data availability

Data will be made available on request.

References

Allen, D.R., Mayuga, M.N., 1970. The Mechanics of Compaction and Rebound. International Hydrological Decade, Symposium on Land Subsidence, Tokyo, Japan 17–22 Sept. Wilmington Oil Field, Long Beach, California, USA.

Anderson, H.R., 1978. Hydrogeologic Reconnaissance of the Mekong Delta in South Vietnam and Cambodia. Contributions to The Hydrology of Asia and Oceania, Geological Survey Water-Supply Paper 1608-R.

Baldan, S., Minderhoud, P.S.J., Xotta, R., Zoccarato, C., Teatini, P., 2025. Data-driven 3D modelling of long-term Holocene delta evolution and sediment compaction: the Mekong Delta. Earth Surf. Process. Landf. 50. https://doi.org/10.1002/esp.6046.

Baú, D., Ferronato, M., Gambolati, G., Teatini, P., 2004. Surface flow boundary conditions in modeling land subsidence due to fluid withdrawal. Groundwater 42, 516–525. https://doi.org/10.1111/j.1745-6584.2004.tb02620.x.

Boone, S.J., 2010. A critical reappraisal of "preconsolidation pressure" interpretations using the oedometer test. Can. Geotech. J. 47, 281–296. https://doi.org/10.1139/T09-093.

Buffardi, C., Minderhoud, P.S.J., Mandolini, A., Ruberti, D., 2025. Characterizing Holocene sediments for assessing coastal-deltaic subsidence: the role of cone penetration tests and geomechanics. Front. Earth Sci. 13. https://doi.org/10.3389/feart.2025.1585388.

Danh, V.T., Khai, H.V., 2015. Household demand and supply for clean groundwater in the Mekong Delta, Vietnam. Renew. Wind Water Sol. 2, 4. https://doi.org/10.1186/s40807-014-0004-7.

Davydzenka, T., Tahmasebi, P., Shokri, N., 2024. Unveiling the global extent of land subsidence: the sinking crisis. Geophys. Res. Lett. 51. https://doi.org/10.1029/2023gl104497.

De Wit, K., Lexmond, B.R., Stouthamer, E., Neussner, O., Dörr, N., Schenk, A., Minderhoud, P.S.J., 2021. Identifying causes of urban differential subsidence in the Vietnamese Mekong Delta by combining InSAR and field observations. Remote Sens. 13, 189. https://doi.org/10.3390/rs13020189.

Domenico, P.A., Schwartz, F.W., 1998. Physical and Chemical Hydrogeology, 2. Ed., paperback. ed. Wiley, New York Chichester Weinheim.

Dörr, N., Schenk, A., Hinz, S., 2024. Land subsidence in the Mekong Delta derived from advanced persistent scatterer interferometry with an infrastructural reference network. IEEE J. Sel. Top. Appl. Earth Obs. Remote Sens. 17, 12077–12091. https://doi.org/10.1109/jstars.2024.3420130.

Dörr, F., Bauer, J., Rau, G.C., Lewi, E., Hoan, V.T., Van, L.T.M., Valois, R., Steinel, A., Nestmann, F., Norra, S., 2026. The recharge illusion: how seasonal surface loading can hide continuing groundwater resource declines in confined deltaic aquifers. J. Hydrol. 665, 134674. https://doi.org/10.1016/j.jhydrol.2025.134674.

Duy, N.L., Nguyen, T.V.K., Nguyen, D.V., Tran, A.T., Nguyen, H.T., Heidbüchel, I., Merz, B., Apel, H., 2021. Groundwater dynamics in the Vietnamese Mekong Delta: trends, memory effects, and response times. J. Hydrol. Reg. Stud. 33, 100746. https://doi.org/10.1016/j.ejrh.2020.100746.

Erban, L.E., Gorelick, S.M., Zebker, H.A., 2014. Groundwater extraction, land subsidence, and sea-level rise in the Mekong Delta, Vietnam. Environ. Res. Lett. 9, 084010. https://doi.org/10.1088/1748-9326/9/8/084010.

Feng, W.-Q., Zheng, X.-C., Yin, J.-H., Chen, W.-B., Tan, D.-Y., 2019. Case study on long-term ground settlement of reclamation project on clay deposits in Nansha of China. Mar. Georesour. Geotechnol. 39, 372–387. https://doi.org/10.1080/1064119X.2019.1704319.

Galavi, V., 2010. Groundwater Flow, Fully Coupled Flow Deformation and Undrained Analyses in PLAXIS 2D and 3D. Plaxis, Delft Neth.

Gambolati, G., Teatini, P., 2021. Land Subsidence and its Mitigation. The Groundwater Project. https://doi.org/10.21083/978-1-77470-001-3.

Gambolati, G., Teatini, P., Baú, D., Ferronato, M., 2000. Importance of poroelastic coupling in dynamically active aquifers of the Po River Basin, Italy. Water Resour. Res. 36, 2443–2459. https://doi.org/10.1029/2000WR900127.

Giao, P.H., Dung, N.T., Long, P.V., 2008. An integrated geotechnical–geophysical investigation of soft clay at a coastal site in the Mekong Delta for oil and gas infrastructure development. Can. Geotech. J. 45, 1514–1524. https://doi.org/10.1139/t08-077.

Hoan, T.V., Richter, K.-G., Börsig, N., Bauer, J., Ha, N.T., Norra, S., 2022. An improved groundwater model framework for aquifer structures of the quaternary-formed sediment body in the southernmost parts of the Mekong Delta, Vietnam. Hydrology 9, 61. https://doi.org/10.3390/hydrology9040061.

Hoan, T.V., Richter, K.-G., Dörr, F., Bauer, J., Börsig, N., Steinel, A., Le, V.T.M., Pham, V. C., Than, D.V., Norra, S., 2025. The utilization of a 3D groundwater flow and transport model for a qualitative investigation of groundwater salinization in the Ca Mau Peninsula (Mekong Delta, Vietnam). Hydrology 12, 126. https://doi.org/10.3390/hydrology12050126.

Holzer, T.L., Johnson, A.I., 1985. Land subsidence caused by ground water withdrawal in urban areas. GeoJournal 11. https://doi.org/10.1007/BF00186338.

Kooi, H., Erkens, G., 2020. Creep consolidation in land subsidence modelling; integrating geotechnical and hydrological approaches in a new MODFLOW package (SUB-CR). Proc. IAHS 382, 499–503. https://doi.org/10.5194/piahs-382-499-2020.

Le, H.-A., Nguyen, T., Gratiot, N., Deleersnijder, E., Soarez-Frazao, S., 2023. The multi-channel system of the Vietnamese Mekong Delta: impacts on the flow dynamics under relative sea-level rise scenarios. Water 15 (20), 3597. https://doi.org/10.3390/w15203597.

Lee, I., Choi, Y.-T., Lee, M., Yune, C.-Y., 2018. Effect of groundwater level variation on residual settlement of Korean high-speed railway on soft ground. KSCE J. Civ. Eng. 22, 3312–3320. https://doi.org/10.1007/s12205-017-0472-6.

Lexmon, B.R., Guzy, A., Torfs, P.J.J.F., Pham, H.V., Essink, G.H.P.O., Teatini, P., Stouthamer, E., Minderhoud, P.S.J., 2025. Simulating Extraction-induced Subsidence in the Mekong Delta: Investigating the Effects of Discretization and Conductivity Uncertainty. https://doi.org/10.21203/rs.3.rs-7609506/v1.

Logan, W.S., 2002. Vietnam's highway no. 1: corridor of power and patrimony. Hist. Environ. 23–27.

Mi, N.V.A., Thongchart, S., Mairaing, W., 2023. Roadway settlement characteristics on Mekong Delta for various landforms. Int. J. GEOMATE 25. https://doi.org/10.21660/2023.111.4006.

Minderhoud, P.S.J., Erkens, G., Pham, V.H., Bui, V.T., Erban, L., Kooi, H., Stouthamer, E., 2017. Impacts of 25 years of groundwater extraction on subsidence in the Mekong Delta, Vietnam. Environ. Res. Lett. 12, 064006. https://doi.org/10.1088/1748-9326/aa7146.

Minderhoud, P.S.J., Coumou, L., Erban, L.E., Middelkoop, H., Stouthamer, E., Addink, E. A., 2018. The relation between land use and subsidence in the Vietnamese Mekong delta. Sci. Total Environ. 634, 715–726. https://doi.org/10.1016/j.scitotenv.2018.03.372.

Minderhoud, P.S.J., Coumou, L., Erkens, G., Middelkoop, H., Stouthamer, E., 2019. Mekong delta much lower than previously assumed in sea-level rise impact assessments. Nat. Commun. 10, 1–13. https://doi.org/10.1038/s41467-019-116021.

Minderhoud, P.S.J., Middelkoop, H., Erkens, G., Stouthamer, E., 2020. Groundwater extraction may drown mega-delta: projections of extraction-induced subsidence and elevation of the Mekong delta for the 21st century. Environ. Res. Commun. 2, 011005. https://doi.org/10.1088/2515-7620/ab5e21.

Montoya-Araque, E.A., Aparicio-Ortube, A.J., Zapata-Medina, D.G., Arboleda-Monsalve, L.G., 2022. An open-source application software to determine the preconsolidation pressure of soils in incremental loading oedometer testing: pySigmaP. SoftwareX 17, 100990. https://doi.org/10.1016/j.softx.2022.100990.

Nguyen Thi, N., Son, B.T., Ngoc, D.M., 2020. Research on horizontal coefficient of consolidation of Vietnam's soft soil. J. Eng. 2020, 1–13. https://doi.org/10.1155/2020/3697689.

Osenbrück, K., Steinel, A., Montcoudiol, N., Manh, L.V., Bäumle, R., 2025. Geochemical evolution and flow of groundwater impacted by long-term abstraction in the Mekong Delta, Vietnam. J. Hydrol. 655, 132881. https://doi.org/10.1016/j.jhydrol.2025.132881.

Qi, J., Xie, Y., Li, C., Guo, H., Wang, Y., 2025. Creep behavior of clayey soil and its model prediction in the Cangzhou land subsidence area. Sci. Rep. 15, 9130. https://doi.org/10.1038/s41598-025-93928-z.

Syvitski, J.P.M., Kettner, A.J., Overeem, I., Hutton, E.W.H., Hannon, M.T., Brakenridge, G.R., Day, J., Vörösmarty, C., Saito, Y., Giosan, L., Nicholls, R.J., 2009. Sinking deltas due to human activities. Nat. Geosci. 2, 681–686. https://doi.org/10.1038/ngeo629.

Tavenas, F., Jean, P., Leblond, P., Leroueil, S., 1983. The permeability of natural soft clays. Part II: permeability characteristics. Can. Geotech. J. 20, 645–660. https://doi.org/10.1139/t83-073.

Tuller, M., Or, D., 2005. Water retention and characteristic curve. In: Encyclopedia of Soils in the Environment. Elsevier, pp. 278–289. https://doi.org/10.1016/B0-12-348530-4/00376-3.

Van, L.T.T., Lertsirivorakul, R., Vuong, B.T., Thang, C.H., 2023. Groundwater recharge in Mekong River Delta: An application of the water-table fluctuation method in the Long Xuyen quadrangle and the Ca Mau peninsula. Songklanakarin J. Sci. Technol. 45.

Vermeer, P.A., Neher, H.P., 1999. A soft soil model that accounts for creep. In: Brinkgreve, R.B.J. (Ed.), Beyond 2000 in Computational Geotechnics. Routledge, pp. 249–261. https://doi.org/10.1201/9781315138206-24.

Wagner, F., Tran, V.B., Renaud, F.G., 2012. Chapter 7, groundwater resources in the Mekong Delta: availability, utilization and risks. In: Renaud .K.C., Fabrice G. (Ed.), The Mekong Delta System - Interdisciplinary Analysis of a River Delta, 1st ed. Springer, Dordrecht, pp. 201–220. https://doi.org/10.1007/978-94-007-3962-8_7.

Xu, J., Jitteh, K., Li, Y., Chen, J., 2025. Predictive model for estimating the weight of existing RC buildings using easily accessible structural parameters. Struct. Control. Health Monit. 2025, 6558932. https://doi.org/10.1155/stc/6558932.
Yuill, B., Lavoie, D., Reed, D.J., 2009. Understanding subsidence processes in coastal Louisiana. J. Coast. Res. 10054, 23–36. https://doi.org/10.2112/SI54-012.1.
Zoccarato, C., Minderhoud, P.S.J., Teatini, P., 2018. The role of sedimentation and natural compaction in a prograding delta: insights from the mega Mekong Delta, Vietnam. Sci. Rep. 8, 11437. https://doi.org/10.1038/s41598-018-29734-7.

A.4. Vietnams Mekong-Delta - Landsenkung infolge von Grundwasserübernutzung (Dörr et al., 2023)

Vietnams Mekong-Delta - Landsenkung infolge von Grundwasserübernutzung

Das Mekong-Delta ist Lebensraum für ca. 21,5 Mio. Menschen und sieht sich seit einigen Jahren mit zunehmend existenzbedrohenden Landsenkungsprozessen (bis zu 3 cm/a) konfrontiert. Als einer der Hauptgründe dafür gilt die starke Grundwasserentnahme. Um die Prozessdynamik besser untersuchen zu können, wurde ein im Mekong-Delta bislang einmaliges Messsystem zur tiefendifferenzierten Landsenkungsmessung an einem Pilot-Standort aufgebaut, dessen vorläufige Messdaten eine Korrelation zwischen Landsenkung und dem fallenden Grundwasserspiegel zeigen.

Felix Dörr, Jonas Bauer, Hoan Viet Tran, Stefan Norra und Franz Nestmann

1 Bisheriger Kenntnisstand zur Landsenkung infolge von Grundwasserübernutzung im Mekong-Delta

1.1 Hydrogeologischer Kontext

Das Grundwassersystem (GW-System) des Mekong-Deltas (MD) ist in seiner Gesamtheit noch nicht vollständig verstanden, da vergleichsweise wenig Daten zur Ausdehnung und komplexen Abfolge von GW-Leitern und -Stauern sowie zu deren Interaktion vorliegen. Grundsätzlich wird im MD zwischen sieben GW-Leitern mit jeweils gespannten GW-Verhältnissen differenziert, deren hydraulische Trennung durch GW-Stauer, wie von Hoan et al. [1] dargelegt, meist als durchgehend gewährleistet angenommen wird. Die im südlichen MD häufig >20 m mächtige Tonschicht, die den oberen GW-Leiter überdeckt, verhindert, wie von Bauer et al. [2] erörtert, eine nennenswerte GW-Neubildung. Die Wechselfolge zwischen GW-Leitern und -Stauern endet in 300-400 m Tiefe, doch selbst die tieferen GW-Leiter weisen GW-Druckspiegel von nur 10-20 m unterhalb der Geländeoberkannte (GOK) auf. GW-Stand, -Dynamik und -Trends der verschiedenen GW-Leiter sind trotz der hydraulischen Trennung oft nahezu identisch, was auf sogenannte Loading Effects in den gespannten GW-Leitern hinweist.

1.2 Landsenkung im Mekong-Delta

In den vergangenen Jahren wurden im MD u. a. von Erban et al. [3] Landsenkungsraten von bis zu 3 cm/a beobachtet. Da sich die GOK des gesamten MD, wie Minderhoud et al. [4] zeigte, im Mittel nur ca. 0,8 m oberhalb des Meeresspiegels befindet, stellt die Landsenkung in Kombination mit dem stetigen Meeresspiegelanstieg ein akutes existenzbedrohendes Problem für die Bewohner dieser Region dar. Die meisten bislang veröffentlichten Datensätze zu Landsenkung im MD basieren auf der Auswertung von Satellitendaten. Die wenigen bestehenden festinstallierten Monitoring-Systeme, wie von Karlsrud et al. [5] vorgestellt, erlauben keine tiefendifferenzierte Messung der Landsenkung.

1.3 Potenzielle Einflussfaktoren auf die Landsenkung

Landsenkung infolge von sinkenden Grundwasserständen ist ein weltweit bekanntes Phänomen, das bereits seit knapp 100 Jahren untersucht wird [6]. Die extensive GW-Übernutzung von >2,5 Mio. m³/d führt im MD zu einer Senkung der GW-Druckspiegel in den gespannten GW-Leitern, so dass der damit einhergehende sinkende hydrostatische Druck im Untergrund zu einer Erhöhung der effektiven Spannung in den Sedimentschichten führt. Insbesondere in den GW-Stauern kann dies zu einer Kompaktion der tonhaltigen Sedimente führen, woraus letztendlich eine Senkung der Landoberfläche resultiert.

Wie stark die Kompaktion einer Sedimentschicht infolge einer Erhöhung der effektiven Spannung ist, kann durch ihren Kompressionsbeiwert C_c beschrieben werden. Bindige Sedimente, wie beispielsweise Ton, weisen deutlich höhere Kompressionsbeiwerte auf als nicht-bindige Sedimente wie Sand.

Modellbasierten Untersuchungen von Minderhoud et al. [7] zufolge ist das MD aufgrund der GW-Entnahme innerhalb von 25 Jahren um durchschnittlich 18 cm abgesunken. Wie groß der Anteil der aus der GW-Entnahme resultierenden Landsenkung an der gesamten Landsenkung tatsächlich ist, konnte bislang jedoch noch nicht anhand von Messdaten belegt werden.

Ein weiterer möglicher Einflussfaktor auf die Landsenkung im MD könnte das Ausbleiben von großflächigen Überflutungen infolge von Dammbauten sein, da dies die Deposition von neuen Sedimenten verhindert und so möglicherweise natürliche Kompaktionen der jüngsten Sedimentlagen nicht mehr durch neue Ablagerungen kompensiert werden können [8]. Im Weiteren gelten, wie Galloway et al. [9] erörtert, der Abbau von organischen Bestandteilen im Untergrund sowie das Austrocknen

Kompakt

- Erstmalig tiefendifferenzierte Landsenkungsmessung im Mekong-Delta.
- Vorläufige Messdaten zeigen mittlere Landsenkungsraten von 9,5 mm/a in 0 m bis 164 m Tiefe.
- Vorläufige Messdaten zeigen Korrelation zwischen Landsenkung und fallendem Grundwasserspiegel.

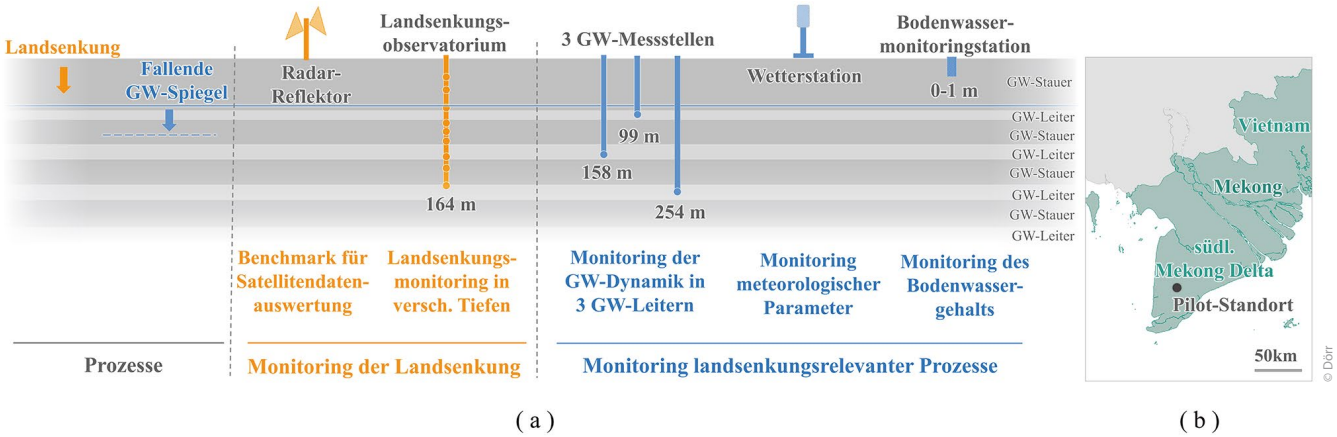


Bild 1: a) Konzeptioneller Querschnitt durch den Pilot-Standort und b) seine Lage im südlichen Mekong-Delta

der oberen Bodenschicht infolge von intensiveren Trockenperioden als potenzielle Einflussfaktoren.

2 Aufbau des Pilot-Standorts

2.1 Konzeptionierung des Pilot-Standorts

Der Pilot-Standort befindet sich im südlichen MD, in der Provinz Ca Mau, südlich der Provinzhauptstadt Ca Mau-Stadt. Ziel des Pilot-Standorts ist es, dort sowohl die Landsenkung selbst als auch relevante Umweltprozesse, die als mögliche Einflussfaktoren auf die Landsenkung gelten, zu messen. Am Pilot-Standort wurden daher u. a. drei GW-Messstellen errichtet, welche in verschiedenen GW-Leitern verfiltert sind (in 99 m, 158 m und 254 m Tiefe). Ebenfalls wurde am Pilot-Standort eine Wetterstation aufgebaut und eine Profilmesssonde zur Messung des Bodenwassergehalts installiert. Durch eine Kernbohrung bis in 254 m Tiefe liegen darüber hinaus ungestörte Sedimentproben aus 57 Tiefenhorizonten vor, die eine genaue Ansprache sowie geochemische, mineralogische und geomechanische Untersuchungen der Sedimente ermöglichen.

Zur Messung der Landsenkung selbst verfügt der Pilot-Standort über einen Radar-Reflektor, welcher die Auswertung der Landsenkung anhand von Satellitendaten verbessern kann, sowie über das Landsenkungsobservatorium (LSO) zur tiefendifferenzierten Messung der Landsenkung, welches nachfolgend genauer erläutert wird. **Bild 1** zeigt einen konzeptionellen Querschnitt durch den Pilot-Standort (a) und seine Lage im südlichen MD (b).

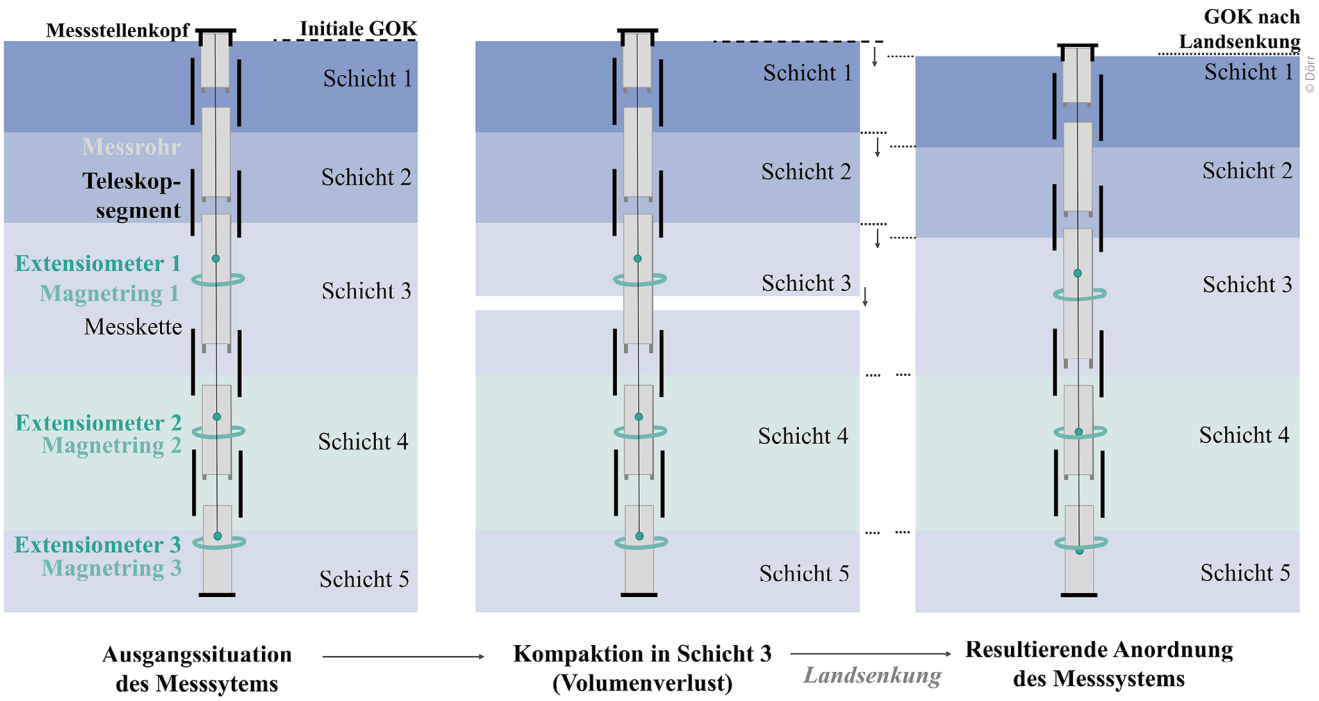


Bild 2: Beispielhafte Darstellung des Messprinzips des Landsenkungsobservatoriums

2.2 Landsenkungsobservatorium

Zur tiefendifferenzierten Messung der Landsenkung wurde am Pilot-Standort ein Messsystem in einer 164 m tiefen Bohrung installiert, das über eine Messkette mit acht digitalen Extensiometern verfügt. Die Messkette hängt frei in einem Messrohr, welches durch Teleskopsegmente in separat bewegliche Abschnitte gegliedert ist. In verschiedenen Tiefen sind Magnetringe am Messrohr befestigt. Der Raum zwischen Messrohr und der Bohrlochwand wurde mit einer Bentonit-Zement-Suspension gemäß ISO 18 674 verfüllt, so dass Festigkeit und Steifigkeit der Verfüllung bestmöglich den Eigenschaften der anstehenden Sedimentschichten entsprechen und sich Kompaktionsprozesse in den Sedimenten auf die Verfüllung und somit das Messrohr übertragen.

Führt eine Kompaktion in einer Sedimentschicht zu Landsenkung, senkt sich die gesamte Messkette, welche über den Messstellenkopf mit der GOK verbunden ist, um das Maß der erfolgten Kompaktion nach unten. Die Abschnitte des Messrohrs, die sich oberhalb des nächsttieferen Teleskopsegments befinden, bewegen sich ebenfalls um das gleiche Maß nach unten und führen zu einer Stauchung des nächsttieferen Teleskopsegments. Die darunterliegenden Messrohrabschnitte mitsamt ihrer Magnetringe verbleiben unbewegt, sodass dort eine relative Bewegung zwischen Magnetring und den Extensiometern an der Messkette zu verzeichnen ist. Oberhalb des gestauchten Teleskopsegments verschieben sich Magnetringe und Extensiometer hingegen parallel, so dass dort keine relative Bewegung zwischen Magnetring und Extensiometer vorliegt. Somit kann eine tiefendifferenzierte Bewertung der Kompaktion zwischen den Tiefenlagen der Teleskopsegmente erfolgen.

Kompaktionen, die im Bereich zwischen dem untersten Teleskopsegment und der Endtiefe des Messrohrs erfolgen, führen zu einer Stauchung des untersten Teleskopsegments. Kompaktionen die unterhalb der Endtiefe des Messrohrs erfolgen, können mit diesem Messsystem nicht erfasst werden. Hierzu kann jedoch grundsätzlich die Differenz zwischen der mit dem LSO ermittelten Landsenkung im Bereich 0-164 m und der mit Satellitendaten ermittelten Gesamtlandsenkung herangezogen werden.

Das Messprinzip ist konzeptionell für ein Beispiel in **Bild 2** dargestellt. Dort führt eine Kompaktion der Schicht 3 zu einer relativen Bewegung zwischen Extensiometer 2 und Magnetring 2 sowie zwischen Extensiometer 3 und Magnetring 3. Extensiometer 1 und Magnetring 1 bewegen sich parallel, sodass dort keine relative Bewegung zu verzeichnen ist.

3 Vorläufige Messdaten und erste Erkenntnisse

3.1 Tiefendifferenzierte Messreihe der Landsenkung

Die vorläufigen Messergebnisse des LSO sind für den Betrachtungszeitraum 11.12.2022-02.04.2023 in **Bild 3** dargestellt. Die Messdaten zeigen in diesem Zeitraum eine Landsenkung von ca. 2,9 mm über den gesamten vom LSO erfassten Messbereich (0-164 m Tiefe). Dies entspricht einer mittleren Landsenkungsrate von ca. 9,5 mm/a.

Bild 3a zeigt die Ganglinien der acht digitalen Extensiometer und somit die Dynamik der Kompaktionsprozesse in den abgegrenzten Tiefenhorizonten. **Bild 3b** fasst die zeitlich kumulierte Landsenkung der jeweiligen Tiefenhorizonte im Betrachtungszeitraum zusammen, welche sich aus der Differenz der entsprechenden Ganglinien ergibt. Die Tiefenzuordnung der Messdaten, die sich aus der Lage der Teleskopsegmente ableitet, ist in **Bild 3b** beschriftet.

Die Auswertung der vorläufigen Messergebnisse des LSO zeigt, dass mehr als 60 % der aufgezeichneten Landsenkung auf

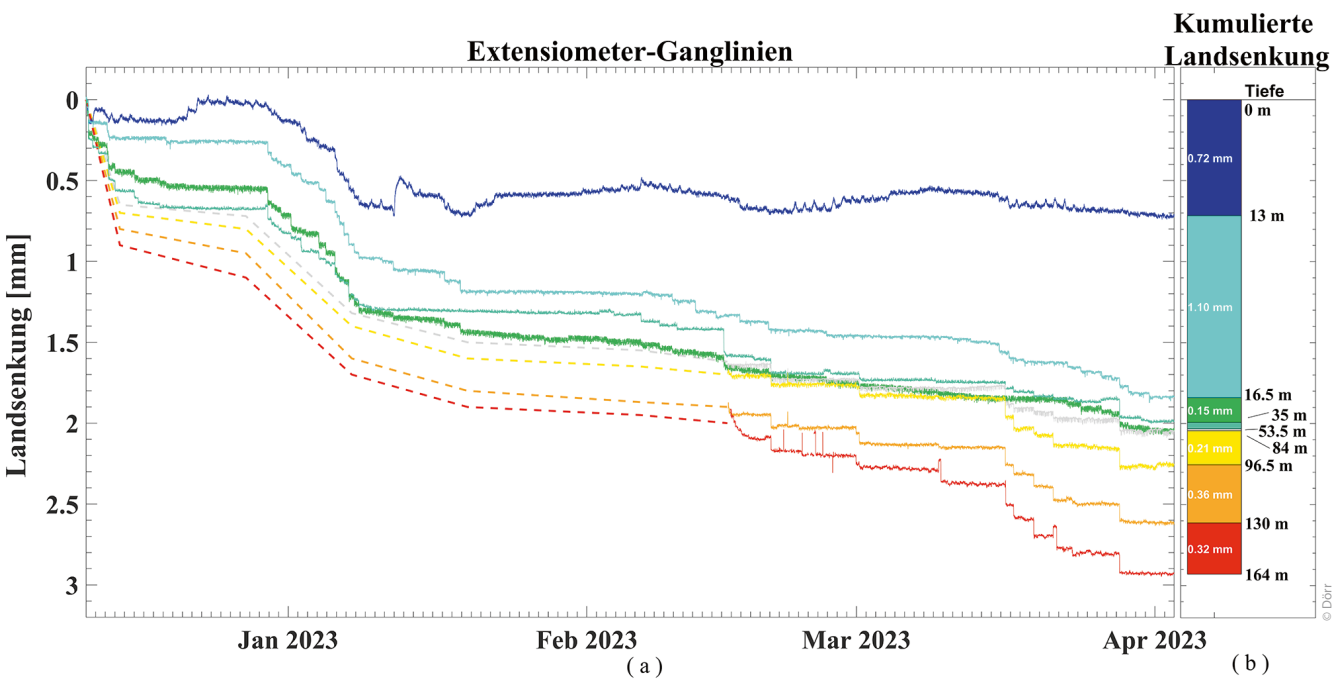


Bild 3: Vorläufige Messdaten des Landsenkungsobservatoriums

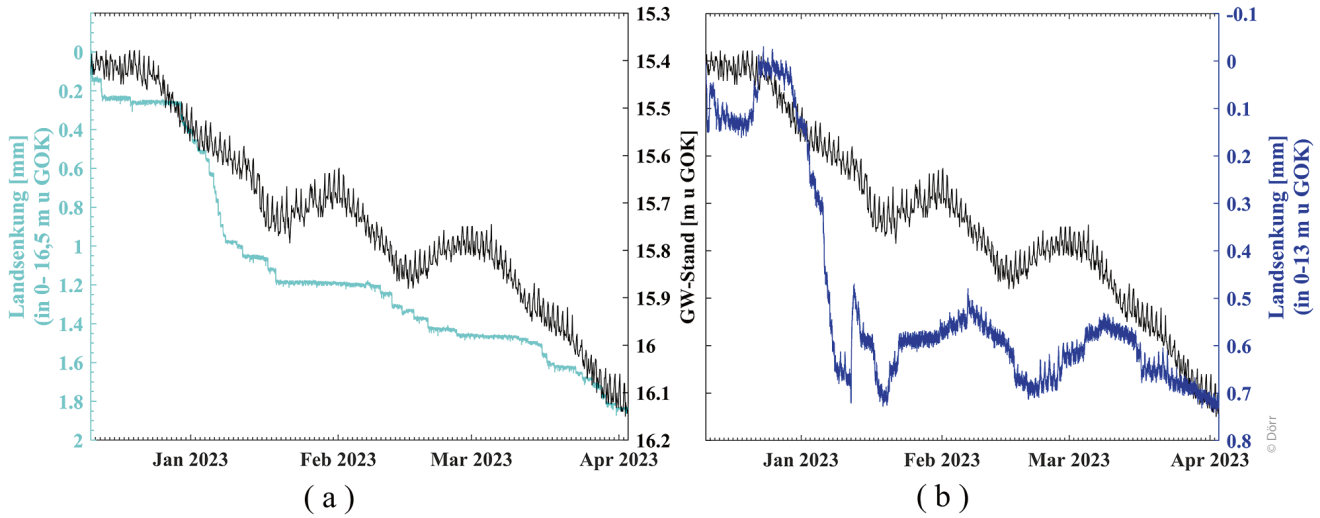


Bild 4: Korrelation zwischen Landsenkung und Grundwasserdruckspiegel

Kompaktionsprozesse in den Tiefenbereichen 0-13 m und 13-16,5 m zurückzuführen sind. Der Tiefenhorizont 13-16,5 m erfasst den aktuellen Schwankungsbereich der GW-Druckspiegel in den drei überwachten GW-Leitern. Die Messdaten weisen also darauf hin, dass ein signifikanter Anteil der Kompaktionsprozesse in den Horizonten der fallenden GW-Druckspiegel erfolgt. Aufgrund ihres geringen Alters sowie eines hohen Tonanteils sind diese Horizonte vermutlich durch hohe Kompressionsbeiwerte charakterisiert und weisen daher wahrscheinlich ein großes Landsenkungspotenzial auf.

In den Tiefenhorizonten 35-84 m zeichnet das LSO kaum signifikante Kompaktionsprozesse auf. Während dies für den Tiefenhorizont 35-53,5 m aufgrund der dort vorliegenden hohen Anteile an Sand in den Sedimenten zu erwarten war, liegen im Tiefenhorizont 53,5-84 m bereichsweise Tonschichten mit organischen Anteilen vor, in denen Kompaktionsprozesse infolge der GW-Druckspiegelsenkung erwartbar gewesen wären.

In den Tiefenhorizonten 84-96,5 m, 96,5-130 m und 130-164 m zeichnet das LSO Kompaktionsprozesse auf, die etwa 30 % der aufgezeichneten Gesamtlandsenkung verursachen. Diese Horizonte sind durch Wechselfolgen aus sandigen und tonigen Sedimenten charakterisiert.

Die Dynamik der vier unteren Extensiometer konnte für die erste Hälfte des Betrachtungszeitraums bis zum 15.02.2023 nicht ausgewertet werden (gestrichelte Linien in **Bild 3**), da die Messkette aufgrund einer lokalen Schrägstellung des Messrohrs und einer daraus resultierenden temporären Blockade eines Extensiometers in diesem Zeitraum nach aktuellem Kenntnisstand nicht frei im Messrohr hing.

3.2 Korrelation zwischen Landsenkung und Grundwasserdruckspiegel

In **Bild 4** sind die Ganglinien der beiden oberen Extensiometer (hellblau und dunkelblau) und die GW-Standsganglinie der in 99 m Tiefe verfilterten GW-Messstelle (schwarz) dargestellt.

Bild 4a zeigt eine deutliche Korrelation zwischen dem fallenden GW-Druckspiegel und den aufgezeichneten Kompaktionsprozessen im Tiefenhorizont 0-16,5 m. Bei temporär ansteigenden GW-Spiegeln stagniert die Landsenkung in **Bild 4a** so lange, bis wieder ein neuer Minimalwert des GW-Stands erreicht wird. Die Messdaten zeigen also, dass eine Absenkung des GW-Druckspiegels zu einer Landsenkung führt. Zukünftige GW-Entnahmen, die zu einer Absenkung des GW-Spiegels führen, werden demnach weitere Landsenkung zur Folge haben.

Bild 4b zeigt ebenfalls eine Korrelation zwischen dem fallenden GW-Spiegel und Kompaktionen im Tiefenhorizont 0-13 m; allerdings zeigt diese Ganglinie darüber hinaus auch eine vermeintliche Landhebung infolge von temporär ansteigenden GW-Ständen. Eine solche ist jedoch nach aktuellem Kenntnisstand nicht erfolgt, da eine tatsächliche Hebung der GOK eine Hebung der gesamten Messkette zur Konsequenz hätte, welche sich wiederum in allen acht Extensiometerganglinien zeigen müssten. Da jedoch nur der oberste Extensiometer eine solche Dynamik aufzeigt, ist nach aktuellem Kenntnisstand davon auszugehen, dass diese vom Extensiometer erfasste relative Bewegung aus einer abwärtsorientierten Bewegung des Magnetrings und nicht aus einer aufwärtsorientierten Bewegung der Messkette resultiert. Diese Messdaten spiegeln somit keine tatsächlichen Hebungsprozesse des Untergrunds wider, sondern resultieren vermutlich allein aus Bewegungsprozessen des Messsystems selbst. Diese vorläufige Interpretation muss in Zukunft anhand von längeren Zeitreihen verifiziert werden.

3.3 Ausblick

Die vorläufigen Messergebnisse sind in Größenordnung und Dynamik plausibel und erlauben erstmals eine tiefendifferenzierte Bewertung der Kompaktionsprozesse im MD sowie deren Korrelation mit möglichen Einflussfaktoren. Die Auswertung längerer Zeitreihen sowie eine manuelle Messung der Lage der Magnetringe sollte in Zukunft zur Verifizierung der Tiefenzuordnung der Messwerte sowie zur Klärung eventueller Hebungsprozesse herangezogen werden. Eine Messreihe von

mindestens 12 Monaten ist hierfür notwendig, um insbesondere auch die Reaktionen des Messystems auf die Monsunniederschläge und steigende GW-Spiegel zu beurteilen.

Darüber hinaus kann durch geomechanische Untersuchungen an den Kernproben ein vertikal hochaufgelöstes Profil der Kompressionsbeiwerte zur Bewertung der Landsenkungsvulnerabilität am Pilotstandort erarbeitet werden, das im Anschluss als Grundlage für numerische Modellierungen der Landsenkung dienen kann.

Mit den in dieser Studie vorgestellten Daten liegt erstmals eine fundierte Grundlage für kommende politische und wissenschaftliche Bewertungen vor, welche Gegenmaßnahmen hinsichtlich durch GW-Entnahme bedingter Landsenkung ergriffen werden sollten, um die Zukunft des südlichen MD zu sichern.

Dank

Die hier vorgestellten Messdaten wurden im Rahmen des Forschungsprojekts ViWaT-Engineering erhoben, gefördert vom Bundesministerium für Bildung und Forschung (BMBF) unter der Fördernummer 02WCL1474A. Ein besonderer Dank gilt an dieser Stelle allen Forschenden des ViWaT-Engineering-Projekts sowie den vietnamesischen Partnern des Vietnamese Ministry of Science and Technology (MOST) und des Department of Natural Resources and Environment Ca Mau (DONRE Ca Mau). Ein weiterer Dank gilt der Hector Fellow Academy, die im Rahmen eines Stipendiumsprogramms die Finanzierung von Personal- und Forschungsmitteln des Erstautors dieser Studie bereitstellt.

Hinweis

Bei den im Rahmen dieser Studie vorgestellten Messdaten und Interpretationen handelt es sich um vorläufige Erkenntnisse, die in Zukunft weiter verifiziert werden müssen und ggfls. von dem hier Dargestellten abweichen können. Die Rohmessdaten können erst nach Abschluss der Forschungsarbeiten der Autoren veröffentlicht werden.

Felix Dörr, Jonas Bauer, Hoan Viet Tran, Stefan Norra und Franz Nestmann

Vietnam's Mekong Delta - Land Subsidence due to Groundwater Overexploitation

The Mekong Delta is home for approx. 21.5 million people and is confronted with existence-threatening land subsidence processes up to 3 cm/a since several years. Groundwater overexploitation is considered to be the main reason for this. In order to investigate the process dynamics of land subsidence, a depth-differentiated land subsidence monitoring system was set up at a pilot site, which is so far unique in the Mekong Delta. The preliminary monitoring data shows a correlation between land subsidence and the lowering groundwater level.

Autoren

Felix Dörr, M. Sc.
Jonas Bauer, M. Sc.
Hoan Viet Tran, M. Sc.
Karlsruher Institut für Technologie
Adenauerring 20b
76131 Karlsruhe
felix.doerr@kit.edu
jonas.bauer@kit.edu
hoan.tran@kit.edu

Prof. Dr. Stefan Norra
Universität Potsdam
Karl-Liebknecht-Str. 24-25
14476 Potsdam-Golm
stefan.norra@uni-potsdam.de

Univ. Prof. Dr.-Ing. Dr. h. c. mult. Franz Nestmann
Karlsruher Institut für Technologie
Engesserstr. 22
76131 Karlsruhe
franz.nestmann@kit.edu

Literatur

[1] Hoan, T. et al.: An Improved Groundwater Model Framework for Aquifer Structures of the Quaternary-Formed Sediment Body in the Southernmost Parts of the Mekong Delta, Vietnam. In: Hydrology 9 (2022), Nr. 4, S. 61.
[2] Bauer, J. et al.: Geochemistry and evolution of groundwater resources in the context of salinization and freshening in the southernmost Mekong Delta, Vietnam. In: Journal of Hydrology: Regional Studies (2022).
[3] Erban, L.; Gorelick, S.; Zebker, H.: Groundwater extraction, land subsidence, and sea-level rise in the Mekong Delta, Vietnam. In: Environ. Res. Lett. 9 (2014), Nr. 8, S. 84 010.
[4] Minderhoud, P. et al.: Mekong delta much lower than previously assumed in sea-level rise impact assessments. In: Nat Commun 10 (2019), Nr. 1, S. 3 847.
[5] Karlsrud, K. et al.: Preliminary results of land subsidence monitoring in the Ca Mau Province. In: Proceedings of the International Association of Hydrological Sciences (2020), Nr. 382, S. 111-115.
[6] Gambolati, G.; Teatini, P.: Geomechanics of subsurface water withdrawal and injection. In: Water Resour. Res. 51 (2015), Nr. 6, S. 3 922-3 955.
[7] Minderhoud, P. et al.: Impacts of 25 years of groundwater extraction on subsidence in the Mekong delta, Vietnam. In: Environ. Res. Lett. 12 (2017), Nr. 6, S. 64 006.
[8] Zoccarato, C.; Minderhoud, P.; Teatini, P.: The role of sedimentation and natural compaction in a prograding delta: insights from the mega Mekong delta, Vietnam. In: Sci Rep 8 (2018), Nr. 1, S. 11 437.
[9] Galloway, D. et al.: Preface: Land subsidence processes. In: Hydrogeol J. 24 (2016), Nr. 3, S. 547-550.

DOI dieses Beitrags: http://doi.org/10.1007/s35147-023-1922-3

Springer Professional

Mekong-Delta

Le Vinh, A. at al.: Overview of Coastal Protection Structures in the Mekong River Delta. In: Proceedings of the 4th International Conference on Sustainability in Civil Engineering: Singapore: Springer Nature Singapore, 2024. https://sn.pub/uMnfgg

Mai, N. P.: Proposed Adaptation Measures for Saltwater Intrusion in the Vietnamese Mekong Delta. In: Proceedings of the 4th International Conference on Sustainability in Civil Engineering: Singapore: Springer Nature Singapore, 2024. https://sn.pub/cRiyZH

Appendix B

Co-author publications

B.1. Summary of Co-authorship scientific publications

B.1.1 Groundwater Use Habits and Environmental Awareness: Pham et al., (2023)



Tite: Groundwater Use Habits and Environmental Awareness in Ca Mau Province, Vietnam: Implications for Sustainable Water Resource Management.

Authors: Van Cam Pham, Jonas Bauer, Nicolas Börsig, Johannes Ho, Long Vu Huu, Hoan Viet Tran, Felix Dörr, Stefan Norra.

Journal: Environmental Challenges 13 (2023).

DOI: https://doi.org/10.1016/j.envc.2023.100742

Authorship statement: In this article, written by Van Cam Pham and published in a peer-reviewed scientific journal, results of conducted questionnaires are presented and evaluated to assess the social perception of groundwater and other water resources as well as the public awareness of associated environmental hazards in the southern Mekong Delta. The questionnaire revealed insufficient public awareness about land subsidence and associated environmental challenges. Complementary to the questionnaire, groundwater samples were taken at selected households wells and later analyzed for selected quality parameters. The results are discussed with regard of national and international regulations as well as the various purposes the water is used for. In this study, Felix Dörr contributed to the design of the questionnaire in particular in regard to land subsidence related questions. Together with regular co-author revisions on the manuscript, the contribution of Felix Dörr to this article can be approximated to 5-10%.

Abstract: The Vietnamese Mekong Delta including Ca Mau province (CMP) is seriously affected by land subsidence. Groundwater over-extraction is considered to be a major driver for this process. To address the reduction of groundwater (GW)

extraction as a potential counter measure for further subsidence, this study focuses on understanding the importance of GW in people's life and water using habits as well as their awareness with current environmental problems in Ca Mau. Therefore, GW sampling campaigns and surveys were conducted in all 9 districts of Ca Mau province in 2019 and 2020. The analyzed water samples showed a connection with information from questionnaires and created a general picture of water using habits. GW plays an important role in people's lives, it is used for washing, cooking, drinking and other activities. People use GW for different purposes depending on their perception of water quality. For important and direct health related purposes, such as cooking or drinking, people prepare to treat water more carefully or choose another alternative water resource. The analytical approach to evaluation results based on viewpoints from general to detail helped to dig deeper into people's stories to explain research results with their behavior in each situation. When people are dependent on GW and have no option to use alternative water resources, the importance level of GW in their life increases and their awareness of GW over-extraction becomes less. If people have another water source to use such as tap water (TW), habits of using GW change. This opens up the idea that a potential alternative water will reduce the dependence of people on GW and protect GW from over-exploitation. Besides, people in Ca Mau do not have much awareness of land subsidence or the reason leading to environmental problems. Therefore, raising the awareness of people by well-design education campaigns should be strongly considered.

© The full article is reprinted with kind permission from Elsevier under the Creative Commons Attribution License and is included in Appendix B.2.

B.1.2 Model-based Investigation of Groundwater Salinization: Hoan et al., (2025)



Tite: The Utilization of a 3D Groundwater Flow and Transport Model for a Qualitative Investigation of Groundwater Salinization in the Ca Mau Peninsula (Mekong Delta, Vietnam)

Authors: Tran Viet Hoan, Karl-Gerd Richter, Felix Dörr, Jonas Bauer, Nicolas Börsig, Anke Steinel, Van Thi Mai Le, Van Cam Pham, Don Van Than, Stefan Norra.

Journal: Hydrology 2025, 12(5), 126.

DOI: https://doi.org/10.3390/hydrology12050126

Authorship statement: This peer-reviewed journal article was written by Hoan Viet Tran and qualitatively explores potential groundwater salinization pathways with a finite-element model for flow and transport. Felix Dörr contributed to this article by sharing experiences in numeric groundwater simulation and proposing the model-based assessment of local salinization processes in the anulus of wells, where improper drilling procedures may cause aquifer interconnectivity, therefore inducing vertical leakage processes from shallow saline groundwater. In total the contribution of Felix Dörr to this article can be approximated to 5-10 %.

Abstract: The Ca Mau Peninsula (CMP), the southernmost region of the Mekong Delta, is increasingly threatened by groundwater salinization, posing severe risks to both the fresh-water supply and land sustainability. This study develops a three-dimensional, density- dependent groundwater flow and salinity transport model to investigate salinization dynamics across the CMP's complex multi-aquifer system. Unlike previous studies that largely rely on model calibration, this research introduces a novel approach by systematically deriving the spatial distribution of longitudinal dispersivity based on sediment

characteristics. Moreover, detailed land use mapping is integrated to assign spatially and temporally variable Total Dissolved Solids (TDS) values to the uppermost layers, thereby enhancing the model realism in areas where monitoring data are limited. The model was utilized not only to simulate the regional salinity evolution, but also to critically evaluate conceptual hypotheses related to the mechanisms driving groundwater salinization. Results reveal a strong influence of seasonal and land use factors on salinity variability in the upper aquifers, while deeper aquifers remain largely stable, affected primarily by paleosalinity and localized pumping. This integrated modeling approach contributes to a better understanding of regional-scale groundwater salinization and highlights both the potential and the limitations of numerical modeling under data-scarce conditions. The findings provide a valuable scientific basis for adaptive water resource management in vulnerable coastal zones.

© The full article is reprinted with kind permission from MDPI under the Creative Commons Attribution License and is included in Appendix B.3.

B.1.3 Seawater Intrusion in River Delta Systems: Bauer et al. (2025)



Tite: Seawater Intrusion in River Delta Systems. Inter-annual Dynamics and Drivers of Salinity Variations in the southern Mekong Delta, Vietnam.

Authors: Jonas Bauer, Felix Dörr, Hoang Thai Duong Vu, Andreas Schenk, Hoan Viet Tran, Van Cam Pham, Nicolas Börsig, Roderick van der Linden, Ngoc Hoa Nguyen, Elisabeth Eiche, Stefan Norra.

Journal: Journal of Hydrology 661 (2025).

DOI: https://doi.org/10.1016/j.jhydrol.2025.133745

Authorship statement: This peer-reviewed journal article was authored by Jonas Bauer and addresses the interannual dynamics of seawater intrusion in the Mekong Delta, a hazard that is ultimately exacerbated by land subsidence, as subsiding river-bed elevations alter the governing hydraulic gradients in the river system. Felix Dörr contributed to this article by sharing experience and insights from frequency analyses and through continuous discussions of the manuscript's scientific content. Overall, the contribution of Felix Dörr to this article is estimated at approximately 10%.

Abstract: Amidst intensifying impacts of climate change and anthropogenic pressure, sea-water intrusion (SWI) emerges as a growing threat for delta systems worldwide, compromising freshwater resources and ecosystem stability. The Mekong Delta (MD) and its southernmost province Ca Mau are at the frontline of climate change impacts and anthropogenic modifications of the hydrological regime. To assess the inter-annual variability of river SWI, factors contributing to changes of the hydraulic pressure gradient between freshwater and seawater are analyzed. By utilizing long-term hydro-meteorological data from 2000 to 2022, the collective impact of catchment-scale and local-scale factors on salinity is evaluated. While salinity gradually increases by more than 10 g/L during the dry season, significant inter-annual differences of up to 15 g/L in peak salinity occur, regularly reaching and exceeding sea-water salinity levels. Upstream freshwater discharge patterns were identified as major control for coastal water levels and resulting salinity levels. While climate variability governs natural upstream discharge fluctuations, dam constructions and operational responses to low-rainfall years lead to unfavorable conditions along the Mekong River, shifting and prolonging the low discharge period in the delta. This intensifies hydro- logical drought conditions and triggers extreme SWI events. Land subsidence of up to 2 cm per year, derived from water level records, is driving relative sea level rise and increasing the MD's vulnerability to future SWI. Mitigation strategies for SWI are examined from new perspectives, highlighting the benefits of increasing early dry- season discharge through rethought

upstream reservoir operations and water storage concepts, as well as adapted local sluice gate management.

© The full article is reprinted with kind permission from Elsevier under the Creative Commons Attribution License and is included in Appendix B.4.

B.1.4 Alternative water resources: Pham et al. (2026)


Environmental Challenges 22 (2026) 101443

Contents lists available at ScienceDirect

Environmental Challenges

journal homepage: www.elsevier.com/locate/envc

The potential of collected rainwater as an alternative water resource for domestic purpose to mitigate groundwater overexploitation in terms of water quality and people's acceptance

Van Cam Pham, Johannes Ho, Jonas Bauer, Nicolas Börsig, Felix Dörr, Tran Viet Hoan, Elisabeth Eiche, Andreas Tiehm, Stefan Norra

ARTICLE INFO

ABSTRACT

1. Introduction

Tite: The potential of collected rainwater as an alternative water resource for domestic purpose to mitigate groundwater over-exploitation in terms of water quality and people's acceptance

Authors: Van Cam Pham, Johannes Ho, Jonas Bauer, Nicolas Börsig, Felix Dörr, Tran Viet Hoan, Elisabeth Eiche, Andreas Tiehm, Stefan Norra.

Journal: Environmental Challenges (2026)

DOI: https://doi.org/10.1016/j.envc.2026.101443

Authorship statement: This peer-reviewed journal article was written by Van Pham and explores the potential of rainwater as an alternative was resource in the Mekong Delta, by a multi-disciplinary approach. This approach includes survey-based evaluations of social perceptions, assessments of rainwater availability and water quality analyses. As ongoing groundwater depletion causes land subsidence, these considerations are of great relevance in the context of land subsidence mitigation strategies. Felix Dörr contributed to the study by participating in the design of the questionnaire and in the revision of the manuscript. The overall contribution of Felix Dörr is estimated at approximately 5–10%.

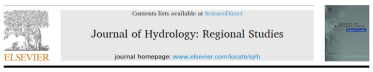
Abstract: Ca Mau province, located in the south of the Mekong Delta, is strongly affected by land subsidence and seawater intrusion. Overexploitation of groundwater has been highlighted as a significant driving factor for these processes. As groundwater currently plays a crucial role in the local water supply, this study examines the potential of rainwater as an alternative water source for domestic use to reduce groundwater extraction and contribute to ensure the safe and sustainable water resource for public use (SDG 6). The present study follows a multi-disciplinary evaluation of the potential of rain water as an alternative water resource, covering an assessment of (i) social perception of rainwater usage, (ii) rainwater availability as well as water quality analyses of rainwater stored under various conditions. For this, a combined survey and sampling campaign throughout Ca Mau province was conducted in two main phases between 2019 and 2022. The survey includes a questionnaire which was completed by 473 participants together with in-depth interviews in several selected locations. Complementary, time series of precipitation were analyzed to determine the potentially available rainwater quantity. Stored rainwater samples were collected and analyzed according to their quality based on physical parameters, chemical parameters using ICP-MS and Ion Chromatography with 49 water samples and biological parameters using the IDEXX Colilert® system and MALDI-TOF-MS with 75 water samples. Based on the results, factors that could affect the quality of rainwater were examined. The results show that in some rainwater samples, threshold values of the standards from Vietnamese regulation were exceeded for some parameters, raising the issue of rainwater treatment before use. The questionnaire revealed that rainwater is considered as a potential water source which can replace groundwater for domestic purposes by participants. Despite concerns about rainwater storage during the dry season, public acceptance of using rainwater is generally high. However, the government's interest in communicating information about current environmental issues as well as support in guiding rainwater storage and economic support during the transition process is an issue

that people are concerned about. The results of this study provide new insights to further identify potential pilot sites in Ca Mau for rainwater harvesting as an alternative to groundwater extraction, as well as to design concepts for optimizing the use of rainwater.

© *The full article is reprinted with kind permission from Elsevier under the Creative Commons Attribution License and is included in Appendix B.5.*

B.1.5 Tidal effects on surface water salinity: Bauer et al. (2026 - under review)

Tite: Tidal Control of Salinity Dynamics and Seawater Intrusion in the Southern Mekong Delta, Vietnam



Authors: Jonas Bauer, Felix Dörr, Andreas Schenk, Vũ Hoàng Thái Dương, Hoan Viet Tran, Van Cam Pham, Nicolas Börsig, Roderick van der Linden, Ngoc Hoa Nguyen, Elisabeth Eiche, Stefan Norra.

under review

Submission information: submitted to the Journal of Hydrology Regional Studies
submission date: 06.01.2026

Authorship statement: This peer-reviewed journal article was written by Jonas Bauer and investigates tide-driven salinity fluctuations on surface water salinity in the Mekong Delta. Through joint evaluations and continuous discussions about the applied methods, results and implications, as well as through reviewing the manuscript, the contribution of Felix Dörr to this study amounts to approximately 10 %.

Abstract: *Study region*: Ca Mau Province, Mekong Delta, Vietnam.

Study focus: As sea levels rise and freshwater resources decline, seawater

intrusion (SWI) poses an increasing threat to many delta systems worldwide. Effective mitigation strategies for SWI require a fundamental understanding of underlying processes, supported by sufficient observational field data. In the Vietnamese Mekong Delta, SWI recurs annually during the dry season, adversely affecting agriculture and ecosystems. While long-term trends and interannual fluctuations represent baseline conditions, short-term, tide-driven salinity fluctuations can push the system over critical management thresholds. This study examines the sub-seasonal interplay between tide-driven water level fluctuations and salinity. Time series analyses, including harmonic analysis, were applied to data from three monitoring stations in Ca Mau Province between January and June in 2017 and in 2018 to identify their dynamics and derive involved processes.

New hydrological insights for the region: Results show that co-oscillations of two different tidal regimes in the east and in the west influence water level patterns and ultimately salinity dynamics. Frequency analyses revealed salinity variations at major tidal frequencies. A sliding window Harmonic Least Squares approach captured the non-stationary behavior expected in estuarine systems at all three stations, with weighted R^2 values of 0.85 to 0.98 for water level and 0.53 to 0.73 for salinity. The findings of this study highlight the spatiotemporal complexity of salinity variations in the study region.

The manuscript is presented in Appendix B.6.

B.2. Groundwater Use Habits and Environmental Awareness: Pham et al., (2023)

Environmental Challenges 13 (2023) 100742



Contents lists available at ScienceDirect

Environmental Challenges

journal homepage: www.elsevier.com/locate/envc



Groundwater Use Habits and Environmental Awareness in Ca Mau Province, Vietnam: Implications for Sustainable Water Resource Management



Van Cam Pham [a,*], Jonas Bauer [a], Nicolas Börsig [a], Johannes Ho [b], Long Vu Huu [d], Hoan Tran Viet [a,c], Felix Dörr [a], Stefan Norra [e]

[a] Karlsruhe Institute of Technology (KIT), Institute of Applied Geosciences, Adenauerring 20b, 76131 Karlsruhe, Germany
[b] Technology Center Water, Karlsruher Straße 84, 76139 Karlsruhe
[c] National Center for Water Resources Planning and Investigation (NAWAPI), No. 93, lane 95, Vu Xuan Thieu Street Sai Dong Ward, Long Bien District, Hanoi, Viet Nam
[d] Karlsruhe Institute of Technology (KIT), Institute of Photogrammetry and Remote Sensing (IPF), Engesserstraße 6, 76131 Karlsruhe
[e] Potsdam University, Institute of Environmental Sciences and Geography, Soil Sciences and Geoecology, Campus Golm, Building 12, 14476 Potsdam Golm, Germany

ARTICLE INFO

Keywords:
groundwater extraction
groundwater use habits
environmental awareness
Ca Mau

ABSTRACT

The Vietnamese Mekong Delta including Ca Mau province (CMP) is seriously affected by land subsidence. Groundwater over-extraction is considered to be a major driver for this process. To address the reduction of groundwater (GW) extraction as a potential counter measure for further subsidence, this study focuses on understanding the importance of GW in people's life and water using habits as well as their awareness with current environmental problems in Ca Mau. Therefore, GW sampling campaigns and surveys were conducted in all 9 districts of Ca Mau province in 2019 and 2020. The analyzed water samples showed a connection with information from questionnaires and created a general picture of water using habits. GW plays an important role in people's lives, it is used for washing, cooking, drinking and other activities. People use GW for different purposes depending on their perception of water quality. For important and direct health related purposes, such as cooking or drinking, people prepare to treat water more carefully or choose another alternative water resource. The analytical approach to evaluation results based on viewpoints from general to detail helped to dig deeper into people's stories to explain research results with their behavior in each situation. When people are dependent on GW and have no option to use alternative water resources, the importance level of GW in their life increases and their awareness of GW over-extraction becomes less. If people have another water source to use such as tap water (TW), habits of using GW change. This opens up the idea that a potential alternative water will reduce the dependence of people on GW and protect GW from over-exploitation. Besides, people in Ca Mau do not have much awareness of land subsidence or the reason leading to environmental problems. Therefore, raising the awareness of people by well-design education campaigns should be strongly considered.

1. Introduction

Vietnam is one of the most threatened area with the effect of sea level rise (Hens et al., 2018) as well as climate change related to the intensity of natural disasters (MONRE, 2016; Oxfarm, 2008). The Vietnamese Mekong Delta, including Ca Mau province (CMP), is located at the Lower Mekong River and forms the very southern edge of Vietnam. The Mekong Delta has an extremely low mean elevation above sea level (around 0.8 m) (Minderhoud et al., 2019, 2017). In addition, the Mekong Delta is facing a great number of environmental challenges and sustainability problems during the twenty first century due to the decrease of sediment supply from its catchment due to upstream dams, saltwater intrusion from the sea, sea level rise and flooding as well as significant land subsidence (Allison et al., 2017; Tran et al., 2021). Human activities and climate change have impacts on saltwater intrusion into GW systems in Mekong Delta (Han et al., 2021). The Mekong delta has to deal with salinity intrusion in the dry season and flooding during the rainy season. For example, in the dry season of 2015/2016, eight provinces in the Mekong delta have announced an emergency situation due to drought and salinization (Bäumle, 2017). In recent years, due to rapid social-economic development and an increase in population, the increasing demand of freshwater led to an increased exploitation of

* Corresponding author.
E-mail address: van.pham@kit.edu (V.C. Pham).

https://doi.org/10.1016/j.envc.2023.100742
Received 10 March 2023; Received in revised form 21 June 2023; Accepted 21 June 2023
2667-0100/© 2023 The Authors. Published by Elsevier B.V. This is an open access article under the CC BY-NC-ND license (http://creativecommons.org/licenses/by-nc-nd/4.0/)

GW without any planning, what causes serious problems in the Mekong Delta in general and Ca Mau Peninsula in particular (Friedrich et al., 2008; Van, 2019). Therefore, water security in the region is seriously endangered due to a decrease in freshwater quantity and quality, mainly caused by salinization, pollution and over-extraction (Ha et al., 2018). GW over-exploitation leading to an average decline of hydraulic heads of around 30 cm per year, potentially plays an important role in ongoing land subsidence (Erban et al., 2014). Land subsidence in Mekong Delta is leading to the unsustainability of area (Gustafson et al., 2018; Di Giusto et al., 2021).

The Vietnamese Mekong Delta has a transition in agriculture from mono-culture (rice farm) to multi production like shrimp-rice to be more sustainable (Nguyen et al., 2021). CMP, is the shrimp basket of Vietnam with a high demand of GW for farming. The export of these goods is of uttermost importance for Vietnam's economy. However, Ca Mau's groundwater resources are intensively affected by saltwater intrusion and a decrease of hydraulic heads resulting in a lack of freshwater for estimated 95,600 households (UN, 2020). Thus, this region urgently needs the identification, development and implementation of adapted relief measures to save it from complete inundation by the sea (Minderhoud et al., 2020). Bauer et al., 2022 described the challenges of the Mekong Delta as "a progressive loss of land and freshwater". One major counter measure to mitigate land subsidence might be to stop or significantly reduce GW extraction from deep, confined aquifers and switching to alternative water resources, such as surface water from the rivers and channels, rainwater, pumped water from the Mekong River, or desalinization of sea water. However, before even starting with one of these measures, it has to be investigated how people would react on such intensive intervention into their daily life. Many previous studies have shown that sustainable adaptation is only successful if the local people fully accept it. People intend to increase their adaptation when they are aware of the risk of climate change to many aspects of their life (Luu et al., 2019).

People in CMP are diverse in terms of living standards as well as access to water resources. To start reducing the use of GW, it is necessary to understand the importance of GW in people's life. Research needs to reflect people's opinions and their assessment of the water they are using. People's perception of GW quality and surrounding factors might influence their usage habits. Some factors affecting the acceptance of water source are public awareness about water supply, distribution, treatment as well as income and other personal factors (Baumann, 1983). Another case study in Bengaluru, India evaluated the factors impacting the acceptance of recycled water. One of the noticeable results was that 89% of the people using surface water were not aware of waste water treatment concepts or water reuse at all (Ravishankar et al., 2018). Another research in Vietnam also indicated that people's choice of water source depend on availability, quality of the water sources and financial situation of the household (Danh and Khai, 2015). In CMP, a recent study showed that people are not fully aware of the danger of submersion by the sea (Di Giusto et al., 2021). In addition, to our best knowledge, facing many problems of water use, there are still no studies on people's perception on water usage habits, with both quantitative and qualitative aspects in Ca Mau. On the one side, quantitative research is a research approach, which evaluates the relationship between variables by numeric data collection and analysis (data can be expressed in numbers or scores). On the other side, qualitative research is a research approach, which concentrates on discovering individual's experiences with phenomena by narrative or text data collection and analysis (data can be expressed in words and images) (Clark et al 2016). The combination of these two approaches creates enhanced methods that can show a more comprehensive view of people's opinion in Ca Mau from a personal perspective as well as statistical analysis (Creswell, 2017). Therefore, in this study a comprehensive GW quality assessment combined with a survey in CMP was conducted. This study emphasizes on the relationship between water quality and people's water use habits with the quantitative approach. At the same time, the open-end questions and group discussion from the qualitative approach open up explanations to the problem, explaining why people in CMP are overusing GW and evaluates their possible alternative options.

2. Methodology

2.1. Study area

The study area in this research focus in Ca Mau province (CMP). Ca Mau is the southernmost province in Vietnam, surrounded by sea in three directions. CMP includes 9 districts (Ca Mau, U Minh, Tran Van Thoi, Dam Doi, Thoi Binh, Cai Nuoc, Phu Tan, Nam Can, Ngoc Hien). This area contains high density of river and canals, it is flat and low area, average elevation is around 0.5 to 1.5 m above sea level. (Pechstein et al., 2018). Ca Mau is located in the monsoonal zone, it has a tropical monsoon climate with two main seasons (rainy and dry seasons). The rainy season is usually from May to November and the dry season is from November to May.

The population of CMP is around 1.2 million people with 603,250 males and 589,150 females in 306999 households. Sex ratio in Ca Mau is around 102.39 male/100 female. According to Ca Mau Statistic Office in 2021, main labor force is in rural area with 535,892 people with 80.01%, labor force in urban area accounts for 19.99% with 133,881 people. The occupation of people in CMP includes high level professionals, mid-level professionals, clerks, personals services, protective workers, sales workers, skilled agricultural, forestry and fishery workers, craft and related trade workers, machine operators, unskilled occupations and others. The most popular occupations are workers related to agricultural, forestry and fishery sector with 214,153 workers accounting 32. 63% and unskilled workers with 254,550 workers accounting 38.78%. The key activities in the development of economy sector is agriculture, especially aquaculture (with a total area of 297,200 ha). GW extraction in Ca Mau is mainly used for agriculture, aquaculture and domestic use in rural area, from mostly small to medium sized wells with pumping rates >200 m^3/day. However, the number of GW extraction wells is approximately 175,710 wells including only 248 centralized wells and 452 licensed extraction wells (Pechstein et al., 2018). It means most wells are illegally extracting GW without any exact estimation of extraction rates.

2.2. Questionnaires

2.2.1. Data collection

The data set was collected on the basis of questionnaires and group discussions with households in CMP. Questionnaires were collected by face-to-face interviews between the authors, an instructor from the local government and a household member. Field trips were implemented by visiting nine districts in CMP to collect data. The first survey was carried out in March 2019 with 87 questionnaires and water samples collected in all nine districts. The second survey took place in December 2019 and January 2020 with 57 questionnaires and water samples focusing on the northern part of CMP. Based on the experiences from the first field trip on March 2019, questionnaires were collected together with groundwater samples at the same location. Groundwater samples were taken systematically to cover all regions in CMP (Fig. 1a, 1b). Following the approach by Ravishankar et al (2018), the authors of this study are aware that some aspects of this study might not be representative for a commune, district or CMP as a whole. However, as this is the first study in the area, it is important to qualitatively focus on basic factors and reasons impacting groundwater extraction as well as the connection between people's story and the respective water quality. In total, 144 questionnaires and 144 GW samples were collected (Fig. 1a). At first, a survey was conducted to get the results and lead to the following up questions in discussion for better understanding of initial finding from quantitative research (Clark et al, 2016). The questionnaire was designed with 28 questions in the first version and was extended by 35

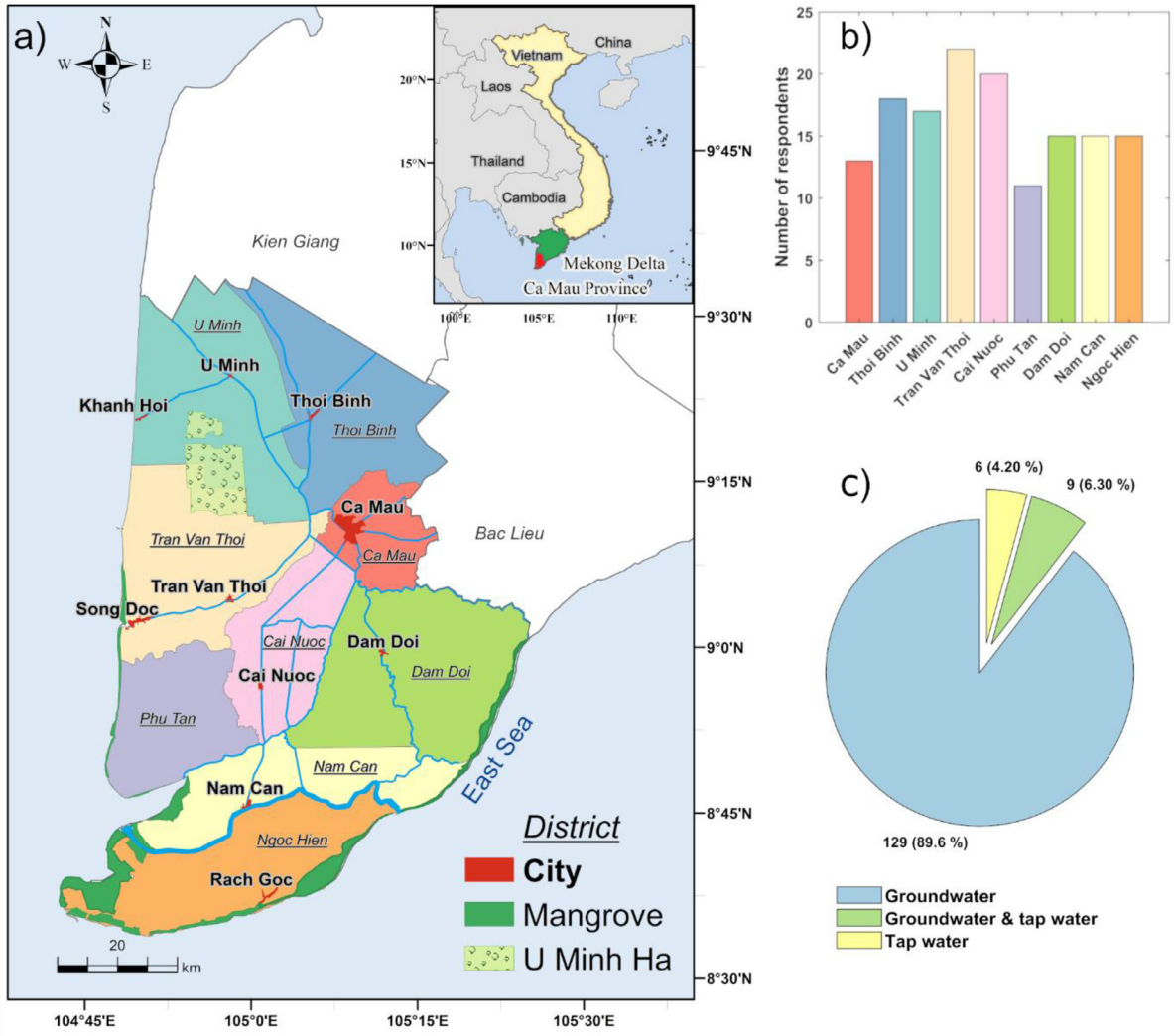


Fig. 1. a. Questionnaire locations in Ca Mau, b. Distribution of respondents in the nine districts of Ca Mau, c. Percentage of households in different groups (GW users and TW users).

questions in the second version after the evaluation of the results of the first survey. The second version focuses more on people's assessment of GW quality and their awareness of negative environmental impacts, such as salinization and land subsidence. All questions were explained and discussed with households directly. The questionnaire system is designed and divided into four main parts with easy to understand contents to match the perceptions of the respondents in CMP. The first part covers basic information surrounding the respondents, such as living conditions. The second part explores information about groundwater extraction and water use habits. The third part describes the potential of alternative water sources and the last part is about people's perceptions and awareness of overexploitation and land subsidence in CMP. The level of awareness of the people is divided by level from 1 to 4, with 1 being the lowest level, meaning that people totally have no knowledge of this issue. Level 2 means that people heard about this issue somewhere but they do not understand it clearly. Level 3 means that people know about the problem and have a basic understanding of the causes. Level 4 is the highest level when the people capture the whole picture, understand the issue and relevant information.

After completing a questionnaire, in the following group discussion part, respondents had a deeper discussion with the interviewer to explain their answers and stories.

2.2.2. Data analysis

To evaluate the outcomes of the questionnaires, well established quantitative and qualitative approaches are applied. The quantitative approach covers statistical evaluation of the questions related to numbers such as amount of water use or number of people using the well etc. Similarly, the qualitative approach consists of a hermeneutical evaluation of questions related to words and text, such as the favorite water source or GW using purpose etc.

The selection of locations was based on the general idea to get a complete overview about the different living conditions and water resources around the whole province rather than a statistical overview based on the distribution of population. Distribution of questionnaires in Ca Mau province is shown in Fig. 1b. Information gained from data collection was expressed with the points of view from general view into detailed explanation.

According to observations and interviews, beside groundwater, there are three other types of water sources used in CMP, including rain water, tap water, and bottled water (from private water supplier). Tap water (TW) is not available for the whole province. TW is obtained from GW, which is treated at a drinking water plant and distributed usually to nearby households in the same ward or commune. Until now, fresh water management and distribution are not effective. GW is the major

water source which is used mainly for domestic purposes (Ha et al., 2015) The number of households that possess the ability to use TW is not as high as compared to households using GW. In this study, although the main research subject are households using groundwater (GW users) and GW samples, tap water households (TW users) are also approached and interviewed to collect further information. For this reason, the respondents (144 questionnaires in total) were divided into two groups. Group 1 includes all households that only have GW as the main source of water called GW users, and group 2 includes households that own a GW well but also have direct access to tap water, or use TW only, called TW users. Results from 2 groups of respondents were selected, analyzed and compared to understand the difference of their thought and behaviors between 2 groups. The distribution of questionnaires in two groups is not the same (Fig. 1c). GW users accounts for 89.6% questionnaires, the percentage of people who use only TW and TW together with GW are 4.20% and 6.20%, respectively. Important reason for this extra subject is that people who get experience in using TW have more diversity in perception and they can evaluate water sources and their consumption habits in a wider view. This study focused on the group of GW users and the number of TW users is used for comparison. The number of TW users is small and do not have the meaning to be a representative for the whole group.

2.3. Water quality

GW samples were collected in parallel to the questionnaires and were analyzed in the frame of the previous study by Bauer et al. (2022), emphasizing on GW evolution and geochemistry. However, only major ions and parameters were considered in this study. The sampling methods are described in Bauer et al. (2022) in detail. Briefly, GW samples were collected from households, small businesses and water supply stations with the aim to cover the whole province. Sampling points were selected based on their spatial relevance, general access as well as permission situation. The number of samples is more than the number of questionnaires. GW was collected after 15 minutes of pumping to ensure that the sample originate from the aquifer and not the stagnant water which was standing in the well casing prior to pumping. GW was taken and measured some parameters on site, or brought back into laboratory for further analysis, as described in Section 2.3.2. To prepare for analysis, 25 mL of GW sample was filtered through a 0.45 µm cellulose-acetate filter (Satorius Stedim Biotech GmbH). 50 µL of high purity nitric acid was added to the filtered sample to prevent the precipitation of cation (APHA AWWA, 2005) and 50 µL of sodium azide was added to inhibit microbiological processes to ensure a correct anion analysis (Vanderford et al., 2011). Physiochemical parameters including temperature, pH, electrical conductivity (EC), Oxygen and redox were determined on site by using a multi parameter portable meter (WTW Multi 3630 IDS). Total alkalinity was also measured on site with a titration kit (Merck KGaA, Germany). Besides, samples after filtration and acid/sodium azide addition were transported to Germany and analyzed with IC (X-Series 2, Thermo Fisher) for anions and ICP-MS (Dionex, ICS-1000; Trennsäule IonPac As14 Supressor ERS 500) for cations at the Karlsruhe Institute of Technology in the laboratories of Institute of Applied Geosciences.

After analysis, the samples of GW were compared with the people's subjective assessment of the water quality from the questionnaires. In addition, the concentration of ions, are compared with the National Technical Regulation on Domestic Water Quality QCVN 01-1/2018 BYT to know whether the water quality meets the usage standards or not. The dashed red line represents the QCVN standards and shows clearly that some parameters of samples are over the permissible standards for domestic water (Fig. 5). If the dashed red line does not appear in the figure, it means all values of each parameter meet QCVN standards. All necessary parameters were analyzed and a comparison was carried out between the group of people using GW for non-drinking and drinking purpose. One more aspect to be discussed is samples where GW is chosen as the best water resource. Not all parameters from the list of Vietnamese standard QCVN 01-1: 2018/BYT are considered. This study focuses on some selected parameters, which are most important to evaluate domestic water quality and are easy for people to realize if they occur in harmful concentration. The parameters include pH, EC, NH_4^+, Cr, As, Cd, Sb, Pb, Al^{3+}, Mn^{2+}, Zn, B, Fe, Ba, Na^+, Ca^{2+}, Cl^-, SO_4^{2-}. pH is the basic parameter, which can affect to value of other parameters. Heavy metals such as cadmium, lead and chromium dissolve more easily in highly acid water (DeZuane, 1997). Besides, iron and manganese are not serious substances, which cause health problems, but can cause bitter taste in drinking water even at very low concentration. When water containing higher amounts of Fe^{2+} and Mn^{2+} are exposed to air, these ion can oxidize and precipitate and the water can turn to be turbid (APHA AWWA, 2005). Zinc is not harmful at small concentration, but it can cause strange taste in drinking water with concentration of above 4 mg/L. Zinc at concentrations between 3 – 5 mg/L in water can cause the greasy film when boiling (WHO, 2018). Besides, using lead pipes increases lead concentration in drinking water and after long term, it could affect children mental health. Arsenic also causes a risk to health after long term exposure (WHO, 2018). Ammonia (NH_4^+) concentration can be over the taste threshold at 35 mg/l (WHO, 2018).

3. Results and discussion

3.1. General information of respondents

In this study, households' information of GW use issues along with perceptions of GW over-exploitation are used for the analysis. Percentage of males and females among the respondents was a ratio of 2 males: 1 female. The average household size is 5.5 people per household. According to the Ca Mau Statistic Office, the population in rural area is much higher than in urban area (920948 with 77.2% in comparison with 271452 people, around 22.8%). In this study, respondents are also focused on rural area with around 91.0% and 9.00% respondents in urban area. Most respondents who used groundwater lived in rural area. In urban area, tap water is supplied to the households from water supplier station.

The interviewed households have a variety of occupations, from growing rice, farming shrimp to doing small business to working as employees of a company or officer in government.

The majority of respondents are farmers (rice or shrimp farming) with 68.1%. There are also small self-employed households including restaurants, bars, selling bottled water with 16.7%. People working in companies and government organization known as officers, accounted for 10.4% of interviewees, and finally 4.86% of interviewees were workers. In Ca Mau population, percentage of these occupations are 32.6%, 8.50%, 2.93% and 8.87% respectively (according to Ca Mau Statistic Office, 2021)

The household's income is difficult to estimate because most interviewees do not have a stable monthly income but their income is determined by the success of the crop or shrimp harvest. Usually, people in Ca Mau have more than one source of income. One person can be an employee but also a small seller or a farmer. According to Ca Mau Statistic Office, average monthly income per capita in urban and rural region in 2018 is 2,985,900 VND/pp/month (around 129.6 USD/pp/month). This income is including wage or salary (798,300 VND) (around 34.7 USD /pp/month), income from agriculture, forestry and fishery (self-employment) (1,015,200 VND) (around 44.1 USD), income from non - agriculture activities (813,400 VND) (approximately 35.4 USD) and others (359,100 VND) (around 15.6 USD). This data fits to the authors' impressions in CMP.

Respondents are mainly normal households where GW is used only for domestic purposes. Besides, there were some other types of households. Some households own their business which require much water such as bike washing, restaurant, shrimp farming. Others are private

Table 1
Purpose of using groundwater in Ca Mau province (N=144 questionnaires).

Purpose of groundwater use	Percentage of respondents using groundwater for this purpose
Washing	97.0%
Cooking	65.7%
Drinking	25.4%
Others (gardening, doing business…)	23.9%

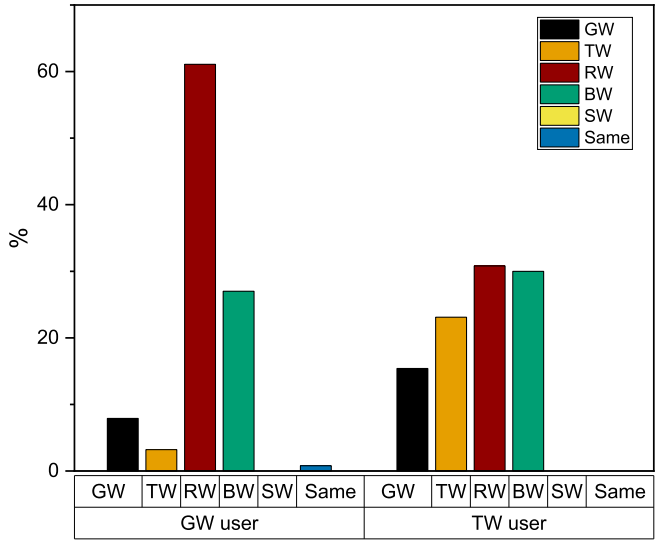


Fig. 2. Best water source in household's opinion.

water suppliers who sell water bottles or owners/managers of water station.

3.2. Current state of using water resource

Groundwater is popular and plays an important role in people's lives in CMP. To understand if people would accept stopping GW usage, it is necessary to understand the importance and specific role of GW in their daily life under social and economic aspects.

According to the results of 144 questionnaires, GW is used for many purposes in CMP, which are listed in Table 1. Households consume GW to wash clothes, dishes, cook or even drink directly. However, washing clothes and dishes consume the highest amount of GW.

Two groups of GW users and TW users have different opinions for certain aspects. For each group, their experience with TW differs, leading to their perception of several different assessments regarding water quality or convenience of use. People have sensory assessments of each water source they use, in terms of water volume, water quality, and as a consequence which water source is the best. Opinions of respondents about the best water source are shown in Fig. 2.

Among GW users, rainwater (RW) is rated as the best quality with 61.1% agreement of households and according to the respondents: "Rainwater is sweet and delicious, is usually boiled to drink tea. Rain water is only used for the main drinking and cooking purpose. Although the water quality is good, the amount of rain water is not enough for another purpose." Their opinions about rain water is based on long-time experiences of using it. According to Đoàn Thu Hà and Hồ (2014), rain water in the Mekong Delta is also considered as high quality water source and it meets Vietnamese standards for almost all parameters. However, contamination of fecal parameters are due to the condition of rain water storage and treatment (Wilbers et al., 2013). Second is bottled water (BW) with 27.0%. In fact, BW comes from groundwater but it is treated in private filtration systems and sold to people. People have confidence in the water quality after treatment with the filtration system and think that BW is of good quality.

In addition, the TW users group believes that RW, BW and TW are the top three with the best water quality, with 30.8%, 30.0% and 23.1% respectively. Even though they have access to TW, they still believe that RW has a better quality in taste. Some interviewees said that TW is sometimes still affected by pipes, strange color changes and its taste is worse than that of RW. Not so many respondents think all water sources have the same quality and no one chose surface water (SW) as the best water source. SW in Ca Mau Peninsula is widely contaminated with organic matters, nutrients, total suspended solids, and microorganisms (Giao, 2022).

On the other hand, both target groups believe that in general GW quality is not really good, with only 7.90% for GW users and 15.4% for TW users voted for GW as the best water resource. The perception of households about groundwater is nearly compatible with the water quality due to the characteristics of some parameters in terms of color, smell and taste (mentioned in Section 3.3). In addition, the role of GW in the life of the household with access to TW has decreased. The importance level of GW in people's life from the results of the survey is shown in Fig. 3.

The question posed to residents is how important GW is in their lives. The answer is divided from level 1 (not important) to level 4 (extremely important, irreplaceable). For the GW users group, none of the people choose level 1, up to 30.3% and 66.4% of the respondents choose the importance level of GW to be level 3 and 4. For the TW users, the importance of GW in people's life is less important, with 22.2% at level 3 and 55.6% at level 4 (Fig. 3). It can be seen that when the group of people is able to use TW, the importance of GW decreases.

Moreover, the use of GW for drinking purposes is a matter of great concern. GW users can be further divided into two subgroups: (i) a group of people who use GW for the purpose of drinking and (ii) a group of people how use GW for non-drinking purposes. If people use GW for the purpose of drinking, people tend to pay more attention to water quality and they usually use some pre-treatment to make water safer for drinking (Fig. 4).

The results show that only 4.2% did not use any pre-treatment before drinking GW, which might be concerning for their health. However, 25% of the subgroup did use a settling process to remove suspended particles before drinking, while 20.8% used both settling and boiling methods to ensure safe water. The majority of the respondents, 50%, relied on filtration systems to remove impurities before drinking GW. Normally, people use mini filtration systems at home. The price of a mini system is in range of 6.000.000 VND (around 260 USD) and they have to change the filter every 3-6 months with a price of around 90.000 VND/filter (around 3.90 USD). These findings highlight the importance of promoting safe water practices to ensure the health and wellbeing of the population, particularly for those who do not currently use any pre-treatment methods (Fig. 4).

The importance of GW in people's lives is affected by their intention in using GW as well as whether they have other water sources such as TW to use. Besides using GW, people also have access to other water sources such as RW, SW, BW or TW for different purposes. The self-assessment question of best quality water opens up potential alternatives to replace GW as main water source. Fig. 2 shows that RW is preferred by people and rated as the best quality water source for both GW users and TW user groups. RW is also a popular drinking water source in the Mekong Delta with positive characteristics of color, taste and smell (G. J. Wilbers et al., 2013b). However, the quantity of RW is not enough for people's demand during the dry season when they only can collect and store rain water in few and rather small containers (Li et al., 2016).

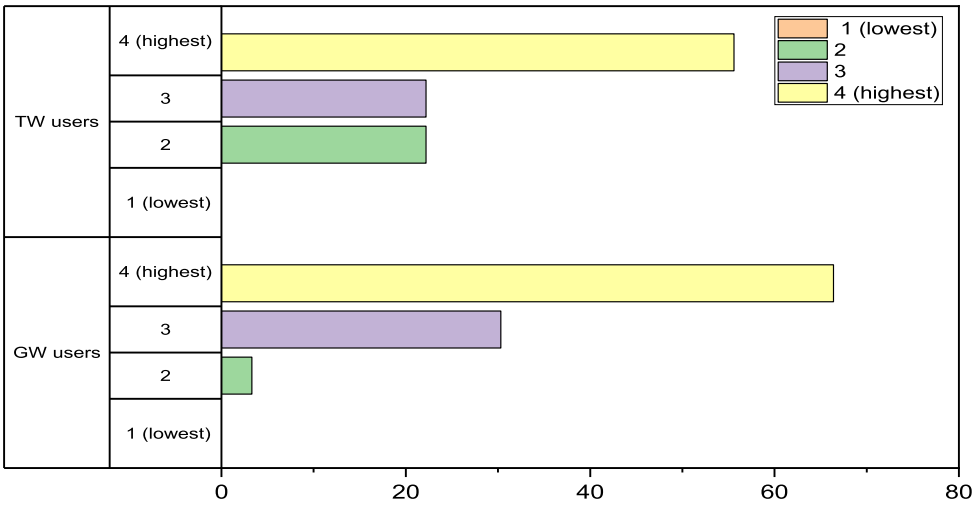


Fig. 3. Importance level of groundwater in 2 groups of households.

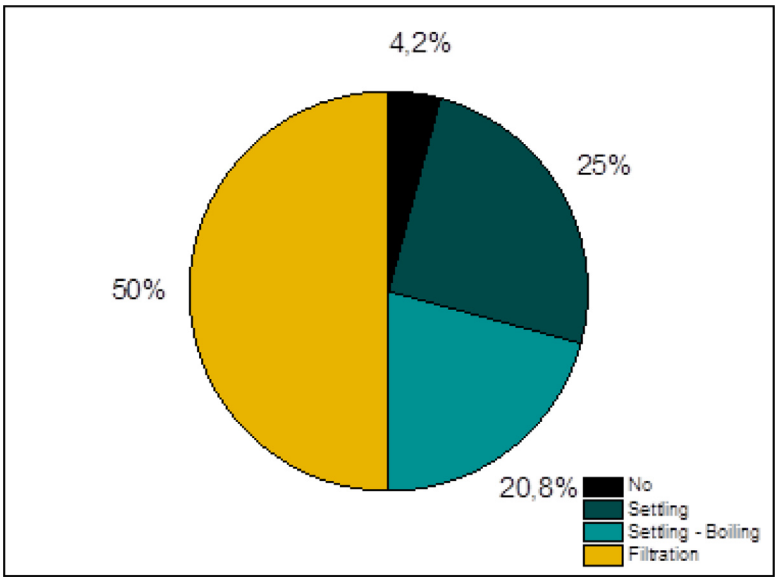


Fig. 4. Treatment practices for groundwater before using for the purpose of drinking.

3.3. Groundwater quality at the locations where GW is used for the purpose of non-drinking and drinking

Since the scientific assessment of water quality through proper measuring equipment is not an option for most of the people in CMP, their decisions and actions in using water depend on their individual gustatory and olfactory senses. According to feedback from residents through interviews, when people perceive strange water quality in regard to taste, color or odor, they will not use GW for drinking. According to the findings of Bauer et al. (2022), the analysis of water samples regarding EC, reveals that certain GW does not meet the necessary standards for direct consumption as drinking water. The graphical representation in Fig. 5 presents a comparative analysis of water quality parameters (as discussed in Chapter 2.3) in areas where GW is used for drinking purposes (blue boxplot) and areas where GW is not utilized for drinking (red boxplot). In general, values where GW is used for non-drinking purpose have a wider range and there are more outliers in the plot. The depth of the GW extraction wells also has to be considered to know which aquifer households use for each purpose. The median depth of 120m for both groups correspond to the upper-middle Pleistocene aquifer qp2-3, which is the common aquifer on a household wells in Ca Mau, accounting for 63.37% amount of exploitation based on the estimation of GW model (Hoan et al., 2022). However, non-drinking purpose wells have few exceptions with deeper wells. This indicates that the depth is not extremely important, this also agrees with Bauer et al., 2022 who identified that water chemistry is more a regional feature rather than a vertical one.

On the one hand, the results state that most samples for non - drinking purpose (red boxplot) show that EC and pH parameters met the regulatory limits. However, many water samples in the study area show concentrations of NH_4^+, B, Fe^{2+}, Ba^{2+}, Na^+, Cl^-, SO_4^{2-} exceeding the threshold value for drinking water in Vietnam (Fig. 5). Due to the noticeable strange taste, color or general appearance of these samples, households evaluated their quality poorly, and thus, did not choose them as a source of drinking water. Non-drinking water have higher pH, also correlated with EC. There are some dependent variables of high EC, mostly Cl^-, pH, SO_4^{2-}, Na^+, $Ca^{2+}$and B. It is interesting that NH_4^+ is higher in the group of samples with higher EC. This could probably support the assumption that presumably contaminated saline GW from the shallow aquifer is leaking into deeper aquifers (Bauer et al., 2022).

Regarding the “easy-to-detect” water quality parameters above, GW samples utilized for drinking purposes (blue boxplot) are comparatively superior to the water quality of samples not used for drinking purposes, as depicted in Fig. 5. However, further investigation into the questionnaires is necessary to explain this result, as there are some exceptions that require deeper analysis.

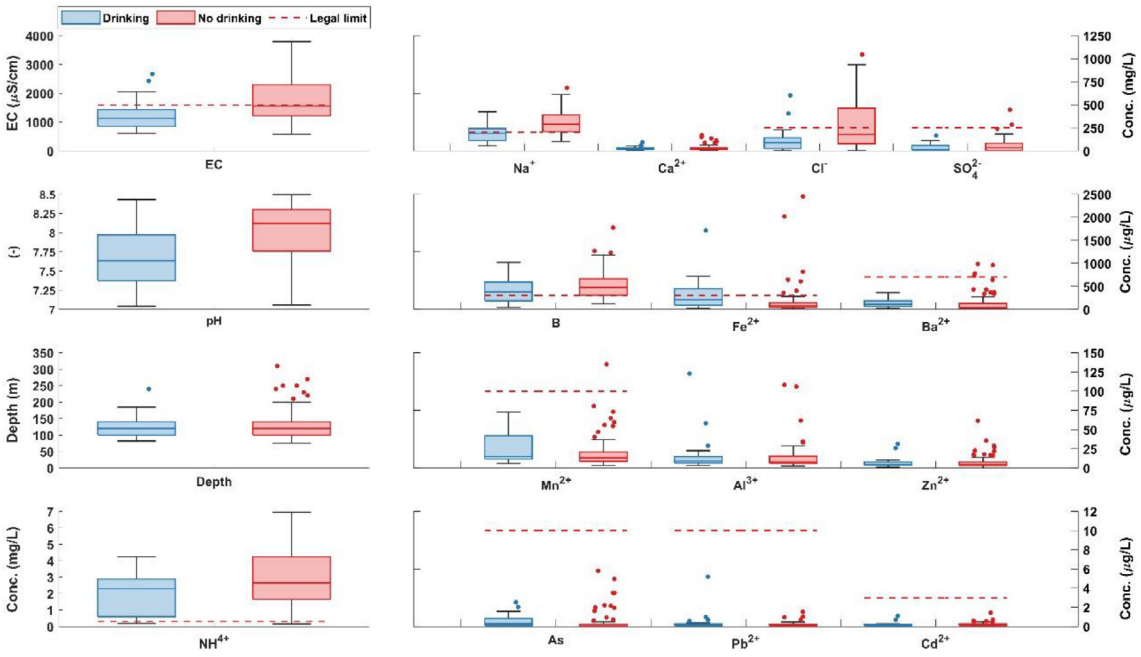


Fig. 5. Groundwater quality at the locations where GW used for the purpose of non – drinking (red boxplot) and drinking (blue boxplot).

For samples with iron (Fe) concentration exceeding the standards (>0.30 mg/L) that people use for the purposes of drinking, people also have different ways of treating GW before consumption as drinking water source. Seven of them use treatment methods before consumption. Of those two households use sedimentation, three use sedimentation with filtration and boiling, and two use a mini filtration system. Two households do not use pre-treatment and rely on other sources like RW and BW for drinking, using GW only as a backup in emergencies.

In the case of samples with Boron (B) levels exceeding the permissible limit (>0.30 mg/L), 15 samples were found to exceed the limit. Among these, two samples were consumed without any pre-treatment, five samples were settled, two were boiled, five were filtered, and one sample was obtained from a water treatment plant. Unlike iron, Boron is a substance that has minimal impact on taste and is challenging to detect for the households by themselves.

For Sodium concentration, there are twelve households exceeding the standard (>200 mg/L). At the same time all twelve households have Boron concentration exceeding the standard, too. Of these twelve samples, one is from a water plant. Two households do not use any measure before using the GW because these households use mainly RW and BW as their primary drinking source, GW is an additional option for them in case of emergency. The other four households are using sedimentation and they also use additional sources for drinking, like RW and BW. Two households boil water, three households treat water with filtration systems and they do not use any other water sources. When households use treatment for GW, it could be assumed that they intend to increase the water quality before they use it for drinking water source.

Similarly, in a household with Chloride concentrations exceeding the standard (>250 mg/L) (concentration of Sodium, Boron also exceeds the standard), there are two locations. One household has a professional water treatment system, filtration and UV disinfection to treat water after extraction and distribute water as a supplier of potable water. Another household uses only a small amount of GW for drinking; they also use BW (filtered water) and RW instead.

Households using GW for both, cooking and drinking purposes, often have high water quality, with chemical parameters in the range of permissible limits. Biological parameters can be discussed further in future studies. For those households that use GW for drinking purposes but do not have good enough water in terms of quality, when digging into the discussion, it could be realized that they only use very little amount of GW for this purpose. In addition, they also have a different amount of water from rain or bottled water as main sources, or they will treat GW with different treatment before use, depending on their ability (Table 2). It is suggested by previous studies that people in CMP should treat GW before drinking (Ha et al., 2022). However, treatment for GW has to be appropriate with current water quality.

People have a certain perception of GW quality leading to their different usage behavior. Therefore, people's perceptions as well as their stories need to be discussed more to find out about what factors can affect their water use habit, perhaps convenience and applicability of water sources, available alternative water sources and economic conditions.

3.4. GW quality of households where GW is perceived as best water resource

Through their perceptions, people identify some uncertainties in the quality of the water they use. It can be said that the perceptions of the people and their responses are important factors in determining water quality as well as the role of GW in people's life and the status of GW extraction.

Figs. 6 and 7 shows that most samples, which are perceived to have the best water quality, adapt with QCVN standards. There are not so many samples to parameters over the thresholds. For each situation there will be a reasonable explanation in Table 2.

For households whose water samples exceed the QCVN standard for Boron, the first sample is from a restaurant. Assuming that the quality of all types of water is same, they use a large amount of GW daily for restaurant business (400 – 500L/day). GW use brings financial benefits to the household at a very low cost, therefore GW is still the best water source in their situation. The remaining three out of five samples from households are using GW as the main source of water for drinking. They believe in the quality of their current water source because two households use a mini-filtration system for private households and one household is a supplier of potable (bottled) water with a professional treatment system. The fifth household uses a sedimentation method. This household still uses GW and RW in combination because of the low cost although TW is available. When RW runs out in the dry season,

Table 2
Reasons why households still appreciate GW although some parameters of GW samples do not meet the standard.

Group	Reasons	Extend explanation for the reasons
GW as drinking water source	Use of basic water treatment before utilization (settling, boiling, filtering via cloth) before drinking	The traditional practices of water treatment brings a sense of assurance regarding the quality of the treated water, thus rise a level of confidence of household when they use GW for drinking.
	Use of mini filtration system at home before drinking	People trust in the water treatment quality of modern filtration devices as advertised.
	Use of professional water treatment system (for private water supplier) before drinking	GW sample is an input of professional water treatment of private water supplier. They treat GW then distribute water bottles to households nearby.
	Use of professional water treatment system (for water station) before drinking	GW sample is an input of professional water treatment plan which is designed for specific GW to guarantee the output can be delivered to people and used for all purposes.
	Use of rain water or tap water mainly, GW is only used in case of emergency	GW is only used with a small amount if people is lack of other water sources (TW, RW). GW is not the first priority water source in these cases.
GW as the best water source	Do business with high amount of water utilization (restaurant, shrimp farm)	People use a considerable amount of water for their business operations. GW has the lowest cost and meets their business water usage demands.
	Use of professional water treatment system (for private water supplier)	GW is an essential input for professional water treatment by private water suppliers. It directly relates to their economic benefit and becomes a significant source of their income.

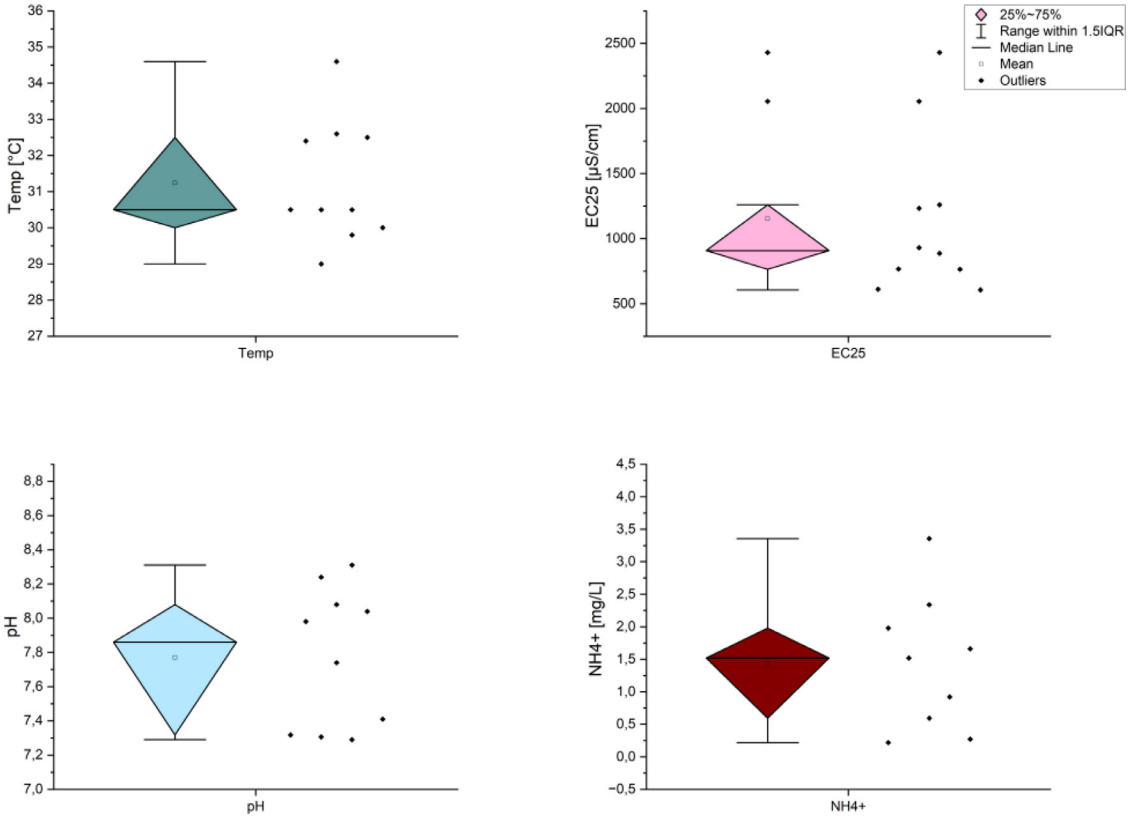


Fig. 6. Groundwater quality at the point of GW as best water source (in people opinion) (Temperature, EC25, pH, NH_4^+).

the main water source could be GW. The last household does not use GW for drinking purposes, GW is used as the main source of water, not only for washing and cooking purposes, but also in shrimp farming. Each month, the household uses much electricity to pump underground water up and the electricity bill to pump groundwater reach to 9.000.000 -10.000.000 VND/month (391 USD to 434.8 USD). GW is used for work that generates a large income for the family, so it is appreciated for its quantity and quality.

Only two samples have chlorine content exceeding the standards. Both use GW as main water source and apply modern filtration systems before use. One uses a mini-filtration system for the household and one uses a large filtration system for bottled water production and distribution. This also explains the simple reason that although the original water quality is not good to reach the standards, GW is mainly used and still is be the best water source.

Depending on the different cases, people always have their own reasons to choose which water source they consider to be the best, even though the water quality does not meet the standards of domestic water. The quality of GW and RW is highly appreciated, but RW has a great limitation in terms of inadequate water storage volume, so it is still used

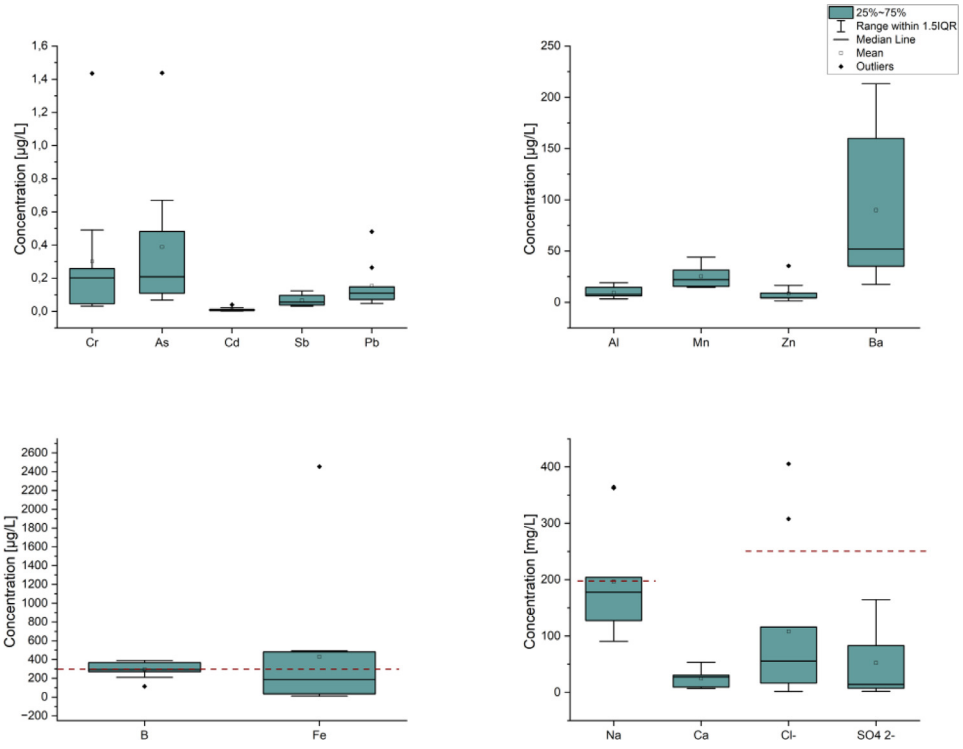


Fig. 7. Groundwater quality at the point of GW as best water source (in people opinion) (other parameters).

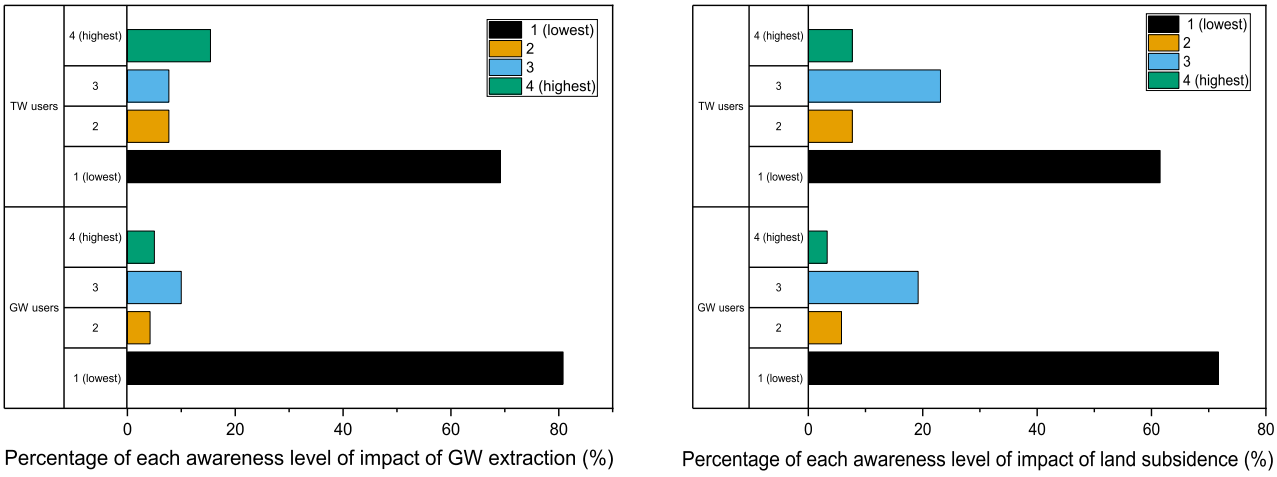


Fig. 8 & 9. Awareness level of people with impact of GW extraction and land subsidence state.

only in the rainy season, in general GW is preferred in comparison with rain water. Seemingly unlimited availability is a strong positive aspect of using GW in people's opinion.

3.5. Evaluation of people awareness about the impact of groundwater extraction on land subsidence

Changing people's living habits is not simple. The priority of this study is to understand people's thoughts and perceptions of their issues. The next question in the questionnaire sheds further light on people's awareness of land subsidence impact and the effects of excessive GW extraction. Most of the people have low or extremely low awareness of these two problems as shown in Figs. 8 and 9.

In the two questions on the awareness issue, the number of households is also divided into two groups as in the previous part: GW users and TW users. According to the results collected, 80.8% of GW users had the lowest level (level 1) of awareness of the impact of GW extraction, 69.2% for the TW users group. With the highest level of awareness about the impact of GW extraction, the GW users group only has 5.00% of the households at this level, while TW users group has 15.4%.

Similar to the question of people's perception of land subsidence in Ca Mau, the level of awareness among GW users on this issue from level 1 to level 4 was 71.7%, 5.8%, 19.2% and 3.30% respectively. As for the TW users, the level of awareness of the people is higher with the rate from low to high of 61.5%, 7.70%, 23.1% and 7.70%.

In general, respondents in this study mainly are not aware of the impact of GW extraction as well as land subsidence in Ca Mau. The level of awareness of people about these issues is extremely low and needs to be promoted. In addition, the importance of GW to people's life is extremely high (Fig. 3), which could lead to a low level of awareness.

The opinions about the importance of GW and people's awareness of excessive GW extraction as well as land subsidence show an inverse relationship. The more people depend on groundwater use, the harder it is to pay attention to the issues surrounding excessive groundwater extrac-

tion. Similar to the farmers in the Red River Delta, people do not have the intention to adapt to climate change when they do not realize any threat to their life and health (Luu et al., 2019). Currently, GW plays an important role in people's lives, while their awareness of overexploitation and land subsidence in Ca Mau is limited, it leads to the lack of attention to climate change issues. According to Eslami et al. (2021) inadequate understanding of environmental systems and processes in the Mekong Delta results in misinterpretation of socio-environmental aspects, ineffective policymaking, and an uninformed public opinion. The latter aspect is important, as only a well educated and informed society may accept change in their daily life.

It can be seen that the TW users and GW users object groups have quite different answers, although the number of TW users' questionnaires is still small compared to GW users. For the next study, it is necessary to expand the number of TW users and focus on making a case study in an area that contains both two subjects for deeper comparison.

The proposed alternative water sources should also be analyzed and applied to each condition, considering the advantages and disadvantages of this water source for each area to get the most accurate results. RW is mentioned frequently in the answers of households as potential alternative water resources. Research on how to overcome the disadvantages of RW subtraction is also very interesting when RW has gained the interest of the people using it.

4. Conclusion

This study has created a general picture of the Ca Mau household's GW using habits. The research approach of evaluating ground water quality parameters and then going into detail about each response of the people has shown more closely and explained the analysis results as well as the connection between the survey and sample analysis data.

The study shows the opinions of households concerning GW use habits based on questionnaires that are reasonably collected according to the spatial and social condition distribution. These results do not claim to be statistically representative for the whole CMP population, however, it is a crucial first step in the evaluation of GW use habits in CMP. GW plays an important role in people's life, it is used for washing, cooking and other activities (restaurant business, shrimp farming, bottled water business, etc.). Depending on the people's perception of different GW qualities, they use GW for different purposes. People estimated the water quality through their perception without knowing the water quality though professional analysis techniques. For important and direct health-related purposes such as cooking and drinking, people have to prepare and treat GW as well as provide alternative water sources to GW if they feel that the water quality is inadequate. As people become more dependent on groundwater (GW users), their awareness of the potential impacts of GW extraction becomes less, and the importance of GW in their lives increases. Besides, people do not have much awareness about land subsidence processes in Ca Mau in general and especially about the potential, that GW extraction can be a major factor for land subsidence. If people have more options to use water, such as TW users, habits of use or dependence on GW as well as their perception of the harmful effects of groundwater extraction change. This opens a research direction to find potential alternative water besides tap water to meet the needs of the people - as a solution to reduce the current excessive exploitation of GW.

Author contributions

Van Cam Pham: Conceptualization, Methodology, Investigation, Formal analysis, Writing - Original Draft, Visualization. **Jonas Bauer:** Investigation, Writing - Review & Editing, Visualization. **Nicolas Börsig:** Investigation, Writing - Review & Editing, Project administration. **Johannes Ho:** Investigation, Review & Editing. **Long Vu Huu:** Investigation & Review. **Hoan Tran Viet:** Review & Editing. **Felix Dörr:** Review & Editing. **Stefan Norra**: Writing - Review & Editing, Supervision, Project administration, Funding acquisition

Declaration of Competing Interest

The authors declare that they have no known competing financial interests or personal relationships that could have appeared to influence the work reported in this paper.

Data availability

Data will be made available on request.

Acknowledgment

This research was carried out as a part of the project ViWaT- Engineering, funded by the German Federal Ministry of Education and Research (BMBF) under grant No. 02WCL1474A. We sincerely thank the Vietnamese National Center for Water Resources Planning and Investigation and the Department of Natural Resources and Environment Ca Mau (DONRE Ca Mau) for their kindly support. We would like to thank the laboratory staffs of the Institute of Applied Geosciences at KIT, Karlsruhe and all project partners working together in this project. I would like to express a special thanks to the financial support of Graduate Funding from the German States (Landesgraduiertenförderung). Finally, we acknowledge support from the KIT-Publication Fund of the Karlsruhe Institute of Technology.

References

Allison, M., Nittrouer, C., Ogston, A., Mullarney, J., Nguyen, T., 2017. Sedimentation and Survival of the Mekong Delta: A Case Study of Decreased Sediment Supply and Accelerating Rates of Relative Sea Level Rise. Oceanography 30, 98–109. doi:10.5670/oceanog.2017.318.

APHA AWWA, W.E.., 2005. Standard methods for examination of water and waste water.

Bauer, J., Börsig, N., Pham, V.C., Hoan, T.V., Nguyen, H.T., Norra, S., 2022. Geochemistry and evolution of groundwater resources in the context of salinization and freshening in the southernmost Mekong Delta. Vietnam. J. Hydrol. Reg. Stud. 40, 101010. doi:10.1016/j.ejrh.2022.101010.

Baumann, D.D., 1983. Social acceptance of water reuse. Appl. Geogr. 3, 79–84. doi:10.1016/0143-6228(83)90007-3.

Bäumle, R., 2017. Final Report IGPVN Activities and Achievements.

Creswell, J.W., Cresswell, J., 2017. Research Design: Qualitative, quantitative, and mixed methods approaches. Sage publications.

Danh, V.T., Khai, H.V., 2015. Household demand and supply for clean groundwater in the Mekong Delta doi:10.1186/s40807-014-0004-7.

Di Giusto, B., Le, T.M.N., Nguyen, T.T.M., Nguyen, T.T.H., Vu, N.U.M., Lavallee, J.P., 2021. Development versus adaptation? Facing climate change in Ca Mau. Vietnam. Atmosphere (Basel). 12. doi:10.3390/atmos12091160.

Đoàn Thu Hà, Hồ, N.H., 2014. Đề xuất giải pháp thu trữ nước mưa hộ gia đình vùng Đồng bằng sông Cửu Long. Khoa Học Kỹ Thuật Thủy Lợi Và Môi Trường 44, 121–125.

Erban, L.E., Gorelick, S.M., Zebker, H.A., 2014. Groundwater extraction, land subsidence, and sea-level rise in the Mekong Delta, Vietnam doi:10.1088/1748-9326/9/8/084010.

Eslami, S., Hoekstra, P., Minderhoud, P.S.J., Trung, N.N., Hoch, J.M., Sutanudjaja, E.H., Dung, D.D., Tho, T.Q., Voepel, H.E., Woillez, M.N., van der Vegt, M., 2021. Projections of salt intrusion in a mega-delta under climatic and anthropogenic stressors. Commun. Earth Environ. 2, 1–11. doi:10.1038/s43247-021-00208-5.

Friedrich, H., Vaessen, V., Himmelsbach, T., Struckmeier, W., 2008. Groundwater and Climate Change: Challenges and Possibilities. In: Geol. Surv. Denmark Greenl. (GEUS), Denmark, p. 20.

Giao, N.T., 2022. Analysis of Surface Water Quality using Multivariate Statistical Approaches : A case study in Ca Mau Peninsula. Vietnam 8, 463–477. doi:10.22059/POLL.2021.329252.1165.

Gustafson, S., Cadena, A.J., Hartman, P., 2018. Adaptation planning in the Lower Mekong Basin: merging scientific data with local perspective to improve community resilience to climate change. Clim. Dev. 10, 152–166. doi:10.1080/17565529.2016.1223593.

Ha, Q.K., Thi, M.V.Le, Vo, P.Le, Nguyen, H.Q., Mekherjee, A., 2022. An assessment of groundwater quality for drinking and agricultural purposes in Ca Mau peninsula, Vietnamese Mekong Delta An assessment of groundwater quality for drinking and agricultural purposes in Ca Mau peninsula, Vietnamese Mekong Delta. IOP Conf. Ser. Earth Environ. Sci. doi:10.1088/1755-1315/964/1/012008.

Ha, T.P., Dieperink, C., Dang Tri, V.P., Otter, H.S., Hoekstra, P., 2018. Governance conditions for adaptive freshwater management in the Vietnamese Mekong Delta. J. Hydrol. 557, 116–127. doi:10.1016/j.jhydrol.2017.12.024.

Han, X., Yin, T., Haiming, L.I., Lu, Z., Thanh, N., Chen, D., 2021. ScienceDirect Saltwater intrusion into groundwater systems in the Mekong Delta and links to global change. Adv. Clim. Chang. Res. 12, 342–352. doi:10.1016/j.accre.2021.04.005.

Hens, L., Thinh, N.A., Hanh, T.H., Cuong, N.S., Lan, T.D., Van Thanh, N., Le, D.T., 2018. Sea-level rise and resilience in Vietnam and the AsiaPacific: A synthesis. Vietnam J. Earth Sci. 40, 126–152. doi:10.15625/0866-7187/40/2/11107.

Hoan, T.V., Richter, K., Börsig, N., Bauer, J., Ha, N.T., 2022. An Improved Groundwater Model Framework for Aquifer Structures of the Quaternary-Formed Sediment Body in the Southernmost Parts of the Mekong Delta, Vietnam doi:10.3390/hydrology9040061.

Li, L., Li, C.S., Wichelns, D., 2016. Assessing household willingness to pay for bottled water in rural areas of the Mekong Delta. Vietnam. Water Resour. Rural Dev. 7, 36–49. doi:10.1016/j.wrr.2016.03.001.

Kyoochul Ha, Nguyen Thi Minh Ngoc, Eunhee Lee, R.J., 2015. Current status and issues of groundwater in the Mekong River Basin.

Luu, T.A., Nguyen, A.T., Trinh, Q.A., Pham, V.T., Le, B.B., Nguyen, D.T., Hoang, Q.N., Pham, H.T.T., Nguyen, T.K., Luu, V.N., Hens, L., 2019. Farmers' intention to climate change adaptation in agriculture in the Red River Delta Biosphere Reserve (Vietnam): A combination of Structural Equation Modeling (SEM) and Protection Motivation Theory (PMT). Sustain. 11. doi:10.3390/su11102993.

Minderhoud, P.S.J., Coumou, L., Erkens, G., Middelkoop, H., Stouthamer, E., 2019. Mekong delta much lower than previously assumed in sea-level rise impact assessments. Nat. Commun. 10, 1–13. doi:10.1038/s41467-019-11602-1.

Minderhoud, P.S.J., Erkens, G., Pham, V.H., Bui, V.T., Erban, L., Kooi, H., Stouthamer, E., 2017. Impacts of 25 years of groundwater extraction on subsidence in the Mekong delta. Vietnam. Environ. Res. Lett. 12. doi:10.1088/1748-9326/aa7146.

Minderhoud, P.S.J., Middelkoop, H., Erkens, G., Stouthamer, E., 2020. Groundwater extraction may drown mega-delta: Projections of extraction-induced subsidence and elevation of the mekong delta for the 21st century. Environ. Res. Commun. 2. doi:10.1088/2515-7620/ab5e21.

MONRE, 2016. Climate Change and Sea Level Rise Scenarios. Minist. Nat. Resour. Environ. 1–126.

Nguyen Thanh, B., Le Van Thuy, T., Nguyen Anh, M., Nguyen Nguyen, M., Nguyen Hieu, T., 2021. Drivers of agricultural transformation in the coastal areas of the Vietnamese Mekong delta. Environ. Sci. Policy 122, 49–58. doi:10.1016/j.envsci.2021.04.010.

Office, C.M.S., 2021. Statistical Yearbook 2020.

Office of the UN Resident Coordinator, 2020. Viet Nam : Drought and Saltwater Intrusion Office of the UN Resident Coordinator 3, 4.

Oxfarm, 2008. In: Viet Nam Climate Change, Adaptation and Poor People, 17. Oxfarm, pp. 413–418.

Pechstein, A., Hanh, H.T., Orilski, J., Nam, L.H., Manh, L. Van, Chi, H., City, M., 2018. Detailed Investigations on the hydrogeological situation in Ca Mau Province, Mekong Delta.

(BYT), QCVN 01-1/2018, 2018. National technical regulation on domestic water quality.

Clark, Plano, Vivky, L., Ivankova, N.V., 2016. Mixed methods research: A guide to the field 118–126.

Ravishankar, C., Nautiyal, S., Seshaiah, M., 2018. Social Acceptance for Reclaimed Water Use: A Case Study in Bengaluru. Recycling 3 (4). doi:10.3390/recycling3010004.

Tran, D.D., Dang, M.M., Du Duong, B., Sea, W., Vo, T.T., 2021. Livelihood vulnerability and adaptability of coastal communities to extreme drought and salinity intrusion in the Vietnamese Mekong Delta. Int. J. Disaster Risk Reduct. 57. doi:10.1016/j.ijdrr.2021.102183.

Van, T.P., Koontanakulvong, S., 2019. Estimation of groundwater use pattern and distribution in the coastal mekong delta, Vietnam via socio-economical survey and groundwater modelling. Eng. J. 23, 487–499. doi:10.4186/ej.2019.23.6.487.

Vanderford, B.J., Mawhinney, D.B., Trenholm, R.A., Zeigler-Holady, J.C., Snyder, S.A., 2011. Assessment of sample preservation techniques for pharmaceuticals, personal care products, and steroids in surface and drinking water. Anal. Bioanal. Chem. 399, 2227–2234. doi:10.1007/s00216-010-4608-5.

WHO, 2018. A global overview of national regulations and standards for drinking-water quality. In: Verordnung über die Qual. t von Wasser für den Menschl. Gebrauch (Trinkwasserverordnung -TrinkwV 2001), p. 100.

Wilbers, G., Sebesvari, Z., Rechenburg, A., Renaud, F.G., 2013. Effects of local and spatial conditions on the quality of harvested rainwater in the Mekong Delta. Vietnam. Environ. Pollut. 182, 225–232. doi:10.1016/j.envpol.2013.07.019.

B.3. Model-based Investigation of Groundwater Salinization: Hoan et al., (2025)

hydrology

MDPI

Article

The Utilization of a 3D Groundwater Flow and Transport Model for a Qualitative Investigation of Groundwater Salinization in the Ca Mau Peninsula (Mekong Delta, Vietnam)

Tran Viet Hoan [1,2,*], Karl-Gerd Richter [3], Felix Dörr [1], Jonas Bauer [1,*], Nicolas Börsig [1], Anke Steinel [4], Van Thi Mai Le [2], Van Cam Pham [1], Don Van Than [2] and Stefan Norra [5]

[1] Institute of Applied Geosciences, Karlsruhe Institute of Technology (KIT), Adenauerring 20b, 76131 Karlsruhe, Germany; nicolas.boersig@kit.edu (N.B.)
[2] National Center for Water Resources Planning and Investigation (NAWAPI), No. 93, lane 95, Vu Xuan Thieu Street, Sai Dong Ward, Long Bien District, Hanoi 100000, Vietnam
[3] Aquantec Company for Water and Environment GmbH, Am Zwinger 5, 76227 Karlsruhe, Germany; richter@aquantec-gmbh.de
[4] German Federal Institute for Geosciences and Natural Resources (BGR), Stilleweg 2, 30655 Hannover, Germany
[5] Institute of Environmental Sciences and Geography, Soil Sciences and Geoecology, Campus Golm, Potsdam University, Building 12, 14476 Potsdam, Germany
* Correspondence: hoan.tran@kit.edu (T.V.H.); jonas.bauer@kit.edu (J.B.)

Abstract: The Ca Mau Peninsula (CMP), the southernmost region of the Mekong Delta, is increasingly threatened by groundwater salinization, posing severe risks to both the freshwater supply and land sustainability. This study develops a three-dimensional, density-dependent groundwater flow and salinity transport model to investigate salinization dynamics across the CMP's complex multi-aquifer system. Unlike previous studies that largely rely on model calibration, this research introduces a novel approach by systematically deriving the spatial distribution of longitudinal dispersivity based on sediment characteristics. Moreover, detailed land use mapping is integrated to assign spatially and temporally variable Total Dissolved Solids (TDS) values to the uppermost layers, thereby enhancing the model realism in areas where monitoring data are limited. The model was utilized not only to simulate the regional salinity evolution, but also to critically evaluate conceptual hypotheses related to the mechanisms driving groundwater salinization. Results reveal a strong influence of seasonal and land use factors on salinity variability in the upper aquifers, while deeper aquifers remain largely stable, affected primarily by paleosalinity and localized pumping. This integrated modeling approach contributes to a better understanding of regional-scale groundwater salinization and highlights both the potential and the limitations of numerical modeling under data-scarce conditions. The findings provide a valuable scientific basis for adaptive water resource management in vulnerable coastal zones.

Keywords: salinity modeling; groundwater transport modeling; hydrogeology; aquifers system; Vietnam; saltwater intrusion; Ca Mau Peninsula; Kien Giang; Bac Lieu

check for updates

Academic Editor: Yong Xiao

Received: 25 March 2025
Revised: 10 May 2025
Accepted: 12 May 2025
Published: 20 May 2025

Citation: Hoan, T.V.; Richter, K.-G.; Dörr, F.; Bauer, J.; Börsig, N.; Steinel, A.; Le, V.T.M.; Pham, V.C.; Than, D.V.; Norra, S. The Utilization of a 3D Groundwater Flow and Transport Model for a Qualitative Investigation of Groundwater Salinization in the Ca Mau Peninsula (Mekong Delta, Vietnam). *Hydrology* **2025**, *12*, 126. https://doi.org/10.3390/hydrology12050126

Copyright: © 2025 by the authors. Licensee MDPI, Basel, Switzerland. This article is an open access article distributed under the terms and conditions of the Creative Commons Attribution (CC BY) license (https://creativecommons.org/licenses/by/4.0/).

1. Introduction

Groundwater salinization is increasingly recognized as a critical global issue, threatening freshwater resources essential for domestic, agricultural, and economic activities in coastal regions [1–4]. This phenomenon is exacerbated by multiple stressors, including

climate change, rising sea levels, and intensive groundwater extraction [5,6], highlighting the need for the improved understanding and management of coastal groundwater resources [7].

The Ca Mau Peninsula (CMP), located at the southernmost region of the Mekong Delta (MKD), is one of the regions most affected by groundwater salinization [8]. For local communities who rely heavily on groundwater, particularly during the dry season [9], excessive groundwater extraction has led to notable declines in groundwater levels (Figure 1). Additionally, upstream dam construction on the Mekong River significantly reduces freshwater inflow, intensifying dry season saltwater intrusion inland [10,11]. However, saltwater intrusion pathways remain inadequately understood due to geological complexity and data limitations, necessitating detailed hydrogeological modeling.

The hydrogeological structure of the CMP comprises seven aquifers and seven aquitards [12,13]. While aquitards were traditionally viewed as continuous barriers, recent studies highlight significant heterogeneity and interconnectedness among aquifers [6,14]. Observations show synchronized dynamics of the groundwater levels across multiple aquifers, suggesting either hydraulic connectivity or loading effects from external stresses [15].

To underscore the urgency of the situation, Figure 1 illustrates the decline in groundwater levels across various aquifers in the CMP, providing direct visual context for the modeling objectives that follow.

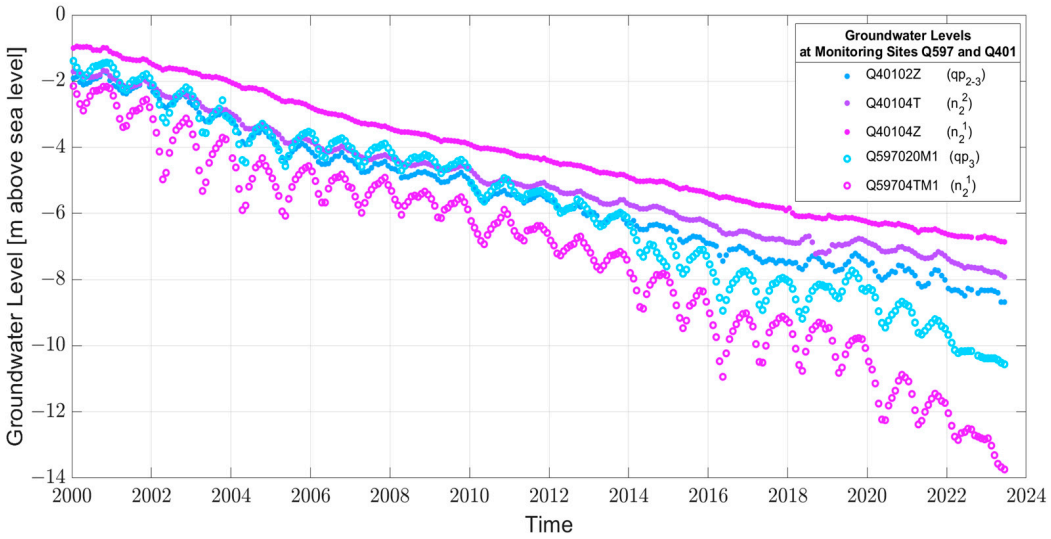


Figure 1. Monthly averaged groundwater levels in monitoring well groups, Q597 and Q401, located in the Ca Mau Peninsula; for the location see Figure 2, and for different aquifers (upper Pleistocene—qp_3; Upper–Middle Pleistocene—qp_{2-3}; Middle Pliocene—n_2^2; Lower Pliocene—n_2^1) see Figure 3 (source of data: the NAWAPI).

Over the past decades, groundwater flow and salinization models have been developed for Vietnam [16–18], as well as for the MKD in particular [13,19,20]. Modeling approaches have primarily employed the MODFLOW software [21] and have mostly covered large areas. However, a recent development includes a local high-resolution groundwater model specifically designed for the CMP by [12].

Due to the limited availability of spatially distributed, continuous salinity measurement data, we propose a salinity transport model based on the hydrogeological model of [12] to assess potential salinity pathways.

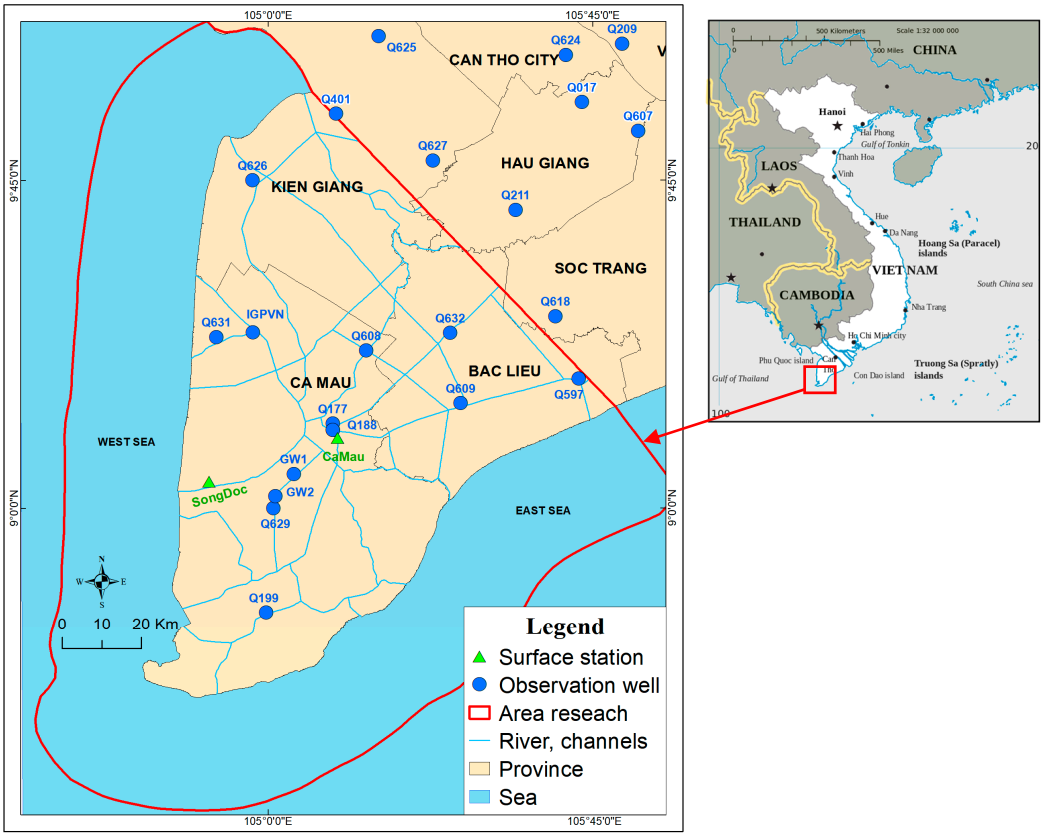


Figure 2. The location of the study area on the Ca Mau Peninsula showing the extent of the model area and observation wells (sources of data: NAWAPI, Esri, HERE, Garmin, © OpenStreetMap contributors, and the GIS user community).

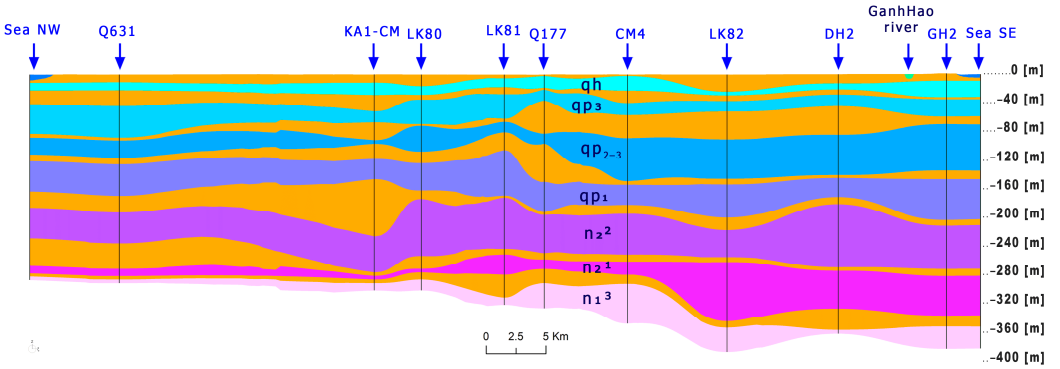


Figure 3. The hydrogeological structure of the Ca Mau Peninsula. Aquitards are shown in orange, and aquifers range in color from blue to magenta (modified after [12]).

Based on the data analysis and the knowledge from the hydrogeological model, we formulate and evaluate the following hypotheses based on observed salinity trends and hydrogeological modeling:

(a) "There is no lateral saline intrusion from the ocean into the deeper aquifer".

This hypothesis suggests no horizontal saltwater movement into the deeper aquifer, depending on the geological and hydrological conditions such as the extent and continuity of the aquitards.

(b) "Different land use classes impact the salinity in the qh aquifer and contribute to the high spatial variability of the salinity in the qh aquifer".

This hypothesis indicates spatial salinity variability driven by land use impacts on infiltration, runoff, and recharge processes.

(c) "Interannual variations in the surface water salinity in the river and channel system, as well as in mangrove, rice, and shrimp farming areas, could cause the high variability in the salinity in the qh aquifer".

This hypothesis emphasizes climatic, precipitation, and anthropogenic influences on salinity dynamics in shallow aquifers.

(d) "Salinity variations in the deeper aquifers might be caused by the extraction of water during pumping".

Based on recent field surveys conducted by the ViWaT research program [9,22] and data collected in Ca Mau Province, there has been a noticeable rise in the groundwater salinity levels over the past decade. This has led farmers and water suppliers to drill deeper wells to access freshwater, as previously utilized sources no longer meet quality standards (personal interviews with local farmers, 2022). However, monitoring data from the Vietnamese national groundwater network show no significant increase in salinity within the deeper aquifers [23]. This discrepancy suggests a need for further investigation to identify whether local factors, such as over-extraction or well-drilling practices, could be causing localized increases in salinity.

This study advances the understanding of saltwater intrusion by systematically deriving the spatial distribution of longitudinal dispersivity instead of relying solely on calibration, as commonly practiced in previous groundwater salinity models. Rather than focusing solely on optimizing the fit to available salinity measurements, our approach prioritizes improving the physical understanding of salinity transport processes through a hypothesis-driven methodology. While many studies traditionally adjust porosity to refine model performance, we highlight the critical role of dispersivity in controlling salinity patterns. A particularly notable contribution is the application of detailed land use maps to assign variable TDS values for the uppermost aquifer layer, where direct monitoring data are limited or unavailable. This method significantly enhances the spatial resolution and accuracy of groundwater salinity characterization at regional scales, providing an efficient and cost-effective alternative to traditional field-based measurements and interpolation techniques. The findings offer valuable insights into interactions between aquifer heterogeneity, dispersivity, and land use-driven salinity variations, establishing a refined methodology highly applicable for regional groundwater salinity assessments.

The primary objectives of this study are as follows: (1) to systematically derive the spatial distribution of longitudinal dispersivity; (2) to integrate detailed land use mapping to assign realistic TDS values in shallow aquifers; (3) to elucidate the dynamics and underlying mechanisms of groundwater salinization within a complex multi-aquifer system at the regional scale; and (4) to assess the practical limitations of applying the modeling approach.

2. Study Area

The study area aligns with that employed in our previous study [12]. It is located in the southernmost region of the MKD, Vietnam, covering the provinces of Ca Mau, Bac Lieu, and the lower part of Kien Giang (see Figure 2). The study area is located in a region strongly affected by climate change [24]. The region faces major challenges, described by [9] as the "loss of land and freshwater", which includes processes such as coastal erosion, land subsidence, and the salinization of the surface and groundwater bodies.

Geologically, there have been multiple transgression and regression periods, resulting in several-hundred-meter-thick sequences of marine and fluvial sediment deposits [14]. In recent geological history, the area was created as a consequence of the uplift of the Himalayan Mountains and the associated erosion. This eroded material was transported by

the Mekong River and deposited in its delta, forming the CMP. These deposits also exhibit a certain degree of salinity from former transgression/regression processes.

With an average elevation of approximately 0.8 m [25] above sea level, the CMP lies at a relatively low altitude. The coastline of the model area is approximately 396 km long. The maximum ocean depth within a range of 30 km beyond the coastline is approximately 80 m. The salinity of the ocean water is 35 g/L on average [13,26]. The channel and river system of the CMP is strongly influenced by the ocean tides. Tidal amplitudes in the western sea reach a maximum of approximately 1 m, whereas in the eastern sea, amplitudes can reach up to 4 m [27]. This causes saline inflow into the channel and river system, with a maximum salinity of nearly 33 g/L in the river system [28]. The river system can be locally connected to the qh aquifer, as described by [29]. However, the surface water–groundwater interaction is considered to be limited in most areas, with the top aquitard being several meters thick [12], Figure 3 (cross-section).

The surface water network comprises a dense system of interlinked channels used for transportation and agricultural and aquacultural activities. However, the hydraulic interaction between the surface water network and the aquifer system does not extend down to qp_{2-3} [30]. The conceptual model of the groundwater system of the CMP consists of seven aquifers (from top to bottom: Holocene—qh; Upper Pleistocene—qp_3; Upper—Middle Pleistocene—qp_{2-3}; Lower Pleistocene—qp_1; Middle Pliocene—n_2^2; Lower Pliocene—n_2^1; and Upper Miocene—n_1^3; Figure 3). These aquifers are separated from each other by aquitards. However, the continuity of these aquitards has not yet been fully clarified and is therefore examined in this evaluation.

The groundwater in the deep aquifers in the MKD region consists of brackish, saline, and fresh types. In previous studies, the determination of the groundwater age was inconclusive, ranging from recent to older than 45 ka, but with an increasing trend from the Pleistocene to Miocene aquifers [26,30]. The saline water in the deep aquifers could result from the diffusion of saline pore water and/or past/present salt intrusion into the freshwater resources. The interaction between the deeper aquifers might be caused by the natural conditions (e.g., locally thin aquitard layer, hydrogeological windows, and hydraulic gradients) or anthropogenic factors (e.g., number of production wells, leakage along the well structure, and underground construction) [9].

This study focuses on qp_{2-3} and n_2^2 aquifers, as these are the most exploited aquifers in the model area, as mentioned in [12]. The qp_{2-3} and n_2^2 accounted for 63.7% (361,580 m^3/day in 2019) and 29.7% (168,600 m^3/day in 2019) of the total pumping in 2011. According to a survey conducted in 2019, residents in Ca Mau mainly use groundwater for diverse domestic purposes. However, only 25.4% of the respondents in the survey used groundwater from local household wells for drinking purposes [22]. The higher salinity in the qp_{2-3} aquifer is one reason for the minor use of its groundwater for drinking. In addition, high concentrations of other parameters (e.g., Fe, Mg, etc.) have been reported [4], leading to a reduced use of water from qp_{2-3} for drinking. Therefore, this study emphasizes the importance of qp_{2-3} and n_2^2.

Due to the presence of a thick clay layer at the top, the recharge to deeper aquifers in the study area is severely restricted. Consequently, groundwater in deeper aquifers primarily comprises paleowater, accumulated tens of thousands of years ago during historical transgression and regression periods. Over thousands of years, variations in transgression and regression have shaped the current salinity patterns in deep aquifers, leading to complex interactions between ancient saline water and present groundwater dynamics. This characteristic strongly influences the groundwater salinity distribution and dynamics within the system.

3. Data Collection

Despite these modeling advancements, the available data for the evaluation of groundwater salinity in the CMP remain limited. Groundwater salinity data in the CMP have been collected primarily through two distinct approaches:

- Sampling campaigns at various observation wells in different aquifers, with the laboratory analysis of Total Dissolved Solids (TDS) since 2011 with two measurements per year (dry and rainy season);
- Electrical Conductivity (EC) measurements (data logging sensor) with a calibration factor for TDS calculations, implemented since 2019, at various observation wells in different aquifers.

To ensure comprehensive data coverage, salinity data were collected from multiple sources, including the national groundwater monitoring network [31] and international research cooperation projects, such as the ViWaT project (https://www.viwat.info/english/21.php (accessed 20 August 2023)) and the IGPVN (https://igpvn.vn/ (accessed 20 August 2023)) project from 2013 to 2022, which cover key study areas, including Ca Mau, Kien Giang, Soc Trang, and Bac Lieu.

For salinity measurements, two distinct methodologies were employed in the study area. The first approach entailed the laboratory analysis of water samples utilizing standard procedures. While some samples were collected biannually during both the dry and rainy seasons [32], others were based on one-time sampling. In contrast, the second method involved continuous measurements using Electrical Conductivity.

It should be noted that EC and TDS values obtained over long-term monitoring periods can exhibit certain inaccuracies due to various factors, including the prolonged observation of well operations, sampling technique, pumping duration, and analytical procedures [33,34]. These factors inherently increase uncertainty in EC and TDS measurements. Nevertheless, this variability reflects the natural complexity and inherent uncertainty of real groundwater systems, particularly in shallow aquifers (qh). Therefore, these discrepancies are considered an inevitable component in the analysis and evaluation of modeling results.

These salinity measurements are crucial for assessing seawater intrusion in coastal areas. The assessment of seawater intrusion into the groundwater in the coastal areas of Vietnam relies predominantly on the TDS and EC measurements. However, our data collection process revealed the existence of numerous conversion factors between the EC and TDS across different studies, which creates a larger uncertainty in the data.

To address this uncertainty and improve the spatial resolution of the salinity data, various interpolation methods can be employed. Saline and freshwater areas can be distinguished using the interpolation method in space for point measurements. Alternatively, regionalizing methods can be used, as presented by [35]. The dataset, available on a 1 km by 1 km grid, incorporated groundwater points with TDS and wells with geophysical logging via indicator kriging. An additional dataset for Ca Mau Province is from [23]. To regionalize these data for each aquifer, a detailed data analysis and interpolation using the "Ordinary kriging [36] in the ArcGIS geostatistical analyst toolbox, as the best linear unbiased estimator" [23] was carried out. The result was a homogenized dataset of salinity distributions for each aquifer. Therefore, in principle, two homogenized datasets are available for the CMP.

The time series of the measured data from 2011 to 2021 did not reveal any significant trend in the lower aquifers regarding salinization [23]. In Figure 4a, the measured TDS data for aquifer qh are presented, illustrating the entire period of observation from 2011 to 2024. While the assessment focuses on the 2011–2021 period, some monitoring wells in aquifer qh, such as Q177 and Q632, exhibited fluctuations in TDS concentrations over time; however, no clear increasing or decreasing trend was evident, particularly for well Q401

(Figure 4a). Overall, the available data do not suggest a long-term increase in salinity in aquifer qh on a regional scale.

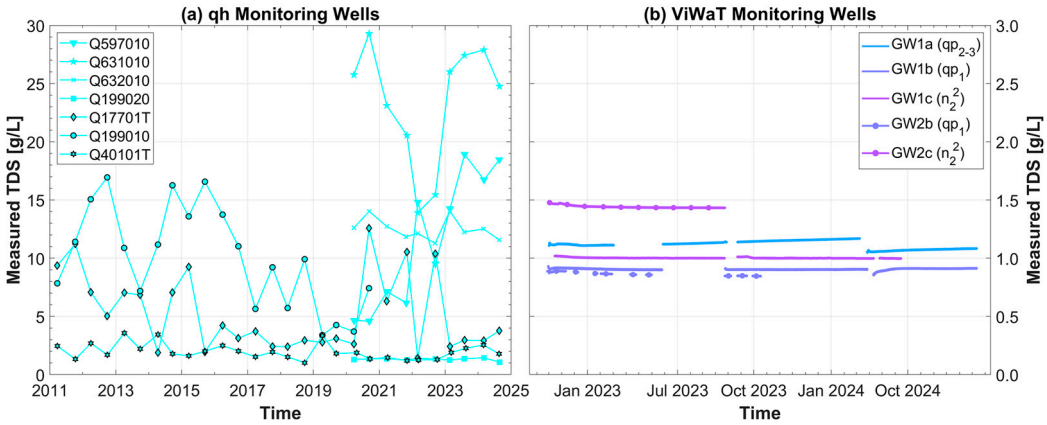


Figure 4. Examples of TDS time series of groundwater monitoring wells from (**a**) the NAWAPI (aquifer qh; period 2011–2024) and (**b**) the ViWaT project (well groups installed in 2022).

In Figure 4b, the automated EC monitoring data (converted to TDS) of groundwater wells in the ViWaT projects at two monitoring locations, GW1 and GW2, are visualized. The data showed that different levels of TDS were established at two sites in different aquifers over time. However, the observed change in the TDS in the aquifers was not significant.

4. Methodology

4.1. Approach to Salinity Transport Modeling

An adapted method for the assessment of saline intrusion was employed, based on numeric modeling but deviating from the conventional approach of calibrating the parameters for a transport model, due to the limited data availability (Figure 5). The method involves developing a simple model to calculate the longitudinal dispersion coefficient using a global dataset and verifying it with regionally developed coefficients, which were derived from the data collected in the study area. The main goal of our approach was to improve the understanding of the physical processes involved, rather than achieving the best fit for the few available salinity measurements.

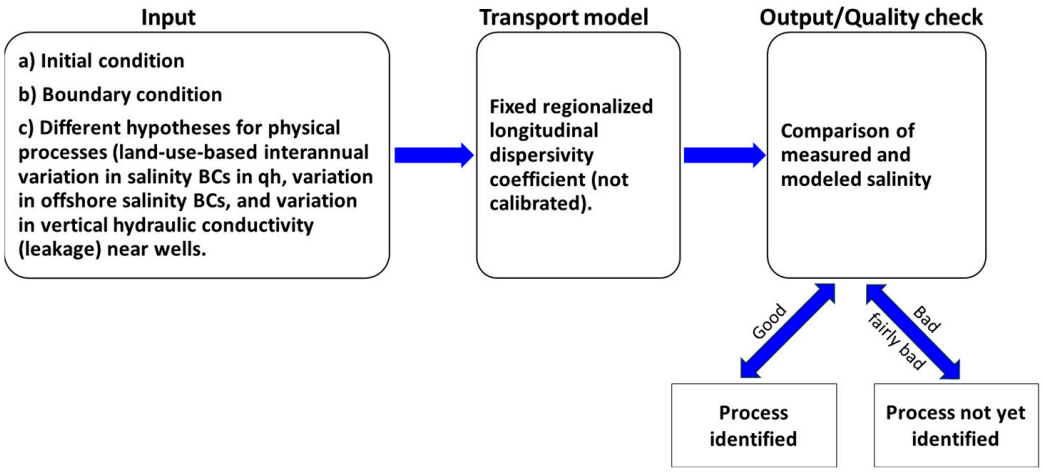


Figure 5. Conceptual framework for evaluating longitudinal dispersion coefficients in saltwater intrusion processes in the Ca Mau Peninsula. *Note: The four processes outlined in the model include additional mechanisms that may not fully correspond to the initial hypotheses but are considered relevant based on field observations.*

Our aim was to assess the significance of these hypotheses and glean insights into the dynamic processes governing groundwater salinization through the examination of various hypotheses against both measured and calculated salinity data. This approach emphasizes a more exploratory and hypothesis-driven analysis of salinity transport, allowing for the identification of important processes. Such an approach is promising and potentially insightful, particularly in situations with limited available salinity data.

Figure 5 illustrates the conceptual framework we used for evaluating salinity transport in the study area. While the initial hypotheses provided a foundational framework for evaluating salinity transport processes, the model incorporates additional mechanisms based on the field data and observed variability in the study area. These mechanisms, including the mixing and dispersion along the flow path and leakage through hydraulic windows, are considered essential for a comprehensive analysis of potential salinization pathways. The conceptual framework also accounts for the historical context of the groundwater system. Given the predominance of paleowater in deeper aquifers, initial salinity conditions in the groundwater model reflect historical salinity patterns resulting from past marine transgression and regression events. This assumption aligns with the field evidence showing distinct salinity interfaces and mixing patterns, as detailed in the Section 4.2.2, which are critical for understanding current salinity dynamics driven by hydraulic gradients from intensive groundwater extraction.

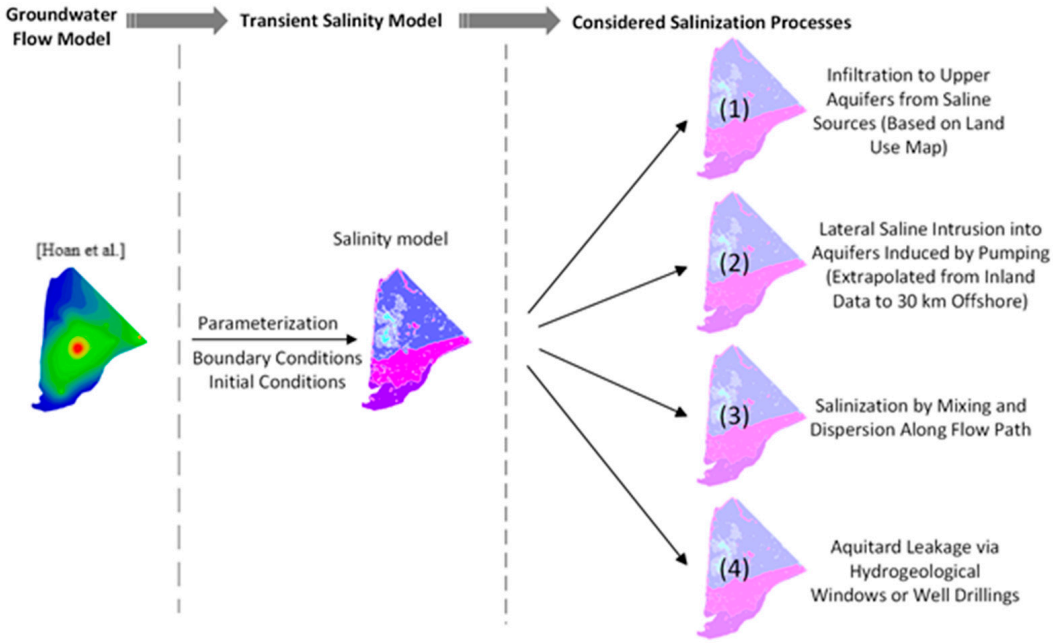
The output of the transient transport model is the concentration at each node in the model domain during the considered time period. The calculated concentration values can be compared to observed concentrations as well as to qualitative information (e.g., reports showing increasing salinity in some production wells). Our approach highlights the iterative nature of model development and refinement. If the simulation results show a good agreement between the measured and calculated salinity in terms of the trend and the order of magnitude, it suggests that the identified processes and the model parameters used could represent real-world conditions. This alignment provides confidence in our model's ability to predict salinity transport within the study area. The spatial discretization of the model was designed to support large-scale and long-term salinity simulations. A spatially variable mesh with local refinement was applied in sensitive areas; the details of the mesh configuration are provided in Section 4.2.1.

In contrast, if the simulation results do not match the measured salinity well, it signals the need for further investigation. This may involve the identification of additional or alternative physical processes that impact salinity transport but were not adequately considered in the initial model. It could also prompt a re-evaluation of the chosen model parameters and assumptions.

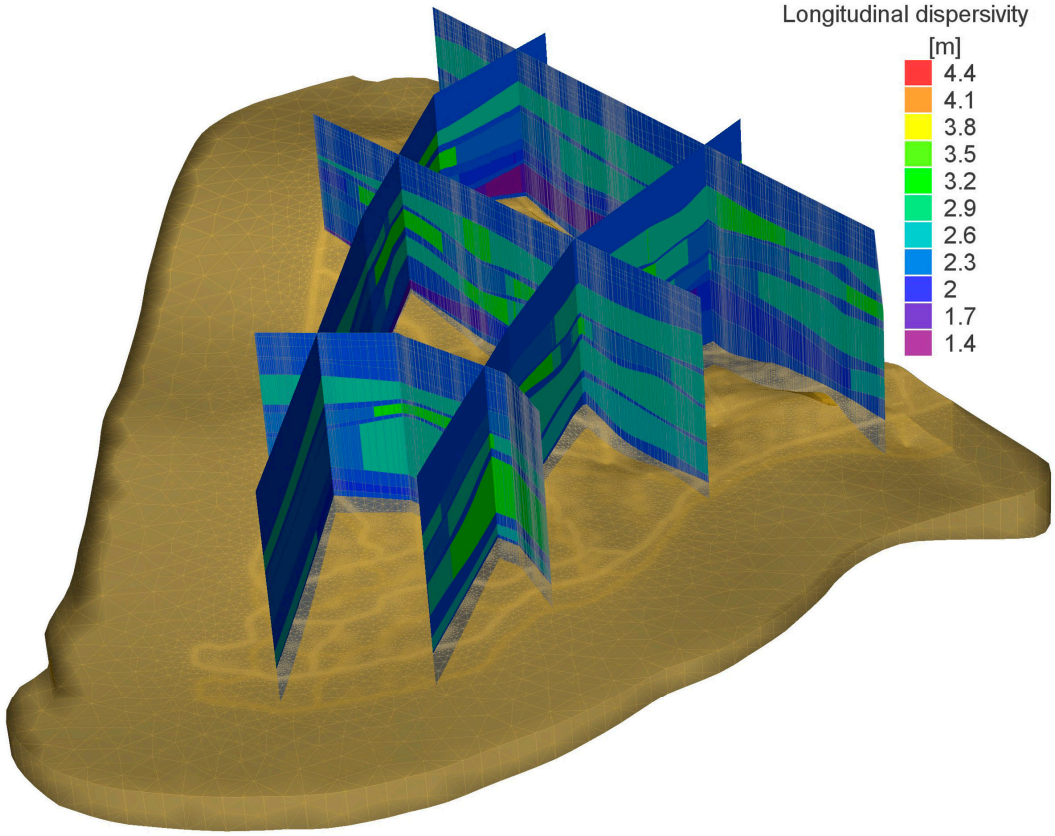
The goal of this study was to continuously refine and improve the model by incorporating new insights, data, and adjustments to better capture the complexities of the salinity transport system. This iterative process is common in scientific modeling, where the feedback loop between model predictions and real-world observations helps enhance the accuracy and reliability of the model over time.

4.2. Saline Intrusion Model Setup

Figure 6a illustrates the process of enhancing the existing flow model [12], transforming it into a variable-density transient transport model with a subsequent sensitivity analysis. Figure 6b provides a three-dimensional conceptual representation of the aquifer–aquitard system used in the model, helping visualize the spatial structure and layering relevant to salinity transport.



(**a**)



(**b**)

Figure 6. (**a**) The flowchart of the integrated groundwater flow [12] and salinity modeling approach for evaluating potential saltwater intrusion processes in the MKD. (**b**) A three-dimensional schematic representation of the hydrogeological model, showing the spatial layering of aquifers and aquitards with corresponding longitudinal dispersivity values assigned to each sediment type.

The density-dependent transient transport model for the CMP was set up with the software FEFLOW [37] for the time period from 2011 to 2024. The following salinization processes in the CMP were considered in the model:

1. Infiltration from saline surface water sources (rivers, canals, aquaculture ponds, salt production, and tidal inundations) into the upper aquifers as identified by the land use map;
2. Lateral saline intrusion from the offshore areas into the aquifer system induced by pumping, assuming that freshwater/saline water in deep aquifers is extrapolated from inland data up to 30 km offshore;
3. Salinization by mixing and dispersion from areas with higher salinity to areas with lower salinity along the flow path;
4. Downward or upward leakage from one aquifer to another through hydraulic windows in the aquitard, either naturally or from drilled wells. Although not included in the current model, this process is considered relevant to understanding salinity changes in the region.

4.2.1. Groundwater Flow Model

The groundwater flow model used as the basis for the salinity transport simulation was originally developed for the CMP by [12]. The original model covers a total area of approximately 19,900 km^2, including Ca Mau Province and parts of adjacent provinces, with approximately 9600 km^2 representing the land area. It was constructed using the finite-element software FEFLOW with a triangular finite-element mesh, featuring a spatially variable resolution. The mesh was refined to element sizes of 2–10 m near monitoring wells, extraction wells, rivers, and channels. Elsewhere, element sizes were gradually increased up to 2.5 km. Vertically, the model is structured into seven aquifers and seven interbedded aquitards. The boundary conditions of the flow model consist of a Dirichlet boundary condition (hydraulic head BC) at the northern boundary based on observed groundwater levels, no-flow boundary conditions along offshore boundaries, and Cauchy-type boundary conditions representing surface water–groundwater interactions in rivers and channels. The groundwater recharge was applied at a rate of approximately 1% of the monthly average precipitation. The flow model was simulated as a transient model from January 2011 to December 2020, using monthly time increments.

The understanding of the salinization process in the CMP is important for the model. Salinization in the upper aquifers (qh, qp_3) is influenced by the intrusion from the river and channel system above and from the interaction between the sea and land beneath the ground surface. Additionally, we assume an influence from shrimp and rice farming practices, salt production, and groundwater abstraction. We also assume the presence of freshwater below the sea floor. These processes are simulated with the model setup.

4.2.2. Mass Transport Model

For the mass transport model, the TDS was used to represent salinity, as it is a widely accepted proxy in groundwater studies, particularly in coastal aquifers where detailed ionic composition data may be limited. This approach follows previous studies [13,26,35], which have demonstrated that the TDS provides a reliable spatial representation of salinity. During the model validation period, the observed TDS values from a total of 14 well groups were used for the period of 2011–2024. The transient transport model was run using monthly time steps to capture seasonal and interannual variations throughout the simulation period. For model comparison and analysis, observed TDS data were incorporated twice per year (representing the dry and rainy seasons) at each monitoring location. This approach enabled the model to effectively reflect seasonal salinity dynamics, particularly strongly

expressed in the shallow aquifer (qh), while also capturing long-term salinization trends observed in deeper aquifers (qp_3, $qp_{2–3}$, qp_1, n_2^2, and n_2^1).

Model Boundary Conditions

The following boundary conditions (BCs) were considered:

(1) Seawater intrusion was implemented as Dirichlet BCs with defined concentrations. For Layer 1–Layer 5, representing aquifers qh and qp_3, this was set to 35 g/L (similar to the current TDS of seawater), while for Layer 6–Layer 14, which represent the main exploited aquifers (freshwater to slightly brackish water), this was set to 3 g/L [38] at the model boundary offshore.

(2) No boundary conditions for salinity were defined at the northern model boundary. As there is a flow boundary condition defined at the northern model boundary, the FEFLOW software automatically generates a salinity boundary condition to adapt the concentration of the inflowing water to maintain the concentration near the boundary.

(3) The land use-based estimation of human activities influencing the salinity in the qh aquifer was determined using land use maps [39] (Figure 7, left side). For most land use classifications, a constant salinity concentration BC was used (see Figure 7, right side) for the top layer and the qh aquifer depending on the predominant land use class in each region. At selected locations, these boundary conditions were refined to time-varying fixed-concentration BCs according to the interannual dynamics illustrated in Figure 8 with monthly data.

(4) Surface water–groundwater interaction: The channel and river system in the CMP is strongly influenced by the tidal system of the ocean as well as seasonal (dry/rainy) interactions. The water levels in the river and channel system were interpolated from measurements based on the mean monthly change in the water level. In addition, we used the measured mean monthly salinity data (Ca Mau and Song Doc stations) to interpolate the interannual variation in the surface water bodies, mangrove, and semi-intensive shrimp and salt production zones and implemented them as time-varying fixed-concentration BCs (shown in Figure 8).

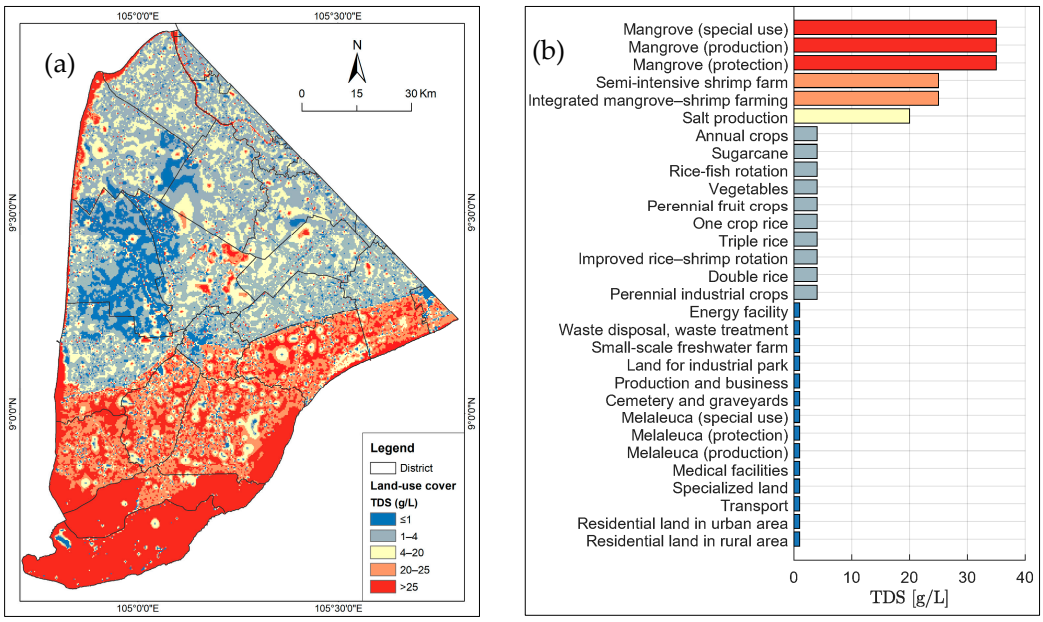


Figure 7. Land use-dependent salinity initialization (**a**) based on [39] and TDS classification based on land use (**b**).

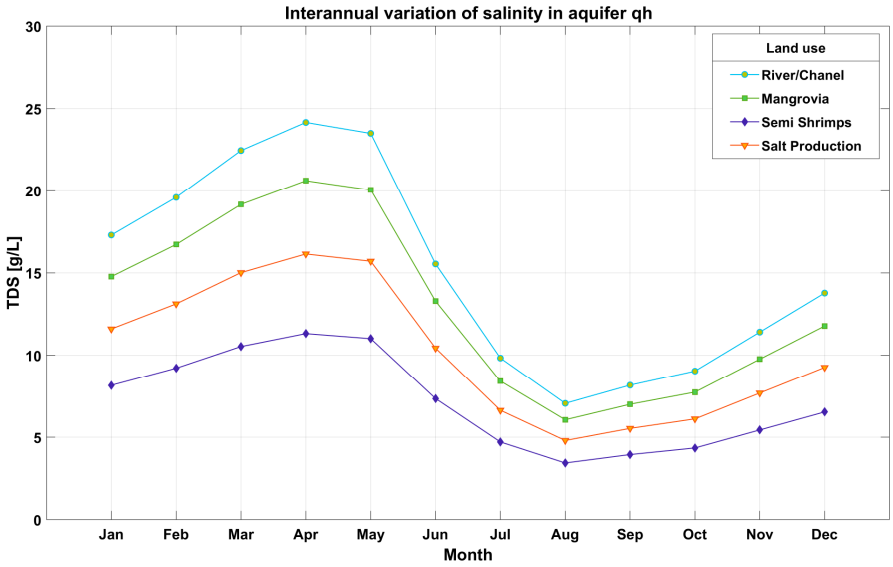


Figure 8. Mean monthly salinity for different land use types applied for model boundary conditions in aquifer qh and the top layer (derived from the salinity of surface water monitoring stations of Song Doc and Ca Mau, period 2012–2020).

Initial Conditions

At the beginning of the simulation (January 2011), the initial TDS concentration had to be defined for every node in the model. The initial conditions were determined based on the limited information available, specifically the salinity data collected simultaneously across different locations. All the salinity data available in different locations were utilized to establish the initial horizontal salinity values.

A combined dataset was established from the regionalized data of the IGPVN project [23] for the aquifers qp_3, qp_{2-3}, qp_1, n_2^2, and n_2^1 inside Ca Mau Province and interpolated values outside of Ca Mau Province based on the values measured during our data collection.

One of the challenges was determining the initial TDS concentration for the upper layers. There are many lakes, ponds, and rivers/channels, covering approximately 60% of the study area. However, their common feature is that the salinity varies seasonally. Data on these changing salinity levels are not available.

Therefore, the salinity in Layer 1 and Layer 2 (qh) was determined according to the zoning of the land use types, combined with survey data from some specific point groups. For the upper aquitards, the same initial conditions as in the upper aquifer were applied. For areas controlled by sluice gates, salinity measurements vary within a relatively small range. Consequently, the TDS value is considered to be a boundary condition that is constant over time for areas controlled by sluice gates. As for the remaining regions and land use types, their salinity variations were estimated through interpolation based on seasonal changes throughout the year (as depicted in Figure 8). The initial conditions for the aquifers are illustrated in Figure 9.

Dispersivity Parameter Adaptation

Flow velocities and hydrodynamic dispersion coefficients are key parameters for the description of fluid and solute transport in porous media. The topic of dispersivity has been of great interest in the scientific community, particularly among those studying hydrology and contaminants and flow through porous media (e.g., [40–43]). Hydrodynamic dispersion includes both mechanical (advective) dispersion and molecular diffusion. For low fluid velocities, solute dispersion is dominated by molecular diffusion; for high velocities,

advection becomes dominant, but the contribution of diffusion cannot be neglected. In this study, we did not calibrate the longitudinal dispersion coefficient but instead derived the spatial distribution of the longitudinal dispersion coefficient.

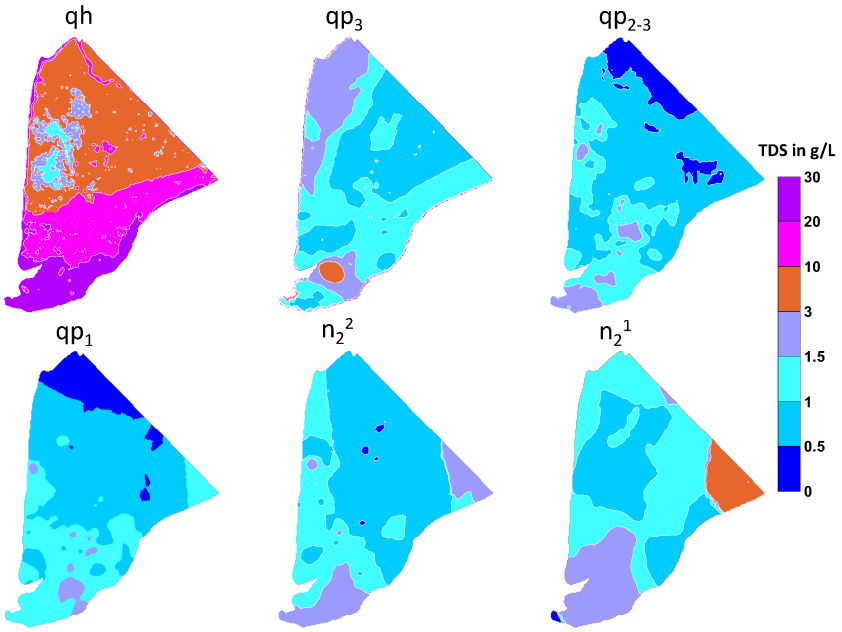


Figure 9. The spatial distribution of the initial salinity (January 2011) for the aquifers qh, qp_3, $qp_{2–3}$, qp_1, $n_2{}^2$, and $n_2{}^1$.

The following dependencies of the longitudinal dispersion on the soil and sediment are known from the literature:

1. The longitudinal dispersivity coefficients for homogeneous soil and layered heterogeneous sediments show that stratification affects the longitudinal dispersivity coefficient, and the longitudinal dispersivity coefficients for layered heterogeneous sediments are nearly half than those in homogeneous sediments [44–47].
2. The longitudinal dispersion coefficient is influenced by the distance of travel, and its values undergo changes as the distance increases. In both homogeneous and layered heterogeneous sediments, the dispersion coefficient's values increase by a factor of 2.5 with the expansion of the horizontal travel distance [47–49].
3. There is also a dependency of the longitudinal dispersivity coefficient on the sediment type. From sand to clay, the longitudinal dispersion coefficient decreases with the smaller grain size of the material.

We set up a simple regionalized model for the calculation of the longitudinal dispersion coefficient in terms of average parameters from the Waterloo Hydrologic Enviro-Base, modified by the mentioned dependencies 1 and 2. We verified this regionalized longitudinal dispersion coefficient with local literature values [50].

Therefore, in this study, the Waterloo Hydrogeologic Enviro-Base [50] was used to calculate the average longitudinal dispersivity coefficients and average flow distances for different sediment types in the multilayered aquifer system of the CMP.

These averaged longitudinal coefficients were normalized (i.e., normalized dispersion coefficient) by dividing by the averaged flow distance (Figure 10a). The dependency of the normalized dispersion coefficient was fitted by the regression shown in Figure 10a. To recalculate the longitudinal dispersion coefficient for every soil type, an estimated flow distance of about 50 m was selected.

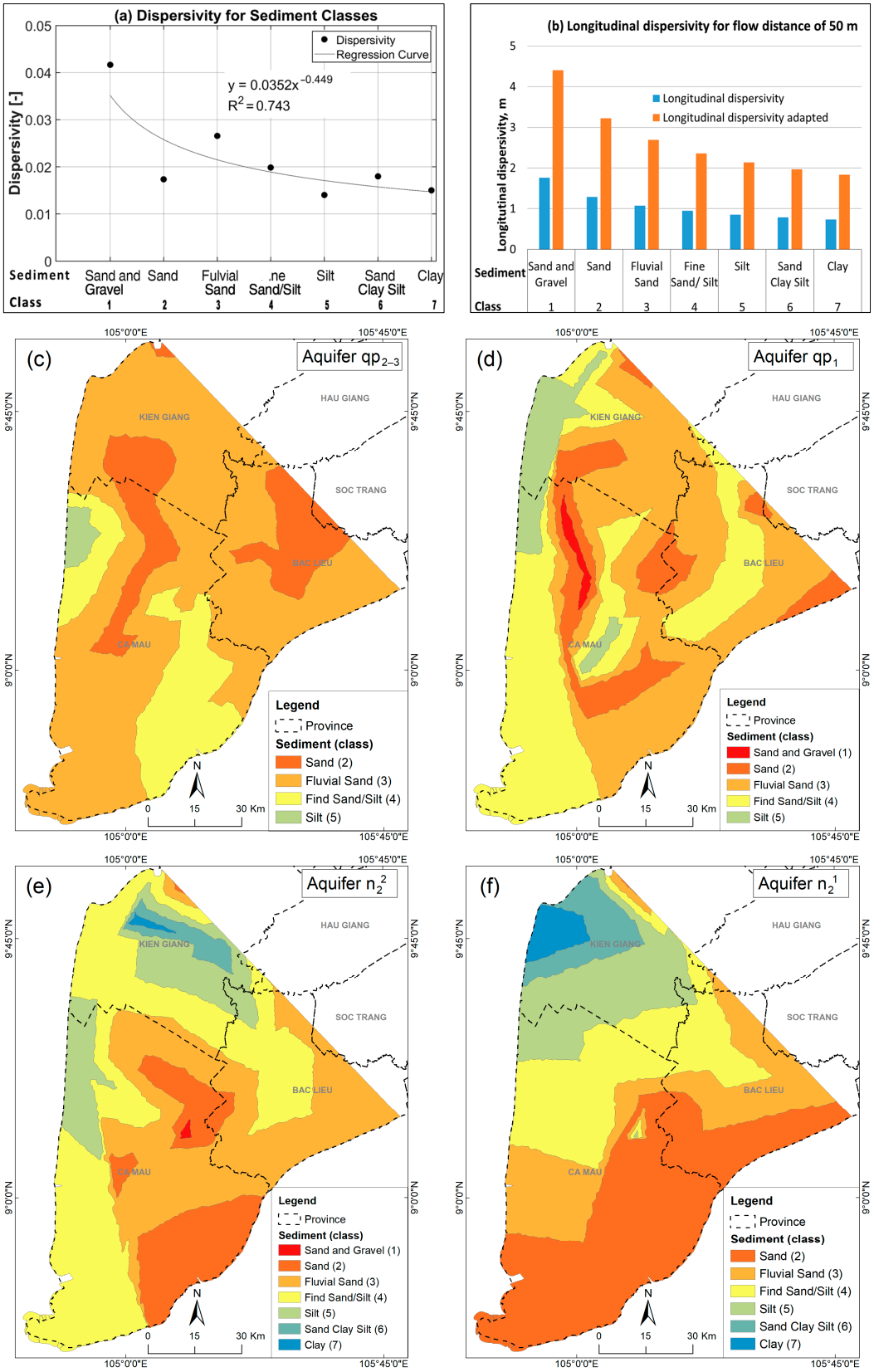


Figure 10. (**a**) The dependency of longitudinal dispersivity on the sediment class as demonstrated by [26], based on flow meter data; (**b**) longitudinal dispersivity coefficient (m) for different sediment classes based on a flow distance of 50 m for different sediment classes; and (**c**–**f**) sediment classes for different aquifers, qp_{2-3}, qp_1, n_2^2, and n_2^1 [51], used for the regionalization of the longitudinal dispersivity coefficient.

According to point one, we assumed that the sediments were homogeneous within the sediment classes presented in Figure 10, because detailed information about the sediment structure was not available. Thus, the longitudinal dispersivity was multiplied by a factor of 2.5 and by a 50 m flow distance. The regional distributions for the sediment type-based coefficients for aquifers qp_{2-3}, qp_1, n_2^2, and n_2^1 are shown in Figure 10c–f.

To validate the derived longitudinal dispersivity coefficients for the study area, they were compared to those in the previous literature. Ref. [52] described a groundwater fieldwork pumping and tracer injection test in the Nghiem Xuyen commune, Thuong Tin district, Hanoi, where a salinized and fresh groundwater boundary exists in the Pleistocene aquifer. The tracer experiment was conducted during a 60 h pumping test. The result was a longitudinal dispersivity value of 2.5 m, with an effective porosity of 0.32. In four other reports [53–56] (Table 1), the longitudinal dispersivity was estimated from 20-day-long tracer tests using 150 kg of salt. The salt was injected during pumping tests after the water level reached a steady state (after 48–72 h). These longitudinal dispersivity coefficient results differ significantly due to many influencing factors, such as the pump rate throughout the pumping test, the pumping well not being cleaned before the experiment, the salt injection process, and asynchronous machinery. In addition, there are natural factors such as the heterogeneous nature of the sediment types.

Table 1. Overview of dispersivity coefficients from different reports in Vietnam.

Well Name	Aquifer	Longitudinal Dispersivity	Effective Porosity	Specific Storage	Average Filtration Velocity	Flow Distance	Location
		αL (m)	ne (%)	μ (m^{-1})	V (m/min)	m	
CM2E [(1)]	n_2^2	1.14	14.0	7.53×10^{-4}	4.54×10^{-2}		Ca Mau
BL4D [(2)]	n_2^2	0.02	16.0	4.58×10^{-3}	4.20×10^{-3}	8.0	Bac Lieu
BL2B [(3)]	qp_{2-3}	0.12	19.4	5.58×10^{-4}	8.90×10^{-4}	8.0	Bac Lieu
IGPVN 1.4 [(4)]	n_2^2	0.09–1.1	11.5–29.50		$4.0–9.9 \times 10^{-5}$	10.09	Ca Mau
CHN5 [(5)]	qp_1	2.5	32.00				Hanoi

Note: [(1)] [56], [(2)] [54], [(3)] [53], [(4)] [57], and [(5)] [52].

The longitudinal dispersivity coefficient varied between 0.02 m and 2.5 m, with an effective porosity between 11.5% and 32%. Thus, the aforementioned dispersion coefficients were within the range of the derived sediment-based coefficient without applying the layer-based factor (blue columns in Figure 10b). The transverse dispersivity in the model was applied as 0.5 m.

In addition to dispersivity, porosity is another critical parameter influencing salinity transport in groundwater systems. In this study, a uniform effective porosity value of 0.3 was applied to both aquifers and aquitards. This choice aligns with values commonly reported for sandy aquifers [58,59] and is consistent with previous regional-scale groundwater models in the Mekong Delta, which typically adopted effective porosity values in the range of 0.25–0.30 without differentiating between aquifers and aquitards [6,13,26]. Although some studies, such as [35], assigned distinct porosity values to aquifers and aquitards based on the sediment type, the application of a single representative value remains a common and acceptable simplification in large-scale models aiming for consistency and tractability.

We acknowledge, however, that the effective porosity of aquitard materials such as clay is generally lower, typically ranging from 0.01 to 0.18 [60,61]. Nevertheless, as our model focuses primarily on horizontal transport processes in sandy aquifers, the impact of this simplification on the overall salinity distribution is expected to be limited. Future studies may benefit from implementing spatially variable porosity fields derived from detailed

lithological data to better capture vertical transport and retardation effects, particularly in fine-grained aquitard layers.

4.3. Limitations of the Model

In order to evaluate the groundwater salinization processes in the CMP, the model was adapted accordingly based on the available dataset. However, the model incorporates some limitations due to the limited available data.

No private household wells are included in the model, since household wells operate with very small flows. Instead, the water consumption for each commune is based on the population and an average rural water demand of 34 L/person/day [12]. This water consumption for each commune is implemented in the model by several wells with a total flow rate equivalent to the derived water demand. With this method, the assumed amount of the water extraction by a large number of private household wells is represented by fewer wells in the model.

The drilling time of wells is not considered during the transient model calculation: all wells are included in the model throughout the whole calculation period. However, in reality, many of the deeper wells are drilled later than the shallow wells. This time dependency could be considered in further evaluations.

Additionally, the use of a spatially uniform effective porosity value for both aquifers and aquitards, while consistent with several previous regional studies, may not fully represent the heterogeneity of fine-grained aquitard layers and their limited contribution to advective transport. Furthermore, the use of uniform porosity values may underestimate the effects of fine-scale heterogeneities, which are especially relevant in layered systems.

5. Salinity Model Results

The groundwater flow model validation was discussed in detail in [12]; thus, the following discussion focuses on the aspects of the transport model only. The longitudinal dispersivity parameters of the transport model are not calibrated. They have been estimated by a regionalized method using representative literature values and correction methods. According to the described validation criteria, salinity modeling can be performed for the purposes of confidence building and scientific validation. As stated by Ref. [62], confidence building "is a measure of the adequacy of the model structure (conceptual model and mathematical model) in describing the system behavior" and "is a measure of the accuracy of the model input parameters relative to experimental results and field observations". For regional validation at different time steps, the scientific view postulated by [63] demands the validation of specific models "that one might reasonably expect someone with relevant technical knowledge to consider the model acceptable".

As described in the Data Collection Section, there are only very limited continuous salinity data available that could be used for a transient model calibration. Therefore, as an alternative approach, the comparison of measured and modeled salinity concentrations was used to validate the implemented salinization processes and assess their relevance. In Figure 11, the values measured twice a year, as well as the modeled TDS concentrations, for different aquifers are shown as time series.

Figure 11 illustrates that the modeled TDS concentrations at the presented monitoring wells align closely with the observed values, both in terms of magnitude and temporal trends. The modeled salinity concentrations at monitoring well Q199 qh (Figure 11a) show seasonal variations as a result of the applied boundary conditions with interannual variations (as shown in Figure 8). This indicates that part of the measured variability may be caused by the interannual variation in salinity assumed in the rivers system. Thus, we identify this process as a potential contributor to the salinization pathway, but other

impacts on the variability remain unclear. This can also be observed in Figure 11b for well Q177 qh, where the model simulates the general trend well but the observed variations in the TDS concentrations are not reflected, indicating that a further consideration of locations with interannual variations in the TDS boundary conditions in qh could improve the model results, such as the Q177 site, where constant TDS boundary conditions are applied.

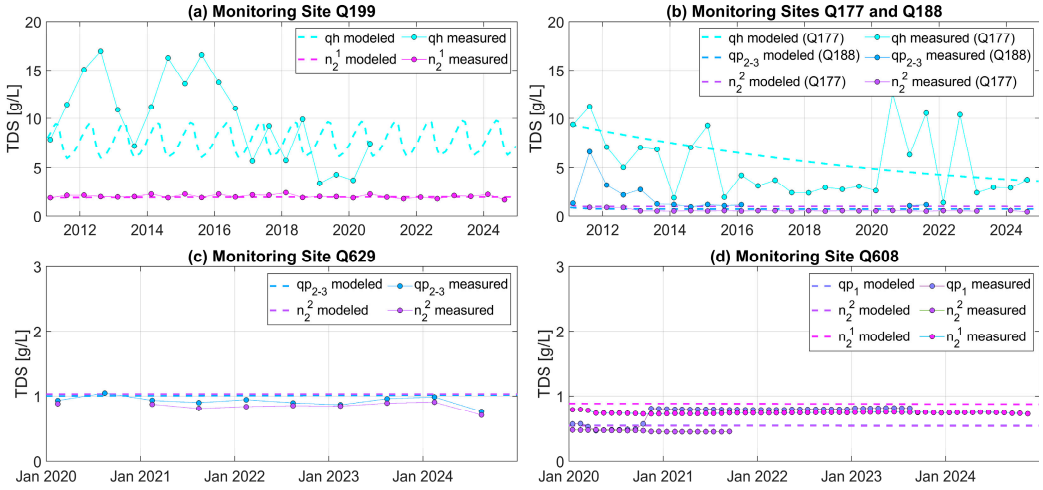


Figure 11. Time-dependent comparison of measured and modeled salinity for different well groups and aquifers. (**a**) Q199 (qh)—Seasonal and interannual variation captured; (**b**) Q177 (qh)—General trend matched; short-term variability not reproduced; (**c**) Q629 (qp2–3, n22)—Stable salinity indicates limited vertical transport; and (**d**) Q608 (deep)—Consistent salinity primarily driven by initial conditions.

Figure 11c (monitoring site Q629) shows a more stable trend in the observed and modeled TDS concentrations for the aquifer layers $qp_{2–3}$ and n_2^2. The model captures the general trend, with slight deviations observed during the period from 2020 to 2024. This consistency suggests that vertical transport processes in deeper aquifers may be limited or occur at a much slower rate. However, minor discrepancies, especially near the end of the time series, may still arise from sampling conditions, laboratory handling, or other external influences that require further investigation.

The salinity in the deeper aquifers qp_1 and n_2^2 tends to be stable in the monitoring wells, without interannual variation. Figure 11a–d show that the simulated (Q199, Q188, Q177, Q629, and Q608) TDS concentrations effectively depict the behavior of the groundwater system over an extended validation period (from 2011 to 2024) in the complex exploitation setting. This indicates that only the initial condition is responsible for the well-simulated salinity in the deeper aquifers. It also suggests that during this extended period, the vertical transport of salinity remains very slow, further confirming the stability observed in deeper aquifer systems.

A common method for evaluating model performance in groundwater modeling is through scatterplots. Figure 12 presents the scatterplot comparing modeled and measured TDS concentrations at observation wells during various time intervals from 2011 to 2024. The 1:1 line represents a perfect agreement between modeled and measured values, while the $\pm$10% and $\pm$20% boundaries highlight regions of underestimation or overestimation by the model. This scatterplot offers a qualitative assessment of the model's performance.

It is important to note that the larger discrepancies seen in Figure 12 are primarily associated with observation wells located in the shallow aquifer (qh), which were deliberately separated from other wells for targeted evaluation. This is due to the high seasonal variability and surface influence affecting TDS concentrations in qh, particularly given the model's reliance on land use data to estimate the recharge salinity in these shallow zones.

In contrast, wells in deeper aquifers show a much closer match to observed values, with the majority falling within the ±10% or ±20% deviation bands. This distinction highlights both the complexity of modeling shallow systems and the overall robustness of the model in representing deeper groundwater salinization processes. Despite some discrepancies in absolute values in qh, as observed in Figure 11a,b, the model effectively captured the overall trends and variability in the TDS at the shallow aquifer level.

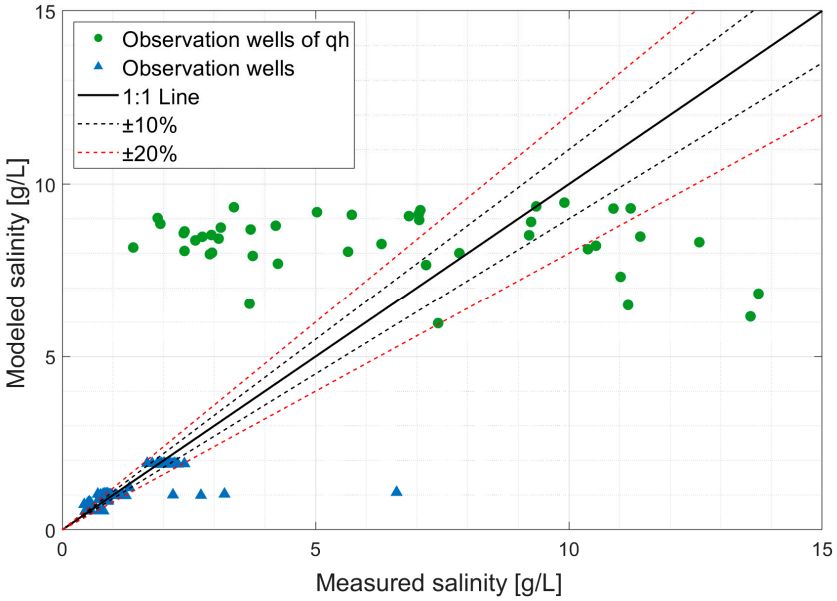


Figure 12. A comparison between measured versus modeled average TDS concentrations (g/L) at observation wells during the simulation period (2011–2024). The solid black line represents a perfect 1:1 match, while dashed lines indicate ±10% and ±20% deviations. Green circles represent qh wells affected by surface processes and land use variability, while blue triangles indicate deeper aquifers with a generally closer agreement.

The salinity distribution in January 2011 served as the initial conditions for aquifers qh and qp_3, as outlined in the Section Initial Conditions. Subsequent simulations captured changes in the TDS concentrations, with Figure 13 providing a visual representation of these variations. In the top-right portion of Figure 13, the influence of the boundary conditions with interannual variations is evident, resulting in a reduction in the salinity of the qh aquifer during the rainy season. This reduction is likely attributed to the dilution caused by the influx of freshwater from precipitation events. Conversely, for August 2022, the bottom-right portion of Figure 13 illustrates an increase in salinity in aquifer qp_3. This increase is attributed to the substantial transport of salinity from aquifer qh to qp_3. Furthermore, the long-term simulation uncovered additional dynamics in the salinity distribution. In the top-right portion of Figure 13, there is an indication of salinity import from the top, possibly influenced by external factors or processes affecting the upper part of the aquifer. Simultaneously, the bottom-right portion shows ongoing salinity transport from the top down, suggesting the continuous downward movement of saline water within the aquifer system.

Figure 13 shows that the salinity transport was dominated by input from the surface, and the modeled salinity in the two upper aquifers qh and qp_3 shows a strong change over the simulation between January 2011 and August 2022. In contrast, the lower aquifers $qp_{2–3}$ and n_2^2 show fewer changes in salinity over time (for comparison, see two lower maps in Figure 14a–e). The scale is defined within an interval of 1.0 g/L. For the deeper aquifers $qp_{2–3}$ and n_2^2 (Figure 14a–e), no significant lateral change in salinity can be obtained from the model results for the simulation period. In the current model described above, only a

small-scale variation in salinity due to pumping can be detected. However, this is consistent with the time series measurement of the salinity, as no significant changes in salinity over time could be observed (see Figure 11). Figure 14c,f show the modeled spatial changes in the freshwater zones (<1 g/L) between 2011 and 2022. Both time steps include the 1 g/L isolines to allow the direct comparison of the salinity extent between 2011 and 2022. In $qp_{2–3}$ (Figure 14c), region 1 shows an increase in salinity along the border of the original salinity inflow from the ocean, while region 2 presents a northward expansion of salinity from the northern boundary (Bac Lieu Province), likely induced by intensive groundwater extraction. In regions 3 and 4, salinity levels exceed 1 g/L due to the lateral transport of brackish water, rendering the groundwater unsuitable for drinking. In aquifer n_2^2 (Figure 14f), changes are less pronounced, but a local increase in salinity is noticeable in the eastern parts (regions 5 and 6), following the direction of the horizontal groundwater flow.

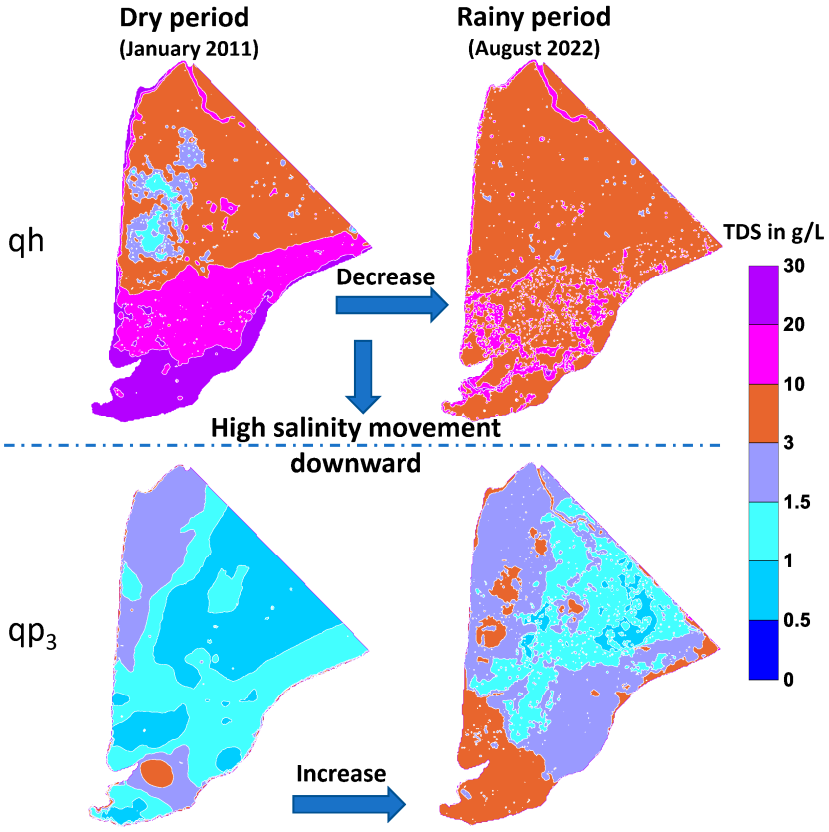


Figure 13. The modeled salinity distribution (TDS in g/L) in aquifers qh and qp_3 during the dry period (January 2011) and the rainy period (August 2022).

These patterns of lateral salinity increase—particularly in the northeast (Bac Lieu) and west—may reflect the influence of anisotropic aquifer properties, where a horizontal hydraulic conductivity dominates. In the Mekong Delta's stratified aquifer systems, interbedded clay or silt layers tend to impede vertical flow while allowing horizontal movement. This likely limits the downward salt transport from qp_3 to deeper units like $qp_{2–3}$ and n_2^2, despite pumping activity. However, due to the coarse resolution of the model, such anisotropic behavior is not explicitly represented.

In the southern part of the CMP, the model also indicates vertical salinity transport from qp_3 to $qp_{2–3}$, originating from the mangrove regions in the upper layers (Figure 9). As a result of the model, we only observe small influences on the vertical salinity movement in $qp_{2–3}$ and n_2^2, which result from pumping. Exploitation is simulated based on area-wide values rather than specific points. In regions with high pumping rates, such as Ca Mau City,

the results therefore suggest a stable salinity as compared to other regions, as illustrated in Figure 14d,e.

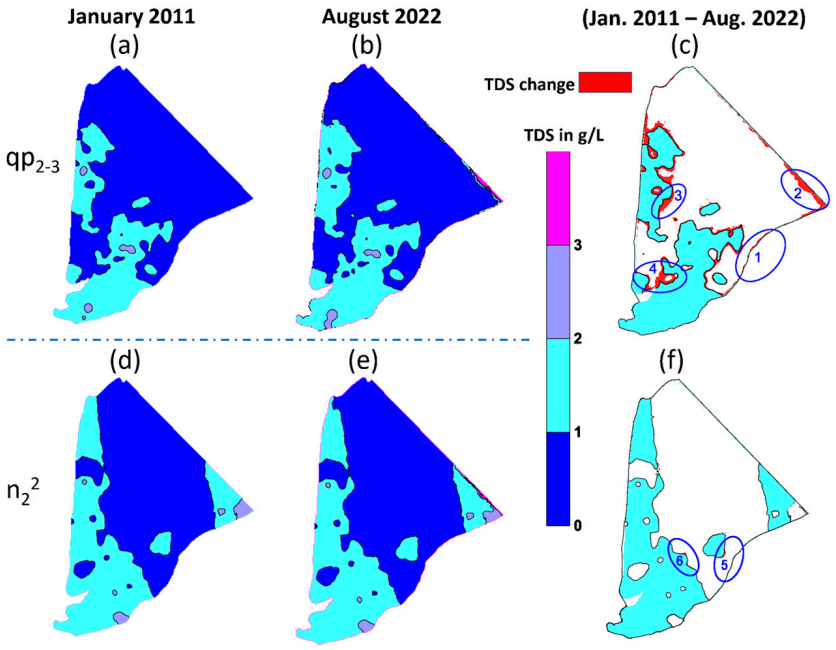


Figure 14. The development of the salinity from 2011 up to 2022 for aquifer $qp_{2–3}$ (**a**,**b**) and n_2^2 (**d**,**e**); (**c**,**f**) illustrate the difference between simulation results from 2011 to 2022.

In the study by [22] it was found, among 144 participants who completed questionnaires in Ca Mau, that the percentage of exploited groundwater allocated for cooking purposes constituted 65.7% of the water usage, while 97% of respondents used groundwater for washing purposes. These freshwater areas are depicted as dark-blue regions in Figure 14a,b, representing the northeastern Ca Mau Province. In the future, the number of areas with higher salinity is likely to increase due to similar pumping-induced effects, as illustrated in Figure 14c. Thus, the possibility of pumping freshwater from $qp_{2–3}$ will decrease. In this area, freshwater has to be substituted from other sources, such as rainwater harvesting or water diversion structures from other sites. In regions with brackish groundwater, with a salinity exceeding 1 g/L but below 3 g/L, it will be possible to use water from the $qp_{2–3}$ aquifer for cleaning and washing in the near future.

For aquifer n_2^2 (Figure 14d,e), the model showed a local increase in the saline water area in the east from January 2011 to August 2022 (Figure 14f, red color), due to the horizontal salinity movement along the direction of the groundwater flow.

6. Discussion

6.1. Key Controls on Salinity Dynamics

As previously mentioned in the Methodology Section, our approach was primarily exploratory, aiming to elucidate dominant physical mechanisms rather than achieving a perfect fit to limited observational data.

The complex interaction between surface water salinity and the upper aquifer qh in the CMP remains inadequately characterized, despite its importance for regional water management. Elevated salinity concentrations in both sediments and water bodies are a ubiquitous problem in the CMP. The salinity varies at the local scale (5–10 m), but the relative effects of land use and surface geology on the salinity variation in the near-surface zone (<5 m) are still unclear. Reference [64] identified that "the influence of surface water salinity (associated with different land uses) on the groundwater salinity regime is

pervasive". They found that areas underlying a shrimp farm/tidal flat displayed a higher salinity regardless of the near-surface sediment characteristics, while areas underlying drinking water ponds or inhabited areas had a relatively low salinity. In this study, the impact of land use and the infiltration of surface water into the qh aquifer was implemented in a numeric model to simulate the relationship between land use and groundwater salinity.

In addition to the spatial variability driven by land use patterns, temporal variations in salinity also present significant complexity, particularly in the shallow aquifer system. Our analysis indicated that significant fluctuations primarily occurred within the shallow qh aquifer, which were strongly influenced by seasonal factors and surface activities such as irrigation, aquaculture, and the tidal-induced salinity intrusion through rivers and canals. Deeper aquifers generally exhibited stable salinity trends both in observational data and model simulations. However, our model also revealed localized temporal variations at certain production wells, where increasing or decreasing trends in TDS were observed (as explicitly presented in Figure 15). These findings underscore the complexity of groundwater salinity dynamics, which are driven by both natural hydrological processes and anthropogenic activities. Beyond surface-driven influences, the internal structure and connectivity of the aquifer system also play a crucial role in shaping salinity behavior.

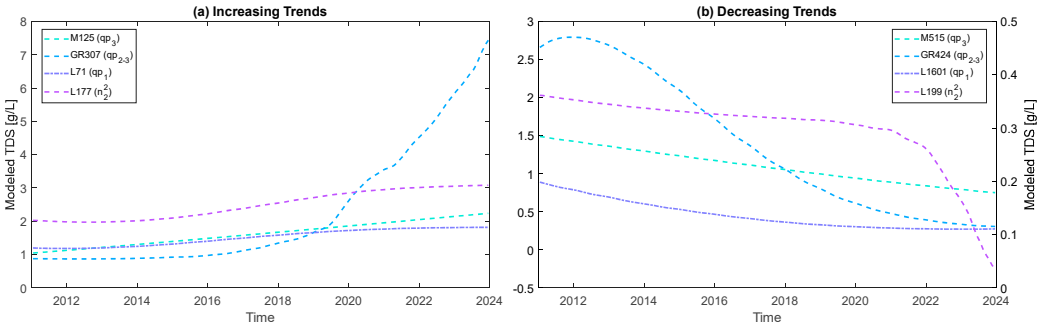


Figure 15. Modeled TDS variations at selected wells across aquifers (2011–2024) (upper Pleistocene—qp_3; Upper–Middle Pleistocene—qp_{2-3}; Middle Pliocene—n_2^2; and Lower Pliocene—n_2^1); see Figure 3 (source of data: NAWAPI).

Other key factors influencing salinity dynamics are geological heterogeneity and anisotropy. Variations in hydraulic conductivity, the presence of semi-permeable aquitards, and preferential flow paths across layers may significantly influence saltwater migration patterns. These physical features, combined with anthropogenic stresses such as intensive groundwater abstraction, can alter vertical and lateral salinity gradients. In multi-aquifer systems like Ca Mau, long-term pumping can enhance inter-aquifer leakage, mobilizing deeper or trapped paleo–saline water towards abstraction zones. Consistent with this, ref. [65] demonstrated through numerical modeling that the presence of preferential flow pathways in heterogeneous aquifers significantly accelerates saltwater intrusion processes under groundwater pumping conditions, emphasizing the combined impact of geological heterogeneity and human-induced stresses.

However, a detailed quantitative assessment of individual parameters, such as the hydraulic conductivity, porosity, and geological structure, was beyond the scope of this exploratory study. In addition, due to the coarse spatial resolution of the regional-scale model, preferential flow processes were not explicitly resolved. These mechanisms are often better captured in high-resolution 2D or localized 3D models. For instance, [65] illustrated the influence of preferential flow on pumping-induced salinity intrusion using a focused modeling approach. Future research should aim to combine detailed vertical salinity analyses, parameter sensitivity assessments, and high-resolution subregional models to

better quantify the roles of aquifer heterogeneity, anisotropy, and preferential pathways in salinity dynamics across the CMP.

6.2. Model Representation and Applicability

As shown in the scatterplot (Figure 12), the modeled salinity values generally align well with the measured data. However, discrepancies are evident, particularly in the qh aquifer, where the errors are more pronounced. These deviations suggest that while the model effectively captures general trends, it does not accurately replicate localized variations in salinity. This limitation can be attributed to the scarcity of detailed observational data for the upper layer, regionalized longitudinal dispersivity parameters, and potential unknown local factors that remain beyond the scope of the current model.

Interannual variations in the TDS concentrations at observation wells are most evident for the qh aquifer. Nevertheless, even in deep aquifers (e.g., in n_2^1 at Q199 (Figure 11a)), such interannual variations are observed. In order to model these dynamics, interannually variable TDS boundary conditions were applied at selected locations in the model for the qh aquifer. Nonetheless, these dynamics in the TDS concentration did not propagate to the lower aquifers in a sufficient magnitude in the model.

To address this, the model's intent is not to focus on the detailed representation of the uppermost layer but to propose a conceptual framework. This framework leverages land use maps with varying salinity levels for the surface layer, combined with seasonal salinity variations, to simulate broader regional patterns effectively. Such an approach is a pragmatic solution for a wide-scale analysis, especially when high-resolution data are unavailable.

As highlighted by ref. [64], the distance from rivers can influence groundwater salinity, but the presence of saline water within the rivers themselves often plays a more significant role. Their study identified that areas located approximately 400–500 m from rivers exhibited groundwater salinity levels ranging from 2.8 to 3.8 g/L (4100–5500 µS/cm, with a conversion factor EC to TDS of k = 0.7). In this study, we observed similar patterns at well Q199010 in the qh aquifer, where interannual salinity levels varied between 6 and 10 g/L (Figure 9, top left). This well, located approximately 100 m from the nearest river, experiences a significant influence from the tidal system and seasonal variations, including rainy and dry periods. The modeled interannual variability in the TDS at this location (4–8 g/L, as shown by the green dashed line in Figure 11a) aligns closely with Rahman et al.'s observations, reinforcing the critical role of river proximity and tidal influences in shaping groundwater salinity dynamics.

6.3. Management Strategies and Research Priorities

Effective groundwater salinity management requires a nuanced understanding of both regional and local dynamics. In this context, Figure 15 below illustrates modeled TDS variations across selected representative wells, helping to visualize localized salinity trends across aquifers. For these wells, salinity increases when pumping induces the movement of saline water from the surrounding areas toward the well due to a steeper hydraulic gradient. Conversely, salinity decreases where freshwater inflow dominates, diluting the salinity in the pumping wells. These localized trends reflect the complexity of salinity dynamics, driven by the interplay between groundwater exploitation, hydrogeological conditions, and the spatial distribution of freshwater and saline water lenses. Field surveys further confirmed that these changes align with the influence of paleowater mixing and extraction-induced hydraulic gradients, emphasizing the need to consider ancient trapped saline water in evaluating long-term salinization risks.

Additionally, Figure 15 demonstrates that among the 1101 pumping wells in the model, salinity fluctuations—both increases and decreases—are observed at many locations, depending on local conditions. These dynamics emphasize the need for site-specific strategies to effectively manage groundwater resources in areas impacted by saltwater intrusion. Such strategies should consider localized variations and the broader regional dynamics to ensure sustainable groundwater use.

Moreover, data resolution plays a crucial role in shaping the observed salinity patterns. According to the ref. [23], salinity maps with higher point densities—such as in the qp_{2-3} aquifer—exhibited greater spatial complexity compared to deeper aquifers like n_2^1, where fewer data points were available. This suggests that some apparent homogeneity may result from data scarcity rather than actual aquifer uniformity. The report recommends acquiring at least 50 spatially distributed sampling points per aquifer for provinces with areas exceeding 5000 km^2. Implementing such monitoring strategies would enhance our ability to characterize heterogeneity and improve model reliability for groundwater salinization assessments.

Based on the criteria detailed in Section 4.2.2, the system's salinization behavior is reasonably well represented in the model from a confidence-building perspective. The calculated salinity was validated against point-measured data, with the simulated results showing a reasonable agreement in terms of magnitude and temporal evolution. This aligns with the operational aspect of model validation, i.e., "that a good, correct, or sufficient representation of reality" in time and space can be achieved with the model. Moreover, the model can be considered acceptable as it incorporates knowledge of the hydrogeological and salinity context in the CMP for its setup.

Ref. [66] obtained salinity forecasts covering the period up to 2026, focusing on a 1.5 g/L shift (below 1.5 g/L and above 1.5 g/L) in the saline boundary line in two different regions. The work described in this study presents a salinity distribution with improved detail. Due to the initialization dataset used for each aquifer, more monitoring data would be needed for a more accurate salinity forecast model. Our model indicated that the salinity movement in the deeper aquifers appeared to be slow, which is consistent with the predictions made by ref. [66].

As illustrated in the cross-section in Figure 3, the aquitard thicknesses vary significantly in the southernmost region of the MKD. This variation in thickness, along with the small number of available drilling logs upon which the layer interpolation is based, can be considered an indicator that hydrogeological windows may indeed exist in different aquitards, even though they have not yet been identified in drilling logs. This observation points to the need for further investigation into the potential salinization pathways in this area.

Building on this finding, as neither the observed TDS concentrations in the monitoring wells nor the modeled concentrations showed a significant increase in salinity during the simulation period from 2011 to 2024, it becomes evident that further potential pathways of groundwater salinization need to be evaluated. To achieve this, a sensitivity analysis of the vertical hydraulic conductivity interaction between the aquifers should be conducted to better understand the dynamics of salinity movement.

Further an investigation regarding the comparison of the TDS concentrations of monitoring wells, active production wells, and abandoned production wells is necessary to better understand the impact of pumping and well construction on the local groundwater salinity.

7. Conclusions

Building on the groundwater flow model of [12], this study developed an enhanced 3D density-dependent transport model to investigate the understanding of saltwater dynamics

and salinization processes in the CMP. The model incorporated new approaches, including the determination of longitudinal dispersivity as a function of sediment type and the inclusion of interannual salinity impacts driven by land use, infiltration from river systems, and mangrove areas.

These advancements enabled the detailed identification of high-salinity regions in aquifer qh and their influence on the salinity dynamics in qp_3 and parts of $qp_{2–3}$. The deeper aquifers predominantly contained freshwater (TDS below 1.0 g/L) with a minimal temporal variation over the analyzed timeframe (2011–2024). However, localized regions in northeast Ca Mau (Bac Lieu) exhibited higher salinity, highlighting potential pathways of salinization through hydrological windows or lateral flow.

Notably, the model results showed a fair correlation between simulated and measured salinity values across different aquifers, validating its reliability in capturing broad salinity trends. The surface salinization from various land use types significantly impacted the qh aquifer, while deeper layers did not exhibit clear top-down salinization trends during the observed period.

Although monitoring wells did not show a clear increase in salinity, the model demonstrated that, based on the analysis of production wells, localized salinity increases were evident in areas impacted by groundwater extraction.

This study confirms that land use-related salinity inputs significantly affect the shallow aquifer, while deeper aquifers remain relatively stable. Model outputs aligned with field observations, indicating the effectiveness of the approach in representing salinization trends across aquifers.

Overall, this study contributes to a nuanced understanding of salinity intrusion pathways and provides valuable insights for managing groundwater resources in regions affected by saltwater intrusion.

Author Contributions: Conceptualization, T.V.H., S.N., K.-G.R. and F.D.; methodology, T.V.H., K.-G.R., F.D. and J.B.; validation, formal analysis, and investigation, T.V.H. and K.-G.R.; resources, V.T.M.L., A.S., N.B. and S.N.; writing—original draft preparation, T.V.H. and K.-G.R.; writing—review and editing, T.V.H., F.D., K.-G.R., J.B., N.B., A.S., V.T.M.L., V.C.P., D.V.T. and S.N.; supervision, S.N.; funding acquisition, S.N.; administrator, S.N. and N.B. All authors have read and agreed to the published version of the manuscript.

Funding: This study was funded by the Karlsruhe Institute of Technology; This work is part ViWaT – Engineering project, funded by the German Ministry of Education and Research (BMBF) under grant No. 02WCL1474A; and the Catholic Academic Exchange Service (KAAD).

Data Availability Statement: The data described in this paper are available upon request to the corresponding author. A permission letter was obtained from the NAWAPI for the collection of the rainfall data, groundwater quality data, surface- and groundwater-level data, and water exploitation data.

Acknowledgments: This paper benefitted substantially from the comments and suggestions of the two anonymous reviewers. This publication was supported by the Publication Fund of the Karlsruhe Institute of Technology, the German Ministry of Education and Research (BMBF), the ViWaT Engineering research project, the Ministry of Science and Technology (MOST), and the Catholic Academic Exchange Service (KAAD). This work is was contribution to German– Vietnamese research initiative ViWaT Mekong (http://www.viwat.info/english/21.php (accessed on 25 April 2025).

Conflicts of Interest: Author Karl-Gerd Richter was employed by the company Aquantec Company for Water and Environment GmbH. The remaining authors declare that the research was conducted in the absence of any commercial or financial relationships that could be construed as a potential conflict of interest.

References

1. Ha, Q.K.; Dang, V.T.; Vo, L.P.; Dang, D.H. Integrated approaches to track saline intrusion for fresh groundwater resource protection in mekong delta. *Groundw. Sustain. Dev.* **2023**, *23*, 101046. [CrossRef]
2. Michael, H.A.; Post, V.E.A.; Wilson, A.M.; Werner, A.D. Science, society, and the coastal groundwater squeeze. *Water Resour. Res.* **2017**, *53*, 2610–2617. [CrossRef]
3. Post, V.E.A.; Groen, J.; Kooi, H.; Person, M.; Ge, S.; Edmunds, W.M. Offshore fresh groundwater reserves as a global phenomenon. *Nature* **2013**, *504*, 71–78. [CrossRef] [PubMed]
4. Werner, A.D.; Bakker, M.; Post, V.E.A.; Vandenbohede, A.; Lu, C.; Ataie-Ashtiani, B.; Simmons, C.T.; Barry, D.A. Seawater intrusion processes, investigation and management: Recent advances and future challenges. *Adv. Water Resour.* **2013**, *51*, 3–26. [CrossRef]
5. Ferguson, G.; Gleeson, T. Vulnerability of coastal aquifers to groundwater use and climate change. *Nat. Clim. Change* **2012**, *2*, 342–345. [CrossRef]
6. Minderhoud, P.S.J.; Erkens, G.; Pham, V.H.; Bui, V.T.; Erban, L.; Kooi, H.; Stouthamer, E. Impacts of 25 years of groundwater extraction on subsidence in the Mekong delta, Vietnam. *Environ. Res. Lett.* **2017**, *12*, 064006. [CrossRef]
7. Custodio, E. Coastal aquifers of Europe: An overview. *Hydrogeol. J.* **2010**, *18*, 269–280. [CrossRef]
8. UN VIETNAM. Viet Nam Drought and Saltwater Intrusion in the Mekong Delta. Joint Assessment Report. January, 15–17. 2020. Available online: https://reliefweb.int/sites/reliefweb.int/files/resources/MekongDeltaDroughandSaltwaterIntrusion_JointAssessmentReport_Feb2020.pdf (accessed on 10 June 2024).
9. Bauer, J.; Börsig, N.; Pham, V.C.; Hoan, T.V.; Nguyen, H.T.; Norra, S. Geochemistry and evolution of groundwater resources in the context of salinization and freshening in the southernmost Mekong Delta, Vietnam. *J. Hydrol. Reg. Stud.* **2022**, *40*, 101010. [CrossRef]
10. Allison, M.A.; Nittrouer, C.A.; Ogston, A.S.; Mullarney, J.C.; Nguyen, T.T. Sedimentation and survival of the Mekong delta: A case study of decreased sediment supply and accelerating rates of relative sea level rise. *Oceanography* **2017**, *30*, 98–109. [CrossRef]
11. Van Binh, D.; Kantoush, S.; Sumi, T. Changes to long-term discharge and sediment loads in the Vietnamese Mekong Delta caused by upstream dams. *Geomorphology* **2020**, *353*, 107011. [CrossRef]
12. Hoan, T.V.; Richter, K.G.; Börsig, N.; Bauer, J.; Ha, N.T.; Norra, S. An Improved Groundwater Model Framework for Aquifer Structures of the Quaternary-Formed Sediment Body in the Southernmost Parts of the Mekong Delta, Vietnam. *Hydrology* **2022**, *9*, 61. [CrossRef]
13. Vuong, B.T.; Chan, N.D.; Nam, L.H.; Bach, T.V.; Long, P.N.; Van Hung, P. Report on Construction of Model of Groundwater Flow and Models of Saline–Fresh Groundwater Interface Movement for Mekong Delta (Issue 434); 2014. Available online: https://www.researchgate.net/publication/375642932_The_Process_of_Groundwater_Salinization_on_the_Ca_Mau_Peninsula_Mekong_Delta_Vietnam_Evaluation_of_Saltwater_Intrusion_Pathways_via_Scenario_Calculations_Applying_a_3D_Groundwater_Model/fulltext/6554b793b86a1d521be6c0af/The-Process-of-Groundwater-Salinization-on-the-Ca-Mau-Peninsula-Mekong-Delta-Vietnam-Evaluation-of-Saltwater-Intrusion-Pathways-via-Scenario-Calculations-Applying-a-3D-Groundwater-Model.pdf (accessed on 10 May 2025).
14. Wagner, F.; Tran, V.B.; Renaud, F.G. Groundwater Resources in the Mekong Delta: Availability, Utilization and Risks. In *The Mekong Delta System*; Springer: Dordrecht, The Netherlands, 2012. [CrossRef]
15. Burgess, W.G.; Shamsudduha, M.; Taylor, R.G.; Zahid, A.; Ahmed, K.M.; Mukherjee, A.; Lapworth, D.J.; Bense, V.F. Terrestrial water load and groundwater fluctuation in the Bengal Basin. *Sci. Rep.* **2017**, *7*, 3872. [CrossRef] [PubMed]
16. Van Hoang, H.; Larsen, F.; Van Lam, N.; Nhan, D.D.; Luu, T.T.; Nhan, P.Q. Salt Groundwater Intrusion in the Pleistocene Aquifer in the Southern Part of the Red River Delta, Vietnam. *VNU J. Sci. Earth Environ. Sci.* **2018**, *34*, 10–22. [CrossRef]
17. Jusseret, S.; Tam, V.T.; Dassargues, A. Groundwater flow modelling in the central zone of Hanoi, Vietnam. *Hydrogeol. J.* **2009**, *17*, 915–934. [CrossRef]
18. Lam, Q.D.; Meon, G.; Pätsch, M. Coupled modelling approach to assess effects of climate change on a coastal groundwater system. *Groundw. Sustain. Dev.* **2021**, *14*, 100633. [CrossRef]
19. Minderhoud, P.S.J.; Middelkoop, H.; Erkens, G.; Stouthamer, E. Groundwater extraction may drown mega-delta: Projections of extraction-induced subsidence and elevation of the Mekong delta for the 21st century. *Environ. Res. Commun.* **2020**, *2*, 011005. [CrossRef]
20. Nam, N.D.G.; Goto, A.; Osawa, K.; Ngan, N.V.C. Modeling for analyzing effects of groundwater pumping in Can Tho city, Vietnam. *Lowl. Technol. Int.* **2019**, *21*, 33–43.
21. Harbaugh, A.W. *MODFLOW-2005, The U.S. Geological Survey Modular Ground-Water Model—the Ground-Water Flow Process MODFLOW-2005*; US Geological Survey: Reston, VI, USA, 2005. [CrossRef]

22. Pham, V.C.; Bauer, J.; Börsig, N.; Ho, J.; Vu, L.; Tran, H.; Dörr, F.; Norra, S. Groundwater Use Habits and Environmental Awareness in Ca Mau Province, Vietnam: Implications for Sustainable Water Resource Management. *Environ. Chall.* **2023**, *13*, 100742. [CrossRef]
23. Manh, L.V.; Steinel, A. *Groundwater Salinity Distribution Mapping for Ca Mau Province*; Technical Note TN-IV-03. Technical Note TN-IV-03. 'Improvement of Groundwater Protection in Vietnam (IGPVN)' Project, Hanoi, Vietnam; National Center for Water Resources Planning and Investigation (NAWAPI), Vietnam & Federal Institute for Geosciences and Natural Resources (BGR): Koblenz, Germany, 2021; p. 63.
24. Li, D.; Long, D.; Zhao, J.; Lu, H.; Hong, Y. Observed changes in flow regimes in the Mekong River basin. *J. Hydrol.* **2017**, *551*, 217–232. [CrossRef]
25. Minderhoud, P.S.J.; Coumou, L.; Erkens, G.; Middelkoop, H.; Stouthamer, E. Mekong delta much lower than previously assumed in sea-level rise impact assessments. *Nat. Commun.* **2019**, *10*, 3847. [CrossRef]
26. Pham, V.H.; Van Geer, F.C.; Bui Tran, V.; Dubelaar, W.; Oude Essink, G.H.P. Paleo-hydrogeological reconstruction of the fresh-saline groundwater distribution in the Vietnamese Mekong Delta since the late Pleistocene. *J. Hydrol. Reg. Stud.* **2019**, *23*, 100594. [CrossRef]
27. Hoanh, C.T.; Phong, N.D.; Gowing, J.W.; Tuong, T.P.; Ngoc, N.V.; Hien, N.X. Hydraulic and water quality modeling: A tool for managing land use conflicts in inland coastal zones. *Water Policy* **2009**, *11* (Suppl. S1), 106–120. [CrossRef]
28. Duong, T.D.; Vo, V.T.; Pham, M.T.; Cuong Kien, D. Dự Báo đỉnh Mặn Tại Các Trạm Đo Chính Của Tỉnh Cà Mau Bằng Mô Hình Chuỗi Thời Gian Mờ. 2016. Available online: https://ctujsvn.ctu.edu.vn/index.php/ctujsvn/article/view/2508 (accessed on 20 December 2024).
29. Le Duy, N.; Nguyen, T.V.K.; Nguyen, D.V.; Tran, A.T.; Nguyen, H.T.; Heidbüchel, I.; Merz, B.; Apel, H. Groundwater dynamics in the Vietnamese Mekong Delta: Trends, memory effects, and response times. *J. Hydrol. Reg. Stud.* **2021**, *33*, 100746. [CrossRef]
30. Doan, V.C.; Dang, D.N.; Nguyen, K.C. Formation and chemistry of the groundwater resource in the Mekong river delta, South Vietnam. *Vietnam J. Sci. Technol. Eng.* **2018**, *60*, 57–67. [CrossRef]
31. NAWAPI. *Bulletins Announcing, Forecasting and Warning Water Resources in the Mekong River Basin*; National Center for Water Resources Planning and Investigation (NAWAPI): Hanoi, Vietnam, 2024.
32. Ha, Q.K.; Tran Ngoc, T.D.; Le Vo, P.; Nguyen, H.Q.; Dang, D.H. Groundwater in Southern Vietnam: Understanding geochemical processes to better preserve the critical water resource. *Sci. Total Environ.* **2022**, *807*, 151345. [CrossRef]
33. Barcelona, M.J.; Wehrraann, H.A.; Varljen, M.D. Reproducible Well-Purging Procedures and VOC Stabilization Criteria for Ground-Water Sampling. *Groundwater* **1994**, *32*, 12–22. [CrossRef]
34. Nielsen, D.M.; Nielsen, G. *The Essential Handbook of Ground-Water Sampling*; CRC Press: Boca Raton, FL, USA, 2006. [CrossRef]
35. Gunnink, J.; Van Pham, H.; Oude Essink, G.; Bierkens, M. The 3D groundwater salinity distribution and fresh groundwater volumes in the Mekong Delta, Vietnam, inferred from geostatistical analyses. *Earth Syst. Sci. Data Discuss.* **2021**, *13*, 3297–3319. [CrossRef]
36. Cressie, N.A.C. Statistics for Spatial Data Revised edition. In *Statistics for Spatial Data*; John Wiley & Sons, Inc.: Hoboken, NJ, USA, 2015; pp. 1–900. [CrossRef]
37. DHI-WASY GmbH. FEFLOW 7.2. 2022. Available online: https://www.mikepoweredbydhi.com/products/feflow (accessed on 20 January 2025).
38. Monre. *Socialist Republic of Vietnam, Technical Regulations for Mapping Groundwater Quality, Scale 1:25,000. 08/2014/TT-BTNMT (Translated)*; Ministry of Natural Resources and Environment: Hanoi, Vietnam, 2014; pp. 20–37.
39. Wehrheim, C.; Lübken, M.; Stolpe, H.; Wichern, M. Identifying key influences on surface water quality in freshwater areas of the Vietnamese Mekong Delta from 2018 to 2020. *Water* **2023**, *15*, 1295. [CrossRef]
40. Bear, J.; Verruijt, A. Modeling Groundwater Pollution. In *Modeling Groundwater Flow and Pollution*; Springer: Dordrecht, The Netherlands, 1987; pp. 153–195. [CrossRef]
41. Grathwohl, P. Diffusion in Natural Porous Media: Contaminant Transport, Sorption/Desorption and Dissolution Kinetics. 1998. Available online: http://www.springer.com/earth+sciences+and+geography/book/978-0-7923-8102-0 (accessed on 15 January 2025).
42. Jacques, W.D. *The Handbook of Groundwater Engineering*, 2nd ed.; T. & F. Group, Ed.; CRC Press: Boca Raton, FL, USA, 2019.
43. Koch, D.L.; Brady, J.F. A Non Local Description of Advection-Diffusion With Application to Dispersion in Porous Media. *J. Fluid Mech.* **1987**, *180*, 387–403. [CrossRef]
44. Al-Tabbaa, A.; Ayotamuno, J.M.; Martin, R.J. One-dimensional solute transport in stratified sands at short travel distances. *J. Hazard. Mater.* **2000**, *73*, 1–15. [CrossRef]
45. Leij, F.J.; Van Genuchten, M.T. Approximate analytical solutions for solute transport in two-layer porous media. *Transp. Porous Media* **1995**, *18*, 65–85. [CrossRef]
46. Sternberg, S.P.K. Dispersion Measurements in Highly Heterogeneous Laboratory Scale Porous Media. *Transp. Porous Media* **2004**, *54*, 107–124. [CrossRef]

47. Zhang, X.; Wu, Y. Laboratory experiments and simulations of MTBE transport in layered heterogeneous porous media. *Environ. Earth Sci.* **2016**, *75*, 836. [CrossRef]
48. Gelhar, L.W.; Welty, C.; Rehfeldt, K.R. A critical review of data on field-scale dispersion in aquifers. *Water Resour. Res.* **1992**, *28*, 1955–1974. [CrossRef]
49. Khan, A.U.H.; Jury, W.A. A laboratory study of the dispersion scale effect in column outflow experiments. *J. Contam. Hydrol.* **1990**, *5*, 119–131. [CrossRef]
50. Guiguer, N.; Horvath, M. Enviro-Base, Waterloo hydrogeologic Inc. 2003, pp. 1–7. Available online: www.waterloohydogeologic.com (accessed on 18 September 2024).
51. Rinkel, P. Methodological Studies on Modeling Land Subsidence with the Help of Feflow Using the Example of the Ca Mau Peninsula in the Mekong Delta (Vietnam). Master's Thesis, Leibnitz Univerity Hannover, Hannover, Germany, 2022.
52. Thanh, T.N.; Huy, T.D.; Van Kenh, N.; Tung, T.T.; Quyen, P.B.; Van Hoang, N. Methodology of determining effective porosity and longitudinal dispersivity of aquifer and the application to field tracer injection test in Southern Hanoi, Vietnam. Vietnam J. *Earth Sci.* **2017**, *39*, 57–75. [CrossRef]
53. DWRPIS. *Report "Results of Experimental Water Pumping Combined Combined with Injecting Salt to BL2B."*; Internal report (in Vietnamese). Department of Water Resources Planning and Investigation South (DWRPIS): Ho Chi Minh City, Vietnam, 2021.
54. DWRPIS. *Report "Results of Experimental Water Pumping Combined Combined with Injecting Salt to BL4D."*; Internal report (in Vietnamese). Department of Water Resources Planning and Investigation South (DWRPIS): Ho Chi Minh City, Vietnam, 2021.
55. DWRPIS. *Report "Results of Experimental Water Pumping Combined Combined with Injecting Salt to BL5C."*; Internal report (in Vietnamese). Department of Water Resources Planning and Investigation South (DWRPIS): Ho Chi Minh City, Vietnam, 2021.
56. DWRPIS. *Report "Results of Experimental Water Pumping Combined Combined with Injecting Salt to CM2E."*; Internal report (in Vietnamese). Department of Water Resources Planning and Investigation South (DWRPIS): Ho Chi Minh City, Vietnam, 2021.
57. Pechstein, A.; Hanh, H.T.; Orilski, J.; Nam, L.H.; Van Manh, L.; Chi, H.; City, M. *Detailed Investigations on the Hydrogeological Situation in Ca Mau Province, Mekong Delta, Vietnam*; Technical Report No III-5 of Technical Cooperation Project "Improving groundwater protection in the Mekong Delta" (Issue December); National Center for Water Resources Planning and Investigation (NAWAPI): Hanoi, Vietnam, 2018.
58. Fitts, C.R. Groundwater Science. In *Groundwater Science*; Academic Press: Cambridge, MA, USA, 2012. [CrossRef]
59. Johnson, A.I. Compilation of Specific Yields for Various Materials—Hydrologic Properties of earth Materials. Geological Survey Water-Supply Paper 1662-D 1967; 80p. Available online: https://pubs.usgs.gov/wsp/1662d/report.pdf (accessed on 20 October 2024).
60. Fetter, C.W. *Applied Hydrogeology*, 4th ed.; Waveland Press Inc.: Long Grove, IL, USA, 2014.
61. Freeze, R.A.; Cherry, J.A. *Groundwater*; Prentice-Hall, Inc.: Hoboken, NJ, USA, 1979.
62. Davis, P.A.; Goodrich, M.T. A proposed strategy for the validation of ground-water flow and solute transport models. In Proceedings of the GEOVAL-90, Symposium on Validation of Geosphere Performance Assessment Models, Stockholm, Sweden, 14–17 May 1990; pp. 580–588.
63. Jackson, C.P.; Lever, D.A.; Sumner, P.J. Validation of transport models for use in repository performance assessments: A view illustrated for INTRAVAL test case 1b. Adv. *Water Resour.* **1992**, *15*, 33–45. [CrossRef]
64. Rahman, A.K.M.M.; Ahmed, K.M.; Butler, A.P.; Hoque, M.A. Influence of surface geology and micro-scale land use on the shallow subsurface salinity in deltaic coastal areas: A case from southwest Bangladesh. *Environ. Earth Sci.* **2018**, *77*, 423. [CrossRef]
65. Geng, X.; Michael, H.A. Preferential Flow Enhances Pumping-Induced Saltwater Intrusion in Volcanic Aquifers. *Water Resour. Res.* **2020**, *56*, e2019WR026390. [CrossRef]
66. NAWAPI. *Forecast of the Risk of Lowering Underground Water Level and Saline Intrusion in the Mekong River Basin, Period 2021–2026*; National Center for Water Resources Planning and Investigation (NAWAPI): Hanoi, Vietnam, 2021.

Disclaimer/Publisher's Note: The statements, opinions and data contained in all publications are solely those of the individual author(s) and contributor(s) and not of MDPI and/or the editor(s). MDPI and/or the editor(s) disclaim responsibility for any injury to people or property resulting from any ideas, methods, instructions or products referred to in the content.

B.4. Seawater Intrusion in River Delta Systems: Bauer et al. (2025)

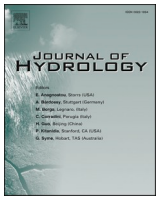
Journal of Hydrology 661 (2025) 133745



Contents lists available at ScienceDirect

Journal of Hydrology

journal homepage: www.elsevier.com/locate/jhydrol



Seawater intrusion in river delta systems. Inter-annual dynamics and drivers of salinity variations in the southern Mekong Delta, Vietnam

Jonas Bauer [a,b,*], Felix Dörr [a,b], Hoang Thai Duong Vu [c], Andreas Schenk [d], Hoan Viet Tran [a,b], Van Cam Pham [a,b], Nicolas Börsig [a], Roderick van der Linden [e], Ngoc Hoa Nguyen [f], Elisabeth Eiche [a,b], Stefan Norra [g]

[a] Karlsruhe Institute of Technology (KIT), Institute of Applied Geosciences, Karlsruhe, Germany
[b] Laboratory of Environmental and Raw Materials Analysis (LERA), Institute of Applied Geosciences, Karlsruhe, Germany
[c] Water Resources University, Ho-Chi-Minh-City, Viet Nam
[d] Karlsruhe Institute of Technology (KIT), Institute of Photogrammetry and Remote Sensing, Germany
[e] Karlsruhe Institute of Technology (KIT), Institute of Meteorology and Climate Research, Germany
[f] National Center for Hydro-Meteorological Forecasting of Vietnam, Hanoi, Viet Nam
[g] Potsdam University, Institute of Environmental Sciences and Geography, Potsdam-Golm, Germany

ARTICLE INFO

This manuscript was handled by D. Han, Editor-in-Chief, with the assistance of Ryan T. Bailey, Associate Editor

Keywords:
Seawater intrusion
Time series analysis
Hydrology of delta systems
Water management
River discharge
Land subsidence

ABSTRACT

Amidst intensifying impacts of climate change and anthropogenic pressure, seawater intrusion (SWI) emerges as a growing threat for delta systems worldwide, compromising freshwater resources and ecosystem stability. The Mekong Delta (MD) and its southernmost province Ca Mau are at the frontline of climate change impacts and anthropogenic modifications of the hydrological regime. To assess the inter-annual variability of river SWI, factors contributing to changes of the hydraulic pressure gradient between freshwater and seawater are analyzed. By utilizing long-term hydro-meteorological data from 2000 to 2022, the collective impact of catchment-scale and local-scale factors on salinity is evaluated. While salinity gradually increases by more than 10 g/L during the dry season, significant inter-annual differences of up to 15 g/L in peak salinity occur, regularly reaching and exceeding seawater salinity levels. Upstream freshwater discharge patterns were identified as major control for coastal water levels and resulting salinity levels. While climate variability governs natural upstream discharge fluctuations, dam constructions and operational responses to low-rainfall years lead to unfavorable conditions along the Mekong River, shifting and prolonging the low discharge period in the delta. This intensifies hydrological drought conditions and triggers extreme SWI events. Land subsidence of up to 2 cm per year, derived from water level records, is driving relative sea level rise and increasing the MD's vulnerability to future SWI. Mitigation strategies for SWI are examined from new perspectives, highlighting the benefits of increasing early dry-season discharge through rethought upstream reservoir operations and water storage concepts, as well as adapted local sluice gate management.

1. Introduction

Freshwater availability is a major challenge worldwide and the occurrence of regions with freshwater scarcity is rapidly increasing (Huggins et al., 2022). Coastal areas and in particular the large delta systems, inhabited by more than 500 million people worldwide, are threatened by progressive seawater intrusion (SWI) accelerated by climate change and anthropogenic interventions (Bucx et al., 2014; Nicholls et al., 2021; Rahman et al., 2019). Seawater is characterized by high concentrations of total dissolved solids with a global average concentration of 35 g/L, which in case of inland progression degrades valuable freshwater resources and ecosystems (Vengosh, 2013; White and Kaplan, 2017).

The pressure gradient between rivers and the sea defines the inland

Abbreviations: CM, Ca Mau; CMP, Ca Mau Province; GH, Ganh Hao; LDP, Low discharge period; MD, Mekong Delta; NAWAPI, National Center for Water Resources Planning and Investigation, Hanoi, Vietnam; NCHMF, National Center for Hydro-Meteorological Forecasting of Vietnam, Hanoi; RSLR, Relative sea level rise; SD, Song Doc; SIWRR, Southern Institute of Water Resources Research, Vietnam; SLR, Sea level rise; SWI, Seawater intrusion.

* Corresponding author at: Karlsruhe Institute of Technology (KIT), Institute of Applied Geosciences, Karlsruhe, Germany.
E-mail address: jonas.bauer@kit.edu (J. Bauer).

https://doi.org/10.1016/j.jhydrol.2025.133745
Received 9 January 2025; Received in revised form 14 June 2025; Accepted 20 June 2025
Available online 26 June 2025
0022-1694/© 2025 The Author(s). Published by Elsevier B.V. This is an open access article under the CC BY license (http://creativecommons.org/licenses/by/4.0/).

extent of SWI (Park et al., 2022; Savenije, 2012). For a given topographic setting, the hydraulic pressure gradient in coastal rivers originating from the sea is regulated by the seawater level, while the freshwater gradient is determined by river discharge. Within this framework, natural and human-induced factors, such as climate variability, water management infrastructure and land subsidence due to groundwater exploitation affect relative seawater levels and river discharge, thereby modifying the hydraulic pressure gradient and influencing SWI dynamics.

The Mekong River Basin and in particular the Mekong Delta (MD) in Vietnam, Southeast-Asia, was classified as a hotspot for severe freshwater stress and storage loss, and ranked amongst the highest social-ecological vulnerable regions globally (Bucx et al., 2014; Huggins et al., 2022). The region is seriously affected by numerous environmental stressors, which contribute to the progressive "loss of land and freshwater" phenomenon (Bauer et al., 2022), inevitably leading to progressive SWI. The causes for SWI are complex and cannot solely be attributed to rising sea levels (Eslami et al., 2019a). Recent studies identified several, interconnected drivers for SWI in the MD: (i) Relative sea level rise (RSLR) comprising sea level rise (SLR) due to global warming (Smajgl et al., 2015) and accelerated land subsidence rates (Erban et al., 2014; Minderhoud et al., 2020), (ii) adverse effects of upstream hydropower dam construction including variations in discharge of the Mekong River (Dang et al., 2019; Lu and Chua, 2021) as well as sediment starvation (Anthony et al., 2015; Brunier et al., 2014; Karlsrud et al., 2017; Liu et al., 2017, Jordan et al. 2020) and (iii) riverbed level incision due to sand mining (Jordan et al. 2019, Eslami et al., 2021a, 2019b; Kumar et al., 2024; Loc et al., 2021a; Park, 2024).

In the coastal areas of the monsoon-influenced MD, SWI is a natural process recurring every dry season, which spans approximately from December to April. Over decades and centuries, people have adapted to that phenomenon by integrating brackish and saltwater aquaculture into their socio-economic activities (Nguyen et al., 2019a). Recent observations of accelerated SWI, with seawater conditions in the coastal zones and brackish water extending more than 90 km upstream (Gugliotta et al., 2017; Park et al., 2022), give rise to great concerns. In the course of El Niño events in 2010, 2015–2016 and 2019–2020, the MD experienced extreme droughts and SWI conditions, which had a severe impact on livelihoods (Binh et al. 2025; Hoang-Phi et al., 2020; Park et al., 2022; Van Tho, 2022). Even though farmers have the adaptive capability to change to salt-tolerant crops or brackish aquaculture, they struggle to cope with the rapid change, and especially the large variability of conditions (Binh et al. 2025; Vu et al., 2022a). For example, SWI directly controls the rice crop calendar in the coastal zones (Ferrer et al., 2022; Hoang-Phi et al., 2020; Tri et al., 2019a) and unpredictable water quality poses a high risk for shrimp farmers (Joffre et al., 2018).

Variations in river discharge driven by factors such as climate variability and precipitation patterns, upstream reservoir management as well as water consumption by agriculture and industry impact the extent of SWI in the MD. In that regard, the occurrence of hydrological drought and SWI conditions is concurrent (Park et al., 2022). Although these drivers of SWI in the MD are widely discussed in literature (e.g. Eslami et al., 2021a), a detailed analysis of inter-annual salinity variability over an extended time period is missing. Previous studies utilized a range of modeling approaches for SWI, typically relying on short time frames of in-situ observations for calibration and validation, sometimes only encompassing a few days (Eslami et al., 2021b; Khang et al., 2008; Lam, 2020; Nhung et al., 2019; Tran et al., 2024a,c). This deficiency in long-term observational data leads to limited confidence in model performance, lacking the capability to encompass the full range of inter-annual salinity variations. Moreover, the southernmost region of the MD is underrepresented in SWI studies, and processes and dynamics there are expected to differ from those in the main estuary zone of the Mekong River.

In April 2024, Ca Mau Province (CMP), along with other regions, announced an emergency in some of its districts due to water scarcity and SWI accelerated by the 2023–2024 El Niño event (VnExpress, 2024). In the light of that event, the present study provides a comprehensive assessment of inter-annual SWI variability and aspects controlling SWI in the southernmost MD on straightforward in-situ monitoring data evaluation from 2000 to 2022. Thereby, the temporal and spatial variability of SWI is investigated in CMP. CMP was selected as the study region for SWI due to its unique geographical characteristics and socio-economic relevance. Surrounded by the sea on three sides and featuring a low topography, CMP is already characterized by a saline environment (Khang et al., 2008, Minderhoud et al., 2019a) and is at the frontline of climate change impacts, facing severe challenges from sea level rise and land subsidence. The convergence of natural and anthropogenic challenges makes CMP a valuable model region for other at-risk coastal areas (Khang et al., 2008; Minderhoud et al., 2019a).

This study incorporates supporting data, including local precipitation, river water levels, and upstream discharge time series, to systematically characterize river salinity dynamics and identify the major drivers of SWI fluctuations and their evolution in the southern MD. Particular emphasis is placed on analyzing the causes of extreme SWI events and understanding their connection to hydrological droughts, land subsidence, and upstream water management practices. Furthermore, the progression of SWI under the combined influence of natural variability and anthropogenic interventions is assessed, and novel perspectives on previously introduced mitigation strategies are critically evaluated. The methods and insights developed here are intended to support evidence-based water management and are transferable to other coastal provinces within the MD, as well as to similar deltaic regions in Southeast Asia and globally.

2. Study area

2.1. Overview

Fig. 1 shows the location of the MD and CMP as well as main features and points of interest relevant for this study. The Vietnamese MD, one of the largest river delta systems globally, and the metropolis Ho-Chi-Minh-City together are inhabited by over 27 million people (GSOV, 2024). Vietnam is the world's third-largest rice exporter, accounting for nearly 15 % of global exports, with the MD contributing up to 90 % of the country's export capacity (Huong et al., 2022; Maitah et al., 2020). The MD is characterized by a tropical monsoon climate where the rainy season lasts approximately from May to November and annual precipitation can reach up to 2500 mm/a in CMP (Dang et al., 2020; Pham-Thanh et al., 2021). The rainy season is followed by a pronounced dry season from December to April. The mean relative humidity is around 80 % throughout the year and mean monthly temperatures range between 25 °C and 30 °C (GSOV, 2024). The study area CMP, inhabited by around 1.2 million people (GSOV, 2024), is the southernmost province of the MD and is located on the Ca Mau Peninsula, which includes the neighboring provinces Bac Lieu in the northeast and Kien Giang in the north. CMP covers an area of 5,221 km^2 with an estimated average elevation below 0.8 m above mean sea level (Minderhoud et al., 2019a; Zoccarato et al., 2018). Land use dynamics in the MD, and in CMP in particular, are key factors to understand the environmental impact, economic aspects, as well as potential social conflicts of progressive SWI (Binh et al. 2025). CMP has a leading role in the agricultural sector of Vietnam, especially for shrimp farming (Nguyen et al., 2019b; Thong et al., 2010). After the land use transformation in the year 2000, high-value brackish and saline aquaculture or other cash-crops basically replaced traditional rice farming (Phan et al., 2021; Vu et al., 2022a). Depending on available freshwater resources, various farming practices exist in CMP, including shrimp permaculture or various aquaculture-rice rotation systems, and rarely two-crop rice cultivation in the protected zones like the U Minh freshwater zone (Le et al., 2018; Loc et al., 2021b; Nguyen et al., 2020).

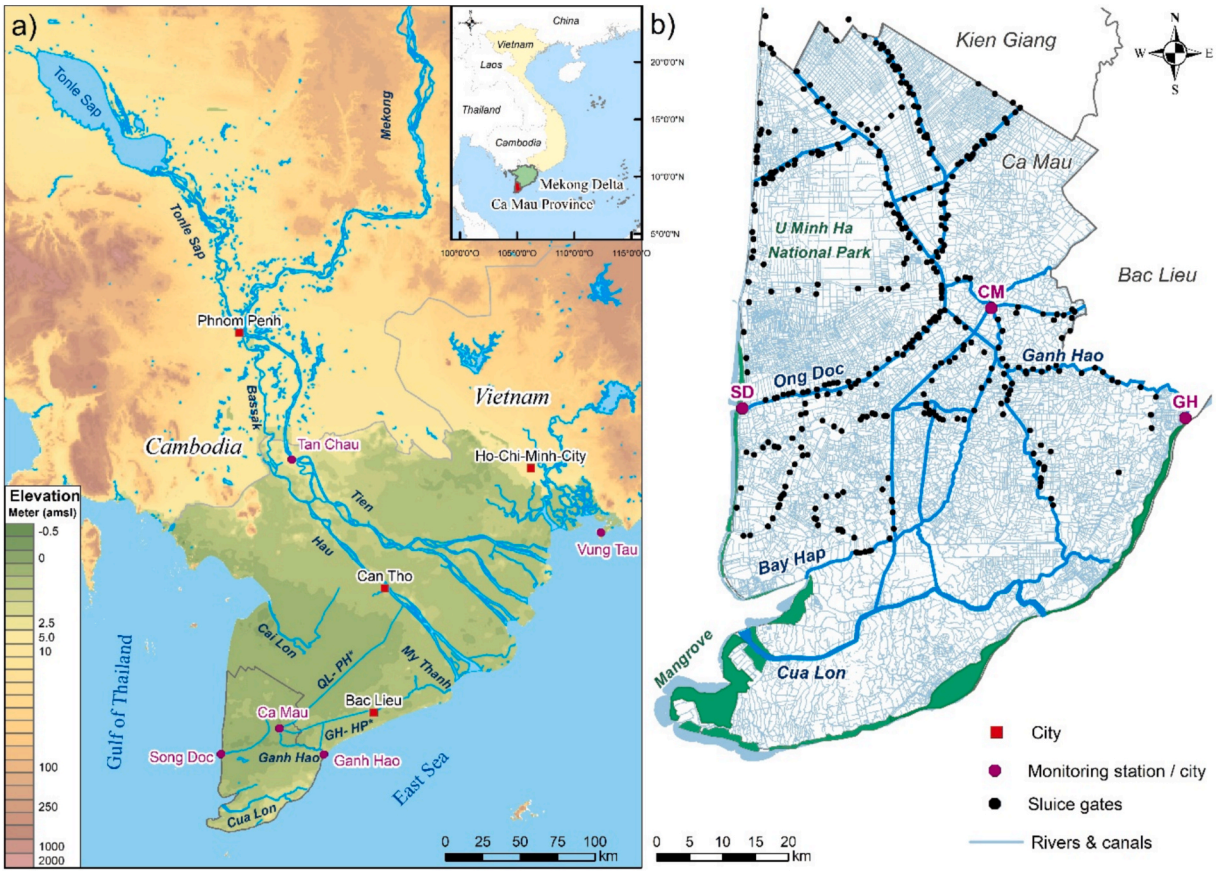


Fig. 1. a) Overview of the Mekong Delta, including points of interest for this study. *QL-PH: Quan Lo – Phung Hiep Canal. BL-CM: Bac Lieu – Ca Mau Canal. GH-HP: Ganh Hao – Ho Phong Canal. Monitoring stations are Song Doc (SD), Ca Mau (CM) and Ganh Hao (GH). Surface elevation (not linear) in the Mekong Delta by Minderhoud et al. (2019a) with a grid size of 500x500 m (Minderhoud et al., 2019b). Surface elevation outside the Mekong Delta from the Global Topographic 30 Arc-Second Digital Elevation Model GTOPO30 (EROS, 2017). b) Ca Mau Province and its hydrological infrastructure 2022 (river network data provided by the National Center for Water Resources Planning and Investigation, Vietnam (NAWAPI)).

2.2. Hydrological regime

In the Vietnamese MD, the quantity of water resources is mainly controlled by the discharge of the Mekong River (Eslami et al., 2021a; Ha et al., 2018). The Mekong River's discharge is governed by precipitation in its catchment area and is subject to significant seasonal and inter-annual variations (Mohammed et al., 2018). Precipitation in the Mekong River Basin is influenced by climate phenomena, like El Niño Southern Oscillation (ENSO) and climate change (Lee and Dang, 2018; van der Linden et al., 2016). Beginning in late April to mid-May, the discharge of the Mekong River in the middle and lower basin undergoes a gradual increase, attributed to higher precipitation rates during the summer monsoon. The peak of river water levels in the coastal zones is observed towards the end of the rainy season, typically between October and November and up to December in the southern Ca Mau Peninsula (Nguyen, 2020; Nguyen et al., 2023). With the beginning of the dry season, discharge of the Mekong River sharply decreases, whereas minimum river water levels in the delta are observed in June to July (Schwarzer et al., 2016). Since the construction of upstream dams in China, Laos and Cambodia, river discharge and seasonality have been altered significantly to ensure stable conditions for hydropower production and water availability (Ang et al., 2024). Dry-season discharge has more than doubled in Cambodia and Laos and increased by around 20 % in the Tien River in Vietnam to accommodate double and triple rice cropping in the Mekong River Basin. On the contrary, discharge is limited during the rainy season to prevent flooding of agricultural areas (Binh et al., 2021; Le Huy et al., 2021; Lu and Chua, 2021). Over 90 % of the river's discharge is directed towards the East Sea, also known as South China Sea, or used for irrigation, with less than 5 % reaching the Gulf of Thailand via the southern MD plain and the Ca Mau Peninsula (Renaud and Kuenzer, 2012).

The southern MD plain is characterized by tidal rivers and an extensive network of man-made channels, intensively utilized for transportation and irrigation purposes. Primary channels convey water from the tidal rivers into agricultural areas, while secondary channels further subdivide these networks, directly supplying water for agriculture and aquaculture. The main rivers in the study region, which particularly contribute to SWI, are Ganh Hao in the east, Ong Doc and Bay Hap in the west as well as Cua Lon, which directly connects the East Sea with the Gulf of Thailand (Fig. 1). On regional scale, the rivers My Than northeast and Cai Lon northwest of CMP in Kien Giang Province contribute to SWI in the area (Hoanh et al., 2009; Tho et al., 2006). These rivers provide water for the secondary channel systems but due to SWI and conflicting demands between freshwater rice farming and saltwater related aquaculture, water flow and quality in tributary channels is controlled by numerous sluice gates of varying size and pumping activities (Di Giusto et al., 2021; Hoanh et al., 2009; Nguyen et al., 2020). The gates and pumps are operated on seasonal or tidal scale. To provide freshwater for the saltwater zones, straight canals parallel or perpendicular to the Hau River were constructed through the Ca Mau Peninsula (Nhung et al., 2019). As soon as SWI is expected, large sluice gates, like in Ho Phong in Bac Lieu Province or the Cai Lon-Cai Be sluice in CMP, are closed, typically near the end of February (Hoanh et al., 2009). Within CMP, no large sluices control SWI in the Ong Doc and Ganh Hao rivers. On average, river depth is about 3–5 m except for Cua Lon River (5–19 m) and Ganh Hao River (5–14 m). The depth of

secondary channels and irrigation canals are generally shallower.

3. Data and methods

In the Vietnamese MD, environmental data is generally scarce, and many studies utilize the same or similar datasets on salinity, water level and discharge provided by governmental institutions to investigate various research questions. Amongst others, parts of the datasets used in this study were previously used to study flow dynamics (Eslami et al., 2019b), water level evolution and tidal characteristics (Nguyen, 2020; Phan et al., 2019), saline intrusion (Dang et al., 2019; Loc et al., 2021a; Tri, 2012), land use impacts and water quality (Minh et al., 2020; Tri et al., 2019b), as well as land subsidence (Nguyen et al., 2023;Khang et al., 2008). To comprehensively assess inter-annual salinity variability in CMP, the utilization of available models as employed in previous studies was intentionally avoided in favor of a straight-forward evaluation of in-situ monitoring data. The time series data was quality-checked, and obviously false values that fell outside reasonable ranges were removed, while decimal errors were corrected manually. These corrections affected only isolated data points and accounted for less than 1 % of the dataset. For the continuous datasets, resulting short-duration gaps were linearly interpolated. To ensure better comparability with previous studies, linear regression analysis was chosen for the trend analysis of the different time series. The figures in this article use *ColorBrewer2*-inspired color schemes (Brewer et al., 2013).

3.1. Salinity

Daily maximum salinity values from 2000 to 2022 are available for three monitoring stations in CMP and were provided by the National Center for Hydro-Meteorological Forecasting of Vietnam (NCHMF). The stations are located in Ca Mau (CM) and Ganh Hao (GH), both situated along the Ganh Hao River, approximately 40 km and 1 km from the East Sea, respectively, and Song Doc (SD), located along the Ong Doc River about 2 km from the Gulf of Thailand (Fig. 1). In the MD, the standard sampling procedure involves collecting grab samples of surface water, followed by measuring salinity concentrations using a handheld meter.

The salinity records contain data gaps of one to four days and typically cover the period from January to July, which includes the dry season when salinity levels are highest. The limited temporal coverage reflects the operational focus of monitoring for water management and SWI control, with less emphasis on long-term scientific continuity. The available records were combined into a dataset of daily maximum salinity values and are presented in Fig. 2. The highest recorded salinity occurred at SD in May 2020 with 44 g/L, followed by peak years 2016 and 2010. In contrast, salinity at CM consistently reached seawater levels in the early 2000 s, with major peaks in 2010 and 2016. No peak was observed at CM in 2020, unlike at SD. At CM, a clear pattern of increasing and decreasing salinity phases is present in most years. Similar dynamics were observed at SD in several years (e.g., 2010, 2015, 2016, and 2020), whereas in other years, such as 2017 to 2001, and more recently in 2021 and 2022, the increase was more gradual. GH, located on the eastern coast, exhibited the lowest inter-annual variability, especially in recent years where salinity measurements were more tightly clustered. The distinct seasonal salinity patterns observed at CM and SD were less pronounced at GH.

To analyze long-term trends, monthly mean values of daily maximum salinity were calculated for February, March, and April, covering the period June 2000 to May 2020. These months were selected to ensure consistent data availability and to focus on the peak dry season. Linear trends for each station and month were derived using the fitlm function in MATLAB.

3.2. Water level

Continuous 1-hourly surface water level data from the river monitoring stations SD and GH were provided by NCHMF and the National Center for Water Resources Planning and Investigation (NAWAPI). For CM, no water level data was available, as continuous measurements over the entire study period are lacking. Sand mining and dredging largely influences water levels in the Tien River (Jordan et al. 2020, Eslami et al., 2021a,), but is considered negligible for CMP due to lower extraction activity in the study area. Continuous RSLR, combining SLR and land subsidence, significantly contributes to SWI in coastal regions, including the MD (Eslami et al., 2021a; Savenije, 2012; Tran et al., 2021; Vu et al., 2018). Therefore, both factors are assessed via trend analysis.

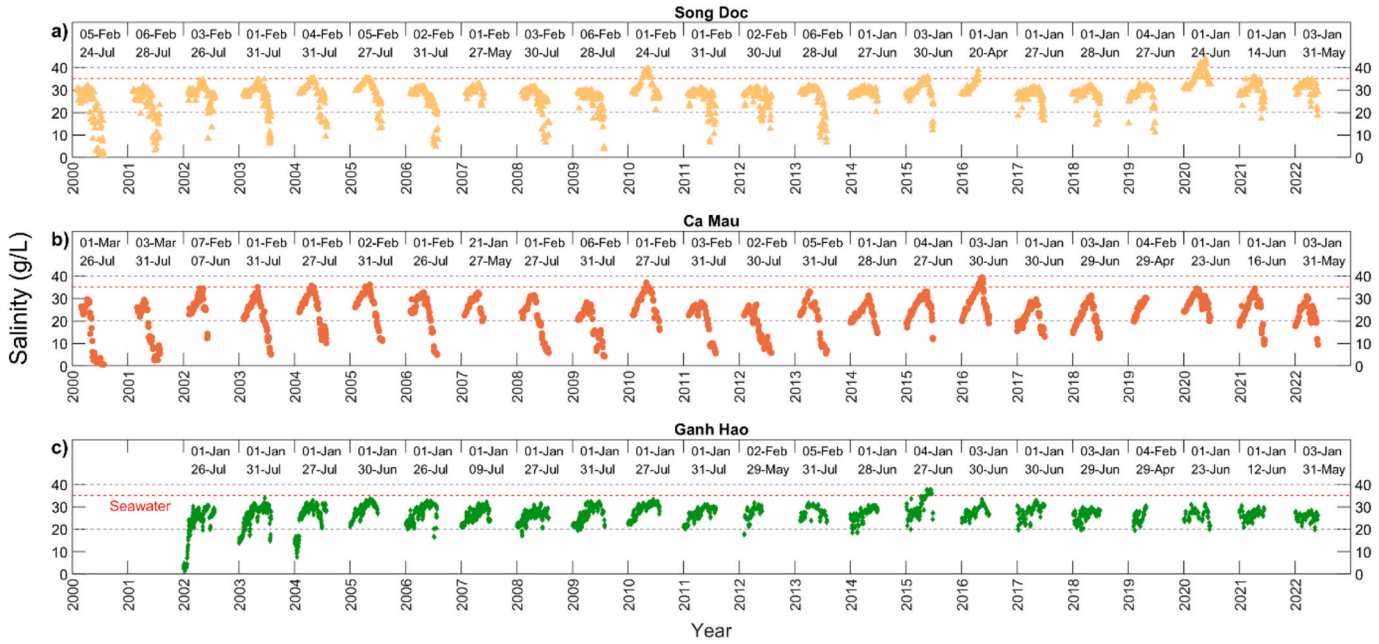


Fig. 2. Daily maximum salinity data for Song Doc, Ca Mau and Ganh Hao from 2000 to 2022. Each year's starting and ending dates are indicated above the time series. Seawater salinity is indicated by the red dashed line. (For interpretation of the references to color in this figure legend, the reader is referred to the web version of this article.)

Land subsidence is one of the most recognized threats to the MD and is locally one magnitude higher than SLR due to global warming (Dörr et al., 2024; Minderhoud, 2019). When assessing SLR by tidal gauge stations, subsidence of the station itself can be a major source of error and contributes to observed SLR at tide gauges in many coastal settings, potentially overestimating SLR (Liu et al., 2020; Saramul and Ezer, 2014). Nguyen et al. (2023) estimated subsidence rates for the time period October 1987 to September 2015 utilizing monthly averaged changes in water level records from eleven stations in the MD by comparing them with rates of SLR at the Vung Tau station, which is considered tectonically stable. At Vung Tau station a RSLR of 2.2 ± 0.3 mm/a was determined, and by subtracting the value at Vung Tau from the RSLR of 13.5 ± 0.7 mm/a in GH, a yearly subsidence of 11.3 mm was obtained. Monthly averages are commonly used in assessing SLR to reduce short-term water level fluctuations and data noise (Church and White, 2011; Kim and Cho, 2016). Therefore, monthly averages of water level data for the two periods January 2000 to December 2019 and January 2010 to December 2019 at GH and SD were used to calculate RSLR by linear regression analysis using Matlabs's *fitlm* function. These two time frames were selected to capture the pre-dam period (before 2009) and the post-dam era, marked by a sharp rise in the number of dams along the Mekong River since 2010 (Tran et al., 2021, Lu and Chua, 2021) To ensure that long-term trends are not influenced by recurring seasonal fluctuations, the data was deseasonalized by subtracting the monthly mean for each calendar month over the study period, providing a clearer identification of inter-annual variability. The resulting anomalies highlight deviations from the long-term seasonal cycle, enabling trend assessment independent of predictable seasonal patterns. Due to varying methodologies and time frames of previous SLR calculations at Vung Tau, an average value of 3.10 mm/year was derived from available studies, including Nguyen et al. (2023: 2.20 ± 0.3 mm/year, linear regression analysis of deseasonalized monthly mean sea-level data, 1987–2015), Hak et al. (2016: 3.50 mm/year, linear regression analysis of annual mean sea-level data, 1985–2010), and MONRE (2016: 3.19 mm/year, linear regression analysis of annual mean sea-level data, 1978–2014). Since land subsidence in the MD locally exceeds 30 mm/year, SLR, which is approximately one order of magnitude lower, plays only a minor role in the overall estimation of RSLR (Minderhoud et al. 2020).

The use of linear regression on deseasonalized monthly mean sea-level data provides an estimate but does not account for other causes of sea level variation, such as large-scale oceanic-atmospheric interactions, including fluctuations driven by the Pacific Decadal Oscillation and ENSO-related wind and circulation changes (Cheng et al., 2023). Nguyen et al. (2023) selected a 28-year analysis period (1987–2015) to effectively eliminate biases from the 18.6-year lunar nodal tidal cycle, which periodically affects tidal amplitudes and coastal water level records. In contrast, the 1.5-cycle timeframe was not applied in this study. Instead, a more recent period was chosen to better capture the influence of increasing subsidence rates on current RSLR estimates (Allison et al., 2017; Dunn and Minderhoud, 2022). Additionally, consistent with the salinity trend analysis, water level trends were calculated separately for the months of February, March, and April. These months represent the peak of the dry season, when water levels are low and SWI effects are most pronounced.

Tides were not explicitly considered in the analysis of inter-annual water level changes and salinity variations, as their predictable short-term fluctuations have minimal influence compared to river discharge and RSLR on longer timescales (Baranes et al., 2023; Kvale, 2006).

3.3. Upstream river discharge and water level at Tan Chau

Since discharge is not measured at the monitoring stations SD, CM, and GH, available data on seasonal streamflow variations from the Mekong River, which supplies freshwater to the delta, is instead used as a proxy. Daily mean discharge [m^3/s] and water level data at the monitoring station in Tan Chau close to the Cambodian border (Fig. 1) was provided by the Southern Institute of Water Resources Research (SIWRR) for the years 2000 to 2022. The station is located at the Tien River, which accounts for more than 80 % of the Mekonǵs annual discharge to the delta (Binh et al., 2021). The discharge of the Tien River at Tan Chau has a linear relationship with that of the parallel Hau River (Le et al., 2007). Even though discharge at Tan Chau does not directly represent discharge at the coastal stations in CMP, it serves as a good proxy for hydrological conditions in the delta. The station captures freshwater inflow before significant tidal effects and local water diversions alter streamflow conditions downstream, making it a representative site for analyzing seasonal discharge variations.

The length of the dry season is an important aspect when assessing SWI in the MD and is associated with the onset and cessation of the monsoon season. In this study, the duration of the dry season was not assessed based on precipitation but instead defined through a low discharge period (LDP). The LDP was identified when the weekly average discharge at Tan Chau station consistently exceeded or fell below a threshold of 4000 m^3/s for two consecutive weeks. To our best knowledge, no universally recognized critical discharge value for SWI in the MD exists. The 4000 m^3/s threshold represents approximately 10 % of the annual average peak flow (Binh et al. 2020) and 20 % of the average monthly discharge during the rainy season. The LDP serves as a reliable proxy for freshwater availability in the system rather than indicating a direct, short-term physical relationship between discharge at Tan Chau and salinity levels at SD, CM, and GH, given the time lag in water transport, which can be a few weeks during low flow conditions in the dry season (Birkinshaw et al., 2010; Hung et al., 2012; Le et al., 2007). As the LDP defined here typically begins between mid-January and late February and ends between late April and mid-May, it encompasses the dry season.

To compare with local surface water levels in CMP, the water level trend at Tan Chau station, which is directly related to discharge, was also calculated. The trend analysis followed the same approach as described for salinity, using linear regression on monthly averages and deseasonalized data to ensure comparability and to identify long-term changes while minimizing short-term fluctuations.

3.4. Precipitation

Daily precipitation data is available for Ca Mau City, close to the river monitoring station CM, and was provided by NCHMF. CMP receives the highest annual rainfall in the MD, reaching up to 2500 mm (Pham-Thanh et al., 2021). By choosing the optimal set of rainy season onset detection parameters, including the total rainfall amount during the initial wet spell, the number of wet days within this period, and the duration of a control period ensuring sustained wet conditions, Pham-Thanh et al. (2021) found that the onset of the rainy season is strongly controlled by local rainfall characteristics and shows significant regional correlation, with the initial wet spell being the most robust indicator. Therefore, it can be assumed that the rainy season begins simultaneously in the southern MD with a mean onset between the end of April and early May and shifts to the northeast part of the delta (Pham-Thanh et al., 2022). Precipitation from the meteorological station in Ca Mau City is thus considered sufficiently representative for the study region CMP.

4. Results

4.1. Inter-annual variability of salinity and hydrometeorological drivers

To understand the progression and severity of SWI in the southernmost MD, seasonal patterns and inter-annual salinity variations from 2000 to 2022 were analyzed in relation to local and catchment-scale hydrometeorological factors. While inter-annual differences in salinity maxima exceed 15 g/L, seasonal dynamics are characterized by gradual increase and decrease phases within each year (Fig. 2), with an abrupt

turning point at the onset of the monsoon season, when continuous rainfall and rising local discharge decrease salinity. The years that stand out in terms of low precipitation and high salinity, described previously as periods of pronounced drought and SWI (Park et al., 2022), are presented in Fig. 3. Fig. 3a-i presents daily maximum salinity for the three monitoring stations and daily precipitation from the Ca Mau meteorological station for the drought years 2010, 2016 and 2020, along with data from the preceding and following years. The average total precipitation in the dry-season months of January to April from 2000 to 2022 is 160 mm, with maximum values reaching up to 400 mm due to an early monsoon onset in April, as occurred in 2012 and 2022 (not shown). In contrast, during the dry years 2010 and 2016, total rainfall was below 10 mm (Fig. 3b, e), while in 2020, rainfall was similarly low except for a single heavy rain event with almost 80 mm in March (Fig. 3h). At the onset of the rainy season in April 2020, the salinity at CM and GH stations, situated along the Ganh Hao River, began to decrease, while the salinity at the SD station continued to rise, culminating in a peak value of 44 g/L. In 2015, salinity at GH almost reached 37.5 g/L, much higher than at the other stations, which only occurred in this particular year. In the drought years, salinity in CM is higher than at GH, but lower than at SD. In contrast, in normal and wetter-than-normal years, salinity in GH is higher than at CM or equal, like in 2011 or 2017. Single, yet strong, irregular rain events amid the dry season, like in 2009 or March 2020, momentarily halt the salinity rise, only for it to resume shortly after at a relatively steady pace.

The Mekong River's discharge significantly contributes to the adverse shift in the pressure gradient impacting SWI. Recent studies showed that SWI in the MD is co-occurring with hydrological drought conditions caused by variations in discharge of the Mekong River (Park et al. 2022). Fig. 4 shows the monthly mean discharge at Tan Chau station (see Fig. 1) and monthly maximum salinity values at the three monitoring stations in CMP (see Fig. 2). The lowest discharge between 1760 m^3/s and 2,200 m^3/s occurred in March and/or April 2004, 2005, 2007 and 2010, followed by February and March of 2020. Dry-season discharge was highest in March 2019 and 2017, with 4,621 m^3/s and 4,182 m^3/s, respectively, and in April 2022 with 5,012 m^3/s and around 4,550 m^3/s in April 2017 and 2019. For comparison, during wet years, the monthly rainy season discharge peaks between 22,000 m^3/s and nearly 25,000 m^3/s. The lowest river discharge in May was measured in the years 2003 to 2006, and 2010, ranging between 2,400 m^3/s and 2,800 m^3/s, while in more recent years 2017 to 2022 discharge is more than doubled in May compared to the pre-2010 period. The lowest discharge in June and July corresponds to the years with the highest salinity. In order of lowest discharge, these years are 2010, 2020, 2019, 2015, 2007, 2005, and 2003. Lowest discharge in December and November occurred in 2019 and 2015, prior to severe drought years 2020 and 2016, indicating the relevance of early dry season conditions.

Fig. 5 illustrates the onset, end, and duration of the LDP, defined as the annual recurring period when the weekly average discharge of the Mekong River at Tan Chau station drops below 4000 m^3/s. In addition, discharge volume during the LDP as well as total discharge volume in the early dry season for the period November to February are shown in

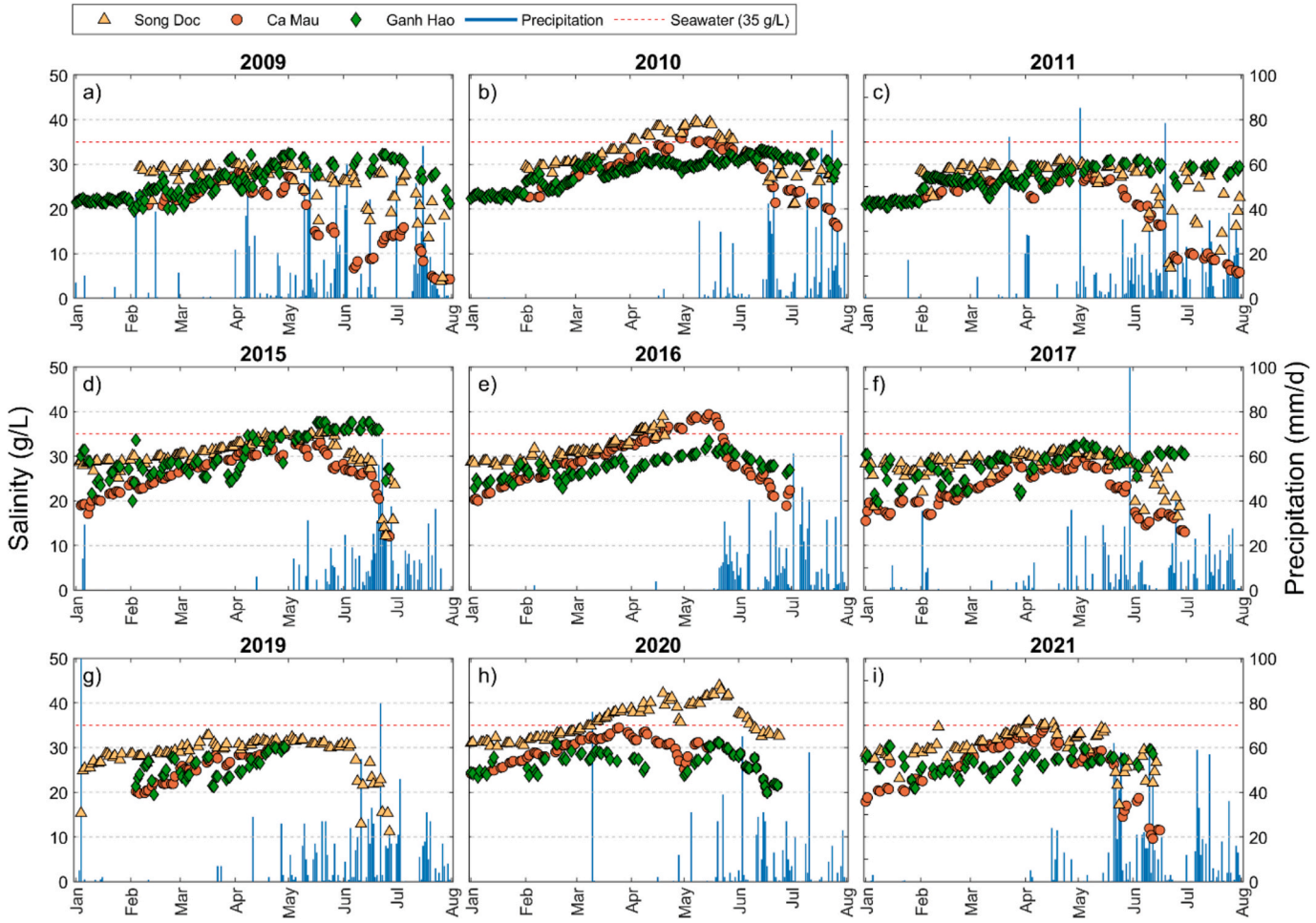


Fig. 3. Daily maximum salinity at Song Doc, Ca Mau and Ganh Hao and precipitation at the Ca Mau meteorological station between January and July in the drought years 2010, 2016 and 2020 as well as the previous and subsequent years. The red dashed line indicates seawater salinity levels with 35 g/L. (For interpretation of the references to color in this figure legend, the reader is referred to the web version of this article.)

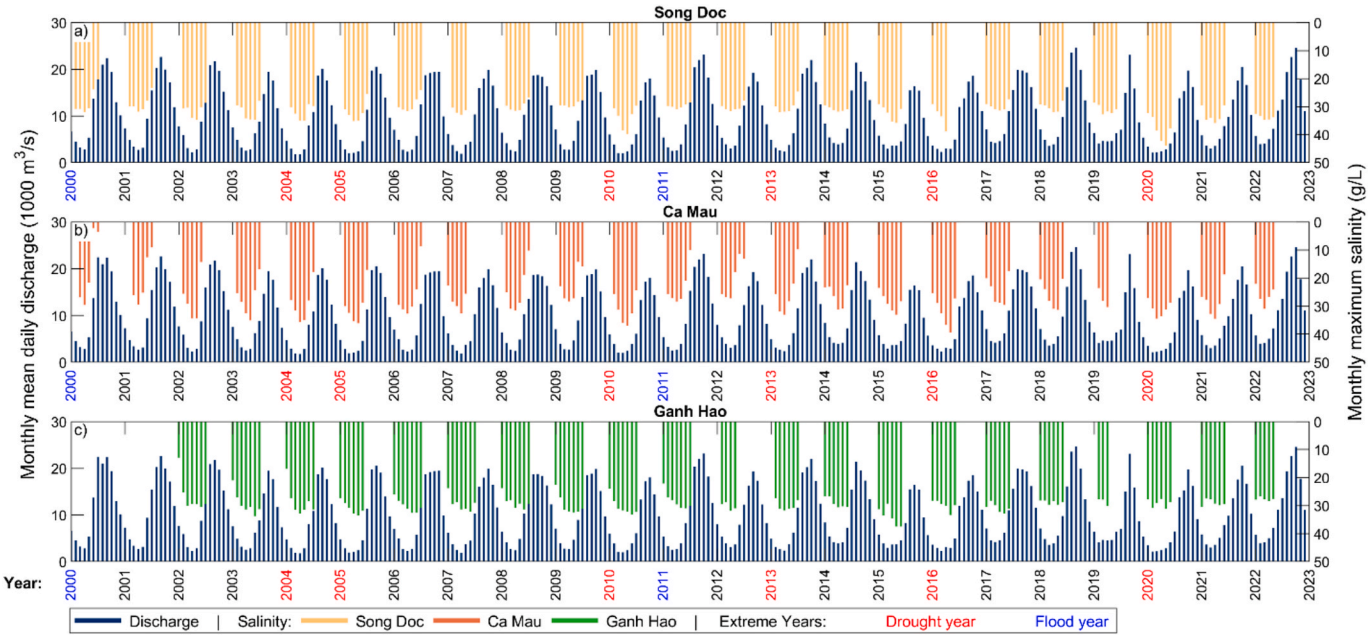


Fig. 4. Monthly mean discharge at Tan Chau station and monthly dry season maximum salinity at Song Doc, Ca Mau and Ganh Hao from 2000 to 2022 (compare Fig. 2). No salinity data are available during the rainy season. Drought and flood years are indicated (Loc et al., 2021a; Van et al., 2024).

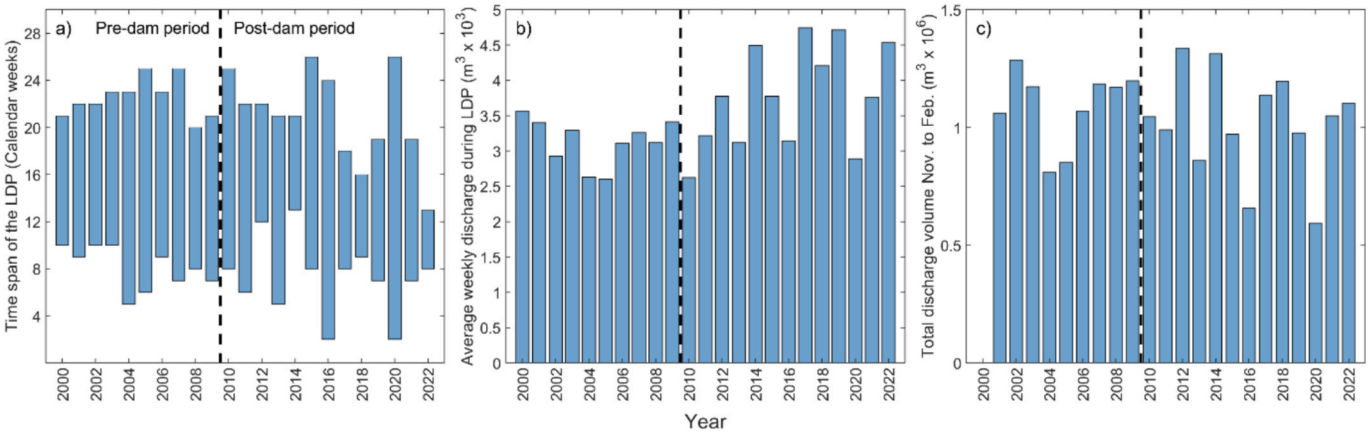


Fig. 5. Discharge patterns at Tan Chau station showing a) starting and ending calendar weeks of the low discharge period, with its duration calculated as the difference between the two, b) average weekly discharge volume during the Low discharge period, and c) total discharge volume between November and February. The black dashed line separates the pre-dam and post-dam era.

Fig. 5*b, c*. The LDP varies significantly between 2000 and 2022, ranging from a minimum of five weeks in the dry season of 2022 to a maximum of 24 weeks in 2020. In the pre-dam era, the data in Fig. 5a–c show relatively stable patterns, whereas the post-dam era is characterized by greater variability, including pronounced minima and maxima and more distinct year-to-year fluctuations. Significant earlier onsets and longer durations of the LDP were observed in 2013 and particularly in 2016 and 2020 (Fig. 5*a*), coinciding with ENSO-related low rainfall during the monsoon seasons of 2015 and 2019. Notably later onsets and earlier ends, resulting in shorter LDP durations, were also recorded in more recent years, such as 2012, 2014, 2018, and 2022, with a tendency of decreasing LDP duration in that order. Lowest average weekly discharge volume was detected in 2004, 2005 and 2010, while in extreme SWI years 2016 and 2020 discharge during the LDP is slightly higher (Fig. 5*b*). In rainy years, average discharge is significantly higher after 2013. The increase of inter-yearly discharge fluctuation is pronounced for the total discharge volume between November and February, with a decrease of discharge from 2010, 2013 to 2016 and finally 2020 (Fig. 5*c*). Although 2004 and 2005 also experienced low discharge during these months, SWI conditions were not as pronounced as in 2016 and 2020.

Fig. 6 shows the duration of the LDP and mean salinity in April, when highest salinity levels are expected, at all three stations. Fig. 6 also shows information about the maximum salinity observed in each year. In years marked by extreme mean and maximum salinity levels, such as 2010, 2016, and 2020, the LDP tends to be longer, indicating a notable relationship between extreme salinity levels and prolonged LDPs. Overall, salinity levels at SD and CM show a moderate to good Spearman correlation, with $\rho = 0.61$ and $\rho = 0.66$, respectively, while GH shows a weaker correlation with $\rho = 0.34$. In years with record low total discharge like 2004 and 2005 (Fig. 4) and a long LDP, salinity levels are high at SD and CM. In the years 2002, 2003 and 2021 salinity levels are increased despite an average LDP. Even though the LDP in 2022 is only five weeks and mean salinity is low, the maximum salinity is high at SD, but low at CM and GH. At GH, highest mean salinity level occurred in 2004, 2005 and 2010. In 2016 and 2020, salinity levels are significantly

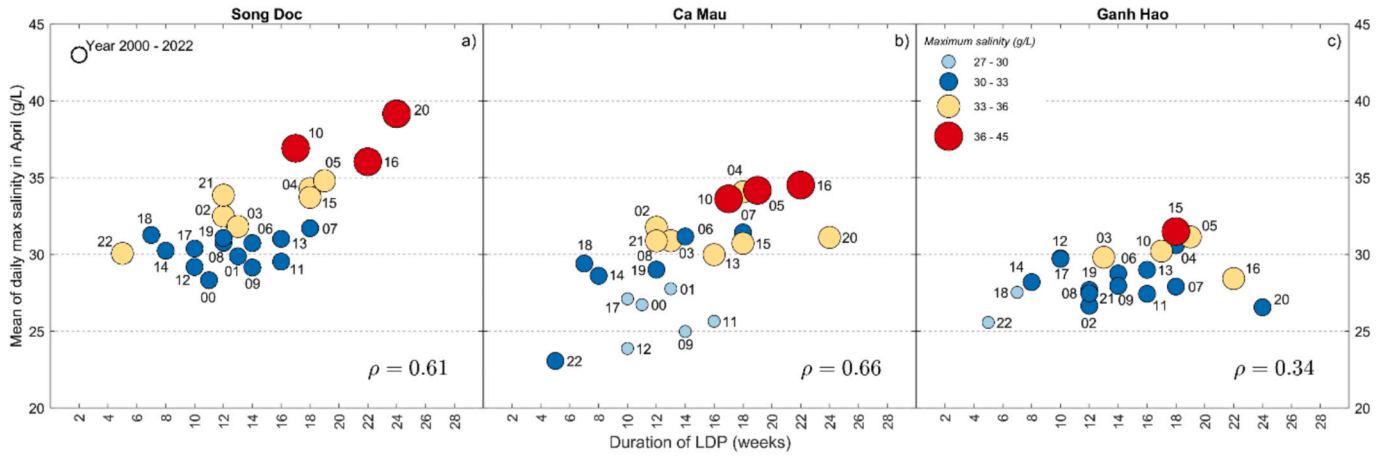


Fig. 6. Correlation (Spearman ρ) between the duration of the low discharge period (as defined in chapter 3.3) and mean of daily maximum salinity in April at Song Doc, Ca Mau and Ganh Hao for the period 2000 to 2022. Years are indicated next to the data points in two-digit format.

lower at GH than at SD and CM, despite the long LDP. The spatial differences in observed salinity levels are discussed further in Chapter 5.1.

4.2. *Trends for salinity, water level and land subsidence*

The analysis of water level trends and land subsidence rates provides valuable insights into long-term hydrological and topographic changes at Tan Chau, located 220 km inland from the river mouth, for the period January 2000 to December 2022, and at the coastal stations SD and GH from June 2000 to May 2020, with implications for salinity trends. Using linear regression on both the original and deseasonalized data, annual rates of change were calculated and are presented in Fig. 7.

At Tan Chau, the long-term trend reveals a steady decline in water levels, with an annual decrease of 2.67 cm based on the original data and 2.72 cm for the deseasonalized data. At SD and GH, the trends show an increase in water levels, with rises of 1.58 cm and 2.06 cm, respectively, for the deseasonalized data, aligning closely with the original data. In the post-dam era (2010–2019), the trends show a more pronounced increase. At SD and GH, water levels have risen at accelerating rates of 2.32 cm and 2.66 cm per year, respectively, since 2010. During the study period from 2000 to 2022, seasonal water level differences at Tan Chau ranged between 300 and 400 cm prior to 2010 (Fig. 7a). In more recent years, this range decreased significantly to below 250 cm, with the smallest seasonal variations observed in 2020 and 2021, both recording less than 100 cm. After deseasonalizing the monthly water level time series, anomalies at Tan Chau reached up to plus 150 cm in 2011 and minus 150 cm in 2020 and 2021 relative to the long-term trend (Fig. 7b). This indicates that a substantial portion of the discharge variability observed in the original water level data upon entering Vietnam is influenced by non-seasonal factors. In comparison, deviations from the trend at the coastal stations are smaller (Fig. 7d, f). Distinct anomalies with negative values in 2010, 2015, and 2016 reaching up to 9 cm, and positive values in 2000 and 2011 between 9 and 11 cm, reflect the non-seasonal influences. These account for approximately one-third to one-half of the total water level fluctuation, similar in relative magnitude to those observed at Tan Chau.

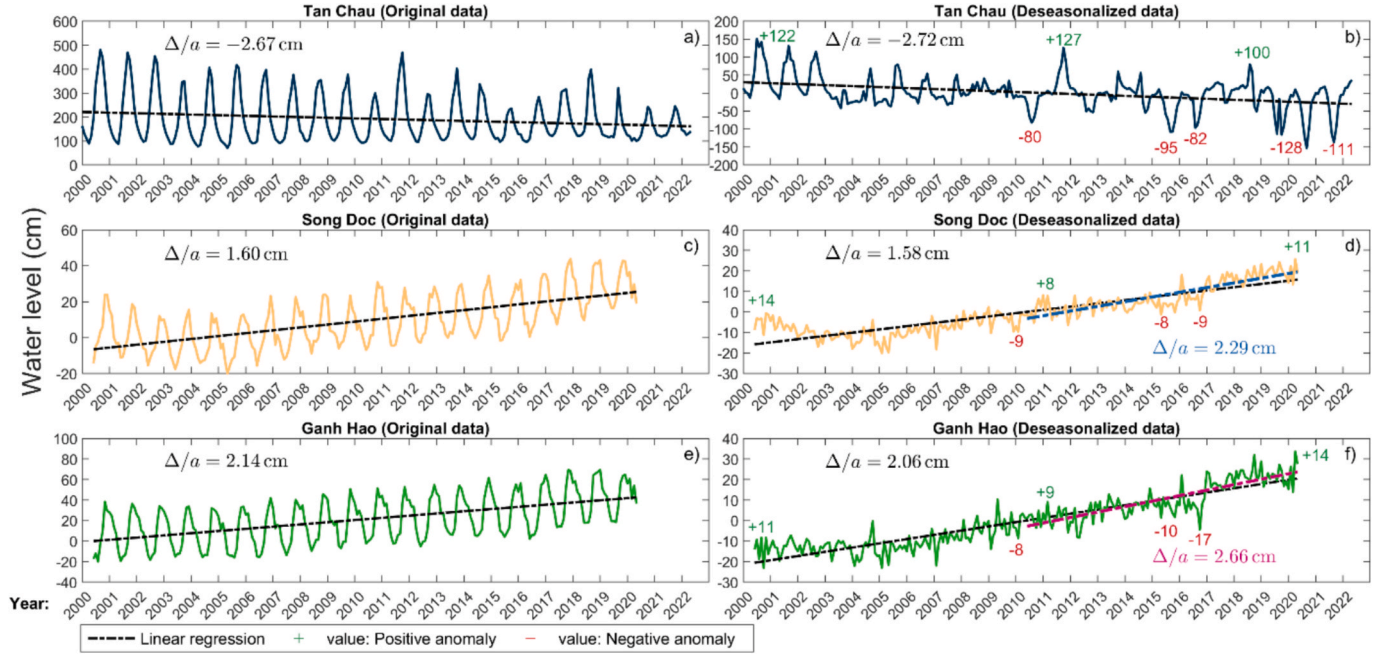


Fig. 7. Water level trend from 2000 to 2020 at the monitoring stations Tan Chau, Song Doc and Ganh Hao. Fig. 7a, c, e show the original data, while Fig. 7b, d, f) show the deseasonalized trend. Fig. 7d, f includes the trend for 2010 to 2019 at SD and GH.

Land subsidence rates were estimated by subtracting the SLR at Vung Tau (0.31 cm/a) from RSLR trends at SD and GH, following the methodology of Nguyen et al. (2023). For the period 2000 to 2019, land subsidence was calculated at 1.27 cm/a at SD and 1.75 cm/a at GH. However, during the more recent period from 2010 to 2019, this used method suggests an increase of land subsidence rates to 1.98 cm/a at SD and 2.35 cm/a at GH, reflecting more pronounced land subsidence rates in the past decade.

To evaluate long-term trends and variability in salinity in relation to water levels and their inter-annual fluctuations, Fig. 8 presents linear trends for monthly mean water levels in February, March, and April, analysed for the period 2000 to 2022 at Tan Chau and 2000 to 2020 at SD and GH. It also shows trends in monthly mean salinity, derived from daily maximum values, for the same months at CM, SD, and GH from 2000 to 2022. Notably, no water level data was available for CM. At Tan Chau, the trends diverge from the overall declining water levels shown in Fig. 7. Water levels exhibit a positive trend, increasing by 0.45 cm/a in February, 0.85 cm/a in March, and 1.75 cm/a in April. For SD, the water level trends in February and April align closely with the annual average rates of increase, while the trend in March shows a comparatively smaller rise. At GH, the increases in February and April are substantially higher than the annual trend, reaching 2.70 cm/a in February. In March, the rate of increase is significantly lower than in the previous and subsequent months. At CM, no significant salinity trend is observed for February, while a 0.09 g/L increase in March and a 0.10 g/L decrease in April are noted. For SD, salinity trends show an annual increase of 0.09 g/L in February, which rises to 0.15 g/L in March before reverting to 0.09 g/L in April. At GH, February salinity increases by 0.05 g/L, while March and April exhibit decreases of 0.03 g/L and 0.10 g/L, respectively.

5. Discussion

5.1. Dynamics and drivers of salinity variability

The inter-annual variability of salinity is of great concern for local stakeholders, governing water management and agricultural practices (Nguyen, 2017). While salinity gradually increases during every dry season, significant inter-annual differences, as shown in Fig. 2, create high uncertainty in regional conditions and, consequently, in the planning of dry-season agricultural practices, including sowing and harvest timing, crop selection, and the management of aquaculture species such as fish and shrimp. The primary factor controlling progressive SWI within many coastal and deltaic environments is the volume of freshwater contributing to river discharge at the river mouth (Pokavanich and Guo, 2024; Savenije, 2012). Naturally and anthropogenically influenced variability of river discharge persists in many large catchments worldwide, causing both periods of flood and drought (Hansford et al., 2020), and eventually SWI. In the Mekong River Basin, peak rainfall during the rainy season, which is typically highest in August and September, triggers the annual rise in water levels at Tan Chau. As the Mekong's discharge propagates downstream, peak water levels on the Ca Mau Peninsula occur between November and December (Nguyen, 2020; Nguyen et al., 2023), with a time lag ranging from one to several weeks relative to Tan Chau due to the low slope of the delta. (Fig. 4). In contrast, local rainfall in CMP provides an immediate freshwater source to counteract the seawater hydraulic gradient, as is evidenced by a pronounced drop in salinity as soon as continuous monsoon rainfall starts (Fig. 3). A time lag occurs between the onset of rainfall in the delta and the rise of discharge in the Mekong River Basin and Tan Chau, and the timing of both freshwater sources influence the salinity gradient. Within the dry season, local rainfall typically plays a minor role, as delta water levels depend mainly on upstream discharge. However, single heavy rain events, like in 2009 or March 2020, can temporarily reduce surface salinity (Fig. 3). This may result from surface dilution or short-term increases in local or upstream discharge due to regionally correlated rainfall. Since salinity is measured from surface grab samples, values at depth may remain high, and the quick return of high salinity suggests limited mixing. This underscores a methodological limitation and points to the need for follow-up studies to better understand how short-term salinity dynamics are affected by rainfall.

The inter-annual variability in water levels and corresponding upstream discharge, including both the total discharge and the timing of the LDP, directly contributes to salinity variability in the delta (Fig. 6). In particular, pronounced negative water level anomalies occurred in 2015–2016 and 2019–2020 (Fig. 7a), coinciding with salinity extremes at the monitoring sites (Fig. 2 and Fig. 4). Therefore, the non-seasonal factors contributing to discharge fluctuations are assessed. While ENSO controls much of the rainfall patterns in the Mekong River Basin and is the primary natural cause of drought and flood conditions, as seen in the monsoon seasons of 2015 and 2019 and their respective subsequent dry seasons (Apel et al., 2020; Fok et al., 2018; Xue et al., 2011), anthropogenic interventions can amplify these discharge fluctuations. This amplification in discharge fluctuations since the onset of the mega-dam era in 2010 has led to either very long or very short LDPs (Fig. 5a). Additionally, early dry-season discharge levels have become highly

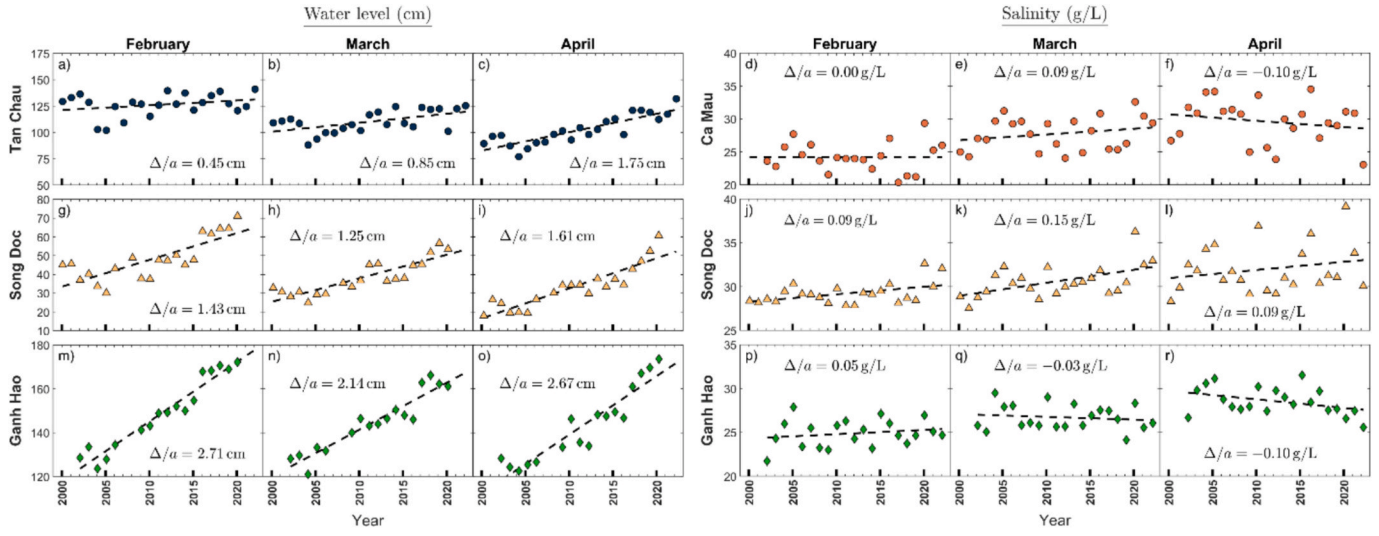


Fig. 8. (a-c, g-I, m-o) Monthly mean water level trend for February, March and April at the monitoring stations Tan Chau, Song Doc and Ganh Hao and (d-f, j-l, p-r) monthly mean salinity trend (of daily maximum values) for February, March and April at the monitoring stations Ca Mau, Song Doc and Ganh Hao.

variable, sometimes being similar to or higher than those of the pre-dam era (e.g., 2012 and 2014), and sometimes reaching unprecedentedly low discharge levels (Fig. 5a, c), promoting extreme SWI (e.g., 2016 and 2020).

Dam operation and the management of reservoirs significantly alter the yearly distribution of discharge volume to mitigate extreme floods and low flows (Binh et al., 2020; Lu and Chua, 2021). As demonstrated by trend analysis, water levels at Tan Chau are increasing in the dry season months February to April (Fig. 8), despite an overall declining trend (Fig. 7). Throughout the study period, early dry season discharge minima have declined steadily, with new record lows reached repeatedly (Fig. 5c), particularly in the post-dam era. At the same time, peaks in higher-discharge years, such as 2012, 2018, and 2022, also show a decreasing volume of early dry season discharge in that chronological order. The coastal stations SD and GH show an increasing trend in salinity in February (Fig. 8j, p), which, based on the analysis presented here, is likely attributable to reduced early dry season discharge between November and February due to upstream water management (Fig. 5c). While CM has also experienced high variability in salinity levels, the trend for February suggests a more consistent pattern (Fig. 8d). In March, the rate of salinity increase becomes significantly more pronounced at CM and SD (Fig. 8e, k). During this month, water levels at SD and GH show notably slower rates of increase compared to the preceding and following months (Fig. 8h, n). At the same time, water levels at Tan Chau continue to rise (Fig. 8b), indicating that the lower water levels at SD and GH are due to local sluice gate management rather than upstream discharge, which typically close at the end of February to prevent SWI (Hoanh et al., 2009). While sluice gates help to reduce SWI in protected zones, they can lead to higher salinity downstream (Danh et al., 2024). This effect is evident in the increased salinity levels, as numerous sluice gates were constructed along the Ganh Hao and Ong Doc Rivers to protect secondary channels from SWI, as well as in the neighbouring provinces of Kien Giang and Bac Lieu, to protect them from SWI originating in CMP. (Nguyen and Nguyen, 2023). At GH station, a slight declining trend is observed for salinity in March (Fig. 8q), which can be explained by the increased upstream discharge starting in February, gradually reaching GH through the canal network connected to the Hau River (Fig. 1), but not at SD or CM yet. In April, the increased discharge begins to affect salinity at CM as well, leading to a shift in the trend to a decline (Fig. 8f), similar to GH (Fig. 8r). However, SD continues to show increasing salinity rates (Fig. 8l), not benefiting from increased upstream discharge. The increase in salinity at SD and the decrease at CM and GH in April, as observed in the long-term trend analysis (Fig. 8f, l, r), are reflected in the 2020 case, where salinity levels at GH and CM decreased rapidly in April, while at SD, salinity continued to rise, reaching nearly 45 g/L in May (Fig. 3h). At SD, hypersaline conditions with salinity well above seawater levels of 35 g/L occurred in 2010, 2016 and 2020 (Fig. 3b, e, h). During periods of low river discharge, high temperature and low humidity conditions, accelerated in those years by El Niño episodes (Nguyen et al., 2014), elevated evaporation rates can lead to the accumulation of solutes and therefore salinity levels well above 35 g/L (Mikhailov and Isupova, 2008). At river mouths, where the monitoring stations are located, the development of a maximum salinity zone can evolve, temporarily blocking freshwater from reaching the sea (Wolanski, 1986). In addition, differences in tidal amplitude between the Gulf of Thailand and the East Sea can alter river flow direction during the dry season, potentially creating stagnant water zones in CMP when opposing forces reach equilibrium (Hoanh et al., 2009; Le et al., 2007), eventually promoting evaporation and concentration of solutes. In addition, while salinity levels are expected to decrease landwards, in the drought years of 2010, 2016, and 2020, salinity levels at the inland station CM exceeded those at the coastal station GH. Since both stations are located along the Ganh Hao River, additional processes, particularly evaporation, are likely factors contributing to this observation. Regarding observed salinity extremes, this phenomenon has not been previously documented for the MD and is typically observed in arid regions, such as the reversed estuaries in Western Africa and Australia (Mikhailov and Isupova, 2008; Wolanski, 1986). These salinity extremes are likely confined to areas near river mouths and further inland, where stratification and evaporation are more pronounced, and are not expected to extend into the Gulf of Thailand or the East Sea, where salinity levels are generally more stable and remain at or below 35 g/L (Aschariyaphotha et al., 2008; Guo et al., 2021; Limsakul et al., 2023, Zeng et al. 2018). Furthermore, complexities of salt transport, such as mixing and stratification as well as estuarine circulation might add to observed salinity conditions (Tran et al., 2024c, Eslami et al., 2021b; Geyer, 2010). However, these processes must be further investigated.

Extreme events can cause abrupt and significant impacts that may be overlooked when focusing solely on trends and gradual changes (Vogel et al., 2019). As shown in Fig. 5, years of extreme salinity share an early onset and long duration of the LDP, along with persistently low water levels and discharge at Tan Chau (Fig. 7). In 2010, 2016 and 2020, discharge remained low over the entire period from November to June (Fig. 4). The large Xiaowan and Nuozhadu reservoirs, together accounting for around 85 % of the Lancang Basin's total storage, operated normally during the 2019–2020 dry season despite low rainfall in 2019 (Vu et al., 2022b). The Lancang Basin, located in China and also referred to as the Upper Mekong River Basin, forms the upper reach of the Mekong River and contributes about 55 % of the average annual flow measured in Northern Thailand, making it a key driver of the river's hydrology. By the end of 2019, most reservoirs showed reduced storage, and it is suggested that, due to concerns over another dry year and its potential impact on hydropower production, water releases were limited (MRC, 2022), which likely contributed to an early onset of the dry season, as indicated by the LDP (Fig. 5*a*). The large reservoirs in China usually start filling up in June and July (MRC, 2022) and are refilled until the end of October (Li et al., 2017). When rainfall began in the monsoon season of 2020, reservoirs were replenished first, rapidly reaching the same storage levels as in the rainy year of 2018 (MRC, 2022), which arguably contributed to the prolongation of the LDP in the delta, resulting in extreme salinity in 2020. In addition, Lu and Chua (2021) noted that the untimely filling of the newly constructed Xayaburi dam in October 2019 in Laos had a significant influence on extreme salinity levels in the MD in the dry season of 2020 as well.

In conclusion, reduced rainfall during the preceding monsoon season results in low reservoir storage levels across the Mekong River Basin, prompting reservoir operators to prioritize reservoir replenishment at the start of the early monsoon season, thus delaying the transition from the LDP to the high discharge period. Since depleted reservoir conditions typically coincide with more intense dry seasons, the reduced early monsoon discharge caused by this management practice exacerbates SWI in the delta, as observed by Bui et al. (2023) and illustrated in Fig. 4. Furthermore, the monsoon onset has been shifting later by approximately two to four days per decade (Pham-Thanh et al., 2021) and the early monsoon period coincides with the lowest annual water levels in the delta (Hoang et al., 2019). The simultaneous occurrence of these conditions prolongs the LDP in some years (Fig. 5a) and causes extreme SWI events (Fig. 6), while in other years the increase in late dry season discharge (Fig. 5c) mitigates SWI.

Similar to the situation observed in 2019–2020, the same processes likely contributed to the severe SWI event of 2015–2016, with 2015 showing reduced rainfall due to El Niño. In the dry season of 2015 to 2016, critical SWI occurred 1.5 months earlier than usual (Nguyen, 2017). The case of the extreme SWI event in 2010 differs slightly as the preceding year 2009 was not particularly dry, but the commissioning of the large Xiaowan dam during this period may have contributed to the late end of the LDP in week 24 (Fig. 5a), and especially to the lowest average discharge recorded during the LDP in the study period, thereby promoting SWI. The Nuozhadu Dam, which has the highest capacity in the entire Mekong River Basin (5,850 MW) and the second largest reservoir volume (23,703 Mm^3), required nearly half a year to fill after

its completion in 2012 (Lu & Chua, 2021; Ang et al., 2023). This may explain the early onset of the LDP in 2013, as no climatic explanation is apparent, given that the period from May 2010 to early 2014 was dominated by La Niña conditions, typically associated with increased rainfall. Together, these examples underscore the critical role of reservoir management in controlling the hydrological regime of the Mekong River and its influence on SWI in the delta.

Another impact of water management becomes evident at the Tonle Sap Lake in Cambodia, where reduced monsoon-season discharge has led to less frequent flood pulses, which historically filled the lake (Lu and Chua, 2021). Therefore, the Tonle Sap Lake does not reach sufficient water levels necessary to discharge freshwater into the delta during the dry season, when the water level in the Mekong River should be lower than that of the lake (Arias et al., 2014; Cochrane et al., 2014; Eslami et al., 2021a). As a result, the reduced discharge from Tonle Sap Lake does not contribute to the freshwater gradient and, therefore, fails to counteract SWI. For instance, during the 2015/2016 drought event, the MD experienced extreme low peak flow and volume, which can be partly explained by the decreased inflow and outflow of the Tonle Sap Lake (MRC, 2022). Data show that the reverse flow from the Tonle Sap Lake into the Mekong River in 2010, 2015 and 2016, as well as 2020, was significantly reduced compared to historical data (MRC, 2022). On the other hand, in rainy years such as 2014, 2017 and 2018, the duration of the LDP was only between seven and ten weeks, much shorter than in the pre-dam era (Fig. 5), highlighting that upstream reservoir management can also be beneficial for SWI control. In conclusion, it appears that upstream reservoir management amplifies discharge patterns in both directions.

Overall, the data analyses indicate that the main drivers altering the hydraulic pressure gradient between freshwater and seawater in favor of SWI events are reduced rainfall in the previous year across the Mekong River Basin, combined with little to no rainfall during the affected dry season. Additionally, an early onset of the dry season and a delayed onset of the rainy season, resulting in a prolonged LDP, appear to have significantly contributed to extreme salinity levels. Finally, these drivers are strongly influenced by anthropogenic interventions, such as upstream dam operations and local sluice gate management, causing substantial inter-annual salinity variability.

5.2. Future development of seawater intrusion

As demonstrated for the locations SD and GH, land subsidence calculated through RSLR trends after Nguyen et al. (2023) amount to 1.27 cm/a and 1.75 cm/a for the period 2000 to 2019, respectively, and increasing rates of 1.98 cm/a and 2.35 cm/a in the period 2010 to 2019. The more recent subsidence rates are notable higher than previously calculated at GH (Nguyen et al., 2023) and in the same value range at SD, which was not assessed before. However, the calculated rates are consistent with recent remote sensing land subsidence studies in the area (Dörr et al., 2021, 2024). In general, continuous land subsidence substantially contributes to increased RSLR and therefore promotes increasing rates of SWI (Loc et al., 2021a; Savenije, 2012). Each successive decrease in total dry-season discharge in 2010, 2016, and 2020 led to progressively higher record salinity levels (Fig. 5), and RSLR can be considered a major factor for this observation. In the aforementioned years, the effect of RSLR could not be compensated for. In addition, after 2016, water levels at SD and GH show no negative anomalies in the long-term trend (Fig. 8d, f), not even in 2020, despite a pronounced negative discharge anomaly at Tan Chau (Fig. 8b), suggesting that land subsidence is having an increasingly significant and lasting impact on coastal water levels and, consequently, salinity. Continuous land subsidence amplifies the impact of extreme events, while extreme events can, in turn, accelerate land subsidence (Miller et al. 2020, Huning et al. 2024). The analysis conducted here suggests such a relationship for the 2016 event, though further investigation using post-2020 water level data is needed to determine whether this also applies to the 2020 event.

From this perspective, three major conclusions can be outlined:

1) To mitigate the impacts of continuous RSLR, maintaining sufficient upstream dry-season discharge in the future is crucial, as current water management practices and competing demands already limit discharge availability. As RSLR continues to increase, discharge must also be increased to balance the hydraulic forces to effectively counteract SWI.
2) The reduction of discharge in the early dry season, November to February, promotes SWI for the southernmost MD. The dry season starts notably earlier in dry years, and while dam operations during the late dry season increase discharge along the main branches of the Mekong River in the MD, these higher discharge levels do not reach CMP quickly enough, causing high SW levels. Sufficient discharge in the early dry season is crucial, which is strongly affected by upstream reservoir filling, predominantly in October (Li et al., 2017). Amongst other negative effects of upstream dams (Binh et al., 2020), altered discharge patterns caused by upstream reservoir operation apparently contribute considerably to hydrological drought and SWI events in the southernmost MD, which was previously suspected but had not been confirmed through salinity data analysis (Lu and Chua, 2021).
3) In years when upstream discharge is significantly reduced, either due to negative rainfall anomalies and/or reservoir management, an immediate salinity rebound effect must be expected, leading to gradually more severe SWI events in the upcoming years, progressively accelerated by RSLR, which is already visible in the data (Fig. 2 and Fig. 5).Overall, cumulative factors, including continuous SLR, land subsidence, a later onset of the rainy season, intensifying rainfall anomalies, rising temperatures and lastly anthropogenic interventions such as sand mining and the construction of additional upstream dams are expected to further exacerbate SWI in the MD and CMP (Allison et al., 2017; Nguyen et al., 2014; Park, 2024; Pham-Thanh et al., 2021; Phan et al., 2020; Tamura et al., 2020; Yuen et al., 2022). The delta has become increasingly vulnerable, even to mild natural events (Eslami et al., 2021b), likely due to these contributing factors that add upon each other. This vulnerability may be amplified by human-induced cascading feedback loops. For instance, reduced rainfall prompts adjustments in upstream reservoir management, as seen in 2019 affecting the 2020 dry season, and increases agricultural water demand, further worsening the initial water shortage. In conclusion, as variability increases, long-term trends become increasingly less reliable. Extreme events have a lasting impact that extends beyond its duration. For example, progressive SWI leads to the accumulation of solutes in farmland soils, which often cannot be flushed out at the same rate as they are being introduced, thereby persistently affecting soil quality adversely (Loc et al., 2021b; Tarolli et al., 2024). In addition, farmers often cannot financially compensate a year of yield loss, which might explain the high rates of outmigration in CMP, with nearly 3 % in 2010 and between 1 % and 2 % after 2018 (GSOV, 2024).

5.3. Mitigation approaches for seawater intrusion

Risks and adaptation strategies are widely discussed for many large delta systems worldwide (Cremin et al., 2023), with the MD and CMP being no exception (Gustafson et al., 2018; Karlsrud et al., 2017; Nhung et al., 2019). In summary, these measures include protective constructions such as sluice gates, seawalls and breakwaters (Danh et al., 2024; Luom et al., 2021; Vu et al., 2022c), as well as natural solutions such as mangrove reforestation and increasing the sediment budged for delta stabilization (Besset et al., 2019; Tinh et al., 2022; Veettil et al., 2021). Adaptation strategies encompass land use and crop change and the utilization of alternative water resources in the dry season, such as rainwater harvesting and storage (Loc et al., 2021b; Pham et al., 2023; Tran et al., 2024b; Vu et al., 2022a). Lastly, research often highlights the

need to reduce or stop sand mining to prevent SWI as well as groundwater overexploitation to mitigate land subsidence (Dörr et al., 2023; Eslami et al., 2019a; Kondolf et al., 2022; Loc et al., 2021a). Building on the findings and insights from this study, concepts for reducing the risk of SWI extremes in the MD can be enhanced and further developed. In particular, Binh et al. (2020) proposed an early release of water from upstream reservoirs in case of emergency. As the present study shows, an increase of early dry-season discharge would greatly benefit the MD and is crucial for CMP to reduce SWI extreme events (e.g., Fig. 5). In the long run, a managed increase of dry-season discharge is necessary in any case, as RSLR will further promote SWI. As shown here, adapted and integrated upstream water management is already reducing SWI in some years and has a large potential for overall SWI control, but mismanagement must be avoided as it triggers and enhances extreme SWI like in 2020. Therefore, storage of sufficient freshwater volumes to overcome critical episodes of water scarcity is crucial. While it is questionable if this can be achieved within the delta alone, transboundary efforts are necessary to rethink upstream reservoir operation. The results of this study suggest that restoring the Tonle Sap Lake's past capacities, as it once played a significant role in supporting dry-season discharge, especially between November and February (Pokhrel et al., 2018). The lake could serve as an optimal buffer for managing discharge variability. This would benefit not only the delta, but also the farmers and ecosystems in Cambodia, which have been struggling with decreasing water levels since major upstream dam operations began in 2010 (Sithirith, 2024). Under the current conditions, the Tonle Sap Lake does not receive enough freshwater to provide these functions (Jiang et al., 2024) and therefore engineering and infrastructure solutions are proposed to sufficiently fill the lake in the rainy season. However, the inland waterway project Funan-Techo Canal in Cambodia, intended to be finalized in 2028 and suspected to further reduce river flow into Vietnam, just recently increased tensions about water resources and environmental impact in the region (Normandin et al., 2024; Tran et al., 2024b). In addition to transboundary solutions, local efforts are necessary to cope with SWI (Tran et al., 2021). Building on previous studies (e.g., Tran et al., 2024b), which suggest that effective sluice gate management is crucial in preventing SW, especially further inland, this study provides new support for this concept from a different perspective. Analyses have shown that river system complexity and vulnerability to water flux variations shows an inverse relationship (Tejedor et al., 2015a,b). In the lower MD, the main pathways for SWI involve relatively few rivers (Fig. 1), characterizing the MD as less complex compared to many other delta systems. This inherent vulnerability, in fact, presents an opportunity for effective management and prevention of SWI by constructing well-managed sluice gates.

6. Conclusion

By combining long-term salinity, upstream discharge, and coastal water level records with a focus on inter-annual dynamics, this study developed a novel and integrated approach to assess the drivers of SWI in the MD. The use of time series analysis, including monthly dry-season trends in water level and salinity, long-term trends from both original and deseasonalized water level records (2000–2022), the introduction of the LDP concept, and the estimation of relative sea level rise proved effective in capturing both natural variability and anthropogenic influences.

The results demonstrate that SWI dynamics are primarily governed by fluctuations in the total volume and timing of upstream freshwater discharge. Non-seasonal fluctuations, driven increasingly by anthropogenic factors such as reservoir operations and flow regulation, now control a significant portion of the Mekong River's hydrological regime. This shift alters the freshwater–seawater gradient and amplifies SWI risks. At the same time, the findings show that rethought and adapted upstream water management presents a strong opportunity to mitigate SWI impacts by strategically increasing freshwater discharge early in the dry season, thereby enhancing the MD's resilience. In parallel, land subsidence continues to accelerate relative sea level rise, further exacerbating salinity intrusion. These findings reveal the cumulative impacts of multiple stressors acting across spatial and temporal scales and underscore the need for adaptive, coordinated water management strategies. The study provides new insights into the long-term vulnerability of monsoon-influenced coastal deltas to SWI. Beyond the MD, the applied approach and identified interactions offer valuable lessons for other regions where climate change, land subsidence, and upstream water use affect the freshwater–saltwater balance.

Within the MD, future work should build on these insights through integrated long-term SWI modelling. At the same time, detailed analyses of short-term salinity fluctuations in relation to tidal regimes and local water management will be essential to complete the understanding of salinity variability across all time scales. The methods applied here can also be extended to additional monitoring stations, and the relative impact of individual contributing factors should be further quantified.

Ultimately, strengthening delta resilience to future SWI challenges will require not only effective local measures but also the recognition of transboundary hydrological linkages and the integration of dynamic pressure factors into flexible responsive water governance frameworks.

Declaration of Generative AI and AI-assisted technologies in the writing process

During the preparation of this work the authors used ChatGPT in order to improve language and readability of the study. After using this tool/service, the authors reviewed and edited the content as needed and take full responsibility for the content of the publication.

CRediT authorship contribution statement

Jonas Bauer: Writing – original draft, Visualization, Methodology, Investigation, Formal analysis, Data curation, Conceptualization. **Felix Dörr:** Writing – review & editing, Methodology, Investigation, Formal analysis. **Hoang Thai Duong Vu:** Writing – review & editing. **Andreas Schenk:** Writing – review & editing, Investigation. **Hoan Viet Tran:** Writing – review & editing, Data curation. **Van Cam Pham:** Writing – review & editing. **Nicolas Börsig:** Writing – review & editing, Project administration. **Roderick van der Linden:** Writing – review & editing. **Ngoc Hoa Nguyen:** Writing – review & editing. **Elisabeth Eiche:** Writing – review & editing, Resources, Project administration. **Stefan Norra:** Writing – review & editing, Supervision, Resources, Project administration, Funding acquisition.

Declaration of competing interest

The authors declare that they have no known competing financial interests or personal relationships that could have appeared to influence the work reported in this paper.

Acknowledgments

We gratefully thank the National Center for Hydro-Meteorological Forecasting of Vietnam, the Southern Institute of Water Resources Research, the National Center for Water Resources Planning and Investigation Vietnam as well as the Department of Natural Resources and Environment Ca Mau for providing monitoring data used in this study as well as their support in the field, scientific and personal exchange. A special thanks goes to all project partners contributing to this work. This research was conducted in the frame of the project "ViWaT – Vietnam Water Technologies" funded by the German Federal Ministry of Education and Research (funding reference: 02WCL1474A). We acknowledge support by the KIT-Publication Fund of the Karlsruhe Institute of Technology, Germany.

Data availability

Data used in this study can be provided on request to NCHMF and/or NAWAPI, Hanoi, Vietnam, or by directly contacting the authors of this study, who can assist with access and facilitate contact with the aforementioned institutions.

References

Allison, M.A., Nittrouer, C.A., Ogston, A.S., Mullarney, J.C., Nguyen, T.T., 2017. Sedimentation and survival of the Mekong delta: a case study of decreased sediment supply and accelerating rates of relative sea level rise. Oceanography 30, 98–109. https://doi.org/10.5670/oceanog.2017.318.

Ang, W.J., Park, E., Pokhrel, Y., Tran, D.D., Loc, H.H., 2023, "Replication Data for: Dams in the Mekong: A comprehensive database, spatiotemporal distribution, and hydropower potentials", doi: 10.21979/N9/ACZIJN, DR-NTU (Data), V2, UNF:6:WPyeXwvCJSNeRzsfLOPd5Q== [fileUNF].

Ang, W.J., Park, E., Pokhrel, Y., Tran, D.D., Loc, H.H., 2024. Dams in the Mekong: a comprehensive database, spatiotemporal distribution, and hydropower potentials. Earth Syst. Sci. Data 16, 1209–1228. https://doi.org/10.5194/essd-16-1209-2024.

Anthony, E.J., Brunier, G., Besset, M., Goichot, M., Dussouillez, P., Nguyen, V.L., 2015. Linking rapid erosion of the Mekong River delta to human activities. Sci. Rep. 5, 1–12. https://doi.org/10.1038/srep14745.

Apel, H., Khiem, M., Hong Quan, N., Quang Toan, T., 2020. Brief communication: seasonal prediction of salinity intrusion in the Mekong Delta. Nat. Hazards Earth Syst. Sci. 20, 1609–1616. https://doi.org/10.5194/nhess-20-1609-2020.

Arias, M.E., Piman, T., Lauri, H., Cochrane, T.A., Kummu, M., 2014. Dams on Mekong tributaries as significant contributors of hydrological alterations to the Tonle Sap Floodplain in Cambodia. Hydrol. Earth Syst. Sci. 18, 5303–5315. https://doi.org/10.5194/hess-18-5303-2014.

Aschariyaphotha, N., Wongwises, P., Wongwises, S., Humphries, U.W., You, X., 2008. Simulation of seasonal circulations and thermohaline variabilities in the Gulf of Thailand. Adv. Atmos. Sci. 25 (3), 489–506. https://doi.org/10.1007/s00376-008-0489-3.

Baranes, H., Dykstra, S.L., Jay, D.A., Talke, S.A., 2023. Sea level rise and the drivers of daily water levels in the Sacramento-San Joaquin Delta. Sci. Rep. 13, 1–15. https://doi.org/10.1038/s41598-023-49204-z.

Bauer, J., Börsig, N., Pham, V.C., Hoan, T.V., Nguyen, H.T., Norra, S., 2022. Geochemistry and evolution of groundwater resources in the context of salinization and freshening in the southernmost Mekong Delta Vietnam. J. Hydrol. Reg. Stud. 40. https://doi.org/10.1016/j.ejrh.2022.101010.

Besset, M., Gratiot, N., Anthony, E.J., Bouchette, F., Goichot, M., Marchesiello, P., 2019. Mangroves and shoreline erosion in the Mekong River delta Viet Nam. Estuar. Coast. Shelf Sci. 226. https://doi.org/10.1016/j.ecss.2019.106263.

Binh, D.V., Kantoush, S.A., Saber, M., Mai, N.P., Maskey, S., Phong, D.T., Sumi, T., 2020. Long-term alterations of flow regimes of the Mekong River and adaptation strategies for the Vietnamese Mekong Delta. J. Hydrol.: Reg. Stud. 32, 100742. https://doi.org/10.1016/j.ejrh.2020.100742.

Binh, D.V., Kantoush, S.A., Sumi, T., Mai, N.P., Ngoc, T.A., Trung, L.V., An, T.D., 2021. Effects of riverbed incision on the hydrology of the Vietnamese Mekong Delta. Hydrol. Process. 35, 1–21. https://doi.org/10.1002/hyp.14030.

Binh, D.V., Tran, D.D., Thái Dương, V.H., Bauer, J., Park, E., Loc, H.H., 2025. Land use change in the Vietnamese Mekong Delta: long-term impacts of drought and salinity intrusion using satellite and monitoring data. Iscience 28 (6). https://doi.org/10.1016/j.isci.2025.112723.

Birkinshaw, S.J., O'Donnell, G.M., Moore, P., Kilsby, C.G., Fowler, H.J., Berry, P.A.M., 2010. Using satellite altimetry data to augment flow estimation techniques on the Mekong River. Hydrol. Process. 24, 3811–3825. https://doi.org/10.1002/hyp.7811.

Brewer, C.A., Harrower, M., Sheesley, B., Woodruff, A., Heyman, D., 2013. ColorBrewer 2.0. Retrieved January 30, 2015.

Brunier, G., Anthony, E.J., Goichot, M., Provansal, M., Dussouillez, P., 2014. Recent morphological changes in the Mekong and Bassac river channels, Mekong delta: the marked impact of river-bed mining and implications for delta destabilisation. Geomorphology 224, 177–191. https://doi.org/10.1016/j.geomorph.2014.07.009.

Bucx, T., van Driel, W., de Boer, H., Graas, S., Langenberg, V.T., Marchand, M., Van de Guchte, C., 2014. Comparative assessment of the vulnerability and resilience of deltas – extended version with 14 deltas - synthesis report. Delta Alliance report number 7. Delta Alliance International, Delft-Wageningen, The Netherlands.

Cheng, X., Zhao, M., Duan, W., Jiang, L., Chen, J., Yang, C., Zhou, Y., 2023. Regime shift of the sea level trend in the south china sea modulated by the tropical pacific decadal variability. Geophys. Res. Lett. 50, 1–8. https://doi.org/10.1029/2022GL102708.

Cochrane, T.A., Arias, M.E., Piman, T., 2014. Historical impact of water infrastructure on water levels of the Mekong River and the Tonle Sap system. Hydrol. Earth Syst. Sci. 18, 4529–4541. https://doi.org/10.5194/hess-18-4529-2014.

Cremin, E., O'Connor, J., Banerjee, S., Bui, L.H., Chanda, A., Hua, H.H., Van Huynh, D., Le, H., Murshed, S.B., Mashfiqus, S., Vu, A., Sebesvari, Z., Large, A., Renaud, F.G., 2023. Aligning the Global Delta Risk Index with SDG and SFDRR global frameworks to assess risk to socio-ecological systems in river deltas. Sustain. Sci. 18, 1871–1891. https://doi.org/10.1007/s11625-023-01295-3.

Dang, V.H., Tran, D.D., Cham, D.D., Hang, P.T.T., Nguyen, H.T., Truong, H.V., Tran, P. H., Duong, M.B., Nguyen, N.T., Le, K.V., Pham, T.B.T., Nguyen, A.H., 2020. Assessment of rainfall distributions and characteristics in coastal provinces of the. Water (Switzerland) 12, 1–34.

Dang, V.H., Tran, D.D., Pham, T.B.T., Khoi, D.N., Tran, P.H., Nguyen, N.T., 2019. Exploring freshwater regimes and impact factors in the coastal estuaries of the Vietnamese mekong delta. Water (Switzerland) 11, 1–17. https://doi.org/10.3390/w11040782.

Danh, V.T., Linh, D.Q., Thuy, N.T.D., 2024. Assessing impact of sluice gate operation on salinity intrusion in Ho Chi Minh City. IOP Conf. Ser.: Earth Environ. Sci 1349. https://doi.org/10.1088/1755-1315/1349/1/012028.

Di Giusto, B., Le, T.M.N., Nguyen, T.T.M., Nguyen, T.T.H., Vu, N.U.M., Lavallee, J.P., 2021. Development versus adaptation? Facing climate change in Ca Mau Vietnam. Atmosphere (Basel). 12. https://doi.org/10.3390/atmos12091160.

Dörr, N., Schenk, A., Hinz, S., 2021. Analysis of heterogeneous ps-insar derived subsidence rates using categorized gis objects - a case study in the Mekong Delta. Int. Geosci. Remote Sens. Symp. 2021-July, 2655–2658. doi: 10.1109/IGARSS47720.2021.9553297.

Dörr, N., Schenk, A., Hinz, S., 2024. Land subsidence in the mekong delta derived from advanced persistent scatterer interferometry with an infrastructural reference network. IEEE J. Sel. Top. Appl. Earth Obs. Remote Sens. 1–19. https://doi.org/10.1109/JSTARS.2024.3420130.

Dörr, F., Bauer, J., Tran, H.V., Norra, S., 2023. Vietnams Mekong-Delta - Landsenkung infolge von Grundwasserübernutzung. Forsch. | WASSERWIRTSCHAFT 64–68. (In German language).

Dunn, F.E., Minderhoud, P.S.J., 2022. Sedimentation strategies provide effective but limited mitigation of relative sea-level rise in the Mekong delta. Commun. Earth Environ. 3. https://doi.org/10.1038/s43247-021-00331-3.

Erban, L.E., Gorelick, S.M., Zebker, H.A., 2014. Groundwater extraction, land subsidence, and sea-level rise in the Mekong Delta Vietnam. Environ. Res. Lett. 9. https://doi.org/10.1088/1748-9326/9/8/084010.

EROS, 2017. Global 30 arc-second elevation (GTOPO30). U.S. Geological Survey. [WWW Document]. Earth Resour. Obs. Sci. Cent. https://doi.org/10.5066/F7DF6PQS.

Eslami, S., Hoekstra, P., Nguyen Trung, N., Ahmed Kantoush, S., Van Binh, D., Duc Dung, D., Tran Quang, T., van der Vegt, M., 2019a. Tidal amplification and salt intrusion in the Mekong Delta driven by anthropogenic sediment starvation. Sci. Rep. 9, 1–10. https://doi.org/10.1038/s41598-019-55018-9.

Eslami, S., Hoekstra, P., Kernkamp, H., Trung, N.N., Do Duc, D., Quang, T.T., Februarianto, M., Van Dam, A., van der Vegt, M., 2019b. Flow division dynamics in the Mekong Delta: Application of a 1D-2D coupled model. Water (Switzerland) 11, 1–25. https://doi.org/10.3390/w11040837.

Eslami, S., Hoekstra, P., Minderhoud, P.S.J., Trung, N.N., Hoch, J.M., Sutanudjaja, E.H., Dung, D.D., Tho, T.Q., Voepel, H.E., Woillez, M.-N., van der Vegt, M., 2021a. Projections of salt intrusion in a mega-delta under climatic and anthropogenic stressors. Commun. Earth Environ. 2, 1–11. https://doi.org/10.1038/s43247-021-00208-5.

Eslami, S., Hoekstra, P., Kernkamp, H.W.J., Nguyen Trung, N., Do Duc, D., Nguyen Nghia, H., Tran Quang, T., Van Dam, A., Darby, S.E., Parsons, D.R., Vasilopoulos, G., Braat, L., Van Der Vegt, M., 2021b. Dynamics of salt intrusion in the Mekong Delta: results of field observations and integrated coastal-inland modelling. Earth Surf. Dyn. 9, 953–976. https://doi.org/10.5194/esurf-9-953-2021.

Ferrer, A.J.G., Thanh, L.H., Kiet, N.T., Chuong, P.H., Trang, V.T., Hopanda, J.C., Carmelita, B.M., Gummadi, S., Bernardo, E.B., 2022. The impact of an adjusted cropping calendar on the welfare of rice farming households in the Mekong River Delta Vietnam. Econ. Anal. Policy 73, 639–652. https://doi.org/10.1016/j.eap.2021.12.018.

Fok, H.S., He, Q., Chun, K.P., Zhou, Z., Chu, T., 2018. Application of ENSO and drought indices for water level reconstruction and prediction: a case study in the lower Mekong River estuary. Water (Switzerland) 10. https://doi.org/10.3390/w10010058.

Geyer, W.R., 2010. Estuarine salinity structure and circulation. In: Valle-Levinson, A. (Ed.), Contemporary Issues in Estuarine Physics. Cambridge University Press, pp. 12–26.

GSOV, 2024. General Statistics Office of Vietnam, URL (10.2024): https://www.gso.gov.vn/en/homepage/.

Gugliotta, M., Saito, Y., Nguyen, V.L., Ta, T.K.O., Nakashima, R., Tamura, T., Uehara, K., Katsuki, K., Yamamoto, S., 2017. Process regime, salinity, morphological, and sedimentary trends along the fluvial to marine transition zone of the mixed-energy Mekong River delta Vietnam. Cont. Shelf Res. 147, 7–26. https://doi.org/10.1016/j.csr.2017.03.001.

Guo, J., Qu, D., Zhang, Z., Sangmanee, C., Chanthasiri, N., Guo, B., 2021. Thermohaline conditions and circulation in the Gulf of Thailand during the northeast monsoon. Cont. Shelf Res. 225 (June), 104487. https://doi.org/10.1016/j.csr.2021.104487.

Gustafson, S., Cadena, A.J., Hartman, P., 2018. Adaptation planning in the lower Mekong Basin: merging scientific data with local perspective to improve community resilience to climate change. Clim. Dev. 10, 152–166. https://doi.org/10.1080/17565529.2016.1223593.

Ha, T.P., Dieperink, C., Dang Tri, V.P., Otter, H.S., Hoekstra, P., 2018. Governance conditions for adaptive freshwater management in the Vietnamese Mekong Delta. J. Hydrol. 557, 116–127. https://doi.org/10.1016/j.jhydrol.2017.12.024.

Hak, D., Nadaoka, K., Patrick Bernado, L., Le Phu, V., Hong Quan, N., Quang Toan, T., Hieu Trung, N., Van Ni, D., Tri, P.D., 2016. Spatio-temporal variations of sea level around the Mekong Delta: their causes and consequences on the coastal environment. Hydrol. Res. Lett. 10, 60–66. https://doi.org/10.3178/hrl.10.60.

Hansford, M.R., Plink-Björklund, P., Jones, E.R., 2020. Global quantitative analyses of river discharge variability and hydrograph shape with respect to climate types. Earth-Science Rev. 200, 102977. https://doi.org/10.1016/j.earscirev.2019.102977.

Hoang-Phi, P., Lam-Dao, N., Pham-Van, C., Chau-Nguyen-xuan, Q., Nguyen-Van-anh, V., Gummadi, S., Le-Van, T., 2020. Sentinel-1 SAR time series-based assessment of the impact of severe salinity intrusion events on spatiotemporal changes in distribution

of rice planting areas in coastal provinces of the mekong delta. Vietnam. Remote Sens. 12, 1–21. https://doi.org/10.3390/rs12193196.
Hoang, L.P., van Vliet, M.T.H., Kummu, M., Lauri, H., Koponen, J., Supit, I., Leemans, R., Kabat, P., Ludwig, F., 2019. The Mekong's future flows under multiple drivers: how climate change, hydropower developments and irrigation expansions drive hydrological changes. Sci. Total Environ. 649, 601–609. https://doi.org/10.1016/j.scitotenv.2018.08.160.
Hoanh, C.T., Phong, N.D., Gowing, J.W., Tuong, T.P., Ngoc, N.V., Hien, N.X., 2009. Hydraulic and water quality modeling: a tool for managing land use conflicts in inland coastal zones. Water Policy 11, 106–120. https://doi.org/10.2166/wp.2009.107.
Hung, N.N., Delgado, J.M., Tri, V.K., Hung, L.M., Merz, B., Bárdossy, A., Apel, H., 2012. Floodplain hydrology of the mekong delta. Vietnam. Hydrol. Process. 26, 674–686. https://doi.org/10.1002/hyp.8183.
Huning, L.S., Love, C.A., Anjileli, H., Vahedifard, F., Zhao, Y., Chaffe, P.L.B., Cooper, K., Alborzi, A., Pleitez, E., Martinez, A., Ashraf, S., Mallakpour, I., Moftakhari, H., AghaKouchak, A., 2024. Global land subsidence: impact of climate extremes and human activities. Rev. Geophys. 62, 1–22. https://doi.org/10.1029/2023RG000817.
Huggins, X., Gleeson, T., Kummu, M., Zipper, S.C., Wada, Y., Troy, T.J., Famiglietti, J.S., 2022. Hotspots for social and ecological impacts from freshwater stress and storage loss. Nat. Commun. 13. https://doi.org/10.1038/s41467-022-28029-w.
Huong, D.T.T., Dieu, P.Q., Anh, D.T., 2022. Market Structure of Rice Export in Vietnam from 2010 to 2020. https://ap.fftc.org.tw/article/2985.
Jiang, W., Dai, Z., Mei, X., Long, C., Binh, N.A., Van, C.M., Cheng, J., 2024. Profiling dynamics of the Southeast Asia's largest lake. Tonle Sap Lake. Sci. Total Environ. 917, 170444. https://doi.org/10.1016/j.scitotenv.2024.170444.
Jordan, C., Tiede, J., Lojek, O., Visscher, J., Apel, H., Nguyen, H.Q., Quang, C.N.X., Schlurmann, T., 2019. Sand mining in the Mekong Delta revisited - current scales of local sediment deficits. Sci. Rep. 9, 1–14. https://doi.org/10.1038/s41598-019-53804-z.
Jordan, C., Visscher, J., Dung, N.V., Apel, H., Schlurmann, T., 2020. Impacts of human activity and global changes on future morphodynamics within the tien river, vietnamese mekong delta. Water (Switzerland) 12. https://doi.org/10.3390/w12082204.
Joffre, O.M., Poortvliet, P.M., Klerkx, L., 2018. Are shrimp farmers actual gamblers? An analysis of risk perception and risk management behaviors among shrimp farmers in the Mekong Delta. Aquaculture 495, 528–537. https://doi.org/10.1016/j.aquaculture.2018.06.012.
Karlsrud, K., Vangelsten, B.V., Frauenfelder, R., 2017. Subsidence and shoreline retreat in the Ca Mau Province - Vietnam causes, consequences and mitigation options. Geotech. Eng. 48, 26–32.
Khang, N.D., Kotera, A., Sakamoto, T., Yokozawa, M., 2008. Sensitivity of salinity intrusion to sea level rise and river flow change in vietnamese mekong delta-impacts on availability of irrigation water for rice cropping. J. Agric. Meteorol. 64, 167–176. https://doi.org/10.2480/agrmet.64.3.4.
Kondolf, G.M., Schmitt, R.J.P., Carling, P.A., Goichot, M., Keskinen, M., Arias, M.E., Bizzi, S., Castelletti, A., Cochrane, T.A., Darby, S.E., Kummu, M., Minderhoud, P.S.J., Nguyen, D., Nguyen, H.T., Nguyen, N.T., Oeurng, C., Opperman, J., Rubin, Z., San, D.C., Schmeier, S., Wild, T., 2022. Save the Mekong Delta from drowning. Science 376, 583–585. https://doi.org/10.1126/science.abm5176.
Kumar, S., Park, E., Tran, D.D., Wang, J., Ho, H.L., Kantoush, S.A., Binh, D.V., Li, D., Switzer, A.D., Kumar, S., Park, E., Tran, D.D., Wang, J., Ho, H.L., 2024. A deep learning framework to map riverbed sand mining budgets in large tropical deltas. Giscience Remote Sens. 61. https://doi.org/10.1080/15481603.2023.2285178.
Kvale, E.P., 2006. The origin of neap-spring tidal cycles. Mar. Geol. 235, 5–18. https://doi.org/10.1016/j.margeo.2006.10.001.
Lam, N.T., 2020. Real-Time Prediction of Salinity in the Mekong River Delta. In: Trung Viet, N., Xiping, D., Thanh Tung, T. (Eds.), APAC 2019. Springer Singapore, Singapore, pp. 1461–1468.
Le, A.T., Chu, T.H., Miller, F., Bach, T.S., 2007. Flood and salinity management in the Mekong Delta. Challenges to Sustain. Dev. Mekong Delta Reg. Natl. policy issues Res. needs Lit. Anal. 15–168.
Le Huy, B., Le, H., Xuan, H.N., 2021. The harmful of the hydroelectric dams in Mekong River upstream on the ecosystems and livelihoods in the Mekong Delta Vietnam. Water Conserv. Manag. 5, 35–45. https://doi.org/10.26480/wcm.01.2021.35.45.
Le, T.N., Bregt, A.K., van Halsema, G.E., Hellegers, P.J.G.J., Nguyen, L.D., 2018. Interplay between land-use dynamics and changes in hydrological regime in the Vietnamese Mekong Delta. Land Use Policy 73, 269–280. https://doi.org/10.1016/j.landusepol.2018.01.030.
Lee, S.K., Dang, T., 2018. Evaluating drought events under influence of El-nino phenomenon: a case study of mekong delta area Vietnam. J. Agrometeorol. 20, 275–279.
Li, D., Long, D., Zhao, J., Lu, H., Hong, Y., 2017. Observed changes in flow regimes in the Mekong River basin. J. Hydrol. 551, 217–232. https://doi.org/10.1016/j.jhydrol.2017.05.061.
Limsakul, A., Kammuang, A., Paengkaew, W., Sooktawee, S., Aroonchan, N., 2023. Changes in slow-onset climate events in Thailand. Environ. Eng. Re. 29 (1), 220784. https://doi.org/10.4491/eer.2022.784.
Liu, J.P., De Master, D.J., Nguyen, T.T., Saito, Y., Nguyen, V.L., Ta, T.K.O., Li, X., 2017. Stratigraphic formation of the Mekong river delta and its recent shoreline changes. Oceanography 30, 72–83. https://doi.org/10.5670/oceanog.2017.316.
Liu, Y., Li, J., Fasullo, J., Galloway, D.L., 2020. Land subsidence contributions to relative sea level rise at tide gauge Galveston Pier 21. Texas. Sci. Rep. 10. https://doi.org/10.1038/s41598-020-74696-4.
Loc, H.H., Van Binh, D., Park, E., Shrestha, S., Dung, T.D., Son, V.H., Truc, N.H.T., Mai, N.P., Seijger, C., 2021a. Intensifying saline water intrusion and drought in the Mekong Delta: from physical evidence to policy outlooks. Sci. Total Environ. 757, 143919. https://doi.org/10.1016/j.scitotenv.2020.143919.
Loc, H.H., Low Lixian, M., Park, E., Dung, T.D., Shrestha, S., Yoon, Y.J., 2021b. How the saline water intrusion has reshaped the agricultural landscape of the Vietnamese Mekong Delta, a review. Sci. Total Environ. 794, 148651. https://doi.org/10.1016/j.scitotenv.2021.148651.
Lu, X.X., Chua, S.D.X., 2021. River discharge and water level changes in the mekong river: droughts in an era of mega-dams. Hydrol. Process. 35, 1–19. https://doi.org/10.1002/hyp.14265.
Luom, T.T., Phong, N.T., Anh, N.T., Tung, N.T., Tu, L.X., Duong, T.A., 2021. Using fine-grained sediment and wave attenuation as a new measure for evaluating the efficacy of offshore breakwaters in stabilizing an eroded muddy coast: Insights from ca mau, the mekong delta of vietnam. Sustain. 13. https://doi.org/10.3390/su13094798.
Maitah, K., Smutka, L., Sahatqija, J., Maitah, M., Anh, N.P., 2020. Rice as a determinant of Vietnamese economic sustainability. Sustainability (Switzerland) 12 (12), 1–12. https://doi.org/10.3390/su12125123.
Mikhailov, V.N., Isupova, M.V., 2008. Hypersalinization of river estuaries in West Africa. Water Resour. 35, 367–385. https://doi.org/10.1134/S0097807808040015.
Miller, M.M., Jones, C.E., Sangha, S.S., Bekaert, D.P., 2020. Rapid drought-induced land subsidence and its impact on the California aqueduct. Remote Sens. Environ. 251, 112063. https://doi.org/10.1016/j.rse.2020.112063.
Minderhoud, P.S.J., 2019. The sinking mega-delta; Present and future subsidence of the Vietnamese Mekong delta. Utrecht Studies in Earth Sciences (ISSN: 2211-4335).
Minderhoud, P.S.J., Coumou, L., Erkens, G., Middelkoop, H., Stouthamer, E., 2019a. Mekong delta much lower than previously assumed in sea-level rise impact assessments. Nat. Commun. 10, 1–13. https://doi.org/10.1038/s41467-019-11602-1.
Minderhoud, Philip S.J., Coumou, L., Erkens, G., Middelkoop, H., Stouthamer, E., 2019. Digital elevation model of the Vietnamese Mekong delta based on elevation points from a national topographical map. doi: 10.1594/PANGAEA.902136.
Minderhoud, P.S.J., Middelkoop, H., Erkens, G., Stouthamer, E., 2020. Groundwater extraction may drown mega-delta: projections of extraction-induced subsidence and elevation of the Mekong delta for the 21st century. Environ. Res. Commun. 2, 011005. https://doi.org/10.1088/2515-7620/ab5e21.
Minh, H.V.T., Avtar, R., Kumar, P., Le, K.N., Kurasaki, M., Van Ty, T., 2020. Impact of rice intensification and urbanization on surface water quality in an giang using a statistical approach. Water (Switzerland) 12, 1–18. https://doi.org/10.3390/W12061710.
Mohammed, I.N., Bolten, J.D., Srinivasan, R., Lakshmi, V., 2018. Satellite observations and modeling to understand the lower Mekong River Basin streamflow variability. J. Hydrol. 564, 559–573. https://doi.org/10.1016/j.jhydrol.2018.07.030.
Ministry of Natural Resources and Environment (MONRE), 2016. Climate Change and Sea Level Rise Scenarios. Science (80-). 294, 1379–1388.
Mekong River Comission (MRC), 2022. Mekong Low Flow and Drought Conditions in2019 - 2021. Hydrological conditions in the Lower Mekong River Basin.
Nguyen, D.Q., Renwick, J., Mcgregor, J., 2014. Variations of surface temperature and rainfall in Vietnam from 1971 to 2010. Int. J. Climatol. 34, 249–264. https://doi.org/10.1002/joc.3684.
Nguyen, M.T., Renaud, F.G., Sebesvari, Z., 2019a. Drivers of change and adaptation pathways of agricultural systems facing increased salinity intrusion in coastal areas of the Mekong and Red River deltas in Vietnam. Environ. Sci. Policy 92, 331–348. https://doi.org/10.1016/j.envsci.2018.10.016.
Nguyen, T.H.O., Tran, T.T.K., Nguyen, C.T.H., 2019b. Shrimp yield in relation to the ecological parameters of an organic shrimp model in the mekong delta of Vietnam: a case study. Asian Fish. Sci. 32, 154–161. https://doi.org/10.33997/j.afs.2019.32.4.003.
Nguyen, N.A., 2017. Historic drought and salinity intrusion in the Mekong Delta in 2016: lessons learned and response solutions Vietnam. J. Sci. Technol. 1, 2015–2018.
Nguyen, Q.H., Tran, D.D., Dang, K.K., Korbee, D., Pham, L.D.M.H., Vu, L.T., Luu, T.T., Ho, L.H., Nguyen, P.T., Trang, T.T., Nguyen, D.T.K., Wyatt, A., van Aalst, M., Tran, T.A., Sea, W.B., 2020. Land-use dynamics in the Mekong delta: from national policy to livelihood sustainability. Sustain. Dev. 28, 448–467. https://doi.org/10.1002/sd.2036.
Nguyen, N.T., 2020. Evolution of Water Levels at Coastal Hydrological Stations of the Mekong Delta. In: Nguyen, K.D., Guillou, S., Gourbesville, P., Thiebot, J. (Eds.), Estuaries and Coastal Zones in times of Global Change. Springer Water, Singapore, pp. 831–843. https://doi.org/10.1007/978-981-15-2081-5_48.
Nguyen, T.C., Nguyen, N.H., 2023. Does the community support the sluice gates in response to salinity intrusion ? The case of Kien Giang province.
Nguyen, T.C., Schwarzer, K., Ricklefs, K., 2023. Water-level changes and subsidence rates along the East Sea coastline of the Saigon-Dong Nai River Estuary and the Mekong Delta. Decis. Support Syst. 113260. https://doi.org/10.1016/j.ecss.2023.108259.
Nhung, T.T., Le Vo, P., Van Nghi, V., Quoc Bang, H., 2019. Salt intrusion adaptation measures for sustainable agricultural development under climate change effects: a case of Ca Mau Peninsula Vietnam. Clim. Risk Manag. 23, 88–100. https://doi.org/10.1016/j.crm.2018.12.002.
Nicholls, R.J., Lincke, D., Hinkel, J., Brown, S., Vafeidis, A.T., Meyssignac, B., Hanson, S.E., Merkens, J.L., Fang, J., 2021. Author Correction: A global analysis of subsidence, relative sea-level change and coastal flood exposure (Nature Climate Change, (2021), 11, 4, (338-342), 10.1038/s41558-021-00993-z). Nat. Clim. Chang. 11, 634. doi: 10.1038/s41558-021-01064-z.
Normandin, C., Frappart, F., Bourrel, L., Blarel, F., Biancamaria, S., Wigneron, J.P., Galenon, L., Bernard, E., Coulon, L., Lubac, B., Marieu, V., Vantrepotte, V., Pham-Duc, B., Do, H.T., Prigent, C., Aires, F., Yamazaki, D., Ciais, P., 2024. Sharp decline in surface water resources for agriculture and fisheries in the lower Mekong Basin

over 2000-2020. Sci. Total Environ. 950. https://doi.org/10.1016/j.scitotenv.2024.175259.
Park, E., 2024. Sand mining in the Mekong Delta: extent and compounded impacts. Sci. Total Environ. 924, 171620. https://doi.org/10.1016/j.scitotenv.2024.171620.
Park, E., Loc, H.H., Van Binh, D., Kantoush, S., 2022. The worst 2020 saline water intrusion disaster of the past century in the Mekong Delta: impacts, causes, and management implications. Ambio 51, 691–699. https://doi.org/10.1007/s13280-021-01577-z.
Pham-Thanh, H., Phan-Van, T., Fink, A.H., van der Linden, R., 2021. Local-scale rainy season onset detection: a new approach based on principal component analysis and its application to Vietnam. Int. J. Climatol. 1–17. https://doi.org/10.1002/joc.7441.
Pham-Thanh, H., Phan-Van, T., Van Der Linden, R., Fink, A.H., 2022. The performance of ECMWF subseasonal forecasts to predict the rainy season onset dates in Vietnam. Weather Forecast. 37, 113–124. https://doi.org/10.1175/WAF-D-21-0144.1.
Pham, V.C., Bauer, J., Börsig, N., Ho, J., Vu, L., Tran, H., Dörr, F., Norra, S., 2023. Groundwater use habits and environmental awareness in Ca Mau Province , Vietnam: implications for sustainable water resource management. Environ. Challenges 13, 100742. https://doi.org/10.1016/j.envc.2023.100742.
Phan, D.C., Trung, T.H., Truong, V.T., Sasagawa, T., Vu, T.P.T., Bui, D.T., Hayashi, M., Tadono, T., Nasahara, K.N., 2021. First comprehensive quantification of annual land use/cover from 1990 to 2020 across mainland Vietnam. Sci. Rep. 11, 1–21. https://doi.org/10.1038/s41598-021-89034-5.
Phan, H.M., Ye, Q., Reniers, A.J.H.M., Stive, M.J.F., 2019. Tidal wave propagation along the Mekong deltaic coast. Estuar. Coast. Shelf Sci. 220, 73–98. https://doi.org/10.1016/j.ecss.2019.01.026.
Phan, V.H., Dinh, V.T., Su, Z., 2020. Trends in long-term drought changes in the Mekong River Delta of Vietnam. Remote Sens. 12, 1–22. https://doi.org/10.3390/RS12182974.
Pokavanich, T., Guo, X., 2024. Saltwater intrusion in Chao Phraya Estuary: a long, narrow and meandering partially mixed estuary influenced by water regulation and abstraction. J. Hydrol. Reg. Stud. 52, 101686. https://doi.org/10.1016/j.ejrh.2024.101686.
Pokhrel, Y., Burbano, M., Roush, J., Kang, H., Sridhar, V., Hyndman, D.W., 2018. A review of the integrated effects of changing climate, land use, and dams on Mekong river hydrology. Water (Switzerland) 10, 1–25. https://doi.org/10.3390/w10030266.
Rahman, M.M., Penny, G., Mondal, M.S., Zaman, M.H., Kryston, A., Salehin, M., Nahar, Q., Islam, M.S., Bolster, D., Tank, J.L., Müller, M.F., 2019. Salinization in large river deltas: drivers, impacts and socio-hydrological feedbacks. Water Secur. 6, 100024. https://doi.org/10.1016/j.wasec.2019.100024.
Renaud, F.G., Kuenzer, C., 2012. The Mekong Delta System. Springer, Netherlands.
Saramul, S., Ezer, T., 2014. Spatial variations of sea level along the coast of Thailand: Impacts of extreme land subsidence, earthquakes and the seasonal monsoon. Glob. Planet. Change 122, 70–81. https://doi.org/10.1016/j.gloplacha.2014.08.012.
Savenije, H.H.G., 2012. Salinity and tides in alluvial estuaries, Second Com. ed, Journal of Hydraulic Engineering. Delft University of Technology, Water Resources Section, Delft, The Netherland. doi: 10.1061/(asce)0733-9429(1988)114:12(1509).
Schwarzer, K., Thanh, N.C., Ricklefs, K., 2016. Sediment re-deposition in the mangrove environment of Can Gio, Saigon River estuary (Vietnam). J. Coast. Res. 1, 138–142. https://doi.org/10.2112/SI75-028.1.
Sithirith, M., 2024. A framework for analysing water security of Tonle Sap Lake in the Mekong River basin: Flow, volume, inundation, productivity and livelihoods. Lakes & Reserv. Sci. Policy Manag. Sustain. Use 29, e12451. https://doi.org/10.1111/lre.12451.
Smajgl, A., Toan, T.Q., Nhan, D.K., Ward, J., Trung, N.H., Tri, L.Q., Tri, V.P.D., Vu, P.T., 2015. Responding to rising sea levels in the Mekong Delta. Nat. Clim. Chang. 5, 167–174. https://doi.org/10.1038/nclimate2469.
Tamura, T., Nguyen, V.L., Ta, T.K.O., Bateman, M.D., Gugliotta, M., Anthony, E.J., Nakashima, R., Saito, Y., 2020. Long-term sediment decline causes ongoing shrinkage of the Mekong megadelta Vietnam. Sci. Rep. 10, 4–10. https://doi.org/10.1038/s41598-020-64630-z.
Tarolli, P., Luo, J., Park, E., Barcaccia, G., Masin, R., 2024. Soil salinization in agriculture: mitigation and adaptation strategies combining nature-based solutions and bioengineering. Iscience 27, 108830. https://doi.org/10.1016/j.isci.2024.108830.
Tejedor, A., Longjas, A., Zaliapin, I., Foufoula-Georgiou, E., 2015a. Delta channel networks: 1. a graph-theoretic approach for studying connectivity and steady state transport on deltaic surfaces. Water Resour. Res. 51, 3998–4018. https://doi.org/10.1002/2014WR016577.
Tejedor, A., Longjas, A., Zaliapin, I., Foufoula-Georgiou, E., 2015b. Delta channel networks: 2. Metrics of topologic and dynamic complexity for delta comparison, physical inference, and vulnerability assessment. Water Resour. Res. 51, 4019–4045. https://doi.org/10.1002/2014WR016604.
Tho, N., Vromant, N., Hung, N.T., Hens, L., 2006. Organic Pollution and salt intrusion in Cai Nuoc District, Ca Mau Province Vietnam. Water Environ. Res. 78, 716–723. https://doi.org/10.2175/106143006x101755.
Thong, M.T., Thanh, X., Huyen, V.N., Trung, L.D., Cuong, L.P., Hung, L. Van, Hung, C.C., Thi, T., Diep, N., Marcille, J., 2010. Expansion of shrimp farming in Ca Mau , Vietnam Ha Thi Phuong Tien , Nguyen Thu Huong, in: Cook, J.A., Cylke, O., Larson, D.F., Nash, J.D., Stedman-Edwards, P. (Eds.), Vulnerable Places, Vulnerable People Trade Liberalization, Rural Poverty and the Environment. pp. 126–144. doi: doi: 10.4337/9781849805193.00015 [Titel anhand dieser DOI in Citavi-Projekt übernehmen].
Tinh, P.H., MacKenzie, R.A., Hung, T.D., Vinh, T.V., Ha, H.T., Lam, M.H., Hanh, N.T.H., Tung, N.X., Hai, P.M., Huyen, B.T., 2022. Mangrove restoration in Vietnamese Mekong Delta during 2015-2020: achievements and challenges. Front. Mar. Sci. 9, 1–11. https://doi.org/10.3389/fmars.2022.1043943.
Tran, T.A., Dang, T.D., Nguyen, T.H., Pham, V.H.T., 2021. Moving towards sustainable coastal adaptation: analysis of hydrological drivers of saltwater intrusion in the Vietnamese Mekong Delta. Sci. Total Environ. 770, 145125. https://doi.org/10.1016/j.scitotenv.2021.145125.
Tran, D.Q., Nguyen, N.N.T., Huynh, M.V.T., Bairagi, S.K., Le, K.N., Tran, T.V., Durand-Morat, A., 2024a. Modeling saltwater intrusion risk in the presence of uncertainty. Sci. Total Environ. 908, 168140. https://doi.org/10.1016/j.scitotenv.2023.168140.
Tran, T.A., Tran, D.D., Van Vo, O., Pham, V.H.T., Van Tran, H., Yong, M.L., Le, P.V., Dang, P.T., 2024b. Evolving pathways towards water security in the Vietnamese Mekong Delta: an adaptive management perspective. Ambio. https://doi.org/10.1007/s13280-024-02045-0.
Tran, D.D., Thi, P., Thuc, B., Park, E., Thi, P., Hang, T., Man, D.B., Wang, J., 2024c. Extent of saltwater intrusion and freshwater exploitability in the coastal Vietnamese Mekong Delta assessed by gauging records and numerical simulations. J. Hydrol. 130655. https://doi.org/10.1016/j.jhydrol.2024.130655.
Tri, N.H., Choowaew, S., Van Ni, D., Kansantisukmongkol, K., 2019a. Impact of saline intrusion and adaptation options on rice- and fish-farming households in the Mekong Delta of Vietnam. Kasetsart J. Soc. Sci. 40, 427–433. https://doi.org/10.34044/j.kjss.2019.40.2.10.
Tri, D.Q., Mai Linh, N.T., Thai, T.H., Kandasamy, J., 2019b. Application of 1D–2D coupled modeling in water quality assessment: a case study in Ca Mau Peninsula Vietnam. Phys. Chem. Earth 113, 83–99. https://doi.org/10.1016/j.pce.2018.10.004.
Tri, V.K., 2012. Hydrology and hydraulic infrastructure systems in the Mekong Delta. Vietnam 49–81. https://doi.org/10.1007/978-94-007-3962-8_3.
Van, C.T., Thuy, H.T.T., Viet, C.T., Anh, L.N., Van Anh, V.T., Tran, D.D., 2024. Unveiling flood vulnerability in the Vietnamese Mekong Delta: a case study of an Giang province. Int. J. Disaster Risk Reduct. 106, 104429. https://doi.org/10.1016/j.ijdrr.2024.104429.
van der Linden, R., Fink, A.H., Pinto, J.G., Phan-Van, T., Kiladis, G.N., 2016. Modulation of daily rainfall in southern Vietnam by the madden-julian oscillation and convectively coupled equatorial waves. J. Clim. 29, 5801–5820. https://doi.org/10.1175/JCLI-D-15-0911.1.
Van Tho, N., 2022. Salinity Intrusion in the Vietnamese Mekong Delta, a Threat: possible Causes, Effects on People's Life and production, and Temporary Solutions and Adaptable strategies. In: Jeon, H.-Y. (Ed.), Sustainable Development of Water and Environment. Springer International Publishing, Cham, pp. 1–10.
Veettil, B.K., Ward, R.D., Dung, N.T.K., Van, D.D., Quang, N.X., Hoai, P.N., Hoang, N.D., 2021. The use of bioshields for coastal protection in Vietnam: current status and potential. Reg. Stud. Mar. Sci. 47, 101945. https://doi.org/10.1016/j.rsma.2021.101945.
Vengosh, A., 2013. Salinization and Saline Environments, Treatise on Geochemistry: Second Edition. Elsevier Ltd. doi: 10.1016/B978-0-08-095975-7.00909-8.
VnExpress, 2024. Ca Mau announced an emergency drought. URL (17.05.2024) https://www.vietnam.vn/en/ca-mau-cong-bo-han-han-khan-cap/.
Vu, H.T.D., Tran, D.D., Schenk, A., Nguyen, C.P., Vu, H.L., Oberle, P., Trinh, V.C., Nestmann, F., 2022a. Land use change in the Vietnamese Mekong Delta: new evidence from remote sensing. Sci. Total Environ. 151918. https://doi.org/10.1016/j.scitotenv.2021.151918.
Vu, D.T., Yamada, T., Ishidaira, H., 2018. Assessing the impact of sea level rise due to climate change on seawater intrusion in Mekong Delta Vietnam. Water Sci. Technol. 77, 1632–1639. https://doi.org/10.2166/wst.2018.038.
Vu, D.T., Dang, T.D., Galelli, S., Hossain, F., 2022b. Satellite observations reveal 13 years of reservoir filling strategies, operating rules, and hydrological alterations in the Upper Mekong River basin. Hydrol. Earth Syst. Sci. 26, 2345–2364. https://doi.org/10.5194/hess-26-2345-2022.
Vu, H.T.D., Zemann, M., Oberle, P., Seidel, F., Nestmann, F., 2022c. Investigating wave transmission through curtain wall breakwaters under. J. Coast. Hydraul. Struct. 2. https://doi.org/10.48438/jchs.2022.0019.
White, E., Kaplan, D., 2017. Restore or retreat? Saltwater intrusion and water management in coastal wetlands. Ecosyst. Heal. Sustain. 3. https://doi.org/10.1002/ehs2.1258.
Wolanski, E., 1986. An evaporation-driven salinity maximum zone in Australian tropical estuaries. Estuar. Coast. Shelf Sci. 22, 415–424. https://doi.org/10.1016/0272-7714(86)90065-X.
Xue, Z., Liu, J.P., Ge, Q., 2011. Changes in hydrology and sediment delivery of the Mekong River in the last 50 years: connection to damming, monsoon, and ENSO. Earth Surf. Process. Landforms 36, 296–308. https://doi.org/10.1002/esp.2036.
Yuen, K.W., Park, E., Duc Tran, D., Huu Loc, H., Switzer, A.D., Feng, L., Wang, J., 2022. Extent of widespread illegal sand mining in the Mekong Delta. AGU Fall Meet. Abstr. 2022, EP51B-02. doi: 10.1038/s43247-023-01161-1.
Zoccarato, C., Minderhoud, P.S.J., Teatini, P., 2018. The role of sedimentation and natural compaction in a prograding delta: insights from the mega Mekong delta Vietnam. Sci. Rep. 8, 1–12. https://doi.org/10.1038/s41598-018-29734-7.
Zeng, L., Chassignet, E.P., Schmitt, R.W., Xu, X., Wang, D., 2018. Salinification in the South China Sea since late 2012: a reversal of the freshening since the 1990s. Geophys. Res. Lett. 45 (6), 2744–2751. https://doi.org/10.1002/2017GL076574.

B.5. Alternative water resources: Pham et al. (2026)

Environmental Challenges 22 (2026) 101443

Contents lists available at ScienceDirect

Environmental Challenges

journal homepage: www.elsevier.com/locate/envc

The potential of collected rainwater as an alternative water resource for domestic purpose to mitigate groundwater overexploitation in terms of water quality and people's acceptance

Van Cam Pham [a,*], Johannes Ho [b], Jonas Bauer [a], Nicolas Börsig [a], Felix Dörr [a], Tran Viet Hoan [a,c], Elisabeth Eiche [a], Andreas Tiehm [b], Stefan Norra [d]

[a] Karlsruhe Institute of Technology (KIT), Institute of Applied Geosciences, Adenauerring 20b, 76131 Karlsruhe, Germany
[b] TZW: DVGW-Technologiezentrum Wasser, Department of Water Microbiology, Karlsruher Straße 84, 76139 Karlsruhe, Germany
[c] National Center for Water Resources Planning and Investigation (NAWAPI), No. 93, lane 95, Vu Xuan Thieu Street Sai Dong Ward, Long Bien District, Hanoi, Vietnam
[d] Potsdam University, Institute of Environmental Sciences and Geography, Soil Sciences and Geoecology, Campus Golm, Building 12, 14476 Potsdam - Golm, Germany

ARTICLE INFO

Keywords:
Groundwater overexploitation
Alternative water resource
Water management
Rain water harvesting
Water quality
Mekong Delta

ABSTRACT

Ca Mau province, located in the south of the Mekong Delta, is strongly affected by land subsidence and seawater intrusion. Overexploitation of groundwater has been highlighted as a significant driving factor for these processes. As groundwater currently plays a crucial role in the local water supply, this study examines the potential of rainwater as an alternative water source for domestic use to reduce groundwater extraction and contribute to ensure the safe and sustainable water resource for public use (SDG 6). The present study follows a multi-disciplinary evaluation of the potential of rain water as an alternative water resource, covering an assessment of (i) social perception of rainwater usage, (ii) rainwater availability as well as water quality analyses of rainwater stored under various conditions. For this, a combined survey and sampling campaign throughout Ca Mau province was conducted in two main phases between 2019 and 2022. The survey includes a questionnaire which was completed by 473 participants together with in-depth interviews in several selected locations. Complementary, time series of precipitation were analyzed to determine the potentially available rainwater quantity. Stored rainwater samples were collected and analyzed according to their quality based on physical parameters, chemical parameters using ICP-MS and Ion Chromatography with 49 water samples and biological parameters using the IDEXX Colilert® system and MALDI-TOF-MS with 75 water samples. Based on the results, factors that could affect the quality of rainwater were examined. The results show that in some rainwater samples, threshold values of the standards from Vietnamese regulation were exceeded for some parameters, raising the issue of rainwater treatment before use. The questionnaire revealed that rainwater is considered as a potential water source which can replace groundwater for domestic purposes by participants. Despite concerns about rainwater storage during the dry season, public acceptance of using rainwater is generally high. However, the government's interest in communicating information about current environmental issues as well as support in guiding rainwater storage and economic support during the transition process is an issue that people are concerned about. The results of this study provide new insights to further identify potential pilot sites in Ca Mau for rainwater harvesting as an alternative to groundwater extraction, as well as to design concepts for optimizing the use of rainwater.

1. Introduction

The Mekong Delta, the third largest delta in the world, is facing severe land subsidence, for which groundwater over-extraction is considered the major driver (Minderhoud et al., 2020). The effect of land subsidence is exacerbated by sea level rise and progressive seawater intrusion into the delta (Bauer et al., 2025). Besides, human activities, including sand mining and regulation of the Mekong river (reservoirs and dams), cause a substantial decline of sediment supply further accelerating land subsidence (Zoccarato et al., 2018). The Vietnamese

* Corresponding author.
E-mail address: van.pham@kit.edu (V.C. Pham).

https://doi.org/10.1016/j.envc.2026.101443
Received 24 December 2025; Received in revised form 18 February 2026; Accepted 24 February 2026
Available online 26 February 2026
2667-0100/© 2026 The Author(s). Published by Elsevier B.V. This is an open access article under the CC BY license (http://creativecommons.org/licenses/by/4.0/).

Mekong Delta has the highest population density in the area with 297 inhabitants per km^2 and is home to around 19.8 million people (Mekong River Commission , 2019). Accordingly, people's demand in water in this area is high. Residents mostly use groundwater for their daily need. For example, in Can Tho province, people use groundwater for many activities such as cooking, drinking and even for washing, bathing and gardening (Danh and Khai, 2015). Similarly, in coastal provinces like Ca Mau province (CMP), groundwater is the main water source used for all purposes including washing, gardening, cooking and drinking (Pham et al., 2023). Because of the high demand, groundwater is extracted uncontrolled without any planning. Of the total 175,710 wells counted in 2017, only 248 wells served centralized drinking water production and only 452 private wells had an abstraction license. The majority of wells were private wells without any license for operation (Pechstein et al., 2018). Groundwater extraction rates from small to medium sized private wells in CMP was around <200 m^3/day (Pechstein et al., 2018). In 2015, the groundwater extraction required to meet the freshwater demand was 0.42 million m^3/day (Pechstein et al., 2018). Hoan et al. (Hoan et al., 2022) revaluated that the groundwater exploitation rate in the Ca Mau Peninsula is approximately 567,364 m^3/day, with the highest abstraction occurring in the upper–middle Pleistocene (qp_{2-3}) and middle Pliocene (n_2^2) aquifers. Bauer et al. (Bauer et al., 2022) indicated that the hydrogeological layers in the Ca Mau Peninsula are hydraulically connected, suggesting that salinization from seawater intrusion or other sources, driven by altered aquifer conditions, may accelerate groundwater degradation. This situation has caused a series of environment challenges in CMP and residents have to cope to many issues arising from groundwater extraction. In particular, significant land subsidence is challenging the low elevated CMP with ongoing subsidence rates of 2–4 cm/year derived from satellite data evaluation (Erban et al., 2014; Dörr et al., 2024) and from on-site measurements (Karlsrud et al., 2017; Dörr et al., 2023). The deep aquifers, which are used most frequently for groundwater extraction, have a low land rebound potential and therefore an insignificant subsidence mitigation potential (Dörr et al., 2025). Groundwater resources are significantly impacted by climate change and hydrological variables (Bui et al., 2017). To ensure sustainable groundwater development, groundwater abstraction should be limited, and groundwater quality should be improved through additional artificial recharge measures (Bui et al., 2017).

In addition, current research shows that groundwater quality in large parts of the Mekong Delta lowland is unsuitable for drinking and irrigation and may lead to long-term non-carcinogenic health effects (Tran et al., 2021). The use of pesticides has led to large-scale problems of surface water contamination, which also has spread to other water sources such as groundwater (Chau et al., 2015). Moreover, specific land use can affect the salinity of shallow aquifers (Hoan et al., 2025). In the rural areas of the Mekong Delta, shallow groundwater is commonly utilized as a drinking water source to replace contaminated surface water (Buschmann et al., 2008). Analysis of several water samples revealed that arsenic and manganese concentrations exceeded the World Health Organization (WHO) guideline values in some areas of the Mekong Delta, potentially leading to chronic poisoning and posing significant risks to human health (Buschmann et al., 2008). There is the possibility that groundwater quality of private tube-wells built before 1975 was better than that of groundwater wells which were recently built (Danh and Khai, 2015). In the context of groundwater over-extraction and the decrease of groundwater quality (Erban et al., 2014; Buschmann et al., 2008), the identification of potential alternative water sources is of great relevance for the study area.

In this study, rainwater is considered as a potential substitute for domestic purposes, which was demonstrated in previous studies worldwide. Rainwater harvesting is practiced in other parts of Southeast Asia and is considered a potential option for local residents, depending on its availability (Özdemir et al., 2011). Rainwater utilization has long history as a drinking water source in rural areas of Vietnam. It is considered a good-quality source of drinking water that is both cost- and energy-efficient (Nguyen et al., 2019). Rainwater harvesting is considered a suitable approach for freshwater supply and management and has, for example, been increasingly adopted across Europe (Wartalska et al., 2024). However, based on the financial situation and specific social characteristics in CMP, the utilization of rainwater for domestic purpose as well as people acceptance need further investigation. Characteristics of household's head (including age, sex, education status and time of settlement) are important factors impacting to their probability of changing the water source (Danh and Khai, 2015). The objective of this study is to assess current rainwater use practices in CMP and to evaluate whether rainwater could serve as an alternative water source to reduce groundwater extraction.

2. Methodology

2.1. Study area

This research was conducted in CMP, the southernmost province in Vietnam. The area covers around 5270 km^2 (General Statistics Office, 2023). CMP has three sides bordering the sea and a dense network of canals connected to the ocean through major river mouths. The elevation is below 0.8 m in 2018 (Minderhoud et al., 2019), with limited freshwater inflow from upstream, resulting in widespread salinization across much of the region (Ca Mau, 2018).

Please note that this work uses the pre-2025 provincial terminology and administrative boundaries, as provinces were substantially restructured in 2025. There are nine districts in CMP with a total population of around 1.2 million people (General Statistics Office, 2022). According to the Statistics Office (General Statistics Office, 2023), the average population density in CMP is 229 persons/km^2. The ratio of male and female is 104.5 male/100 female. The population in urban areas is 275,812 people which accounts for 22.8 % of the total population, compared with the population in rural area where 931,766 people live which equals a share of 77.2 %. The main occupation of CMP residents is high and mid - level professionals, clerks, personal services, workers, sale workers, skilled agricultural, forestry and fishery workers or have unskilled occupations (General Statistics Office, 2023).

Under the effect of the tropical monsoon climate, CMP has two distinct seasons, which are the dry season and the rainy season. Significant rainfall mainly occurs in the rainy season from May to November with the total amount of 2413.4 mm, while the dry season lasts from December to April with relatively little amount of precipitation with 505.1 mm in 2022 (General Statistics Office, 2023). The water demand is extremely high even though the water sources are limited. The current freshwater supply sources in CMP are groundwater, tap water and bottled water (produced mainly from groundwater) and rain water (Pham et al., 2023; Vinh et al., 2024). However, given that tap water (water distributed by water supply station) is not available for the whole area, some people do not really have the opportunity to use this water source and tap water is originated from groundwater after treatment in some places (Pham et al., 2023). Surface water is not used due to high salinity and pollution resulting from land use practices, particularly extensive shrimp farming and wastewater (Van Muoi et al., 2022).

2.2. Questionnaire collection and analysis

In order to assess the acceptance of using rain water as an alternative water resource, two surveys in two main phases between 2019 and 2022 were conducted. Questionnaires were collected during the face-to-face interviews between the corresponding author, instructors and surveyed households in different locations in CMP. The questionnaire was first introduced in 2019 and revised in subsequent versions in 2021 and 2022 based on the initial interview results. For the first survey campaigns in 2019 and 2020, questionnaires were deployed across all nine districts in CMP with the content focusing on the importance of

groundwater, the potential of available water sources and people's awareness of land subsidence. 144 questionnaires were implemented together with the collection of groundwater samples at the same location, providing an initial comprehensive overview of the study area (Pham et al., 2023). Afterwards, in 2021 and 2022, subsequent surveys were conducted based on the results of the first campaigns. During this period, 329 participants were interviewed in eight districts of CMP, resulting in a total number of interview participants to 473. To ensure the representativeness, the Yamane's formula for calculating sample size was applied (Yamane, 1973; Ahmed, 2024):

$$n = \frac{N}{1 + N(e)^2}$$

N: population e: standard deviation n: number of samples to reach the level of representativeness

Based on the information provided by the general statistics office (General Statistics Office 2022), the number of samples needed for representativeness is around 400.

Thus, the number of interview participants during field trips meets the conditions to represent the region. During the second field trip, the number of questions in the questionnaire was increased to 62 questions in order to capture people's opinion in greater detail by broadening the research topics addressed. The questionnaire consisted of six parts, including general information of respondents, importance of groundwater, importance of water supply, potential use of rainwater, potential use of surface water and people's awareness about the problem of land subsidence in CMP. This study focuses on the information gathered that is related to the potential for using rainwater for households, especially in exchange to using groundwater. The questions with regard to satisfaction with using other water sources instead of groundwater and people's self - evaluation of rain water quality were evaluated in this study. The answer options were divided into five levels (Likert scale) with the level of satisfaction gradually increasing from 1 (people don't want to replace groundwater under any circumstances) to 5 (people are highly motivated to substitute groundwater or are already doing so). Respondent's perceptions of rainwater quality were categorized into five levels, ranging from level 1 (lowest quality) to level 5 (highest quality). After completing the questionnaire, the interviewer as well as the author of this study had an in-depth discussion about the reason behind the answers, therefore this study provides also information on the related context of people's opinions.

In parallel with the questionnaire, 49 stored rainwater samples were collected randomly at the interview locations to evaluate the people's opinions of using rain water together with the quality of rainwater at the current locations as well as figure out a relationship between usage habits and people's assessment of rainwater quality in term of physico-chemical parameters. Moreover, for collected rainwater, hygiene issues are very important when people use it for drinking purposes. Therefore, the number of samples collected to evaluate the microbiological quality was even higher (74 samples).

Similar with the methodology used in the previous study (Pham et al., 2023), the survey and questionnaires were evaluated with regard to various aspects including quantitative and qualitative assessments. For the quantitative approach, answers to questions related to quantity such as the number of people using water in the household, the maximum amount of rainwater stored in the household, etc. were statistically evaluated. For the qualitative approach, answers related to people's subjective perception are mentioned, for example the purpose of water use, the level of people's interest for different water sources as well as the level of people's satisfaction with changing water sources, etc. The multi-dimensional approach allows the authors to capture the different points of view of the interview participants, as well as the overall context.

The primary data set from the 2019 and 2020 survey provided general information and an overview of the research area, leading to the selection of focused locations for the next survey. Based on the initial results with data analysis from general to in-depth details in 2019, together with people's opinion, groundwater quality in the southern of CMP was getting salinized. Tapwater was distributed by centralized water stations and supplied for households in southern area. It's a reason why the next surveys were only focused on the northern and central of CMP. The distribution of survey questionnaires is shown in Fig. 1. The questions dug deeper into the potential of each type of water, current usage status and people's opinion for each option.

2.3. Water sample collection and analysis

2.3.1. Water sampling and chemical analysis

In this study, rainwater samples were collected from selected households participating in the survey. Rainwater was collected directly at the respective water storage vessels and tanks of the households participating in the survey. Physicochemical parameters, such as pH, electrical conductivity (EC) and temperature were measured onsite using a portable multi parameter meter (WTW Multi 3630 IDS). In addition, the rainwater samples were taken and preserved for chemical analysis in the laboratory. The procedure of sample collection and preservation was similar to the way described in our previous publications for groundwater samples (Pham et al., 2023; Bauer et al., 2022). For cation analysis, 50 µL of high purity nitric acid was added to the samples to prevent metal precipitation (W. E. APHA AWWA, 2005), while for anion analysis, 50 µL of sodium azide was added to prevent microbial growth (Vanderford et al., 2011). Cations were analyzed using ICP-MS (Thermo Fisher X-Series 2 and ICap RQ) and anions with Ion Chromatography (Dionex ICS-1000 with column IonPac As Supressor ERS 500 and Methrom Compact IC 930 with column Metrosep A Supp 5–150) at the Laboratory for Environmental and Raw Material Analysis at the Institute of Applied Geosciences at the Karlsruhe Institute of Technology (Bauer et al., 2022).

Following the analysis, the rainwater quality was compared with the National Technical Regulation on Domestic Water Quality QCVN 01–1/2018 BYT (the regulation was applied for domestic water quality and people used it as standard when this research was carried out) and the newest updated version QCVN 01–1/2024. In the updated version of 2024, the threshold of some parameters have been adjusted. Of the parameters mentioned in the National Technical Regulation on Domestic Water Quality QCVN 01- 1/2018 BYT and QCVN 01–1/2024 BYT, the following parameters were used in this study: pH, EC, NH_4^+, Cr, As, Cd, Sb, Pb, Al, Mn, Zn, B, Fe, Ba, Na, Ca, Cl^-, SO_4^{2-}. The parameters are characterized by the fact that humans can recognize abnormalities when water concentrations exceed certain thresholds (WHO, 2022). For instance, at levels above 5 mg/L, cooper (Cu) can impact color of the water and cause undesired bitter taste. At levels above 0.3 mg/L, iron (Fe) can stain laundry and sanitary fixtures. At levels above 0.02 mg/L, manganese (Mn) can form insoluble manganese oxides in water supplies and may cause discolored water and staining like iron (Fe). When concentrations of zinc (Zn) exceed 3–5 mg/L, it may cause a greasy film when water is boiled. In addition, sulfate can cause noticeable taste. Taste thresholds range from 250 mg/L for sodium sulfate and 1000 mg/L for calcium sulfate (WHO, 2022). Statistical evaluation, data processing and visualization were performed with Origin 2022b software.

2.3.2. Water sampling and micro-biological analysis

Samples were collected in sterilized 50 mL plastic bottles (VWR International GmbH, Darmstadt, Germany) and stored cooled (4 °C) until shipment. After completion of the sampling campaign, all samples were transported under cooled conditions to Germany and subsequently analyzed at the TZW German Water Centre Laboratory. Rainwater storage samples were analyzed for *Escherichia coli*, coliform bacteria and enterococci. Enumeration of *E. coli* and total coliform bacteria was performed using the IDEXX Colilert® system (IDEXX Laboratories, Inc., Westbrook, ME, USA) according to the manufacturer's instructions.

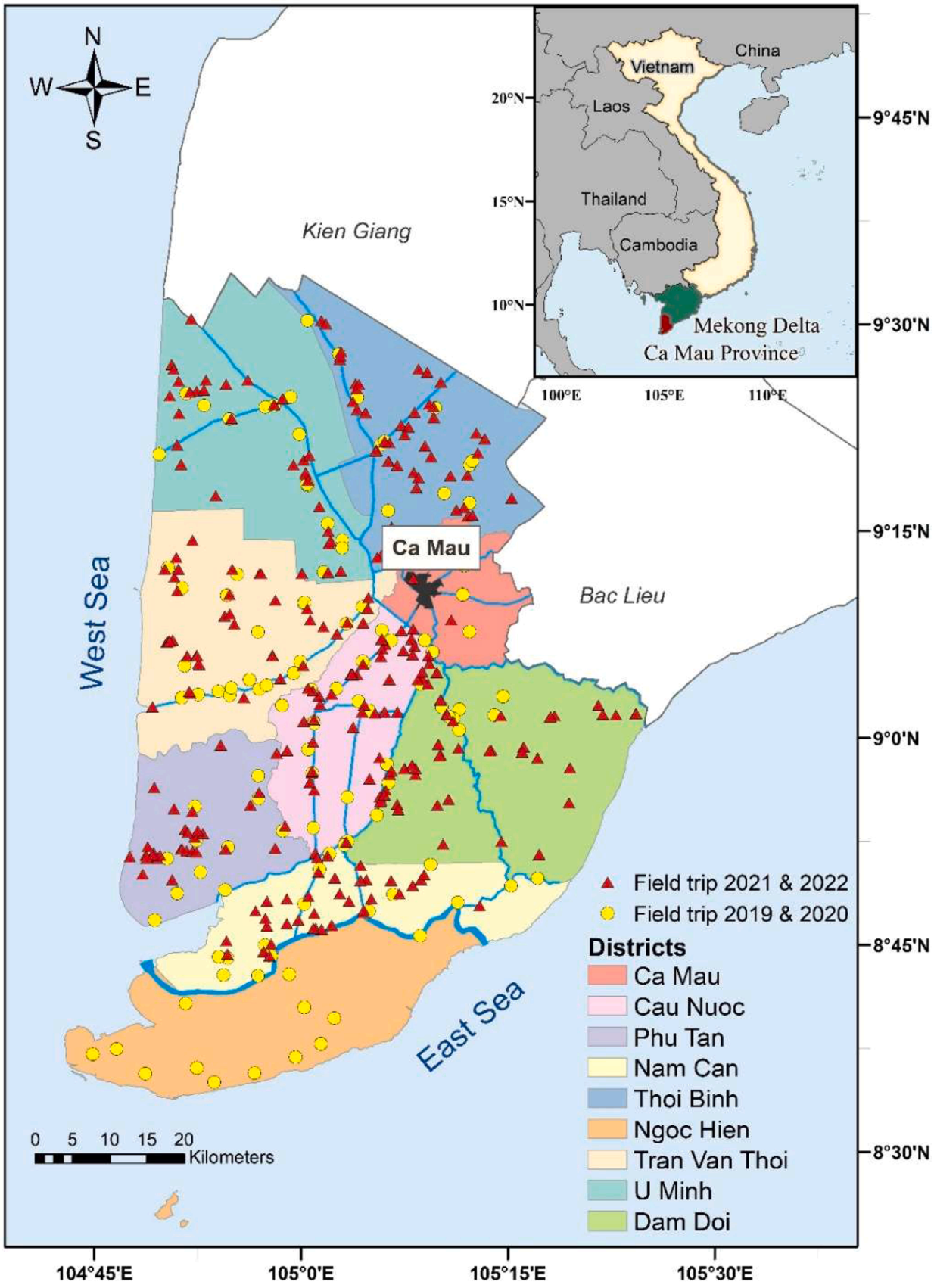


Fig. 1. Map of questionnaire location in Ca Mau province.

Enterococci were quantified using the IDEXX Enterolert® system (IDEXX Laboratories, Inc., Westbrook, ME, USA). For confirmation and further identification, up to 15 wells per sample were picked with sterile tips and analyzed using MALDI-TOF-MS (Microflex LT, Bruker Daltonics GmbH, Bremen, Germany) as described previously (Reitter et al., 2021). Relative species frequencies were obtained by normalizing species counts to the total number of identified isolates. Statistical evaluations were performed using Python 3.11. The Kruskal–Wallis test (scipy.stats.kruskal) was used to assess differences in microbial concentrations across roof types, and chi-squared tests (scipy.stats.chi2_contingency) were applied to evaluate species composition and detection frequencies. Data processing and visualization were conducted using pandas (v2.2.2), numpy (v1.26.4), matplotlib (v3.9.1), and seaborn (v0.13.2).

3. Results

3.1. Current state of rainwater storage in Ca Mau and people's habit in using rainwater

It was found that people use different ways to store rain water and use rain water for different purposes. The containers for storing rainwater of the majority of people interviewed in 2019 were mainly ceramic tanks with covers (with 52.8 % of respondents). Besides, 21.5 % of respondents used plastic tanks and 11.8 % people used concrete tanks. Only 3.5 % of people did not use any covers when storing rainwater in ceramic tanks and 20.1 % of people participating in the survey used rainwater directly without long term storage. They took rainwater that is collected in a small basin after heavy rain (Fig. 2). In addition, the survey results provide insights into the role of rainwater in people's lives. People use rainwater for multi-purposes. 72.9 % of people participating in the survey use rainwater for drinking, while 56.3 % of people utilize rainwater for cooking. Only 6.3 % of people use rainwater for cleaning and washing purposes (Fig. 3).

From this initial information about the potential of using rainwater, the second survey was conducted and focused on rural areas of 8 northern districts in CMP (Fig. 1). A total of 329 people participated in the survey, of which 62.0 % of respondents were men and 38.0 % were women. Respondents' ages range from 19 to 85 years, with the average age of survey participants being 47 years. The occupations of the interviewees were very diverse. Because the research area is concentrated in rural areas, the majority of people working as farmers account for 53.5 %, followed by small household businesses (grocery shop, car washes etc.) with 22.8 %. The remaining people are carrying out occupations such as officers with 12.2 %, or are workers with 5.8 %, housewives with 3.0 %, retired with 1.8 % and unemployed person with rates of 0.3 %. Similar to the information from 2019, people in CMP usually have more than one source of income (Pham et al., 2023). Based on 329 interviews, the average household income is around 9 million VND per month (around 341 USD per month). In 2021, 53.2 % of interviewees use plastic tanks to store rainwater, while 48 % of people use ceramic tanks with cover (Fig. 4). 64.7 % of respondents use rainwater for drinking purposes, while 52.6 % and 59.6 % of respondents use rainwater also for both washing and cooking purposes (Fig. 5).

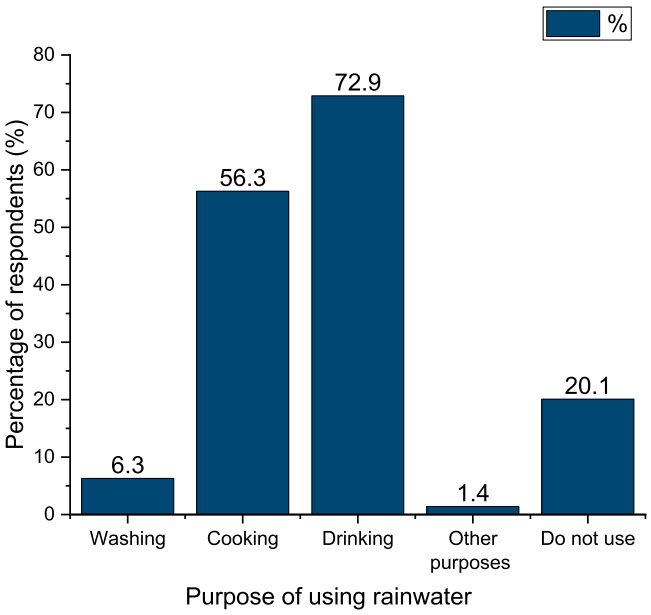


Fig. 3. Purpose of using rainwater in CMP (data from field trip in 2019, $n = 144$).

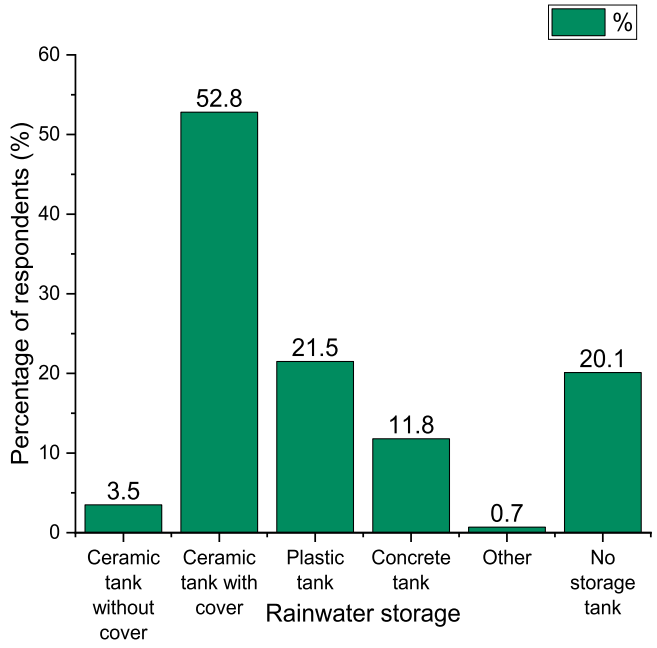


Fig. 2. Types of devices used for rainwater storage in CMP (data from field trip in 2019, $n = 144$).

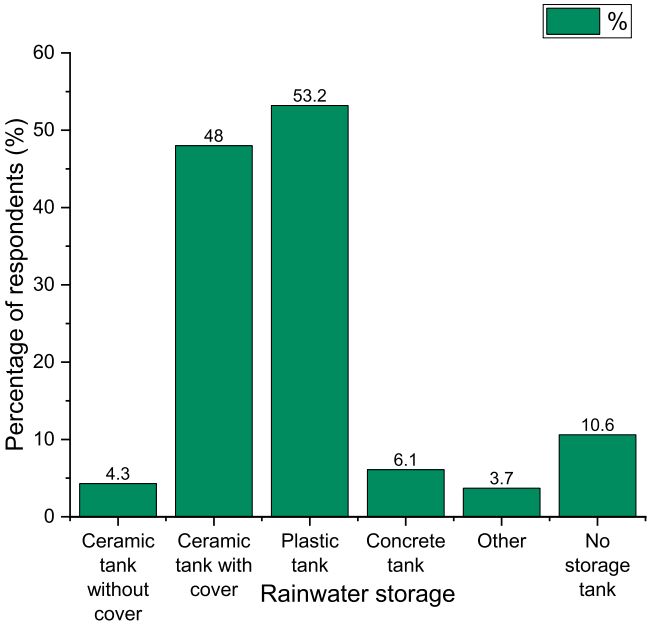


Fig. 4. Types of devices used for rainwater storage in CMP (data from field trip in 2021, $n = 329$).

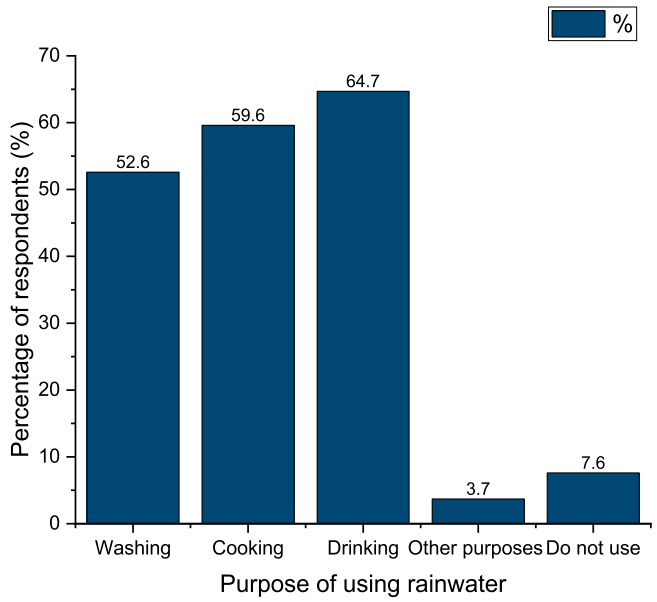


Fig. 5. Purpose of using rainwater in CMP (data from field trip in 2021, $n = 329$).

After determining the changes of rainwater storage habits and rainwater using purposes in the 2021 survey, information surrounding the state of using rain water was further investigated. The capacity of storing rainwater depends on the available storage facilities at their home. With the responses from 329 households, the current average amount of rainwater stored by each of them is around 2.5 m^3 per year. Rain water is mainly collected via roof systems with 98.3 % of the people who answered the questionnaire. Rainwater has been used for a long time and based on people's experience, rainwater is collected from the roof only after discharging the first few rains of the season. According to information from discussion with households, the first rainwater of the season is not collected but used to clean the roof from dirt and impurities. After that, rainwater is collected through pipe systems in tanks. In many households, different roof materials are used in house constructions. Regarding the results obtained from the latest survey in 2021/2022, before using, most people use different measures to treat and improve water quality such as settling, filtering through cloth, boiling and using filtration systems (Table 1).

57.9 % households who do not treat rainwater use this source exclusively for washing and gardening purposes. 71.1 % of those who do not apply any forms of treatment for rainwater refrain from using rainwater for drinking. For the group of household who use common and cost-effective treatment such as settling, filtration via cloth or boiling, 89.5 % people utilize treated rainwater for cooking and direct consumption. Furthermore, 100 % of respondents who apply filtration systems consume rainwater for both cooking and drinking purpose while 90 % of this group use treated rainwater specifically for drinking purpose.

Table 1
Rainwater treatment options used in Ca Mau province. results compiled in the survey in 2021/2022.

Rainwater treatment methods	Percentage of households using this treatment
No treatment	11.6 %
Settling	55.3 %
Basic filtration via cloth	41.3 %
Boiling	44.4 %
Mini filtration system	3.7 %
Other treatment	0.9 %

3.2. Evaluation of collected rainwater quality

3.2.1. Chemical quality of rainwater

Collected rainwater samples were analyzed, objective parameters like legal regulations (the Vietnamese regulation QCVN 01–1:2018/BYT and QCVN 01–1:2024/BYT) on domestic water quality standards (Table 2) have to be used for quality evaluation.

According to the results shown in Table 2, most parameters are below the thresholds of QCVN 01–1:2018 and QCVN 01–1:2024. Overall, inorganic quality of rainwater is therefore appropriate for drinking water or other domestic use. However, there are three parameters whose values partially exceed the allowable thresholds in QCVN 01–1:2018, which are pH, nitrate and aluminum (Al) (Fig. 6). With the new updated regulation in 2024, the threshold of Nitrate is higher, for this reason, some samples which had exceeded the threshold in 2018, have become acceptable in 2024. Measured aluminum (Al) concentrations however exceed the allowable thresholds in both regulations.

In total 49 rainwater samples were analyzed, including 10 samples harvested from asbestos tiles/fibre-cement roofs, 37 samples from galvanized steel sheet roof systems and 2 samples from thatch roofs. This categorization reveals that samples exceeding the QCVN standard in 2024 for Al is in the group representing samples harvested from the galvanized steel sheet roof (Fig. 7). For further investigation, values of Al were statistically evaluated to figure out the connection with roof type category. The Kruskal-Wallis test is applied, results ($p = 0.33 > 0.05$) showing that there are no statistically significant differences between three different types of roof. Regarding the impact of the storage technique, it could also be demonstrated that collected rainwater samples from the ceramic tank with a cover and plastic tank currently exceed the standard of aluminum concentration of some samples (Fig. 7). However, a similar statistically equation was applied to Al concentration values in different water storage category. The Kruskal-Wallis test was implemented and resulted in $p = 0.62{,}781 > 0.05$. Thus, there is no significant difference between different water storage tanks (ceramic tank without cover, ceramic tank with cover, plastic tank and concrete tank).

3.2.2. Microbiological quality of rainwater

Together with the chemical parameters listed in chapter 3.2.1, microbiological contaminants are crucial parameters regarding water quality. Indicator organisms such as *E. coli*, enterococci, and coliform bacteria express possible contamination and the potential presence of pathogenic microorganisms (WHO, 2022). Threshold values for these microbial indicators are specified in Vietnamese national regulations (2018 and 2024) for domestic water, covering drinking, cooking and hygiene purposes Table 3.

Coliform bacteria showed the highest concentrations among the analyzed indicators, with maximum values up to around 5×10^5 MPN/100 mL and a mean of approximately 3×10^4 MPN/100 mL, with a detection rate of 75 % (Fig. 8). Enterococci were detected less frequently, with maximum counts of 9×10^2 MPN/100 mL and a positive rate of 43 %. In contrast, *E. coli* was rarely detected (7 % of samples), likely due to the prolonged storage (up to 14 days at 4 °C) and transport to Germany before analysis. *E. coli* is commonly used as a short-term indicator of recent fecal contamination (WHO, 2022) and microbiological water samples should ideally be analyzed within 24 h to avoid underestimation of indicator bacteria (Canada, 2024). To improve the precision of *E. coli* measurements and avoid die-off effects, we recommend on-site microbiological testing within 24 h in Vietnam; however, this was not logistically feasible in our study.

When comparing samples from different roof materials, microbial concentrations exhibited high variability and no consistent trend indicating differences between roof types was observed. This was confirmed by Kruskal–Wallis test results ($p > 0.05$), indicating no statistically significant differences among roof categories (Fig. 8). An analogous analysis across storage types (ceramic tank with cover/without cover,

Table 2
Comparison of rain water quality with threshold values that are compiled in the Vietnamese regulations QCVN 01–1:2018 and QCVN 01–1:2024.

Parameter (unit)	Unit	Concentration				QCVN 01–1:2018/BYT	QCVN 01–1:2024/BYT
		Min	Max	Median	SD		
pH		4.7	9.1	7	0.99	6–8.5	6–8.5
As	µg/L	0.06	1.46	0.24	0.28	10	10
B	µg/L	1.10	54.1	10.4	10.9	300	2400
Sb	µg/L	0.04	0.38	0.05	0.08	20	20
Ba	µg/L	0.35	66.0	3.24	13.1	700	1300
Cd	µg/L	0.002	2.17	0.01	0.33	3	3
Pb	µg/L	0.01	2.31	0.08	0.35	10	10
Cl^-	mg/L	0.45	17.1	3.26	3.76	250 (300)	250 (300)
Cr	µg/L	0.04	3.87	0.27	0.64	50	50
Cu	µg/L	0.11	4.53	0.64	1.06	1000	1000
Ca	mg/L	0.18	36.0	3.48	7.83	120	120
F	mg/L	0.01	0.05	0.02	0.01	1.5	1.5
Zn	µg/L	5.10	905	67.3	252	2000	2000
Mn	µg/L	0.18	27.3	2.01	4.79	100	100
Na	mg/L	0.29	23.94	1.72	5.14	200	200
Al	µg/L	1.81	387	27.4	74.6	200	200
Ni	mg/L	0.07	1.75	0.21	0.42	70	70
NO_3^-	mg/L	0.18	7.17	1.4	1.42	2	11
Fe	µg/L	1.33	47.6	5.76	7.12	300	300
SO_4^{2-}	mg/L	0.28	13.3	1.34	3.16	250	250

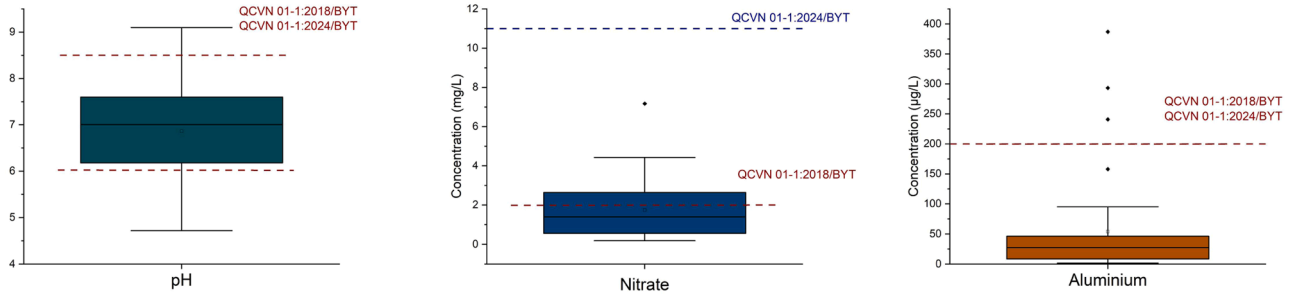


Fig. 6. Concentrations and distribution of water parameters in samples that are partially above the thresholds of QCVN 01–1:2018/BYT and QCVN 01–1:2024/BYT.

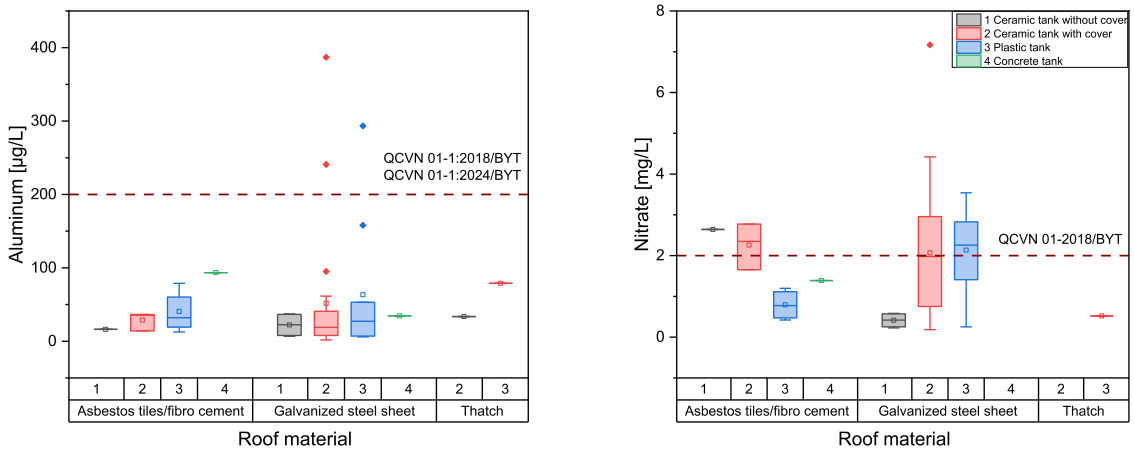


Fig. 7. Concentration and distribution of the parameters aluminum, nitrate in samples representing different roof materials and water storage techniques.

plastic, concrete) likewise yielded no statistically significant differences in concentrations of coliforms, or enterococci after multiple-testing correction (Kruskal–Wallis, $p > 0.05$ for all pairwise comparisons). For *E. coli*, a Kruskal–Wallis comparison yielded a nominally significant p-value ($p = 0.02$) (Fig. 9). However, this result is not considered interpretable, as almost all groups consisted exclusively of non-detects. In a more detailed analysis, all storage-type and roof-material groups were jointly evaluated, yielding similar results without significant differences (Fig. S1 in supplementary material).

MALDI-TOF-MS analysis identified various coliform species (Fig. 10) in rainwater tanks, with *Enterobacter cloacae* and *Klebsiella pneumoniae* dominating across roof types. Additional species such as *Serratia marcescens* and *Citrobacter freundii* occurred only in samples from metal roofs. The two samples from thatched roofs contained exclusively *Enterobacter asburiae*. However, this finding remains exploratory due to the very small sample size.

Statistical analysis revealed no significant differences in species composition between roof types after correction for multiple testing.

Table 3
Comparison of microbiological water quality standards for different uses according to Vietnamese QCVN regulations. "Not specified" indicates that no explicit limit is provided in the respective guideline.

Parameter	Positive rate,mean, min, max	QCVN 01–1:2018/BYT	QCVN 01–1:2024/ BYT
E. coli	**7 %** **9 MPN/100 mL** 5–15.5 MPN/100 mL	< 1 CFU/100 mL	<1 CFU/100 mL (must not be detectable)
Total Coliforms	**75 %** **30.000 MPN/100 mL** 5–500.000 MPN/100 mL	< 3 CFU/100 mL	< 1 CFU/100 mL
Enterococci	**43 %** **250 MPN/100 mL** 15–940 MPN/100 mL	*Not specified*	*Not specified*

Although the overall chi-squared test ($p = 0.0127$) suggested potential variation, small group sizes limit the interpretability of this result. Thus, no robust association between roof material and microbial profile could be established. The detected species point to general environmental contamination rather than clear fecal pollution.

A weak, non-significant correlation between enterococci and coliform counts (Pearson $r = 0.46$, $p = 0.076$) suggests a possible trend, but high variability and limited sample size prevent firm conclusions. Notably, coliform species composition differed significantly between samples with and without enterococci ($Chi^2 = 32.42$, $p = 0.020$), though the practical relevance of these differences appears limited.

In addition to the roof-type comparison, we evaluated MALDI-TOF-MS species profiles across storage types (Fig. 11). A chi-squared test on the full species-by-storage contingency table indicated statistically significant differences ($p < 0.001$). However, we caution against causal interpretation: multiple isolates originated from the same tank (non-independence), colony picking introduces stochasticity in MALDI-TOF profiling, and storage type co-varies with unmeasured factors (e.g., tank age, cleaning frequency, shading, inflow characteristics). Consistent with this, fecal indicator bacteria (***E. coli***, coliforms, enterococci) did not differ significantly across storage types. We therefore report the statistical result but refrain from inferring a storage-type–specific microbial signature.

3.3. Perceptions of people about rainwater

The survey campaigns conducted in CMP also included questions about people's needs and their perception of water usage. In terms of quality of stored rainwater, 55.0 % of the participants think that rainwater quality is at the highest level (Fig. 12). Only 1.8 % and 4.0 % of the participants think that rainwater has a poor quality with scores 1 and 2. Similar results were obtained when people were asked how satisfied they are with using rainwater as an alternative to groundwater. 18.8 % and 31.3 % of respondents have the highest level of satisfaction at levels 4 and 5 in this regard, respectively. Those who do not feel satisfied if they completely used rainwater to replace groundwater (level 1 and 2) accounted for 17.6 % and 14.3 %. Furthermore, Kruskal-Wallis test were applied to evaluate the effect of roof material and water storage on people's perceptions of water quality. The test result ($p = 0.65$ for roof material and $p = 0.45$ for water storage, > 0.05) indicates that no significant differences were detected in Likert- scale ratings of perceived water quality across different roof material and water storage tank. These findings suggest that, within the current sample size, roof material and water storage tank are not a statistically significant factors impacting on the people's perception of rainwater quality.

To delve deeper into people's thoughts about the quality of different water sources, they were asked to choose their favorite type of water. Among available water sources, rainwater is the most popular choice, with 41.0 % of the participants selecting this option, followed by bottled water with 33.7 % (Fig. 13). Although it is considered the best water source in people's opinion, people have their own reasons for not using rainwater for all purposes. 58.7 % of people think they do not have sufficient rainwater, 36.2 % of the participants think that rainwater supply is not reliable all year around, particularly during the dry season (Fig. 14).

Moreover, according to the results of the field trip in 2019, 61.1 % of respondents said that rainwater was the best quality water source (Pham et al., 2023). Two years later, in the context of the world facing to the Covid 19 epidemic, people changed their assessment of the quality of rainwater. After having a more in-depth interview with the people, they shared rumors saying that the Covid 19 virus can spread through the air and enter into rainwater. There were additional rumors that the disposal of human remains during the Covid 19 epidemic could create dust entering the air and rainwater, causing water pollution. From these rumors, a part of people began to form prejudices against the use of

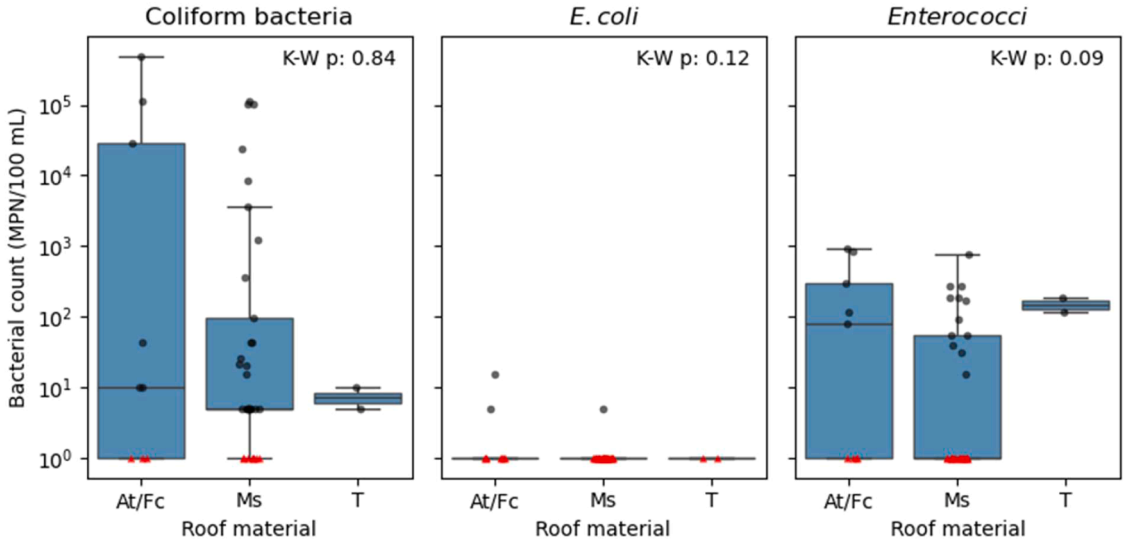


Fig. 8. Concentrations of coliform bacteria, *E. coli*, and enterococci in rainwater storage samples collected from different roof types (At/Fc: asbestos tiles/fibre cement; Ms: metal sheets; T: thatch). Dots represent positive detections; triangles indicate the detection limit for non-detects. Statistical differences between roof types were assessed using the Kruskal–Wallis test; p-values are shown in each plot.

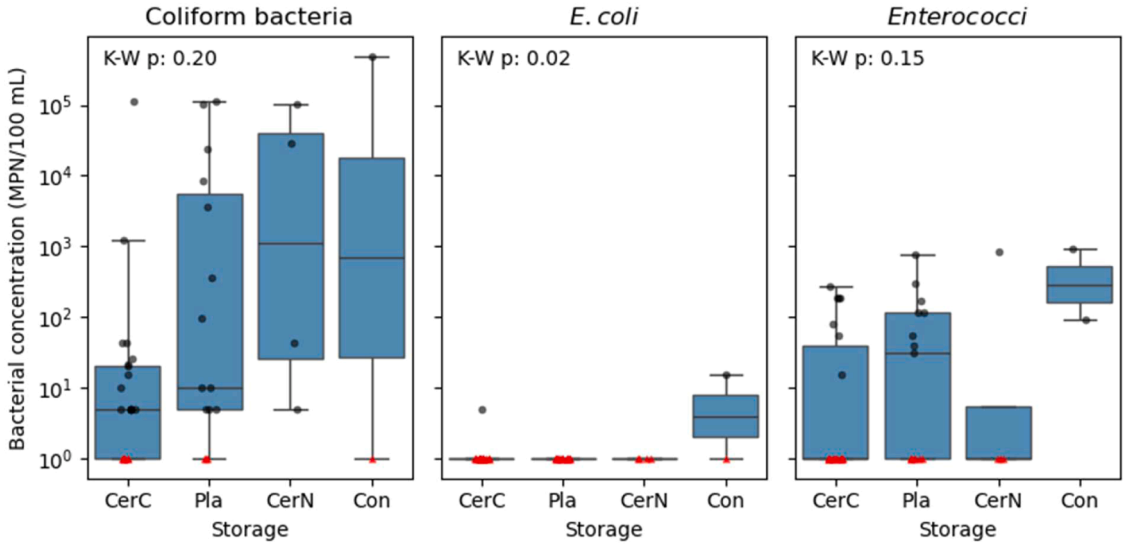


Fig. 9. Concentrations of coliform bacteria, *E. coli*, and enterococci by storage type (CerC: Ceramic with cover, CerN: Ceramic without cover, Pla: Plastic, Con: Concrete); dots indicate positive detections; triangles indicate the detection limit for non-detects. Kruskal–Wallis p-values (Bonferroni-adjusted) are annotated per panel.

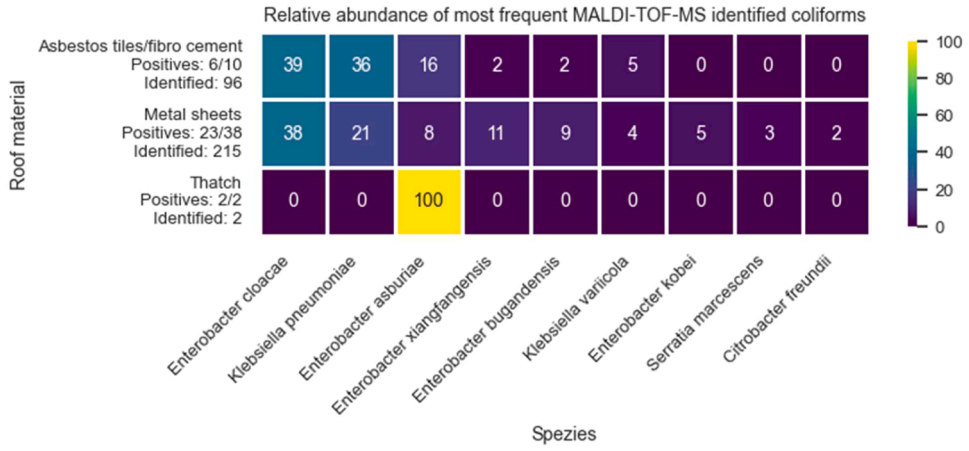


Fig. 10. Relative abundance of coliform bacterial species identified via MALDI-TOF-MS in rainwater samples collected from three roof types. For each group, the number of positive and total samples as well as the total number of identified bacteria is given.

rainwater.

4. Discussion

4.1. Potential of rainwater quantity

Based on time series data from the Integrated Surface Dataset published by the National Oceanic and Atmospheric Administration (NOAA), Fig. 15 shows the changes in the amount of rainwater in both seasons in CMP from the years 1990 to 2021. The dataset highlights the significant difference between the dry season and rainy season. In 2022, total precipitation was 2919 mm, which, taking into account the area of CMP (5274.5 km^2; (General Statistics Office, 2023)), corresponds to a water volume of around 15.4 billion m^3.

The population in CMP in 2022 is 1207,578 people with 275,812 people living in urban area and 931,766 people living in rural area (General Statistics Office, 2022). According to Vietnam Regulation TCXD-VN33:2006/BXD, water demand of people living in rural area is around 40 to 60 liters/person/day, the demand in urban areas considerably higher with around 80 to 150 liters/person/day. The total water demand of residents in the CMP is around 78,306 m^3/day, with 31,718 m^3/d consumed in urban areas and 46,588 m^3/d in rural areas. In one year, the total amount of water that people need for domestic use is therefore around 28.6 million m^3. This calculation indicates, that, if collected and stored efficiently, rainwater could cover people's water demand in CMP.

In addition, Vinh et al. (2024) evaluated potential water availability using a water balance equation under four different scenarios with varying conditions in CMP, including roof catchment area, storage tank capacity requirements, essential domestic water demand during the dry season, and integration with groundwater resources. This study confirmed that the existing roof catchment area is sufficient to meet domestic water demand; however, storage tank capacity must be increased, particularly to ensure water supply during the dry season. Additionally, under the scenario integrating rainwater harvesting with groundwater use, rainwater was able to supply 48 % of domestic water demand, while the extracted groundwater could be effectively recharged by the excess rainwater discharged (Vinh et al., 2024).

4.2. Change in rainwater storage habit for more effective usage

Based on the results from chapter 3.1 and 3.3, it can be concluded

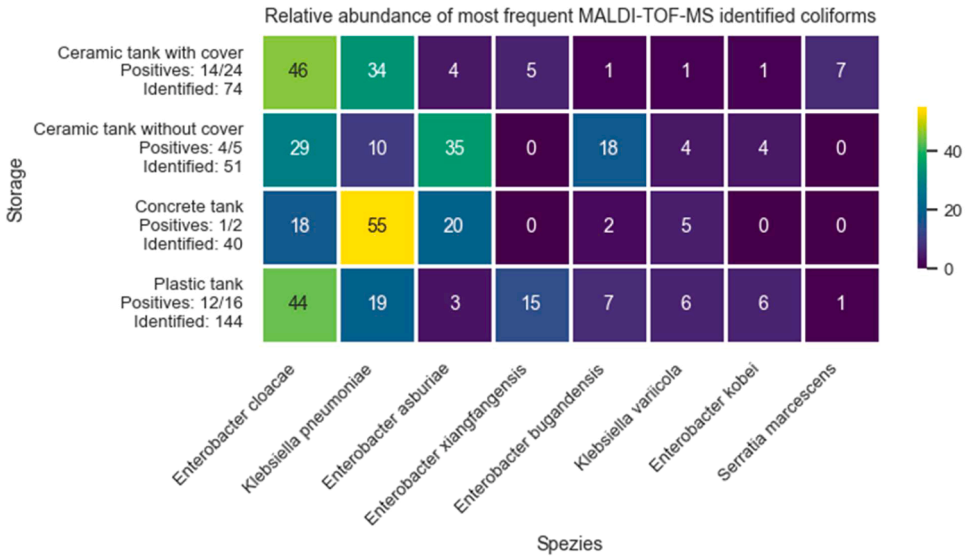


Fig. 11. Relative abundance of coliform bacterial species identified via MALDI-TOF-MS in rainwater samples grouped by storage types. For each group, the number of positive and total samples as well as the total number of identified bacteria is given.

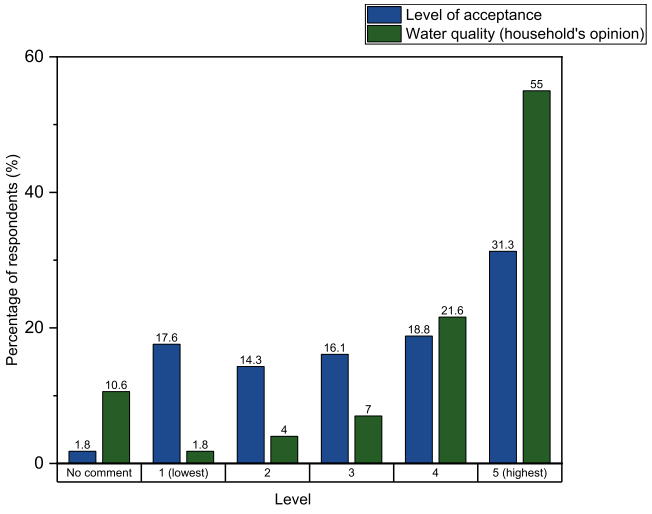


Fig. 12. Household's opinion of rain water quality (green column) and their level of acceptance to use rainwater as a substitute for groundwater (blue column).

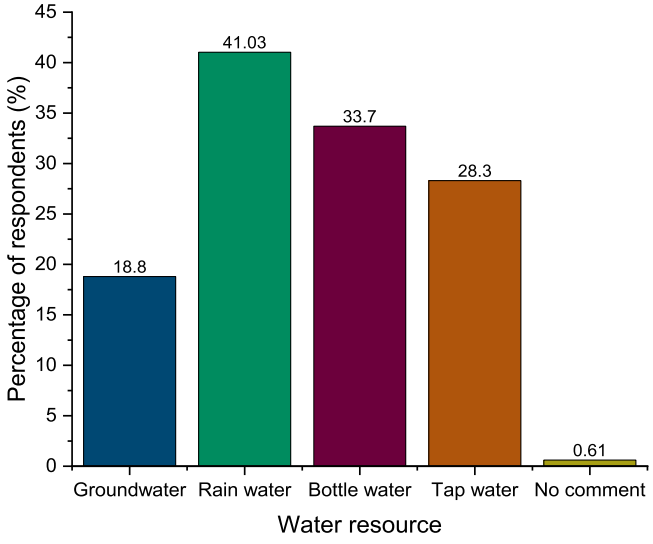


Fig. 13. Best water source in household's opinions.

that CMP residents consider the quality and taste of rainwater to be appropriate, which is why they prefer using it for high-quality purposes such as drinking. In previous studies, direct rainwater quality in the Mekong delta was evaluated as high, with no signs of air pollution and rain quality meets Vietnam National Standard QCVN 02:2009/BYT for most of the parameters (Thu Ha and Hoang, 2014). Most people perceived rain water to be clean, which is why they often use it without further treatment after harvesting. In addition, rainwater quantity stored in vessels and tanks is insufficient for high-consumption purposes such as cleaning and washing. Another study conducted in Tra Vinh province (located in the Mekong Delta) also indicated that rainwater was highly valued for its better taste and its availability during the rainy season. People in Tra Vinh province did not have sufficient containers to collect and store rainwater for use during the dry season (Li et al., 2016). With current storage capacity in Ca Mau, rainwater could not meet the people's demand in the dry season to reduce the groundwater extraction (Vinh et al., 2024).

According to the results of the second survey, rainwater using purposes and rainwater storage equipment changed significantly compared to the result from the first survey in 2019 (Figs. 2,3,4,5). Most obvious is that the number of people using large plastic tanks to store rainwater has clearly increased within two years. Some people use several ways to store rainwater to increase the amount of rainwater. Ceramic tanks were the most commonly utilized and convenient means of rainwater storage in 2019; they were typically covered to maintain water hygiene and to prevent contamination from dust and insects. Plastic tanks with higher quality become currently more popular which also implies that people have invested a certain amount of money in their rainwater storage system. Furthermore, when people have the ability to store more rainwater, their usage purposes also change. Based on the results from Table 1 and the detailed information about water treatment and water use in chapter 3.1, some households use multiple options to treat rainwater before consuming rainwater. The method of treatment depends on the intended use and the economic conditions of households.

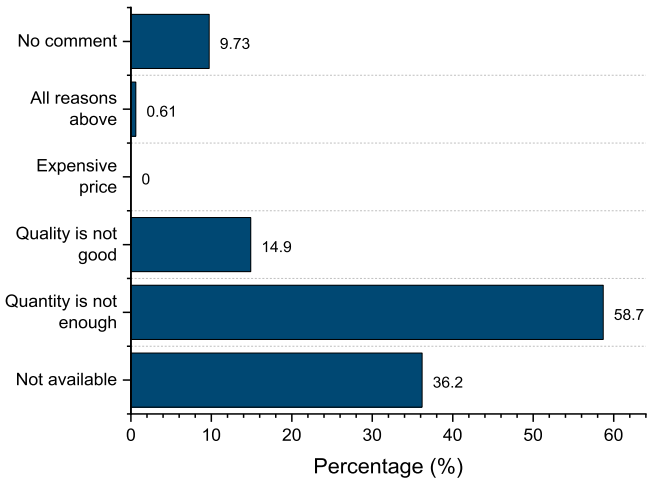


Fig. 14. Reasons why people think rainwater is not suitable for all domestic purposes.

4.3. Potential of rainwater as an alternative to mitigate the impact of groundwater over-extraction

Based on the previous discussion from chapter 4.1, the amount of rainwater can completely serve the water needs of people in Ca Mau, and the Mekong Delta in general. In addition, the study of Vinh et al. (Vinh et al., 2024) also gave similar results on the potential of rainwater in meeting the needs of people based on data from 10 rainwater monitoring stations. According to the assessment of the long term rainfall trend in 2025, the Ca Mau station recorded the highest average annual rainfall in the Mekong Delta of Vietnam (Vuong et al., 2025). However, due to the impacts of climate change, the annual rainfall has shown a decreasing trend. Therefore, it is necessary to implement integrated water resource management and climate adaptation measures to ensure sustainable water use (Vuong et al., 2025).

These results from chapter 3.2 raise the question of why some parameters exceed the limitations. In general, the regular rainwater collection system includes the roofs, pipe systems and storage tanks. When rainwater is harvested, the quality of rain water is affected by roof materials (Olaoye and R.A, 2019). Roof material properties can be one important factor which leads to nonpoint water pollution (Chang et al., 2004). There are three popular roof types including concrete/asbestos tiles, thatch and galvanized metal sheet (Wilbers et al., 2013). In 2019, rain water harvested from asbestos roofing sheet had highest mean value for pH, total hardness, aluminum, cooper, nitrate and sulphate in comparison with another roof types (Olaoye and R.A, 2019). Similarly, rainwater samples in Ca Mau were divided into three different groups based on information from the survey. The difference between the numbers of samples in each group give information on the popularity of different types of roof materials. The difference between the numbers of samples in each group give information on the popularity of different types of roof materials. Water samples with Aluminum concentrations exceeding the standard were in the group from galvanized roofs, contrary to the results of a previous study that rainwater from asbestos roofs had the highest Aluminum and nitrate concentrations (Olaoye and R.A, 2019). After being verified by Kruskal-Wallis statistic, these results indicate that the collected rainwater quality can be influenced by several interacting factors, not only roof types or rain water storage. This supports the assumption that several factors can affect collected rainwater quality, not only roof types, but also pipe system, handling practice, storage duration, people's activities and habits to collect and store water.

Similar findings were reported by Wilbers (Wilbers et al., 2013), who observed that microbial contamination in harvested rainwater was not primarily influenced by roof material but rather by factors such as storage cover type, location, handling practices, and overall hygiene conditions. The presence of coliform bacteria and enterococci in roof-harvested rainwater in chapter 3.2.2 is not unexpected. Fresh rainwater is generally microbiologically clean when it falls, but contamination typically occurs during collection and storage, especially through contact with roof surfaces, bird droppings, gutters, and accumulated debris. Several studies have reported frequent detection of *E. coli*, total coliform and enterococci in rainwater storage tanks, often at concentrations exceeding drinking water standards (Hamilton et al., 2019; Chidamba and Korsten, 2015). Under tropical conditions, such as those in CMP, warm temperatures (25–35 °C), organic matter from roof runoff and stagnant water in storage tanks can create favorable conditions for bacterial persistence and even regrowth (Lleò et al., 2005; Zdeb et al., 2021). While *E. coli* generally declines over time due to its sensitivity to environmental stress, other coliforms such as Klebsiella and Enterobacter identified in this study by MALDI-TOF-MS are more

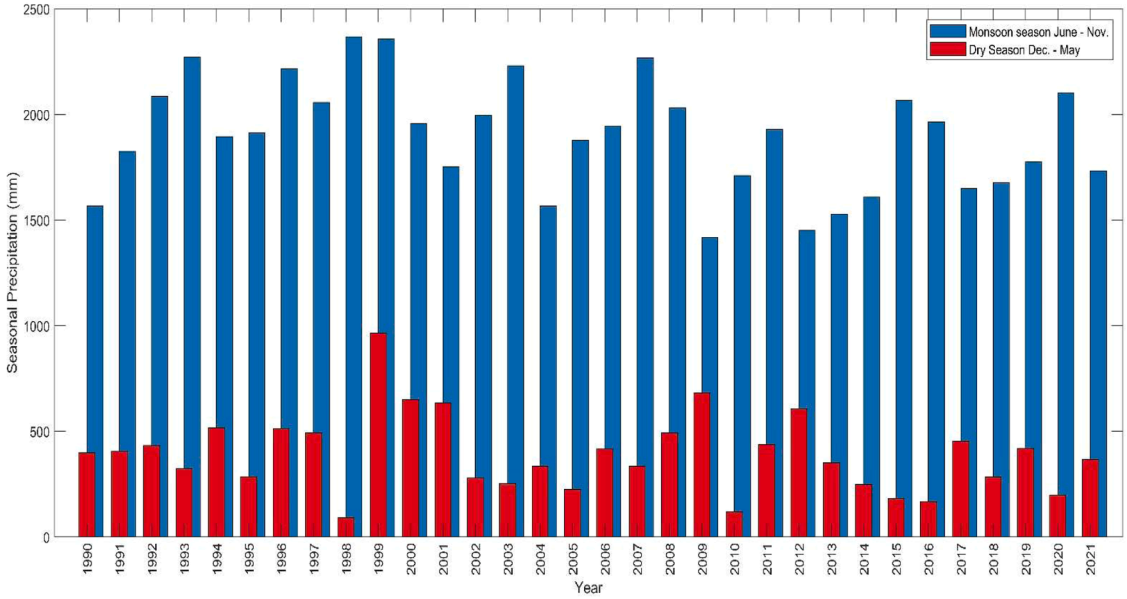


Fig. 15. Changes in rainwater quantity in Ca Mau province during the rainy and dry seasons from 1990 to 2021.

resilient and capable of multiplying in nutrient-rich sediments and biofilms (Martin et al., 2010). Enterococci, although traditionally considered indicators of fecal contamination, are not exclusively of human origin and can also derive from animals or environmental sources (Leister et al., 2023). They are relatively stress-tolerant and can persist for extended periods in stored water. Some studies suggest that under warm, nutrient-enriched conditions, enterococci may survive and even proliferate within biofilms on tank surfaces (Sadanandan and Yogendraiah, 2025; Willett and Dunny, 2024). This highlights the importance of proper tank hygiene and simple treatment measures (e.g., boiling, filtration, or chlorination) before using rainwater for drinking or cooking purposes (Olaoye and Olaniyan, 2019).

In summary, the microbiological analysis indicates that rainwater contamination is primarily due to general environmental exposure rather than specific roof materials or clear fecal sources. No consistent influence of roof type on microbial load was observed. Instead, contamination likely occurs via roof surfaces, and handling practices. Consistent with these findings, the dominance of Enterobacter cloacae in our samples aligns with global assessments of microbial communities in roof-harvested rainwater. Hamilton et al. (Hamilton et al., 2019) reported that environmental coliforms—particularly Enterobacter, Klebsiella, Citrobacter and Serratia—are the most commonly detected genera in rainwater tanks worldwide, whereas *E. coli* typically occurs only sporadically and mainly after recent contamination events. The species profile observed in Ca Mau therefore reflects globally recognized contamination pathways related to dust deposition, plant material, insects and roof biofilms rather than clear fecal pollution. This overlap with global patterns supports the interpretation that microbial contamination in the study area is primarily driven by environmental exposure. According to Vietnamese regulation on drinking water guidelines, the presence of coliform bacteria or enterococci disqualifies rainwater from being considered safe for direct consumption without treatment. To ensure safe use, especially for drinking, basic hygienic standards and appropriate treatment methods such as boiling or filtration are essential. Other studies around the world, which were compiled and reviewed recently, confirmed the high quality of rainwater together with the necessity of treatment before using (Sakati et al., 2023).

In addition, the relationship of groundwater use and rainfall is inversely correlated. For example, a reduction of groundwater extraction was observed during the rainy season in Kenya (Thomson et al., 2019). In Israel, using rainwater for toilet flushing contributed to the reduction of groundwater recharge (Nachson et al., 2022). In addition, groundwater extraction in Ca Mau will become increasingly difficult as shallow aquifers become exhausted or saline (Van Tuan et al., 2024). Water conservation through rainwater harvesting, driven by limited water availability, represents a pathway toward environmental sustainability in many regions of the world (Sakati et al., 2023).

4.4. Attitudes toward rainwater use as alternative water for groundwater and role of government communication in promoting rainwater usage

Following the results from chapter 3.3, the reason behind this perception of water usage is mainly related to concerns about rain water quantity. Some people doubt the feasibility of using rainwater, as the amount of water is inconsistent and not sufficiently available year-round and for all purposes. In another similar study in other provinces of the Vietnam Mekong Delta, rainwater amount is sufficient for households during the rainy season, while during the dry season it is only enough for drinking purpose (Özdemir et al., 2011). Rainwater did not meet the requirements of the local people due to insufficient storage capacity (Vinh et al., 2024). This finding leads to the conclusion that more effective solutions for storing rainwater for domestic use are required. There are several barriers that impede the development of rainwater harvesting in Vietnam, including technical, economic, and social obstacles. Public awareness remains limited due to the spread of unverified information about rainwater quality, lack of knowledge, and insufficient understanding of legal regulations (Nguyen et al., 2019). Peoples lack of system that provides comprehensive information in an easy-to-understand, simple format. In order to prevent misinformation mentioned in chapter 3.3, promoting accurate information to people in a timely manner is very important to raise people's knowledge and awareness. Similar issues arise in many documents dealing with the current state of climate change, but the acute danger posed by land subsidence together with rising sea levels receives less attention (Vo et al., 2025). Vietnam faces water scarcity and saline intrusion, particularly in coastal communities (Bauer et al., 2025; Bauer et al., 2022; Tran and Yong, 2025). Dependence on groundwater among local households increases along the spatial gradient from the northern to the coastal areas. Poor households are particularly vulnerable to domestic water scarcity due to issues such as saline intrusion in groundwater and the lack of alternative water sources (Van Tuan et al., 2024). At the first conference about sustainable development in Mekong Delta, the Vietnamese government emphasized the importance of respecting and adapting to the laws of nature (Linh et al., 2023). To prevent or reduce the over-extraction of groundwater and assure safe water supply also in the future, clear regulation from the government should be formulated and clear benefits of alternative water sources like rainwater should be comprehensively communicated. Our survey together with further discussion with people highlight the factors that affect to people's opinion on changing water resources. Official government announcements are the most important prerequisite for people to comply. It is necessary to implement local-level water management policies, accompanied by proactive actions from local governments, to mitigate environmental impacts and ensure long-term water security in the Mekong Delta (Tran and Yong, 2025). In addition, the high initial investment required for rainwater harvesting systems poses a significant challenge for low-income households (Nguyen et al., 2019). For that reason, residents in CMP expect the encouragement from government to support their change in water sources through financial support to invest e.g. in rainwater storage or tap water distribution.

4.5. Limitations, strengths and future perspectives of the study

This study is based on a limited number of water samples, with relatively few samples corresponding to specific roof materials and storage containers. The number of samples for each material group is uneven due to differences in local prevalence, as some materials have become increasingly scarce in the study area. In addition, microbiological analyses ideally should be conducted directly in the study area; the inability to do so represents a further limitation of this research.

This study adopts a multidisciplinary approach by integrating data from questionnaires, water quality analyses and discussions with local residents to evaluate the potential of rainwater harvesting under specific conditions in CMP. The authors directly collected water samples and engaged with local communities, allowing for a deeper understanding of local perspectives and actual practices. As a result, the methods and findings are highly practical and transferable, and can be applied to similar contexts in other regions. The outcomes of this research contribute to improved water resource management for domestic use and support progress toward Sustainable Development Goal 6.

Future research should expand the study scope by increasing the number of samples and considering additional influencing factors beyond roof materials and storage devices to provide a more comprehensive assessment of rainwater quality. Implementing pilot studies on rainwater harvesting systems would help evaluate their effectiveness in practice. Further investigation into specific case groups using different rainwater storage models tailored to local conditions also represents a promising direction for future work.

5. Conclusion

This study has presented a multi-disciplinary assessment of the

potential of collected rainwater as alternative water source for domestic purpose to reduce the groundwater overexploitation in the southern Mekong Delta. Following the results of a previous study (Pham et al., 2023), the present study expanded the number of surveys to improve regional representativeness and the distribution of social and spatial conditions. This study reaffirms the extremely important role of groundwater in people's lives in CMP. In addition, the habit of using alternative water sources such as rainwater was investigated and showed a significant change in the using purpose from mostly using rainwater for drinking purposes in 2019 to other purposes (drinking, cooking and washing) in 2021 and 2022. Along with that, the rain water storage systems also changed; plastic containers became more popular in the most recent years. Respondents typically discard the first flush of rainwater in the beginning of the rainy season to clean the roof and improve the quality of subsequently collected rainwater. The study showed that residents in CMP currently treat rainwater with quite simple methods, mainly settling and filtering through cloth. Based on the evaluation of time-series data, quantity of rainwater in CMP appears sufficient to meet people's demands; nevertheless, appropriate storage infrastructure must be considered. Water quality testing indicates that rainwater is of relatively good quality. However, some physical and chemical parameters, such as pH, nitrate and aluminum, as well as some biological parameters, such as *E. coli* and coliform, exceeded the thresholds in a few samples. In general, the extension of thresholds for certain parameters in the updated version QCVN 01–1:2024 increases the compatibility of rainwater for domestic use. Subsequently, the study examined factors affecting rainwater quality including roof materials and storage tanks. However, it is also necessary to consider additional causes affecting water quality such as the pipe system, the cleaning process of water containers and people's activity. Microbiological analysis showed that contamination was not clearly linked to roof materials or storage conditions but rather to general environmental exposure and human activities. Although various coliform species were detected, the lack of consistent fecal indicators points to non-specific contamination. This observation is particularly relevant given the stricter microbiological standards that will apply from 2024. Therefore, hygienic handling and basic treatment - such as boiling or filtration - remain essential, especially for drinking purposes. According to the individual perceptions of residents in CMP, the quality of rainwater is highly valued and there is a high level of acceptance of using rainwater instead of groundwater. Nonetheless, people would like clearer information from local authorities about the current environmental problems as well as governmental financial support and guidance on water storage practices. This study has opened up a new research direction in selecting suitable pilot locations and designing utilization concept of rainwater to be used as a potential alternative water source to contribute to the reduction of groundwater overexploitation in CMP.

Declaration of generative AI and AI-assisted technologies in the manuscript preparation process

During the preparation of this work the author(s) used ChatGPT in order to improve language and readability. After using this tool/service, the author(s) reviewed and edited the content as needed and take(s) full responsibility for the content of the published article.

CRediT authorship contribution statement

Van Cam Pham: Writing – original draft, Visualization, Methodology, Investigation, Formal analysis, Conceptualization. **Johannes Ho:** Writing – review & editing, Visualization, Methodology, Investigation. **Jonas Bauer:** Writing – review & editing, Visualization, Investigation. **Nicolas Börsig:** Writing – review & editing, Project administration, Investigation. **Felix Dörr:** Writing – review & editing. **Tran Viet Hoan:** Writing – review & editing. **Elisabeth Eiche:** Writing – review & editing, Resources. **Andreas Tiehm:** Writing – review & editing. **Stefan Norra:** Writing – review & editing, Supervision, Project administration, Funding acquisition.

Declaration of competing interest

The authors declare that they have no known competing financial interests or personal relationships that could have appeared to influence the work reported in this paper.

Acknowledgment

This research was conducted as part of the ViWaT- Engineering project, funded by the German Federal Ministry of Education and Research (BMBF) under Grant No. 02WCL1474A. We gratefully acknowledge the Vietnamese National Center for Water Resources Planning and Investigation and the Department of Natural Resources and Environment of Ca Mau Province (DONRE Ca Mau) for their kind support. We also thank the laboratory staff of the Institute of Applied Geosciences at Karlsruhe Institute of Technology (KIT), as well as all project partners for their valuable collaboration. Special thanks are extended for the financial support provided through the Graduate Funding from the German States program (Landesgraduiertenförderung) and additional support from the Graduate School for Climate and Environment (GRACE – KIT). Finally, we acknowledge support from the KIT-Publication Fund of the Karlsruhe Institute of Technology.

Supplementary materials

Supplementary material associated with this article can be found, in the online version, at doi:10.1016/j.envc.2026.101443.

Data availability

Data will be made available on request.

References

Ahmed, S.K., 2024. How to choose a sampling technique and determine sample size for research: a simplified guide for researchers. Oral Oncol. Rep. 12, 100662. https://doi.org/10.1016/j.oor.2024.100662. September.

APHA AWWA, W. E. *Standard methods for examination of water and waste water*. 2005.

Bauer, J., Börsig, N., Pham, V.C., Hoan, T.V., Nguyen, H.T., Norra, S., 2022. Geochemistry and evolution of groundwater resources in the context of salinization and freshening in the southernmost Mekong Delta, Vietnam. J. Hydrol. Reg. Stud. 40. https://doi.org/10.1016/j.ejrh.2022.101010.

Bauer, J. et al., "Seawater intrusion in river delta systems. Inter-annual dynamics and drivers of salinity variations in the southern Mekong Delta, Vietnam," vol. 661, no. June, 2025, doi: 10.1016/j.jhydrol.2025.133745.

Bui, D.D., Nguyen, N.C., Bui, N.T., Le, A.T.T., Le, D.T., 2017. Climate change and groundwater resources in Mekong Delta, Vietnam. J. Groundw. Sci. Eng. 4 (2).

Buschmann, J. et al., "Contamination of drinking water resources in the Mekong delta floodplains : arsenic and other trace metals pose serious health risks to population," vol. 34, pp. 756–764, 2008, doi: 10.1016/j.envint.2007.12.025.

Canada, H. *Guidelines for Canadian recreational water quality*. 2024.

Chang, M., McBroom, M.W., Beasley, R.S., 2004. Roofing as a source of nonpoint water pollution. J. Environ. Manag. 73 (4), 307–315. https://doi.org/10.1016/j.jenvman.2004.06.014.

Chau, N.D.G., Sebesvari, Z., Amelung, W., Renaud, F.G., 2015. Pesticide pollution of multiple drinking water sources in the Mekong Delta, Vietnam: evidence from two provinces. Environ. Sci. Pollut. Res. 22 (12), 9042–9058. https://doi.org/10.1007/s11356-014-4034-x.

Chidamba, L., Korsten, L., 2015. A scoping study on the prevalence of *Escherichia coli* and Enterococcus species in harvested rainwater stored in tanks. Water SA 41 (4), 501–508. https://doi.org/10.4314/wsa.v41i4.09.

DONRE Ca Mau, "Ca Mau province water resources master plan to 2025, with orientation toward 2035," 2018.

Dörr, F., Bauer, J., Tran, H.V., Norra, S., Nestmann, F., 2023. Vietnams Mekong-Delta - Landsenkung infolge von Grundwasserübernutzung. Wasserwirtschaft 113 (11), 52–56. https://doi.org/10.1007/s35147-023-1922-3.

Dörr, N., Schenk, A., Hinz, S., 2024. Land subsidence in the Mekong Delta derived from advanced persistent scatterer interferometry with an infrastructural reference network. IEEE J. Sel. Top. Appl. Earth Obs. Remote Sens. 17, 12077–12091. https://doi.org/10.1109/JSTARS.2024.3420130.

Dörr, F., et al., 2025. Passive subsurface characterization in subsiding deltas: assessing land subsidence mitigation potential with frequency analyses of groundwater heads and superposing harmonic drivers. J. Hydrol. 662. https://doi.org/10.1016/j.jhydrol.2025.133844. July.

Danh, V.T. and Khai, H.V. "Household demand and supply for clean groundwater in the Mekong Delta, Vietnam," 2015, doi: 10.1186/s40807-014-0004-7.

Erban, L.E., Gorelick, S.M., Zebker, H.A., 2014. Groundwater extraction, land subsidence, and sea-level rise in the Mekong Delta, Vietnam. Environ. Res. Lett. 9 (8). https://doi.org/10.1088/1748-9326/9/8/084010.

General Statistics Office, "Ca Mau." pp. 69–70, 2022.

General Statistics Office, "Statistical yearbook of Vietnam 2022." pp. 0–1268, 2023.

Hamilton, K., et al., 2019. A global review of the microbiological quality and potential health risks associated with roof-harvested rainwater tanks. NPJ Clean Water 2 (1). https://doi.org/10.1038/s41545-019-0030-5.

Hoan, T.V., Richter, K., Börsig, N., Bauer, J. and Ha, N.T. "An Improved Groundwater Model Framework For Aquifer Structures of the Quaternary-Formed Sediment Body in the Southernmost Parts of the Mekong Delta, Vietnam," 2022, doi: 10.3390/hydrology9040061.

Hoan, T.V., et al., 2025. The utilization of a 3D groundwater flow and transport model for a qualitative investigation of groundwater salinization in the Ca Mau Peninsula (Mekong Delta, Vietnam). Hydrology 12 (5), 1–27. https://doi.org/10.3390/hydrology12050126.

Karlsrud, K., Vangelsten, B.V., Frauenfelder, R., 2017. Subsidence and shoreline retreat in the Ca mau province - vietnam causes, consequences and mitigation options. Geotech. Eng. 48 (1), 26–32.

Leister, C., Reiner, J.E., Grießmeier, V., Gescher, J., Hügler, M., 2023. Gastropods as a source for fecal indicator bacteria in drinking water. Water Res. 244. https://doi.org/10.1016/j.watres.2023.120494. June.

Li, L., Li, C.S., Wichelns, D., 2016. Assessing household willingness to pay for bottled water in rural areas of the Mekong Delta, Vietnam. Water Resour. Rural Dev. 7, 36–49. https://doi.org/10.1016/j.wrr.2016.03.001.

Linh, T., Tran, L., Anh, T., Nguyen, H., 2023. Navigating water policy : vietnam ' s strategic shift in the mekong river basin (2017-2021). Resolusi J. Sos. Polit 6 (1), 60–75. http://doi.org/10.32699/resolusi.v6i1.3704.

Lleò, M.D.M., Bonato, B., Benedetti, D., Canepari, P., 2005. Survival of enterococcal species in aquatic environments. FEMS Microbiol. Ecol. 54 (2), 189–196. https://doi.org/10.1016/j.femsec.2005.03.016.

Martin, A.R., Coombes, P.J., Harrison, T.L., Dunstan, H.R., 2010. Changes in abundance of heterotrophic and coliform bacteria resident in stored water bodies in relation to incoming bacterial loads following rain events. J. Environ. Monit. 12 (1), 255–260. https://doi.org/10.1039/b904042k.

Mekong River Commission, 2019. State of the Basin Report 2018. Mekong River Comm, pp. 1–274 [Online]. Available: http://www.mrcmekong.org/assets/Publications/SOBR-v8_Final-for-web.pdf.

Minderhoud, P.S.J., Coumou, L., Erkens, G., Middelkoop, H., Stouthamer, E., 2019. Mekong delta much lower than previously assumed in sea-level rise impact assessments. Nat. Commun. 10 (1), 1–13. https://doi.org/10.1038/s41467-019-11602-1.

Minderhoud, P.S.J., Middelkoop, H., Erkens, G., Stouthamer, E., 2020. Groundwater extraction may drown mega-delta: projections of extraction-induced subsidence and elevation of the mekong delta for the 21st century. Environ. Res. Commun. 2 (1). https://doi.org/10.1088/2515-7620/ab5e21.

Nachson, U., et al., 2022. New modelling approach to optimize rainwater harvesting system for non-potable uses and groundwater recharge : a case study from Israel. Sustain. Cities Soc. 85, 104097. https://doi.org/10.1016/j.scs.2022.104097. May.

Nguyen, D.C. "Rainwater For Drinking in Vietnam : Barriers and Strategies Bui Thi Thuy, Anh Dung Dao, Mooyong Han Viet Anh Nguyen, Hyunju Park, Pham Dang Manh Hong Luan, Nguyen Thi Thanh Duyen and Hong Quan Nguyen," pp. 585–594, 2019, doi: 10.2166/aqua.2019.054.

Olaoye, O., Olaniyan, R.A, 2019. Quality of rainwater from different roof material. Int. J. Eng. Technol. 2 (8), 1413–1421.

Özdemir, S., Elliott, M., Brown, J., Nam, P.K., Hien, V.T., Sobsey, M.D., 2011. Rainwater harvesting practices and attitudes in the mekong delta of Vietnam. J. Water Sanit. Hyg. Dev. 1 (3), 171–177. https://doi.org/10.2166/washdev.2011.024.

Pechstein, A. et al., "Detailed investigations on the hydrogeological situation in Ca Mau province, Mekong Delta, Vietnam. Technical Report No III-5 of Technical Cooperation Project 'Improving groundwater protection in the Mekong Delta,'" no. December, 2018.

Pham, V.C., et al., 2023. Groundwater use habits and environmental awareness in ca mau province, Vietnam : implications for sustainable water resource management. Environ. Challenges 13, 100742. https://doi.org/10.1016/j.envc.2023.100742. March.

Sadanandan, B. and Yogendraiah, K.M. "Enterococcus faecalis biofilm: a clinical and environmental hazard," p. 5, 2025, doi: 10.3390/msf2025035005.

Sakati, S.N., Mallongi, A., Ibrahim, E., Palutturi, S., Mallongi, A., 2023. Utilization of rainwater as consumable water with rainwater harvesting methods : a literature review. Pharmacognosy 15 (6), 1254–1257. https://doi.org/10.5530/pj.2023.15.227.

Thomson, P., et al., 2019. Science of the total environment rainfall and groundwater use in rural Kenya. Sci. Total Environ. 649, 722–730. https://doi.org/10.1016/j.scitotenv.2018.08.330.

Thu Ha, D., Hoang, H.N., 2014. Proposed solutions for household rainwater collection and storage in the Mekong Delta. Water Resour. Eng. Environ. Vietnam 44, 121–125.

Tran, T.A.N.H., Yong, M.L.I., 2025. Navigating water challenges in the Vietnamese Mekong Delta : how can a shift in water management help? Asia Pac. Issues. 29 (172).

Tran, D.A., et al., 2021. Groundwater quality evaluation and health risk assessment in coastal lowland areas of the Mekong Delta, Vietnam. Groundw. Sustain. Dev. 15, 100679. https://doi.org/10.1016/j.gsd.2021.100679. December 2020.

Van Muoi, L., Srilert, C., Dang, V.P., Van, T.P., 2022. Journal of hydrology : regional studies spatial and temporal variabilities of surface water and sediment pollution at the main tidal-influenced river in Ca mau peninsular, vietnamese mekong delta. J. Hydrol. Reg. Stud. 41, 101082. https://doi.org/10.1016/j.ejrh.2022.101082. April.

Van Tuan, P., Jiang, Y., Stigter, T., Zhou, Y., 2024. Groundwater for sustainable development understanding groundwater use and vulnerability of rural communities in the Mekong Delta : the case of Tra Vinh province, Vietnam. Groundw. Sustain. Dev. 25, 101095. https://doi.org/10.1016/j.gsd.2024.101095. December 2023.

Vanderford, B.J., Mawhinney, D.B., Trenholm, R.A., Zeigler-Holady, J.C., Snyder, S.A., 2011. Assessment of sample preservation techniques for pharmaceuticals, personal care products, and steroids in surface and drinking water. Anal. Bioanal. Chem. 399 (6), 2227–2234. https://doi.org/10.1007/s00216-010-4608-5.

Vinh, D.H., Tran, D.D., Cham, D.D., Thi, P., Hang, T., Man, D.B., 2024. Integrated exploitation of rainwater and groundwater : a strategy for water self-sufficiency in Ca Mau province of the Mekong Delta. Hydrology. https://doi.org/10.3390/hydrology11040055.

Vo, T.M.H., et al., 2025. How consistent are adaptation strategies with ongoing climatic and environmental changes in the Vietnamese Mekong Delta: a systematic review. Environ. Sci. Policy 168. https://doi.org/10.1016/j.envsci.2025.104064. January.

Vuong, H., et al., 2025. Assessment of long - term rainfall trends and variability in the vietnamese mekong delta : implications for water resources management strategies. Discov. Environ. https://doi.org/10.1007/s44274-025-00233-7.

Wartalska, K., et al., 2024. The potential of rainwater harvesting systems in europe – current state of art and future perspectives. Water Resour. Manag. 38 (12), 4657–4683. https://doi.org/10.1007/s11269-024-03882-0.

WHO, 2022. Guidelines For Drinking-Water quality: Fourth edition Incorporating the First and Second Addenda. World Health Organization, pp. 1–614.

Wilbers, G.J., Sebesvari, Z., Rechenburg, A., Renaud, F.G., 2013. Effects of local and spatial conditions on the quality of harvested rainwater in the Mekong Delta, Vietnam. Environ. Pollut. 182, 225–232. https://doi.org/10.1016/j.envpol.2013.07.019.

Willett, J.L.E., Dunny, G.M., 2024. Insights into ecology pathogenesis, and biofilm formatio of Enterococcus faecalis from functional genomics. Microbiol. Mol. Biol. Rev. 89. https://doi.org/10.1128/mmbr.00081-2323.

Yamane, T. *Introductory analysis*. 1973. doi: 10.2307/2311831.

Zdeb, M., Zamorska, J., Papciak, D., Skwarczyńska-Wojsa, A., 2021. Investigation of microbiological quality changes of roof-harvested rainwater stored in the tanks. Resources 10 (10). https://doi.org/10.3390/resources10100103.

Zoccarato, C., Minderhoud, P.S.J., Teatini, P., 2018. The role of sedimentation and natural compaction in a prograding delta : insights from the mega mekong delta, Vietnam. Sci. Rep. 1–13. https://doi.org/10.1038/s41598-018-29734-7. January.

B.6. Tidal effects on surface water salinity: Bauer et al. (2026 - under review)

Tidal Control of Salinity Dynamics and Seawater Intrusion in the Southern Mekong Delta, Vietnam

Jonas Bauer[a*], Felix Dörr[a], Andreas Schenk[b], Vũ Hoàng Thái Dương[c], Hoan Viet Tran[a], Van Cam Pham[a], Nicolas Börsig[a], Roderick van der Linden[d], Ngoc Hoa Nguyen[e], Elisabeth Eiche[a], Stefan Norra[f]

[a] Karlsruhe Institute of Technology (KIT), Institute of Applied Geosciences, Karlsruhe, Germany

[c] Water Resources University, Ho-Chi-Minh-City, Viet Nam

[b] Karlsruhe Institute of Technology (KIT), Institute of Photogrammetry and Remote Sensing

[d] Karlsruhe Institute of Technology (KIT), Institute of Meteorology and Climate Research

[e] National Center for Hydro-Meteorological Forecasting of Vietnam, Hanoi

[f] Potsdam University, Institute of Environmental Sciences and Geography, Potsdam - Golm, Germany

*Corresponding author. E-mail address: jonas.bauer@kit.edu (J. Bauer).

Abstract

Study region: Ca Mau Province, Mekong Delta, Vietnam.

Study focus: As sea levels rise and freshwater resources decline, seawater intrusion (SWI) poses an increasing threat to many delta systems worldwide. Effective mitigation strategies for SWI require a fundamental understanding of underlying processes, supported by sufficient observational field data. In the Vietnamese Mekong Delta, SWI recurs annually during the dry season, adversely affecting agriculture and ecosystems. While long-term trends and interannual fluctuations represent baseline conditions, short-term, tide-driven salinity fluctuations can push the system over critical management thresholds. This study examines the sub-seasonal interplay between tide-driven water level fluctuations and salinity. Time series analyses, including harmonic analysis, were applied to data from three monitoring stations in Ca Mau Province between January and June in 2017 and in 2018 to identify their dynamics and derive involved processes.

New hydrological insights for the region: Results show that co-oscillations of two different tidal regimes in the east and in the west influence water level patterns and ultimately salinity dynamics. Frequency analyses revealed salinity variations at major tidal frequencies. A sliding window Harmonic Least Squares approach captured the non-stationary behavior expected in estuarine systems at all three stations, with weighted R^2 values of 0.85 to 0.98 for water level and 0.53 to 0.73 for salinity. The findings of this study highlight the spatiotemporal complexity of salinity variations in the study region.

Keywords: Seawater Intrusion, Estuaries, Time Series Analysis, Harmonic Analysis, Tides, Ca Mau Province

1 Introduction

Seawater intrusion (SWI) amplified by climate change and anthropogenic modifications of hydrological regimes is a major challenge for coastal regions and delta systems globally (Lee et al., 2025; Mohammed and Scholz, 2017). The inland progression of seawater into river and surface water systems is a dynamic and complex process with distinct temporal and spatial characteristics. SWI leads to the degradation of valuable freshwater resources and agricultural farmland (Bucx et al., 2014; Nicholls et al., 2021; Rahman et al., 2019). The high socio-ecological impact of SWI is particularly pronounced in the low-lying Asian mega-deltas (Bucx et al., 2014), adversely affecting drinking water resources and agricultural production, threatening food security both regionally and beyond (Schneider and Asch, 2020). The Vietnamese Mekong Delta (MD) inhabits more than 17 million people and ranks among the most agriculturally productive river deltas in the world (Eslami et al., 2021b; GSOV, 2024; Park et al., 2022). Farmers in the MD critically depend on sufficient freshwater resources for agriculture (Pham et al., 2023), but these resources are sharply declining due to SWI (Binh et al., 2025; Normandin et al., 2024). Meanwhile, groundwater is being heavily overexploited, leading to a sharp decline in hydraulic heads (Dörr et al., 2026; Duy et al., 2021; Hoan et al., 2025) and triggering both land subsidence and salinization (Bauer

et al., 2022; Dörr et al., 2025a; Minderhoud et al., 2017). As land subsidence is an existential threat in the low-lying MD (Dörr et al., 2025b; Kondolf et al., 2022), a further decline of freshwater resources due to riverine SWI must be prevented.

Consequently, given that progressive SWI driven by multiple factors poses a major challenge to sustainable development in the MD, research efforts in recent years have intensified to identify its drivers and to develop mitigation strategies (Bauer et al., 2025; Loc et al., 2021b; Park et al., 2022; Tran et al., 2024a).

In estuarine systems, riverine SWI occurs across multiple time scales as a result of variations in the hydraulic pressure gradient between river discharge and sea levels (Savenije, 2012). Understanding long-term trends and interannual fluctuations is critical for establishing baseline conditions, detecting emerging risks, and for informing sustainable development strategies. In the MD, seasonal salinity levels and interannual variations are primarily controlled by upstream river discharge (Bauer et al., 2025; Binh et al., 2020a), but due to anthropogenic interventions, interannual variations increased substiantially over the last decades, amounting to more than 15 g/L in peak dry season salinity in CMP (Bauer et al., 2025).
Superimposed on these large-scale patterns are high-frequency salinity variations driven by tide-controlled water level fluctuations on the diurnal to fortnightly scale, which are equally essential to understand (Cai et al., 2025), particularly in a complex multi-channel system such as the MD (Eslami et al., 2019; Nguyen and Savenije, 2006). Short-term, tide-driven water level dynamics influence key estuarine processes, which are not simple residuals of gravitational forcing but result from nonlinear interactions, which can reshape the net salt transport and modulate the inland extent of SWI even under stable upstream conditions (Geyer and MacCready, 2014). Nonlinear interactions between tidal forcing and river discharge can amplify or dampen SWI (Savenije, 2012). Short-term excursions, especially during spring-neap cycles or low-discharge periods, can push the system over critical ecological or management thresholds, exposing freshwater-dependent ecosystems, agricultural areas or water supply facilities to sudden and extreme salinity levels that cannot be predicted from long-term averages alone

(Wang et al., 2022). In periods that are characterized by reduced river discharge and precipitation, the tidal influence on salinity levels increases (Gaiolini et al., 2023). Due to upstream reservoir management and intensifying hydrological droughts, low discharge periods of the Mekong River can emerge earlier and last longer (Bauer et al., 2025). Accordingly, a recent study found that the tidal influence along the Mekong River is accelerating due to anthropogenic influences (Nguyen et al., 2025).

Understanding short-term dynamics is essential for improving process-based models and numerical simulations under both current and changing boundary conditions, thereby supporting adaptive management, early warning systems, and community resilience (Chen, 2023). In the MD, this is particularly crucial because hydrological conditions are heavily influenced by ongoing extensive dam development, sand mining and canal projects (Jordan et al., 2020, 2019; Kumar et al., 2024; Tran et al., 2024b), resulting in alterations to the Mekong River´s discharge and coastal morphology (Ang et al., 2024; Lu and Chua, 2021).

Most previous studies directly employed various modelling approaches to simulate and predict water-level-dependent salinity levels and the extent of SWI in different areas of the MD, but mostly relied on short periods of in-situ observations used for calibration and validation, often ranging between a few days to weeks (Eslami et al., 2021a; Khang et al., 2008; Lam, 2020; Tran et al., 2024b; Tran et al., 2019). Assuming a straightforward relationship between the two parameters and extrapolating it over the long term may result in inaccuracies and potentially false predictions, as this approach overlooks the full spectrum of sub-seasonal variability driven by spring-neap cycles and nonlinear interactions between tidal forcing and upstream discharge. So far, tidal characteristics along the MD and water level fluctuations in the tide influenced rivers are mostly described with a seasonal resolution (Nguyen et al., 2023; Phan et al., 2019), overlooking finer-scale diurnal and fortnightly tidal dynamics.

In this context, machine learning techniques hold considerable potential for both short- and long-term predictions (e.g. Guillou et al., 2023; Qian et al., 2022). But without a

fundamental understanding of the underlying processes, the implementation of countermeasures will remain ineffective.

Therefore, the objective of this study is to understand the processes controlling tide-driven salinity fluctuations by analyzing short-term, high-frequency salinity variations and the hydrodynamic interactions that govern them. Harmonic analyses are employed to identify major periodicities and to delineate stationary as well as non-stationary dynamics for water level and salinity in the periods January to June in 2017 and in 2018. This work complements previous work on interannual SWI dynamics in CMP (Bauer et al., 2025), and completes the picture of salinity dynamics in the southern MD across multiple timescales.

The methods and insights developed in this study will support the implementation and improvement of current SWI mitigation strategies and are transferable to other coastal provinces of the MD, as well as to comparable deltaic regions across Southeast Asia and beyond where similar tidal and hydrological dynamics prevail.

2 Study area

2.1 Overview

Figure 1 shows the location of the MD in Southeast-Asia as well as the river network and the location of the monitoring stations in CMP used in this study. The Vietnamese MD, one of the largest river delta systems globally, together with the adjacent metropolis of Ho-Chi-Minh-City, is home to 27 million people (GSOV, 2024). The region is renowned for its vast patches of rice fields and aquaculture production, which play a crucial role in ensuring the nation's food security and enhancing its export capacity. Located on the Ca Mau Peninsula, CMP is the southernmost province of Vietnam, covers an area of 5,221 km^2 and inhabits around 1.2 million people (GSOV, 2024). Please note that the administrative structure of the MD provinces was

reorganized in 2025. The nomenclature and representation used in this study refer to the former provincial boundaries.

Outside the provincial capital, Ca Mau City, most residents live in rural areas along an extensive network of rivers and channels (Figure 1b). They are primarily engaged in diverse small-scale aquaculture and agricultural activities, including traditional rice farming in areas protected from SWI and various forms of aquaculture and adapted crop rotation systems, with shrimp farming being particularly prominent (Nguyen et al., 2019a; Thong et al., 2010; Vu et al., 2022). These activities depend on sufficient water resources, and in the past, local water conflicts have emerged over the competing needs for freshwater in rice farming and brackish water in shrimp farming (Hoanh et al., 2009; Nguyen et al., 2019b).

The region's climate is governed by the tropical monsoon, characterized by a dry season from approximately December to April and a rainy season from May to November. Most precipitation occurs during the rainy season, with annual rainfall reaching up to 2,500 mm in CMP (Dang et al., 2020; Pham-Thanh et al., 2021). Mean monthly temperatures range between 25 °C and 30 °C with humidity levels above 80 % throughout the year (GSOV, 2024). The average elevation in 2018 was below 0.8 m above mean sea level, with many areas in CMP below that average (Minderhoud et al., 2019a; Zoccarato et al., 2018). The study area is surrounded by the sea on three sides, making it exceptionally prone to SWI and coastal erosion.

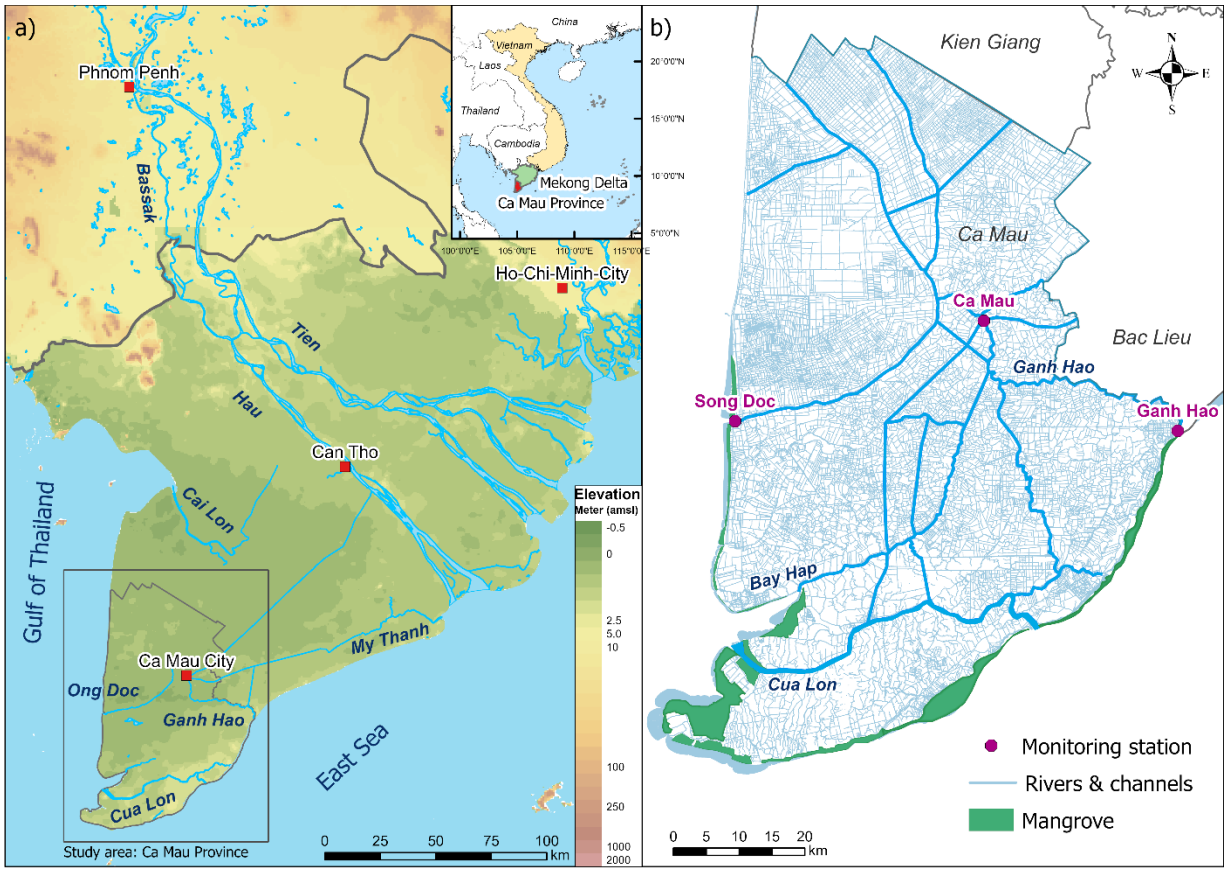


Figure 1 a) Overview of the Mekong Delta and its location in Southeast Asia. Surface elevation in 2018 (not linear) in the Mekong Delta from Minderhoud et al. (2019b). *Surface elevation outside the MD from the Global Topographic 30 Arc-Second Digital Elevation Model GTOPO30* (EROS, 2017). *b) Ca Mau Province and its river network as well as the location of the monitoring stations Song Doc, Ca Mau and Ganh Hao.*

2.2 Hydrological regime and seawater intrusion

Originating from the Tibetan Plateau and flowing through China, Thailand, Laos, and Cambodia, the Mekong River finally enters Vietnam, delivering freshwater and sediments to the delta before ultimately discharging into the East Sea (South China Sea). Discharge of the Mekong River controls water levels in the delta and is subject to strong seasonal as well as interannual variations (Mohammed et al., 2018). Peak water levels in the coastal areas occur at the end of the rainy season, typically between October in the upper delta and in December in the Ca Mau Peninsula. As the dry season begins, discharge sharply decreases, resulting in lowest annual water levels in the coastal areas in June to July (Schwarzer et al., 2016). The largest proportion of

the Mekong River's discharge, almost 90 %, is discharging into the East Sea via its eight main branches, while only a small proportion is flowing through the southern MD plain via the large irrigation canals parallel and perpendicular to the Hau River (Renaud and Kuenzer, 2012). Water infrastructure is omnipresent as the region is characterized by tidal rivers and an extremely dense network of man-made canals, which are used for transportation and irrigation purposes.

Since 2010 an increasing number of upstream hydropower dams and reservoirs substantially alter the discharge patterns of the Mekong River (Binh et al., 2020a). To ensure hydropower production and to mitigate downstream water shortages for agriculture, discharge in the dry season almost doubled in the upper and middle Mekong River Basin and decreased in the rainy season to prevent floods. As a consequence, however, discharge from the Mekong River entering Vietnam slightly decreased in the early dry season (Binh et al., 2021, 2020b), promoting an early dry season onset, an increased duration of the dry season and therefore higher salinity levels (Bauer et al. 2025).

Beyond the seasonal impact of Mekong River discharge on deltaic water levels, tidal forces drive fluctuations on timescales ranging from daily to fortnightly. The MD is classified as a tide-wave dominated regime (Ta et al., 2002b), with the western part at the Gulf of Thailand (GOT) being more influenced by waves attributed to the southwest monsoon and the eastern part by the tidal regime of the East Sea (Phan et al., 2019). Tidal signals in the dry season, when river discharge is low, can reach as far as Phnom Penh, the capital of Cambodia, which is located 300 km upstream (Hung et al., 2012; Nguyen et al., 2023). Tidal fluctuations are significantly affected by bathymetry and the shape of the coast or basin they propagate (Phan et al., 2019). In the study area, two distinct tidal regimes can be distinguished, with the GOT having a mixed, mainly diurnal system and the East Sea having a mixed semi-diurnal system (Nguyen et al., 1998; Phan et al., 2019). The mixed semi-diurnal tide in the East Sea is identified by two high waters and two low waters of varying amplitude per tidal day. Due to seasonal effects and the spring-neap tide cycles, tidal amplitudes at the eastern

coast vary between 1.0 m and 3.8 m, while at the western coast in the GOT tidal amplitudes are much lower with a maximum of about 0.7 m (Hoanh et al., 2009; Phan et al., 2019). In general, the tidal range decreases from the central MD coast along the East Sea southwestward, with lowest tidal ranges at the West Coast and in the GOT (Vu et al., 2025).

In CMP, the rivers Ong Doc and Bay Hap in the west, Ganh Hao in the east, and Cua Long directly connecting the GOT and the East Sea are the primary rivers in the study area affected by SWI (Figure 1). The secondary irrigation channels along these rivers are locally managed via sluice gates and pumping operation to control salinity levels for freshwater rice farming and saltwater related aquaculture (Di Giusto et al., 2021; Hoanh et al., 2009; Nguyen et al., 2020).

On average, river depth is about 3-5 m except for Cua Lon River (5-19 m) and Ganh Hao River (5-14 m). The depths of secondary channels and irrigation canals is generally shallower.

3 Data and Methods

3.1 Monitoring sites and data acquisition

Salinity and water level data from January to June in 2017 and 2018 were obtained by the National Center for Hydro-Meteorological Forecasting of Vietnam, Hanoi, from three hydrological monitoring stations in CMP: Song Doc (SD), Ca Mau (CM), and Ganh Hao (GH) (Figure 1). These two years were chosen as they provide the most recent continuous datasets for the region and were not affected by severe droughts, reducing complexity in analyzing the salinity–water-level relationship and involved processes. SD lies about one kilometer upstream on the Ong Doc River near the Gulf of Thailand, GH is located two kilometers upstream on the Ganh Hao River adjacent to the East Sea, and CM is situated roughly 40 kilometers further inland along Ganh Hao River, centrally within CMP (Figure 1). Salinity was measured manually or semi-automatically every two hours, at odd-numbered hours, over approximately three

consecutive days, followed by pauses of two to four days. Therefore, approximately half of the days within the measurement period are missing.

Measurements were conducted during the dry season and at the onset of the rainy season, between January and June, when data were used to directly support local water management decisions, particularly sluice gate operations. Water levels were available in 1-hourly resolution without gaps.

Shape files for the river network (Figure 1) were provided by the National Center for Water Resources Planning and Investigation, Hanoi, Vietnam.

3.2 Time series preprocessing

In order to evaluate diurnal to fortnightly salinity variations via harmonic analysis, where 1-hourly timesteps are generally recommended in the context of tidal analysis (e.g. Foreman, 2004), and for the purpose of better overall comparability with the 1-h water level data set, a continuous 1-hour data set for 2017 to 2018 was obtained from the original 2-hour data record with missing days intervals by a two-step linear interpolation. First, data from missing days were interpolated using linear interpolation with tidal phase alignment to ensure tide-synchronous reconstruction. Missing observations at a given time of a missing day (e.g., measurements at 01:00 am) were estimated by linearly interpolating data recorded at the same time on adjacent days with available observations.

Subsequently, the data was recombined to a continuous 2-hour dataset and linear interpolation was used once more to obtain a continuous salinity dataset with 1-hour sampling. Examples of a two-week period and a one-week period at SD, CM and GH stations with missing days in between is displayed in Figure 2. Nguyen et al. (2023) presented an alternative approach to obtain a continuous dataset, in which missing consecutive days of less than one week were spatially interpolated from neighboring monitoring stations. For the present study, this approach is considered inappropriate because local differences between stations in regard to water

level dynamics and differences in salinity, as well as different tidal regimes, are too high to justify cross-station interpolation. In addition, data gaps at other monitoring stations in the MD may further impair interpolation. Eslami et al. (2021a) employed model computations to generate 1-hourly datasets for six stations at the mouth of the Mekong River, yet there is potential to enhance the accuracy of their method as the model encountered some challenges to accurately represent the scattered observation values derived from the irregular 2-hourly data. The method presented here can very well replicate the salinity dynamics for missing days at all three stations. However, it must be noted that this interpolation naturally cannot replicate extremes caused by short-term events, such as heavy precipitation or storm surges, and assumes a day-to-day periodicity. Heavy, localized precipitation can temporarily enhance seaward flow, thereby dampening tidal control and diluting river water salinity. Storm surges are episodic events that drive seawater landward and may superimpose on tidal signals but are not part of the regular high-frequency tidal variability. As such events occur infrequently, they are assumed not to substantially influence the overall interpretation of the analysis over the study period.

In the last step the dataset was synchronized so that each time series spans the period from 4th January to 21st June of 2017 and 2018, respectively, ensuring consistency for direct comparisons.

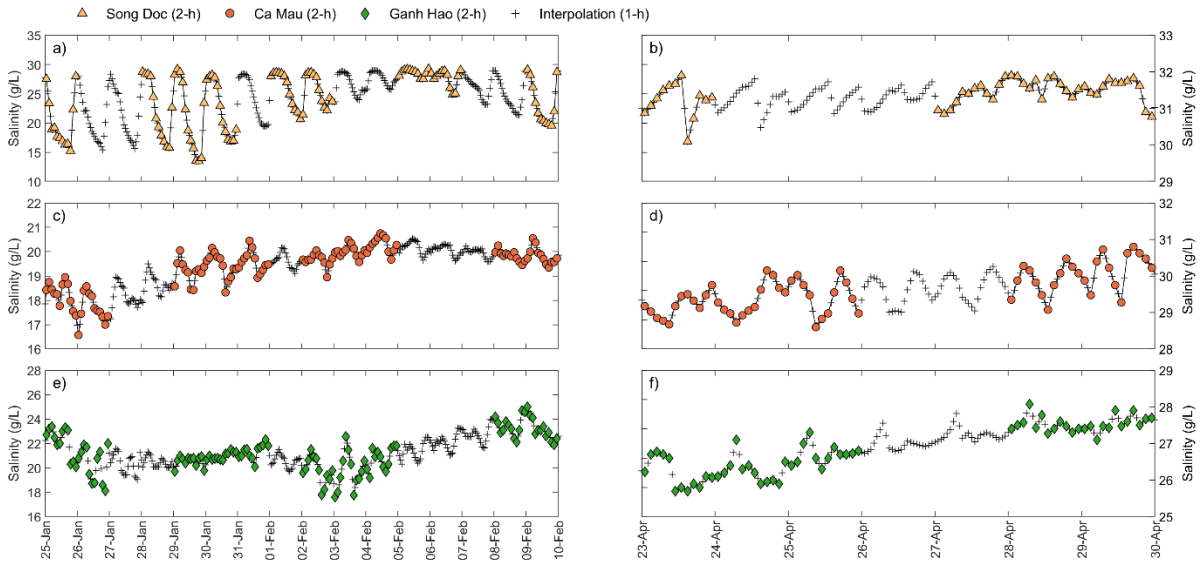


Figure 2. Representative examples of interpolation of discontinuous salinity data at Song Doc, Ca Mau and Ganh Hao monitoring sites in 2018 from 25 January to 10 February (a, c, e) and 23 April to 30 April (b, d, f).

The relationship between tidal water level fluctuations and salinity changes was analyzed using harmonic analysis. The timeseries were detrended using a 45-day moving average (MATLAB´s *movmean* function). Detrending improves frequency, amplitude and phase estimates, which can be masked or biased by long-term trends and low-frequency variations, and is a common step in harmonic analysis (e.g. Baranes et al., 2023). A 45-day window is commonly used as a filter or window length in tidal analysis, as it captures three cycles of fortnightly modulation and adequately resolves the major tidal constituents (Lobo et al., 2024). The original time series, the trendline and the detrended time series are shown in Figure 3.

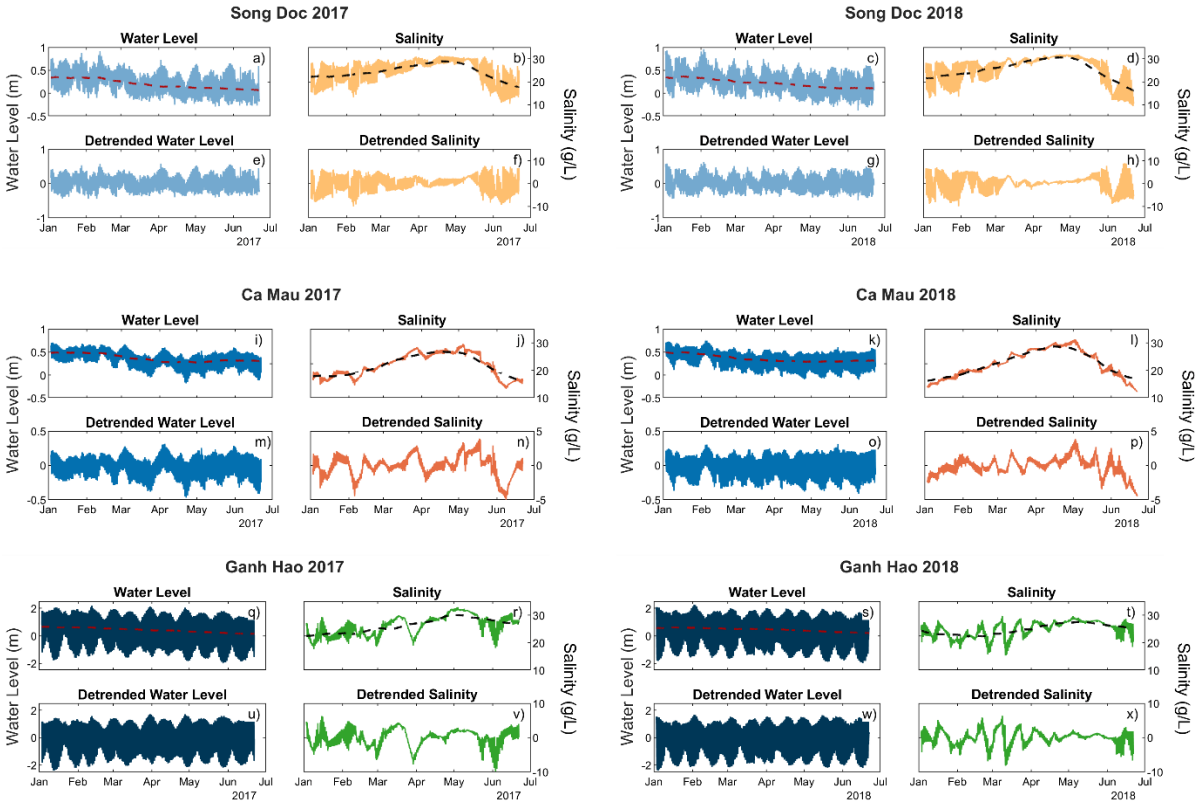


Figure 3 Original time series for water level and salinity at Song Doc (a) to (h), Ca Mau (i) to (p) and Ganh Hao (q) to (x) for January to June 2017 and 2018. The original time series were detrended with a 45-day moving mean. For each station and year, the upper charts show the original data with dashed trendlines and the lower charts the detrended time series respectively.

3.3 Harmonic analysis

In this study, Fast Fourier Transform (FFT) was used to identify dominant periodicities, whereas Harmonic Least Squares (HLS) provided more accurate amplitude estimates, enabled time-series reconstruction to quantify tidal control on salinity, and facilitated the computation of transfer functions to determine time lags of selected tidal frequencies between water level and salinity. All tidal frequencies considered in this study across the different analytical approaches are listed in Annex A.

FFT was applied on the interpolated and detrended timeseries (MATLAB´s *fft* function), effectively converting time-domain data into its frequency-domain representation (e.g. Foreman et al., 2009). Dominant frequencies for salinity and water level were identified and well-known tidal constituents (in cycles per day, cpd),

including M2 (1.9323 cpd, semi-diurnal lunar), S2 (2.0000 cpd, semi-diurnal solar), K1 (1.0027 cpd, diurnal lunar/solar) and O1 (0.9295 cpd, diurnal lunar) (Kvale et al., 1995; Pawlowicz et al., 2002; Phan et al., 2019) were assigned to obtained dominant peaks. Both amplitudes as well as phases were obtained for each constituent. FFT decomposes the signal into fixed, equally-spaced frequency bins and the obtained frequencies might differ from theoretical frequencies, and across stations and years. However, for the calculation of phase lag between water level (input) and salinity (output), uniform and precise frequencies are necessary, as otherwise the direct relationship is not accessible. To overcome this, HLS estimation was used. HLS is fitting a set of sinusoidal functions with precise and predefined target frequencies, e.g. tidal constituents, to the time series and estimates their amplitudes and phases. HLS has the advantage that it fits exact frequencies into the time series rather than scanning over fixed frequency bins like FFT, effectively separating noise and other non-target constituents to avoid amplitude loss. In addition, HLS can handle gaps and irregular sampling (Schweizer et al., 2021). Therefore, HLS amplitudes are assumed to be closer to the real physical oscillation.

HLS was configured with a comprehensive set of fixed astronomical constituents (Mm, MSf, Q1, O1, M1, K1, N2, M2, S2, M3, MK3, M4, MS4). Tidal constituents P1, K2 and MF are not considered individually to meet the Rayleigh criterion, as constituents should be separated by 1/T, where T is the length of the time series (Foreman et al., 2009; Pawlowicz et al., 2002). If two fitted frequencies are closer than df=1/T=0.0059, the columns of the HLS design matrix become nearly collinear, causing large parameter covariance, unstable amplitudes, phases and producing noise-sensitive fits (Codiga, 2011).

HLS was applied to multiple salinity datasets, including (i) the original 2-hourly timeseries with gaps, (ii) the original 2-hourly timeseries with gaps but detrended, and (iii) the interpolated 1-hourly detrended timeseries previously used for FFT. For each dataset, HLS amplitudes at O1, K1, M2, and S2 were extracted from the full-basis fit and compared with FFT amplitudes. Based on the results (see chapter 4.3.2), the 1-

hourly detrended series was selected for subsequent analysis as 1-hourly timesteps are generally recommended for tidal analysis (e.g. Foreman, 2004) and obtained amplitudes are the most consistent. Tidal components were reconstructed from the HLS coefficients and tidal control was quantified as explained variance (R^2) relative to the detrended series. HLS reconstruction was done with two separate approaches to answer two research questions. First, a stationary HLS model over the full time series record was estimated, e.g. SD 2017, and R^2 was calculated for water level and salinity. With this approach it is clarified how well one stationary harmonic model explains the whole time series. Nguyen et al. (2025) pointed out that non-stationary analyses are necessary to capture more dynamics. Therefore, the second approach involves a sliding HLS calculation to investigate how well a local harmonic model explains the water level and salinity data, as non-stationary behavior and phase shifts can be expected in an estuary setting (Lobo et al., 2024; Matte et al., 2013). While longer time series separate frequencies more effectively, shorter windows are able to resolve time variations of tidal patterns (Lobo et al., 2024).

Additionally, for each tidal constituent, a transfer function derived from the HLS coefficients summarizes the salinity response in time, expressed as phase lag, relative to water-level forcing at that frequency. The phase lag was translated into a time lag by taking the fraction of the constituent's cycle represented by the phase and converting it to hours using that constituent's period. Lags were wrapped to the range minus half to plus half a cycle.

For the sliding HLS approach, the harmonic regression in overlapping 45-day windows, advancing by one day, was calculated in the same way as the global HLS fit was calculated. Even though frequency resolution decreases for T=45 days, the Rayleigh criterion is still met for the used tidal frequencies.

In each window, a weighted HLS fit was calculated using a Hann taper, where points near the center are weighted higher to effectively reduce spectral leakage and edge artefacts (Babadi and Brown, 2014). The Rayleigh criterion is still met considering a

potential increase up to 1.5/T, as tapering reduces the nominal spectral resolution (Harris, 1978).

Each window's fitted tidal components were then used to generate predictions for every original timestep of that window. As windows overlap, most timesteps receive multiple predictions. To form the final HLS reconstruction, the multiple results for each individual timestep were averaged, improving overall robustness of the fit. As coverage increases in the first 22.5 days and is then constant until it decreases in the last 22.5 days, timesteps in the beginning and end of the time series have less predictions. Therefore, model performance was summarized for each station and year for water level and salinity using two global coefficients of determination. The first is the straightforward unweighted R^2 computed over all timesteps, assigning each timestep equal weights. The second is a coverage-weighted R^2 that uses the number of overlapping windows as weights, giving more weight to time periods supported by more window fits where the estimator is best supported. The coverage-weighted method effectively suppresses poor model performance at edges.

Uncertainty of the 45-day sliding HLS reconstruction was quantified using the analytic covariance of the regression coefficients in each window. From this, two complementary uncertainty measures were derived for every timestep (Matte et al., 2013; Pawlowicz et al., 2002): (i) the *mean-fit uncertainty*, describing uncertainty of the reconstructed harmonic signal itself, and (ii) the *prediction uncertainty*, which additionally includes residual variability and thus represents the expected scatter of observations around the HLS reconstruction. In addition, per-constituent amplitude and phase standard errors were estimated using linear error propagation via the delta method (Oehlert, 1992; Pawlowicz et al., 2002). Median values per station and year were summarized to characterize overall HLS reconstruction precision.

4 Results

4.1 Salinity variability

The diurnal amplitude of maximum and minimum salinity values for the 1-hourly salinity time series for January to mid of June in 2017 and in 2018 is shown in Figure 4. Salinity dynamics vary distinctly across the three sites SD, CM and GH. Varying between around 10 g/L and 30 g/L, the maximum diurnal differences of up to 16 g/L are observed in SD during the early dry season in January and the transition period between the dry and rainy seasons in June (Figure 4a). As the dry season progresses, salinity levels at all stations increase in both years, leading to a prominent decrease in the diurnal range. In the course of the dry season, the daily minimum salinities increase faster than the maximum values at all stations in 2017 and 2018. The CM inland station exhibited the smallest diurnal range, not exceeding 5 g/L for the observed years (Figure 4b). In both years and at all stations, salinity does not reach seawater salinity levels of 35 g/L, which was previously observed in years with hydrological drought (Bauer et al., 2025; Park et al., 2022).

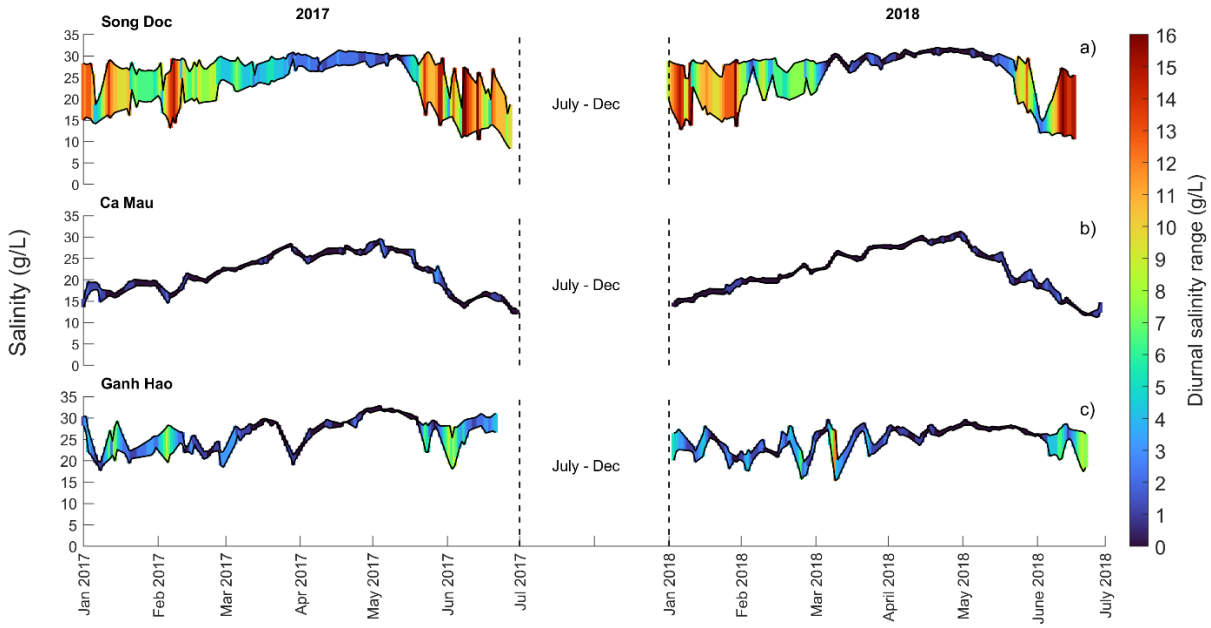


Figure 4. Diurnal salinity range of the continuous 1-h dataset at the three monitoring stations (a) Song Doc, (b) Ca Mau and (c) and Ganh Hao for 2017 and 2018.

4.2 Water level and tides

Variations in water levels and their dynamics can greatly influence salinity in tide-affected rivers, with salinity often responding to the periodic shifts in water levels (van Keulen et al., 2025). To explain the different diurnal salinity dynamics, a detailed characterization of the two tidal regimes in the GOT and East Sea was conducted, represented by SD and GH. Additionally, the water level characteristics at CM were analyzed. Results are presented in Figure 5 exemplary for the year 2018. At GH a tidal cycle with two highs and two lows of different magnitude are observed, while at SD both diurnal and sometimes semi-diurnal tides are present. Tides in the East Sea have a higher amplitude of almost 4 m at GH compared to SD with maximum amplitudes of less than 1 m. Spring tides in the East Sea, when water level and amplitude are highest, occur one to a few days after full and new moon, when the gravitational forces on Earth are at their peak due to the alignment of the moon and the sun (Kvale, 2006). Subsequently, neap tides with lower water levels and amplitudes occur after the first and third quarter. In contrast, at SD station located at the GOT, highest and lowest water levels respond to the declination change of the moon (Figure 5b).

Another aspect observed at GH is diurnal inequality, where one high tide is either higher or lower than the subsequent high tide within the same day (Figure 5f). In addition, semi-monthly inequality is caused by constituents M2 and N2 being in phase every 27.55 days (Kvale, 2006). This can be well observed at GH, as a weaker spring tide is followed by a stronger spring tide (Figure 5*e, f*). Therefore, the tide at GH can be referred to as mixed tide (Mukherjee et al., 2023). In conclusion, tides in the East Sea can be characterized as synodical, mixed-semidiurnal tides with an ideal cycle of 29.53 days and the tides in the GOT as tropical mainly diurnal tides, or equatorial tides, with an ideal cycle of 27.32 days.

In general, these findings are consistent with previous studies (Hoanh et al., 2009; Nguyet-Minh et al., 2025; Phan et al., 2019). However, while previous studies mainly analyzed the tidal regimes on the seasonal scale (Phan et al., 2019), this study analyzed the tidal characteristics in higher resolution for 2017 and 2018, evaluating sub-seasonal

deviations. Notable variations in these patterns due to the interaction of both tidal regimes are evident, and resulting tidal characteristics for CM can be described. Sea water flows from the East Sea to the GOT and vice versa (Cui et al., 2019; Hoanh et al., 2009), around and through CMP, and seem to cause complex tidal interaction observed at the coastal stations and connecting rivers. The gradual interplay of synchronous and asynchronous occurrences of spring and neap tides in the East Sea and the GOT results in complex water level responses at all three stations. The co-oscillation of both tides is particularly visible during spring tides at GH, for example mid of April 2018, as during this time mixed-semi-diurnal features replace the diurnal tides at SD (Figure 5a, c). In the subsequent neap tide at GH, the diurnal features at SD are restored. Water level fluctuations at CM seem to respond to both the East Sea and the GOT tidal patterns. Around the 26^{th} of March and the 9^{th} of April 2018, water levels at CM remained elevated as spring tides from the East Sea and the GOT occurred in close succession, overlapping during the low-water phase and amplifying water levels (Figure 5d).

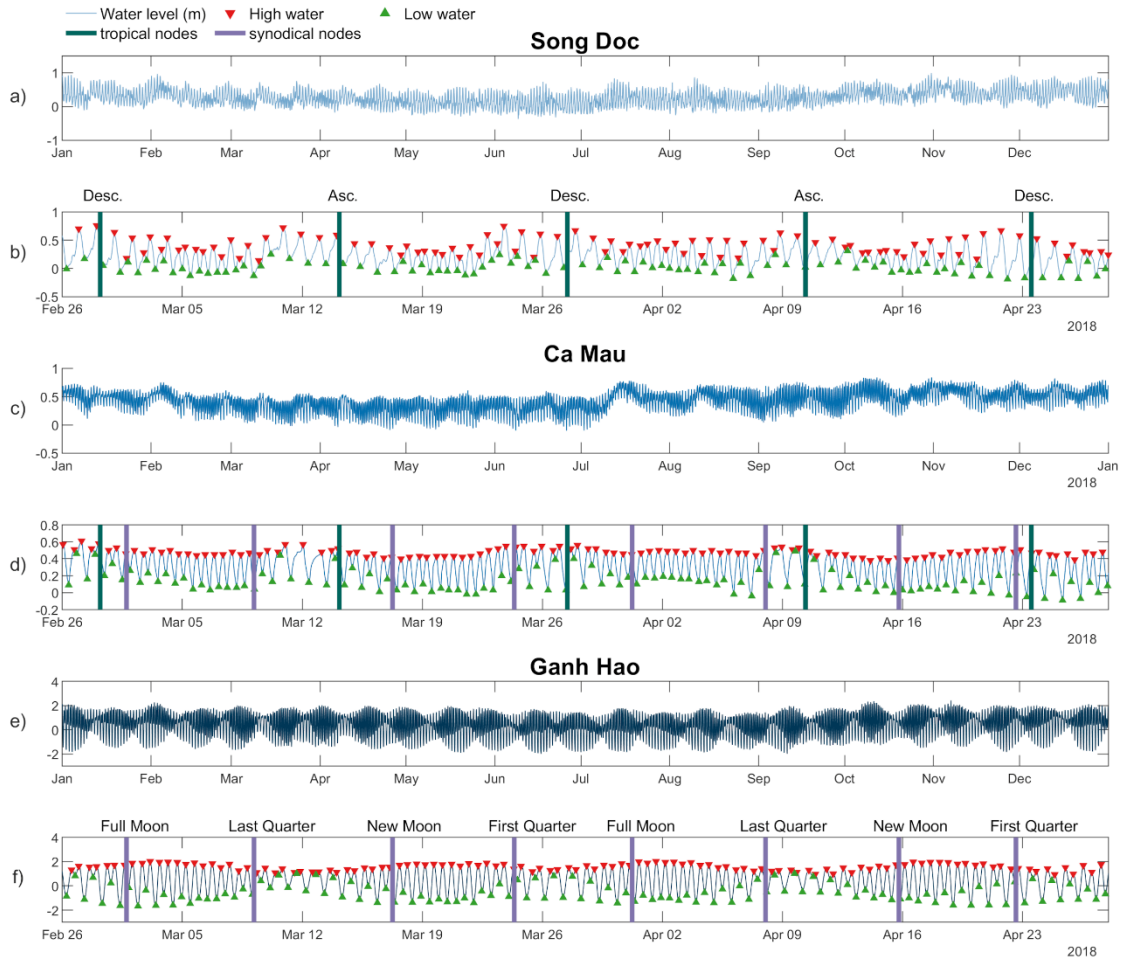


Figure 5. Changes of water levels due to tidal influence in 2018 at the monitoring sites of Song Doc, Ca Mau and Ganh Hao. Tiles b, d, f include indicators for high and low water peaks as well as bars representing moon cycle nodes for synodical and tropical tides.

4.3 The relationship between water level and salinity

4.3.1 General observations

Figure 6 shows the relationship between water levels and salinity during representative spring and neap tides at SD, CM, and GH in January and April 2018. In mid-January (Figure 6a), spring tides occur at SD and GH. At SD, diurnal water level peaks coincide with salinity peaks, although salinity decreases more slowly than the water level. The time lag between peak water level and peak salinity is approximately four hours at SD. At GH, semi-diurnal water level peaks are observed, where two peaks form a plateau until the water level drops to its minimum, and salinity follows the same pattern. In

terms of response times, the first peak has an immediate salinity response, while the second peak shows a response delay of about four hours. A third salinity peak at GH appears concurrent with the water level minimum. At CM, the water level pattern is similar to GH, with a plateau and an immediate salinity response after the first peak, followed by a four-hour delay for the second peak. However, a distinct third salinity peak during ebb tide is absent. The concurrent water level peak at SD and GH occurs at 2 AM local time on January 16$^{\text{th}}$, with the peak at CM happening six hours later at 8 AM.

During the subsequent neap tide at the end of January (Figure 6b), semi-diurnal features develop at SD for both water level and salinity, with salinity peaks delayed by two to three hours. At GH, besides a small increase in salinity during water level peak, highest salinity peaks occur during ebb tides every twelve hours and appear uncorrelated with the preceding water level peaks.

In early April 2018 (Figure 6c), spring tides in the East Sea, with pronounced semi-diurnal water level peaks, result in semi-diurnal water level peaks at SD, where neap tides are present. The delay between water level and salinity peaks at SD remains four hours, but only every second water level peak leads to a distinct salinity peak. At CM, well-defined semi-diurnal features dominate for both water level and salinity, with an almost immediate response. During the subsequent spring tide in the GOT (Figure 6*d*), diurnal water level patterns are restored at SD, and double-peak plateaus form at GH and CM during neap tides. While salinity at CM closely follows water level changes, at GH, several salinity peaks occur with some responding to water level peaks, while others appear unrelated and irregular.

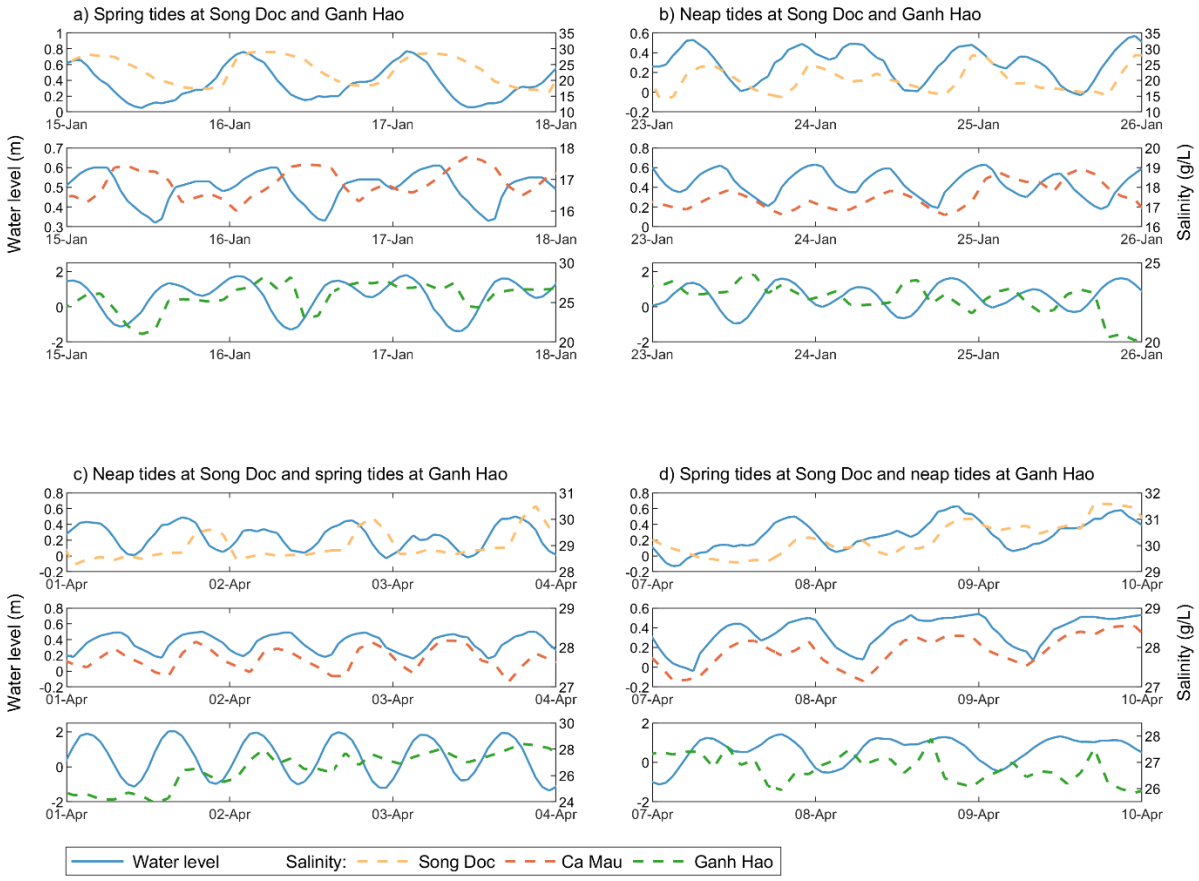


Figure 6. Water level (blue) and salinity at Song Doc, Ca Mau and Ganh Hao (colored) during synchronous and asynchronous spring tides in January and April 2018. Please *note that y-axis scales differ.*

4.3.2 Frequency analysis – Identifying periodic patterns

To further assess the periodic patterns of both water level and salinity, and to quantify their relationship displayed in Figure 6, harmonic analyses were performed. Results are presented in Figure 7, showing the FFT amplitude spectra for water level and salinity in 2017 and 2018. The most prominent diurnal (O1, K1), semidiurnal (M2, S2) and compound tides at around 3 cpd (MK3) and 4 cpd (MS4) are indicated. In addition, fortnightly constituents Mf and MSf, which are close to each other and cannot be resolved by FFT resolution here, are indicated by "F". Other constituents, like N2 or P1 are not labeled, but are present.

The water level at SD is mainly controlled by the diurnal tidal constituent K1, and to a lesser extent by O1. The semi-diurnal constituents M2 and S2 are also significant.

Conversely, at GH the semi-diurnal constituent M2 shows the highest amplitude. This result is consistent with results shown in Figure 6. For the salinity time series, K1 is also dominant at SD, and M2 has a four times smaller amplitude. At GH, while water level is dominated by M2, K1 and M2 are almost equal for salinity (Figure 7f). For CM, salinity frequencies are comparable to GH with much smaller amplitudes and M2 explains more of the variability than K1. For water levels, the semi-monthly frequencies noted as "F" have smaller magnitudes compared to the high-frequency components. On the other side, for salinity the fortnightly band shows high magnitudes and the low-frequency peaks are higher than the high-frequency peaks. At CM, peaks at diurnal and semi-diurnal tidal frequencies are smaller than the peaks occurring in the low-frequency part. In general, salinity peaks in the low-frequency domain beyond fortnightly frequencies hint to a seasonal trend, representing the gradual increase of salinity in the dry season associated with changes in river discharge and precipitation. Detrending with a 45-day window (see section 3.2) could not completely remove longer trends, manifesting as high peaks in the low-frequency domain. These peaks are much smaller for water levels, which are also subject to strong seasonality (Binh et al., 2020b).

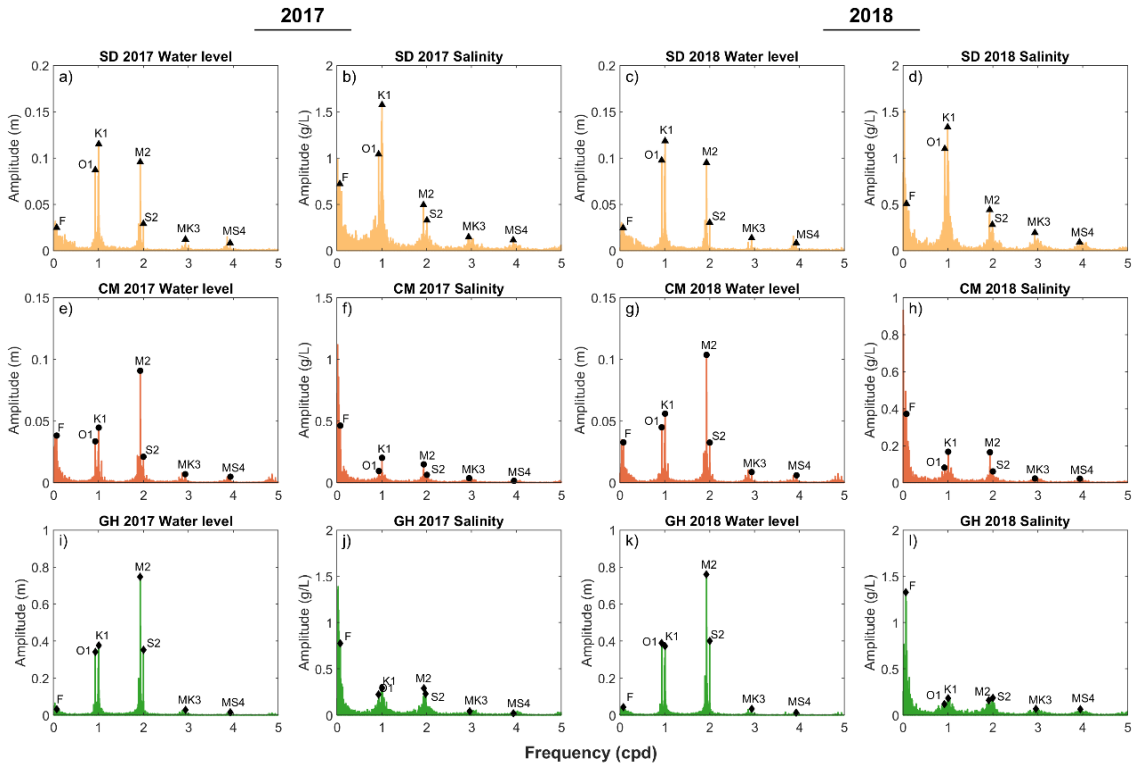


Figure 7. FFT analysis of water level and salinity at Song Doc (a-d), Ca Mau (e-h) and Ganh Hao (i-l). Significant tidal constituents are indicated for frequency ranges between 1 cpd to 4 cpd as well as fortnightly.

In addition to FFT, HLS was applied on differently pre-processed versions of the dataset to compare amplitudes, select the optimal dataset to assess HLS model performance and to compute the transfer function. In Figure 8, the amplitudes of FFT and HLS calculations are shown. For SD the O1 and M2 amplitudes are close to each other, while the HLS results for all datasets collectively are substantially higher at K1, and lower at S2. The HLS results using the original untreated salinity dataset is inconsistent. For example, at CM, using this dataset for HLS results in the highest amplitude for M2 in 2017, but the lowest amplitude in 2018. At CM and GH, the HLS amplitudes for O1 are unreasonably high, suggesting a diurnal dominance. Typically, K1 would indicate diurnal dominance and the water level record is clearly not diurnal for both locations (Figure 6).

The HLS results on the 1-hourly interpolated detrended dataset align well with the FFT results. At GH, the HLS amplitudes show a more pronounced variance. K1 and

M2 amplitudes are notably higher than the FFT amplitudes in both years, while HLS S2 amplitudes are low in 2017. At CM and SD, the 1-hourly interpolated detrended dataset is closest to the FFT result. For consistency with the water-level records and due to more consistent amplitudes (Figure 8), the detrended, interpolated 1-hourly salinity series was further analyzed and evaluated with HLS.

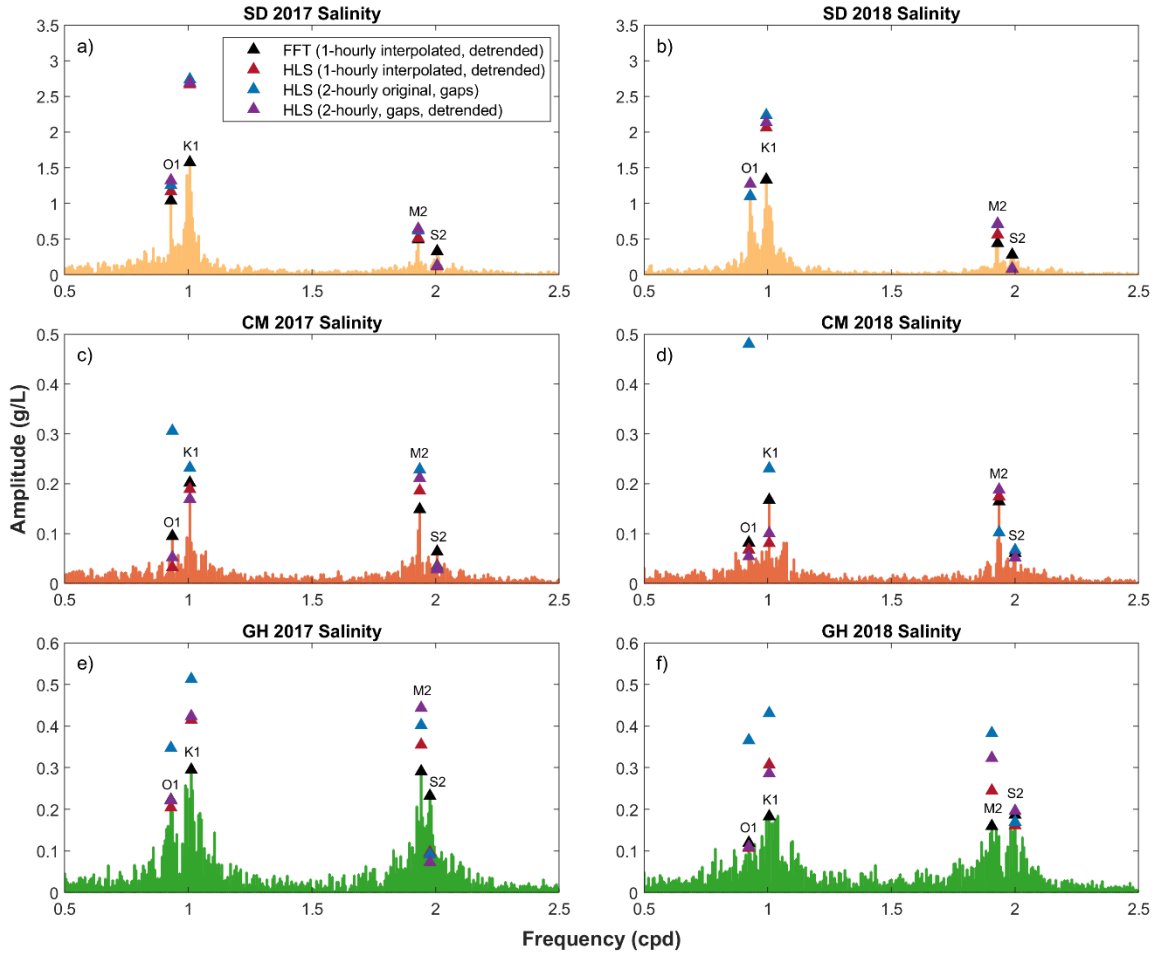


Figure 8 Comparison of amplitudes calculated by Fast Fourier Transform and Harmonic Least Squares for different versions of the salinity timeseries in 2017 and 2018 at Song Doc, Ca Mau and Ganh Hao.

4.3.3 Harmonic Least Square approaches to determine tidal control on water level and salinity

Tidal control was quantified as the explained variance (R^2) of the HLS reconstructions, and constituent-specific phase lags were derived from the transfer function relating water level (input) to salinity (output). Results for the global R^2 and phase lag are

presented in Table 1, and the global HLS fit is shown in Annex B. All R^2 values refer to the detrended timeseries and quantify variance explained by the tidal-band HLS reconstruction. HLS reconstructions of water level reproduced the observed records well across all stations. Maximum R^2 was 0.94 in both 2017 and 2018 at GH. At SD, R^2 was 0.77 (2017) and 0.78 (2018), with slightly lower values at CM. In contrast, salinity R^2 varied more across the stations. At SD, R^2 is 0.40 for 2017 and 0.29 for 2018, while CM 2017 and 2018 as well as GH 2017 have R^2 values below 0.15, and GH 2018 R^2 is 0.34.

Time lags between water level and salinity are also shown in Table 1. In general, the M2 responses are faster compared to the diurnal frequencies at all stations, at around two hours at SD, below one hour at CM and in average three hours at GH. At the K_1 frequency, water level leads salinity by approximately four to five hours, and by about one hour less at CM. For O1 negative values were obtained for GH.

Table 1. R^2 for the global Harmonic Least Squares approach for water level and salinity and time lag (h) between water level (input) and salinity (output) for main tidal components for Song Doc, Ca Mau and Ganh Hao for 2017 and 2018.

		HLS R^2 global		Time lag (h)			
Station	Year	Water level	Salinity	O1	K1	M2	S2
SD	2017	0.77	0.40	4.96	4.20	2.08	5.09
	2018	0.78	0.29	6.08	4.39	2.10	2.48
CM	2017	0.69	0.13	0.93	2.74	-0.05	0.08
	2018	0.76	0.07	3.01	3.98	0.60	0.57
GH	2017	0.94	0.11	-4.50	4.65	2.73	3.70
	2018	0.94	0.34	-9.90	5.04	3.50	1.95

Across all stations and years, mean-fit uncertainties for the sliding windows HLS reconstruction were small, ranging from 4–13 mm for water level and 0.07–0.18 g/L for salinity, indicating a well-constrained harmonic signal. Prediction uncertainties, which include observational noise, were larger, ranging from 4–12 cm and 0.37–1.53 g/L,

respectively. The prediction uncertainties reflect natural short-term variability not captured by the HLS reconstruction. Median amplitude standard errors were 2–5 mm for water level and 0.02–0.05 g/L for salinity, while phase standard errors corresponded to 5-7° and 10–21°, equivalent to timing uncertainties of roughly 10–40 min for the M_2 constituent.

To assess the sub-seasonal tidal control on water level and salinity, the fits for the 45-day-windowed HLS reconstructions are shown in Figure 9, and R^2 are reported (also see Annex C). The sliding HLS approach results in even higher R^2 for water level compared to the global HLS fit, ranging between 0.84 and 0.98, with only slight differences between unweighted and coverage-weighted R^2. For salinity, the sliding HLS fits improve R^2 substantially. For SD and GH, unweighted R^2 ranges between 0.50 and 0.60 in both years, and around 0.30 at CM. Largest differences in scale and amplitudes occur in the end of the time series, from end of May to end of June. As the coverage-weighted approach suppresses this time frame, the coverage-weighted R^2 is notable higher, with all stations showing R^2 between 0.51 and 0.73 for salinity (Figure 9, Annex C).

The temporal evolution of R^2 as a proxy for tidal control for the sliding window fit is shown in Figure 10 with the detrended, interpolated salinity time series in the background. A version of the figure with water level shown as background is provided in Annex D. While R^2 for water level is stable throughout the time series, R^2 for salinity shows larger variations. In mid of April 2017, R^2 for salinity at CM and GH drop sharply from around 0.9 to 0.2 and below, and at SD from slightly above 0.8 to almost 0.5. A few days later, R^2 increases again, followed by another, smaller drop, and another increasing phase. A similar drop occurs at SD in April 2018 and to a lesser extent at CM, while at GH R^2 decreases more gradually. Positive peaks of R^2 seem to correlate with peaks of salinity itself as well as phases of higher fortnightly amplitudes, as seen mid of March 2017 at CM and GH (Figure 10c, e), beginning of May 2018 at CM (Figure 10d), or in general at GH in 2018 (Figure 10f).

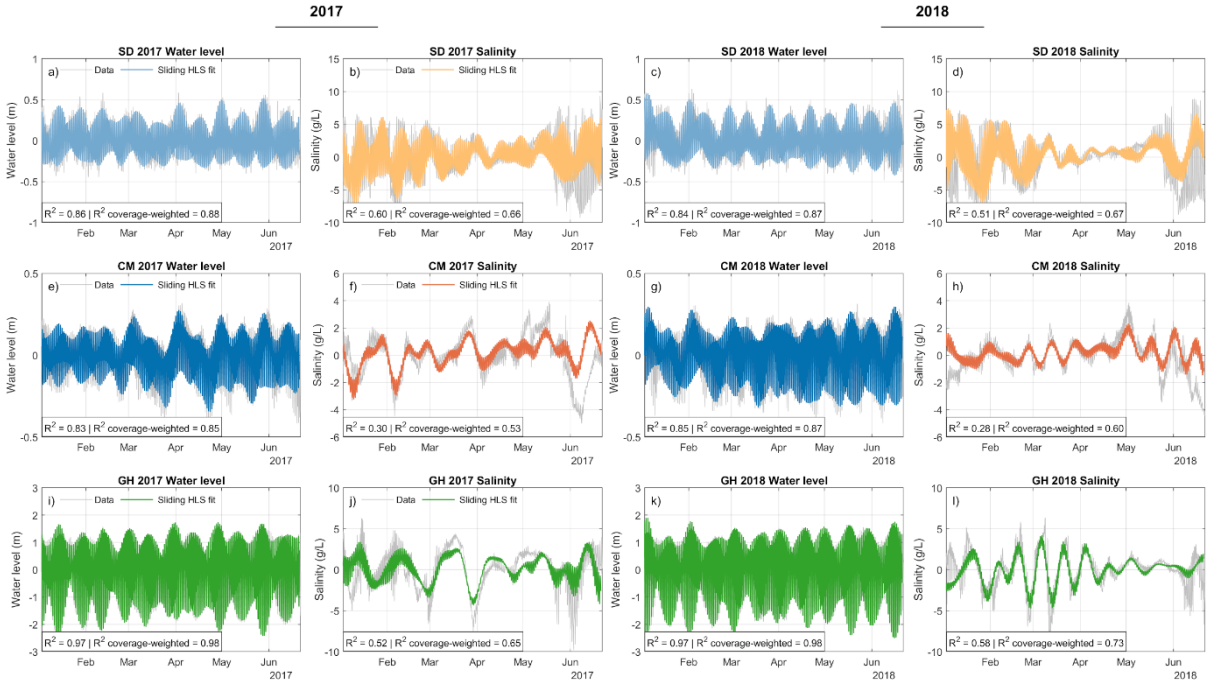


Figure 9 HLS reconstruction (sliding 45-day window, step size of 24h) using 13 tidal constituents (see section 3.3) and fit for water level and salinity at Song Doc, Ca Mau and Ganh Hao for 2017 and 2018.

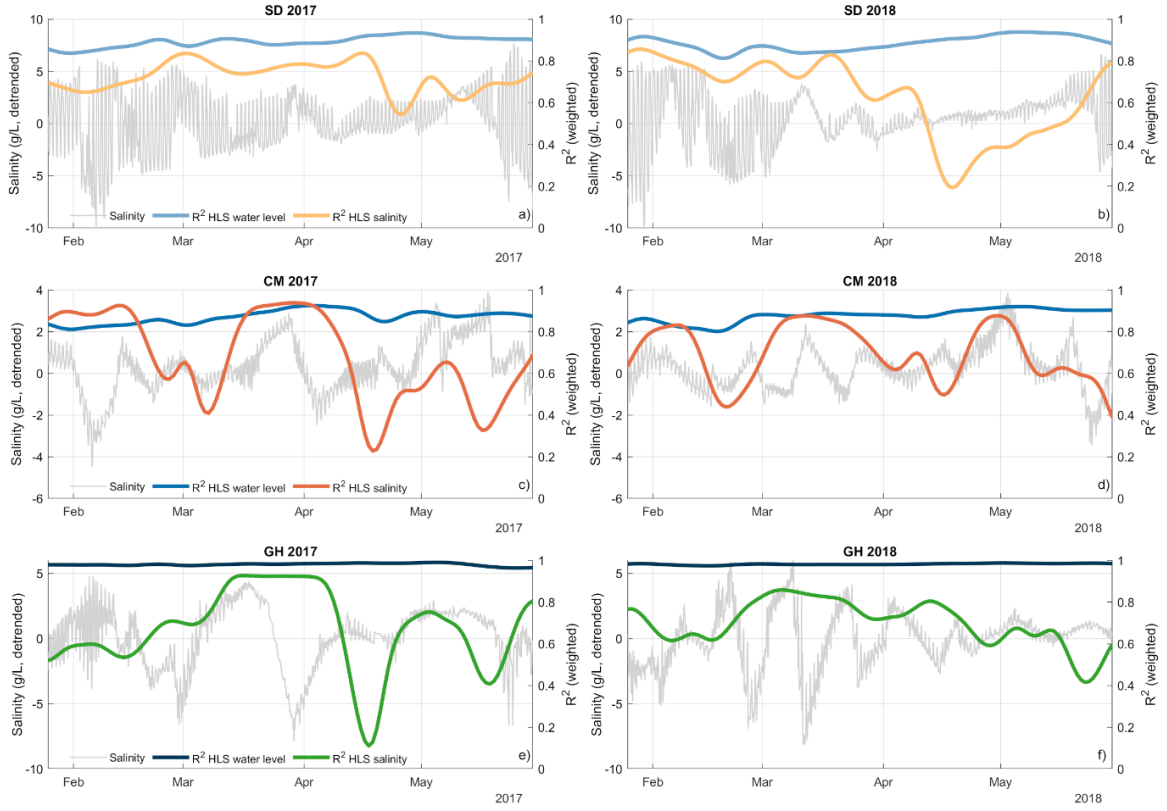


Figure 10 Tidal control expressed as explained variance R^2 of the sliding HLS reconstruction (45-day window, 24h step size) for water level and salinity at Song Doc, Ca Mau and Ganh Hao for 2017 and 2018.

5 Discussion

5.1 Salinity variability in response to tidal regimes

Superimposing seasonal trends, the salinity time series at SD, CM, and GH for January to June in 2017 and in 2018 reveal pronounced diurnal variation of salinity amplitudes, which are highest at the beginning of the dry and rainy seasons, reaching up to 16 g/L at SD, but stay below 5 g/L at the other two stations. (Figure 4). In addition, spring-neap cycles cause fortnightly variations (Figure 6). Farmers must plan ahead when using surface water for agriculture and aquaculture due to specific salinity requirements. However, as the results show, salinity fluctuations and the underlying dynamics are complex. This is especially crucial at the saline-freshwater boundary, where water may be suitable for rice farming during ebb tide or neap tide conditions but not six hours later during flood tide or during strong spring tides in general (Figure 6). This is also true for persistently brackish conditions during the dry season in aquaculture, as different fish and shrimp species require distinct salinity conditions for growth and survival (Duy et al., 2012; Gao et al., 2016; Li et al., 2017), as well as for disease resilience (Duc et al., 2015). Water in ponds, regardless of the farming practice, whether intensive, extensive or natural, needs to be replaced every few weeks (Duy et al., 2012). Unpredictable salinity conditions pose a substantial threat to yield stability. This study shows that salinity condition uncertainty is not exclusive to strong interannual salinity variations but also occurs on diurnal to fortnightly scales.

To better understand the causes for observed salinity variations, tidal influences on water level and salinity in the region were examined. Harmonic analyses show that salinity responds to the same tidal constituents as water level (Figure 7) and follows water level fluctuations (Figure 6) with a time lag ranging between two and six hours at the coastal stations and with more immediate responses inland at CM (Table 1, Figure 6). However, as shown in Figure 5, the different tidal regimes in the GOT and the East Sea, particularly their interaction caused by differences in amplitude and synchronous and asynchronous spring tides, result in complex water level and salinity

patterns across a fortnightly scale (Figure 6). Most notably, during spring tides in the East Sea, semi-diurnal water level and salinity patterns dominate in the GOT, which otherwise experiences diurnal tides. This pattern is pronounced during synchronous neap tides and weakens during spring tides in the GOT. During weaker neap tides in the East Sea, the east to west flow appears to reverse, restoring the original diurnal tide and salinity patterns in the GOT. While previous studies examined the interaction between the GOT and the East Sea, particularly resonant frequencies and amplitude responses (Cui et al., 2019; Phan et al., 2019), the impact of this interaction on salinity variation has not yet been addressed before.

The changes in hydraulic pressure gradients caused by tidal forcing and differences in tidal amplitudes between the GOT and the East Sea result in dynamic water flow conditions and varying solute transport in CMP (Phan et al., 2019). The changing water flow conditions cause the east-to-west freshwater-seawater front to not only shift in response to tidal forcing but to sometimes disappear on the southern peninsula, particularly during the dry season. Thereby, water flows directly through CMP, from the East Sea to the GOT, and vice versa, via large rivers, such as Ganh Hao, Ong Doc and Cua Lon (Figure 1) (Hoanh et al., 2009). Consequently, depending which tidal regime is dominant, both semi-diurnal and diurnal water level and salinity patterns occur at CM, representing the inland areas (Figure 6). The occurrence of changing water flow conditions in CMP has been reported before (Hoanh et al., 2009) and is also well-known among local people navigating these rivers, as the strong currents can pose significant danger to small boats. Changing water flow conditions, referred to reversing estuarine conditions, underscore the complexity of the hydrological regime in CMP and partly explain the observed irregular salinity patterns.

Furthermore, the interaction between the tidal regimes can create stagnant water zones in CMP when the opposing forces reach equilibrium (Le et al., 2007). During periods of extremely low river discharge, high temperature and low humidity, conditions that are exacerbated in El Niño years (Nguyen et al., 2014), elevated evaporation rates can lead to the accumulation of solutes and therefore salinity levels well above 35 g/L. At

SD and CM, salinity levels exceeded seawater salinity levels in the El Niño years 2010, 2016 and reached 45 g/L at SD in May 2020 (Bauer et al. 2025). These high salinity levels cause adverse effects on the ecosystem and agriculture, potentially having a lasting impact that extends beyond its duration as solutes accumulate in soils and sediments (Loc et al., 2021a; Tarolli et al., 2024).

5.2 The complexities of tides and its effect on seawater intrusion

Changes of water level and salinity patterns caused by changes in the hydraulic pressure gradient between river discharge and seawater due to tidal forcing account for much of the observed diurnal to fortnightly salinity variability. Tidal control on both water level and salinity was quantified as the explained variance (R^2) of the HLS reconstruction using a comprehensive set of tidal constituents. Water level can already be well described by the global fit over the whole time series, with R^2 ranging between 0.69 and 0.94, while the sliding-window HLS approach, which allows to incorporate non-stationary variations, elevates the explained variance slightly (Figure 9).

In contrast, in the stationary model, tides do only partly explain salinity variations at SD and GH and only in 2018, and not at all in CM (Table 1). The low explained variance shows that other effects and processes influence salinity variations, especially further inland. The complexities of salt transport, such as mixing and stratification, as well as tidal amplification and tidal asymmetry, and estuarine circulation in general, can alter observed salinity levels and dynamics substantially (Eslami et al., 2021a; Geyer, 2010; Geyer and MacCready, 2014). In shallow coastal rivers and estuarine zones, asymmetric tidal cycles, storage effects, tidal distortion and non-linearities can occur (Simpson et al., 1990; Speer and Aubrey, 1985; Zhang et al., 2025). In addition, human-controlled water diversions and sluice gate operations introduce additional non-linear behavior, further complicating the system response.
For that reason, the non-stationary HLS approach, using a sliding window of 45 days combined with a Hann taper and reporting coverage-weighted R^2, substantially improves the model fit for salinity and therefore the explained variance caused by tides.

R^2 (weighted) for salinity was calculated at 0.53 and 0.60 for CM in 2017 and 2018, respectively, and ranges between 0.65 and 0.73 at SD and GH (Figure 9). This improvement reflects better representation of the temporal variability and is indicative for a strong tidal control, but due to unexplained variances between 27 % to 47 % the non-stationary HLS approach can still not capture the entirety of processes involved. Due to the lack of data on vertical salinity profiles at the monitoring stations and the absence of detailed information on morphology and river geometry, processes such as stratification and mixing could not be directly investigated with the data used in this study. However, such processes have been documented in many estuaries worldwide, including the MD (Eslami et al., 2019; Hendrickx et al., 2023; Hendrickx and Pearson, 2024; Wünsche et al., 2024). The analyses conducted in this study suggest that certain observed water-level and salinity patterns may reflect these processes and are thus inferred.

In particular, quadratic friction and estuarine geometry lead to non-linear effects, which, for example, are manifested as pronounced overtides, such as M4, and compound tides, including MS4 and MK3 (Friedrichs and Aubrey, 1988; Lafta, 2022; Ray et al., 2023). At SD, located at the shallow Ong Doc River, the amplitudes of the exemplary compound tides MS4 and MK3 are relatively high for salinity and water level (Figure 7) and are also distinctly visible at CM and GH. Another compound tide, which can be pronounced in shallow water, is the fortnightly constituent MSf, which reflects the spring–neap modulation of semidiurnal tides with a frequency of 14.765 days, originating from the difference between M2 and S2 (2.00000 cpd - 1.93227 cpd = 0.06773 cpd = 14.765 days) (Garel et al., 2021). At GH and CM, where M2 is more dominant than K1, salinity at CM and GH as well as water level at GH show significant peaks at the fortnightly frequency band, indicating a strong neap-spring tide control on salinity (Figure 7), which is also clearly visible in the time domain (Figure 6, Figure 3m-p, u-x).

In case of large salinity gradients, which can be expected in the MD, density-induced pressure differences in the water column promote gravitational circulation, also known as estuarine circulation, meaning that less saline water at the surface is directed towards the sea, while the saline water at the river bottom moves further upstream, creating complex mixing patterns (Geyer, 2010; Savenije, 2012). This behavior can be observed in many estuary systems, such as the Danshuei River estuary in northern Taiwan, where strong salinity stratification was observed in a deep river during ebb flow when river discharge from upstream was largest (Liu et al., 2022). Another shallower river in the Danshuei River estuary did not show this behavior (Liu et al., 2022). In the Amazon estuary, strong stratification and estuarine circulation is favored during neap tides (Molinas et al., 2014). These effects can largely impact observed salinity levels in CMP. The reduction of vertical mixing and the evolution of stratification caused by the described estuarine circulations (Geyer, 2010), especially during ebb tides and neap tides (MacCready and Geyer, 2010), is estimated to also apply to the MD and the Ganh Hao river (GH station), which is significantly deeper compared to the Ong Doc River (SD station), with a mean depth of 5 to 14 m compared to 3 to 5 m, respectively. In general, deeper river channels promote the extent of SWI and stratification (Ralston and Geyer, 2019), which is also why channel deepening due to sand mining in the main branches of the Mekong River is extremely critical (Park, 2024).

In the beginning of April 2016, a particularly dry year with reduced discharge from the Mekong River, Eslami et al. (2021a) encountered that during neap tide, when tidal forcing is reduced, salinity at the river mouth and up to 40 km upstream in the Dinh An channel, a secondary channel of the Mekong River, was actually higher compared to the subsequent spring tide. During neap tide, strong salinity stratification was observed in the deeper Dinh An channel, but not in the neighboring, shallower Tran De channel, where highest salinity levels were indeed measured during the spring tide. The authors concluded that salinity cannot solely be attributed to simple discharge and tidal forcing but that other physical processes, such as stratification, are involved

as well (Eslami et al., 2021a). Similar observations were made in the Ben Tre Province at the river mouth of the Hau River (Tran et al., 2024c). Elaborating on these patterns, at GH, salinity peaks can be observed concurrent or shortly after the ebb tide during neap tides in the East Sea (Figure 6b, d). Such a peak was also observed by Muoi et al. (2022) during a one-day field campaign on the 5th of September 2019 during the rainy season only a few kilometers upstream Ganh Hao River, but not on the 22nd of March 2019 in the dry season. Based on the current evaluation of the issue, the observation by Muoi et al. (2022) can be explained, as the 22nd of March 2019 coincided with a strong spring tide in the East Sea (not shown), and therefore the salinity peak during ebb tide does not occur.

The low slope of the MD amplifies estuarine circulation by allowing denser saline water to intrude more easily and remain in the deeper river channels, as the gentle gradient provides insufficient gravitational force to push the saline water seaward, particularly in the dry season. Near-shore stratification of salinity is characteristic during periods of reduced water movement (Pokavanich and Guo, 2024), which in case of the MD is true in the dry season, further altering observed salinity dynamics. Additionally, intertidal flats, defined as areas submerged during high tides and exposed during ebb tides, may significantly affect the salinity patterns (Hendrickx and Pearson, 2024). In CMP, these flats are especially abundant along the Ong Doc and Ganh Hao rivers, where they temporarily store already saline water, which is subject to strong evaporation during the dry season. This evaporated saline water flows back into the rivers during low tide, potentially contributing to elevated salinity levels und irregular timings of salinity peaks.

Additionally, sluice gates, designed to protect certain areas of the MD from SWI during the dry season (Nguyen and Nguyen, 2023), also influence observed salinity patterns. By potentially cutting off some coastal areas from freshwater influx and altering water flow, these structures can reduce buffer zones and allow seawater to persist in the system (Binh et al., 2020b; Danh et al., 2024). A recent study for the Hudson River showed that closing gates for three or more days, stopping or limiting streamflow,

promotes SWI and stratification well above naturally occurring extremes (Chen, 2023). As neighboring provinces of CMP operate sluice gates to prevent SWI originating from CMP to protect agricultural areas, SWI and stratification could be increased downstream in CMP.

The sliding HLS approach employed here was able to capture some of the non-stationary processes and substantially improved the overall salinity model fit compared to the stationary fit over the entire time series, which could not capture non-linear effects. The temporal evolution of R^2 was also considered here, showing that in mid of April 2017 and 2018, marking the peak of the dry season, R^2 sharply drops. During this time, water levels are low, diurnal salinity amplitudes are lowest (Figure 4), and salinity levels almost reach seawater conditions (Figure 3). During this time, storage effects, stratification and other non-linear effects can be expected, potentially causing the sharp drop of R^2. In addition, water management, such as sluice gate management and water diversion practices impact total water levels (Bauer et al., 2025), and potentially influence periodic patters as well.

Lastly, during the Holocene, the MD transitioned from a tide-dominated system to a wave-tide dominated system (Ta et al., 2002a), meaning that waves driven by wind also add to water level fluctuations and can alter salinity patterns and SWI, increasing the non-tidal signal.

In the future, monitoring strategies in CMP and the MD should be adapted to qualitatively and quantitively validate the processes inferred in this study. Subsequently, the sliding window HLS approach can be extended to increase model performance and allow robust salinity prediction.

5.3 Implications for modelling and mitigation measures

The findings of this study demonstrate that the depth of monitoring equipment installation, the measurement period as well as the frequency of water sampling must follow a standardized protocol to ensure robust and meaningful results. Without such

consistency, models and predictions risk being weakened or misleading, particularly given the large diurnal amplitudes, fortnightly fluctuations, and seasonal trends observed. (Figure 4). Modeling salinity using short in-situ observation periods of just a few days for calibration and validation, taken during random time intervals, is inadequate. This study suggests that a simple stationary water level to salinity relationship is oversimplified, with significant irregularities caused by complex interaction of tidal regimes, physical processes and human infrastructure. For instance, Vu et al. (2024) calibrated a MIKE 21 SW model with multiple station data in the MD utilizing data limited to February 2020, and achieved an acceptable R^2 of 0.74 and good fits for water level, salinity and current speed. However, the short calibration time certainly did not capture all the variability and irregularities of the considered system. Therefore, the certainty of model results for the SLR-salinity relationship up to the year 2100 should be carefully reconsidered, especially when combining sub-seasonal salinity variability with interannual salinity variability. Analyzing varying time scales reveals an ambivalent relationship between water level and salinity. Simplified, it is shown that high tides drive salinity peaks on a diurnal scale, while seasonal water level highs from river discharge counteract SWI. However, long-term water level increases due to RSLR ultimately promote SWI (Mohammed and Scholz, 2017). Based on the results of this study, model calibration should span at least a hydrological year, incorporating several spring-neap cycles in the dry season and varying upstream discharge variations.

The susceptibility to salinity fluctuations can be regarded as a proxy for system vulnerability and exposure to seawater (Guillou et al., 2023). Therefore, as salinity variability is very high on all considered time scales, the vulnerability of the MD must be considered as very high, particularly in the broader context of the numerous environmental stressors threatening the region (e.g. Binh et al., 2020b; Kondolf et al., 2022; Minderhoud et al., 2021; Park, 2024; Park et al., 2022). Hendrickx et al. (2023) concluded that the complex interplay of estuarine processes and features controls SWI events. Identifying these processes and evaluating their relevance allows for developing

meaningful models and effective, evidence-based mitigation measures. A purely data- or model- driven approach could be misleading. In general, there is consensus that measures counteracting RLSR, negative river discharge anomalies caused by climate change and upstream reservoirs as well as a stop to sand mining are essential to mitigate long-term SWI and stabilize salinity conditions for local stakeholders, or at least make them predictable (e.g. Kondolf et al., 2022). On a local scale, within the delta and within CMP, sluice gates operating on a seasonal to tidal scale are often the solution of choice, but they are also often managed only locally and potentially less effective (Hoanh et al., 2009). Based on the tidal analysis and salinity patterns presented in this work, further options should be explored. Observations from other estuaries and modeling approaches suggest several options in addition to measures that aim to increase upstream river discharge during critical periods. For instance, the tidal rivers and especially the canals in CMP are often straight, but meanders would enhance ebb-dominance and reduce SWI as they increase turbulence and mixing (Pein et al., 2018). This effectively counteracts gravitational circulation with high density saline water moving upstream at the river bottom. Furthermore, intertidal areas play an important role for SWI, but depending on the mixing processes of the river, they can enhance or mitigate SWI (Hendrickx and Pearson, 2024), which should be carefully considered when implementing measures that alter the extent of these areas. In areas where estuarine circulation is dominant and the river is partially mixed or forms a salt wedge, assumable in the deeper Ganh Hao River, intertidal flats can disrupt this circulation and thereby limit salt transport. Conversely, in well-mixed rivers, where tidal oscillation is the dominant process, such as the shallow Ong Doc River, intertidal flats can enhance SWI (Hendrickx and Pearson, 2024), which is arguably supported by salinity levels beyond 35 g/L in dry years (Bauer et al., 2025). In addition, increasing hydraulic drag dampens tidal energy and limits intrusion lengths. This can be achieved by modifying river characteristics, such as increasing bed roughness and bottom friction, reducing water depth and stop dredging as well as widening the river through floodplains and wetlands (Winterwerp et al., 2013). Studies show that increasing bottom friction reduces tidal energy, enhanced vertical mixing and weakens tidal

propagation, ultimately mitigating SWI (Veerapaga et al., 2020). Increasing hydraulic drag can be achieved through various approaches, including engineering solutions such as the construction of inclined roughness elements in the river (Badr and Azzubaidi, 2023), air curtains like inflatable dams or gates (Haralambidou et al., 2018), submerged weir and rubber dams (Sriratana and Bisalyaputra, 2019) but also nature-based solutions, including earthen sills, sand dunes and water diversions (Geerts et al., 2025; Hendrickx et al., 2024; Sriratana and Bisalyaputra, 2019). This abundance of options shows that stakeholders in the MD have various tools to mitigate SWI, besides sluice gates and other hard measures often preferred (Nguyen et al., 2024). To date, none of these options have been implemented on a larger scale. The main obstacles stem from fragmented administrative structures and conflicting stakeholder interests, but also from limited expertise, public awareness, and financial resources (Ha et al., 2018; Minkman et al., 2022; Quang et al., 2024).

Through an in-depth analysis of tidal water level fluctuations and salinity responses in CMP, this study provides fundamental insights needed to develop and evaluate effective countermeasures, and to transfer these approaches to other areas along the Mekong Delta coastline.

6. Conclusion

Salinity levels were found to vary substantially on the sub-seasonal scale in the southern MD. Estuarine tidal dynamics are inherently complex and non-stationary, leading to equally complex spatiotemporal salinity patterns. The results presented here are indicative of some of these processes. A sliding HLS approach is capable of reconstructing water level and salinity dynamics. While this approach captures more of the non-stationary process dynamics compared to a global HLS fit, the gain in statistical representation cannot substitute for process-based understanding. Shallow-water effects revealed through frequency analysis, as well as indications of stratification and tidal co-oscillations, were inferred from distinct time series patterns but require follow-up field investigations for confirmation. The insights gained in this study provide

a foundation for further sub-seasonal SWI investigations in the MD. They offer a framework for deepening the understanding of the water level–salinity relationship and encourage the development of more reliable, explainable models for SWI prediction that incorporate both stationary and non-stationary effects. Short-term salinity variability is as critical as long-term trends, since sudden events can push the system beyond ecological or management thresholds, threatening freshwater-dependent livelihoods and economic stability. Predictive models and mitigation strategies must therefore account for both temporal scales.

Finally, the findings of this study are transferable to other estuarine systems worldwide, particularly low-lying deltas strongly influenced by tides, where non-stationary salinity dynamics pose similar challenges for water resources planning.

CRediT authorship contribution statement

Jonas Bauer: Conceptualization, Data curation, Methodology, Formal analysis, Investigation, Writing – original draft, Visualization.
Felix Dörr: Formal analysis, Investigation, Writing – review & editing
Andreas Schenk: Formal analysis, Writing – review & editing
Vũ Hoàng Thái Dương: Writing – review & editing
Hoan Tran Viet: Investigation, Writing – review & editing
Van Cam Pham: Writing – review & editing
Nicolas Börsig: Writing – review & editing, Project administration.
Roderick van der Linden: Writing – review & editing,
Ngoc Hoa Nguyen: Writing – review & editing,
Elisabeth Eiche: Writing – review & editing, Resources, Project administration
Stefan Norra: Writing – review & editing, Resources, Supervision, Project administration, Funding acquisition

Declaration of Competing Interest

The authors declare that they have no known competing financial interests or personal relationships that could have appeared to influence the work reported in this paper.

Declaration of generative AI and AI-assisted technologies in the writing process

During the preparation of this work the authors used ChatGPT in order to improve language and readability of the study. After using this tool/service, the authors reviewed and edited the content as needed and take full responsibility for the content of the publication.

Data availability

Data used in this study can be provided on request to NCHMF and/or NAWAPI, Hanoi, Vietnam, or by directly contacting the authors of this study, who can assist with access and facilitate contact with the afore- mentioned institutions.

Acronyms and Abbreviations

CM: Ca Mau
CMP: Ca Mau Province
FFT: Fast Fourier Transform
GH: Ganh Hao
GOT: Gulf of Thailand
HLS: Harmonic Least Squares
MD: Mekong Delta
NCHMF: National Center for Hydro-Meteorological Forecasting of Vietnam, Hanoi
RSLR: Relative sea level rise
SD: Song Doc
SLR: Sea level rise

SWI: Seawater intrusion

Acknowledgments

The authors thank the National Center for Hydro-Meteorological Forecasting of Vietnam, the Southern Institute of Water Resources Research, the National Center for Water Resources Planning and Investigation Vietnam, and the Department of Natural Resources and Environment Ca Mau for providing the monitoring data used in this study and for their valuable support during fieldwork, as well as for the scientific and personal exchange. We also gratefully acknowledge the contributions of all project partners involved in this work. This research was carried out within the framework of the project "ViWaT – Vietnam Water Technologies," funded by the German Federal Ministry of Education and Research (funding reference: 02WCL1474A). Publication support was provided by the KIT-Publication Fund of the Karlsruhe Institute of Technology, Germany.

Literature

Ang, W.J., Park, E., Pokhrel, Y., Tran, D.D., Loc, H.H., 2024. Dams in the Mekong: a comprehensive database, spatiotemporal distribution, and hydropower potentials. Earth Syst. Sci. Data 16, 1209–1228. https://doi.org/10.5194/essd-16-1209-2024

Babadi, B., Brown, E.N., 2014. A review of multitaper spectral analysis. IEEE Trans. Biomed. Eng. 61, 1555–1564. https://doi.org/10.1109/TBME.2014.2311996

Badr, S.H., Azzubaidi, R.Z., 2023. Using CFD Modeling to Simulate the Control of the Propagation of Salt Wedge using Inclined Roughness Elements. E3S Web Conf. 427. https://doi.org/10.1051/e3sconf/202342704008

Baranes, H., Dykstra, S.L., Jay, D.A., Talke, S.A., 2023. Sea level rise and the drivers of daily water levels in the Sacramento-San Joaquin Delta. Sci. Rep. 13, 1–15. https://doi.org/10.1038/s41598-023-49204-z

Bauer, J., Börsig, N., Pham, V.C., Hoan, T.V., Nguyen, H.T., Norra, S., 2022. Geochemistry and evolution of groundwater resources in the context of salinization and freshening in the southernmost Mekong Delta, Vietnam. J. Hydrol. Reg. Stud. 40. https://doi.org/10.1016/j.ejrh.2022.101010

Bauer, J., Dörr, F., Duong Vu, H.T., Schenk, A., Tran, H.V., Pham, V.C., Börsig, N., van der Linden, R., Nguyen, N.H., Eiche, E., Norra, S., 2025. Seawater intrusion in river delta systems. Inter-annual dynamics and drivers of salinity variations in the southern Mekong Delta, Vietnam. J. Hydrol. 661, 133745. https://doi.org/https://doi.org/10.1016/j.jhydrol.2025.133745

Binh, D. Van, Kantoush, S., Sumi, T., 2020a. Changes to long-term discharge and sediment loads in the Vietnamese Mekong Delta caused by upstream dams. Geomorphology 353. https://doi.org/10.1016/j.geomorph.2019.107011

Binh, D. Van, Kantoush, S.A., Saber, M., Mai, N.P., Maskey, S., Phong, D.T., Sumi, T., 2020b. Long-term alterations of flow regimes of the Mekong River and adaptation strategies for the Vietnamese Mekong Delta. J. Hydrol. Reg. Stud. 32, 100742. https://doi.org/10.1016/j.ejrh.2020.100742

Binh, D. Van, Kantoush, S.A., Sumi, T., Mai, N.P., Ngoc, T.A., Trung, L.V., An, T.D., 2021. Effects of riverbed incision on the hydrology of the Vietnamese Mekong Delta. Hydrol. Process. 35, 1–21. https://doi.org/10.1002/hyp.14030

Binh, D. Van, Tran, D.D., Thái Dương, V.H., Bauer, J., Park, E., Loc, H.H., 2025. Land use change in the Vietnamese Mekong Delta: Long-term impacts of drought and salinity intrusion using satellite and monitoring data. iScience 28. https://doi.org/10.1016/j.isci.2025.112723

Bucx, T., van Driel, W., de Boer, H., Graas, S., Langenberg, V.T., Marchand, M., Van de Guchte, C., 2014. Comparative assessment of the vulnerability and resilience of deltas – extended version with 14 deltas - synthesis report. Delta Alliance report number 7. Delta Alliance International, Delft-Wageningen, The Netherlands.

Cai, X., Qin, Q., Kirwan, M., Michael, H., Shen, J., Mach, K.J., Raymond, P., 2025. Recognizing Salt Wave Events in Coastal Systems.

Chen, Z., 2023. Effects of Storm Surge Barrier Closures on Estuary Saltwater Intrusion and Stratification Water Resources Research. https://doi.org/10.1029/2022WR032317

Codiga, D., 2011. Unified Tidal Analysis and Prediction Using the UTide Matlab Functions. Tech. Rep. 2011-01. Grad. Sch. Oceanogr. Univ. Rhode Island, Narragansett, RI. 59pp 1–60.

Cui, X., Fang, G., Wu, D., 2019. Tidal resonance in the Gulf of Thailand. Ocean Sci. 15, 321–331. https://doi.org/10.5194/os-15-321-2019

Dang, V.H., Tran, D.D., Cham, D.D., Hang, P.T.T., Nguyen, H.T., Truong, H. Van, Tran, P.H., Duong, M.B., Nguyen, N.T., Le, K. Van, Pham, T.B.T., Nguyen, A.H., 2020. Assessment of Rainfall Distributions and Characteristics in Coastal Provinces of the. Water (Switzerland) 12, 1–34.

Danh, V.T., Linh, D.Q., Thuy, N.T.D., 2024. Assessing impact of sluice gate operation on salinity intrusion in Ho Chi Minh City. IOP Conf. Ser. Earth Environ. Sci. 1349. https://doi.org/10.1088/1755-1315/1349/1/012028

Di Giusto, B., Le, T.M.N., Nguyen, T.T.M., Nguyen, T.T.H., Vu, N.U.M., Lavallee, J.P., 2021. Development versus adaptation? Facing climate change in Ca Mau, Vietnam. Atmosphere (Basel). 12. https://doi.org/10.3390/atmos12091160

Dörr, F., Bauer, J., Rau, G.C., Lewi, E., Hoan, V.T., Van, L.T.M., Valois, R., Steinel, A., Nestmann, F., Norra, S., 2026. The recharge illusion: How seasonal surface loading can hide continuing groundwater resource declines in confined deltaic aquifers. J. Hydrol. 665, 134674. https://doi.org/https://doi.org/10.1016/j.jhydrol.2025.134674

Dörr, F., Bauer, J., Rau, G.C., Valois, R., Hoan, T.V., Pham, V.C., Van, L.T.M., Steinel, A., Nestmann, F., Norra, S., 2025. Passive subsurface characterization in subsiding deltas: assessing land subsidence mitigation potential with frequency analyses of groundwater heads and superposing harmonic drivers. J. Hydrol. 662. https://doi.org/10.1016/j.jhydrol.2025.133844

Dörr, N., Huu, L.V., Schenk, A., Hinz, S., 2025. Drought - Induced Land Subsidence in the Mekong Delta , Vietnam : Insights From SAR Interferometry. Geophys. Res. Lett. 52. https://doi.org/10.1029/2025GL117096

Duc, P.M., Thi Tuyet Hoa, T., Thanh Phuong, N., Bosma, R., Van Hien, H., Ngoc Tuan, T., 2015. Virus diseases risk-factors associated with shrimp farming practices in

rice-shrimp and intensive culture systems in Mekong Delta Viet Nam. Int. J. Sci. Res. Publ. 5, 1–6.

Duy, H.N., Coman, G.J., Wille, M., Wouters, R., Nguyen Quoc, H., Vu, T., Tran Kim, D., Nguyen Van, H., Sorgeloos, P., 2012. Effect of water exchange, salinity regime, stocking density and diets on growth and survival of domesticated black tiger shrimp Penaeus monodon (Fabricius, 1798) reared in sand-based recirculating systems. Aquaculture 338–341, 253–259. https://doi.org/10.1016/j.aquaculture.2012.01.021

Duy, N. Le, Nguyen, T.V.K., Nguyen, D.V., Tran, A.T., Nguyen, H.T., Heidbüchel, I., Merz, B., Apel, H., 2021. Groundwater dynamics in the Vietnamese Mekong Delta: Trends, memory effects, and response times. J. Hydrol. Reg. Stud. 33, 100746. https://doi.org/10.1016/j.ejrh.2020.100746

EROS, 2017. Global 30 Arc-Second Elevation (GTOPO30) [Data set]. U.S. Geological Survey. [WWW Document]. Earth Resour. Obs. Sci. Cent. https://doi.org/https://doi.org/10.5066/F7DF6PQS

Eslami, S., Hoekstra, P., Kernkamp, H.W.J., Nguyen Trung, N., Do Duc, D., Nguyen Nghia, H., Tran Quang, T., Van Dam, A., Darby, S.E., Parsons, D.R., Vasilopoulos, G., Braat, L., Van Der Vegt, M., 2021a. Dynamics of salt intrusion in the Mekong Delta: Results of field observations and integrated coastal-inland modelling. Earth Surf. Dyn. 9, 953–976. https://doi.org/10.5194/esurf-9-953-2021

Eslami, S., Hoekstra, P., Minderhoud, P.S.J., Trung, N.N., Hoch, J.M., Sutanudjaja, E.H., Dung, D.D., Tho, T.Q., Voepel, H.E., Woillez, M.-N., van der Vegt, M., 2021b. Projections of salt intrusion in a mega-delta under climatic and anthropogenic stressors. Commun. Earth Environ. 2, 1–11. https://doi.org/10.1038/s43247-021-00208-5

Eslami, S., Hoekstra, P., Nguyen Trung, N., Ahmed Kantoush, S., Van Binh, D., Duc Dung, D., Tran Quang, T., van der Vegt, M., 2019. Tidal amplification and salt intrusion in the Mekong Delta driven by anthropogenic sediment starvation. Sci. Rep. 9, 1–10. https://doi.org/10.1038/s41598-019-55018-9

Foreman, M.G.G., 2004. Manual for Tidal Heights Analysis and Prediction. Pacific Mar. Sci. Rep.

Foreman, M.G.G., Cherniawsky, J.Y., Ballantyne, V.A., 2009. Versatile harmonic tidal analysis: Improvements and applications. J. Atmos. Ocean. Technol. 26, 806–817. https://doi.org/10.1175/2008JTECHO615.1

Friedrichs, C.T., Aubrey, D.G., 1988. Non-linear tidal distortion in shallow well-mixed estuaries: a synthesis. Estuar. Coast. Shelf Sci. 27, 521–545. https://doi.org/10.1016/0272-7714(88)90082-0

Gaiolini, M., Colombani, N., Mastrocicco, M., Postacchini, M., 2023. Seawater intrusion assessment along the Volturno River (Italy) via numerical modeling and spectral analysis. J. Hydrol. 626. https://doi.org/10.1016/j.jhydrol.2023.130289

Gao, W., Tian, L., Huang, T., Yao, M., Hu, W., Xu, Q., 2016. Effect of salinity on the growth performance, osmolarity and metabolism-related gene expression in white shrimp Litopenaeus vannamei. Aquac. Reports 4, 125–129. https://doi.org/10.1016/j.aqrep.2016.09.001

Garel, E., Zhang, P., Cai, H., 2021. Dynamics of fortnightly water level variations along a tide-dominated estuary with negligible river discharge. Ocean Sci. 17, 1605–1621. https://doi.org/10.5194/os-17-1605-2021

Geerts, S.J., van der Sande, W.M., Hulscher, S.J.M.H., Geurts, B.J., Roos, P.C., 2025. Sand Dunes as a Nature-Based Solution to Mitigate Salt Intrusion in Stratified Estuaries. J. Geophys. Res. Ocean. 130. https://doi.org/10.1029/2024JC021103

Geyer, W.R., 2010. Estuarine salinity structure and circulation, in: Valle-Levinson, A. (Ed.), Contemporary Issues in Estuarine Physics. Cambridge University Press, pp. 12–26.

Geyer, W.R., MacCready, P., 2014. The estuarine circulation. Annu. Rev. Fluid Mech. 46, 175–197. https://doi.org/10.1146/annurev-fluid-010313-141302

GSOV, 2024. General Statistics Office of Vietnam, URL (10.2024): https://www.gso.gov.vn/en/homepage/.

Guillou, N., Chapalain, G., Petton, S., 2023. Predicting sea surface salinity in a tidal estuary with machine learning. Oceanologia 65, 318–332. https://doi.org/10.1016/j.oceano.2022.07.007

Ha, T.P., Dieperink, C., Dang Tri, V.P., Otter, H.S., Hoekstra, P., 2018. Governance conditions for adaptive freshwater management in the Vietnamese Mekong Delta. J. Hydrol. 557, 116–127. https://doi.org/10.1016/j.jhydrol.2017.12.024

Haralambidou, K.I., Sylaios, G.K., Tsihrintzis, V.A., 2018. Testing Alternatives for Salt Wedge Management in an Estuary with the Use of Monitoring and a Mathematical Model. Glob. NEST J. 5, 107–118. https://doi.org/10.30955/gnj.000295

Harris, F.J., 1978. On the Use of Windows for Harmonic Analysis with the Discrete Fourier Transform. Proc. IEEE 66, 51–83.

Hendrickx, G.G., Kranenburg, W.M., Antolínez, J.A.A., Huismans, Y., Aarninkhof, S.G.J., Herman, P.M.J., 2023. Sensitivity of salt intrusion to estuary-scale changes: A systematic modelling study towards nature-based mitigation measures. Estuar. Coast. Shelf Sci. 295, 108564. https://doi.org/10.1016/j.ecss.2023.108564

Hendrickx, G.G., Manuel, L.A., Pearson, S.G., Aarninkhof, S.G.J., Meselhe, E.A., 2024. An Earthen Sill as a Measure to Mitigate Salt Intrusion in Estuaries. Estuaries and Coasts 47, 1199–1208. https://doi.org/10.1007/s12237-024-01359-2

Hendrickx, G.G., Pearson, S.G., 2024. On the Effects of Intertidal Area on Estuarine Salt Intrusion. J. Geophys. Res. Ocean. https://doi.org/10.1029/2023JC020750

Hoan, T.V., Richter, K., Dörr, F., Bauer, J., Börsig, N., Steinel, A., Le, V.T.M., Pham, V.C., Than, D. Van, Norra, S., 2025. The Utilization of a 3D Groundwater Flow and Transport Model for a Qualitative Investigation of Groundwater Salinization in the Ca Mau Peninsula (Mekong Delta , Vietnam) 1–27.

Hoanh, C.T., Phong, N.D., Gowing, J.W., Tuong, T.P., Ngoc, N. V., Hien, N.X., 2009. Hydraulic and water quality modeling: A tool for managing land use conflicts in inland coastal zones. Water Policy 11, 106–120. https://doi.org/10.2166/wp.2009.107

Hung, N.N., Delgado, J.M., Tri, V.K., Hung, L.M., Merz, B., Bárdossy, A., Apel, H., 2012. Floodplain hydrology of the mekong delta, Vietnam. Hydrol. Process. 26, 674–686. https://doi.org/10.1002/hyp.8183

Jordan, C., Tiede, J., Lojek, O., Visscher, J., Apel, H., Nguyen, H.Q., Quang, C.N.X., Schlurmann, T., 2019. Sand mining in the Mekong Delta revisited - current scales of local sediment deficits. Sci. Rep. 9, 1–14. https://doi.org/10.1038/s41598-019-53804-z

Jordan, C., Visscher, J., Dung, N.V., Apel, H., Schlurmann, T., 2020. Impacts of human activity and global changes on future morphodynamics within the tien river, vietnamese mekong delta. Water (Switzerland) 12. https://doi.org/10.3390/w12082204

Khang, N.D., Kotera, A., Sakamoto, T., Yokozawa, M., 2008. Sensitivity of Salinity Intrusion to Sea Level Rise and River Flow Change in Vietnamese Mekong Delta-Impacts on Availability of Irrigation Water for Rice Cropping. J. Agric. Meteorol. 64, 167–176. https://doi.org/10.2480/agrmet.64.3.4

Kondolf, G.M., Schmitt, R.J.P., Carling, P.A., Goichot, M., Keskinen, M., Arias, M.E., Bizzi, S., Castelletti, A., Cochrane, T.A., Darby, S.E., Kummu, M., Minderhoud, P.S.J., Nguyen, D., Nguyen, H.T., Nguyen, N.T., Oeurng, C., Opperman, J., Rubin, Z., San, D.C., Schmeier, S., Wild, T., 2022. Save the Mekong Delta from drowning. Science (80-.). 376, 583–585. https://doi.org/10.1126/science.abm5176

Kumar, S., Park, E., Tran, D.D., Wang, J., Ho, H.L., Kantoush, S.A., Binh, D. Van, Li, D., Switzer, A.D., 2024. A deep learning framework to map riverbed sand mining budgets in large tropical deltas. GIScience Remote Sens. 61. https://doi.org/10.1080/15481603.2023.2285178*

Kvale, E.P., 2006. The origin of neap-spring tidal cycles. Mar. Geol. 235, 5–18. https://doi.org/10.1016/j.margeo.2006.10.001

Kvale, E.P., Cutright, J., BIlodeau, D., Archer, A., Johnson, H.R., Pickett, B., 1995. Analysis of modern tides and implications for ancient tidalites. Cont. Shelf Res. 15. https://doi.org/10.1016/0278-4343(95)00001-H

Lafta, A.A., 2022. Investigation of tidal asymmetry in the Shatt Al-Arab river estuary, Northwest of Arabian Gulf. Oceanologia 64, 376–386. https://doi.org/10.1016/j.oceano.2022.01.005

Lam, N.T., 2020. Real-Time Prediction of Salinity in the Mekong River Delta, in: Trung Viet, N., Xiping, D., Thanh Tung, T. (Eds.), APAC 2019. Springer Singapore, Singapore, pp. 1461–1468.

Le, A.T., Chu, T.H., Miller, F., Bach, T.S., 2007. Flood and salinity management in the Mekong Delta. Challenges to Sustain. Dev. Mekong Delta Reg. Natl. policy issues Res. needs Lit. Anal. 15–168.

Lee, J., Biemond, B., van Keulen, D., Huismans, Y., van Westen, R.M., de Swart, H.E., Dijkstra, H.A., Kranenburg, W.M., 2025. Global increases of salt intrusion in estuaries under future environmental conditions. Nat. Commun. 16, 1–9. https://doi.org/10.1038/s41467-025-58783-6

Li, E., Wang, X., Chen, K., Xu, C., Qin, J.G., Chen, L., 2017. Physiological change and nutritional requirement of Pacific white shrimp Litopenaeus vannamei at low salinity. Rev. Aquac. 9, 57–75. https://doi.org/10.1111/raq.12104

Liu, W.-C., Liu, H.-M., Huang, W.-C., 2022. Flood–Ebb and Discharge Variations in Observed Salinity and Suspended Sediment in a Mesotidal Estuary. Standards 2, 209–225. https://doi.org/10.3390/standards2020016

Lobo, M., Jay, D.A., Innocenti, S., Talke, S.A., Dykstra, S.L., 2024. Implementing Superresolution of Nonstationary Tides with Wavelets: An Introduction to CWT_Multi. J. Atmos. Ocean. Technol. 41, 969–989. https://doi.org/10.1175/JTECH-D-23-0144.1

Loc, H.H., Low Lixian, M., Park, E., Dung, T.D., Shrestha, S., Yoon, Y.J., 2021a. How the saline water intrusion has reshaped the agricultural landscape of the Vietnamese Mekong Delta, a review. Sci. Total Environ. 794, 148651. https://doi.org/10.1016/j.scitotenv.2021.148651

Loc, H.H., Van Binh, D., Park, E., Shrestha, S., Dung, T.D., Son, V.H., Truc, N.H.T., Mai, N.P., Seijger, C., 2021b. Intensifying saline water intrusion and drought in the Mekong Delta: From physical evidence to policy outlooks. Sci. Total Environ. 757, 143919. https://doi.org/https://doi.org/10.1016/j.scitotenv.2020.143919

Lu, X.X., Chua, S.D.X., 2021. River Discharge and Water Level Changes in the Mekong River: Droughts in an Era of Mega-Dams. Hydrol. Process. 35, 1–19. https://doi.org/10.1002/hyp.14265

MacCready, P., Geyer, W.R., 2010. Advances in estuarine physics. Ann. Rev. Mar. Sci. 2, 35–58. https://doi.org/10.1146/annurev-marine-120308-081015

Matte, P., Jay, D.A., Zaron, E.D., 2013. Adaptation of classical tidal harmonic analysis to nonstationary tides, with application to river tides. J. Atmos. Ocean. Technol. 30, 569–589. https://doi.org/10.1175/JTECH-D-12-00016.1

Minderhoud, P. S.J., Coumou, L., Erkens, G., Middelkoop, H., Stouthamer, E., 2019. Mekong delta much lower than previously assumed in sea-level rise impact assessments. Nat. Commun. 10, 1–13. https://doi.org/10.1038/s41467-019-11602-1

Minderhoud, Philip S.J., Coumou, L., Erkens, G., Middelkoop, H., Stouthamer, E., 2019. Digital elevation model of the Vietnamese Mekong delta based on elevation points from a national topographical map. https://doi.org/10.1594/PANGAEA.902136

Minderhoud, P.S.J., Erkens, G., Middelkoop, H., Stouthamer, E., 2021. The existential crisis of the Mekong delta : Impact of accelerating land subsidence 9841.

Minderhoud, P.S.J., Erkens, G., Pham, V.H., Bui, V.T., Erban, L., Kooi, H., Stouthamer, E., 2017. Impacts of 25 years of groundwater extraction on subsidence in the Mekong delta, Vietnam. Environ. Res. Lett. 12. https://doi.org/10.1088/1748-9326/aa7146

Minkman, E., Nguyen, H.Q., Luu, T., Dang, K.K., Nguyen, S.L., Du, H., Huizer, T., Rijke, J., 2022. From national vision to implementation: governance challenges in sustainable agriculture transitions in the Vietnamese Mekong Delta region. Reg. Environ. Chang. 22, 1–13. https://doi.org/10.1007/s10113-022-01898-z

Mohammed, I.N., Bolten, J.D., Srinivasan, R., Lakshmi, V., 2018. Satellite observations and modeling to understand the Lower Mekong River Basin streamflow variability. J. Hydrol. 564, 559–573. https://doi.org/10.1016/j.jhydrol.2018.07.030

Mohammed, R., Scholz, M., 2017. Critical review of salinity intrusion in rivers and estuaries. J. Water Clim. Chang. 9, 1–16. https://doi.org/10.2166/wcc.2017.334

Molinas, E., Vinzon, S.B., de Paula Xavier Vilela, C., Gallo, M.N., 2014. Structure and position of the bottom salinity front in the Amazon Estuary. Ocean Dyn. 64, 1583–1599. https://doi.org/10.1007/s10236-014-0763-0

Mukherjee, S., Ghosh, K.K., Chanda, A., 2023. Environmental Oceanography and Coastal Dynamics: Current Scenario and Future Trends, Environmental Oceanography and Coastal Dynamics: Current Scenario and Future Trends. https://doi.org/10.1007/978-3-031-34422-0

Nguyen, A.D., Savenije, H.H.G., 2006. Hydrology and Earth System Sciences Salt intrusion in multi-channel estuaries: a case study in the Mekong Delta, Vietnam. Hydrol. Earth Syst. Sci 10, 743–754.

Nguyen, C.T., Tran, V.X., Nguyen, N.H., Dang, T.A., 2025. Recent acceleration of tidal amplification in the Vietnamese Mekong Delta: drivers and environmental change implication. Ocean Sci. J. (accepted Artic.

Nguyen, D.Q., Renwick, J., Mcgregor, J., 2014. Variations of surface temperature and rainfall in Vietnam from 1971 to 2010. Int. J. Climatol. 34, 249–264. https://doi.org/10.1002/joc.3684

Nguyen, K.D., Guillou, N., Pham, N.N., 1998. A 3-D numerical study of the tidal circulation in the Mekong Delta Coastal Zones, Vietnam. Int. Work. Mekong Delta, 23-27 Febr. 1998, Chiang Rai, Thail. 57 – 71.

Nguyen, M.T., Renaud, F.G., Sebesvari, Z., 2019. Drivers of change and adaptation pathways of agricultural systems facing increased salinity intrusion in coastal areas of the Mekong and Red River deltas in Vietnam. Environ. Sci. Policy 92, 331–348. https://doi.org/10.1016/j.envsci.2018.10.016

Nguyen, Q., Borton, J., Hout, W., 2024. Understanding the Politics of Vietnamese Climate Adaptation: The Case of Dyke Policies in Ca Mau Province. Asian Perspect.

Nguyen, Q.H., Tran, D.D., Dang, K.K., Korbee, D., Pham, L.D.M.H., Vu, L.T., Luu, T.T., Ho, L.H., Nguyen, P.T., Trang, T.T., Nguyen, D.T.K., Wyatt, A., van Aalst, M., Tran, T.A., Sea, W.B., 2020. Land-use dynamics in the Mekong delta: From national policy to livelihood sustainability. Sustain. Dev. 28, 448–467. https://doi.org/10.1002/sd.2036

Nguyen, T.A.T., Nguyen, K.A.T., Jolly, C., 2019. Is super-intensification the solution to shrimp production and export sustainability? Sustain. 11, 1–22. https://doi.org/10.3390/su11195277

Nguyen, T.C., Nguyen, N.H., 2023. Does the community support the sluice gates in response to salinity intrusion ? The case of Kien Giang province.

Nguyen, T.C., Schwarzer, K., Ricklefs, K., 2023. Water-level changes and subsidence rates along the East Sea coastline of the Saigon-Dong Nai River Estuary and the Mekong Delta. Decis. Support Syst. 113260. https://doi.org/10.1016/j.ecss.2023.108259

Nguyet-Minh, N., Le, T.D., Pham, H. Van, Vu, H.T.D., Ouillon, S., Nguyen, T.C., 2025. Suspended sediment pattern along the Mekong Delta's west coast induced by strong southwest monsoon activities and extreme events. Mar. Geol. 485, 107563. https://doi.org/10.1016/j.margeo.2025.107563

Nicholls, R.J., Lincke, D., Hinkel, J., Brown, S., Vafeidis, A.T., Meyssignac, B., Hanson, S.E., Merkens, J.L., Fang, J., 2021. Author Correction: A global analysis of subsidence, relative sea-level change and coastal flood exposure (Nature Climate Change, (2021), 11, 4, (338-342), 10.1038/s41558-021-00993-z). Nat. Clim. Chang. 11, 634. https://doi.org/10.1038/s41558-021-01064-z

Normandin, C., Frappart, F., Bourrel, L., Blarel, F., Biancamaria, S., Wigneron, J.P., Galenon, L., Bernard, E., Coulon, L., Lubac, B., Marieu, V., Vantrepotte, V., Pham-Duc, B., Do, H.T., Prigent, C., Aires, F., Yamazaki, D., Ciais, P., 2024. Sharp decline in surface water resources for agriculture and fisheries in the Lower Mekong Basin over 2000-2020. Sci. Total Environ. 950. https://doi.org/10.1016/j.scitotenv.2024.175259

Oehlert, G.W., 1992. A Note on the Delta Method. Am. Stat. 46, 27–29. https://doi.org/10.1080/00031305.1992.10475842

Park, E., 2024. Sand mining in the Mekong Delta: Extent and compounded impacts. Sci. Total Environ. 924, 171620. https://doi.org/10.1016/j.scitotenv.2024.171620

Park, E., Loc, H.H., Van Binh, D., Kantoush, S., 2022. The worst 2020 saline water intrusion disaster of the past century in the Mekong Delta: Impacts, causes, and management implications. Ambio 51, 691–699. https://doi.org/10.1007/s13280-021-01577-z

Pawlowicz, R., Beardsley, B., Lentz, S., 2002. Classical tidal harmonic analysis including error estimates in MATLAB using TDE. Comput. Geosci. 28, 929–937. https://doi.org/10.1016/S0098-3004(02)00013-4

Pein, J., Valle-Levinson, A., Stanev, E. V., 2018. Secondary Circulation Asymmetry in a Meandering, Partially Stratified Estuary. J. Geophys. Res. Ocean. 123, 1670–1683. https://doi.org/10.1002/2016JC012623

Pham-Thanh, H., Phan-Van, T., Fink, A.H., van der Linden, R., 2021. Local-scale rainy season onset detection: A new approach based on principal component analysis and its application to Vietnam. Int. J. Climatol. 1–17. https://doi.org/10.1002/joc.7441

Pham, V.C., Bauer, J., Börsig, N., Ho, J., Vu, L., Tran, H., Dörr, F., Norra, S., 2023. Groundwater Use Habits and Environmental Awareness in Ca Mau Province , Vietnam : Implications for Sustainable Water Resource Management. Environ. Challenges 13, 100742. https://doi.org/10.1016/j.envc.2023.100742

Phan, H.M., Ye, Q., Reniers, A.J.H.M., Stive, M.J.F., 2019. Tidal wave propagation along The Mekong deltaic coast. Estuar. Coast. Shelf Sci. 220, 73–98. https://doi.org/10.1016/j.ecss.2019.01.026

Pokavanich, T., Guo, X., 2024. Saltwater intrusion in Chao Phraya Estuary: A long, narrow and meandering partially mixed estuary influenced by water regulation and

abstraction. J. Hydrol. Reg. Stud. 52, 101686 .
https://doi.org/10.1016/j.ejrh.2024.101686

Qian, J., Liu, H., Qian, L., Bauer, J., Xue, X., Yu, G., He, Q., Zhou, Q., Bi, Y., Norra, S., 2022. Water quality monitoring and assessment based on cruise monitoring, remote sensing, and deep learning: A case study of Qingcaosha Reservoir. Front. Environ. Sci. 10, 1–13. https://doi.org/10.3389/fenvs.2022.979133

Quang, N.M., Kawarazuka, N., Nguyen-Pham, T.N., Nguyen, T.H., Le, H.M., Tran, T.T.M., Huynh, T.T.N., 2024. Why adaptation falters: principles for climate change adaptation policy assessment in Vietnam. Int. J. Clim. Chang. Strateg. Manag. 16, 19–43. https://doi.org/10.1108/IJCCSM-05-2023-0063

Rahman, M.M., Penny, G., Mondal, M.S., Zaman, M.H., Kryston, A., Salehin, M., Nahar, Q., Islam, M.S., Bolster, D., Tank, J.L., Müller, M.F., 2019. Salinization in large river deltas: Drivers, impacts and socio-hydrological feedbacks. Water Secur. 6, 100024. https://doi.org/https://doi.org/10.1016/j.wasec.2019.100024

Ralston, D.K., Geyer, W.R., 2019. Response to Channel Deepening of the Salinity Intrusion, Estuarine Circulation, and Stratification in an Urbanized Estuary. J. Geophys. Res. Ocean. 124, 4784–4802. https://doi.org/10.1029/2019JC015006

Ray, R.D., Boy, J.P., Erofeeva, S.Y., Egbert, G.D., 2023. Terdiurnal Radiational Tides. J. Phys. Oceanogr. 53, 1139–1150. https://doi.org/10.1175/JPO-D-22-0175.1

Renaud, F.G., Kuenzer, C., 2012. The Mekong Delta System. Springer, Netherlands.

Savenije, H.H.G., 2012. Salinity and tides in alluvial estuaries, Second Com. ed, Journal of Hydraulic Engineering. Delft University of Technology, Water Resources Section, Delft, The Netherland. https://doi.org/10.1061/(asce)0733-9429(1988)114:12(1509)

Schneider, P., Asch, F., 2020. Rice production and food security in Asian Mega deltas — A review on characteristics , vulnerabilities and agricultural adaptation options to cope with climate change 491–503. https://doi.org/10.1111/jac.12415

Schwarzer, K., Thanh, N.C., Ricklefs, K., 2016. Sediment re-deposition in the mangrove environment of Can Gio, Saigon River estuary (Vietnam). J. Coast. Res. 1, 138–142. https://doi.org/10.2112/SI75-028.1

Schweizer, D., Ried, V., Rau, G.C., Tuck, J.E., Stoica, P., 2021. Comparing Methods and Defining Practical Requirements for Extracting Harmonic Tidal Components from

Groundwater Level Measurements. Math. Geosci. 53, 1147–1169. https://doi.org/10.1007/s11004-020-09915-9

Simpson, J.H., Brown, J., Matthews, J., Allen, G., 1990. Tidal straining, density currents, and stirring in the control of estuarine stratification. Estuaries 13, 125–132. https://doi.org/10.2307/1351581

Speer, P.E., Aubrey, D.G., 1985. A study of non-linear tidal propagation in shallow inlet/estuarine systems Part II: Theory. Estuar. Coast. Shelf Sci. 21, 207–224. https://doi.org/10.1016/0272-7714(85)90097-6

Sriratana, L., Bisalyaputra, K., 2019. Reconnaissance Study on Saltwater Intrusion Control at Main Raw Water Pumping Station of Metropolitan Waterworks Authority (Thailand). Int. J. Eng. Technol. 11, 33–38. https://doi.org/10.7763/ijet.2019.v11.1119

Ta, T.K.O., Nguyen, V.L., Tateishi, M., Kobayashi, I., Saito, Y., Nakamura, T., 2002a. Sediment facies and Late Holocene progradation of the Mekong River Delta in Bentre Province , southern Vietnam : An example of ... Sediment facies and Late Holocene progradation of the Mekong River Delta in Bentre Province , southern Vietnam : an example. Sediment. Geol. 152, 313–325.

Ta, T.K.O., Nguyen, V.L., Tateishi, M., Kobayashi, I., Tanabe, S., Saito, Y., 2002b. Holocene delta evolution and sediment discharge of the Mekong River, southern Vietnam. Quat. Sci. Rev. 21, 1807–1819. https://doi.org/10.1016/S0277-3791(02)00007-0

Tarolli, P., Luo, J., Park, E., Barcaccia, G., Masin, R., 2024. Soil salinization in agriculture : Mitigation and adaptation strategies combining nature-based solutions and bioengineering. ISCIENCE 27, 108830. https://doi.org/10.1016/j.isci.2024.108830

Thong, M.T., Thanh, X., Huyen, V.N., Trung, L.D., Cuong, L.P., Hung, L. Van, Hung, C.C., Thi, T., Diep, N., Marcille, J., 2010. Expansion of shrimp farming in Ca Mau , Vietnam Ha Thi Phuong Tien , Nguyen Thu Huong, in: Cook, J.A., Cylke, O., Larson, D.F., Nash, J.D., Stedman-Edwards, P. (Eds.), Vulnerable Places, Vulnerable People Trade Liberalization, Rural Poverty and the Environment. pp. 126–144. https://doi.org/https://doi.org/10.4337/9781849805193.00015 [Titel anhand dieser DOI in Citavi-Projekt übernehmen]

Tran, D.D., Thi, Pham, Thuc, B., Park, E., Thi, Phan, Hang, T., Man, D.B., Wang, J., 2024. Extent of saltwater intrusion and freshwater exploitability in the coastal Viet-

namese Mekong Delta assessed by gauging records and numerical simulations. J. Hydrol. 130655. https://doi.org/10.1016/j.jhydrol.2024.130655

Tran, D.Q., Nguyen, N.N.T., Huynh, M.V.T., Bairagi, S.K., Le, K.N., Tran, T. V., Durand-Morat, A., 2024. Modeling saltwater intrusion risk in the presence of uncertainty. Sci. Total Environ. 908, 168140. https://doi.org/10.1016/j.scitotenv.2023.168140

Tran, T.A., Tran, D.D., Van Vo, O., Pham, V.H.T., Van Tran, H., Yong, M.L., Le, P.V., Dang, P.T., 2024. Evolving pathways towards water security in the Vietnamese Mekong Delta: An adaptive management perspective. Ambio. https://doi.org/10.1007/s13280-024-02045-0

Tran, T.N., Le Vo, P., Van Nghi, V., Quoc Bang, H., 2019. Salt intrusion adaptation measures for sustainable agricultural development under climate change effects: A case of Ca Mau Peninsula, Vietnam. Clim. Risk Manag. 23, 88–100. https://doi.org/10.1016/j.crm.2018.12.002

van Keulen, D., Kranenburg, W.M., Hoitink, A.J.F., 2025. A New Harmonic Regression Approach to Interpret and Predict Estuarine Salinity Variation. J. Geophys. Res. Ocean. 130. https://doi.org/10.1029/2024JC022185

Veerapaga, N., Shintani, T., Azhikodan, G., Yokoyama, K., 2020. Estuaries and coastal zones in times of global change : proceedings of ICEC-2018, in: Nguyen, K.D., Guillou, S., Gourbesville, P., Thiébot, J. (Eds.), . Springe Singapore, Singapore. https://doi.org/https://doi.org/10.1007/978-981-15-2081-5

Vu, H.T.D., Tran, D.D., Schenk, A., Nguyen, C.P., Vu, H.L., Oberle, P., Trinh, V.C., Nestmann, F., 2022. Land use change in the Vietnamese Mekong Delta: New evidence from remote sensing. Sci. Total Environ. 151918. https://doi.org/10.1016/j.scitotenv.2021.151918

Vu, H.T.D., Zemann, M., van der Linden, R., Dan, T.C., Oberle, P., Seidel, F., Nguyen, N.M., Tu, L.X., 2025. Modeling Ocean Wave Conditions at a Shallow Coast Under Scarce Data Availability: A Case Study in the Mekong Delta, Vietnam. J. Mar. Sci. Eng. 13. https://doi.org/10.3390/jmse13020265

Vu, M.T., Luu, C., Bui, D.Q., Vu, Q.H., Pham, M.Q., 2024. Simulation of hydrodynamic changes and salinity intrusion in the lower Vietnamese Mekong Delta

under climate change-induced sea level rise and upstream river discharge. Reg. Stud. Mar. Sci. 78, 103749. https://doi.org/10.1016/j.rsma.2024.103749

Wang, J., Hong, B., Gong, W., 2022. Study of an abnormally strong saltwater intrusion in the Humen Channel of the Pearl River estuary. Anthr. Coasts. https://doi.org/10.1007/s44218-022-00008-0

Winterwerp, J.C., Wang, Z.B., Van Braeckel, A., Van Holland, G., Kösters, F., 2013. Man-induced regime shifts in small estuaries - II: A comparison of rivers. Ocean Dyn. 63, 1293–1306. https://doi.org/10.1007/s10236-013-0663-8

Wünsche, A., Becker, M., Fritzsch, R., Kelln, J., Winter, C., 2024. The sensitivity of tidal asymmetry descriptors in the Ems estuary. Ocean Dyn. 74, 613–627. https://doi.org/10.1007/s10236-024-01622-x

Zhang, Y., Jiao, S., Zhou, W., Wang, Y., Lv, X., 2025. Exploration the effect of nonstationary signals on the tidal phenomenon using F_TIDE part I. Sci. Rep. 15, 1–15. https://doi.org/10.1038/s41598-025-90490-6

Zoccarato, C., Minderhoud, P.S.J., Teatini, P., 2018. The role of sedimentation and natural compaction in a prograding delta: insights from the mega Mekong delta, Vietnam. Sci. Rep. 8, 1–12. https://doi.org/10.1038/s41598-018-29734-7